POLITECNICO DI MILANO
Department of Civil and Environmental Engineering
Doctoral School in Structural, Earthquake and Geotechnical Engineering

SEISMIC PERFORMANCE OF PRECAST STRUCTURES WITH DISSIPATIVE CLADDING PANEL CONNECTIONS

Doctoral Dissertation of:
Bruno Alberto Dal Lago

Supervisor:
Prof. Fabio Biondini

The Chair of the Doctoral Program:
Prof. Roberto Paolucci

Year 2015 – Cycle XXVI

This page is left intentionally blank

Seismic Performance of Precast Structures with Dissipative Cladding Panel Connections

PhD thesis by: Bruno Alberto Dal Lago
Supervisor: Prof. Fabio Biondini

February 2015

Doctoral School in Structural, Earthquake and Geotechnical Engineering
Department of Civil and Environmental Engineering
Politecnico di Milano

This page is left intentionally blank

Acknowledgements

I am very grateful to prof. Fabio Biondini for his constant scientific advisement and tutoring activity. Special thanks go to my two old masters, my father and prof. Giandomenico Toniolo. Marco Lamperti also deserves special acknowledgements for his fundamental contribution.

The work developed during the Research activity at Politecnico di Milano related to my thesis has been funded by the European Commission within the Safecast and especially the Safecladding projects and by the Italian Department of Civil Protection through the ReLUIS program. Both funding institutions are gratefully acknowledged.

Many acknowledges go to the team of researchers, technicians and students with whom I have been cooperating at Politecnico di Milano. They are prof. Liberato Ferrara, prof. Roberto Felicetti, dr Andrea Titi, dr Francesco Foti and Giulia Carozzi, Giovanni Lobina, Antonio Cocco and Paolo Broglia, Silvia Bianchi, Giulia Marelli, Roberto Segala, Giulia Mariani Orlandi, Alessandro Rocci, Nicola Zoeddu and Marjo Cerriku.

For what concerns the Safecladding consortium, Antonella Colombo from Assobeton, Alessio Rimoldi from BIBM, Paolo Negro and Francisco Javier Molina from ELSA/JRC, prof. Matej Fischinger, prof. Tatjana Isakovic and Blaž Zoubek from the University of Ljubljana, prof. Joannis Psycharis and Joannis Kaliviotis from the Technical University of Athens, prof. Faruk Karadogan, prof. Ercan Yuksel, Ihsan Egin Bal and Eleni Smyrou from the Istanbul Technical University, Bulent Tokman from TPCA and Alejandro Lopez Vidal from ANDECE are gratefully acknowledged, among the others.

The following partners from the industry are also acknowledged: Antonello Gasperi, Claudio Pagani and Enzo Ruggeri from BS-Italia, Uberto Marchetti and Massimo Martinetti from DLC, Roberto Ragozzini and Ivan Marinelli from Ruredil, Stefano Terletti and Diego Carminati from Halfen, Mauro and Luciano Nava from MC prefabbricati.

A hug goes to Beatrice for her collaboration in the layout of the book cover graphics.

Abstract

The inadequate seismic behaviour of the cladding panel connections of precast structures and the consequent failures occurred under recent earthquakes in Southern Europe showed that a revision of the technology and design philosophies adopted for this type of systems is necessary. To solve this problem, a general framework for the seismic design of precast structures based on innovative fastening systems of the cladding panels is proposed. In this framework, the stability of the cladding panels under seismic action is ensured by means of a dissipative system of connections in between the panels that allows to control the level of forces and to limit the displacements. The proposed connection systems consist of friction-based or plasticity-based devices inserted in between panels, that are connected to the structure through a statically determined arrangement. In this way, the panel-to-panel connections lead the cladding panels to become integral part of the whole façade, making it much stiffer up to the limit force associated with the friction threshold or yielding of the devices. Plasticity-based dissipative connectors to be inserted between columns and panels are also proposed and investigated. The technological aspects and design choices of materials and shapes leading to a stable hysteretic behaviour of the dissipative devices are discussed and subjected to experimental verification at Politecnico di Milano by means of monotonic and cyclic tests carried out on single devices, as well as on full scale two-panel structural sub-assemblies with dissipative connections. The silicone sealant, that is generally interposed in between the panels, is also mechanically characterised through experimental testing. Design guidelines for single devices are derived based on the interpretation of the experimental results. Capacity design procedures for structural sub-assemblies and systems are also developed based on the mechanical characteristics of the dissipative connectors. The efficiency of the proposed approach is demonstrated by means of non-linear dynamic analyses of typical precast frame-panel structural systems, as well as through a further experimental campaign carried out at ELSA Laboratory of the Joint Research Centre of the European Commission on a full-scale prototype of a precast building with cladding panels. This experimental program includes pseudo-dynamic and cyclic tests on structural assemblies provided with vertical and horizontal panels and different types of connection systems, including the friction-based panel-to-panel dissipative connections tested at Politecnico di Milano. Numerical simulation of the pseudo-dynamic and cyclic tests is performed to calibrate the modelling criteria provided in the design guidelines and to validate simplified procedures for the estimation of the maximum drift attained during a seismic event. The role of the diaphragm action on the efficiency of the proposed connection systems is finally investigated by means of dynamic nonlinear analyses carried out on a set of precast buildings with different plan geometry and distribution of the earthquake-resisting system. The results confirm the remarkable improvement of the seismic performance of precast structures based on the beneficial effects of dissipative cladding connections, which can provide suitable energy dissipation capacity and limit forces and displacements when the effectiveness of the horizontal diaphragms is ensured.

Sommario

L'inadeguato comportamento sismico delle connessioni dei pannelli di parete delle strutture prefabbricate e i conseguenti fenomeni di collasso che si sono verificati durante recenti eventi sismici in Europa meridionale evidenziano la necessità di una revisione delle metodologie di progetto e delle tecnologie realizzative di tali sistemi. In questo lavoro si propone una soluzione del problema attraverso una nuova impostazione della progettazione sismica di strutture prefabbricate basata sull'impiego di sistemi innovativi di connessione dei pannelli di parete. In tale impostazione, la stabilità sotto sisma dei pannelli viene garantita mediante un sistema di connessioni dissipative che consente il controllo di forze e spostamenti. Si tratta di semplici dispositivi metallici con funzionamento ad attrito o a comportamento plastico da inserire nei giunti tra i pannelli, che sono vincolati alla struttura con un assetto isostatico. Con l'introduzione dei dispositivi si ottiene l'integrazione dei pannelli nel sistema sismo-resistente, che presenta quindi una elevata rigidezza fino al raggiungimento della soglia di attrito o del limite di snervamento dei dispositivi stessi. Nella tesi vengono inoltre proposte e studiate connessioni dissipative da inserire tra pannelli e pilastri. Si presentano le scelte tecnologiche di materiali e forme che assicurano un efficace comportamento isteretico dei dispositivi e si mostrano i risultati di una campagna sperimentale svolta presso il Politecnico di Milano con prove monotone e cicliche sia su singoli connettori, sia su sottoinsiemi strutturali costituiti da due pannelli in scala reale. Nell'ambito di tale campagna vengono svolte prove sperimentali anche per studiare le caratteristiche meccaniche dei sigillanti siliconici generalmente interposti tra i pannelli. Sulla base dei risultati sperimentali vengono quindi definite delle linee guida di progetto sia per i singoli dispositivi di connessione, sia per assiemi strutturali di pannelli mediante criteri di gerarchia delle resistenze. L'efficacia dell'approccio proposto viene mostrata sia con analisi dinamiche non lineari di strutture telaio-pannelli, sia con ulteriori prove sperimentali svolte presso il laboratorio ELSA del Centro Comune di Ricerca della Commissione Europea su un prototipo in scala reale di un edificio prefabbricato con pannelli di parete. Il programma sperimentale comprende prove pseudo-dinamiche e cicliche su assiemi strutturali con pannelli verticali e orizzontali e differenti sistemi di connessione dei pannelli, tra cui i connettori dissipativi ad attrito studiati al Politecnico di Milano. La simulazione numerica delle prove pseudo-dinamiche e cicliche consente inoltre di validare i criteri di modellazione proposti nelle linee guida e le procedure per la stima degli spostamenti massimi attesi. Il lavoro si conclude con lo studio del ruolo dei diaframmi di piano sull'efficienza del sistema di connessione proposto, svolto mediante analisi dinamiche non lineari di edifici prefabbricati con diversa geometria e distribuzione del sistema sismo-resistente. I risultati delle analisi confermano il significativo miglioramento delle prestazioni sismiche di strutture prefabbricate con sistemi di connessioni dissipative, che con una efficace azione diaframma possono conferire una elevata capacità di dissipazione e limitare in modo significativo l'entità di forze e spostamenti.

Contents

List of Figures

List of Tables

This page is left intentionally blank

Foreword

The work presented in this thesis has been funded by the European Commission within the FP7-SME-2011 SAFECLADDING research project (Grant agreement No. 314122, 2012) and jointly by the Italian Department of Civil Protection (DPC) and the Italian Laboratories University Network of Earthquake Engineering (ReLUIS) within the research programs DPC-ReLUIS 2010-2013 and DPC-ReLUIS 2014-2015. The funding institutions are gratefully acknowledged. Although such projects have been contributed by research and industry consortia, it is noted that the numerical and experimental research activities presented herein have been developed at Politecnico di Milano by the POLIMI team with full involvement of the thesis' author, with the exception of the execution of the full scale prototype experimental tests performed at the ELSA laboratory of the Joint Research Centre of the European Commission. The ELSA-JRC team is also gratefully acknowledged.

This page is left intentionally blank

Chapter 1

Introduction

The present chapter introduces the relevance of the research activity carried out related to the thesis. Motivation, objectives and scope of the study are described. A seismic design framing of precast structures with cladding panels is proposed. Finally, a brief outline of the document is provided.

1.1. Motivation of the study

Precast concrete buildings have been diffusing worldwide since the decade of 1960s, gaining a large diffusion for industrial and commercial buildings with frame structures, and also for residential buildings mainly with large panel structures, especially diffused in Eastern Europe, Russian federation and Commonwealth of Independent States (CIS). The large diffusion of such structures highlights the crucial importance that they have on the safety of people working or living in those buildings and on the economy of a nation or a continent.

The latest version of the European design standard, Eurocode 8 (CEN-EN 1998:2004), recognizes that precast frame structures can be designed with the energy dissipation capacity comparable to that of the corresponding cast-in-situ structures. Based on this view, the current design practice of precast buildings is based on a bare frame model where the peripheral cladding panels enter only as masses without any stiffness.

For what concerns the practice of the structural connections of cladding panels, P.J. Harrison starts its description of cladding panels fixings with the following statement (Taylor 1992): "*Fixings are generally the most misunderstood and misused items involved in the cladding of any building*". Actually, precast concrete cladding panels have always been considered as non-structural elements. The panels are then connected to the structure with fastenings dimensioned with a local calculation on the base of their mass for anchorage forces orthogonal to the plane of the panels. The technology available in practice offers, however, connections that are designed to be fixed and distributed in several locations over the cladding panel. This approach does not work, as it was recently dramatically shown by several recent violent shakes in Southern Europe, including L'Aquila in 2009, Grenada in 2010 and Emilia in 2012. The panels, fixed in this way to the structure, come to be integral part of the resisting system conditioning its seismic response. The high stiffness of this resisting system leads to forces much higher than those calculated from the frame model. These forces are related to the global mass of the floors and are primarily directed in the plane of the walls, as it is normally

disregarded by designers. Furthermore, the seismic force reduction in the type of precast structures of concern relies on energy dissipation in plastic hinges formed in the columns. Very large drifts of the columns are needed to activate the energy dissipation assumed in design. However, typically the displacement capacity of the connections, even if specifically designed in order to allow mutual displacements, which is unusual, is exhausted well before such large drifts can develop. Therefore the design of these connections cannot rely on the seismic reduction factor used for design of the bare frame. The actual intensity and direction of the forces and the limited energy dissipation may lead fastenings to failure, leaving the frame columns and beams practically undamaged. Figure 1.1a shows an emblematic image after L'Aquila earthquake in 2009: a building of recent construction of which the structure (columns, beams, roof elements) kept substantially its integrity, while a whole wall of vertical panels, on the contrary, has collapsed. The cause of the collapse is shown in Figure 1.1b: the fastenings of the panels failed under forces for which they were not designed.

(a) (b)

Figure 1.1 – Cladding failure during L'Aquila earthquake: (a) view of the whole line of vertical panels that collapsed, (b) particular view of the failed connections

Numerous have been the collapses of wall panels caused by the failure of their fastenings. These collapses concerned a relevant portion of existing buildings in proximity of the epicentres. The forces received under the earthquake have been much higher than those calculated in the design stage on the base of a local behaviour. In fact the wall system provides the construction with a much higher stiffness than that of the bare frame made of columns and beams modelled in the structural analysis. The actual seismic response has been therefore characterised by a high acceleration that brought strong distortion forces on the fastenings in the plane of the walls. Such collapses occurred in different buildings, involving both vertical and horizontal panels, as shown respectively in Figure 1.2a and Figure 1.2b.

Figure 1.3a shows the interior of a factory: the structure of columns, beams and roof elements had no damages; a whole line of horizontal cladding panels fell down. The same cause of the collapse is shown in Figure 1.3b, that is the failure of the fastening devices. Figure 1.4 shows

the strengthening promptly applied to the remaining panels after the earthquake with strong bolted steel angles.

Failures did not involve only channel bars but also other types of fastenings, as shown in Figure 1.5a and Figure 1.5b. It has been not a question of product inadequacy, but of inadequate design of the connection. In fact the design followed the specific rules of the code, quantifying the forces with a local analysis on the base of the mass of the single panel considered as a non-structural element. Actually the panels received much higher forces differently directed with respect to what considered in design. This happened because their fixed connection to the structure made them integral part of the resisting structural system, taking it to a much higher stiffness. The design approach itself, as proposed by the codes, shall be improved in its principles and new adequate specific solutions shall be proposed by the manufacturers.

(a) (b)

Figure 1.2 – Collapse of single panels: (a) horizontal panels, (b) vertical panels

(a) (b)

Figure 1.3 – Cladding failure during L'Aquila earthquake: (a) view of the whole line of horizontal panels that collapsed, (b) particular view of the failed connections

Figure 1.4 – Emergency intervention on horizontal cladding panels with several thick steel angles per panel connected with post-installed fasteners

(a) (b)

Figure 1.5 – Failure of panel connections: (a) strong strap, (b) standard strap and bearing bracket

Finally, Figure 1.6a and Figure 1.6b show two additional images of L'Aquila earthquake effects. The former shows a building under construction where the cladding panels dragged to collapse two floor TT elements to which they were connected, the latter shows a building just completed: no relevant damages occurred, but the large base panel, 12 by 2,5 metres for 10 tons of weight with upper panels placed over it, moved 10 centimetres from its original position.

From the above considerations it is clear that the current design criteria, leaving the walls to collapse since after their failure the remaining structure will resist anyway by itself, does not work when the failure implies the fall of panels up to 12 tons of weight. The mortal danger of these collapses requires a different approach. And this considerations hold true for all, precast and cast-in-situ concrete, steel and timber structures: even the fall of a traditional masonry large cladding wall represents a serious hazard for human life. New technological solutions for connectors with proper design approaches are therefore urgently required.

(a) (b)

Figure 1.6 – Behaviour of cladding panels: (a) the collapse of vertical panels dragged the floor member to failure, (b) undamaged building with large permanent relative displacements among panels

1.2. Objectives and scope

The present dissertation is related to several objectives that have to be achieved in order to propose proper solutions and to significantly improve the actual knowledge and technical practice related to precast concrete panel connections. A systematic framing of the problem is needed in order to establish proper procedures for the seismic design of precast structures with cladding panels. This framing shall start from the structural arrangement of the panels, including them as fully structural elements. Dissipative solutions based on friction or on plasticity will be studied in order to ensure a safe and proper application. Innovative connection devices will be subjected to experimentation in order to characterise their mechanical behaviour by performing local tests on the single connectors. Furthermore, proper rules for their application in panel structural sub-assemblies will be assessed and tested, in order to provide reliable solutions. The effect of dissipative cladding panel connection systems in enhancing the overall structure will be studied through numerical analyses under dynamic seismic excitation, investigating the problem of the seismic performance of coupled wall/frame structures, and experimental tests on full scale prototypes of precast structures will be performed in order to verify the predicted structural responses and to validate design procedures. The effect of the diaphragm action on the seismic response of precast buildings with dissipative cladding panel connections will be assessed by means of parametric analyses, studying the seismic response of a set of buildings with different plan geometry and distribution of the earthquake-resisting system.

1.3. Innovative concepts for seimic design of cladding panel connection systems

1.3.1. Types of panel connection systems

Regardless of the shape of the cladding panels, they are typically designed to carry only the self-weight, wind forces to which the panels are directly exposed, and seismic forces associated to the panel self-weight. In most cases, the forces generated in the panel during the manufacturing and erection stages of construction govern the reinforcement design of the panel (PCI 1989). According to Arnold (1989), there are four degrees of façade structural participation with the lateral load resisting system of a building, namely:

1) Theoretical Detachment (push-pull connections). While, in theory, push-pull connections detach the cladding from the structure, in a building with hundreds of cladding panels it is likely that the detachment is not complete, and there is some transmission of forces from the structure to the panels and vice versa.

2) Accidental Participation (slotted connections and sliding joints). Because of deterioration or errors in installation, the separation between the cladding and structure is not effective. This is uncontrolled participation.

3) Controlled Stiffening or Damping. This involves the use of devices to connect the cladding to the structure in such a way that the damping of the structure is modified (usually increased) or the structure is stiffened.

4) Full Structural Participation. The cladding and the structure become a new integrated composite structure in which each element performs an assigned role. The cladding may participate in vertical support, and definitely contributes to lateral resistance.

This classification, which is very reasonable, is referred to existing cladding panels, while the accidental participation solution shall be disregarded for a new intervention, since it may cause serious problems in the seismic behaviour of the building. Special attention shall be given to sliding connection in order to make their behaviour stable and reliable, granting an efficient detachment effect.

A new classification based on the panel structural sub-assembly is proposed to define the possible connection systems that can be employed in a new construction from the structural participation point of view. The proposal is also reported in Biondini *et al.* (2010a, 2013b), Colombo & Toniolo (2010, 2012c) and Toniolo (2014). The following four options are considered:

(a) Isostatic systems. The isostatic connection system involves a rigid motion of the panel. All actions on the connections depend exclusively on the statically determined arrangement chosen, while building deformation and dynamics plays a secondary role on in-plane actions. Damage is not expected to occur within the panel and all connections are likely to remain in elastic field, although slight damage is admitted in ductile connections. Within the building design the cladding panels may be omitted, but their contribution in terms of seismic mass and, eventually, stiffness, shall be taken into account, according to the chosen isostatic mechanism. The panel connections may then be designed according to their sub-assembly static scheme only.

(b) Integrated systems. The integrated connection system provides a full participation of the panel in the lateral load resisting system of the building. It is desirable that panels and connections remain elastic, but slight damage is admitted in ductile connections and/or in the panels (provided with ductile reinforcement detailing). Within the building design the cladding panels shall be explicitly considered, and their connections shall be adequately proportioned on the base of the combined seismic actions.

(c) Dissipative systems. The dissipative connection system is an evolution of the isostatic, where dissipative connections are added between cladding and structure or within the cladding panels. All energy dissipation is likely to occur within the specific dissipative devices, with the panel and those connections that create the isostatic system remaining elastic. The cladding participates to the lateral load resisting system with forces that are controlled by the dissipative connections. Within the building design the cladding panels may be considered explicitly or with simplified methods, and their connections may be designed according to their sub-assembly static scheme.

(d) Second-line systems. Second-line systems consist in additional safety devices that link the structure and the panel in order to restrain it from falling once the primary load-bearing system fails. This solution can be added to one of the previous, and can not substitute none of them. It can be used for the temporary safe restraint of existing panels linked with possible deficiencies. Since the devices enter in use only after the panel tends to fail, they can be omitted in the building design. They can be designed according to the panel sub-assembly static scheme only. Some technological examples of such connections are included in Protezione Civile (2012).

Conceptual sketches of the working principle of a precast frame with isostatic or integrated cladding panel connection systems are illustrated in Figure 1.7 for vertical panels and in Figure 1.8 for horizontal panels. A typical precast frame structure is highly flexible, due to its un-braced cantilever-type column static scheme. An isostatic solution, for instance provided with fixed hinge connections positioned in order to create a truss element, fully allows the structure to displace without inducing stiffness. On the contrary, an integrated solution, for instance provided with four fixed connections placed at the panel corners in order to create a double clamped beam element, introduces a large in-plane additional stiffness associated to the displacement of the frame, to which correspond large forces arising in the connections and in the panels.

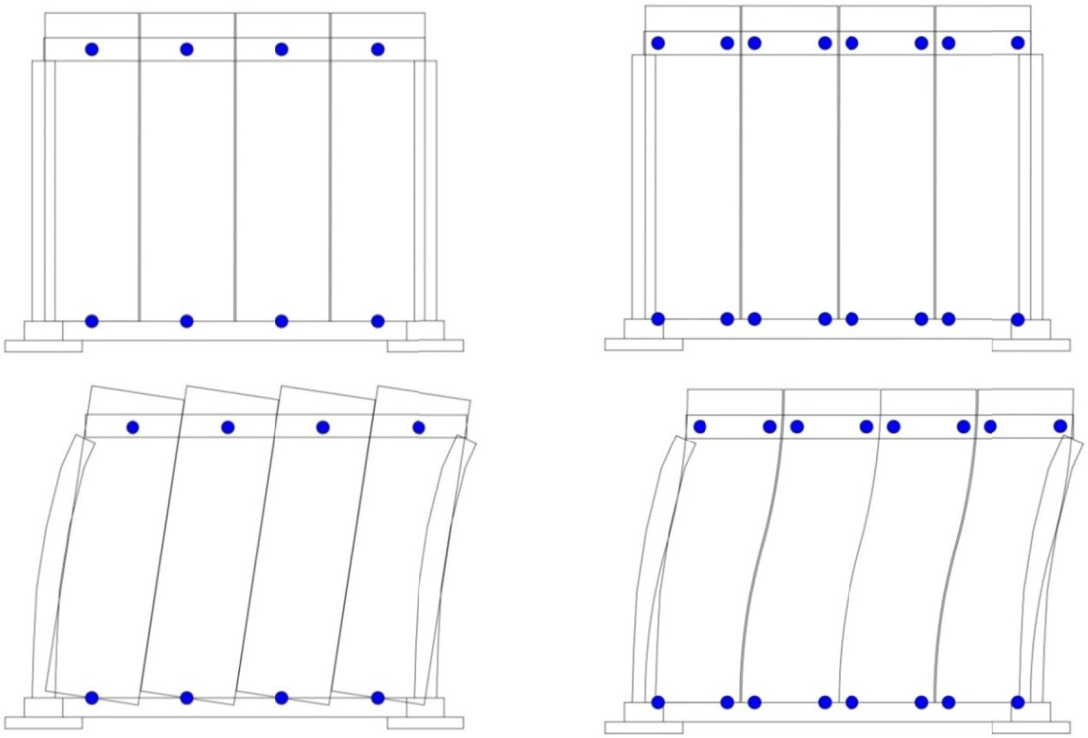

(a) (b)

Figure 1.7 – Vertical cladding panels: (a) isostatic connection system and (b) integrated connection system

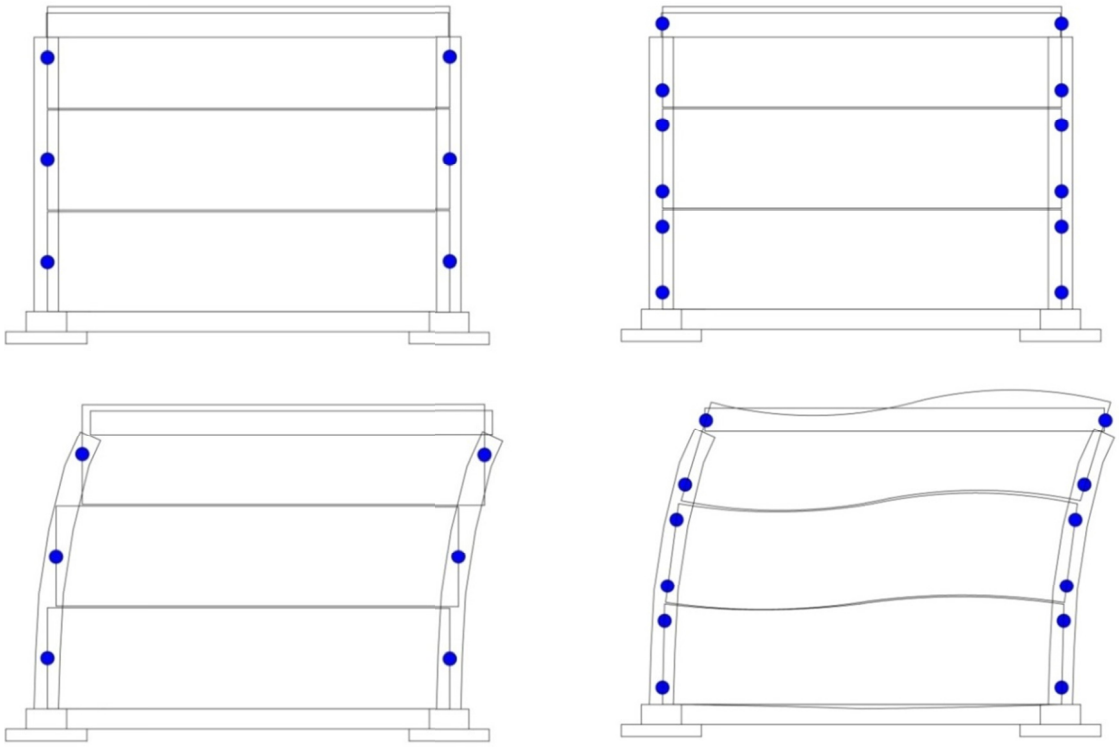

(a) (b)

Figure 1.8 – Horizontal cladding panels: (a) isostatic connection system and (b) integrated connection system

The following symbology is used in order to identify the degrees of freedom and of restraint of a connection:

◀ restrained displacement in the direction of the triangle enlargement.

⟶ free displacement in the arrow direction. High speed displacement is expected to occur.

→ free displacement in the arrow direction. Slow speed displacement may occur.

^^^ displacement direction of work of dissipative connection.

⇉ Restrained rotation around the axis indicated by the double arrow.

1.3.2. Isostatic systems

Several isostatic connection arrangements can be adopted for both vertical and horizontal panels. The suggested isostatic connection arrangements for vertical panels are presented hereafter. Additional degrees of restraint can be added only in case they do not modify the correct kinematic of the panel.

- Pendulum arrangement. The pendulum connection system for vertical panels consists in a base central support around which the panel rotates in-plane and a top shear panel-to-beam connection that allows slow-speed vertical deformation. For the correct functioning of this system it is of main importance to leave the panel displace vertically also in the downward direction at its base, which can be ensured by protecting the joint or adding soft material. This structural arrangement shall also restrain rotation around the vertical axis of the panel or torsion of the panel. Two solutions are foreseen to solve this issue, which may also be combined. Figure 1.9a shows a solution with a rotational restrainer included in the base connection, while Figure 1.9b show a configuration with added push-pull connections that shall allow high speed vertical displacements.

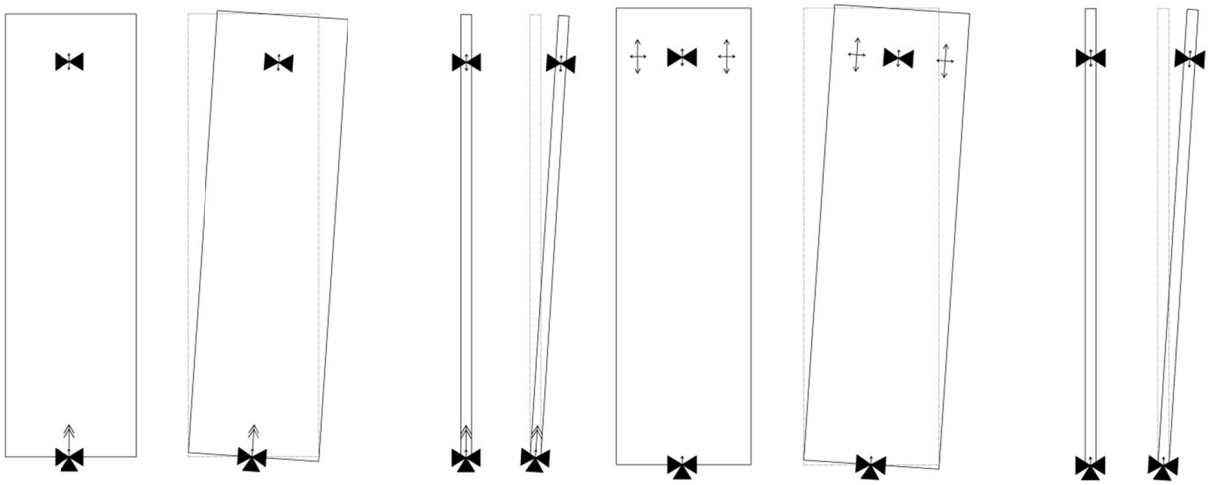

(a) (b)

Figure 1.9 – Isostatic pendulum arrangements for vertical panels: (a) base torsional clamp and (b) with additional push-pull connections

- Rocking arrangement. The rocking connection system for vertical panels consists in base supports and top shear panel-to-beam connections that shall allow high speed vertical displacement. The panel can be simply supported on its foundation. In case of a simple support, additional out-of-plane displacement restrainers are suggested to be used. Figure 1.10 shows the in-plane and out-of-plane behaviour of the rocking arrangement.

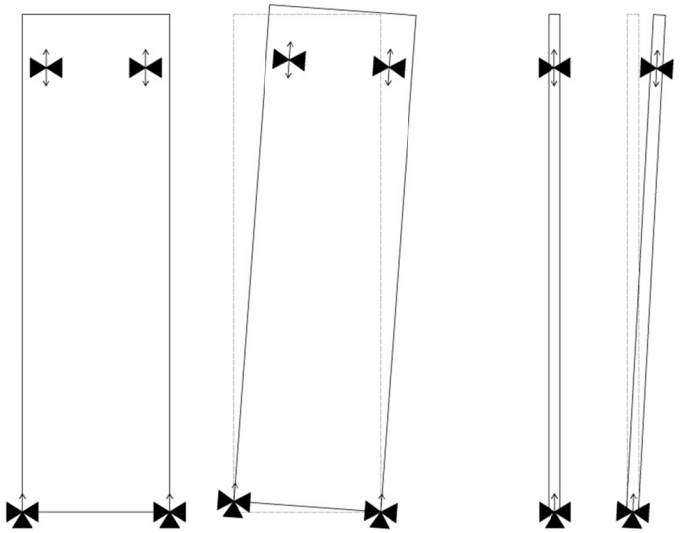

Figure 1.10 – Isostatic rocking arrangement for vertical panels

- Cantilever arrangement. The cantilever connection system for vertical panels consists in base supports and top horizontally sliding connections that shall allow high speed relative displacement between the beam and the panel. The panel can be simply supported on its foundation. Figure 1.11 shows the in-plane and out-of-plane behaviour of the cantilever arrangement.

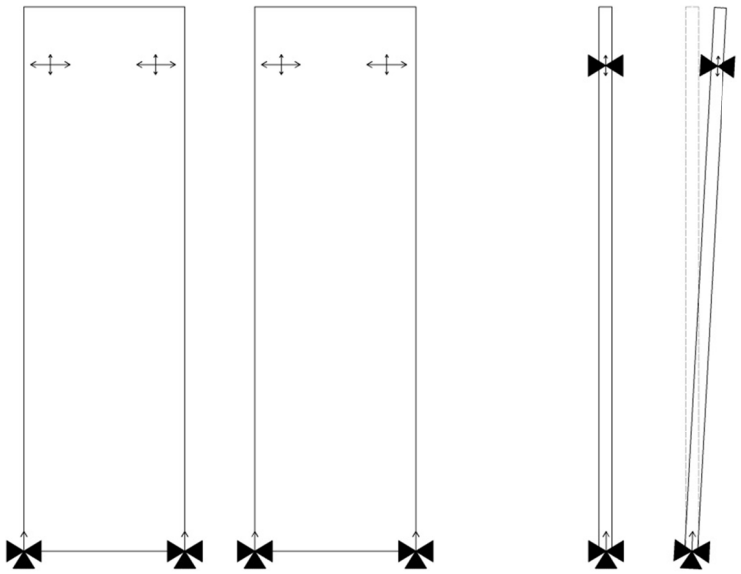

Figure 1.11 – Isostatic cantilever arrangement for vertical panels

- Swaying arrangement. The swaying connection system for horizontal panels consists in panel-to-foundation or panel-to-column supports and horizontally sliding connections that shall allow high speed relative displacement between the panel and the column or the beam. Four solutions are foreseen. Figure 1.12a shows a solution with bottom sliding supports and top shear connection, provided with additional push-pull connections, Figure 1.12b solution is similar to the previous with supports at the top and shear and push-pull connections at the bottom, Figure 1.12c shows a solution with bottom supports and horizontal restrainers and top sliding connections and Figure 1.12d solution is similar to the previous with supports at the top and shear and sliding connections at the bottom.

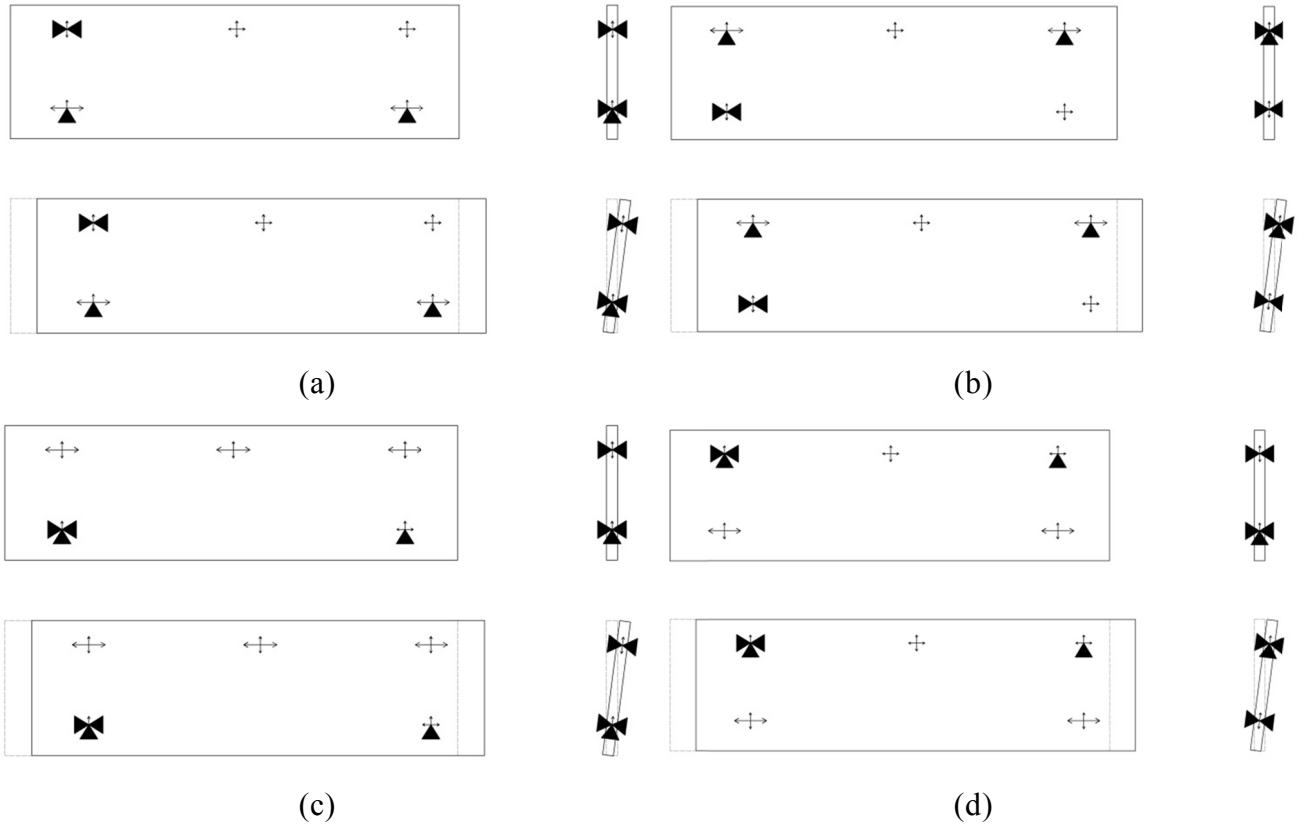

Figure 1.12 – Isostatic swaying arrangements for horizontal panels: (a) sliding bottom supports, (b) sliding top supports, (c) sliding top connections and (d) sliding bottom connections

- Stacked panels arrangement. This connection system for horizontal panels consists in panel-to-foundation or panel-to-panel fixed connections, that may also be simple supports on the panel underneath or on the foundation, and horizontally sliding connections that shall allow high speed relative displacement between the panel and the column or the beam. Figure 1.13 shows the in-plane and out-of-plane behaviour of the stacked panels arrangement. This solution may be used only for a low number of stacked panels.

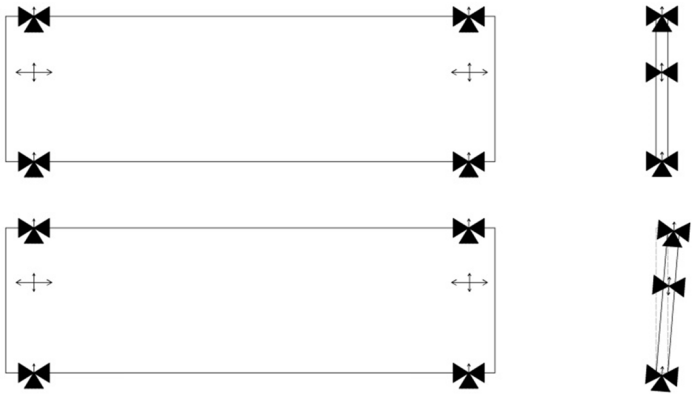

Figure 1.13 – Isostatic stacked panels isostatic arrangement for horizontal panels

1.3.3. Integrated systems

Several integrated connection arrangements can be adopted for both vertical and horizontal panels. Few suggested integrated connection arrangements for vertical panels are presented hereafter. Additional degrees of restraint can be added to strengthen the system.

- Hampered rocking arrangement. The hampered rocking connection system for vertical panels can be obtained with two solutions. Figure 1.14a shows a solution with clamped panel base and top shear connection. Figure 1.14b shows a solution with supported base and top fixed connection. In the latter case, only non-composite panels are suggested to be used to compensate for the hampered temperature deformation.

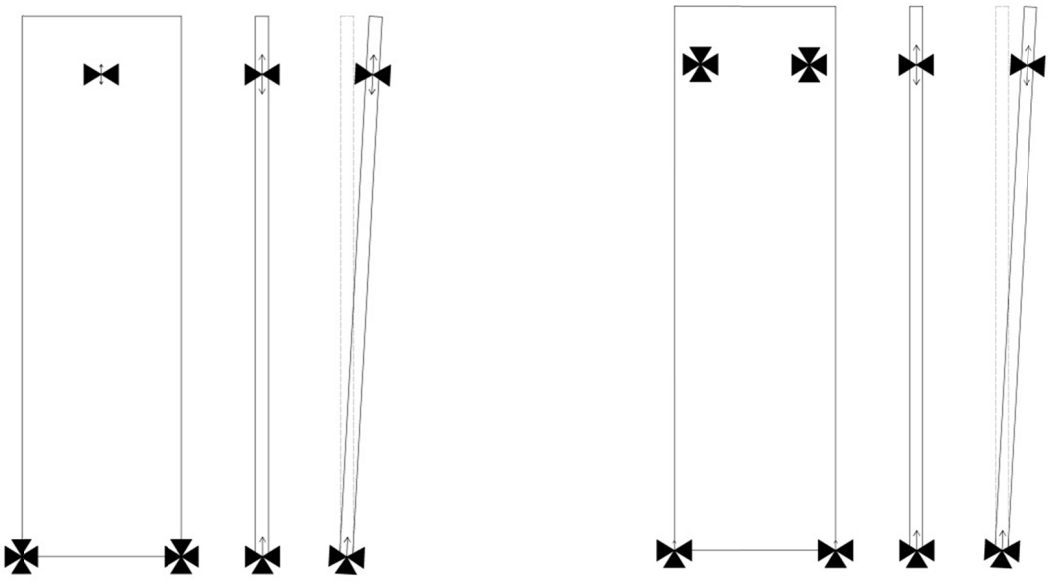

(a) (b)

Figure 1.14 – Integrated hampered rocking arrangements for vertical panels: (a) base clamp and (b) top clamp

- Fixed arrangement. The fixed connection system for horizontal panels consists in the application of fixed connections in correspondence of the panel corners. Figure 1.15 illustrates a possible solution. Only non-composite panels are suggested to be used to compensate for the hampered temperature deformation.

Figure 1.15 – Integrated fixed arrangement proposed for horizontal panels

1.3.4. Dissipative systems

Dissipative connections may be inserted in between the panels or in between panels and frame members (or its foundation). Not all isostatic solutions are suitable for the insertion of panel-to-panel dissipative connections. In particular, only the pendulum and rocking arrangement for vertical panels and only the swaying arrangement for horizontal panels are taken into consideration. Panel-to-frame dissipative connections can be used in all configurations, even if the above cited are suggested. Additional degrees of restraint can be added only in case they do not modify the correct kinematic of the panel.

- Pendulum arrangement. The pendulum dissipative connection system for vertical panels can be obtained on each of the solutions considered for isostatic configuration. Figure 1.16a shows the relative panel displacement that can be used for the exploitation of shear dissipative devices.
- Rocking arrangement. The rocking dissipative connection system functioning scheme is illustrated in Figure 1.16b together with the relative panel displacement that can be used for the exploitation of shear dissipative devices.

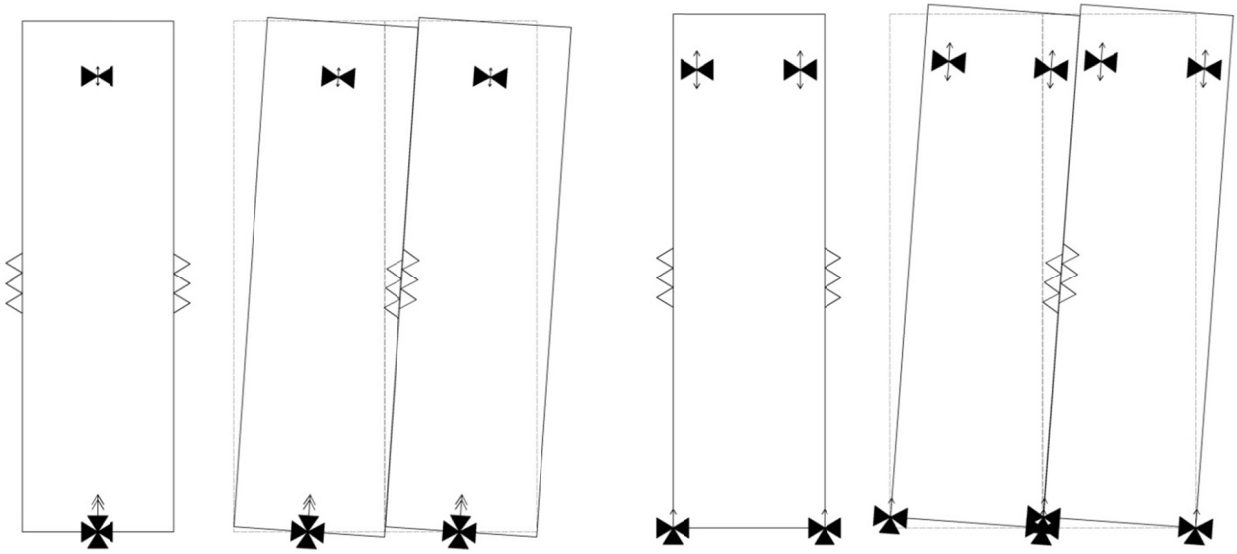

(a) (b)

Figure 1.16 – Dissipative arrangements proposed for vertical panels: (a) pendulum and (b) rocking

- Swaying arrangement. The swaying dissipative connection system for horizontal panels working scheme is illustrated in Figure 1.17 together with the relative panel displacement that can be used for the exploitation of shear dissipative devices.

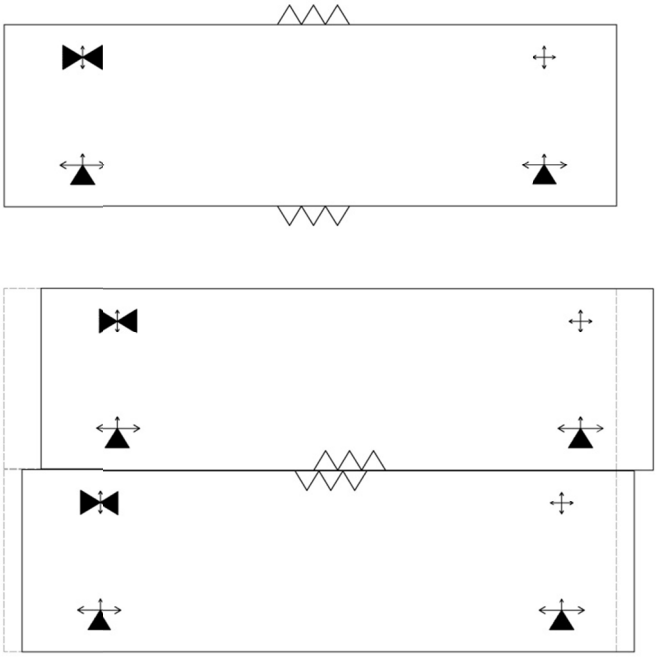

Figure 1.17 – Dissipative swaying arrangement for horizontal panels

1.4. Outline

The dissertation is divided into seven chapters.

The first chapter presents the description of the problem and the proposed framing of the seismic design of precast structures with cladding panels.

The second chapter presents the state of the art regarding both precast concrete structures technologies and related research devoted to their seismic behaviour, with focus on research related to cladding panels.

The third chapter illustrates the experimental activity performed on innovative cladding panel dissipative connections based on friction or on plasticity, together with considerations on their design.

The fourth chapter illustrates the experimental activity performed on panel structural sub-assemblies provided with dissipative and isostatic connection systems under different arrangements, together with the experimental characterisation of silicone sealant on both local and panel sub-assembly scale. Design guidelines are proposed.

The fifth chapter presents a numerical investigation of the efficiency of dissipative cladding panel connections on the seismic enhancement of a case study precast structure with rigid diaphragm. Furthermore, the results of an experimental campaign on a full scale precast

prototype structure provided with different cladding panel systems and subjected to pseudo-dynamic and cyclic tests are presented, together with numerical simulation. Simplified performance-based procedures for the estimation of the maximum drift are also applied and their efficiency is commented.

The sixth chapter is dedicated to the study of the influence of the diaphragm stiffness on the seismic response of precast structures through non-linear dynamic analysis of a case sudy precast structure and a parametric investigation for buildings with different plan geometries.

The seventh chapter contains the conclusions, together with the expected future developments and challenges.

Chapter 2

Seismic behaviour of precast concrete frame structures

The state of the art for what concerns both practice and research on precast concrete structures is summarised in the present chapter. The precast concrete structural arrangements that have been developing in practice are illustrated. A brief overview of the research history performed on dry-assembled precast frame concrete structures is also provided. The specific behaviour of classical precast frame connections and their role on the seismic response of the structure is addressed, followed by a deepening about the practice of cladding panel arrangements, the research activity performed on dissipative cladding panel connections and the existing design philosophies and methods.

2.1. Precast structural arrangements

Precast concrete structures can be divided into three main categories based on the typology of bearing members, namely frame, panel and block structures.

Each typology can further be subdivided into two categories, according to the technology of joints, wet and dry assembled. Wet assembled structures are conceived in order to emulate cast-in-situ concrete structures, by realising clamped connections with in-situ concrete pouring of the connection zone, usually provided with rebars protruding from the precast members. Dry assembled structures are connected by mechanical devices that couple the precast members. The latter denomination also includes semi-dry connections, with an in-situ completion procedure involving a small amount of mortar pouring.

Dry assembled frame structures are the most typical technology developed and used in Europe (see Mandelli Contegni *et al.* 2008 and Bonfanti *et al.* 2008 for details about typical Italian precast structural systems).

2.2. Research on seismic behaviour of precast structures

Traditional cast-in-situ frame structures have been largely investigated in past researches, as for their seismic behaviour: with the currently gathered knowledge, their seismic performance can now be reliably predicted and appropriately “governed” in the design stage, even when complex and/or irregular structures are concerned; also, a unified design philosophy for

optimum seismic performance of traditional concrete structures has been developed: the so–called "capacity design" approach, which has also been codified in the most recent versions of the relevant normative documents, such as Eurocode 8 (ENV 1998: 1994).

The same cannot be said for precast structures: in fact, in spite of the overgrowing diffusion of this kind of structures, their peculiar characteristics and, in particular, their response to seismic excitation, have not been so thoroughly investigated and univocally determined at present. Detailed review of the available literature has shown that only a few state-of-the-art reports related to seismic design of precast concrete building structures exist. Important work was done in the 1980s in the frame of two major initiatives:

- ATC-8 action – "Design of prefabricated concrete buildings for earthquake loads". The proceedings of the workshop (ATC-8:1981) contain eighteen state-of-practice and research papers and six summary papers in particular related to the precast systems in New Zealand, Japan, USA and Europe.
- Building construction under seismic conditions in the Balkan region (Simeonov 1985).

The connection and fastening systems addressed in these two works are predominantly limited to equivalent monolithic connections in frame structures and specific joints in large panel walls (wet assembled structures).

The most recent state-of-art report was published by the fib Task group 7.3 in Bulletin No. 27 "Seismic design of precast concrete building structures" (Park et al, 2003) reporting on (at that time) latest developments in New Zealand, Mexico, Indonesia, Chile, USA, Slovenia, Japan and Italy. A separate chapter is devoted to modelling and analytical methods.

In all these and related documents (in particular Sheppard 1981, Restrepo *et al*. 1993, Shiohara & Watanabe 2000) special attention is given to the seismic behaviour and analytical modelling of the connections. However, although these are the most comprehensive existing documents, they cover only some specific precast structural systems and connections. The Balkan project was strongly oriented to large panel systems, which were extensively used in Eastern Europe and Russian Federation.

The capacity design concepts, providing the designer with a relatively easy and powerful tool to govern ductility resources channelling them to dissipative failure mechanisms, can be properly applied to precast structures, in order to over-proportion non ductile connections with respect to the critical regions of the columns (e.g. Ferrara *et al.* 2004, Biondini *et al.* 2010b).

2.2.1. Precast frame structures

Over the last two decades an extensive research activity aimed to investigate the seismic behaviour of precast concrete frame structures has been carried out at European scale. The results of this activity allowed to consolidate a good knowledge of the seismic behaviour of precast systems and contributed to the achievement of prefabrication in Europe with outstanding realizations in terms of both quality and reliability (Biondini & Toniolo 2010).

The first stage of this research developed between 1992 and 1996 during the drafting of the first ENV version of Eurocode 8. The initial draft of the specific rules for precast structures gave them the presumption of a very bad seismic behaviour. Industrial mono-storey precast buildings were defined as inverted pendulum systems to which a very low value of the

maximum behaviour factor was attributed. This was in conflict with the national codes that did not make any difference between cast-in-situ and precast frames and also with the experience of past earthquakes, where precast structures, with the exception of systems with unconnected members, showed a good ductile behaviour despite their non-seismic design. The lack of experimental data was adduced to justify the heavy penalisation of precast structures in the first version of Eurocode 8.

In order to demonstrate the good seismic performance of precast structures, experimental tests and numerical analyses were performed within several Research Projects. The Italian Association of prefabrication industry (Assobeton) promoted a campaign of analytical investigations developed at Politecnico di Milano. The first stage of these investigations started with a set of cyclic tests on precast columns. Figure 2.1 shows one of the prototypes of precast columns tested at ELSA Laboratory of the Joint Research Center of the European Commission at Ispra, Italy (Saisi & Toniolo 1998). Cyclic and pseudodynamic tests were performed for different reinforcement amount and axial actions.

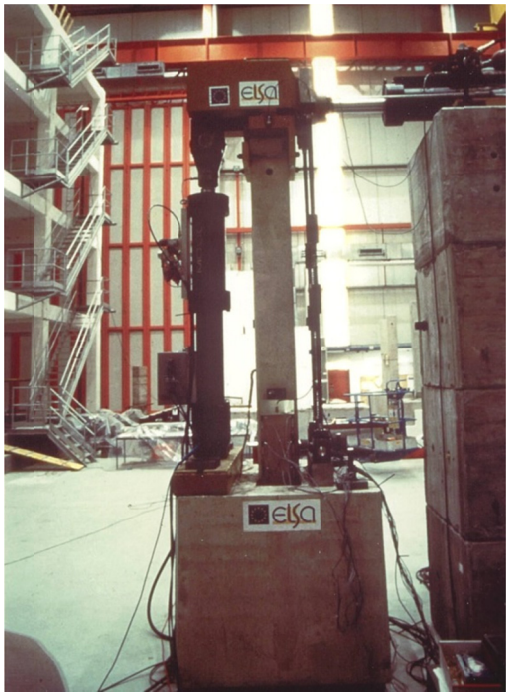

Figure 2.1 – Mono-axial cyclic and pseudo-dynamic tests on cantilever columns with different imposed axial load performed at ELSA/JRC within the Assobeton test campaign

The results of these tests confirmed:

- a good ductile behaviour with specific dissipation around 0,4 (comparison with perfect elastic-plastic equivalent behaviour), as typical for cast-in-situ columns;
- a more reliable behaviour with respect to cast-in-situ columns due to the absence of bar splices and to the stable position of stirrups during casting of concrete (precast columns are cast in horizontal position);
- the fundamental importance of a narrow spacing of the stirrups against the early buckling of longitudinal bars;

- displacement ductility ratios between 3,5 and 4,5 consistent with the code provisions for cast-in-situ frames.

Based on these results, the Eurocode 8 was therefore published with precast structures no more treated as inverted pendulum, but still penalised with a lower behaviour factor with respect to cast-in-situ systems.

The seismic behaviour of cast-in-situ and precast structures has been investigated in a second stage of the research by means of proper numerical models on probabilistic bases (Biondini & Toniolo 2002, 2003, 2004, 2009). This investigation was carried out by means of non linear dynamic analyses reproducing the real vibratory behaviour of the structures under earthquake conditions. Two prototypes were considered, the first cast-in-situ with monolithic connections, the second precast with beam-to-column hinged connections. They have the same overall dimensions, with the size and reinforcement of the columns chosen to achieve the same vibration periods and the same design seismic capacity in terms of base shear strength. The seismic response of these prototype was investigated in probabilistic terms for lognormally distributed material strengths and under artificial accelerograms, randomly generated so to comply with the design response spectrum. A Monte Carlo simulation based on a large sample of incremental nonlinear dynamic analyses taken up to collapse was therefore carried out for each prototype to compute the statistical parameters of the seismic performance. The results proved that precast structures have the same seismic capacity of the corresponding cast-in-situ structures, and confirmed the adequacy of the values given by the code to the behaviour factor of concrete frames (q=4,5).

The third stage of the research developed during the revision of Eurocode 8 for its conversion to the final EN version. The preceding analytical demonstration was effective, but an experimental confirmation was still necessary. Therefore, taking advantage of the Ecoleader programme for the free use of the large European testing facilities, two pseudodynamic tests on full scale prototypes have been performed at ELSA Laboratory (Biondini *et al.* 2004). Figure 2.2 shows a view of the full scale prototypes. The aim of the tests was the experimental comparison of the seismic capacities of cast-in-situ and precast structures, and at the same time the validation of the analytical model used in the numerical investigations (Biondini & Toniolo 2004). The results of the tests highlighted the expected large seismic capacities (critical PGA equal to about 1,0g) of this type of structures and confirmed the overall equivalence of the seismic behaviour of precast and cast-in-situ structures.

The fourth stage of the research was developed within the Growth programme. Two prototypes consisting of six columns and a mesh of beams and roof elements were designed to investigate the seismic behaviour of precast structures with roof elements placed side by side (Ferrara *et al.* 2006, Biondini *et al.* 2008, Biondini & Toniolo 2008). Figure 2.3 shows a view of the prototypes and of the testing plants. The prototypes differ only for the orientation of the beams and roof elements with respect to the seismic action.

(a)

(b)

Figure 2.2 – Ecoleader Project: (a) cast-in-situ frame and (b) equivalent cantilever columns frame tested at ELSA/JRC

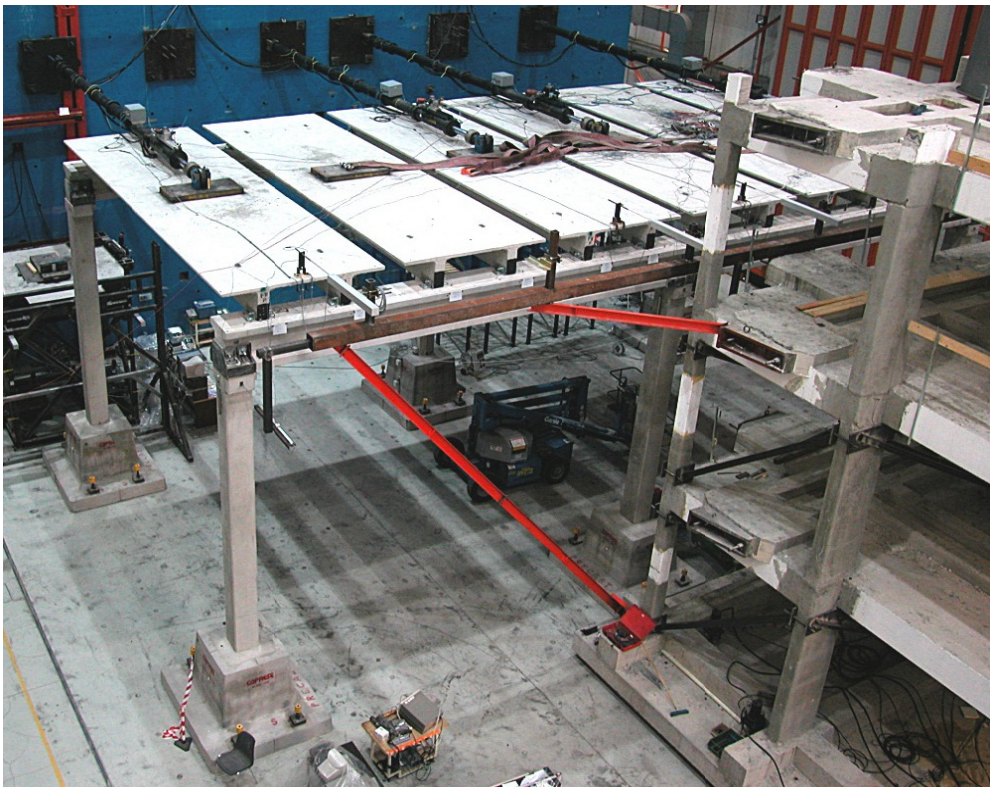

(a)

(b)

Figure 2.3 – Growth Project: pseudo-dynamic tested precast frame specimens at ELSA/JRC with (a) diaphragm members oriented parallel and (b) orthogonal to the direction of seismic action

Hinged connections are used between roof elements, beams and columns. The control of the pseudodynamic tests is based on two degree of freedoms, associated with the top horizontal displacements of the lateral frames, and of the central frame. The measured top displacements of lateral and central columns during the pseudodynamic tests resulted practically coincident. This result proves that double connections between beams and roof elements gives a rotational restraint in the roof plane which enables the activation of an effective diaphragm action, even if the roof elements are not connected among them.

The results of the tests have been also used for a further validation of the analytical model used in the numerical analyses (Biondini & Toniolo 2009). After the pseudodynamic tests, both prototypes have been subjected to a cyclic test under imposed displacements up to collapse. With a ultimate displacement $d_u \approx 360$ mm and a yielding displacement $d_y \approx 80$ mm, a global displacement ductility equal to 4,5 is evaluated, as assumed by the final version of Eurocode 8 for the behaviour factor of precast frame systems.

The results of the investigations carried out under the Ecoleader and Growth research projects showed the good seismic performance of precast structures provided that the connections are properly over-dimensioned (Biondini 2009). The last aspect to be still clarified is therefore the actual behaviour of connections under seismic excitation. Based on these needs, the European research program Safecast has been performed to investigate the seismic performance of connections in precast systems, exploring possible innovative structural solutions.

This project involved a campaign of experimental static tests carried out on single specimens, such as those shown in Figure 2.4, as well as pseudo-dynamic tests on a three-storey full-scale prototype shown in Figure 2.5. The problem of the influence of the connections is also addressed in Fabbrocino *et al.* (2006) and Biondini *et al.* (2013c), where the seismic response of industrial precast buildings with poor connections is addressed. Fischinger *et al.* (2008) and Magliulo *et al.* (2008) provide indications for the seismic assessment of existing industrial buildings. In particular, Biondini *et al.* (2011b), Titi (2012), Camnasio (2013) and Titi & Biondini (2013, 2014) cover the life-cycle assessment of concrete structures exposed to corrosion, with specific reference to precast concrete structures.

Investigations that proceeded to the Safecast project proved that the precast systems can have comparable energy dissipation capacity/seismic performance as cast-in-situ systems but only if the connections are properly designed and drift limitations and other minimum requirements provided by Eurocode 8 are respected. The analytical investigations described in Kramar *et al.* (2010) support the previous assumption, highlighting also the large seismic resistance that precast frames can provide.

Another important outcome is that very large column rotations (corresponding to very large drifts, in some cases over 5%) are needed to fully exploit columns and/or structural energy dissipation capacity. This arises the problem of the displacement compatibility in real structures with claddings installed.

In general, in recent years the problem of the seismic behaviour of the so-called non-structural elements, not only with reference to cladding panels, is gaining interest from the scientific community (e.g. Filiatrault & Sullivan 2014).

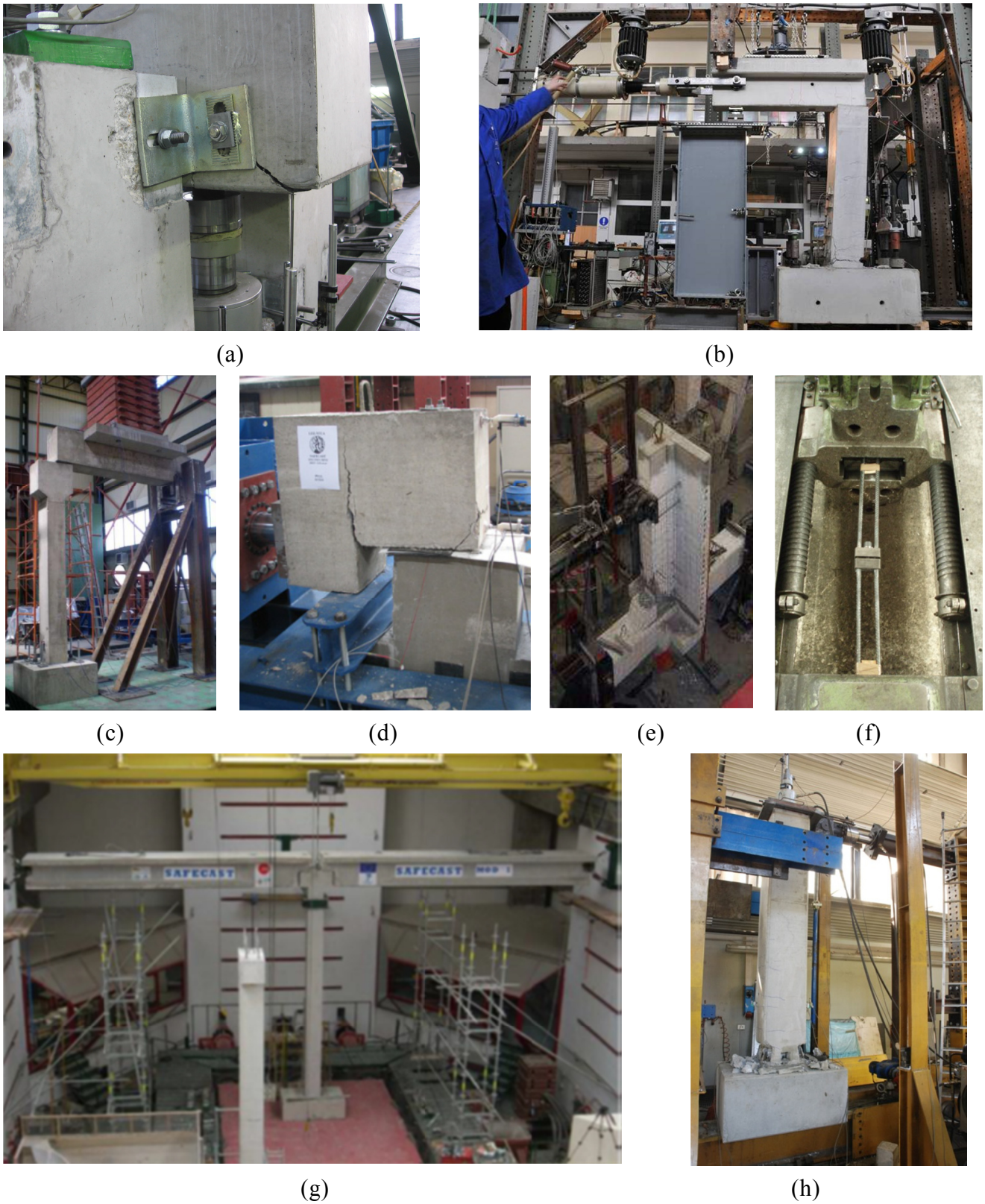

(a) (b) (c) (d) (e) (f) (g) (h)

Figure 2.4 – Safecast Project: Experimental testing on (a) floor-to-beam connections at Politecnico di Milano, (b) beam-to-column connections at University of Ljubljana, (c,d) Technical University of Athens, (e) Technical University if Istanbul, (f) Politecnico di Milano, (g) frame sub-assembly at LNEC and (h) column-to-foundation connections at Politecnico di Milano

(a)

(b)

Figure 2.5 – Safecast Project: experimental testing on full scale 3-storey prototype at ELSA/JRC (a) under construction and (b) completed

2.2.2. Innovative solutions for dry-assembled precast structures

Several structural concept solutions have been conceived in order to limit the deformability of dry-assembled precast frame structures, among them the possibility to realise dry-assembled clamped beam-to-column connections with mechanical devices and the possibility to insert dry or wet assembled precast structural bracing walls within the precast frame (Dal Lago & Dal Lago 2011, 2012b and Toniolo 2012a). Both the solutions have been detailed and experimentally assessed within the ELSA/JRC full scale prototype testing.

Alternative precast concrete structural arrangements based on the use of precast dry-assembled rocking walls and frames have been deeply studied, as it can be found in Wiebe & Christopoulos 2014. The use of re-centring unbonded strands and dissipative connections is the base of the PreSSS system, to which a large experimental campaign has been devoted at the end of the 1990s and further (Stanton *et al.* 1991, Priestley 1991, Priestley 1996, Priestley *et al.* 1999, Kurama 2000, Pampanin 2000, Kurama 2001, Pampanin *et al*. 2001, Kam *et al.* 2010, Smith *et al.* 2011). The results show that a large ductility is obtained with this hybrid system, associated to a low-moderate damage of the concrete components. Numerical models for rocking systems are also provided in Roh & Reinhorn 2009.

The Research has been developing, bringing to the PREWEC system (Aaleti *et al.* 2008), in which a combined wall-external columns member with intermediate dissipative devices provides a large energy dissipation together with re-centring capability and low damage at large displacements.

2.3. Connections in precast frame systems

The connections play a fundamental role in the seismic response of precast frames, as pointed out in Toniolo (2012b). The frame connections in a precast building can be classified as:

- Column-to-foundation,
- Beam-to-column,
- Floor-to-beam,
- Floor-to-floor.

2.3.1. Column-to-foundation connections

The column-to-foundation connection plays a key role in the traditional static scheme typical of European precast frame practice, where cantilever columns concentrate at their base all the ductility and energy dissipation seismic demand. Wet assembled equivalent monolithic connections with pocket foundations have been widely studied in Saisi & Toniolo (1998), taking advantage of the large crop of results gained within the Assobeton leaded research project in collaboration with ELSA/JRC laboratory. The results of this research activity have been previously summarised.

In Dal Lago *et al.* (2010, 2012c, 2013) the behaviour of mechanical dry-assembled connections, that are facing a large spreading within the precast practice due to their

advantages in terms of speed and ease of erection, has been studied within a comprehensive experimental campaign comparing the cyclic behaviour of bolted sockets, mechanical couplers and semi-dry solutions like protruding bars. Also few innovative bolted socket solutions have been designed and tested with the aim to improve their mechanical behaviour. The research pointed out similar results obtained for different technologies, although their failure mode suggested different behaviours, like the concentration of the plastic hinge within the partially threaded rebar going in foundation (bolted sockets), or the free development of plastic hinge within the column (couplers). The design guidelines, proposed by the authors and inserted in Negro & Toniolo (2012) design book, show however that on typical tall and slender columns the effects of the shortening of the plastic hinge effective length become remarkable, completely changing the ductility capacity of the member and, correspondily, of the building.

Metelli *et al.* (2011) proposed a solution with concentration of damage in the foundation rebars, that are however provided with a debonding tube, pre-defining then the plastic segment of the rebar.

2.3.2. Beam-to-column and floor-to-beam connections

In non-seismic European areas, it has been commonly used as beam-to-column and floor-to-beam connections a simple dry support, consisting in the simple juxtaposing of members one on top of the other with interposed a support layer (usually in neoprene or plumb) in order to better distribute the load and to admit room for in-plane edge rotations. This poor technology has been demonstrated to be largely inadequate for seismic loading, among the others by Magliulo *et al.* (2011) and Biondini *et al.* (2013c).

Typical beam-to-column and floor-to-beam connections largely diffused in all dry-assembled precast frames all around the world are dowel connections, made with large diameter rebars protruding from the bearing member (or screwed in pre-installed bushes) and grouted once the supported member is placed in position. The dowel shows negligible purely flexural stiffness, allowing relative rotations between the members, but is able to provide a considerable shear resistance with a combined shear-flexure-axial behaviour of the dowel itself. Vintzeleou & Tassios (1985, 1987), Soroushian *et al.* (1987a, 1987b) and Tsoukantas & Tassios (1989) were among the first to experimentally study this kind of connection and to propose design methodologies specifically referred to its use in precast frames. Dei Poli *et al.* (1992, 1993) performed an experimental investigation on dowel connections with special regard to thin concrete covers, proposing design values for the subgrade stiffness of the concrete embedment. Capozzi *et al.* (2010) performed monotonic tests on precast dowel connections, developing also an analytical model able to catch the experimental behaviour. Psycharis & Mouzakis (2012a, 2012b) recently performed an extensive experimental campaign with local pure shear tests and full-scale shaking table tests on beam-to-column structural sub-assemblies provided with dowel connections with different geometries within the Safecast project, highlighting the large resistance reduction in case of cyclic load in comparison with monotonic and the ductile behaviour of the connection if adequately provided with a considerable amount of transversal reinforcement around the dowel. Easily applicable design guidelines are also proposed. Fischinger *et al.* (2012b and 2013) and Zoubek *et al.* (2014) performed an experimental campaign within the same research project regarding the behaviour of dowel connections at

large relative rotations, through monotonic and cyclic tests. They found that a non-negligible resistance reduction occurs at large relative rotations, identifying similar failure modes with respect to pure shear tests. A robust numerical 3D model has been used to catch and to interprete the experimental results and to exptrapolate them in order to produce more reliable design guidelines for these connections.

Another typical solution to connect dry-assembled floor and beam members only is made with post-installed angles in correspondence of the floor member ribs. The complex flexural-torsional-shear behaviour of such a connection has been studied by Felicetti *et al.* (2010) with monotonic and cyclic experimental tests on floor-beam precast structural sub-assemblies, showing that the behaviour is in general over-resisting and highlighting the danger of using typical hot-rolled thick angles, with which it has been observed a brittle failure of concrete. Cold-formed profiles have been proposed and tested in order to ensure a ductile behaviour of the connection. An experimental investigation on the horizontal dowel connection resistance of the precast member rib is reported in Dal Lago *et al.* (2012a).

Design guidelines for all the connections cited above are provided in Negro & Toniolo (2012).

Other types of dry assembled beam-to-column connections, such as moment resisting (Dal Lago & Dal Lago 2012a) or hybrid (Karadogan *et al.* 2012) are not considered in the present chapter, due to their limited use.

2.3.3. Floor-to-floor connections

Floor-to-floor connections can be performed only in those slabs in which the floor members are placed in adjacent position. Tipically, welded connections are used. A large experimental research with monotonic and cyclic tests specifically devoted to the mechanical characterisation of floor-to-floor welded (dry) and topping (wet) connections has been performed by Naito *et al.* (2009) and Cao & Naito (2009) with regards to both axial and shear behaviour. The majority of the connections subjected to shear with opening restrained exhibited high compression forces coupled with high shear capacity. However, a tension action compromises the shear strength. Topping connections made with welded wire meshes exhibited brittle behaviour.

2.3.4. Precast diaphragms

Storey diaphragms are traditionally made with in-situ concrete screed pouring, which are likely to be avoided in the perspective of totally dry-assembled precast structures. Pushed by the observation of the poor seismic behaviour of large dry-assembled precast parking facilities in the USA (Fleischman *et al.* 1998), especially during the Northridge earthquake in 1994, for problems mainly induced by the diaphragms, an extended research on the subject has been developing in the country. Tena-Colunga & Abrams (1996) performed a general numerical work involving masonry, timber and concrete structures, analysing the increase of the natural periods of the structures with the diaphragm flexibility, together with the accentuation of torsional effects on the lateral load resisting systems. In Fleischman & Farrow (2001, 2003) and Fleischman *et al.* (2002) an extensive numerical study on dry-assembled precast diaphragms inserted in wall-frame or frame structures is reported. They concluded that

perimeter lateral-system structures with flexible diaphragms can produce inadequate seismic performance due to excessive drifts in the gravity-system remote to lateral-system elements, or large unintended ductility demand on the diaphragm, and that the results from dynamic non-linear analyses reach much larger values with respect to what suggested by the code, especially considering wall-frame structures. Furthermore, the larger storey forces have been computed at the lower storeys, in contradiction with what is suggested in the code. The authors suggest to adopt an elastic-plastic design of diaphragm, with the insertion of ductile connection between the members, and suggest improvements for the evaluation of diaphragm seismic loads. They also suggest not to use largely flexible diaphragms in any construction.

The Diaphragm Seismic Design Methodology consortium promoted research activities in the field of design guidelines draft (Fleischman *et al.* 2005b) and experimental validation (Fleischman *et al.* 2005a). While elastic behaviour of the diaphragm is required for serviceability limit state, plasticity behaviour can be exploited in order to sustain larger earthquakes, employing a full diaphragm capacity design from the diaphragm level to the joint and the detail level. An extensive experimental activity has been performed within the research project, the most challenging of which regards a series of shaking table tests on a full-scale 3-storey totally dry assembled precast concrete building provided with external post-tensioned rocking walls that act as lateral load resisting system, performed at the NEES facility. The results are described in Schoettler *et al.* (2009). The prototype showed an elastic behaviour of diaphragm under the serviceability limit state, while it faced flexural yielding damage of the connections under ultimate limit state seismic action. Also innovative ductile steel welded wire meshes floor-to-floor connections performed satisfactorily, facing several strong damage cycles without breaking. Diaphragm design procedures are contained in Nakaki (1998).

Recent research has been devoted to the interaction of spandrel cladding panels with the diaphragm mechanism, highlighting through a numerical investigation (Wan *et al.* 2012) the influence of diffused welded panel connections in the modification of strength, stiffness and deformation capacity of the diaphragm.

Peculiar characteristics of multi-storey dry-assembled precast frame structures have been studied within numerical and large scale experimental projects. Those research projects, including Safecast (Bournas *et al.* 2012a, 2012b, 2013a, 2013b and Biondini *et al.* 2012b, 2012c), showed how the contribution of higher mode effect, which becomes important for flexible structures like multi-storey contilever column precast structure, leads to a dramatic enlargement of diaphragm forces and column shear with respect to what predicted with dynamic modal analysis with response spectrum. Formulas that properly take into account this effect have been proposed by Fischinger *et al.* (2012a) following the approach that Keintzel (1992) and Eberhard & Sozen (1993) developed for reinforced concrete walls.

Valente (2010) also contains information about the seismic behaviour of precast systems with different degrees of diaphragm stiffness.

2.4. Precast concrete cladding panels

2.4.1. Typical cladding panel and connection elements

Cladding panels are typically provided with thermal insulation and ventilation air chamber, with an internal bearing screed (often ribbed) and an external one. In case the external screed is suspended on the inner with connection systems that allow for relative thermal deformation, or in general its stiffness is negligible if compared to the inner, the panel is non-composite. In case the screeds are strongly connected, for instance in case of hollow core panels, the element is composite. Even if different technologies of connections are generally used in many countries, a common distinction is made among bearing, shear and tie-back connections. Bearing connections have the function of sustaining the gravity weight of the panel, shear connections restrain horizontal relative displacements between panel and structure and tie-back connections restrain out-of-plane relative displacements. A single connector can provide multiple functions.

European practice concerns in general simple bearing foundation connections for both vertical (on panel foundation beams) and horizontal stacked (on column foundation) panels. Suspended horizontal panels are generally provided with inclined bracket bearing connections. All panels are then equipped with tie-back connections of various technologies, the most diffused of which is the strap type. It is important to note that, while some brackets are designed to allow horizontal sliding, tie-back connections are for the large majority fixed, possibly acting unintentionally as shear connectors. An overview of the Italian typical cladding connections with reference to their specific technology is available in Mandelli Contegni *et al.* 2007). Furthermore, reference to the specific technologic products available in Europe can be found within the official reports of the Safecladding project.

Traditionally, US cladding panels are designed with two combined bearing-shear connections positioned in a row and several tie-back connections, positioned in order to leave the panel in its position during a lateral load event. This static configuration is referred to the “cantilever” statically determined scheme for vertical panels and to the “swaying” statically determined scheme for horizontal panels. Usually the tie-back connections are made with fixed slender steel rods that can provide large out-of-plane axial resistance while sustaining large in-plane deformation demand, or with sliding devices obtained through slotted profiles.

Several technical details of typical connections can be found in Hegle (1989), Iverson (1989), PCI (1989), McCann (1991), NIST (1995) and NPCA (2012).

Japanese connections are largely devoted to bring to a static scheme that allows the panel to rock around the base connections. This static configuration is referred to the “rocking” statically determined scheme. The typical connections are placed in four symmetric positions along the panel, two at the top and two at the base, and all of them are load-bearing. Technical details can be found in NIST (1995) among others.

2.4.2. Frame-cladding interaction

The claddings are usually conceived as non-structural components (considering the seismic load), which are completely detached from the load-bearing structure. Therefore, they are usually completely neglected when the seismic analysis of the frame precast structures is performed, with an exception of their mass, which is added to the total mass of the structure according to the panel static scheme. However, in many past and recent investigations it was realized that typical connections between claddings and the bearing structure cannot ensure the design assumption. Therefore, claddings can have a significant influence to the stiffness of the structure and consequently to the overall seismic response of the building.

Comprehensive state of the art collections can be found in Hunt & Stojadinovic (2010), Maneetes (2007) and NIST GCR 95-681. Goodno & Craig (1989, 1998) provide an overview on the studies devoted to the cladding-frame collaboration.

Weidlinger (1973), Gjelvik (1973) and Oppenheim (1973) were among the first to promote the idea to use the cladding panels as part of the lateral load resisting system of a building, also noting an existing interaction between cladding and structure with the available common technologies of that time (that are not dramatically changed up to today). An extensive research of the influence of the cladding systems to the vibration and seismic response properties of multistory buildings was performed by the research team at the Georgia Institute of Technology (Goodno *et al.* 1980, Palsson & Goodno 1982, Goodno *et al.* 1983, Palsson *et al.* 1984, Goodno & Palsson 1986, Palsson & Goodno 1988, Goodno *et al.* 1988) also through the study of a 25-storey steel-framed office structure. Three sets of ambient tests and one forced vibration test were performed, and the building was also investigated analytically. Since the analytical and measured periods did not agree, the research of the effects of the claddings to the overall structural response was performed. The analytical periods of the bare frame structure without claddings were up to 34% and 48% greater than the measured translational and torsional periods, respectively. The corrected numerical model with added claddings gave the similar results if compared to the experimental. The above references include also the study of the claddings to the roof displacements and damping.

The effect of a simple cladding system on the modal properties of a multistory concrete framed building was investigated analytically by Henry & Roll (1986) through a case study. They investigated two-dimensional, nine-storey, three-bay concrete moment-framed structure. The cladding system consisted of spandrel panels attached to the structural frame at the panel corners. The following properties of analysed structure were varied: 1) bay widths (35 ft, 25 ft, and 15 ft.), 2) panel heights (0 ft, 3 ft, 5 ft, 7 ft, and 9,5 ft.), and 3) weight of the panels (150 pcf and 100 pcf). The storey height was taken as 10 ft. The fundamental period of the model with cladding was 18% - 55% smaller than the fundamental period of the bare frame model, depending on the bay width, panel height and weight. Hunt & Stojadinović (2010) criticised these analysis. In their opinion the disadvantage of the Henry & Roll modelling approach was that the authors assumed that all of the deformations in the cladding system occurred in the panels themselves. Modelling the cladding system in this manner overestimates the contribution of the cladding to the lateral stiffness of the building. In reality, the shear stiffness of the cladding connectors is much lower than the panels, which can be assumed to act as rigid blocks. Henry & Roll tested also the influence of the claddings to the frame drifts. The lateral

roof displacement decreased as the height of the panel increased. The lateral roof displacement decreased up to the 75% comparing to the model, which consisted of bare frame only.

The contribution of cladding to the lateral stiffness of bare frame structures was also studied by comparing the drifts of frames with and without cladding in Smith & Gaiotti (1989) and Gaiotti & Smith (1992). A single-storey structure, representing a typical end-bay-width story of the frame was analysed. The cladding system, described as typical of low seismicity areas, consisted of one panel constructed over the full storey high and a full bay width with two window openings. The cladding panels reduced the displacement from 12,6 cm to 3,6 mm. These results seem to be, however, unrealistic, since the stiffness values assigned to the connectors were unrealistically large.

The effect of precast concrete cladding on the lateral response of multistory buildings was also investigated by Charney & Harris (1989). They performed analytical studies of a four-storey, two-bay steel moment-resisting frame building. The two inches thick panel decreased the lateral displacement for about 28%. The connectors and panels contributed 14,4% and 8,4%, respectively, to the total drift. When the panel thickness was increased to 6 inches, these contributions were changed to 20,3% and 4,3% for the connectors and panels, respectively. For the 60 inches. thick panel (which represents the infinitely rigid case), the connector was responsible for 24,4% of the total drift.

Thiel et al. (1986) studied the effect that the cladding system has on the damping properties of a ductile steel moment-frame. The researchers performed nonlinear time-history analyses of a benchmark 15-storey building. The cladding was modelled as dampers lumped at each floor and idealized as having elastic-perfectly plastic behaviour. The main conclusions were that the effectiveness of the dampers, which represented the cladding system, increased with increasing yield level. The cladding dampers required relatively high stiffness, comparable to the structure's stiffness to be most effective. For high yield levels and 2% viscous damping in the frame, the cladding damper reduced the response of the structure by approximately 40% of the maximum roof displacement and 45% of the base shear. In summary, the authors argue that the effective damping of a building can be increased through activation of part of the lateral force resistance capacity of the cladding panels and controlled hysteretic behavior of their connections to the structure. However, as stated in their paper, the cladding connections require very high stiffness to be effective, which is not feasible given the connection details and design approach currently used at that time and today.

Wolz *et al.* (1992) used an analytical model and time-history analyses to study the response of a six-storey, 1:4 scale model of a moment-resisting frame provided with two cladding panels per bay. The time-history of the roof displacement of the bare frame model and the model with cladding were recorded. The maximum roof displacement of the model with cladding was approximately 33% less than the roof displacement of the bare frame model.

Cohen & Powell (1993) conducted a design study to explore the use of structural cladding panels with energy dissipating cladding-to-frame connections in order to enhance the seismic behaviour of the frame itself, showing through the results of non-linear dynamic analyses how a dissipative cladding solution could improve the global seismic behaviour of the building.

Pinelli *et al.* (1993, 1995) developped a design method aimed to the optimisation of dissipative cladding connections in energetical terms, by choosing the device that provides the largest

energy dissipation within the building façade. The validity of the proposed design criterion has been validated through a parametric investigation on case studies, with non-linear dynamic analyses and with reference to a plasticity-based tapered connector, which mechanical behaviour can be defined according to the elastic stiffness and the yield force.

Memari *et al.* (2004) carried out a numerical investigation on the effect of near-source vertical ground motion on the demand on cladding connections, finding that forces in the connection can significantly increase in occurrence of a near-source seismic event and suggesting to explicitly include the vertical acceleration component in the formulas for the evaluation of actions on connections.

De Matteis (2005) focused on the seismic design of moment resisting steel frames with structural lightweight cladding panels. The main purpose of the study was to investigate the possible beneficial effects of the claddings in the serviceability and the ultimate limit states of the structure. An original design procedure was proposed, where the stiffening of the structure due to the cladding panels was taken into account. Several non-linear dynamic time-history analyses have been performed. The main parameters affecting the seismic performance of the structure have been investigated: the frame configuration, the mechanical and hysteretic characteristics of cladding panels and their distribution. It was concluded that cladding panels provided an improvement of the global seismic performance. A simplified procedure to account for such an effect was also proposed.

In Singh *et al.* (2006a, 2006b) comprehensive work has been done in order to validate and enhance the methodology of evaluation of the out-of-plane forces of building non-structural components, both for rigid and flexible components. At the end of a large parametric numerical investigation on forces on non-structural components arising in tall buildings carried out with non-linear dynamic analyses, the formulation provided by the US standards seems to be very conservative, since it does not take into account the real complex dynamic interaction between structure and component. More accurate formulations are provided in the cited papers. Recently, a parametric study of the interaction between cladding panels and the bearing structure was performed by Baird *et al*. (2011a). Different failure mechanisms and various configurations were considered in order to show the effect of the entire cladding system upon a structure's seismic behavior. The results showed that there was an increase in strength of at least 10-20% for all systems when the influence of cladding panels was taken into account. This contribution was greater when panels were attached to the columns rather than to the beams because the beams deflected more and activated the connections later.

An increase in hysteretic damping for all systems has also been observed. Frame height to span ratio did not largely affect the yield force of the system. However, increasing it allowed for a higher deflection/drift of the system at yield. When both panel and connections were strong the capacity of the system was increased but the ductility was decreased. They further concluded that it was apparently more advantageous to design for a connection governed failure mechanism instead that for a failure mechanism governed by either the panel or the frame. Connection governed failure allowed greater damping, strength and stiffness over many cycles, provided that the connections are able to achieve large ductility. The post-earthquake substitution of failed connections is seen to be more favourable than having to replace entire damaged panels or to repair the frame.

The same authors (Baird *et al*. 2012), performed a special study, which had the main goal to explain more precisely the damage sustained by cladding systems in the earthquake that struck Christchurch on the 22nd of February 2011. The cladding panels were attached to the frame using two fixed connections at the base and two flexible tie-back connections at the top. Static push-over analyses were used to determine the change in strength and stiffness of the system. Results showed that when cladding interaction is taken into account, the frame is provided with larger stiffness and strength, though with an earlier onset of collapse. Dynamic nonlinear response history analysis was also performed. The maximum inter-storey drift and subsequent cladding connection damage was inferred. Results confirmed the high influence of cladding systems upon the seismic behaviour of multi-storey buildings. Some additional details about these studies can also be found in Baird *et al*. (2011b) and Diaferia *et al*. (2011).

Hobelmann *et al.* (2012) report about the design and the realisation of a set of buildings ranging from four to six stories in which the lateral force resisting system consisted in horizontal stacked cladding panels with strong panel-to-structure and panel-to-panel shear connections. The cladding panels used have all the same shape and are provided with two large punched window openings. Forces in shear connections have been extimated to be up to 330 kN.

With specific reference to the technology used in Southern Europe, Ercolino *et al.* (2013) carried out a numerical investigation on the influence of infilled vertical cladding panels on the dynamic behaviour of one-storey precast industrial buildings. The parametric study shows a high influence of the panels on the first period of the structure, as well as the inadequacy of the code relationships for the evaluation of the natural period for such typology of structure. More suitable relations are proposed in order to evaluate the seismic demand of one story precast buildings both in the case of bare and infilled system.

The stiffening effect of cladding panels provided with interactive connection systems provides a shift in the vibration frequencies of precast buildings, possibily enlarging the seismic demand on them, as presented in Magliulo *et al.* (2014a).

General overviews about dissipative devices can be found in Symans *et al.* (2002, 2008) and Whittaker & Constantinou (2004), among many, and in Towashiraporn *et al.* (2002) with specific reference and application to precast cladding panels.

2.4.3. Field observation of precast cladding seismic peformance

The most comprehensive and reliable data about the response of the panel connections, typically used in Southern Europe, were obtained during the recent L'Aquila (2009), Lorca (2010) and Emilia (2012) earthquakes. In the L'Aquila (Menegotto 2010, Colombo & Toniolo 2012a, 2012b) and Lorca (Espín 2011) earthquakes the precast frame structures behave satisfactorily, with heavy damage observed only in very few buildings. The same cannot be said for the precast concrete cladding panels, that suffered from generalysed problems in a large amount of buildings located nearby the earthquake epicentres. The Emilia earthquake provided quite a different scenario (Savoia *et al.* 2012, Magliulo *et al.* 2014b), with a poor performance of both precast structures, with many global collapses occurred, and cladding panels. It has to be pointed out that, while L'Aquila area has been considered seismically active in the Italian national standards since the beginning of diffusion of precast structures,

the area surrounding Modena has been classified as significantly seismically active only since 2005.

Practically in all cases the failure of the connection between panels and bearing structure was followed by the collapse of the panels. Although in majority of the cases the main reason of the failure of the claddings was the failure of the connector body, in some cases the failure of the anchors between connector and panel was also noted.

For what concerns the observation of the behaviour of cladding panels under earthquake in USA, Cohen (1995) and Iverson & Hawkins (1994) reported the damage of cladding panels observed during the Northridge earthquake. They concluded that cladding panels and connections unintentionally participated in lateral load-resisting structural systems. As a consequence, unanticipated cladding damage occurred, including life-safety problems when dozens of panels fell and others were left hanging precariously. Nevertheless the experimental and analytical investigation proved that the claddings had an important role to the overall response of the buildings, they were usually completely ignored by the designers. Cohen further concluded that multidisciplinary efforts are needed to change the codes and practice in order to ensure predictable, reliable, and safe performance of cladding during seismic events.

Schoettler *et al.* (2012) reported the behaviour of precast structures, with focus on parkeing facilities, that have been subjected to the Christchurch (New Zealand) earthquake of February 2011.

2.4.4. Laboratory experimentation on cladding panel and connection elements

There are several experimental works reported in the literature, where mostly cladding connections typical for US and Japan practice were examined.

In 1979, a cooperative US–Japan testing program was performed on a full-scale steel structure to determine the seismic performance of non-structural elements (Wang 1986a, 1986b, 1987, 1992). A full scale six-storey steel building was tested. It consisted of two bays frame in each direction of the building. Free vibration tests were performed before and after the construction of the non-bearing components. The non-structural elements reduced the natural period of the building by 30%, which suggested that the overall structural stiffness was increased by more than 100%. The stiffness decreased when the non-structural elements were damaged. At storey drift of 0,3%, most of the additional stiffness was lost. Despite these insights from the free vibration tests, it was not possible to separate the contribution of the cladding because the free vibration tests included either all or none of the non-structural components. Both swaying (US) and rocking (Japan) static schemes were tested, considering typical construction details of both countries. The main observations obtained within the presented tests are summarized below.

Long ductile rods used for lateral connections, can accommodate very large story drift, but sliding connections may have problems either due to insufficient slot length or impedence of the sliding mechanism. Although it is possible to design a sliding connection that enhances their reliability, they are still potentially fraught with problems ranging from weathering and ageing of the connection, to improper installation, or poor detailing. Lateral connections, in particular, should not depend upon subjective criteria for installation such as tightening of nuts which cannot be easily perceived during inspections. Once the connection's sliding mechanism gets tangled, the failure of the connection may be sudden and dangerous. If sliding connections

are to be allowed, they must be detailed such that correct installation does not require great experience and skill on the part of the installer. Slot length needs to be large, to avoid imposition of large stresses in panels and connections.

Bearing connections must be sufficiently flexible to avoid conveying stress to the panel, resulting from interstory drift in regard of both in-plane and out-of-plane components of direction. The choice of tube or angle connections makes a great difference in the degree of cracking of the panels. Care should be taken to not inadvertently stiffen connections, such as pouring new concrete around the connection body.

Panels should be "hung" such that bearing connections are at the top and lateral connections are at the bottom, whenever possible. The common practice of bottom bearing connections may result in falling out of panels if the tie-back connections fail.

Connections from a panel to frame should be oriented in the same horizontal direction, otherwise extensive warping and cracking of the panel will occur. This caution is particularly noteworthy in design of cladding for corner conditions.

Joints must be wide enough to avoid contact between panels as a result of drift. Adjacent panels should be designed to respond to drift, in a similar manner whenever possible. Thus, placing wall panels attached to girders, next to column covers attached to columns, must be detailed with extreme caution, to avoid "bumping" of adjacent panels.

The general concepts and specific design recommendations, which resulted from this project are stated in full cognizance of the limitations of testing. Thus, the evidence from the test is overwhelming before a conclusion is stated. The findings, nonetheless, narrow the broad range of opinion on a number of aspects regarding cladding performance, and give a basis to decision making in seismic design of cladding.

Meyyappa *et al.* (1981) tested a 24-storey steel office tower with a lightweight precast cladding and glazing system under free vibrations. They measured the free vibration modes before and after installation of the claddings. The fundamental period of the structure increased after the cladding were fully attached, mainly due to the addition of mass.

Sakamoto *et al.* (1987) performed an experimental evaluation of the correct functioning of rocking connections, diffused in the Japanese practice with the use of Autoclave Light-weight Concrete (ALC) panels, proving a satisfactorily behaviour.

The vibration properties of a two-storey structure with and without cladding were experimentally investigated by Rihal (1988, 1989). The test structure was a two-storey steel moment-resisting frame structure with one bay in each direction. The cladding configuration and connection details were developed in consultation with a precast manufacturer who fabricated the cladding system in accordance with the practices. The modal response of the structure was measured experimentally. When claddings were attached to the bearing structure the first two modal periods were increased for about 20%. One possible explanation offered by Rihal for the increase in period after adding the cladding is that the effects of the added mass of the precast panels seems to have overcome the additional stiffening offered by the cladding panels and connection assemblies to the test structure. The same author performed static tests on typical threaded-rod lateral (push-pull) cladding connections in order to investigate the strength and behaviour of these connections. Cyclic in-plane racking tests of a precast concrete

cladding panel with bearing connections at the bottom and threaded-rod lateral connections at the top was carried out. The in-plane resistance was controlled by the binding deformation of the top threaded rod connections. The 8-inches long threaded rod failed at an applied load of 1,2 kips and an interstorey drift ratio of 1,2%. The in-plane lateral forces in the top connections were approximately 0,25–0,40 times the panel weight at a drift ratio of 1,0%. The load capacity of the push-pull connectors decreased with increasing rod length.

Sack *et al*. (1989) performed experimental tests on simple cladding connections to determine their force-deformation behaviour and energy dissipation characteristics. They tested one-storey, single-bay frame assemblage containing two precast panels. The panels were connected to the frame with bearing connections at the base and slotted and threaded rod connections at the top. The results of the experimental tests of the connectors were used to model the cladding system analytically. A non-linear static analysis was performed assuming the structural frame behaving linear elastically and the panel-frame connections behaving with material non-linearity. The analytical studies showed that the model with cladding had 17% greater stiffness than the bare frame. However, the experimental measurements of stiffness showed no appreciable increase in lateral stiffness when the panel was attached, due to the low stiffness of the threaded rod connections and slotted connections.

In Craig *et al.* (1986) and Craig *et al.* (1988) particular tests of behaviour of steel inserts in cladding panels are reported. These tests were carried out in order to determine their lateral stiffness, energy dissipation, and ductility. The method of failure was the undesirable mode of concrete fracture, and therefore the authors point out how an improvement in the connections should be performed. A correlated numerical work is reported in Craig *et al.* (1992).

Pinelli & Craig (1989) examined seven concrete panels with steel plate inserts. The embedded inserts were supported with either welded 90-degree rebar J-hooks or welded rebar parallel to the surface of the concrete. The inserts showed limited energy dissipation. The cyclic load tests revealed pinching in the hysteretic loops. Low levels of load were resisted primarily by the surrounding concrete, and as the lateral movement increased, the stiffness increased as the rebar engaged the concrete. After failure of the surrounding concrete, the inserts behaved as a hinge. Failure resulted from either failure of the concrete or fracture of the weld between the rebar and plate.

Pinelli *et al.* (1992, 1996) performed experimental testing devoted to the mechanical characterisation of a cladding-to-structure dissipative connection based on plasticity called tapered tube. The results obtained showed that the connection behaviour is satisfactory for what concerns ductility, strength, dissipation and cyclic stability. The authors provide a design guideline and a design chart for the connection.

The Japanese rocking system has been further experimentally investigated by Itoh *et al.* (1998) with tests on full scale panels with regards to the connection hardware, and by Matsumiya *et al.* (2004) and Okazaki *et al.* (2007) by analysing the interaction between the external wall cladding and the seismic load resisting frame of a three-storey steel building structure. Full cyclic tests were performed. The building specimen had Autoclaved Lightweight Concrete (ALC) panels installed and anchored to the structural frame as external wall cladding, using a standard Japanese method developed following the 1995 Kobe earthquake. During the tests it was observed that the ALC panel claddings had negligible influence to the overall stiffness and

strength, even under a very large storey drifts. No visible damage was noted in the ALC panels other than minor cracks and spalling of the bottom of the panels in the first storey. However, the authors point out that special zones of the cladding system, such as corners and openings, should be deeper investigated. The authors also suggest that a real situation with dynamic multi-directional loads may have detrimental effects on claddings.

The response of Autoclaved Aerated Concrete panels was also investigated by Getz and Memari (2006). They used the conventional USA connectors to attach the panels to the structure. The study found that conventional connectors have not been designed for in-plane seismic resistance and would need to be redesigned in order to safely satisfy building code's allowable drift.

Chan (2003) performed four monotonic experiments on push-pull connections in two orthogonal directions. The goal was to investigate the behaviour under bending and axial load. Axial tension and compression occurs as a result of out-of-plane panel movements, and represent the forces that the rods are intended to resist. Bending of the rods occurred as a result of in-plane panel movements. Although push-pull rods were not intended to resist lateral forces on panels via shear, their bending was significant, particularly if they were short. Concerns about their fracture due to bending would not seem justified until deflections exceed 25% of their length.

McMullin *et al.* (2004) carried out eight full-scale tests of cladding connections. Tie-back push-pull threaded rod connections and welded plate lateral seismic connections were subjected to monotonic loading. All connections tested showed ductile failure modes, with some amount of energy dissipation before final failure. Weld fracture was always the failure mode for the lateral seismic connection except for the threaded rod tie-back push-pull connections. Slipping of the push-pull connections was seen only in the axial tests and then only after significant plate bending had occurred. This happened even though the plate washers were not tack-welded to the support. Push-pull connections were dominated by the strength and stiffness of their supports. While showing significant energy dissipation, these connections had very low stiffness to resist both intended and unintended modes of loading. The lateral seismic connection resulted in the plate carrying a significant amount of load when the panel moves out-of-plane, which is not intended by the original design. This resulted from the large flexibility developed by local dishing of the supporting tube. When large displacements occur, the weld of the plate fractured, resulting in a lack of in-plane resistance. It was demonstrated that the complexity of the geometric configurations of many cladding connections did not allow for accurate prediction of the force-displacement relationship based upon traditional structural models. Maximum strengths, initial and plastic stiffnesses and overall ductilities were all significantly different than expected.

Hans *et al*. (2005) performed in situ measurements of existing buildings. The main goal was to identify the dynamic behaviour of ordinary intact buildings built in a conventional practice. Taking advantage of their demolition, it was possible to experimentally extimate the actual influence of the light work elements, full precast façade panels, bearing masonry walls, and the presence of neighbouring joined buildings to the dynamic properties. They concluded that comparative tests performed on intact and modified structures enabled to identify and quantify the leading and negligible phenomena that may influence the actual quasi-elastic behaviour. It

is shown that full precast façade panels or masonry shear walls do have a significant role in the building response.

At the San Diego University (UCSD), in the cooperation with the Network for Earthquake Engineering Simulation (NEES), a shaking table experimental campaign of a benchmark full scale 5-storey precast building provided with non-structural components was performed (Chen *et al.* 2010, Hutchinson *et al.* 2012, Pantoli *et al.* 2013). Complementary testing and conceptual project design are illustrated in McMullin & Nguyen (2008) and McMullin & Ortiz (2009). The cladding panels were installed at upper two storeys. Three full-scale experiments have been carried out, two of which include precast concrete cladding panels. Seismic base isolation has been tested, together with clamped foundations. Different types of damage and failure are investigated, including loss of air seal at joints, closing of the slip connection at the top of column cover panels, damage to the corners of concrete panels when excessive rotation results in the contact between adjoining panels, damage including possible bolt fracture to the pin connections at the base of the column cover panels, cracking of the window glass due to crushing and damage to the connections supporting the return panels resulting in potential instability of panels. Two types of push-pull connections were tested and their capability to accommodate in-plane storey drifts was assessed. Namely, fixed rod and sliding rod connections of varying rod lengths were installed and tested in an effort to understand the relationship between rod length and connection performance. Inspection of residual damage after each test motion revealed that the connections did not undergo any substantial damage in the isolated configurations. During the clamped foundation tests, however, plastic yielding of both the fixed rod and sliding rod connections were observed, with the exception of the sliding short rod connections, which showed no signs of damage under any test. The developed analytical models are reported in (Hunt and Stojadinović 2010).

Studies of the typical connectors used in Europe are quite limited. Belleri *et al.* (2010) carried out four mono-axial cyclic tests on typical European full scale horizontal panel structural sub-assemblies with concrete columns, testing three different connections: rotational and translational bearing brackets, providing lower support to the panel, and tie-back connections (also commented in Piras *et al.* 2010). The panels were intended to have a swaying type static scheme. In the first test a large tightening torque has been applied without control to the tie-back connection, made of a vertical anchor channel at the column side connected through a short threaded rod to a horizontally slotted Ω-shaped profile at the panel side, as representative of a typical non-accured installation that may occur in practice. As a result, the panel interacted with the columns, bringing to large forces and failure of the tie-back connection, that unintentionally acted as a shear connector, at low drift. In all other tests, in which an improved bracket solution with low-friction pads has also been tested, the sub-assembly showed negligible stiffness up to the maximum stroke allowed by the horizontal slot. It was concluded that the amount of dissipated energy within the cladding provided by distortion of the threaded rod or unintentioned friction is negligible if compared to the dissipation capacities of a precast column base, and that it is of fundamental importance to not tightenen the threaded rod of the connection, to which a complete change of the static scheme of the panel would be associated.

A significant in-plane interaction between panels and the main structure was observed during the Growth project (Ferrara *et al.* 2004, 2006, a picture of the structure is reported in Figure

2.3b). The vertical panels, connected with the typical hampered rocking scheme, significantly influenced the cyclic behaviour of the precast building, introducing a large additional shear contribution. However, this interaction was experimentally investigated only for the serviceability limit state.

Several shaking table tests of cladding connections were performed at LNEC (Lisbon) by the team leaded by Ema Coelho in the frame of the Safecast project (Toniolo 2012) with the aim of evaluating both in-plane and out-of-plane behaviour of the panel connections. Two configurations of the horizontal cladding panels, and two types of the connections were investigated, with reference to existing solutions. Six tests were performed, were the seismic load was applied in different directions; in-plane, out-of-plane and bidirectional tests were carried out. The global results, showing a large interaction of the panels with the frame and several connection failures, again suggest that the traditional cladding connection systems shall be reviewed.

2.4.5. Code requirements for cladding panels

An extended chapter of NIST GCR 95-681 provides information about the practice for precast concrete cladding panel seismic design in several countries all over the world up to 1995. In Villaverde (1997), Sielaff (2005) and Filiatrault & Sullivan (2014) the evolution of the USA standard requirements on the subject is traced.

Up to the present, all code requirements about cladding panels and related connections refer to a statically determined connection system and provide resistance requirements with respect to the out-of-plane seismic excitation on the base of the single panel mass. Equivalent static forces method is used in all cases. Some standards also provide minimum drift accommodation distances. In any case, none of them explicitly considers forces acting in the in-plane direction. Furthermore, most codes include cladding panels as non-structural elements, which definition is matter of debate (Bachman & Dowty 2008). Standard rules from Europe and USA will be illustrated in the following, neglecting contributions from other countries that are, however, aligned with one of those illustrated.

2.4.5.1. European standards

Eurocode 8 includes cladding panels among non-structural elements. The out-of-plane equivalent static action is calculated according to the following equation:

$$F_a = \frac{S_a W_a \gamma_a}{q_a} \tag{2.1}$$

where F_a is the out-of-plane horizontal force, W_a is the weight of the element, q_a is the maximum behaviour factor (equal to 2,0 for façade elements), γ_a is the importance factor (equal to 1,0 for façade elements) and S_a is the seismic coefficient, which can be determined according to the following equation:

$$S_a = \alpha S \left[\frac{3\left(1+\frac{z}{H}\right)}{1+\left(1-\frac{T_a}{T_1}\right)^2} - 0{,}5 \right] \geq \alpha S \tag{2.2}$$

where α is the ratio of the design ground acceleration on subsoil type A, a_g, to the acceleration of gravity g, S is the soil factor, z is the height of the non-structural element (centre of mass) above the level of application of the seismic action, H is the building height measured from the foundation or from the top of a rigid basement, T_a is the fundamental period of the element and T_1 is the fundamental vibration period of the building in the relevant direction.

The Italian construction standards up to D.M.L.P. 1996 only referred to the necessity to verify that under seismic/wind drift the stability of non structural elements is granted. No explicit information or instruction was provided according to the calculation of seismic loading on the non structural members. European member nations have accepted Eurocode 8 rules for the design of cladding panels and related connections as non structural elements. In the Italian Nuove norme tecniche delle costruzioni (2008) it is kept in addition to the seismic resistance calculation the consideration that non-structural elements shall accommodate the drift of the structure subjected to the design seismic excitation.

2.4.5.2. US standards

The 1967 *Uniform Building Code* already introduced regulatons about the cladding panel connections. For what concerns drift allowance, it was indicated to be larger than twice the maximum drift caused by wind or seismic load or one fourth of an inch (6,4 mm), whichever is the greater. The seismic forces acting on the single panel were estimated according to the following equation:

$$F_p = ZC_pW_p \tag{2.3}$$

where F_p is the total lateral design seismic force acting on the component, Z is the seismic zone factor, C_p is the horizontal force factor (equal to 1,0 for non-structural components) and W_p is the panel weight. In the 1979 *UBC* version, only the introduction of the multiplying factor I, namely the importance factor, has been adopted as a modification of the previous formula. The value of the importance factor was suggested to be equal to 1,0. However, an important distinction is added for what concerns the force factor. In fact, a unity value is given for all elastic portions of the connections, while the body of the connection could be made with ductile devices which could be calculated according to a larger force factor, equal to 3,0.

In the following 1991 *UBC* version, the formula for lateral forces remained unchanged, while the drift allowance lower limit doubled to half on an inch.

The 1997 *UBC* version introduced several important changes in the calculation methodology. While the drift allowance remained unchanged but with indications on how to compute the drift, two alternative formulae were provided for the evaluation of seismic lateral forces, described in the following equations, together with a lower and higher limitation.

$$4{,}0C_aI_pW_p \geq F_p = 4{,}0C_aI_pW_p \geq 0{,}7C_aI_pW_p \tag{2.4}$$

$$4{,}0C_aI_pW_p \geq F_p = \frac{a_pI_pC_a}{R_p}\left(1+\frac{3h_x}{h_r}\right)W_p \geq 0{,}7C_aI_pW_p \tag{2.5}$$

where a_p is the in-structure component amplification factor (equal to 1,00 for rigid components), R_p is the component response modification factor (equal to 3,00 for the body of the connection and to 1,00 for other non-ductile connections), h_x is the element attachment elevation with respect to grade and h_r is the structure roof elevation with respect to grade.

The 2000 and 2003 *UBC* versions converged on a slightly different version, introducing the design earthquake spectral design acceleration at short period S_{DS}. The calculation is then modified as per the following equation.

$$1{,}6S_{DS}I_pW_p \geq F_p = \frac{0{,}4a_pS_{DS}I_pC_a}{R_p}\left(1+\frac{2z}{h}\right)W_p \geq 0{,}3S_{DS}I_pW_p \quad (2.6)$$

The most recent version of the *IBC* refers to *ASCE 7* Standard for the seismic requirements on non-structural components. The most recent version, *ASCE 7-10*, includes the calculation of the vertical seismic component F_{pv}, calculated as per the following equation.

$$F_{pv} = \pm 0{,}2S_{DS}W_p \quad (2.7)$$

In addition to the calculation rules, *FEMA 461* provides instructions about standard experimental tests aimed to assess the correct functioning of non-structural elements and connections. Finally, general approaches for non-structural buiding components can be found in Filiatrault *et al.* (2001).

2.4.6. Seismic design methodologies

Different approaches have been formulated and are available in literature regarding the seismic design of structures. Those approaches may be divided in very general terms into force based and displacement based.

Equivalent static forces and modal analysis with response spectrum are the most typical seismic design methodologies that use a force based approach (Biondini *et al.* 2010b). Those types of analysis are derived from elastic structural analysis, with which designers are very comfortable, and have been adapted to inelastic structural behaviour through the definition of a behaviour factor that, taking into account the large dissipation of energy provided by hysteretic damping during ductile plastic behaviour (unless explicit displacement rate-dependant devices are used, e.g. viscous dampers), reduces the fictitious elastic force demand on the structure. Several proposals for the evaluation of the behaviour factor are available in literature (Miranda & Bertero 1994 among others), from which the Eurocode 8 adopted the concept of equal elastic and anelastic displacement for flexible structures and equal dissipated energy for stiff structures (Fajfar & Fischinger 1988), with reference to well known standard construction technologies and relative bearing member cyclic behaviour. The maximum expected displacement can be determined at the end of the procedure.

The scientific and technical community has been focusing during the last 30 years to the development of different approaches, recognising the larger importance of a correct evaluation of the displacement demand induced by the seismic event, to which structural damage and seismic performance is strictly related. The main feature of those approaches is to use a static non-linear procedure and to compare the obtained capacity curve with the demand curve, that can be expressed according to different methodologies.

Fajfar & Gaspersic (1996) approach combines the pushover analysis of a multi-degree-of-freedom model with inelastic response spectrum analysis of an equivalent single-degree-of-freedom system. The inelastic response spectrum relies again on the behaviour factor, which is consistent from a physical point of view, since it represents the effect of a hysteretic dissipation of energy (Fajfar 1999).

Since the definition of the maximum behaviour factor allowed for a certain structure is based on experimental and numerical experience that the scientific community gained through time and is mainly dependant on probability based large crops of analysis, this approach is not suitable for non-standard structural technologies, unless new analysis campaigns based on experimental evidence are performed every time with a probabilistic procedure.

Another approach is the so-called Capacity Spectrum Method (Freeman 1978), in which the static non-linear analysis of the structure is performed not only monotically (pushover), but also cyclically. The capacity curve, corresponding to the monotonic plot, is then compared with the demand in the form of an over-damped elastic spectrum, where the over-damping is viscous and is calculated with reference to the equivalent hysteretic energy dissipated at a cycle of a certain amplitude. The method ends when convergence between the performance point (the intersection between capacity and demand curves) and the displacement considered for the calculation of the equivalent damping ratio are close, providing the expected drift of the equivalent single-degree-of-freedom structure. The procedure may be plotted in a unique diagram in the Acceleration-Displacement-Response-Spectrum (ADRS) format (Freeman 1998).

This method, although translating the hysteretic energy in an equivalent viscous (adapted from Jacobsen 1930), which is not physically consistent, has been proved to be effective in the quantification of the performance displacement and, unlikely the previous, may be used to determine the seismic performance of structural systems having whichever hysteretic shape, without the need of defining any initial stiffness, yielding displacement or hysteretic property. A version of the method has been adopted by the US standard ATC-40 (1996).

The definition of equivalent viscous damping is of main importance within the capacity spectrum method. The dissipated energy is adimensionalised with respect to the specific energy, which is generally calculated in accordance with the elastic deformation energy. Its definition has been usually provided for symmetric hardening structural systems (Freeman 1998, Kim *et al.* 2003, Chopra 2006, Priestley *et al.* 2007, Filiatrault *et al.* 2013), while in Priestley *et al.* (1996) is provided a more general definition. However, some authors (Tsopelas *et al.* 1997) suggest to refer to an explicit viscous-type related specific energy.

In Chopra & Goel (1999), Fajfar (2000), Priestley *et al.* (2007), Belleri & Riva (2008) and Martinelli & Faella (2010) a critical comparison of the above mentioned methods is available.

An innovative design procedure that starts from the demand definition in displacement form is called Direct Displacement Based Design (Sullivan *et al.* 2005, Priestley *et al.* 2007), where to acceleration spectra are directly substituted displacement spectra.

All the above-mentioned performance-oriented methods rely on the transformation of a complex structural system into a single-degree-of-freedom equivalent structure (Shibata & Sozen 1976), and then to the performance of a static non-linear analysis. It is clear that, as

stated in Krawinkler & Severinatna (1998), the validity of the methods is respected the more the natural vibration mode is predominant. Even if efforts have been provided to cover the case of multi-modal pushover analyses (Chopra & Goel 2002, Antoniou & Pinho 2004a and 2004b), precast industrial or commercial mono-storey buildings, generally featured by a highly symmetric structure, are in the majority of cases easily modellable with a single translational degree of freedom in each horizontal direction, and therefore the applicability of the performance based design seems to be promising.

For what concerns methods explicitly developed for friction damped structures, Fu & Cherry (2000) provide a tri-linear model to simulate the seismic resisting mechanism of single degree-of-freedom structures provided with double yielding displacements (of the friction connections and of the frame). The method is based on an evolution of the ASE method for bi-linear systems (Iwan & Gates 1979). Levy *et al.* (2001) provide a design methodology originally developed for friction damped steel frames concerning a two-phase iterative force-based modal analysis scheme. Bhaskararao & Jangid (2006) explore two numerical models to represent the dynamic behaviour of structures provided with friction dampers, together with indications on how to obtain an optimised slip threshold load distribution among the connections at different levels. With direct reference to a particular precast concrete system, Morgen & Kurama (2007) illustrate a design procedure to determine joint rotational friction damper slip threshold loads, assuming a linear elastic analysis of the structure under equivalent lateral forces.

Chapter 3

Innovative dissipative connections for cladding panels

The present chapter illustrates the experimental work concerning the mechanical characterisation of the cyclic behaviour of proposed dissipative connection devices. Design rules for the single devices are provided.

The Research activity has been focused on three types of innovative dissipative connections specifically designed to be used in between precast concrete panels, namely Friction Based Devices (FBD) that dissipate energy through friction and Multiple Slit Devices (MSD) and Folded Plate Devices (FPD) that dissipate energy through plasticity. The theoretical investigation on their behaviour and on their design has been accompanied by an experimental campaign aimed to characterise their mechanical behaviour under both monotonic and cyclic loading.

3.1. Local test setup and displacement protocols

The local tests on single devices have been carried out on a uniaxial ± 1000 kN Schenck test machine at the Laboratorio Prove e Materiali of Politecnico di Milano and subjected to vertical displacement histories. The tests are performed in displacement control, thruogh a ± 150 mm control transducer installed on the machine.

The connections are tightened through bolts to a strong support made by two L-shaped HEA steel profiles welded together. The L-shaped profiles are then tightened through nailed thick steel plates provided with large diameter bolts to the machine. Figure 3.1 shows pictures of the test setup with the different connections under testing. In addition to the standard machine instrumentation, two redundant ± 150 mm displacement transducers are always installed with magnetic bases in order to measure the exact drift between the L-shaped profiles. Other additional instruments have been placed depending on the needs of each connection. The data acquisition is performed through an external logger and the control is performed by the standard machine controller.

Monotonic tests are performed with a constant speed of 0,25 mm/s. Five different cyclic protocols have been used, the first three of which consist of increasing displacement amplitudes (Figure 3.2), expecting to provide information about the evolution of the connection behaviour and its low-cycle stability, and the latter two of which consist in constant large amplitude displacements (Figure 3.3) cycled several times in order to investigate the oligo-cyclic stability of the connection subjected to large deformation:

- Protocol A provides increasing displacements up to an amplitude of 10 mm with amplitude increments of 0,5 mm. Each amplitude is cycled three times. The test speed is kept constant at 2 mm/s except where slow speed tests are performed.

- Protocol B provides increasing displacements for the following amplitudes: 2,5 – 5,0 – 10,0 – 20,0 – 40,0 mm. Each amplitude is cycled three times. The test speed is kept constant at 2 mm/s except where slow speed tests are performed.

- Protocol C provides increasing displacement amplitudes from 5 up to 70 mm with a 5 mm step and a single cycle. The test speed is kept constant at 2 mm/s.

- Protocol D provides constant displacement amplitudes of ± 20 mm repeated ten times. The test speed is kept constant at 2 mm/s.

- Protocol E provides constant displacement amplitudes of ± 40 mm repeated ten times. The test speed is kept constant at 2 mm/s.

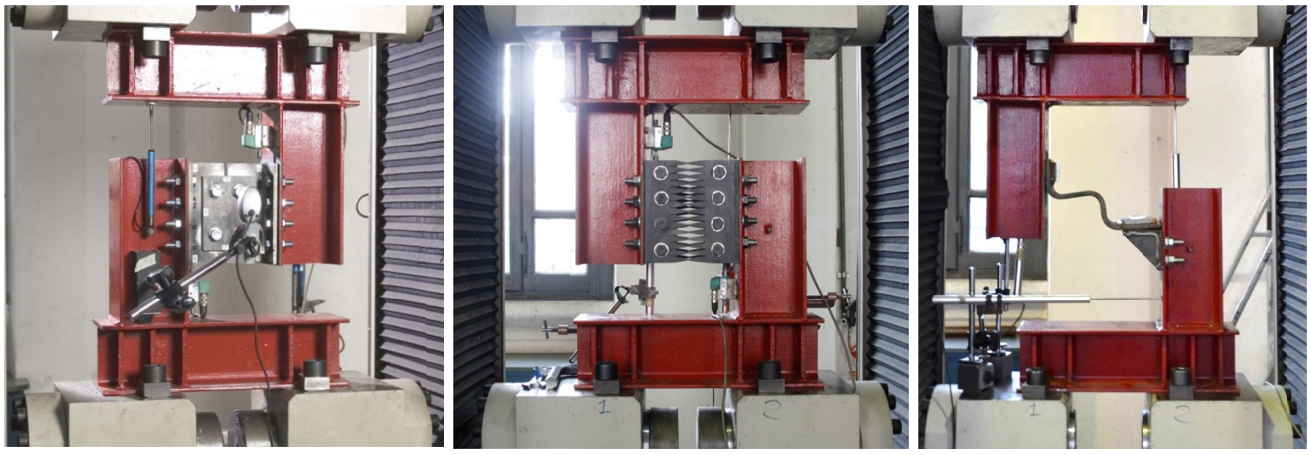

(a) (b) (c)

Figure 3.1 – Test setup with (a) FBD, (b) MSD, (c) FPD connections

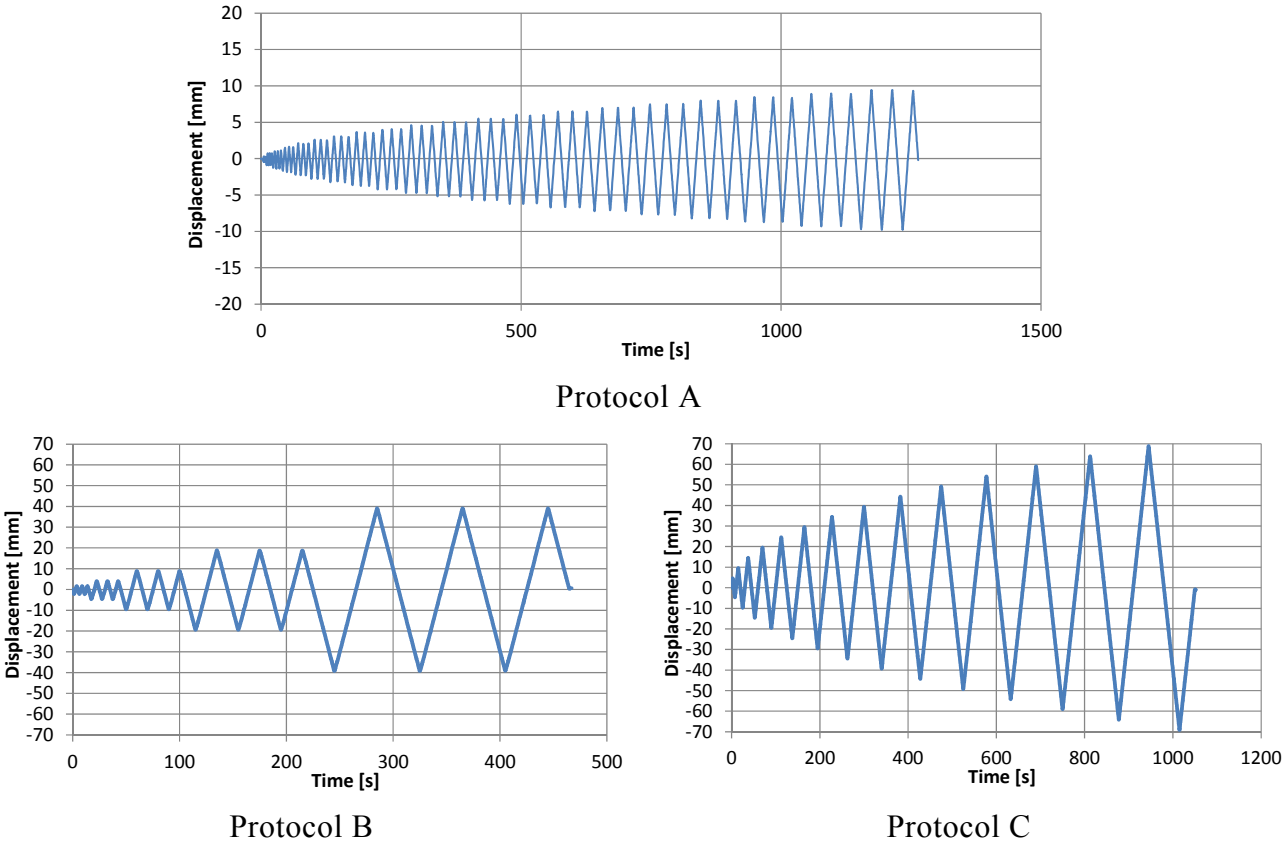

Figure 3.2 – Increasing displacement amplitudes cyclic protocols A, B and C

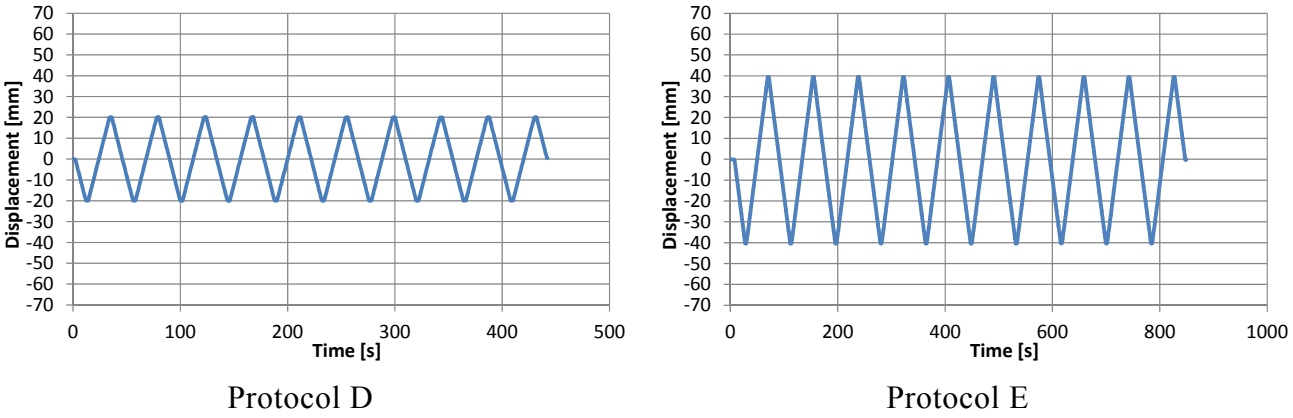

Figure 3.3 – Constant displacement amplitudes cyclic protocols D and E

For calculations of dissipated or specific energy the raw data has been truncated at the drift limit of each cycle, making therefore a more precise comparison between different systems.

For instance, if one cycle reached 15.1 mm instead of 15, the curve is truncated at 15 mm and all the consequent energy calculation is made on the new curve.

The dissipated energy is calculated as the area contained in each semi-cycle curve (Figure 3.4).

The specific energy is calculated as the dissipated energy over an equivalent cycle, defined according to two different ways, namely comparison with equivalent perfect elastic-plastic systems (with the area of a trapezoid surrounding higher force and higher displacement attained with the experimental initial stiffness as slope for the lateral sides as per Figure 3.5a) and comparison with equivalent perfect rigid-plastic systems (with the area of a rectangle surrounding higher force and higher displacement attained as per Figure 3.5b).

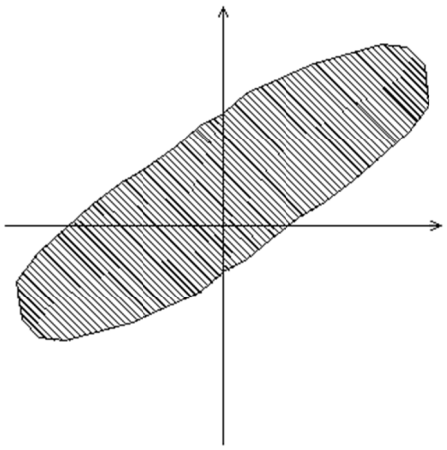

Figure 3.4 – Dissipated energy for each cycle

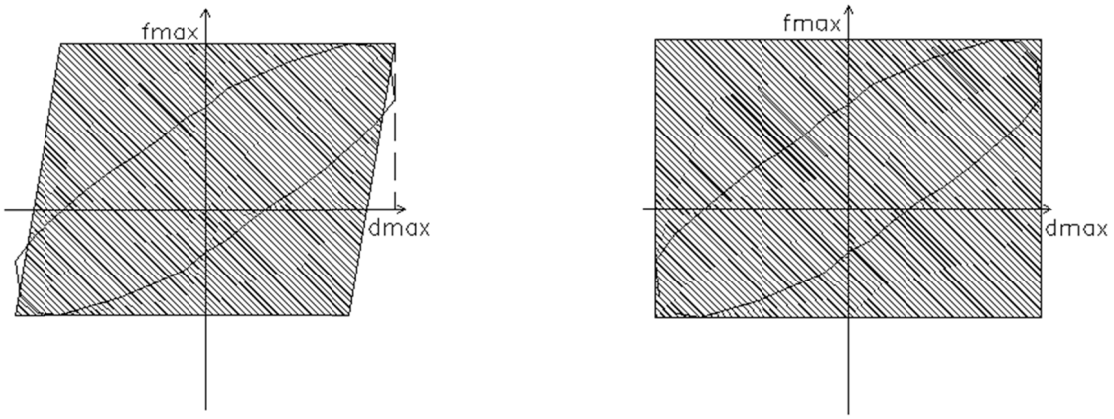

(a) (b)

Figure 3.5 – Specific energy: (a) perfect elastic-plastic equivalent systems, (b) perfect plastic equivalent systems

3.2. Friction Based Device (FBD)

The Friction Based Device, hereinafter FBD, is a connection designed to dissipate energy through friction and to be installed in between concrete panels. Some of the examples in literature are provided by Tyler (1977), Palsson (1982), Grigorian *et al*. (1987), Pall (1989), Cherry & Filiatrault (1993), Mualla (1999), Mualla *et al*. (2002). This kind of connection, based on the presence of a brass plate to stabilize the hysteretic cycles, can be considered also

a Brass Friction Device, in accordance with the classification made by Schultz *et al* (1994). Martinelli & Mulas (2010) and Valente (2013) provided a numerical work based on the use of a friction device working in torque in between columns and beams showing how the seismic behaviour improves through non-linear dynamic analyses on a precast building prototype. The particular set of the shear connection considered hereinafter has been previously tuned by Ferrara *et al* (2011) and applied to structural systems in Biondini *et al.* (2010a, 2013b). The work here presented considers several technological improvements with respect to the original version, together with a theoretical design procedure that has been generalized to different connection geometries.

The FBD is made by three elements assembled through bolts:

- *Support profile*, made with mild steel, which connects the device to the concrete panel. It can be T-shaped, in such a way to obtain a symmetric device-to-panel connection, or L-shaped, for an asymmetric connection. The member is provided with vertical slots that allow the mutual vertical displacement between the two adjacent support profiles and with holes or short horizontal slots on the panel side for a bolted device-to-panel connection or for temporary support for a welded device-to-panel connection. A symmetric profile can be symmetrically connected with the panel side, leading to a distribution of forces that disregards any torsion, however forcing the assemblage to be performed from two sides, in order to tighten all bolts. An asymmetric profile leads to torsional components in the panel connection, though allowing the assemblage to be performed from one side only (in general, the inner side of the building). Figure 3.6 shows that the force distribution related to a shear force V applied to the connection brings to an additional inclined torsional component for the L-shaped support profile.
- *Brass sheet*, made with brass, provided with two round holes in a column and with two horizontal slots in the other column, which realise the bolted connection with the support profiles, providing also an horizontal mounting tolerance which is a related to the length of the slots.
- *Cover plate*, made with mild steel, having the same geometry of the brass sheet.

The connection can be pre-assembled by mounting two support profiles, two brass sheets and two cover plates with bolts, nuts and washers without tightening, placed in position and then tightened, or assembled with each component at a time (an exploded assonometry of the connection mounted on L-shaped support profiles with inverted plate configuration is shown in Figure 3.7). The former solution eases the assemblage from one side only. Figure 3.8 shows the assembled device subjected to imposed displacement and Figure 3.9 shows a technical drawing of the assembled connection. The vertical tolerances are very large, since in vertical direction large slots are provided. Horizontal in-plane tolerance is provided by the horizontal slots on brass and cover plates. The horizontal out-of-plane tolerance s provided by the short horizontal slots on the support profile. Brass and cover plates can be mounted in mirrored or inverted configuration. The first configuration yields to a symmetric distribution of forces up to the sliding shear threshold, after which all horizontal reactions due to shear increments coming from the rotational equilibrium of the plates are taken by the support profile adjacent to the round holes of the plates. The second configuration always provides a symmetric distribution of forces.

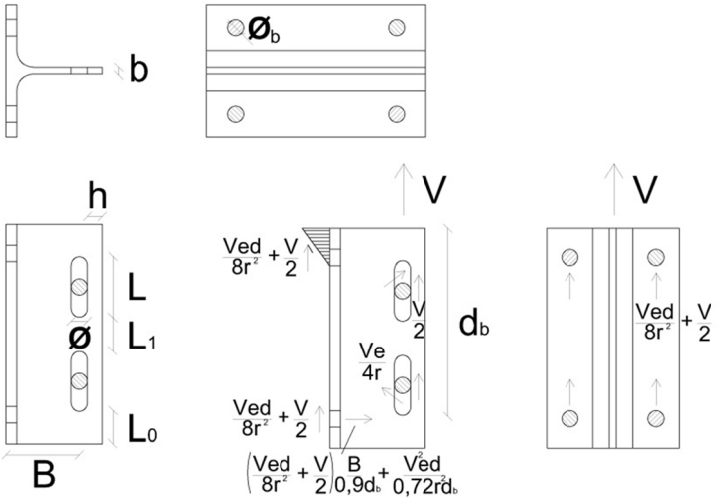

(a)

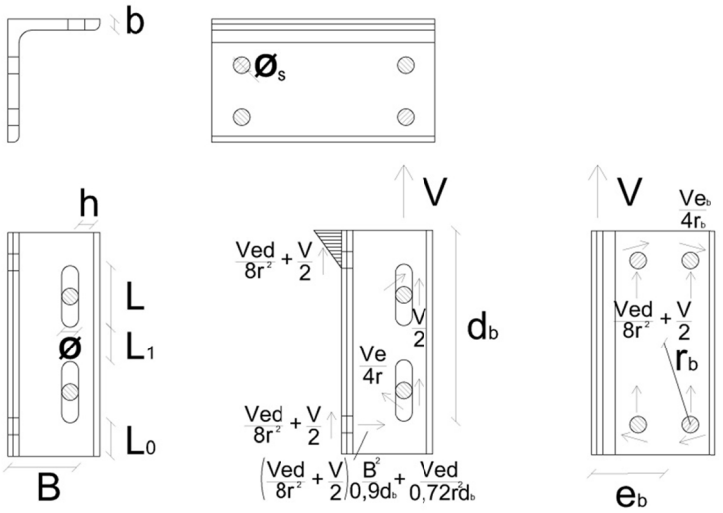

(b)

Figure 3.6 – Geometry and force distribution of (a) T-shaped support profile and (b) L-shaped support profile

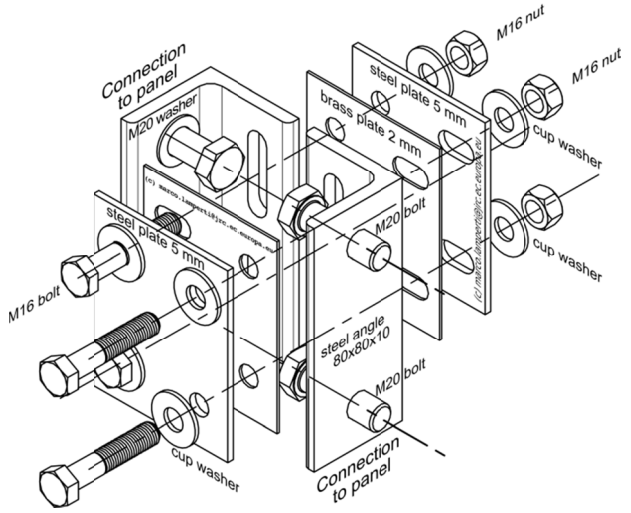

Figure 3.7 – Exploded assonometry of a FBD on L-shaped support profile with inverted plate configuration

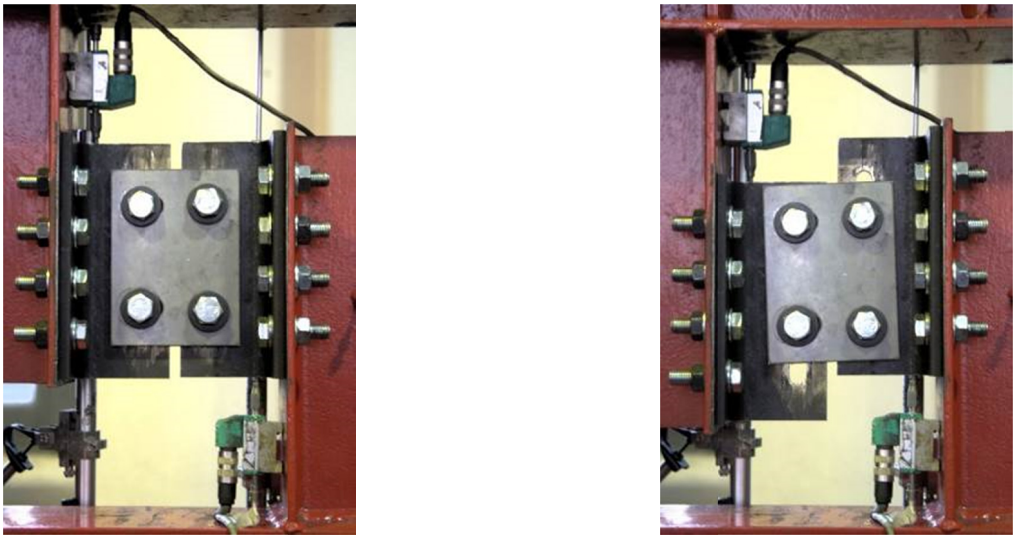

(a) (b)

Figure 3.8 – Friction Based Device (a) assembled and (b) subjected to maximum drift

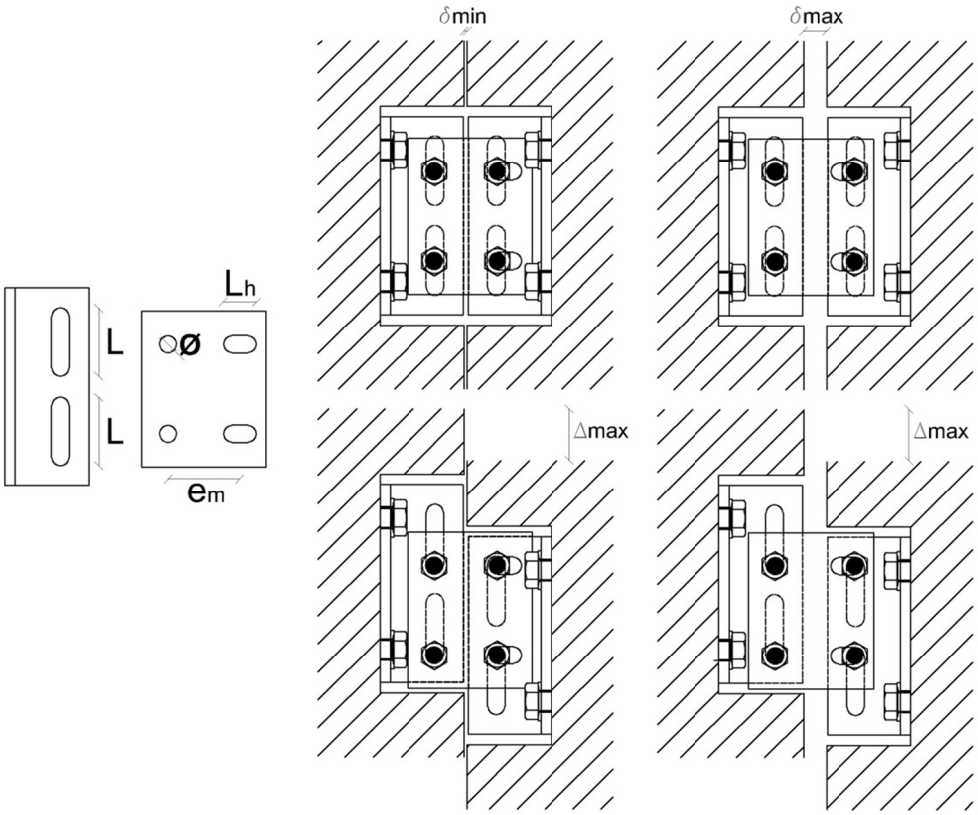

Figure 3.9 – Assemblage tolerances and maximum relative sliding

3.2.1. Experimental programme

The cyclic tests that have been carried out are listed in Table 3-1. The tests have been carried out with the aim to set the best configuration of the device and to investigate several technological issues, both regarding the performance of the connection and its operability (Biondini *et al.* 2014b, 2014e). Those issues regard:

- The necessity of using the brass plates;
- The behaviour under different velocities of displacement application;
- The efficiency of sandblasting surface treatment, aimed to enlarge the steel-brass friction coefficient;
- The necessity of controlling the torque;
- The possibility of re-use of the same components also after several cycles;
- The behaviour considering different types of washers;
- The behaviour with symmetric or asymmetric support profiles.

Table 3-1 – List of the performed tests on FBD

DEVICE	TEST TYPE	CYCLIC LOAD PROTOCOL	SPEED	KIND OF SAMPLE	BOLTS	TIGHTENING TORQUE	WASHER	TEST ID
FBD	CYCLIC	D	SLOW	NEW	8.8	134	THIN	1
			SLOW	USED		134	THIN	2
			FAST	USED		134	THIN	3
			FAST	NEW		134	THIN	4
			FAST	SANDBLASTED1		134	THIN	5
			FAST	SANDBLASTED2		134	THIN	6
			FAST	REVERSED		134	THICK	7
			FAST	NEW		134	THICK	8
		E	FAST	NEW		80	THICK	9
			FAST	USED		134	THICK	10
			FAST	NEW		134	BELLEVILLE	11
			FAST	NEW		134	ELASTIC	12
			FAST	NEW	10.9	190	BELLEVILLE	13
			FAST	REVERSED_NEW		190	BELLEVILLE	14
			FAST	REVERSED_USED		190	BELLEVILLE	15
			FAST	ANGLES - NEW		190	BELLEVILLE	18
			FAST	ANGLES - USED		190	BELLEVILLE	19
		B	FAST	NEW	8.8	134	THICK	20
			FAST	NEW		134	BELLEVILLE	21
			FAST	NEW		134	ELASTIC	22
			FAST	NEW	10.9	190	BELLEVILLE	23
			FAST	USED		190	BELLEVILLE	24
			FAST	REVERSED(NO BRASS)		190	BELLEVILLE	25
			FAST	ANGLES-NEW		190	BELLEVILLE	28
			FAST	ANGLES-USED		190	BELLEVILLE	29

3.2.2. Necessity of brass plates

While none of the performed tests with the traditional configuration of a brass friction device showed cyclic instability, the only test performed without the use of the brass plates, which means that the sliding occurs between the steel surfaces of the support profile and the plate, thus reducing the cost of the device, showed a clear tendency of cyclic instability. Figure 3.10 shows the load vs displacement experimental cycles of the specimen without brass sheets, and it can be noted that a cyclic instability occurred, since the slip load rapidly increases with large drifts. This happened because of tangling of the steel surfaces, which is also called "mechanical welding" effect. Figure 3.11 shows the load vs displacement experimental diagram of a "traditional" connection provided with brass sheets, where tendencies to instability are not observed. The entanglement of the connection without brass sheet caused a large increase in the force, which moved the deformation from the sliding of the central portion to the plastic deformation of the support profiles, as shown in Figure 3.12.

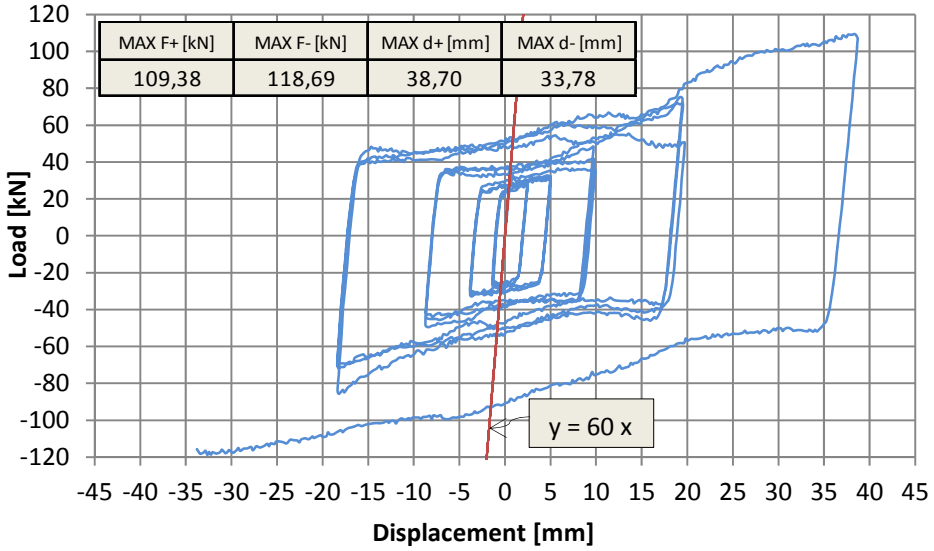

Figure 3.10 – Load vs displacement for specimen without brass sheet (test 25)

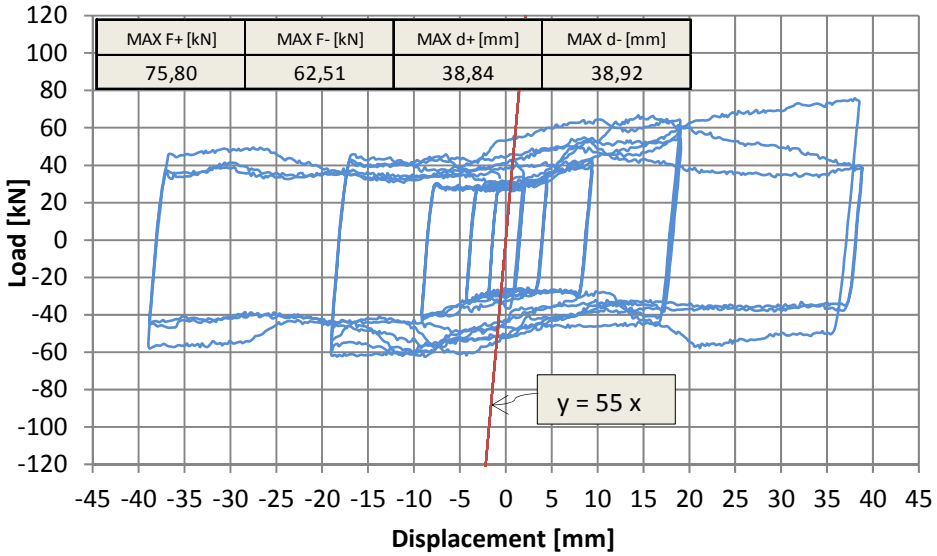

Figure 3.11 – Load vs displacement for specimen provided with brass sheet (test 23)

Figure 3.12 – Strong plastic deformation of the T-shaped support profile after tangling

3.2.3. Load rate

The comparison between the cyclic behaviour of two identical specimens tested with imposed displacements with different load rates, equal to 0,1 mm/s (Figure 3.13) and 2,0 mm/s (Figure 3.14), shows that the behaviour is not influenced by velocity within this speed range.

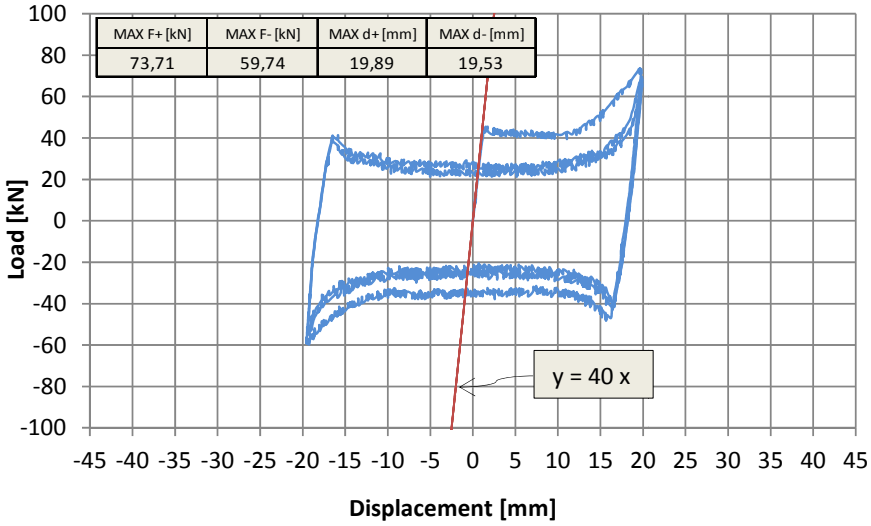

Figure 3.13 – Load vs displacement for specimen tested at a speed of 0,1 mm/s (test 1)

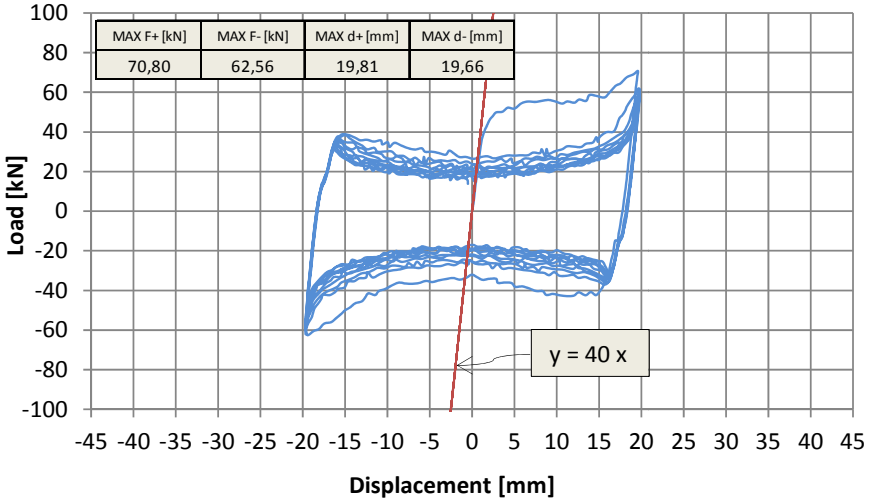

Figure 3.14 – Load vs displacement for specimen tested at a speed of 2,0 mm/s (test 4)

3.2.4. Effect of sandblasting surface treatment

Sandblasting surface treatment has been applied to both the inner sides of the brass sheets in order to increase the friction coefficient between steel and brass, trying to maximize the slip load threshold. The cyclic behaviour that has been reported in Figure 3.15 shows that the surface treatment is efficient in increasing the slip load threshold, both static and dynamic. However, the results show that this effect is strongly active only for monotonic loading, since after the first semi-cycle the behaviour quickly tends to that of a specimen provided with a regular brass sheet (Figure 3.16), which is due to the abrasion of the sandblasting, occurring very soon. Figure 3.17 shows the comparison between a sandblasted and a regular brass sheet after a test with protocol C. The sandblasted surface is strongly abraded, exposing the smooth surface under the treated.

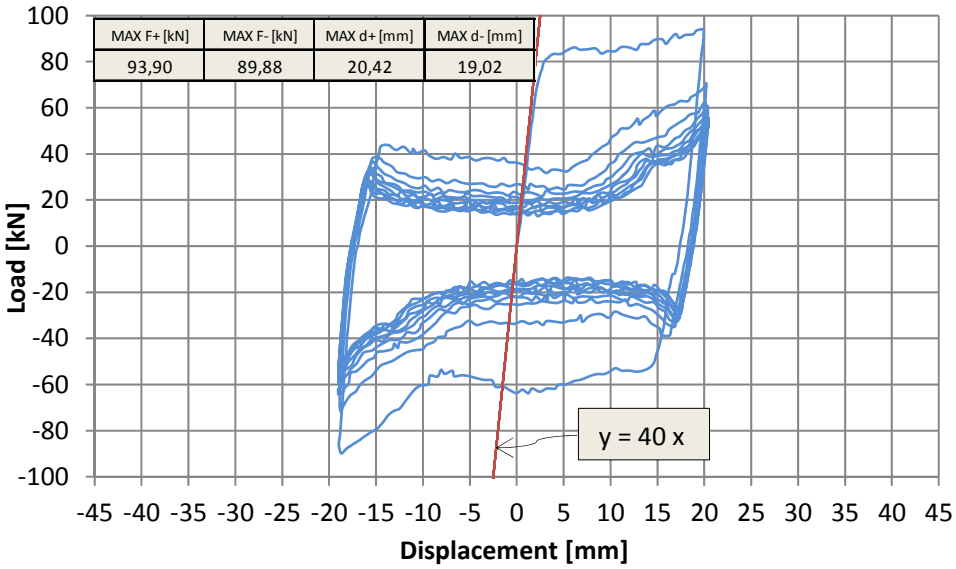

Figure 3.15 – Load vs displacement for specimen with inner sandblasted brass sheets (test 5)

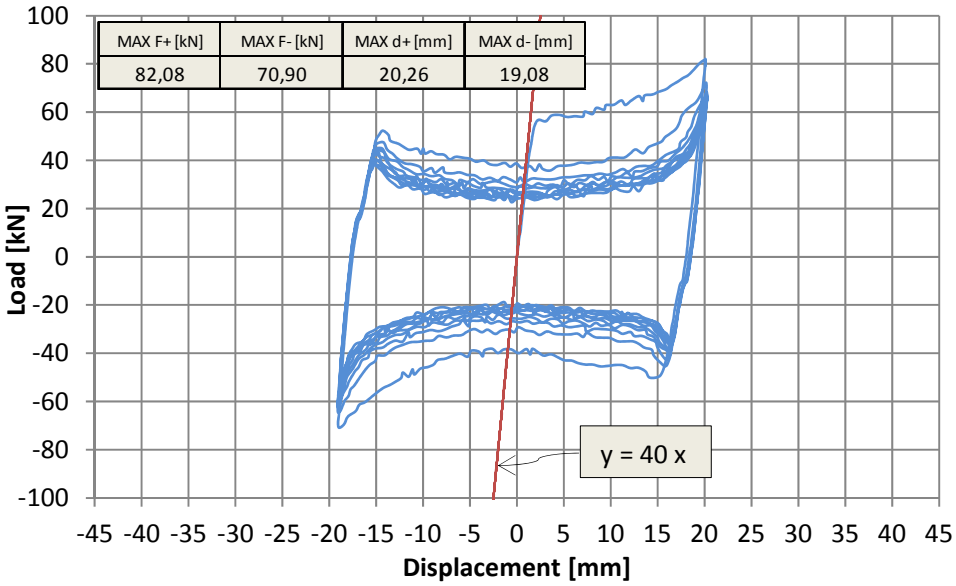

Figure 3.16 – Load vs displacement for specimen with untreated brass sheets (test 3)

(a) (b)

Figure 3.17 – Brass sheets after testing: (a) sandblasted and (b) regular

3.2.5. Importance of torque control

The connection has been tuned to be used with a large axial load provided by the bolts tightening. The higher is the tightening torque, and subsequently the axial load, the higher is the load slip threshold, given that the friction coefficient is constant. Therefore, it is highly important to verify that the torque given to the bolts correspond to what has been considered in the design, for instance using a dynamometric wrench. A larger torque with respect to the maximum prescribed could damage the bolts and the components, also increasing the slip load thresholds with danger for the other panel connections designed according with the connection capacity. A lower torque would lead to a lower slip load threshold, against safety side with respect to the seismic design of the whole structure.

For specimens equipped with 8.8 class M14 bolts the tightening torque has been tuned in accordance with the standard maximum, calculated on the base of standard metric thread and a friction coefficient equal to 0,14 (non-lubricated), which is 136 Nm, corresponding to an axial pre-load of 50 kN. For comparison, a lower torque equal to 80 Nm has been applied with the dynamometric wrench to the bolts of the connection which test results are shown in Figure 3.18. The comparison with a specimen tightened at 136 Nm, which results are collected in Figure 3.19, shows that the load slip threshold proportionally lowers with a lower torque (the static threshold is about 50 kN for the specimen with 136 Nm of torque and 30 kN for the specimen with 80 Nm of torque, which relationship is equal to 1,7 both for loads and torques), confirming the assumptions of above.

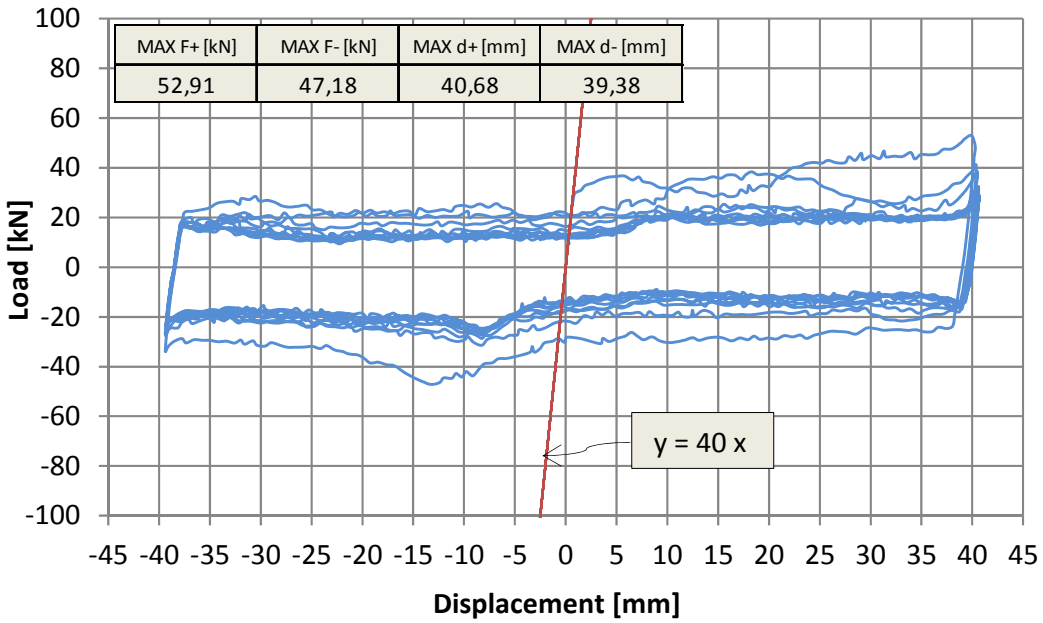

Figure 3.18 – Load vs displacement for specimen with 80 Nm torque (test 9)

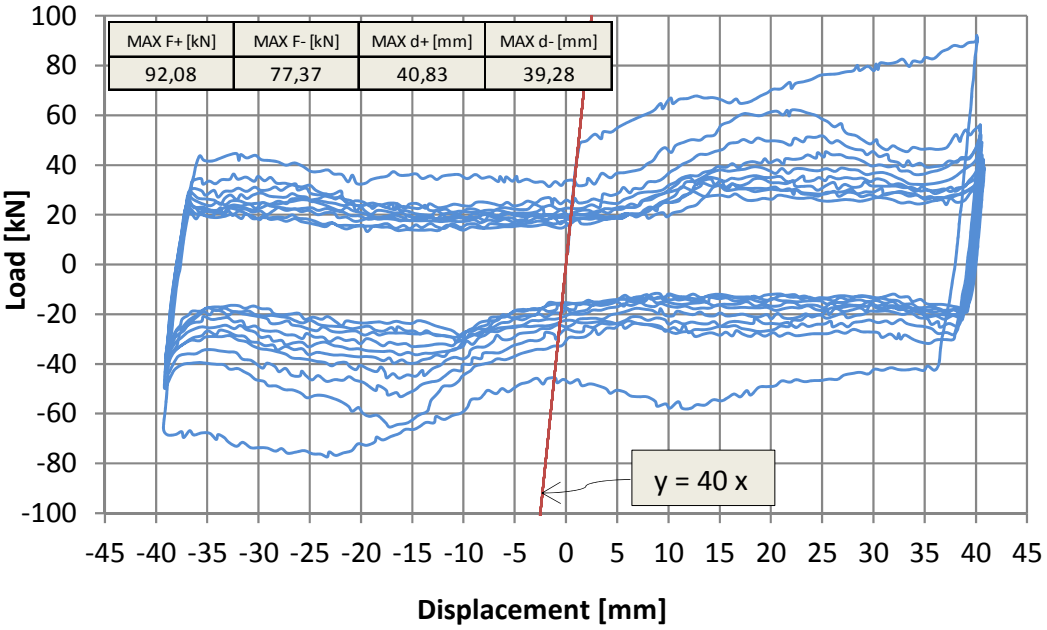

Figure 3.19 – Load vs displacement for specimen with 136 Nm torque (test 10)

3.2.6. Re-use of the connection after several cycles

The global cost of the connection shall take into account the operations and substitutions that need to be done after service to make the connection fully operative again. In particular, special regard has been dedicated to the brass sheets, since they are subjected to abrasion during the motion (Figure 3.20) and they also represent a large part of the connection global cost. Several tests have then been repeated twice using the same components, without dismounting the connection, with the only operation of re-tightening it. The comparison between the hysteretic cycles of a used connection (Figure 3.21) and a new one (Figure 3.11) shows that the performance of the connection is not substantially influenced by the previous strong abrasion of the connection. Similar results have been obtained with all tests repeated with new and used specimens. Thus, it is possible to state that the components of the connection can be re-used after a heavy motion without the need of substitution of whichever component. However, re-tightening is needed in order to restore the original axial load in the bolts, which could have lowered due to abrasion of the brass sheet and subsequent bolt shortening with axial load losses.

Figure 3.20 – Brass sheet after testing with protocol E

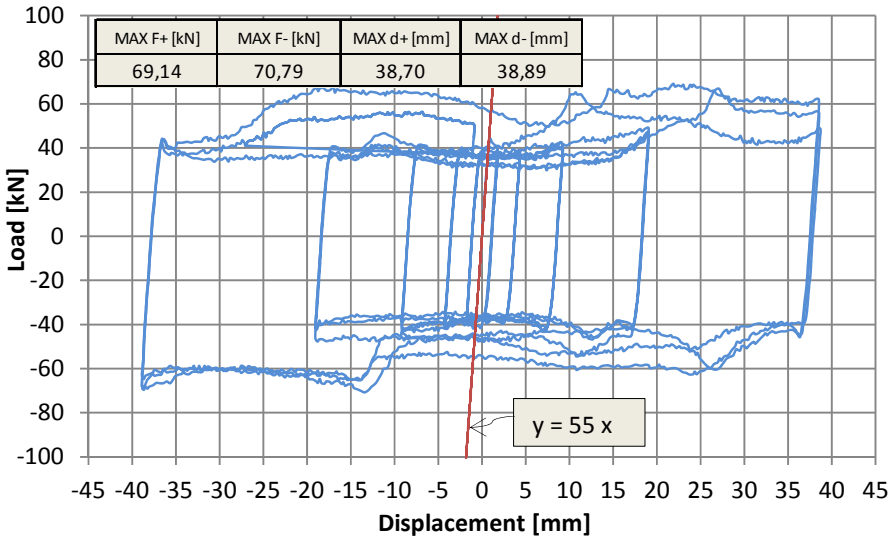

Figure 3.21 – Load vs displacement for specimen with used components (test 24)

3.2.7. Use of different types of washer

A comparison among specimens provided with different types of washer show that this component can have a large influence on the cyclic response of the connection. Four different types of washers have been considered, from normal thin M14 washers to thick M14 washers, up to improved types of washers such as elastic (spiral-shaped cut washer) and belleville (with spherical profile). The hysteretic cycles of the specimen with standard thin washers (Figure 3.14) show a large loss of dynamic load slip threshold through cycles, with a lowering that reaches about 20 kN within the second and the third cycles. At the end of the test, the residual axial load in the bolts has been approximated caught by using again the mechanical wrench for unscrewing. At the only side subjected to slippage, a residual torque of less than 50 Nm, the minimum allowed by the wrench, has been measured for both bolts, while a higher torque of about 100 Nm has been measured for the bolts of the side not subjected to slippage. The energy dissipation properties of this connection are reported in the charts of Figure 3.22, from which it can be deduced that the energy dissipation decay through cycles is rapidly occurring. Looking at the specific energy computed with reference to a perfect plastic cycle having the same maxima drifts and loads of the analysed, again a noticeable decay is occurring, starting from about 0,6 down to 0,35. The specimen with thick washers (Figure 3.19) also shows large losses, reaching a threshold of about 20 kN within the second and third cycles. Residual torques measured at both sides are equal to 60 – 70 – 70 – 100 Nm. The energy dissipation properties reported in the charts of Figure 3.22 show that the energy dissipation decay through cycles is rapidly occurring. Looking at the specific energy, an improvement of the behaviour is noticed, with values that float around 0,6.

Some improvements can be noticed at the specimen provided with elastic washers (Figure 3.24), with which three to four cycles can develop before the threshold lowers down to 20 kN. Residual torques are as follows: 50 – 90 – 90 – 110 Nm. Figure 3.25 shows that the energy dissipation decay through cycles is occurring more softly. Looking at the specific energy, an improvement of the behaviour is noticed, with values that float around 0,6.

The best performance is noticed with the specimen equipped with belleville washers (Figure 3.26), which also shows a tendency to lower the threshold, reducing though losses in such a way that the threshold is of about 30 kN also after the full performance of ten large displacement cycles. The residual torques that have been measured are equal to 70 -110 – 110 – 110 Nm for the other three. Figure 3.27 shows that the energy dissipation decay through cycles is occurring much more softly with respect to the tests with other types of washers. Looking at the specific energy, a stable behaviour is noticed, with values that float around 0,6. Those losses are due to the abrasion of the brass sheet. The bolts are tightened within a short length, between 24 and 28 mm in the performed tests, and thus a superficial abrasion of several hundredths of millimetres can cause a shortening in the bolt that corresponds to a strong loss. Traditional flat washers do not provide a restraint for the bolt shortening, but improved washers, such as elastic and belleville, are aimed to keep the pre-load even under small shortening, as per their stiffness. A slight increase of elastic stiffness of the connection with stiffer washers is also noticed, from a value of about 40 kN/mm with thin washers, to 45 kN/mm with thick washers, to 50 kN/mm with elastic washers up to 55 kN/mm with belleville washers.

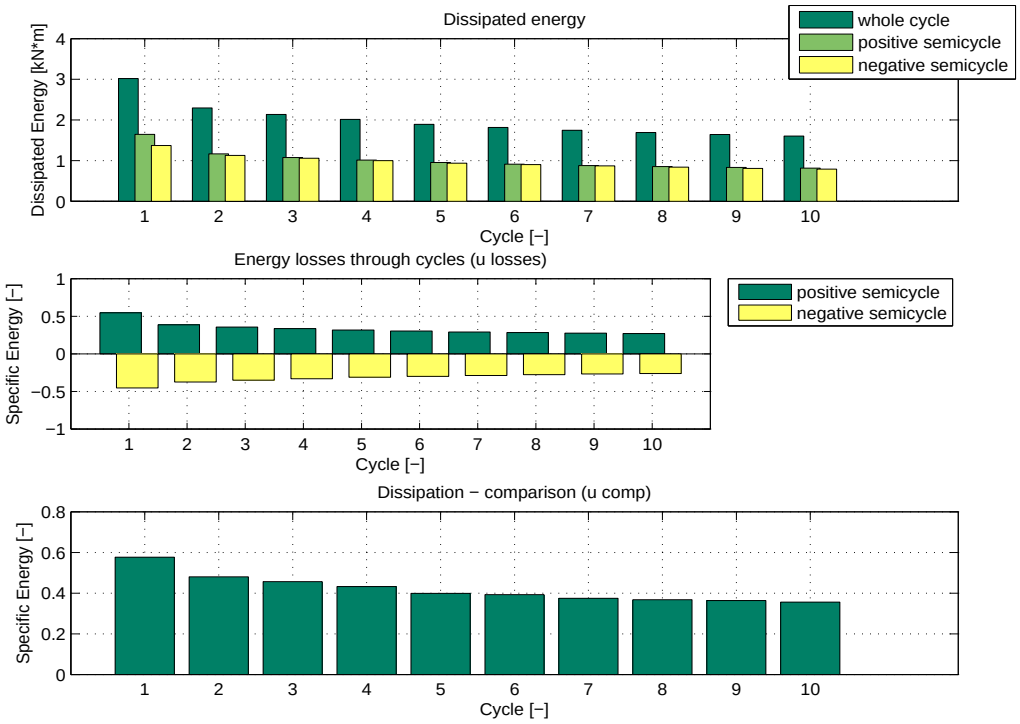

Figure 3.22 – Energy dissipation properties for specimen with thin washers (test 4)

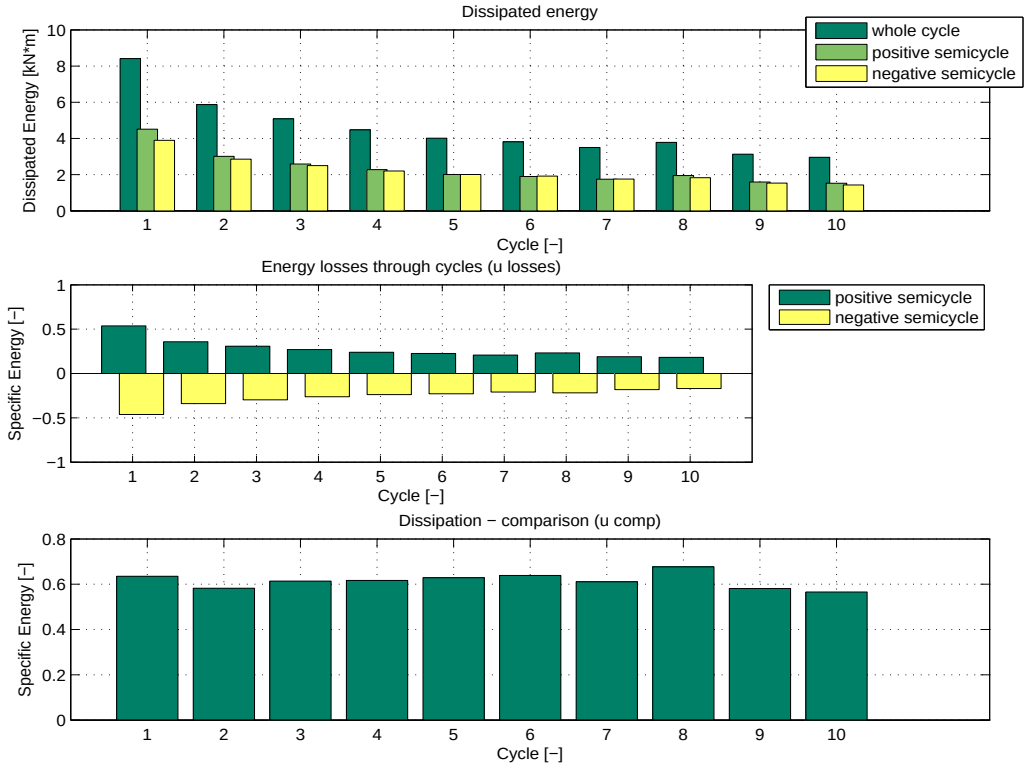

Figure 3.23 – Energy dissipation properties for specimen with thick washers (test 10)

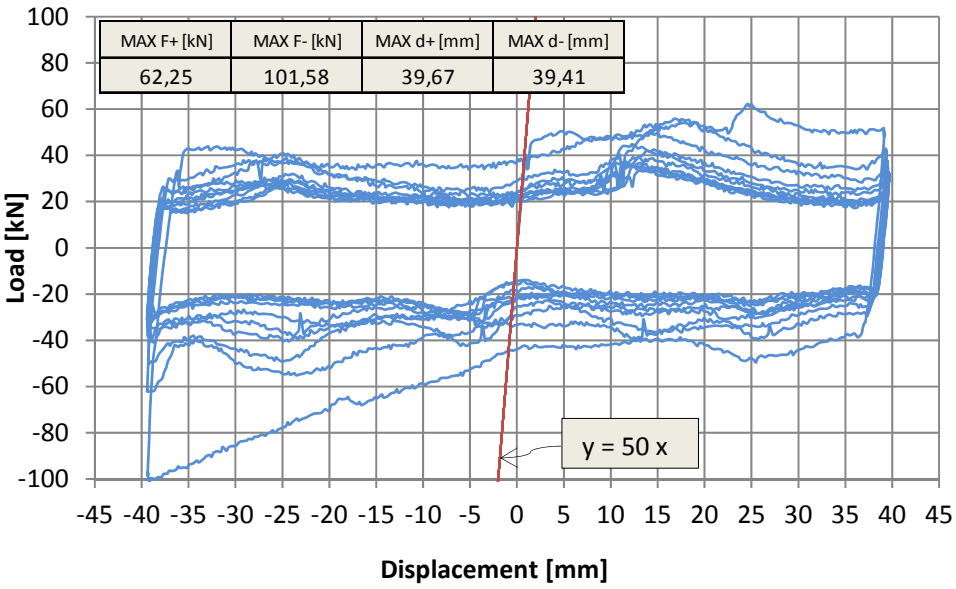

Figure 3.24 – Load vs displacement for specimen with elastic washers (test 12)

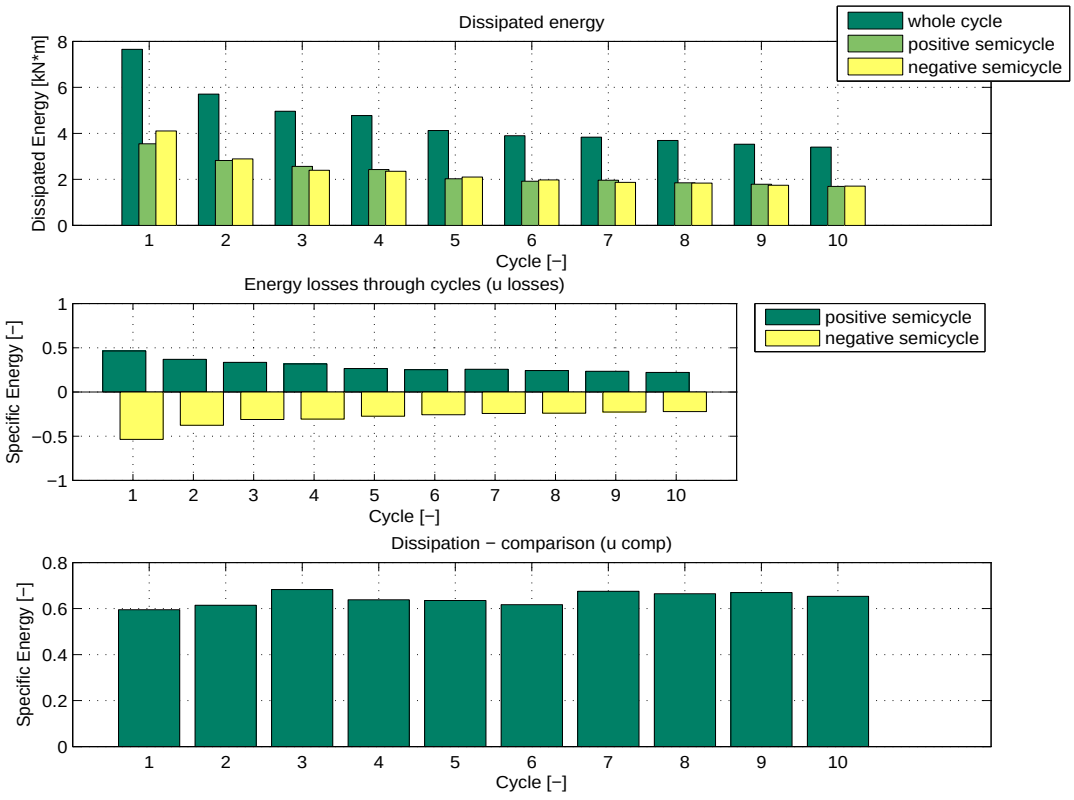

Figure 3.25 – Energy dissipation properties for specimen with elastic washers (test 12)

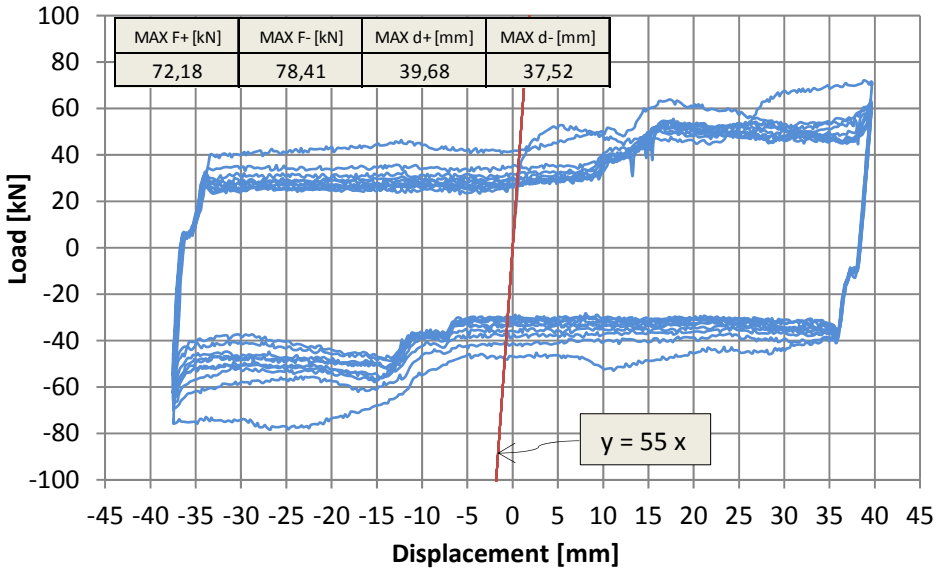

Figure 3.26 – Load vs displacement for specimen with belleville washers (test 11)

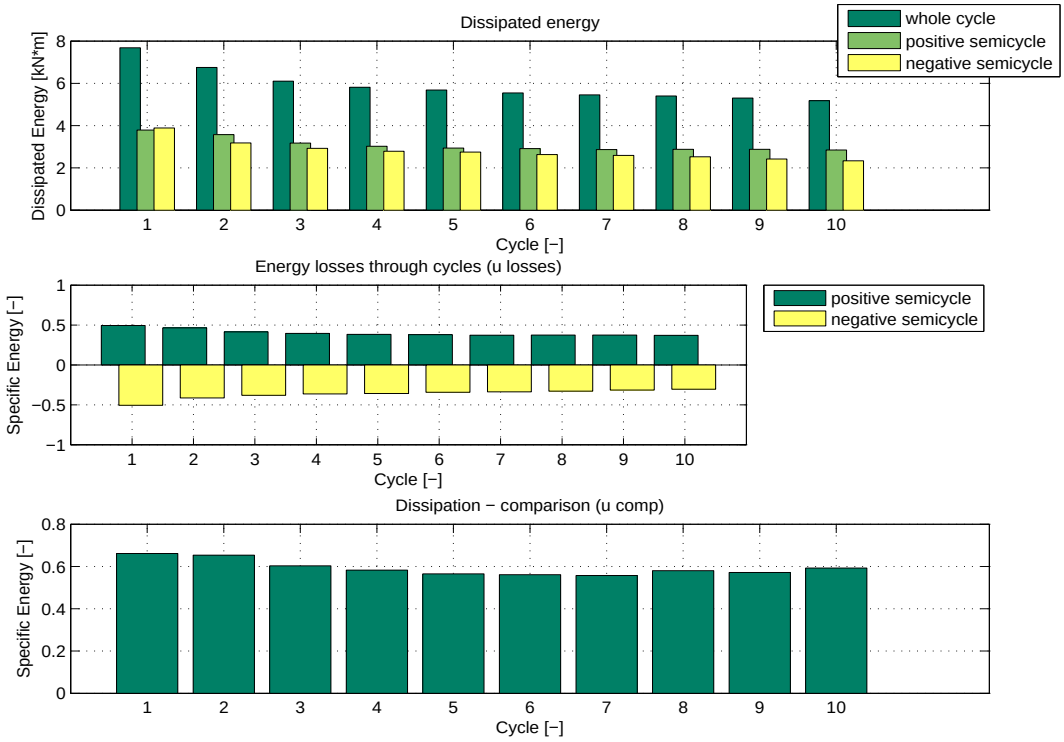

Figure 3.27 – Energy dissipation properties for specimen with belleville washers (test 11)

3.2.8. Asymmetric support profiles

The best configuration of the device has been tuned with asymmetric support profiles, so to be able to mount and dismount the connection from one panel side only. Thick angle profiles have been used with the final technological configuration coming from the previous tests, with belleville washers and untreated brass sheets. M14 class 10.9 bolts are used and tightened at 190 Nm. Figure 3.28 shows the load vs displacement diagram of the new specimen tested with

protocol E and Figure 3.29 shows the energy dissipation properties. A large cyclic stability is achieved, together with a very large specific energy. Similar results are obtained from the same test with used components (Figure 3.30 and Figure 3.31). The tests performed with protocol B also show a large cyclic stability and dissipation properties, both for the new specimen (Figure 3.32and Figure 3.33) and for the used (Figure 3.34 and Figure 3.35).

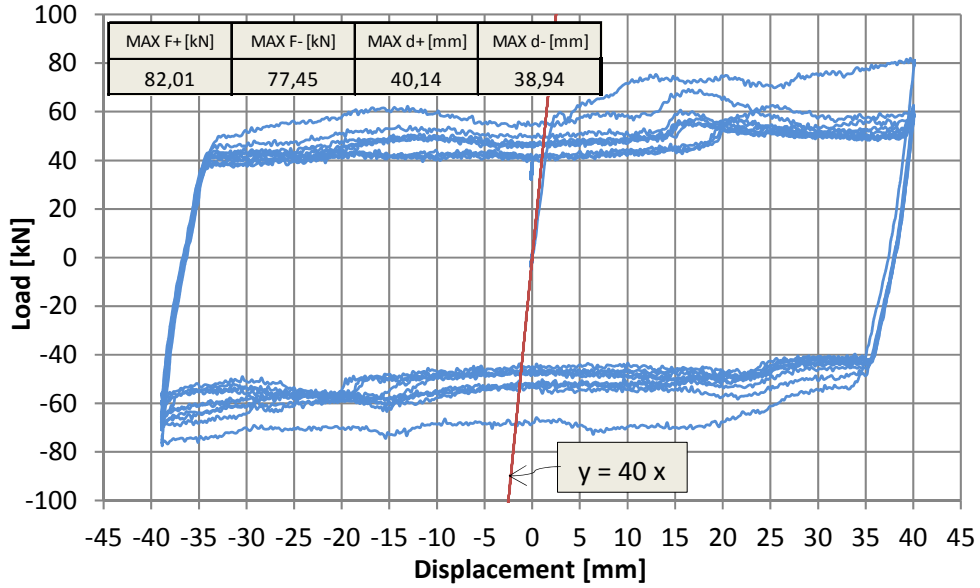

Figure 3.28 – Load vs displacement (test 18)

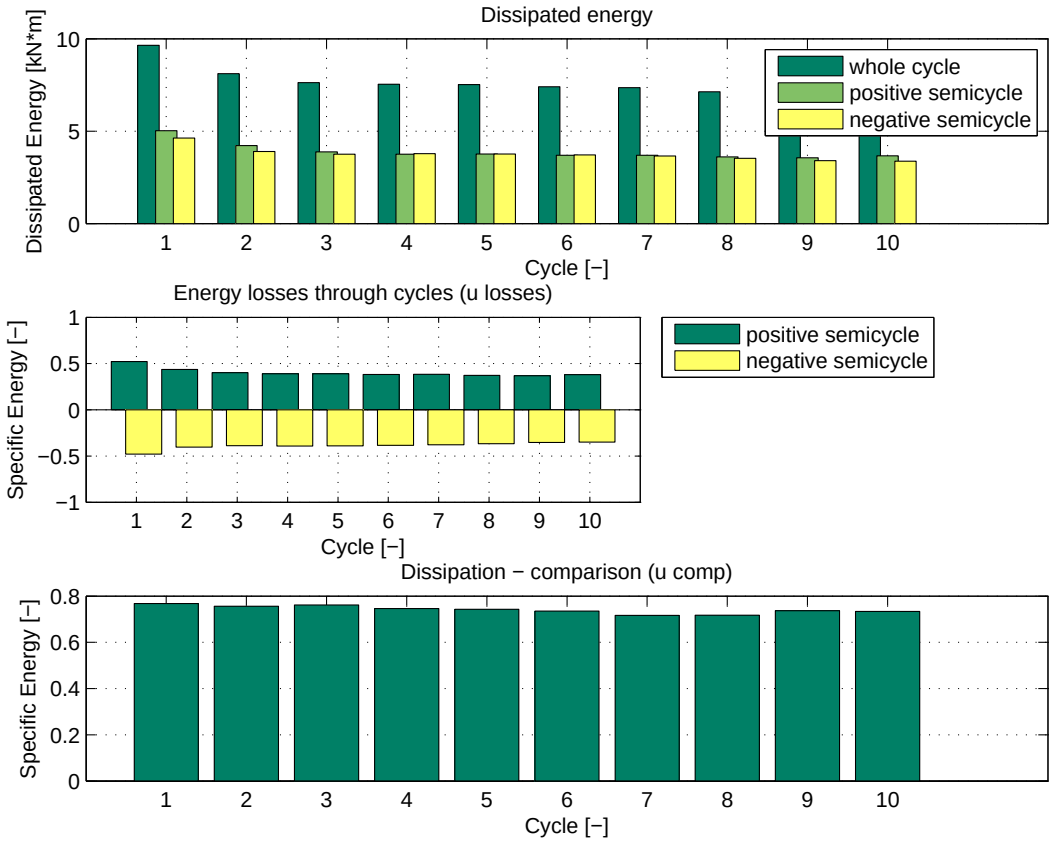

Figure 3.29 – Energy dissipation properties (test 18)

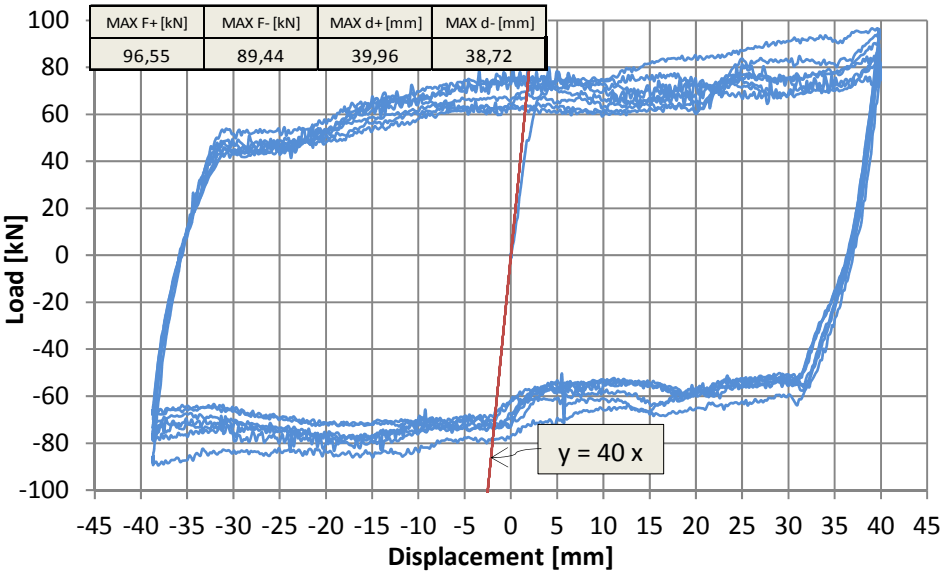

Figure 3.30 – Load vs displacement (test 19)

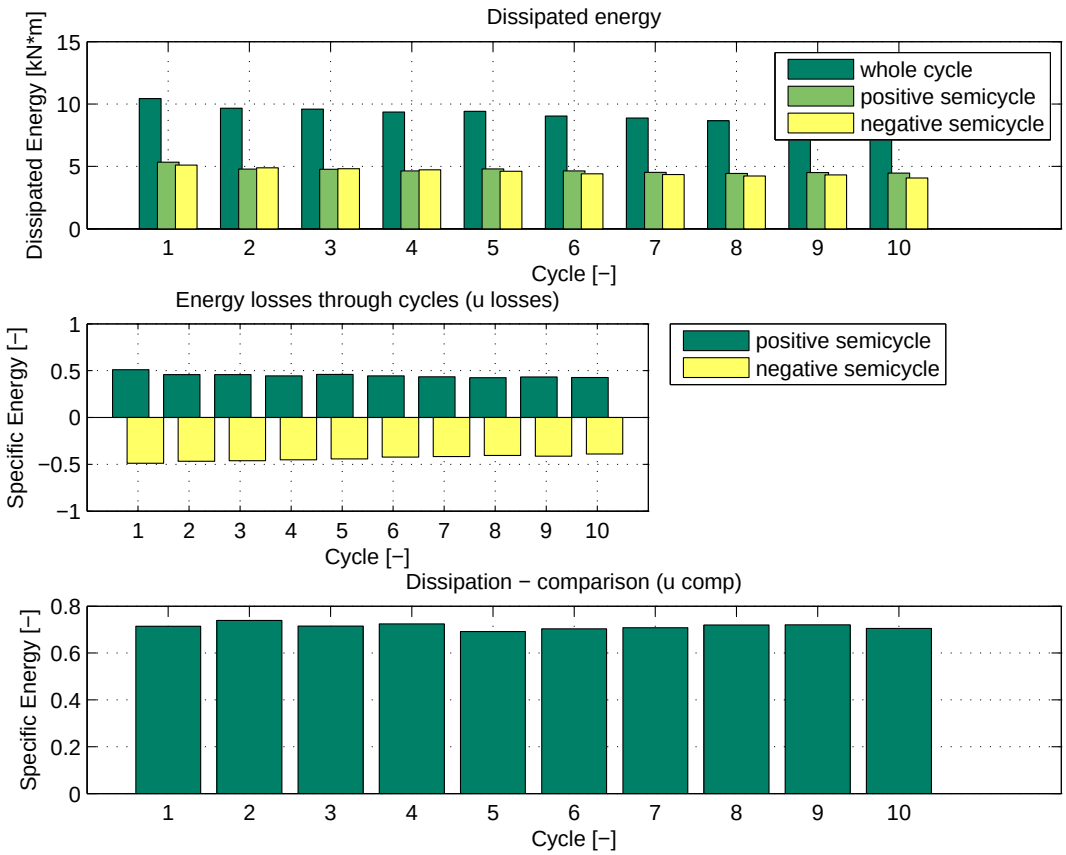

Figure 3.31 – Energy dissipation properties (test 19)

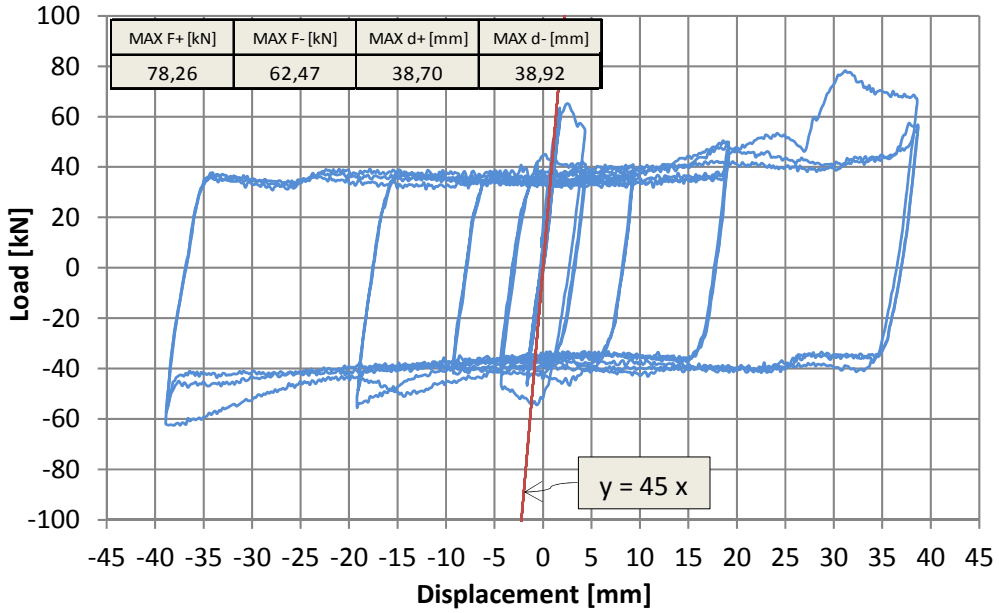

Figure 3.32 – Load vs displacement (test 28)

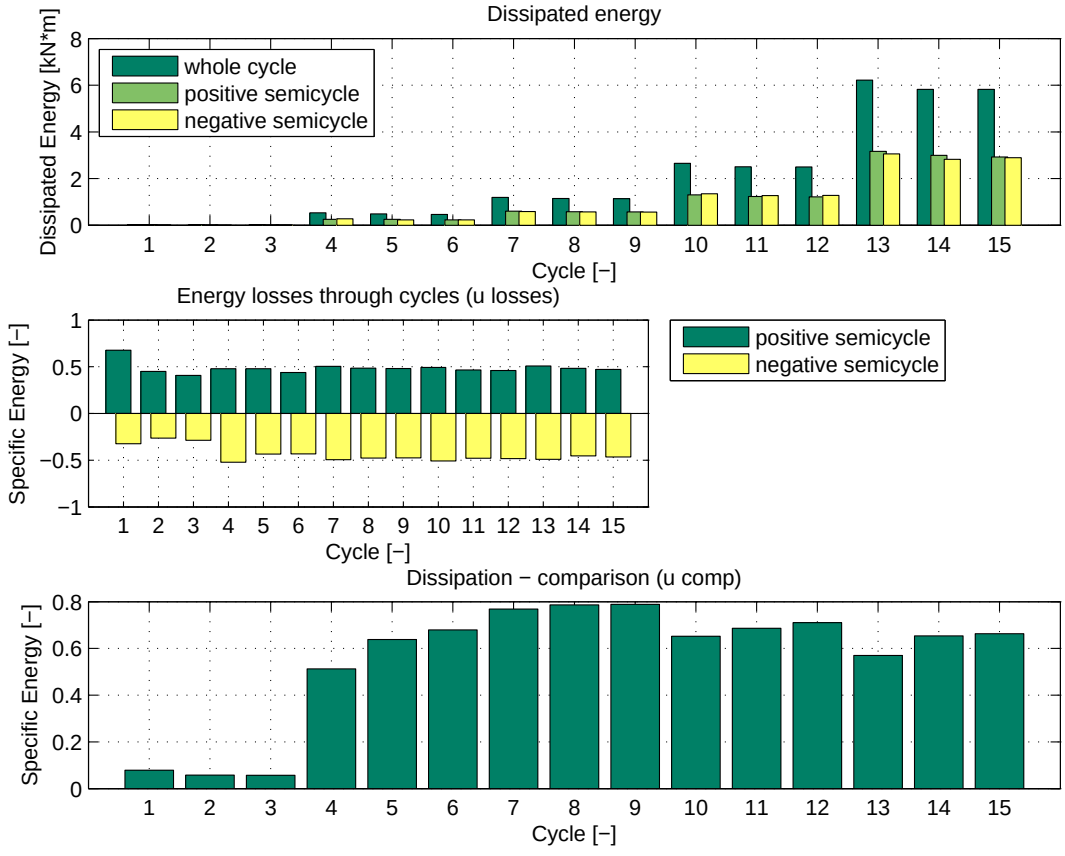

Figure 3.33 – Energy dissipation properties (test 28)

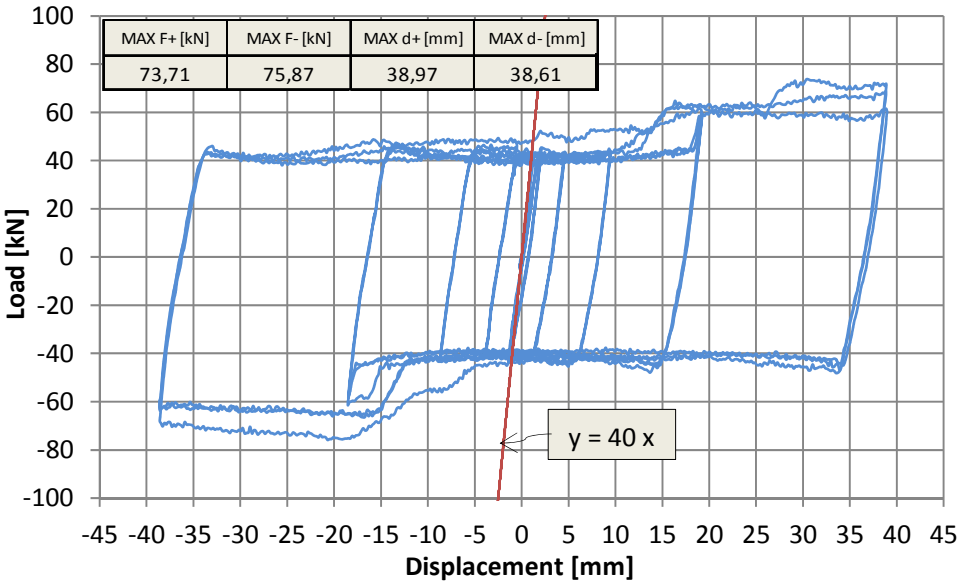

Figure 3.34 – Load vs displacement (test 29)

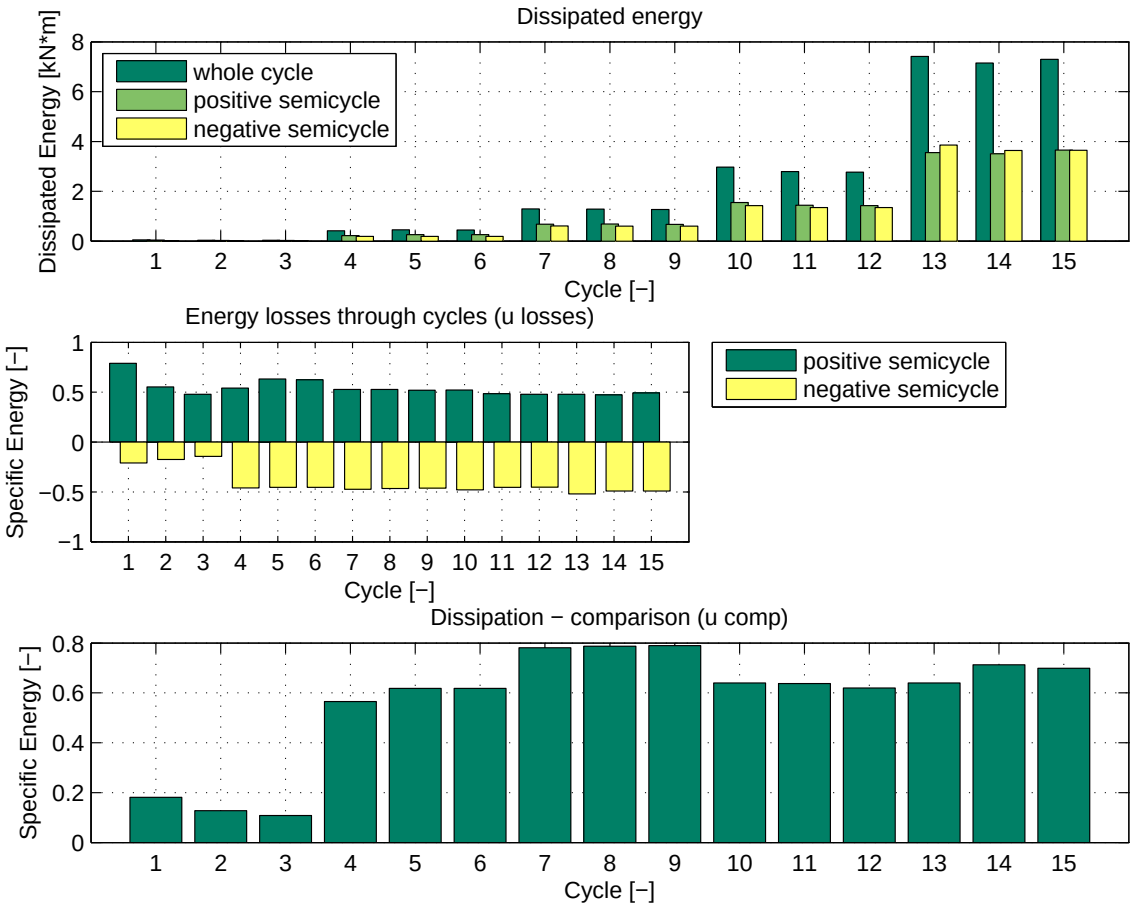

Figure 3.35 – Energy dissipation properties (test 29)

3.2.9. Design recommendations

From the analysis of the experimental data, it is noticeable how similar tests yielded to different results in terms of maximum load, depending on complex local random phenomena related to friction. Anyhow, the tendency of the cyclic behaviour of the connection can be identified as elastic-plastic, with an elastic stiffness within the range 40~60 kN/mm and a plastic branch up to the maximum allowed drift. The maximum drift is equal to the gross length of the vertical slots diminished by the bolt diameter and by the vertical assemblage tolerance. The calculation of the plateau value to be used for the design of the device should take into account three different necessities: a mean value for a serviceability design, a safe side value for the design of the overall structure in which the FBDs improve the seismic response and, finally, a safe side value for the design of the components stressed by the FBD and designed according to its capacity. Direct reference to the shear force transmitted by the connection is made, with a lower value V, corresponding to the dynamic shear force on which the connection stabilises after several cycles, and an upper $V+\Delta V$, corresponding to the maximum expected shear force. The forces arising in the connection are displayed in Figure 3.36 with reference to regular 4 bolted plates connected with two bolts to the panel side and the following geometrical parameters:

e: horizontal distance between bolts considering the maximum tolerance on the safe side

d: vertical distance between bolts

B: horizontal distance between vertical slots and panel

e_b: horizontal distance between connecting bolts and centre of mass of sliding surfaces

d_b: vertical distance between connecting bolts and panel

d_s: useful height of the connecting section

The rotational equilibrium of the plate, subjected to counter-acting shear forces distanced by e brings to inclined actions on the bolts. The vertical component is always equal to half the shear force, while the horizontal component depends on the polar moment of inertia of the connection. In the regular case with four bolts, this component is equal to the ratio between the moment and twice the vertical distance d. It is then possible to relate the axial load N acting in the bolt with the shear force V transmitted by friction. The following equation shows this relationship with reference to the static load threshold V_s:

$$V_s = N \frac{2\mu_s n k_s}{\sqrt{1+\frac{e^2}{d^2}}} \tag{3.1}$$

where μ_s is the static friction coefficient between brass and steel, that can be considered equal to 0,51, n is the number of sliding surfaces (standard connection has two sliding surfaces), k_s is a coefficient depending on the shape of the hole (for slots it can be assumed equal to 0,63 according to EN 1993-1-8:2005).

The mean dynamic slip load threshold can be obtained by substituting μ_d to μ_s, where μ_d is the dynamic friction coefficient between brass and steel, that can be considered equal to 0,44.

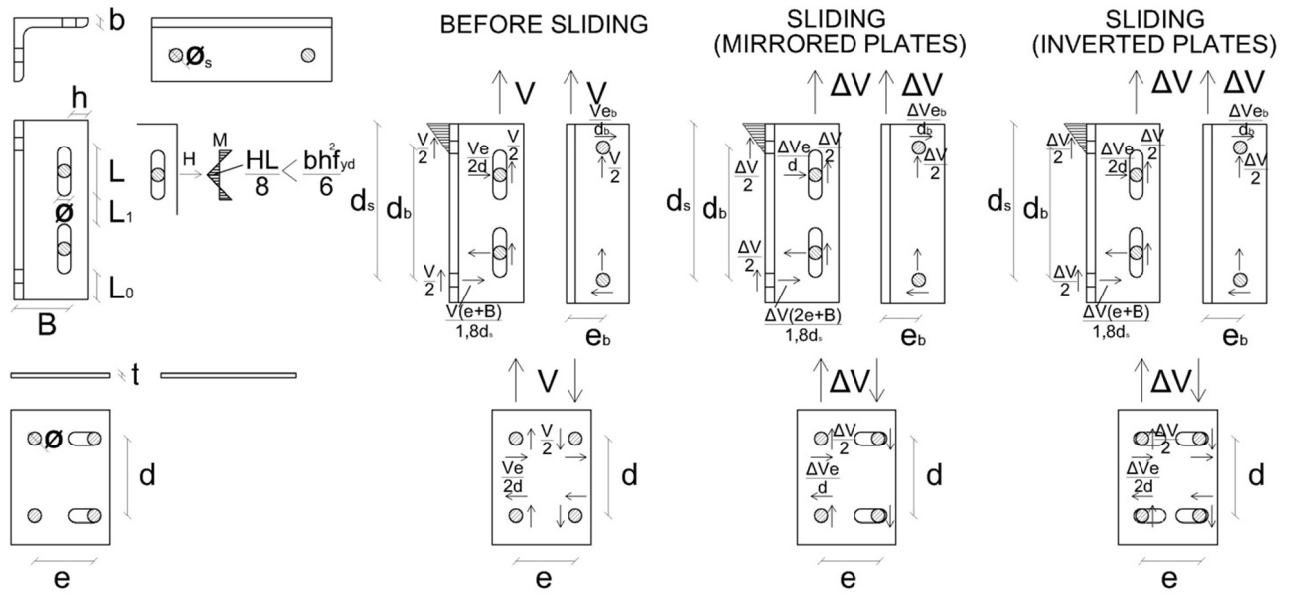

Figure 3.36 – Force distribution in the FBD

The lower bound dynamic slip load threshold can be obtained by considering the oligo-cyclic losses due to bolt shortening for abrasion of brass surface. Including thus a factor ϕ that can be considered on experimental base equal to 1,5 with the use of belleville washers and to 3,0 with the use of traditional washers and reversing the formulation, the design axial load N to be applied to a single bolt can be found as per the following equation:

$$N = \frac{V\phi}{2\mu_d n k_s}\sqrt{1+\frac{e^2}{d^2}} \tag{3.2}$$

The experimental campaign shows that loads larger than the static threshold can occur during motion, and therefore the upper bound load should be higher than this limit. Based on the experimental campaign, and on the safe side, the following equation is proposed in order to evaluate the maximum $V+\Delta V$ shear load that can occur during motion. Such value could be used for the design of other connections and members depending on the capacity of the FBD.

$$V+\Delta V = \rho N \frac{2\mu_d n k_s}{\sqrt{1+\frac{e^2}{d^2}}} \tag{3.3}$$

where the coefficient ρ indicates the accidental increase of load and can be taken equal to 1,6 on experimental base.

For a correct connection functioning, the bolts shall be able to slide through the slot without deformation of the latter, otherwise sudden force peaks or tangling (mechanical welding) can arise. Thus, the outer portion of the support profile in correspondence of the vertical slots shall be verified in order to be stiff and resistant enough. In the frequent case of a slender element, simple double-clamped beam equilibrium can be used considering the horizontal load H, as shown in Figure 3.36, depending also on the configuration of the plates (if mirrored, the additional shear component ΔV is taken only by one side of the support profile).

The resistance of the bolts subjected to contemporary shear and axial loading and the bearing resistance of the profile can be calculated on the base of traditional standards. In the case in which also the FPD-to-panel connection is bolted, the bolts are subjected to combined vertical shear and axial load if support profiles are symmetric, and to an additional torsional shear component if supports are asymmetric.

3.3. Multiple Slit Device (MSD)

Multiple Slit Devices are steel plates with slits of various shapes and sizes that allow to move the stiff shear behaviour of a compact square or rectangular plate to a flexural type, which is more suitable for energy dissipation. MSD have been developed as dissipative connections mainly within the field of structural steel seismic engineering, and can be considered as an evolution of the ADAS devices (Aiken *et al*. 1993, Soong & Spencer Jr 2002), in which several slender steel beams are linked together in a row and dissipate energy through plasticity, by means of juxtaposing the beams in a column instead of a row, by performing cuts in a steel plate. Several types of plate dissipating devices have been experimented by Chan *et al*., from buckling restrained plain (Chan & Albermani 2008) to constant section beams multiple slit (Chan *et al.* 2009) to perforated (Chan *et al.* 2013). Oh *et al.* (2009) carried out experimental testing on a full scale beam-to-column steel joint enhanced with a MSD. An analytical study on shape optimization of a multiple slit device carried out by Ghabraie et al. (2010) brought to the definition of an optimized hourglass-shaped beam device, that has also been tested and reported within the same work. Also Ma et al. (2010) devoted efforts to the design procedures and the experimentation of MSDs with different beam shapes, from constant to butterfly. Analytical tools for the design are also provided in Karavasilis *et al.* (2012). The concept of the device is shown in Figure 3.37, where a set of elementary beams are formed by making linear laser cuts. In such a way, the yield force and displacement of the device can be calibrated on the basis of the design need.

The aim of the work developed is mainly to traduce this type of connection to a proper use within precast concrete cladding panels, by reducing its dimensions with respect to what considered in the previously cited works and introducing large mounting tolerances to the device with the separation of the connection in multiple slit plate and support profile, then bolted together to get the final connection. This new way of assemblage of MSDs allows to introduce several technological improvements, among which the avoidance of axial induced stresses due to the axial elongation restraint thanks to the introduction of a slot and the possibility of combining a friction mechanism with the plastic (Biondini *et al.* 2014d, 2014e).

The conception of the specimens illustrated in the following is based on the trial to avoid a depth vs width ratio of the single beam higher than four, in order to farther the risk of flexural-torsional buckling, that occurred in most of the previously tested specimens, due to their dimensions. Large drifts can be achieved with large profiles also by forming multiple column beams, with the possibility to fulfil the avoidance of lateral buckling, since the thickness of the plate shall be handled by the laser cutter. Furthermore, the size effect can increase the ductility of smaller beams, since to equal imposed curvatures correspond lower maximum strains.

Figure 3.38 shows the functioning scheme of the connection under imposed vertical displacement. The horizontal tolerances can be provided by horizontal slots cut on the plate, while vertical tolerances can be obtained by the support profile, in which vertical slots can be cut. Device-to-panel connecting bolts shall be strongly tightened in order to avoid vertical slippage. In addition to the support profiles shown in Figure 3.6, also UPN symmetric profiles have been considered for the tests on the MSD specimens with horizontal slots. Both UPN flanges are provided with threaded holes for the direct application of the bolt from the external side with one plate only.

Figure 3.37 – Multiple slit connection devices

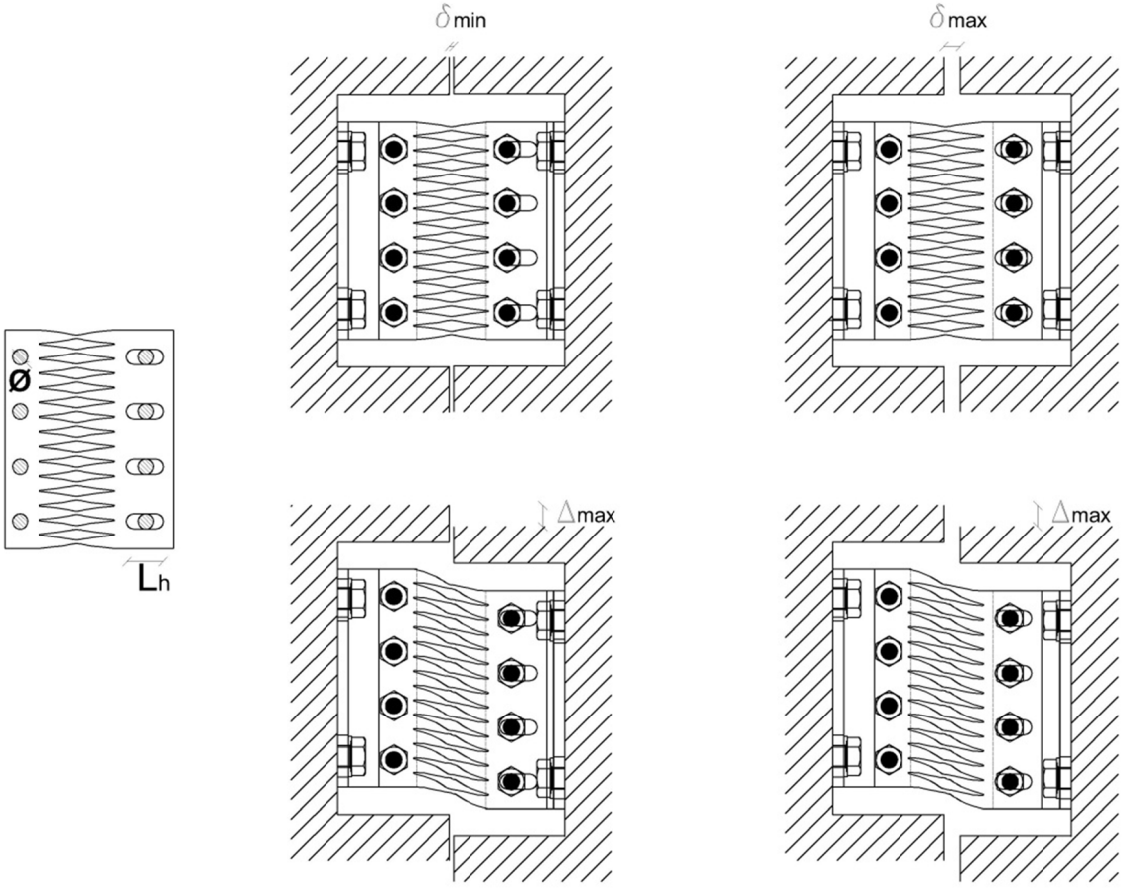

Figure 3.38 – Functioning scheme of the MSD

3.3.1. Test programme

Figure 3.39 shows the device shapes that have been constructed and tested under imposed lateral displacements. The need of maximizing the area of steel that had to yield brought to devices with not more than two columns of slender beams. Also hourglass shapes, based on the optimization of the beam profile, have been tested. Such profiles are conceived in such a way that all beam sections can yield at the same time under an imposed lateral displacement, following therefore a height lowering which is proportional to the square root of the length, except for the very central portion, that cannot undergo a certain minimum height. The yield and ultimate force are therefore not expected to be lowered with respect to a straight beam having the same base height, while its flexibility gets improved, as previously shown. When undergoing large deformation, a second order axial component may arise, decreasing ductility. Thus, also plates provided with horizontal slots have been tested, granting also the needed horizontal mounting tolerance. All the plates have been designed in order to achieve a similar resistance. All plates are made with steel grade S235, except that with hourglass shape and horizontal slots, which is made with a steel grade S355.

The complete list of the performed tests is reported in Table 3-5, for a total of 16.

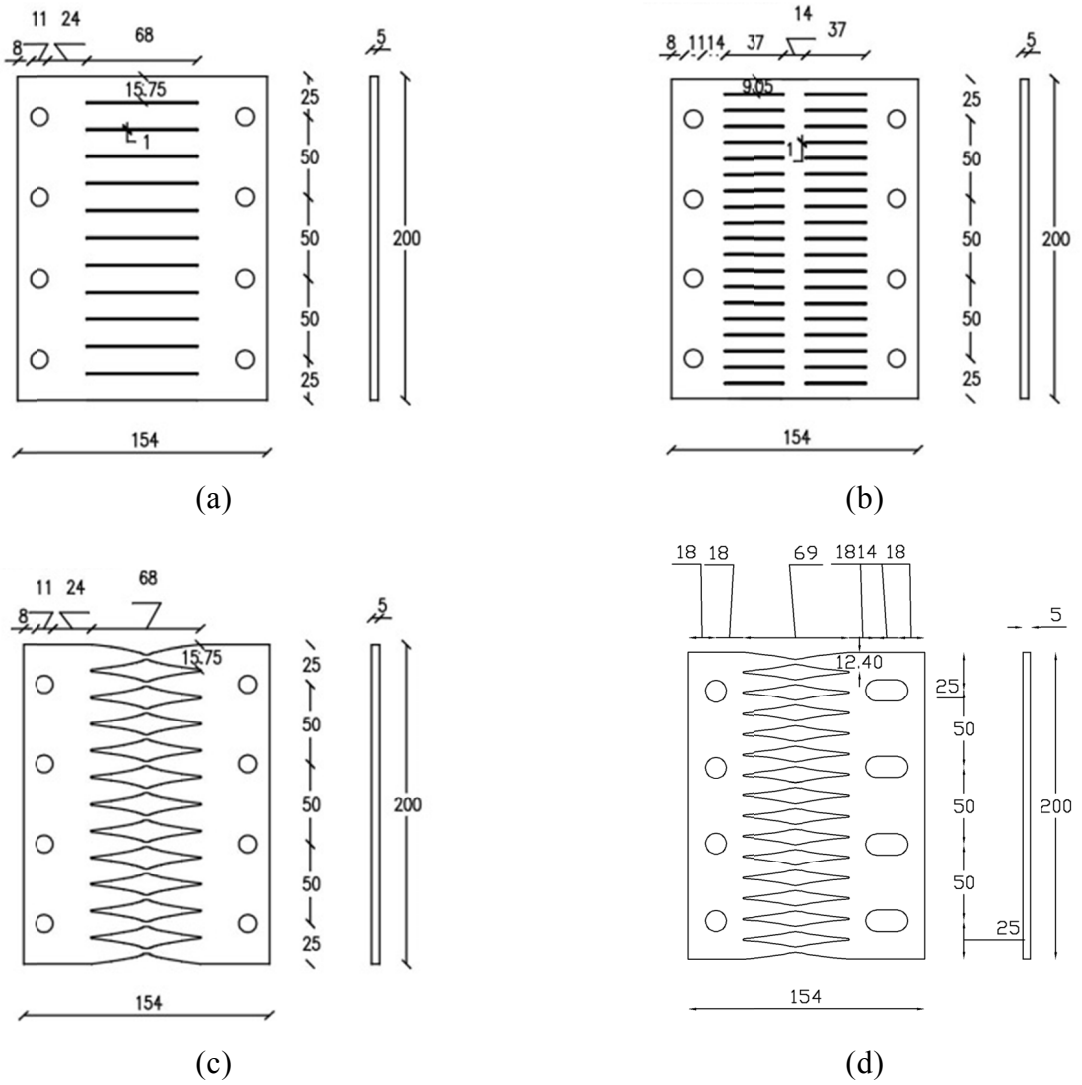

Figure 3.39 – Multiple slit connection devices tested devices: (a) single column, (b) double column, (c) hourglass, (d) hourglass with horizontal slots

Table 3-2 – Performed cyclic tests on multiple slits devices

DEVICE		TEST TYPE	CYCLIC LOAD PROTOCOL	BOLT CLASS	TEST SPEED
MSD	1 COLUMN	CYCLIC	A	8.8	2mm/s
				12.9	2mm/s
			D	12.9	2mm/s
		PUSHOVER	-	12.9	0,25 mm/s
	2 COLUMNS	CYCLIC	A	8.8	2mm/s
				12.9	2mm/s
			D	12.9	2mm/s
		PUSHOVER	-	12.9	0,25 mm/s
	HOURGLASS	CYCLIC	A	8.8	2mm/s
				12.9	2mm/s
			A	12.9	2mm/s
		PUSHOVER	-	12.9	0,25 mm/s
	HOURGLASS WITH SLOTS	CYCLIC	A	10.9	2mm/s
			D	10.9	2mm/s
		PUSHOVER	-	10.9	0,25 mm/s
MSD+FBD		CYCLIC	B	10.9	2mm/s

3.3.2. Monotonic behaviour

Monotonic tests have been carried out on the four different typologies of Multiple Slit Device. Figure 3.40 shows the devices before the test and under the maximum imposed drift. The specimens with constant height beams are subjected to a large plastic deformation at the edges and an almost rigid rotation of the central portion. A large diffused plasticity is observed on the contrary within the hourglass-shaped specimens, providing a better exploitation of the device.

The results are collected in Figure 3.41. The curves show that the response is initially very stiff, with stiffness depending on the profile for very low displacement, after which all curves show a linear branch with an average stiffness of about 12 kN/mm, with a smooth stiffness softening up to a final hardening branch with an average stiffness of about 1,4 kN/mm. Stiffness softening started for all specimens at around 5~6 mm of drift, which corresponds to 7,4~8,8% of ratio with respect to the length of the elementary beam (doubled for the 2-columns specimen). All specimens show a very large residual plastic deformation after the test, as noticeable from Figure 3.42. The specimens with constant height beam show that a plastic deformation of the plate around the corner holes occurred, due to the combination of a vertical reactions due to shear and a radius-wise inclined reaction due to rotational equilibrium. The resulting component is inclined, as clearly shown by the hole deformation.

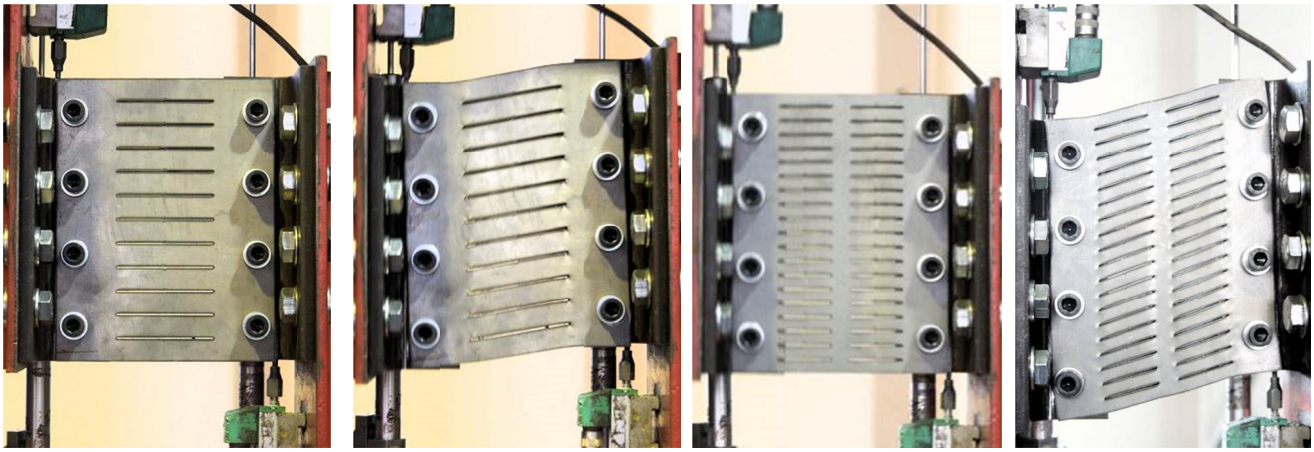

(a) (b) (c) (d)

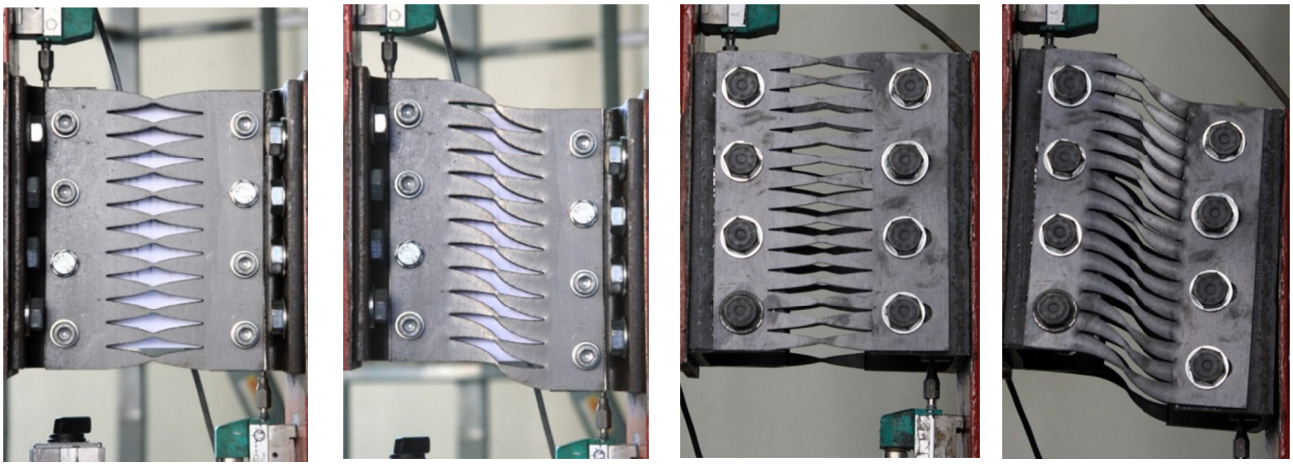

(e) (f) (g) (h)

Figure 3.40 – MSDs under monotonic test from undeformed to maximum drift: (a-b) single column, (c-d) double column, (e-f) hourglass and (g-h) hourglass with horizontal slots

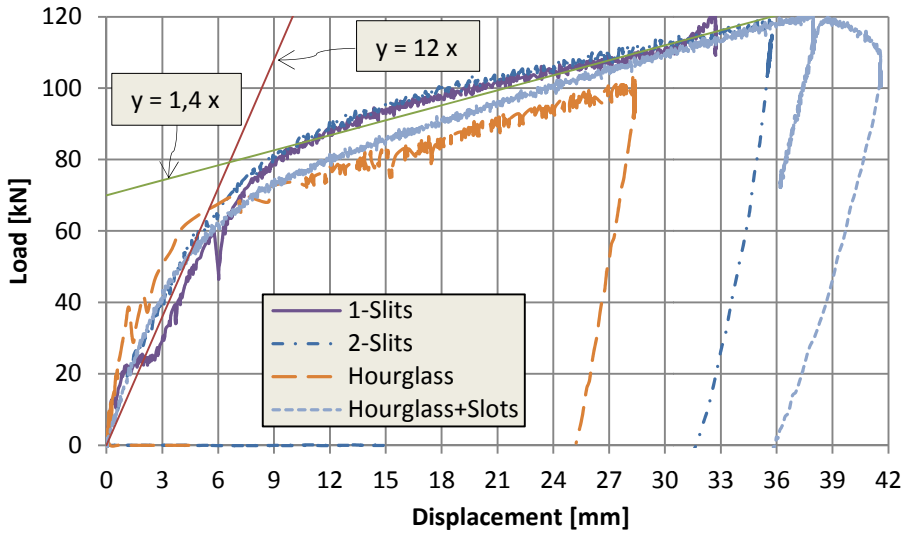

Figure 3.41 – Pushover test results for all specimens

(a) (b) (c) (d)

Figure 3.42 – MSDs under monotonic test residual plastic deformation: (a) single column, (b) double column, (c) hourglass and (d) hourglass with horizontal slots

3.3.3. Low displacement cyclic behaviour

Cyclic tests with low displacement cyclic protocol A have been carried out in order to investigate the device behaviour and its stability under low displacement, which is also useful for serviceability horizontal loads (e.g. wind loads). All specimens show a large reliability for low displacement range (within approximately 10% of drift).

The results of the test performed on the constant height beam devices are shown in Figure 3.43 with the relative energy dissipation property diagrams in Figure 3.44 for the single column device and in Figure 3.45 with the relative energy dissipation property diagrams in Figure 3.46 for the specimen with double columns.

Regarding the single column device, an initial elastic stiffness of about 27 kN/mm could be deduced, with an yielding load of about 33 kN occurred at about 1,2 mm. After yielding, a hardening branch is observed, with a smooth stiffness softening starting at around 6 mm of drift. The specific energy in comparison with perfect rigid-plastic equivalent systems leads to values floating between 0,22 and 0,30.

The test on the double columns device shows an initial elastic stiffness of about 32 kN/mm, with an yielding load of about 20 kN occurred at about 0,8 mm. After yielding, a hardening branch is observed, with a smooth stiffness softening starting at around 5 mm of drift. The specific energy in comparison with perfect rigid-plastic equivalent systems leads to values floating between 0,25 and 0,35.

On both specimen results, a pinching effect is observed, affecting energy dissipation, probably due to small rigid rotations of the plates occurred because of standard bolt-hole tolerance of one millimetre enlarged by plastic local deformation.

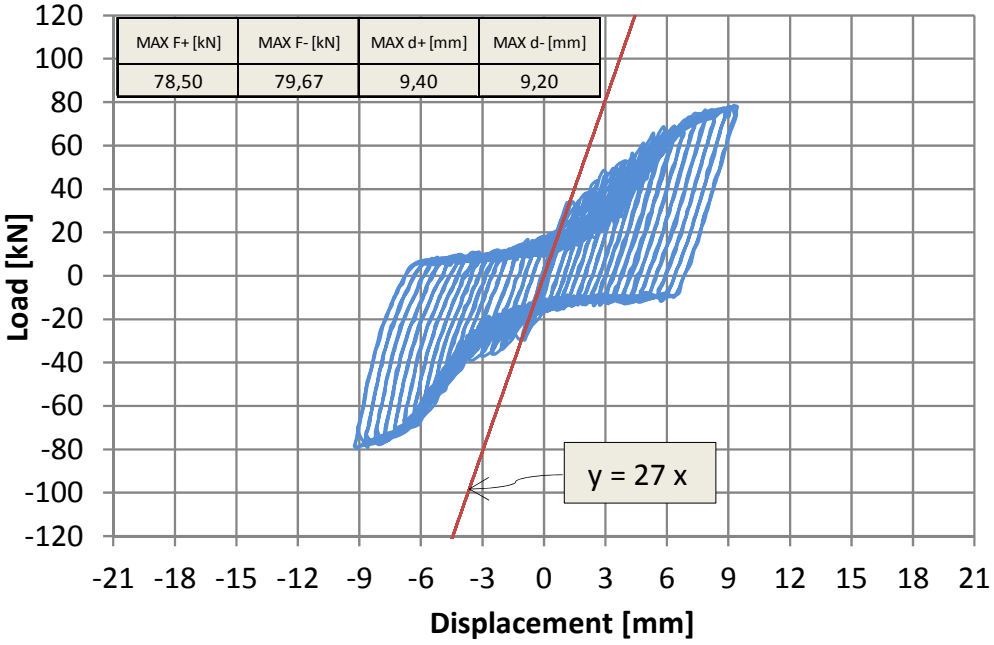

Figure 3.43 – Single column device: load vs displacement

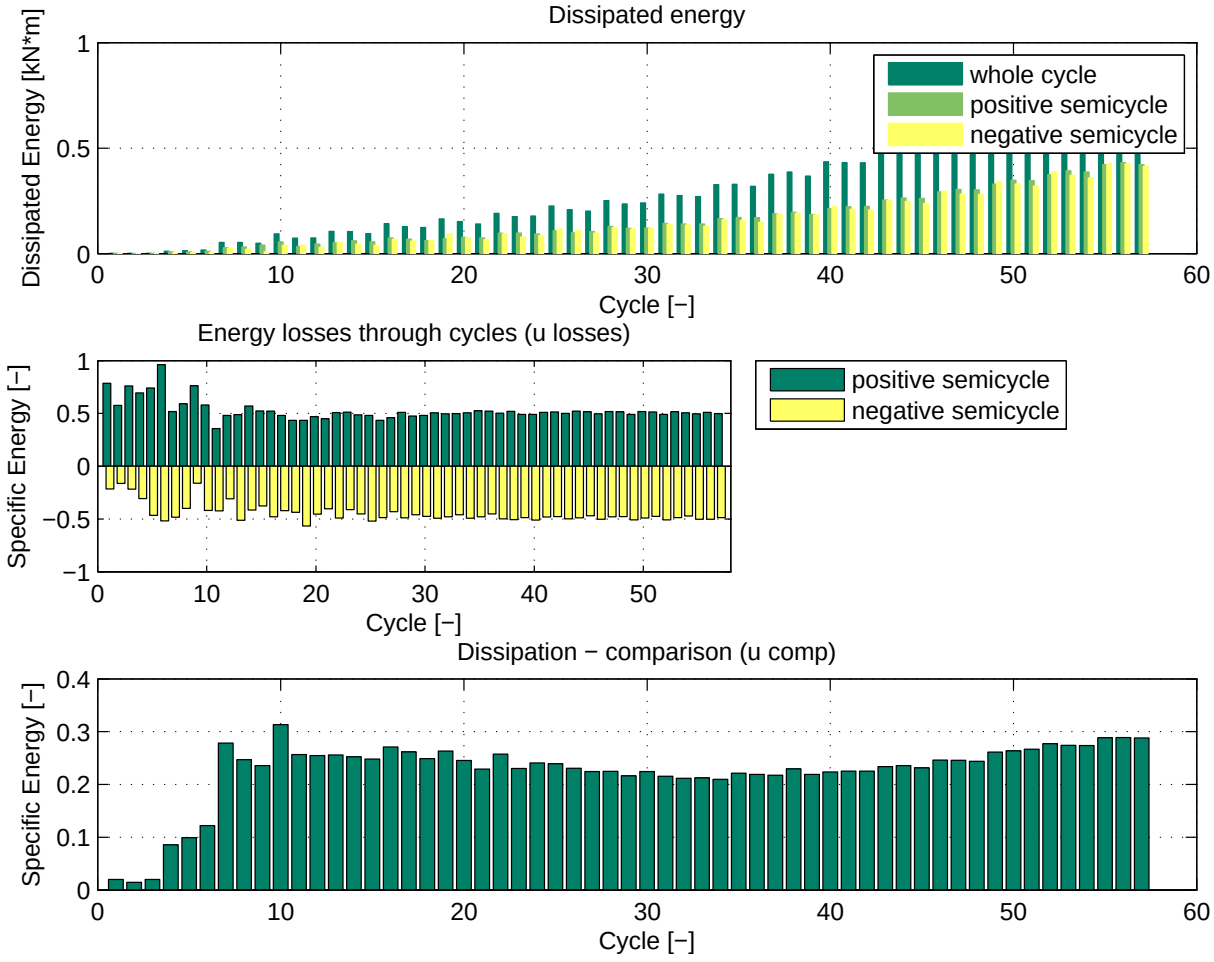

Figure 3.44 – Single column device: energy dissipation properties

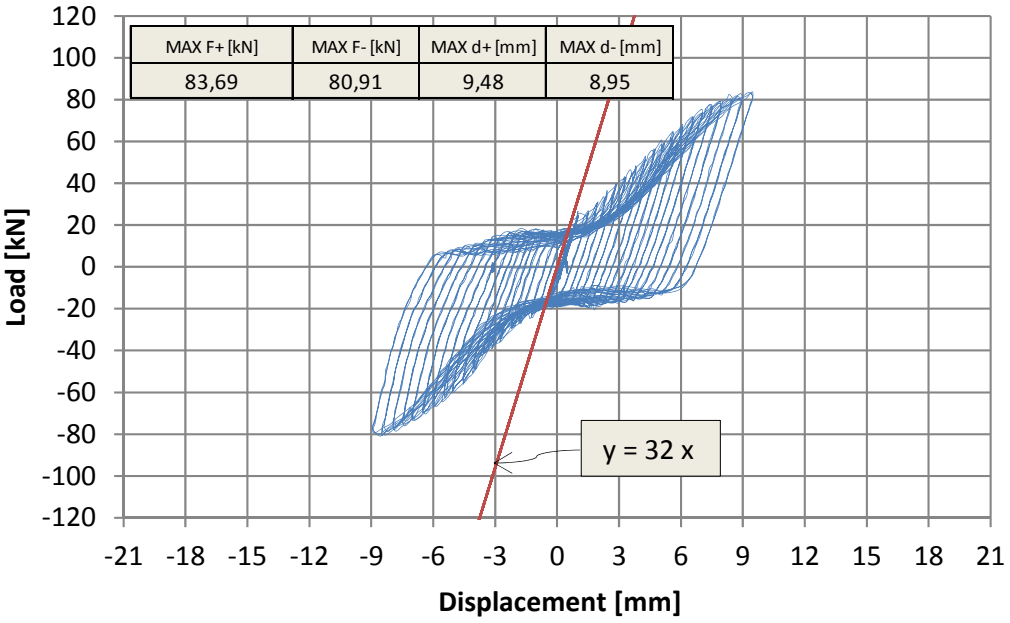

Figure 3.45 – Double column device: load vs displacement

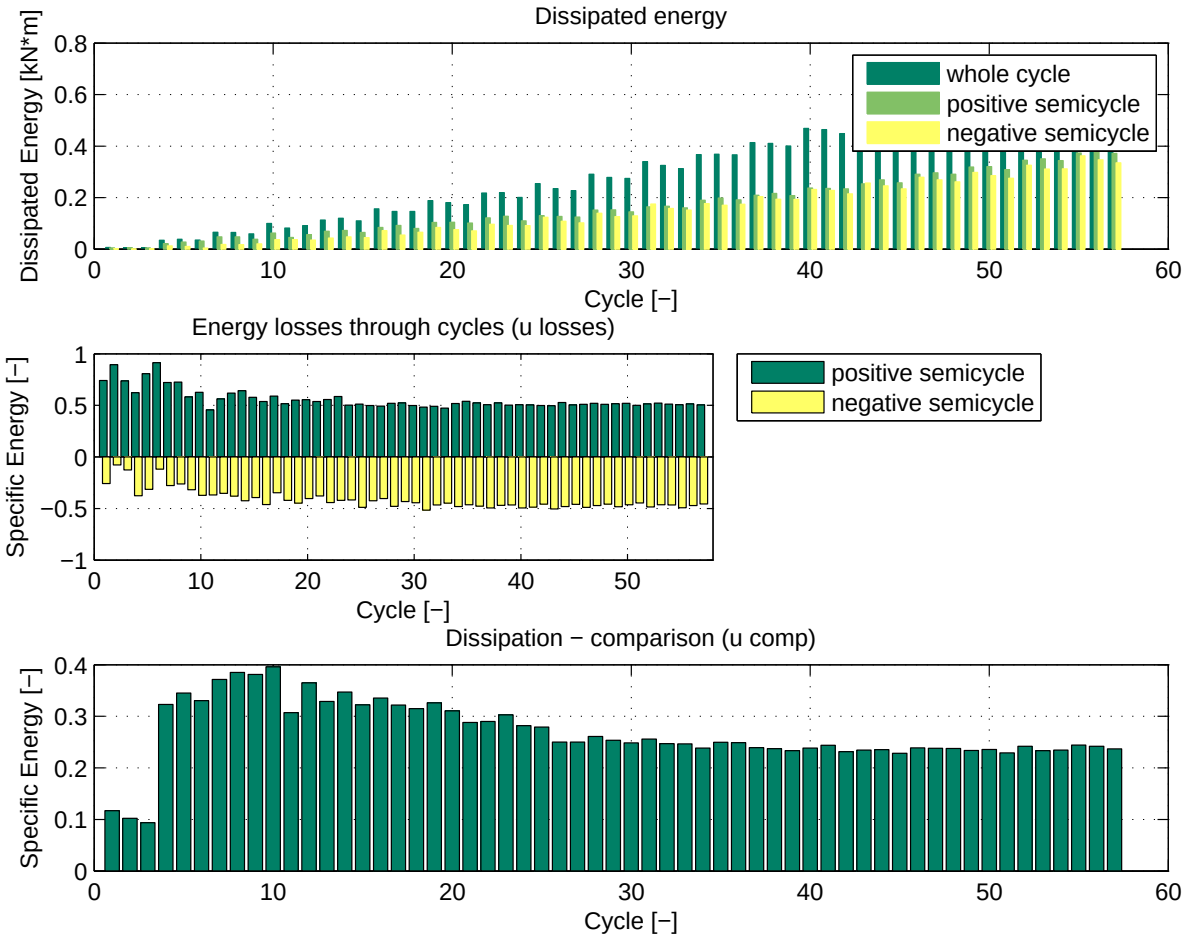

Figure 3.46 – Double column device: energy dissipation properties

The results of the test performed on the hourglass-shaped beam devices are shown in Figure 3.47 for the single column device with the relative energy dissipation property diagrams in Figure 3.48 and in Figure 3.49 with the relative energy dissipation property diagrams in Figure 3.50 for the specimen with double columns. The tests have been performed according to protocol A, after which enlarged displacement amplitudes at 1 mm step cycled three times have been performed up to failure.

Regarding the hourglass-shaped device, an initial elastic stiffness of about 28 kN/mm could be deduced, with an yielding load of about 25 kN occurred at about 1,0 mm. After yielding, a hardening branch is observed, with a smooth stiffness softening starting at around 5 mm of drift. Failure has been attained with rupture of the central portion of the beams, at a section of about 2 mm from midspan, that started at the last semi-cycle with displacement amplitude of 10 mm. The specific energy in comparison with perfect rigid-plastic equivalent systems leads to values floating between 0,30 and 0,50.

The test on the hourglass-shaped device with horizontal slots shows a lower initial elastic stiffness of about 25 kN/mm, with an yielding load of about 30 kN occurred at about 1,2 mm. After yielding, a hardening branch is observed, with a smooth stiffness softening starting at around 6 mm of drift. Failure has been obtained with rupture of the beam edges that started at 16 mm displacement cycles. The specific energy in comparison with perfect rigid-plastic equivalent systems leads to values floating between 0,15 and 0,30.

Pinching is less pronounced on hourglass-shaped devices, providing a better dissipation of energy. Figure 3.51 shows the specimens after the tests. Hourglass-shaped devices are broken, since they have been taken to a larger drift with respect to constant section beam profiles.

A small enlargement in the elementary beam midspan depth over the edge depth, fro 5,2 (hourglass) to 5,0 (hourglass with horizontal slots) moves the failure from midspan to the edge, showing that the otimised ratio is in between those values. Failure of the edge is suggested to be adopted in the design, since it is associated with the maximum attainable displacement.

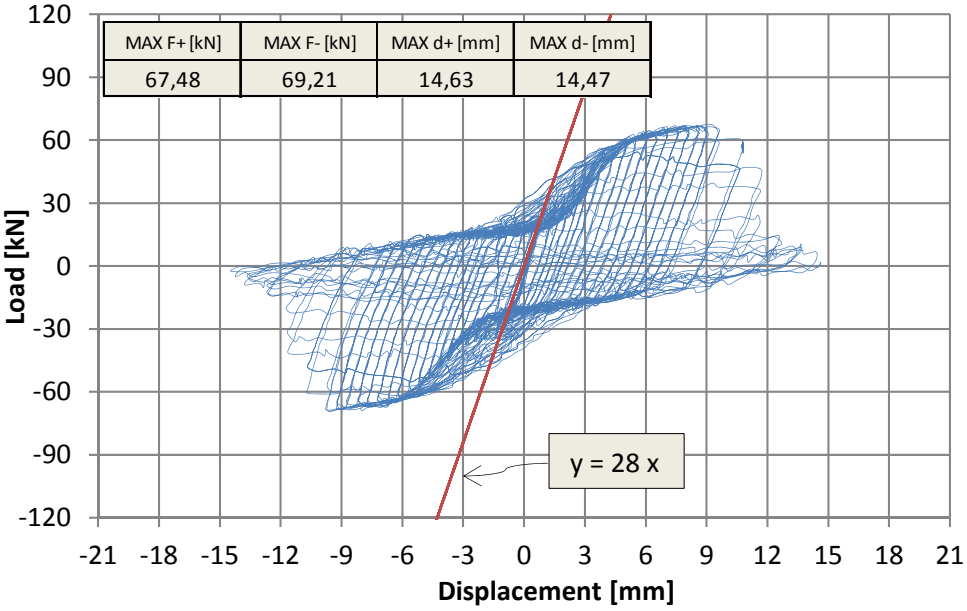

Figure 3.47 – Hourglass device: load vs displacement

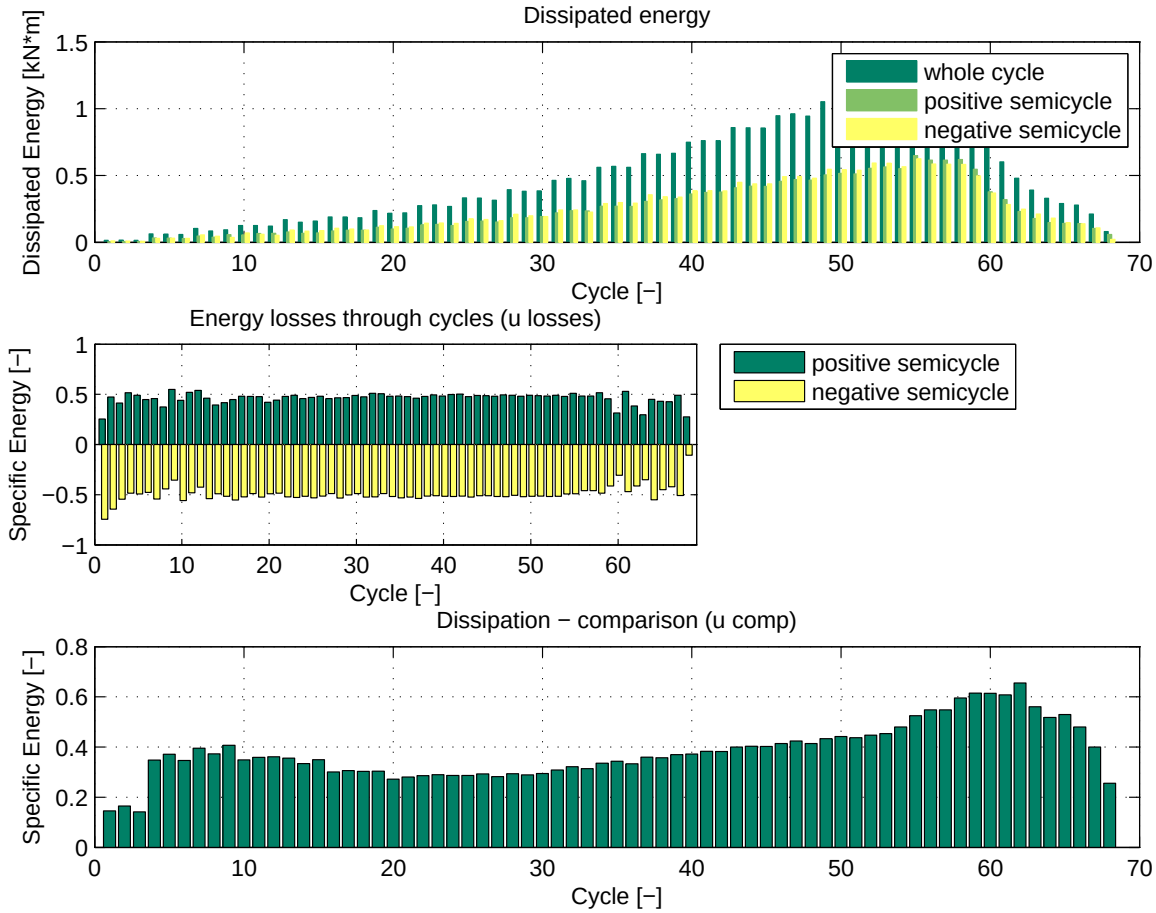

Figure 3.48 – Hourglass device: energy dissipation properties

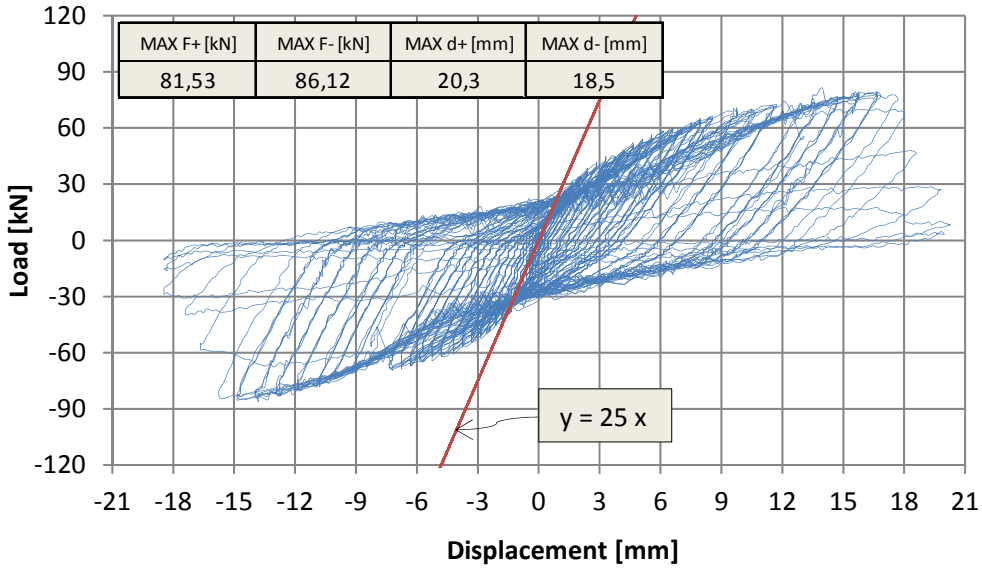

Figure 3.49 – Hourglass device with horizontal slots: load vs displacement

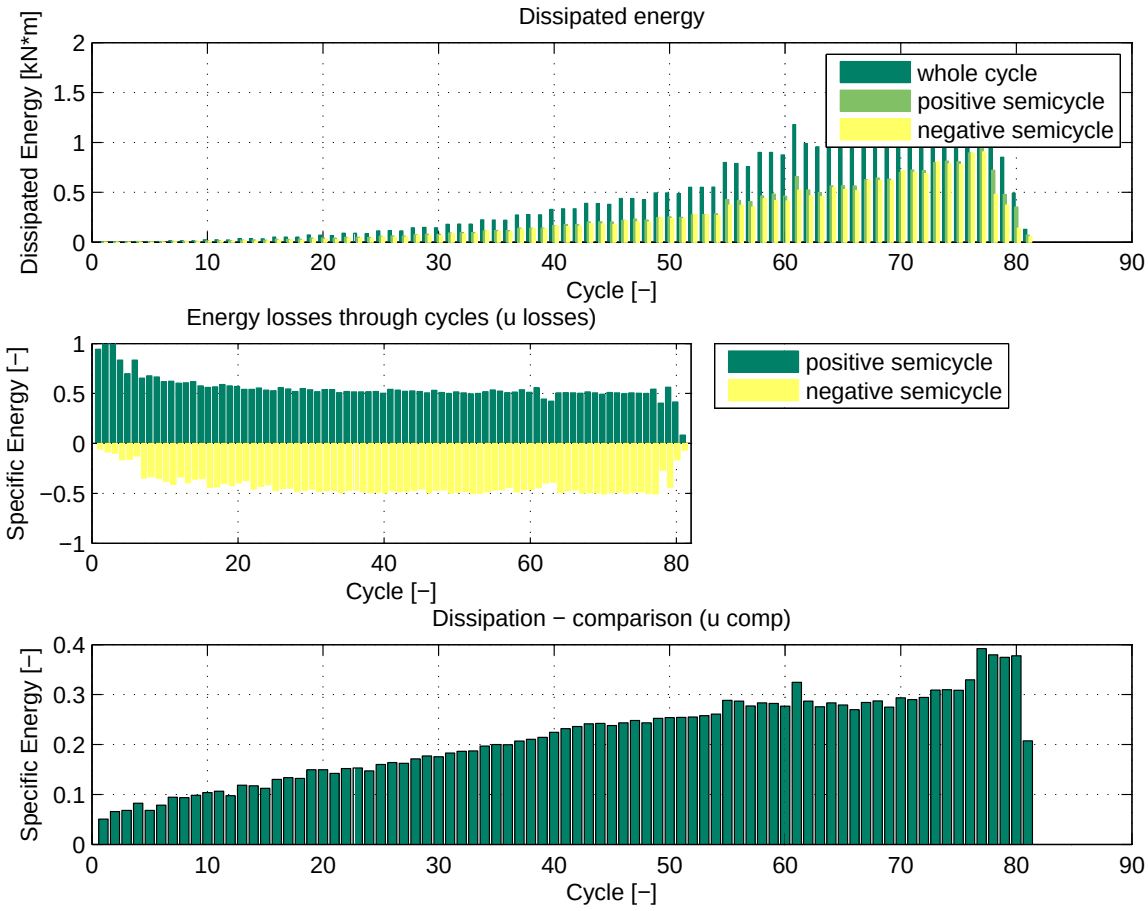

Figure 3.50 – Hourglass device with horizontal slots: energy dissipation properties

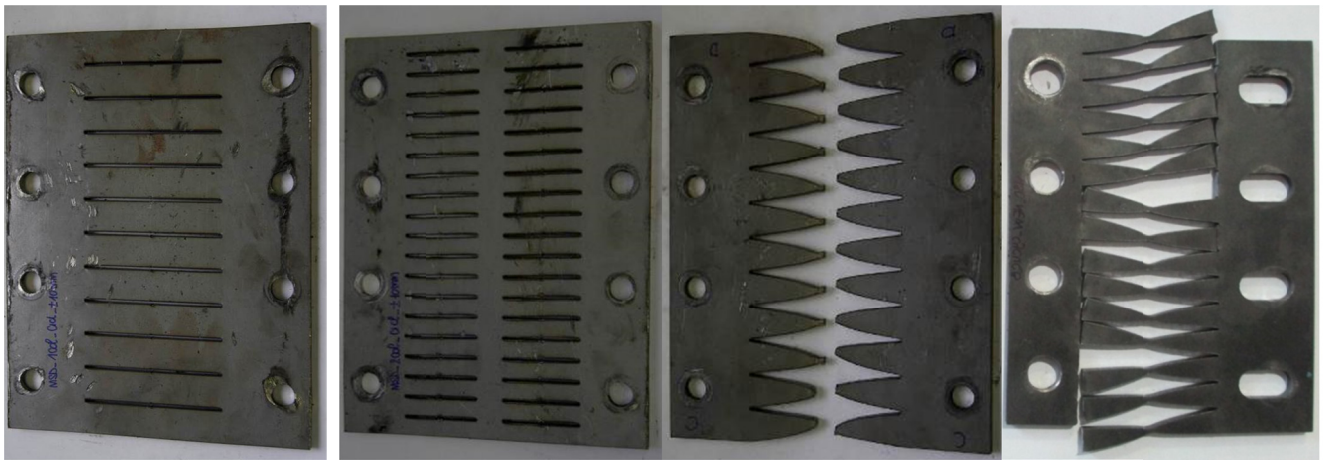

(a) (b) (c) (d)

Figure 3.51 – MSDs after low displacement cyclic test: (a) single column, (b) double column, (c) hourglass and (d) hourglass with horizontal slots

3.3.4. Oligo-cyclic behaviour for large displacements

Cyclic tests with large displacement amplitude cycled ten times (protocol D) have been carried out in order to investigate the oligo-cyclic stability of the specimens. The results show that the specimens suffer from oligo-cyclic fatigue at large displacements, since failure or strong resistance loss have been attained after few cycles for all device shapes. A picture showing the failure mode of each device is reported in Figure 3.52.

The results are shown in Figure 3.53 for the single column device, in Figure 3.55 for the specimen with double columns and in Figure 3.57 for the specimen with hourglass-shaped beams and horizontal slots. Regarding the single column device, the monotonic behaviour confirms what previously observed, showing that failure starts and rapidly develops at the third cycle. Flexural failure occurs at the edge sections of each beam. The specific energy in comparison with perfect rigid-plastic equivalent systems leads to values of about 0,40 before failure (Figure 3.54). The test on the double columns device also provides confirmation of the previously observed monotonic behaviour, though showing a progressive resistance loss that started at the fourth cycle. Flexural failure occurs at the edge section of each beam. The specific energy in comparison with perfect rigid-plastic equivalent systems leads to values of about 0,35 before failure (Figure 3.56). On both constant height beam specimens the pinching effect is confirmed.

The test on the hourglass-shaped device with horizontal slots, which results are shown in Figure 3.57 provides a much better cyclic shape, practically without any pinching, at the first cycles, though showing a rapid failure development that started at the third cycle. The specific energy in comparison with perfect rigid-plastic equivalent systems is improved with respect to the other MSDs up to values of about 0,55 before failure (Figure 3.58). For this specimen, too, flexural failure occurs at the edge sections of each beam, though involving the whole length of the beam in large plastic hysteresis, as pointed out by the large plastic residual deformation noticeable along the whole length of the beams.

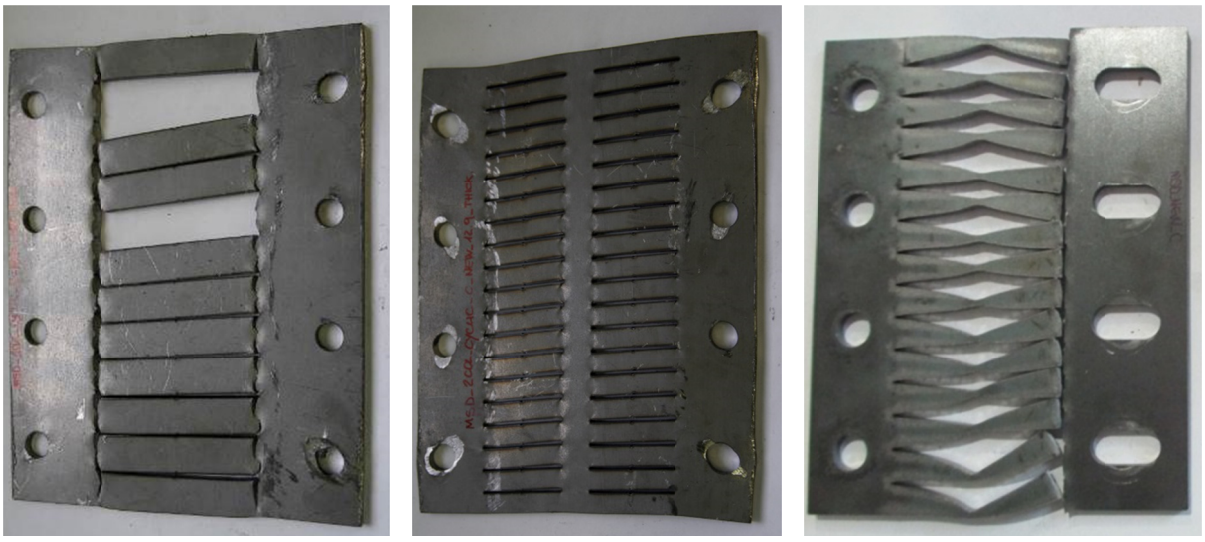

(a) (b) (c)

Figure 3.52 – Failure mode for three different MSDs: (a) single column, (b) double column and (c) hourglass with horizontal slots

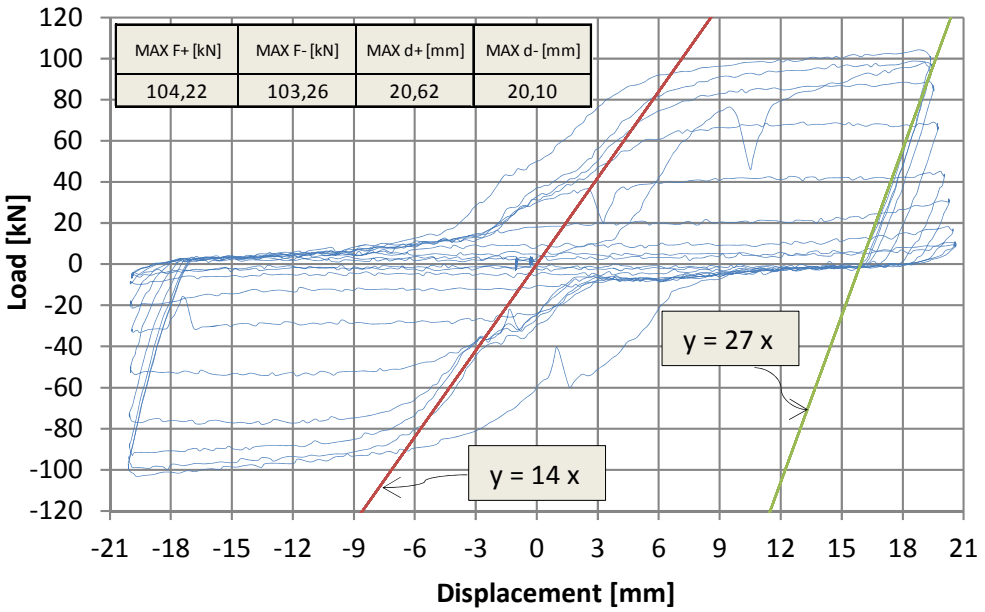

Figure 3.53 – Single column device: load vs displacement

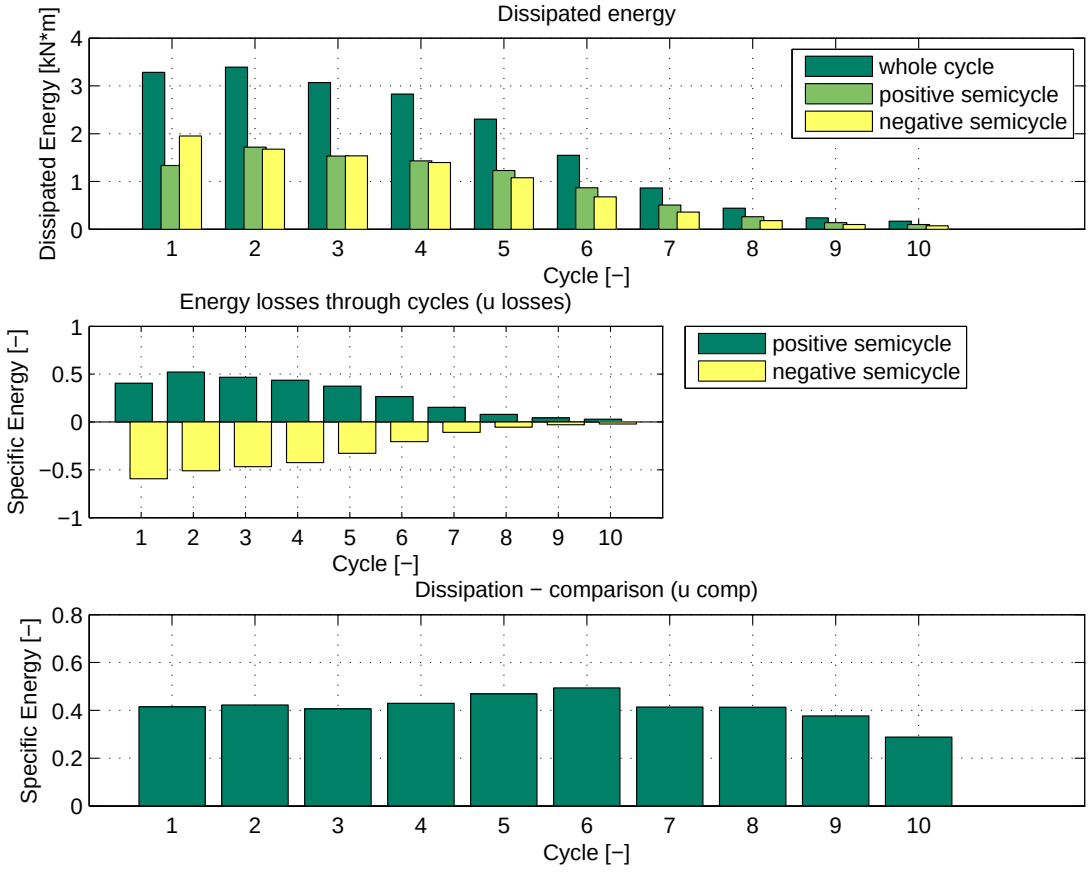

Figure 3.54 – Single column device: energy dissipation properties

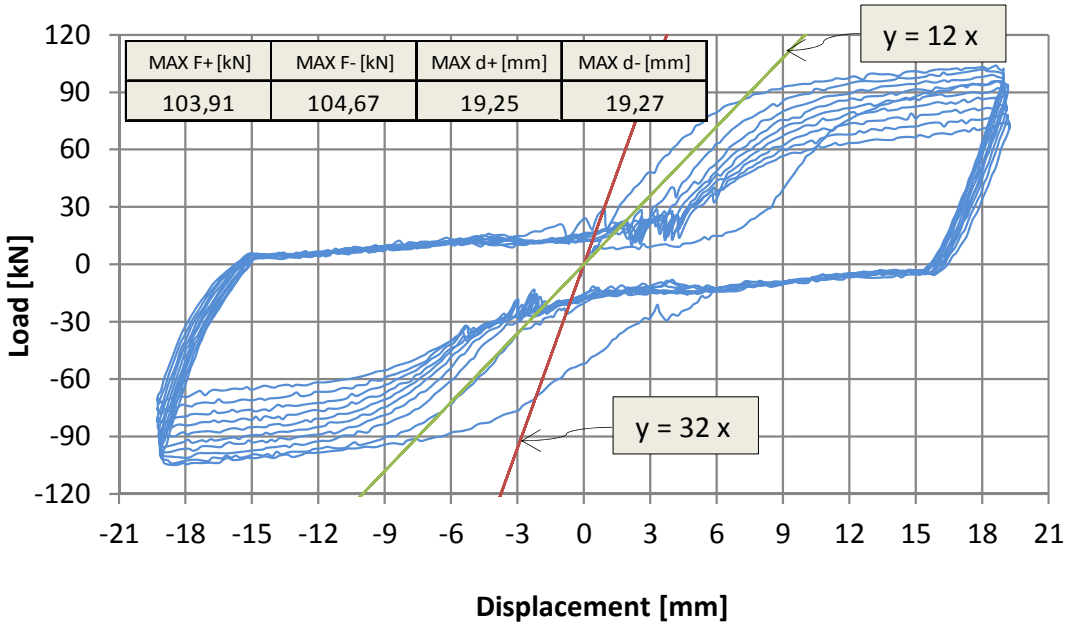

Figure 3.55 – Double column device: load vs displacement

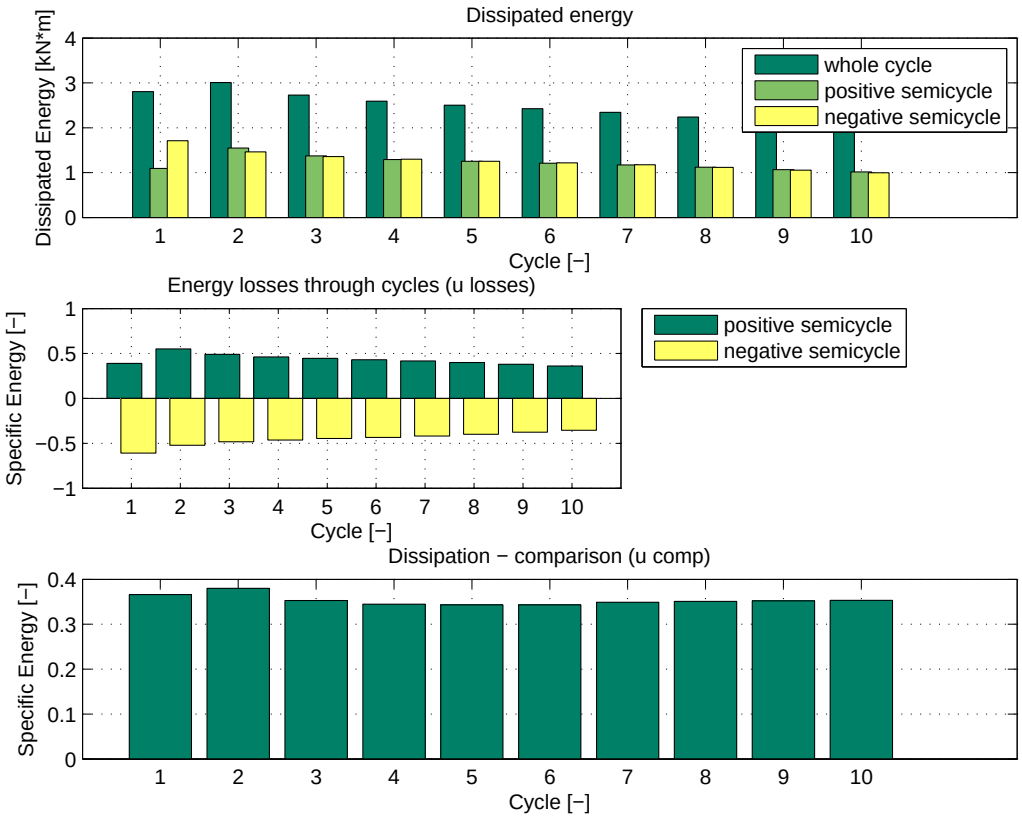

Figure 3.56 – Double column device: energy dissipation properties

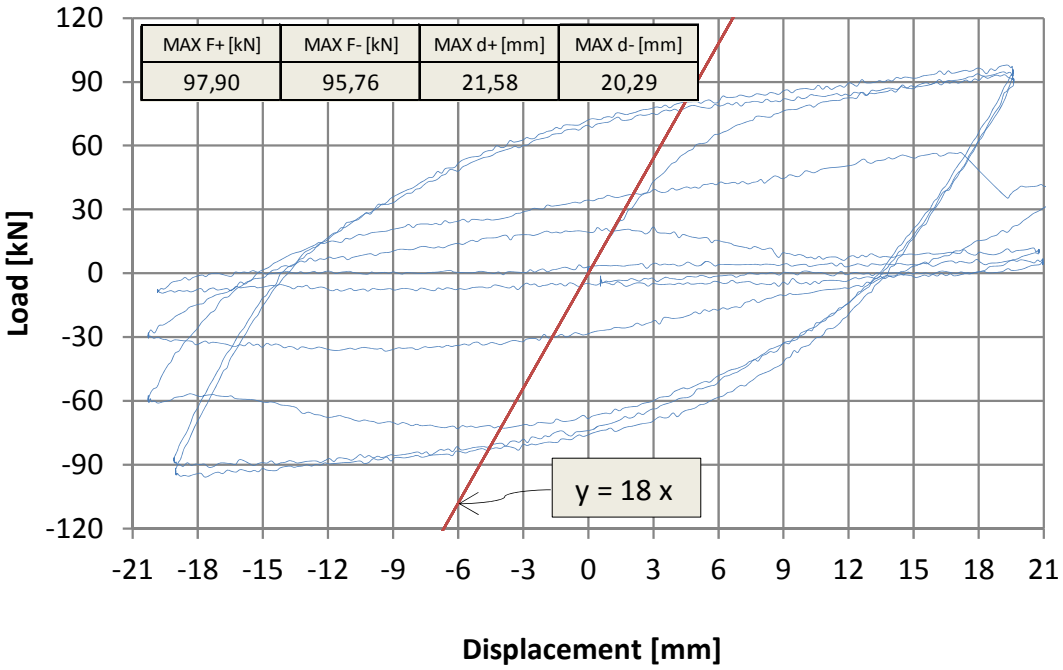

Figure 3.57 – Hourglass device with horizontal slots: load vs displacement

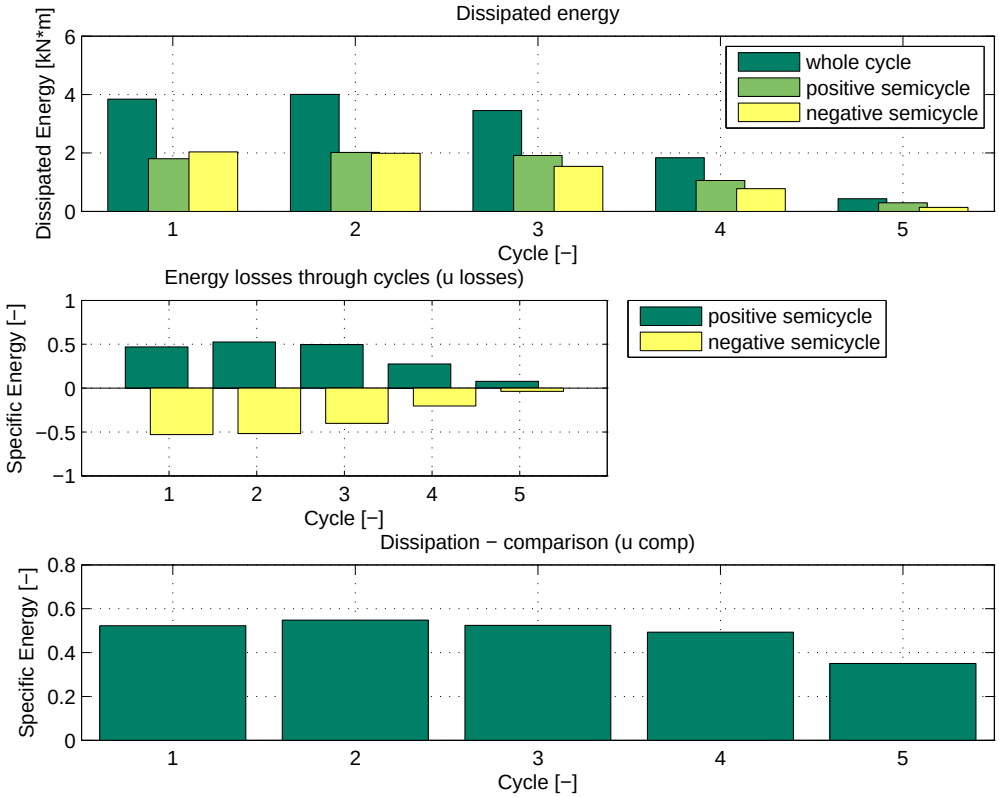

Figure 3.58 – Hourglass device with horizontal slots: energy dissipation properties

3.3.5. Combined MSD and FBD

A comparison between MSD and FBD shows that the first has a softer initial branch, with a well-defined and smooth hardening branch, an ultimate drift that depends on several geometric parameters, the most important of which is the length of the beams, and an ultimate load which corresponds to the breaking of the beams, while the latter has a step-wise sudden activation, an ultimate drift that depends only on the length of the vertical slots (therefore in theory without limitations) and an ultimate load that increases without control due to the attainment of the end of the slots.

The design of a FBD with MSD cover plates could be calibrated in order to have a smooth and flexible elastic branch, due to the functioning of the MSD, and to largely increase its drift by designing a slip load threshold after the MSD yield load and the load at start of the unstable branch. Pushing further the device, it works according to a FBD mechanism, and once the maximum slip is reached, the device turns again into a MSD, allowing a controlled rupture. Figure 3.59b illustrates the theoretical behaviour.

A single pilot test with protocol B has been carried out on a specimen mounted on UPN support profiles provided with net 2 cm long vertical slots (Figure 3.59a) on which two hourglass MSD with horizontal slots have been screwed with internal hollowed square brass sheets and external belleville washers. Each of the 16 M14 8.8 bolts per side have been tightened at 100 Nm, in order to obtain the same total axial load of the regular FBD (provided with 4 M14 acting on two sides). The results are displayed in Figure 3.60. The combination of friction and plastic mechanisms brought to a large dissipation of energy, with an initial smooth branch depending only on the MSD properties and a final controlled failure of the MSD that occurred at a much larger displacement with respect to what attained by the MSD alone, increased by the friction slide. The energy dissipation properties of the connection are reported in Figure 3.61, showing a specific energy in comparison with a perfect rigid-plastic equivalent system, increasing from 0,20 to 0,40 from low displacement cycles to larger. Figure 3.62 shows the components after the test, from which it can be observed that failure had occurred at the edge sections of the beams. The hollowed square brass sheets show that strong abrasion has occurred.

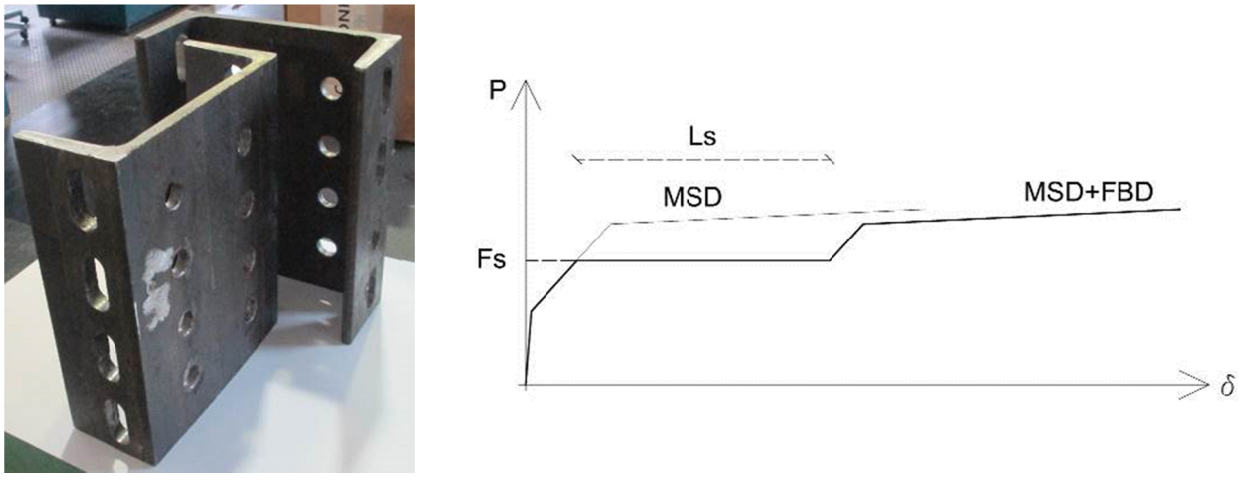

(a) (b)

Figure 3.59 – Combined MSD and FBD: (a) support UPN profiles with net 2 cm vertical millings and (b) theoretical monotonic behaviour

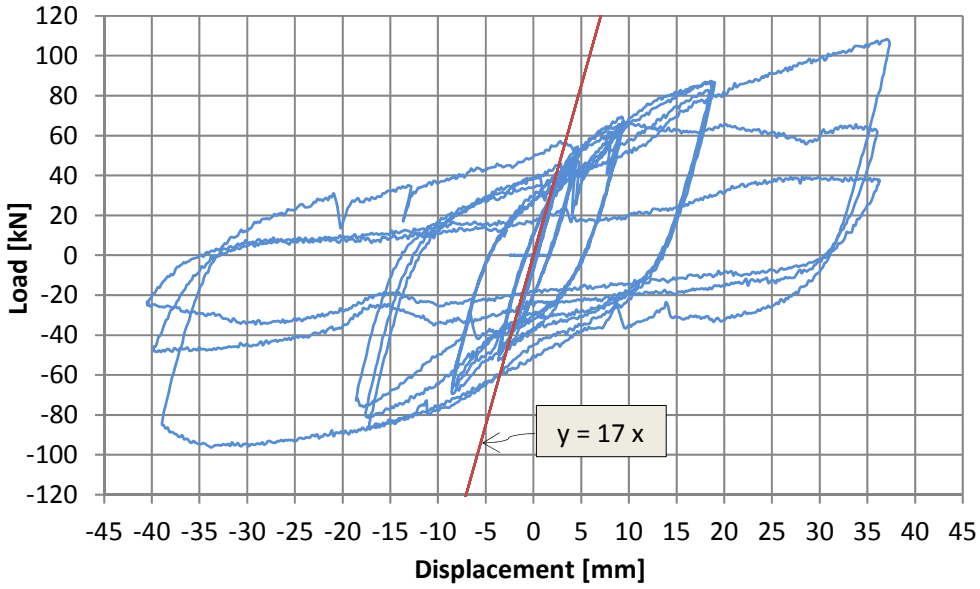

Figure 3.60 – Combined FBD and hourglass with horizontal slots MSD device: load vs displacement

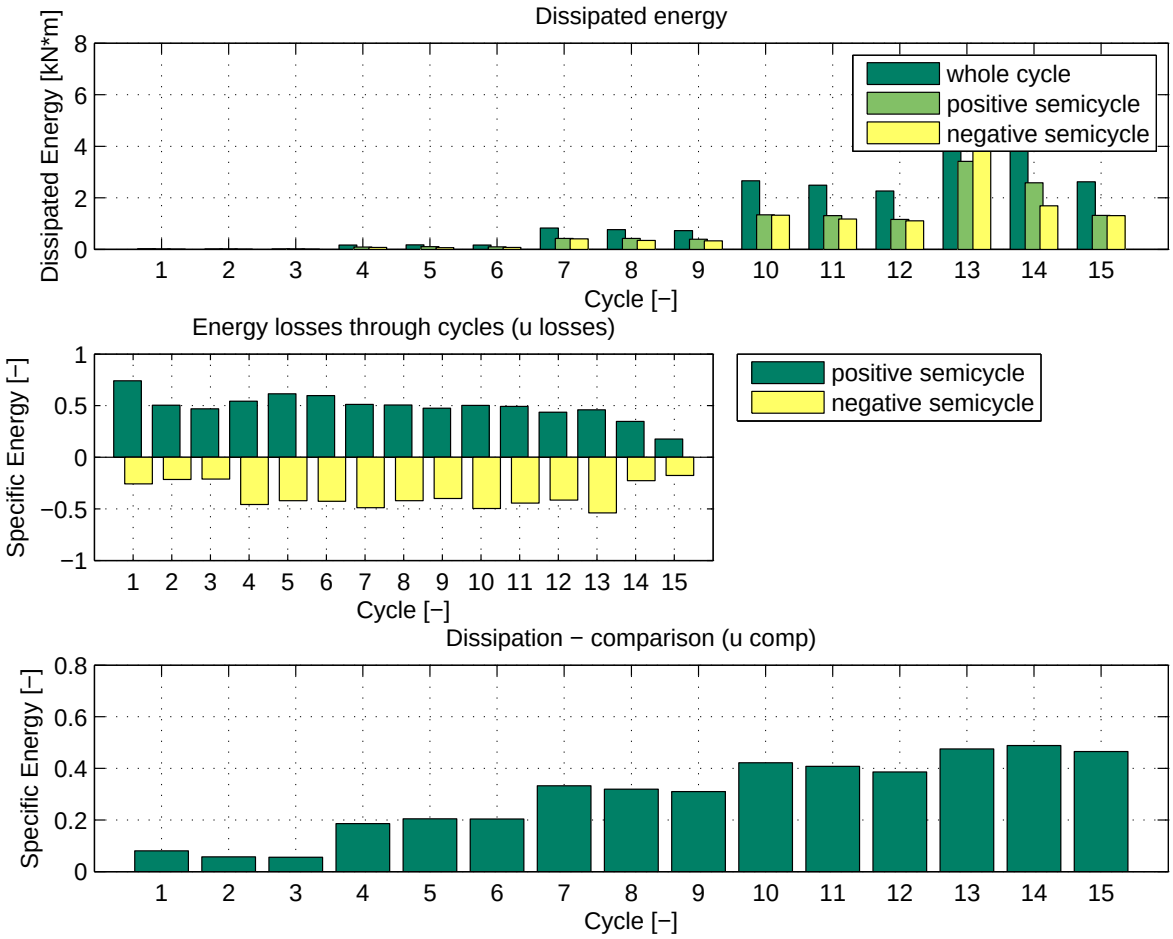

Figure 3.61 – Combined FBD and hourglass with horizontal slots MSD device: energy dissipation properties

Figure 3.62 – Components after the test

3.3.6. Design recommendations

A simplified procedure for the design of MSDs is described in the following with reference to Figure 3.63. Starting from the analysis of a single elementary beam, that can be considered double clamped, an imposed vertical displacement causes the rotational and translational reactions shown in Figure 3.64. If the beam has a constant rectangular cross section, a unitary moment and a unitary shear load as per the following equations arise if considering a Timoshenko beam:

$$k_m = 6\frac{EI}{L^2}\left(\frac{1}{1+\frac{6\chi EI}{L^2GA}}\right) = \frac{Ebh^3}{2L^2}\left(\frac{1}{1+\frac{\chi Eh^2}{2L^2G}}\right) \quad \text{for constant height profile} \quad (3.4)$$

$$k_v = 12\frac{EI}{L^3}\left(\frac{1}{1+\frac{12\chi EI}{L^2GA}}\right) = \frac{Ebh^3}{L^3}\left(\frac{1}{1+\frac{\chi Eh^2}{L^2G}}\right) \quad \text{for constant height profile} \quad (3.5)$$

While, if the beam has a hourglass shape, with a mid-span height equal to a fifth of the edge, the approximated reactions as per the follwogin equations arise considering a Timoshenko beam:

$$k_m = 2{,}58\frac{EI_0}{L^2} = 0{,}22\frac{Ebh_0^{\,3}}{L^2} \quad \text{for hourglass height profile} \quad (3.6)$$

$$k_v = 5{,}16\frac{EI_0}{L^3} = 0{,}43\frac{Ebh_0^{\,3}}{L^3} \quad \text{for hourglass height profile} \quad (3.7)$$

where the second moment of the section I is taken with reference to the edge section (I_0).

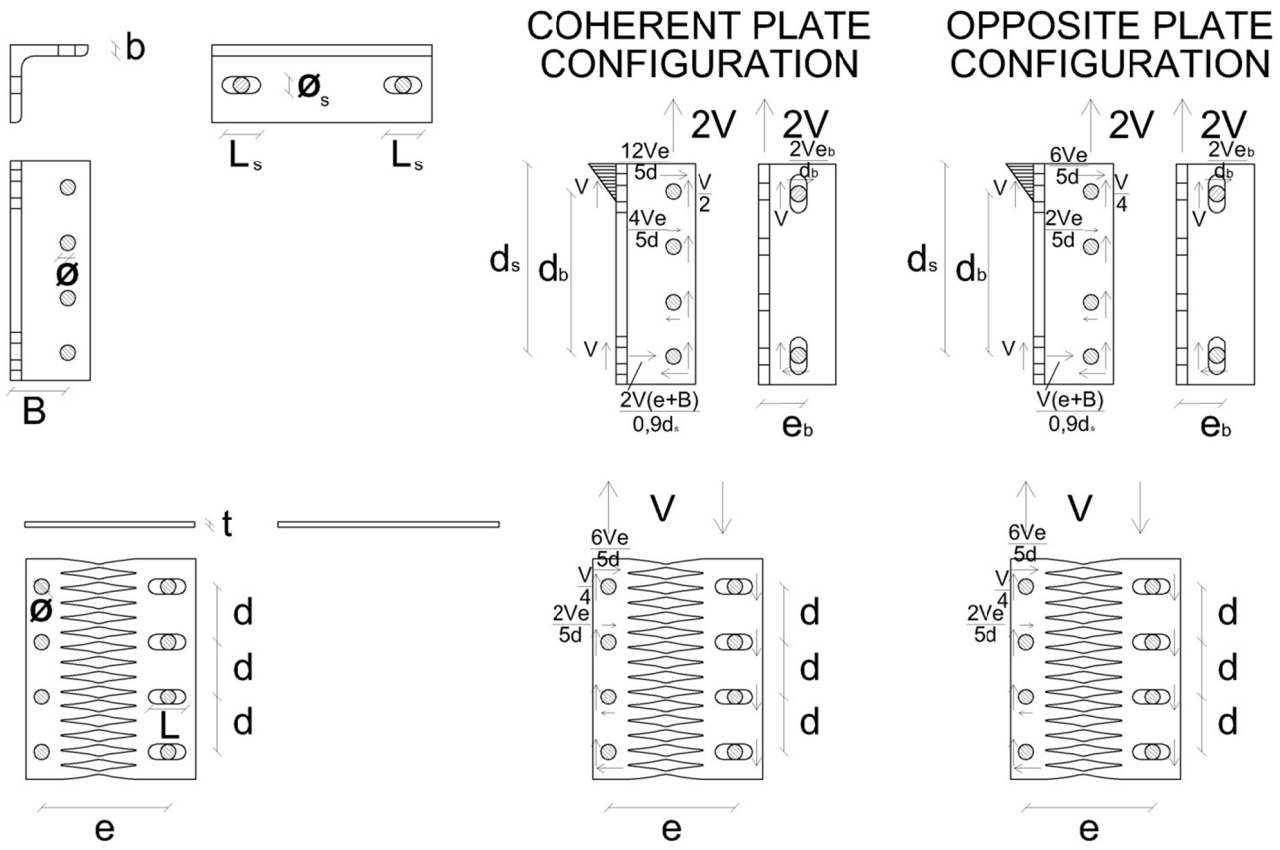

Figure 3.63 – Components of the connection and design forces

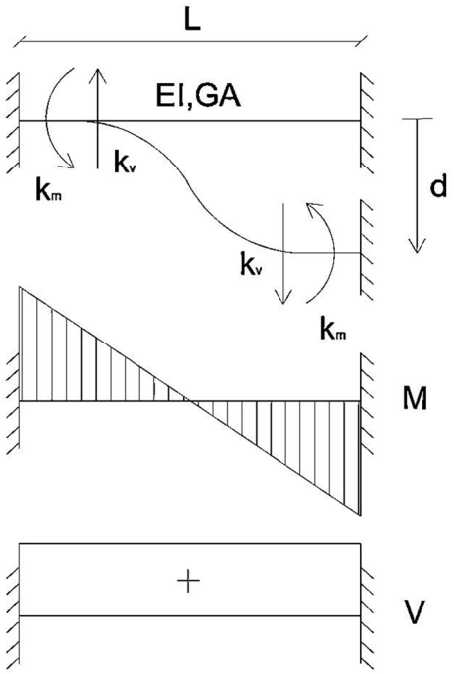

Figure 3.64 – Single beam analysis

The yielding displacement can then be found by imposing that the maximum bending moment along the beam is equal to the yield moment of that cross section:

$$d_y 6\frac{EI}{L^2}\left(\frac{1}{1+\frac{6\chi EI}{L^2 GA}}\right) = f_y \frac{bh^2}{6}$$

That leads to:

$$d_y = f_y \frac{L^2}{3Eh\left(1-\frac{Eh^2\chi}{2LG}\right)} \qquad \text{for constant height profile} \qquad (3.8)$$

$$d_y = 0{,}78 f_y \frac{L^2}{Eh} \qquad \text{for hourglass height profile} \qquad (3.9)$$

And the corresponding yield vertical load can be obtained by multiplying the yield displacement by the translational stiffness:

$$P_y = d_y k_v \qquad (3.10)$$

The ultimate load increases with respect to the yield because of the combination of the diffusion of plasticity along the cross section height and the material over-resistance. The edge chord of the cross section fails when the maximum longitudinal stress reaches the ultimate resistance. All the lower chords, however, are subjected to a lower stress and therefore a contemporaneity factor should be applied to the coefficients referring to those phenomena. The formulation of the ultimate load can be expressed according to the following equation.

$$P_u = P_y \Phi_{pl} \Phi_{or} \Psi \qquad (3.11)$$

where the plastic and over-resistance factors are defined as follows:

$$\Phi_{pl} = \frac{W_{pl}}{W_{el}} = 1{,}5 \qquad \text{For rectangular section only} \qquad (3.12)$$

$$\Phi_{or} = \frac{f_u}{f_y} \qquad (3.13)$$

While the contemporaneity factor Ψ depends on the stress-strain relationship of the material. If considering a linear-plateau-parabola model for steel as shown in Figure 3.65, the development of longitudinal stresses along the section for increasing applied bending moments is shown in Figure 3.66, with reference to the yield and the ultimate stress distribution and to a rectangular section made with steel S275 with nominal resistance values.

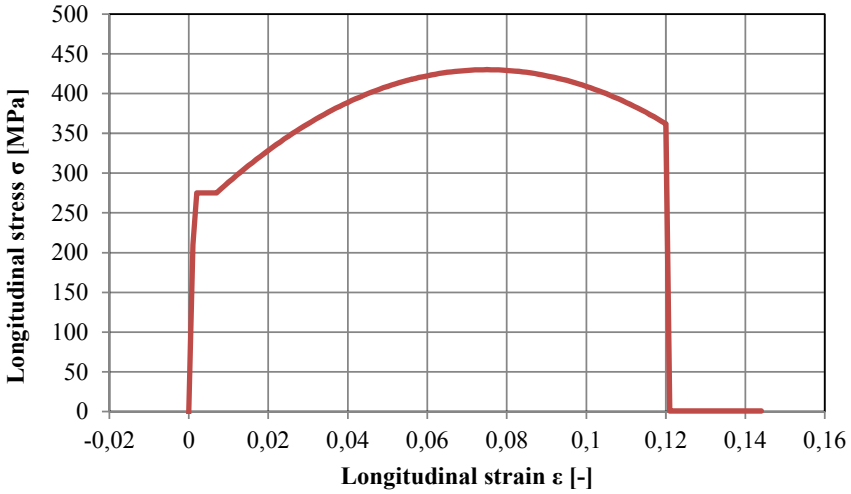

Figure 3.65 – Longitudinal stress-strain relationship for steel (S275 with nominal resistance values in Figure)

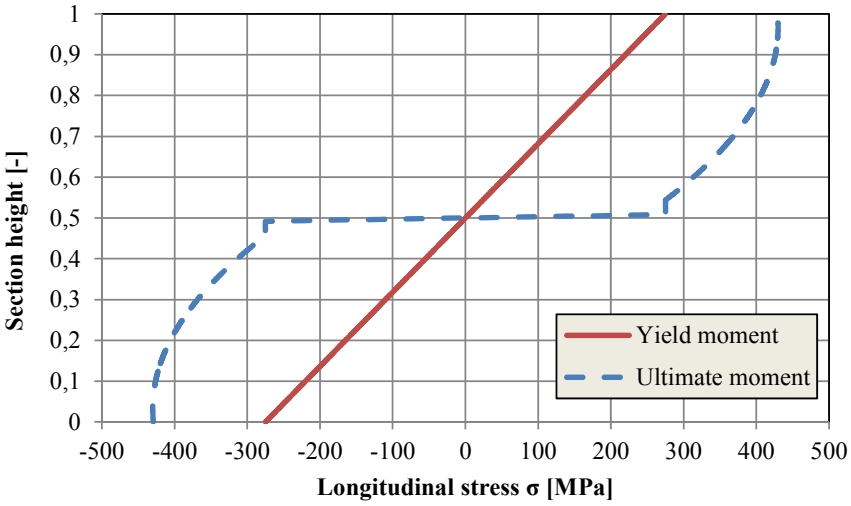

Figure 3.66 – Yield and ultimate stress distribution along the cross section height due to pure bending

The results for different steel grades are collected in Table 3-3. They show that the contemporaneity factor Ψ can be taken with a small approximation equal to 0,94 for all grades.

Table 3-3 – Determination of Ψ factor for different steel grades

Steel grade	$f_{y,nom}$	$f_{u,nom}$	$f_{u,min}$	$f_{u,max}$	Φ_{or}	Φ_{pl}	$\Psi = M_{u,nom}/M_y\Phi_{or}\Phi_{pl}$
	MPa	MPa	MPa	MPa	-	-	-
S235	235	360	360*	510*	1,53	1,5	0,939
S275	275	430	410*	560*	1,56	1,5	0,936
S355	355	510	470*	630*	1,44	1,5	0,946

* for thickness > 3 mm and < 100 mm

Studying the whole device, that can be made with a combination of several elementary beams in parallel with m rows and in series with *n* columns, the following can be written considering the average properties:

$$d_{y,tot} = \frac{\sum_{j=1}^{n} \overline{d}_{y_j}}{n} \tag{3.14}$$

$$P_{y,tot} = \frac{\sum_{i=1}^{m} \overline{P}_{y_i}}{m} \tag{3.15}$$

$$k_{y,tot} = \frac{d_{y,tot}}{P_{y,tot}} \tag{3.16}$$

$$d_{u,tot} = \min(d_{u_j}) \tag{3.17}$$

and the total ultimate load can be calculated as the sum of all beam loads corresponding to the ultimate displacement $d_{u,tot}$.

$$P_{u,tot} = \sum_{i=1}^{m} P_{u_i}(d_{u,tot}) \tag{3.18}$$

By comparing the experimental results with the analytical according to the described procedure, as shown in Table 3-4, good accordance is found only for what concerns the ultimate shear load, calculated according to characteristic mechanical values, satisfactorily predicting the low-displacement cyclic test ultimate load. Important differences are observed if comparing the ultimate load with that of the monotonic behaviour, which is significantly larger than the predicted. Anyhow, the design procedure leads to safe-side estimations. The yield load values differ significantly from the experimental results, but it has to be pointed out that the experimental yield point has only been estimated, while a smooth passage to the plastic branch occurs due to the diffusion of plasticity along the section. The expected yield displacement calculated according to the simplified procedure is largely under-estimating the experimental, which is predominantly influenced by the contribution of bolt tolerances. Both monotonic and cyclic experimental tests are suggested to be performed to characterise the behaviour of new devices.

Table 3-4 – Comparison among experimental and simplified design procedure results

	MONOTONIC BEHAVIOUR								LOW-DISPL CYCLIC BEHAVIOUR					DESIGN PROCEDURE*		
	d_y		P_y	d_u		P_u	μ	ϕ	d_u		P_u	μ	ϕ	d_y	P_y	P_u
	[mm]	[%]	[kN]	[mm]	[%]	[kN]	[-]	[-]	[mm]	[%]	[kN]	[-]	[-]	[mm]	[kN]	[kN]
1-slits	1,2	1,8	33	29	43	100	16,4	3,0	9,4	14	80	7,8	2,4	0,1	34	73,4
2-slits	0,6	0,8	20	31	42	115	38,2	5,8	9,5	13	84	15,8	4,2	0,1	35	75,6
hourglass	1,0	1,5	28	35	51	120	23,8	4,3	10	15	69	10,0	2,5	0,2	34	73,4
hourglass with slots	1,2	1,8	30	37	54	120	21,0	4,0	16	24	86	13,3	2,9	0,2	40	81,6

* The design procedure neglects the influence of rigid rotations due to bolt tolerances

3.4. Folded Plate Device (FPD)

Folded Plate Devices are steel plates bent at 90° in correspondence of three sections, so to have an asymmetric W shape (Biondini *et al.* 2014c, Dal Lago 2014). They are conceived to be installed in between precast horizontal panels and concrete columns. The longer central segment is oriented parallel to the column side, while the shorter is oriented parallel to the panel surface. They provide smaller stiffness and resistance for the relative horizontal displacement, that represents the mutual horizontal displacement between panel and column, while larger stiffness and resistance are provided in the out-of-plane direction. All plates are equipped with welded 10 mm gross thick toothed plates at the edges with passing horizontal slots at column side and passing vertical slots at panel side. The slots allow horizontal and vertical tolerances and their length is designed in order to allow the installation of a M16 fastener avoiding a ϕ 24 rebar in the middle of the column side slot and a ϕ 5 net in the middle of the panel side slot. Tolerances are then eliminated with the application of the closing nut with toothed washer.

Figure 3.67 shows a sketch of the device and Figure 3.68 shows the functioning scheme of the connection.

The maximum drift that the device can sustain depends on its ductility and is limited to the net distance between the column side and the orthogonal-to-panel plate portion, after which an unintended contact between plate and column would occur, changing the response to very stiff. The behaviour of the connections is symmetric only for low displacements, while for large deformations a second order effect tends to arise. Torsional forces directed as per Figure 3.69 would arise in case the out-of-plane panel displacements are perfectly restrained by other panel connections, else a controlled panel torsional rotation is expected to occur.

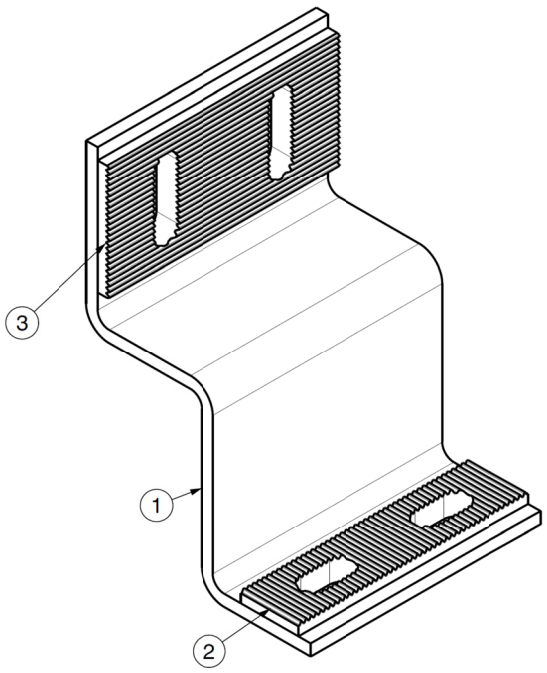

Figure 3.67 – Folded Plate Device

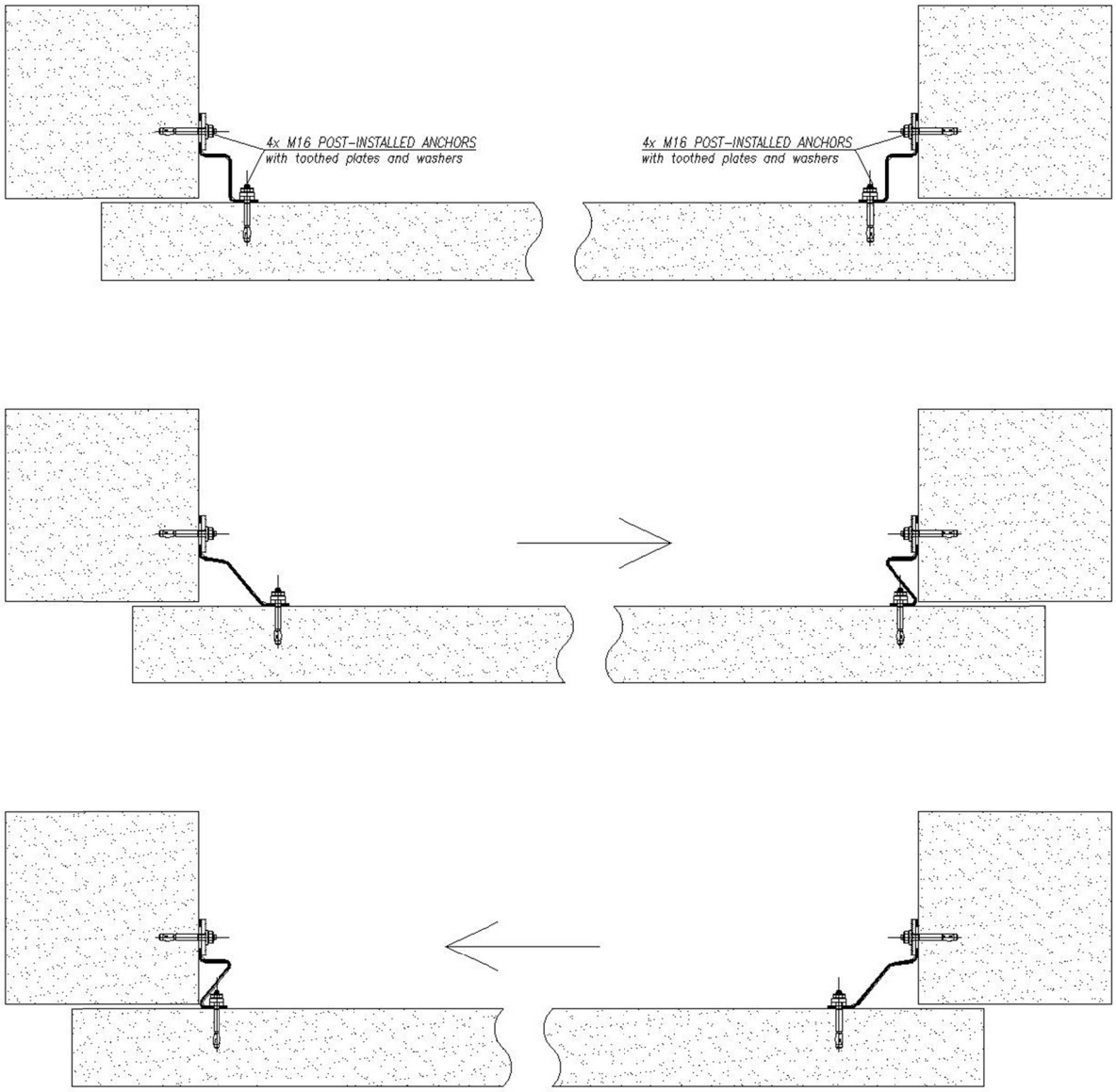

Figure 3.68 – Functioning scheme of the FPD

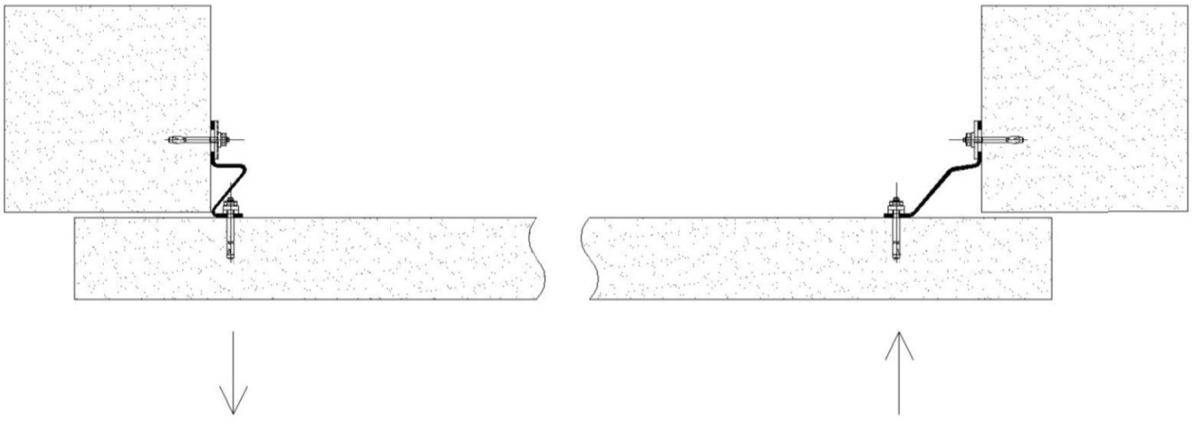

Figure 3.69 – Torsional action due to large device deformation

3.4.1. Test programme

Figure 3.70 shows the device shapes that have been constructed and tested under imposed lateral displacements. All plates are 160 mm wide, with different thicknesses and bending diameters. A picture of four representative samples is shown in Figure 3.71.

M16 class 8.8 bolts have been used to connect the FPD to the setup. The setup is able to simulate both restrained and non-restrained conditions. For the non-restrained condition, the upper metallic angle is strongly tightened to the machine, while the horizontal displacement is allowed by leaving the lower metallic angle slightly tightened. In the tests with restrained horizontal displacement, also the lower angle has been strongly tightened. Three additional displacement transducers are installed on the steel frame that supports the specimens. Two redundant ± 75 mm potentiometers measure the machine vertical displacements, while a third ± 75 mm potentiometers measures the horizontal displacement of the lower HE angle.

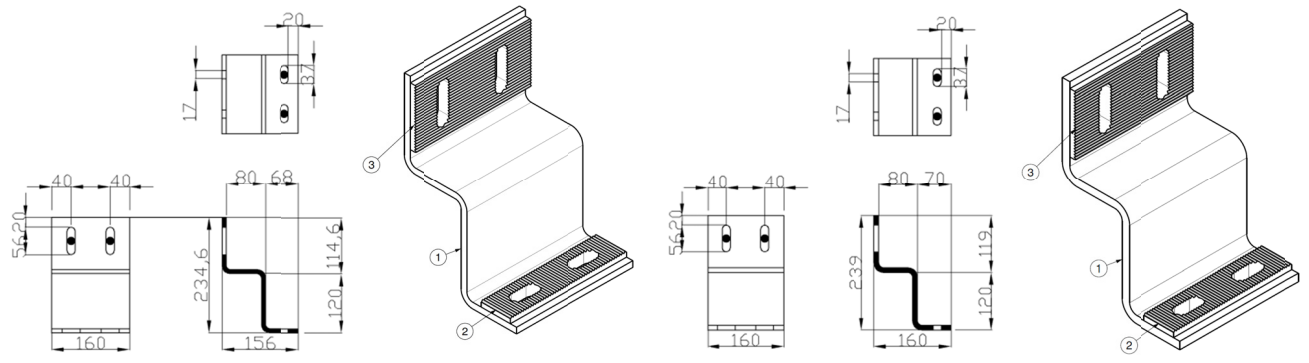

(a) Plate 1

(b) Plate 2

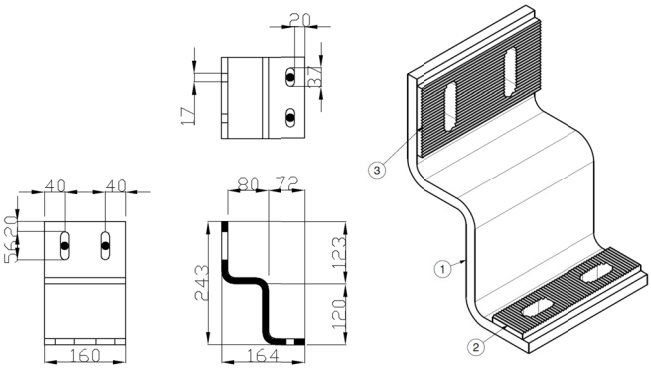

(c) Plate 3

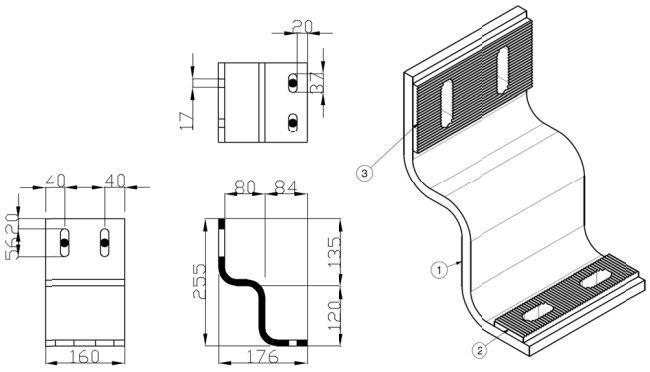

(d) Plate 4

Figure 3.70 – Folded plates: (a) t = 8 mm, Φ = 2t; (b) t = 10 mm, Φ = 2t; (c) t = 12 mm, Φ = 2t; (d) t = 8 mm, Φ = 4t

Figure 3.71 – Folded plates specimens before testing

The complete list of the performed tests is reported in Table 3-5.

Table 3-5 – Performed cyclic tests on folded plate devices

DEVICE	TEST TYPE	CYCLIC LOAD PROTOCOL	KIND OF SAMPLE	HORIZONTAL DISPLACEMENT
FPD	CYCLIC	B	PLATE 1	FREE
			PLATE 1	RESTRAINED
			PLATE 2	FREE
			PLATE 2	RESTRAINED
			PLATE 3	FREE
			PLATE 3	RESTRAINED
			PLATE 4	FREE
			PLATE 4	RESTRAINED
		C	PLATE 1	FREE
			PLATE 1	RESTRAINED
			PLATE 2	FREE

For the sake of brevity, only the results referred to plate 1 are shown and commented in detail.

3.4.2. Cyclic behaviour

The initial and maximum drift shape of FPD 1 subjected to cyclic protocol C are shown in Figure 3.72. While the formation of a plastic hinge can be clearly identified at the left edge of the horizontal segment of the plate (panel side), leaving that segment rotate rigidly, a diffused plasticity occurs within the vertical shorter segment with plastic rotations at both up and bottom edges, together with bending deformation of the segment. A tendency to large out-of-plane displacements is noticed at large drifts.

(a)

(b)

(c)

Figure 3.72 – FPD 1, protocol C with free horizontal displacements: (a) undeformed shape, (b) maximum downwards drift and (c) maximum upwards drift

Figure 3.73 shows the load vs displacement diagram of the cyclic test performed with protocol C. Failure has not been attained. The cyclic behaviour is asymmetric: elastic–plateau for the downward direction and elastic–over-resisting for the upward direction, with different maxima load attained, equal to 23 kN and 37 kN, respectively. This asymmetric behaviour occurs only at relatively large displacement. When the imposed drift tends to extend the plate (upwards direction in the test), the behaviour tends to harden, due to adding second order axial stiffness and resistance to the pure bending behaviour. On the opposite, when the imposed drift tends to contract the plate (downwards direction in the test), the curvature imposed by cold bending

tends to emphasize, weakening the critical sections. It is possible to evaluate an approximated elastic stiffness equal to 1,5 kN/mm. The unload branch at the upwards drift side shows a progressive stiffness degradation from almost rigid to flexible, due to the second order effect and the passage from a stiff combined axial-flexural behaviour to a purely flexural.
Figure 3.74 shows the energy dissipation properties of the connection. Up to the maximum displacement cycles, the positive and negative semi-cycles seem to dissipate about the same amount of energy. The specific energy, if compared to a perfect plastic equivalent system with equal maximum displacements and forces, rises up to about 0,48 for the ± 40 mm cycle and 0,52 for the ± 60 mm cycle, as shown in the energy diagram, while a perfect elasto-plastic equivalent system with the same elastic stiffness as identified above gives a comparison of about 0,86 for the ± 40 mm cycle and 0,77 for the ± 60 mm cycle. The large out-of-plane displacement tendency is confirmed by looking at its history in Figure 3.75.

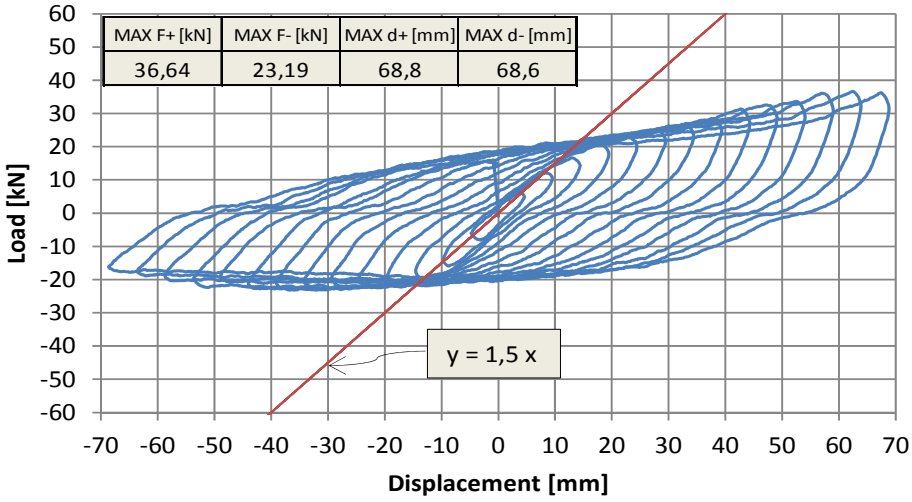

Figure 3.73 – Load vs displacement

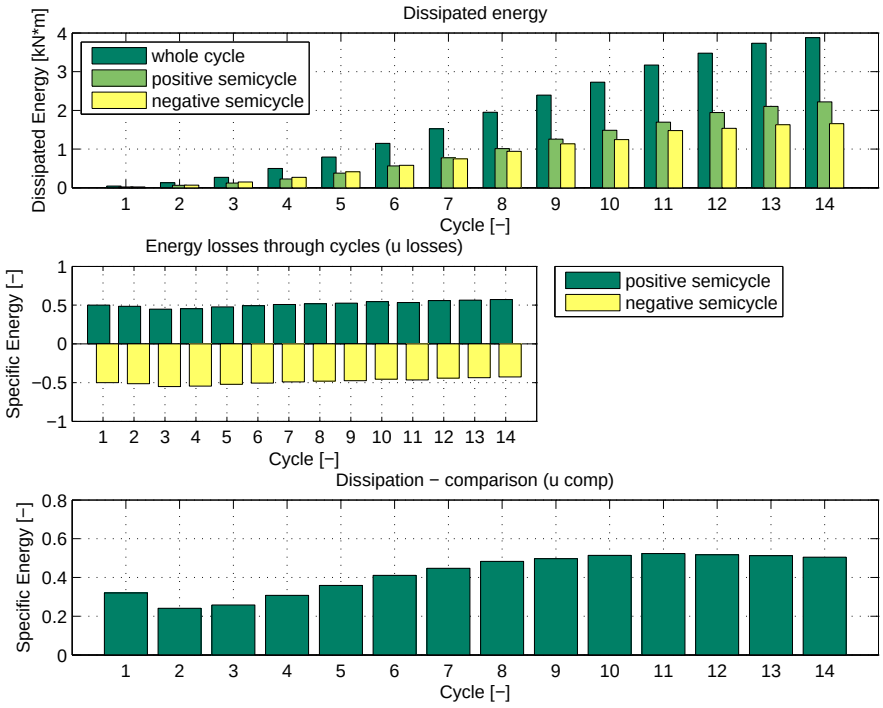

Figure 3.74 – Energy dissipation properties

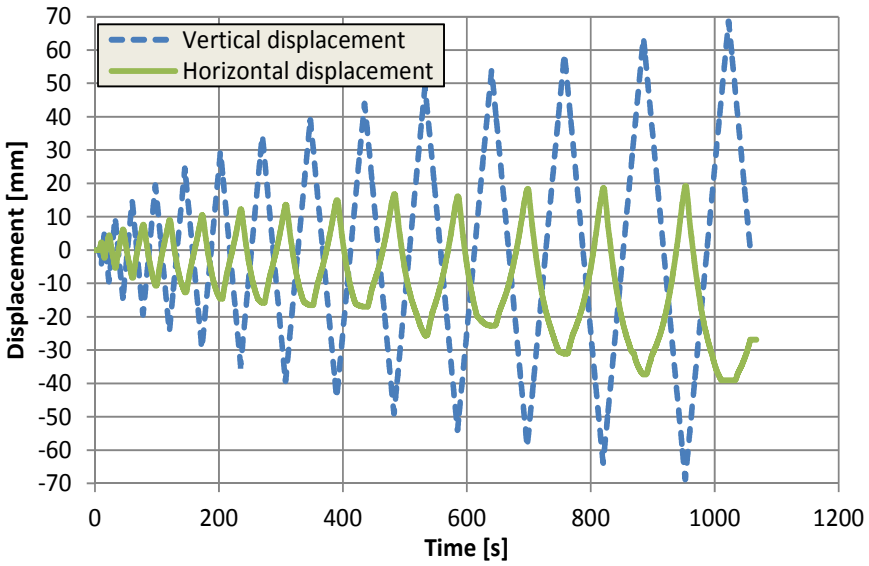

Figure 3.75 – Comparison between the vertical and horizontal displacement components with protocol C

Similar results are obtained within the test on a similar specimen subjected to cyclic protocol B. Figure 3.76 shows the load vs displacement diagram. Failure has not been attained. The cyclic behaviour is confirmed but less emphasised because of the lower drift achieved, with different maxima load attained, equal to 22 kN and 29 kN, respectively. The yield load and displacement could not be clearly identified, also because a pinching effect has been recorded, mainly due to rigid rotation of the horizontal plate-support connection that occurred because of mounting tolerances. It is possible to evaluate an approximated elastic stiffness equal to the previous.

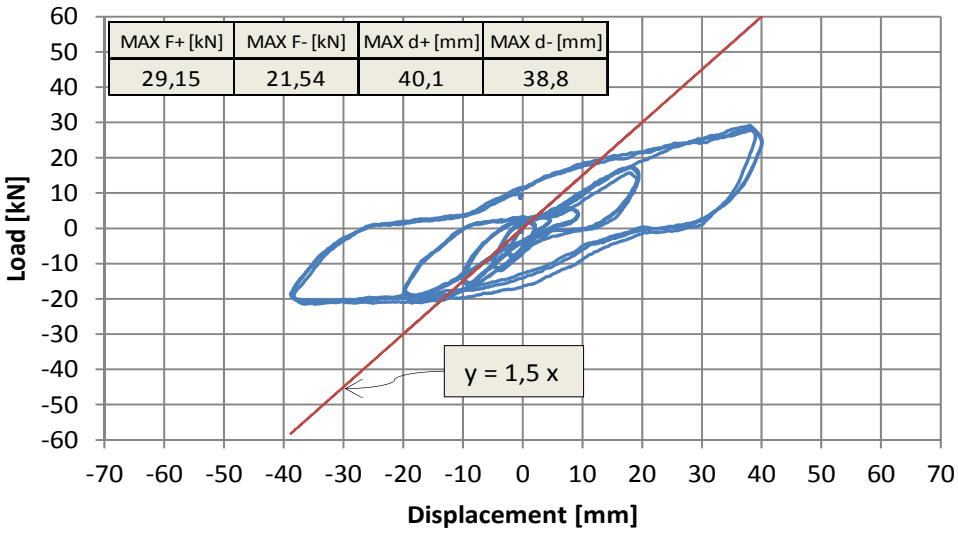

Figure 3.76 – Load vs displacement

Figure 3.77 shows the energy dissipation properties of the connection. Up to the maximum displacement cycles, the positive and negative semi-cycles seem to dissipate about the same amount of energy. The specific energy, if compared to a perfect plastic equivalent system with equal maximum displacements and forces, rises up to about 0,40 for the ± 40 mm cycles, as shown in the energy diagram, while a perfect elasto-plastic equivalent system with the same elastic stiffness as identified above gives a comparison of about 0,70 for the same cycles.
The results are in very good agreement with those obtained from the same specimen subjected to the cyclic protocol C, as showed by the superposition of the experimental loops in Figure 3.78, which suggests that the behaviour of the connection is reliable and cyclically stable.

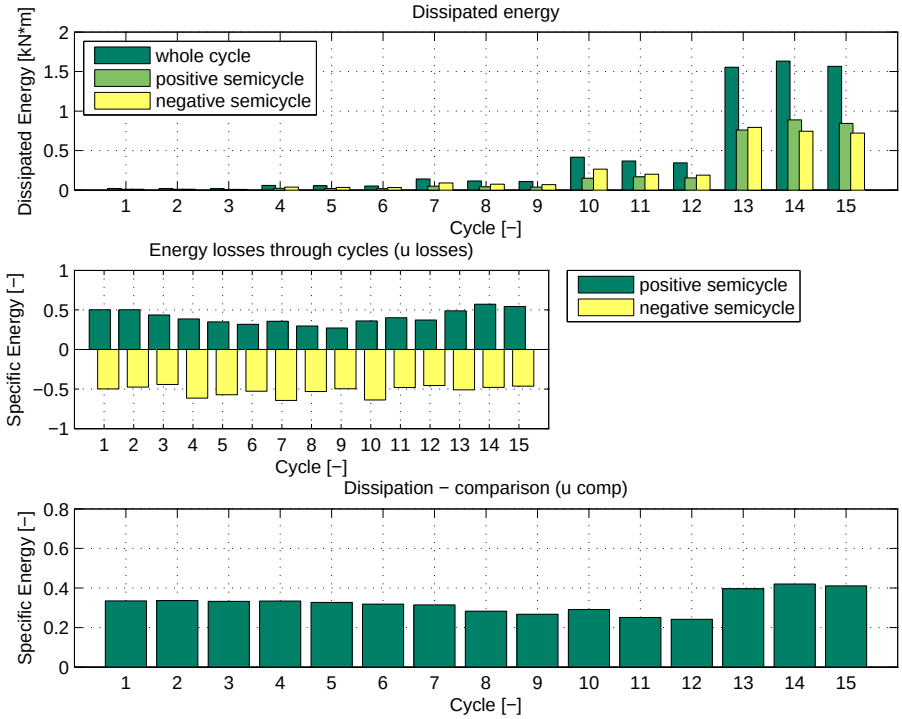

Figure 3.77 – Energy dissipation properties

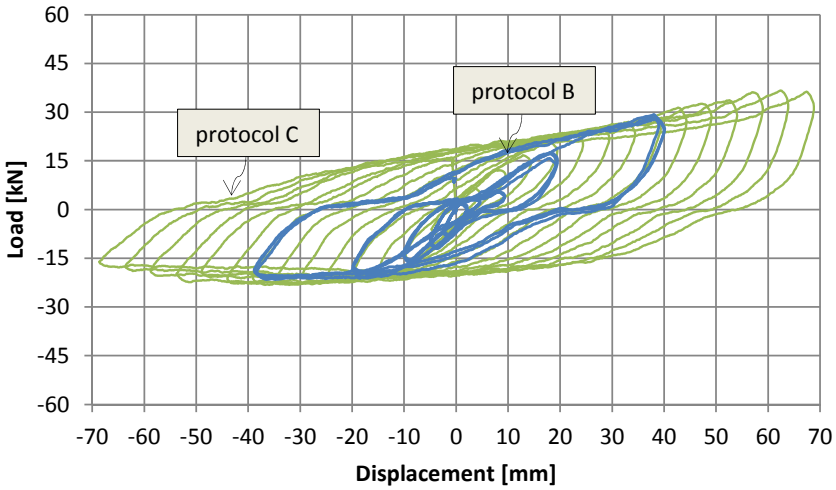

Figure 3.78 – FPD 1 under cyclic test with non-restrained out-of-plane displacement: comparison between the curves obtained with protocols B and C

3.4.3. **Effect of horizontal restraint**

The effect of a horizontal restraint has been studied by repeating the tests with a mechanical blockage of the lower L-shaped support profile. An effective horizontal displacement restraint could also be technologically provided on the specimen by welding diagonal plates between the column-laying portion and the shorter free portion of the device.

The initial and maximum drift shape of FPD 1 subjected to cyclic protocol C are shown in Figure 3.72. The formation of plastic hinges can be clearly identified at both edges of the horizontal segment of the plate (panel side), leaving that segment rotate rigidly. As a result of the restraint of horizontal displacements, the vertical shorter segment does not deform.

(a)

(b)

(c)

Figure 3.79 – FPD 1, protocol C with restrained horizontal displacements: (a) undeformed shape, (b) maximum downwards drift and (c) maximum upwards drift

Figure 3.80 shows the load vs displacement diagram. Failure occurred at the last cycle (± 70 mm) at the left edge of the horizontal segment of the plate (panel side). Figure 3.81 shows the ductile failure mechanism of the plate.

The cyclic behaviour is asymmetric: elastic–under-resisting for the downward direction and elastic–over-resisting for the upward direction, with very different maxima load attained, equal to 37 kN and 60 kN, respectively, which are much larger with respect to those attained within the same test with non-restrained horizontal displacement.

The yield load and displacement could not be clearly identified, while it is possible to evaluate an approximated elastic stiffness equal to 2,6 kN/mm. As also shown by previous tests, the unload branch at the upwards drift side shows a progressive stiffness degradation from almost rigid to flexible, due to the second order effect and the passage from a stiff combined axial-flexural behaviour to a purely flexural.

Figure 3.82 shows the energy dissipation properties of the connection. Up to about half of the maximum displacement cycles, the positive and negative semi-cycles seem to dissipate about the same amount of energy, while the balance tends towards the positive semi-cycles for larger amplitudes.
The specific energy, if compared to a perfect plastic equivalent system with equal maximum displacements and forces, rises up to 0,48 for the ± 40 mm cycle and 0,46 for the ± 60 mm cycle, as shown in the energy diagram, while a perfect elasto-plastic equivalent system with the same elastic stiffness as identified above gives a comparison of 0,78 for the ± 40 mm cycle and 0,66 for the ± 60 mm cycle.

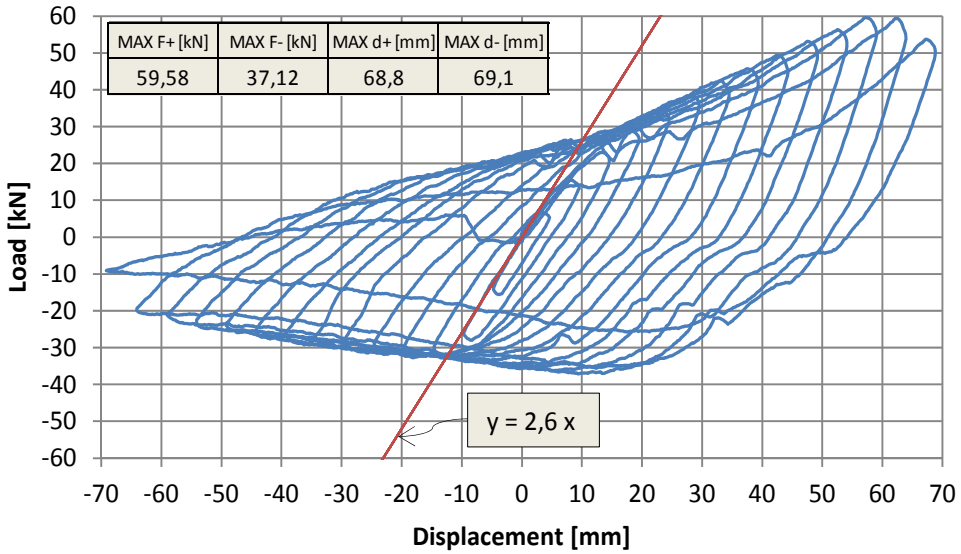

Figure 3.80 – Load vs displacement

Fracture initiation at 70 mm downwards displacement — Failure at the end of the 70 mm cycle

Figure 3.81 – Failure of the plate

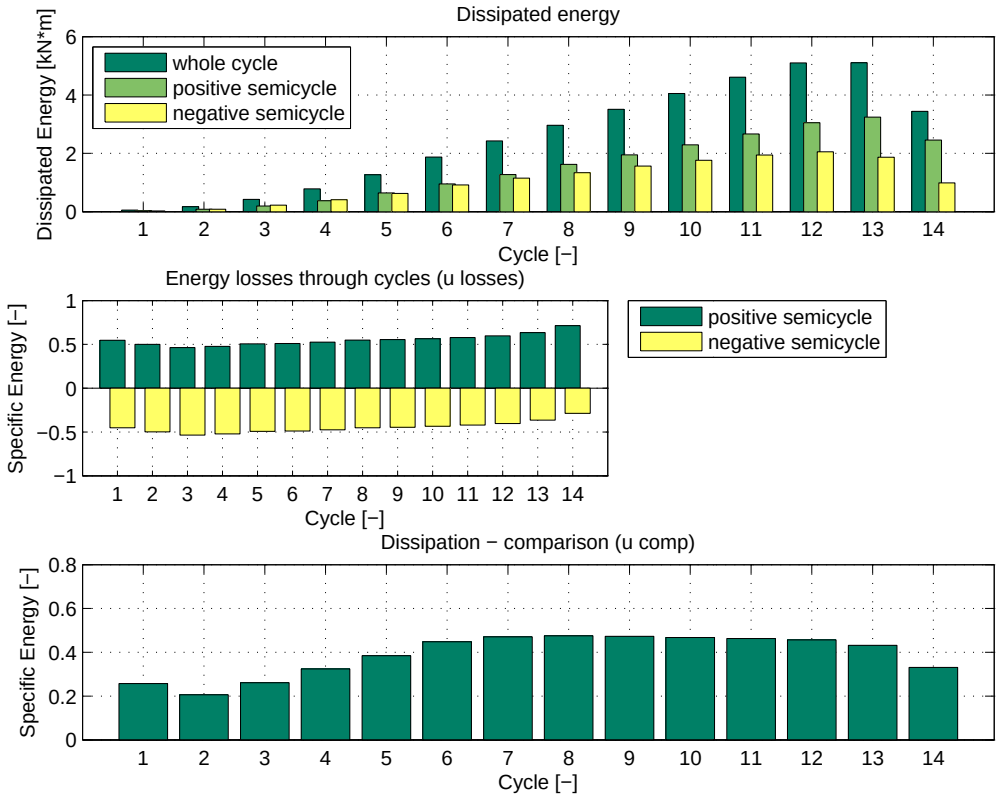

Figure 3.82 – Energy dissipation properties

Figure 3.83 shows the FPD 1 after testing with cyclic protocol C. At the right side, the specimen tested with free horizontal displacements show large residual deformation of the shorter segment, that is negligible for the specimen with restrained horizontal displacements (left side).

Side view Top view

Figure 3.83 – Steel plates after testing

Figure 3.84 shows the load vs displacement diagram from the test on the restrained displacement configuration with cyclic protocol B. Failure has not been attained. The cyclic behaviour is similar to what previously described, with different maxima load attained, equal to 34 kN and 47 kN, respectively. The yield load and displacement could not be clearly identified, while it is possible to evaluate an approximated elastic stiffness equal to 2,6 kN/mm.

Figure 3.85 shows the energy dissipation properties of the connection. Up to the maximum displacement cycles, the positive and negative semi-cycles seem to dissipate about the same amount of energy. The specific energy, if compared to a perfect plastic equivalent system with equal maximum displacements and forces, rises up to about 0,44 for the ± 40 mm cycles, as shown in the energy diagram, while a perfect elasto-plastic equivalent system with the same elastic stiffness as identified above gives a comparison of about 0,73 for the same cycles.

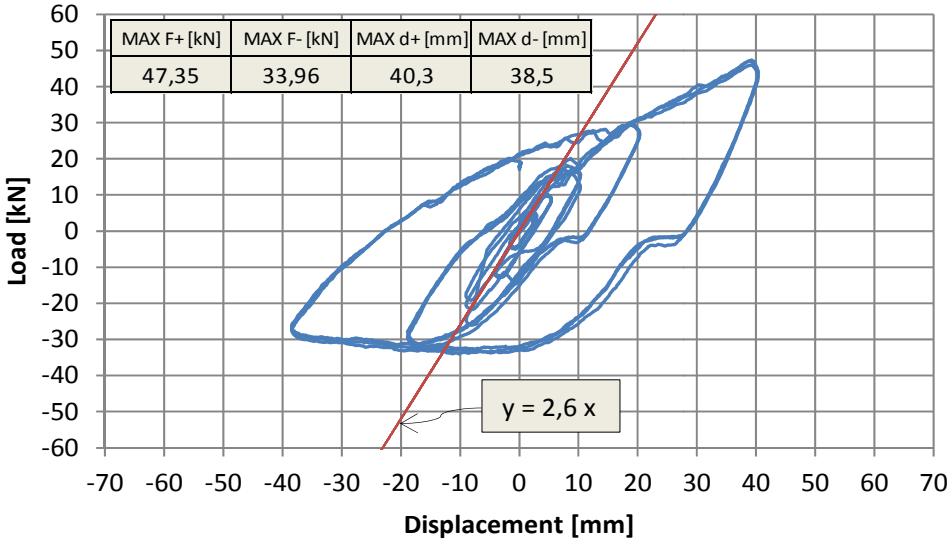

Figure 3.84 – Load vs displacement

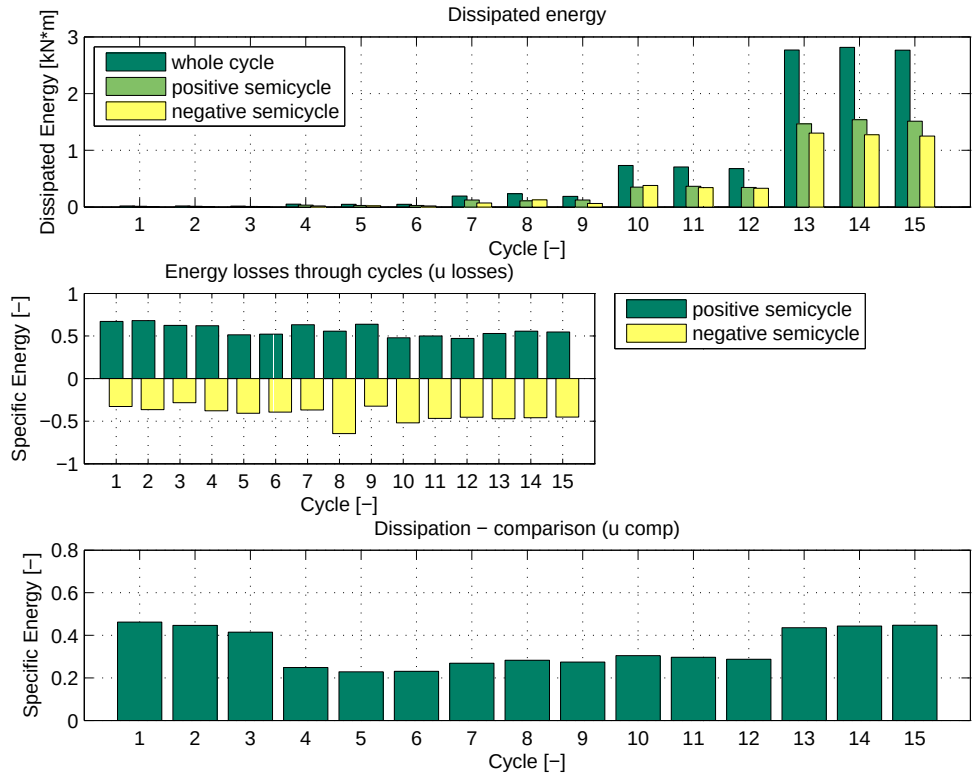

Figure 3.85 – Energy dissipation properties

Figure 3.86 shows the steel plates 1 after testing with cyclic protocol B. At the right side, the specimen tested with free horizontal displacements show large residual deformation of the shorter segment, that is negligible for the specimen with restrained horizontal displacements (left side).

Also with this configuration, the results are in very good agreement with those obtained from the same specimen subjected to the cyclic protocol C, as showed by the superposition of the experimental loops in Figure 3.87.

Side view Top view

Figure 3.86 – Steel plates after testing

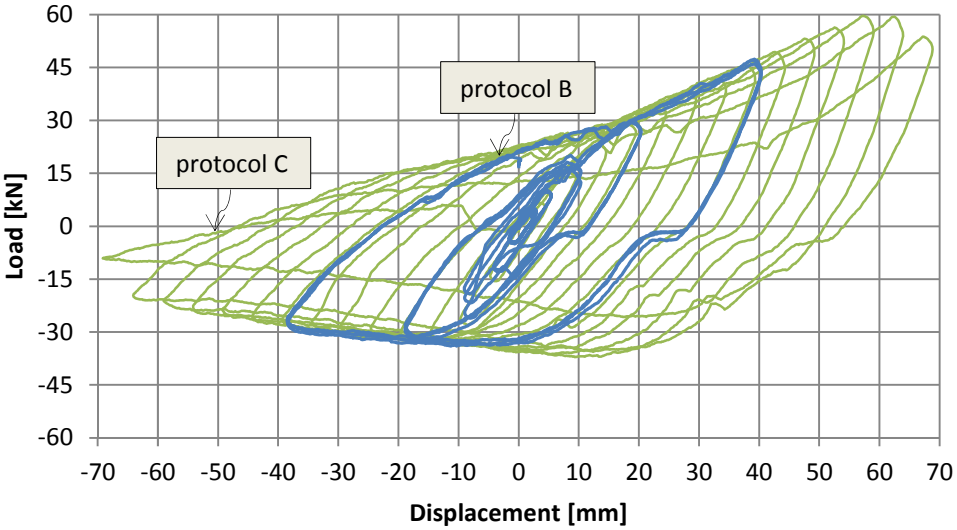

Figure 3.87 – FPD 1 under cyclic test with restrained out-of-plane displacement: comparison between the curves obtained with protocols B and C

3.4.4. Results from additional tests

Thicker specimens provided similar results if compared with those shown above, in terms of cyclic behaviour. A larger initial pinching is detected, due to the difficulty to avoid small rigid body rotations due to tolerances for stiffer profiles.

Considering only the results with cyclic protocol D and free horizontal displacement, larger elastic stiffness, of about 2,0 kN/mm for the 10 mm thick specimens and in about 2,3 kN/mm for the 12 mm thick specimens, have been achieved, together with larger maximum loads, of about 50 kN for positive semi-cycles and 40 kN for negative semi-cycles for the 10 mm thick specimens and of about 65 kN for positive semi-cycles and 50 kN for negative semi-cycles for the 12 mm thick specimens. Figure 3.88 and Figure 3.89 show the results of the tests performed on FPD 2 with cyclic protocol D and C limited to ± 40 mm, respectively.

As it can be noticed by the comparison of the results collected in Figure 3.90 and in Figure 3.91, the cyclic behaviour of the profiles with different bending diameter is very similar. A temporary partial block of the horizontal slider, occurred at the first negative semi-cycle with amplitude 40 mm of the test on FPD 4, as shown in Figure 3.92, clarifies how the load can increase when out-of-plane deformation is prevented.

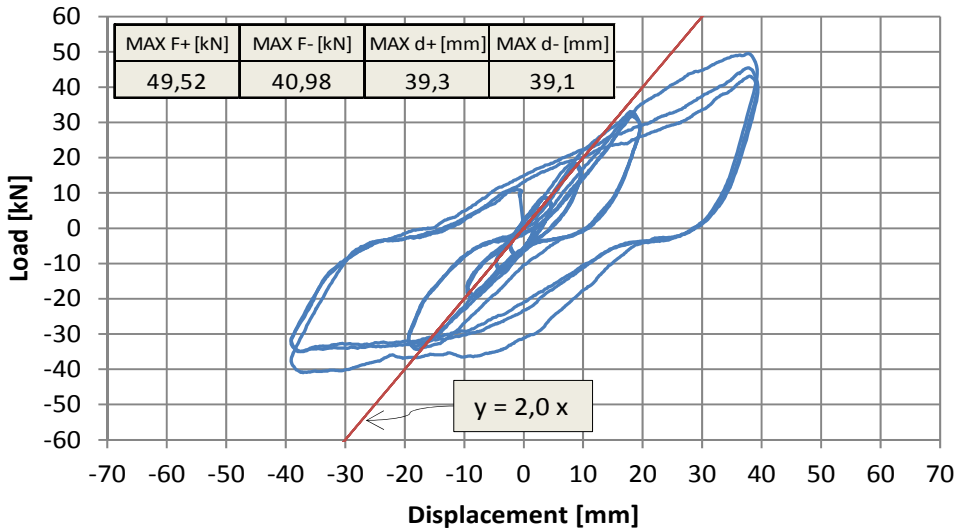

Figure 3.88 – Load vs displacement for cyclic protocol E on FPD 2

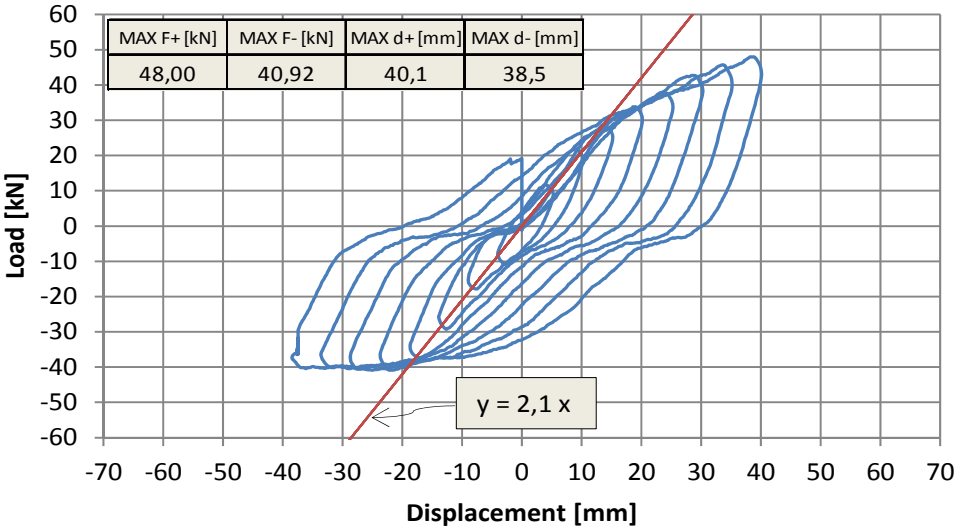

Figure 3.89 – Load vs displacement for cyclic protocol N limited to ± 40 mm on FPD 2

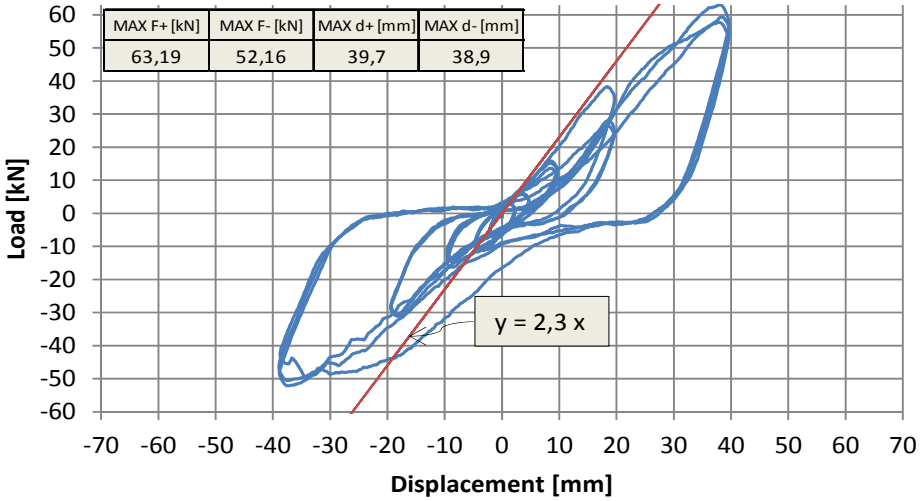

Figure 3.90 – Load vs displacement for cyclic protocol E on FPD 3

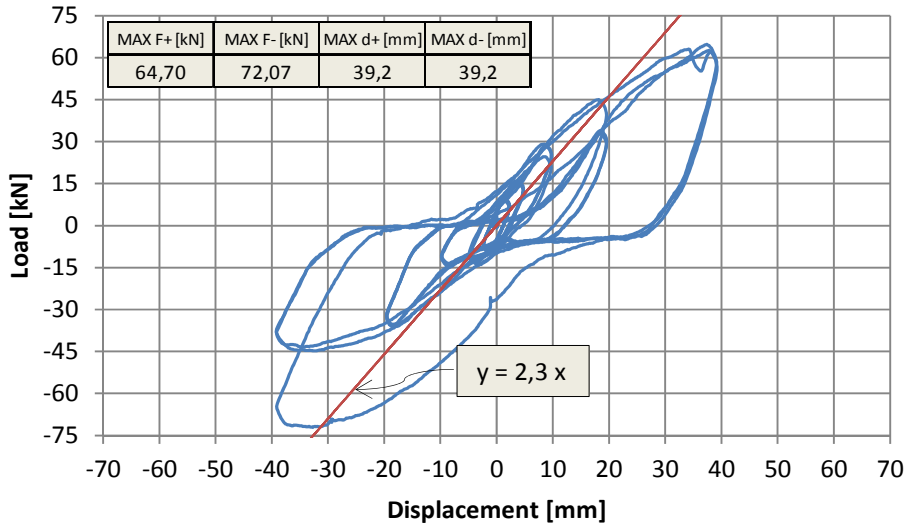

Figure 3.91 – Load vs displacement for cyclic protocol E on FPD 4

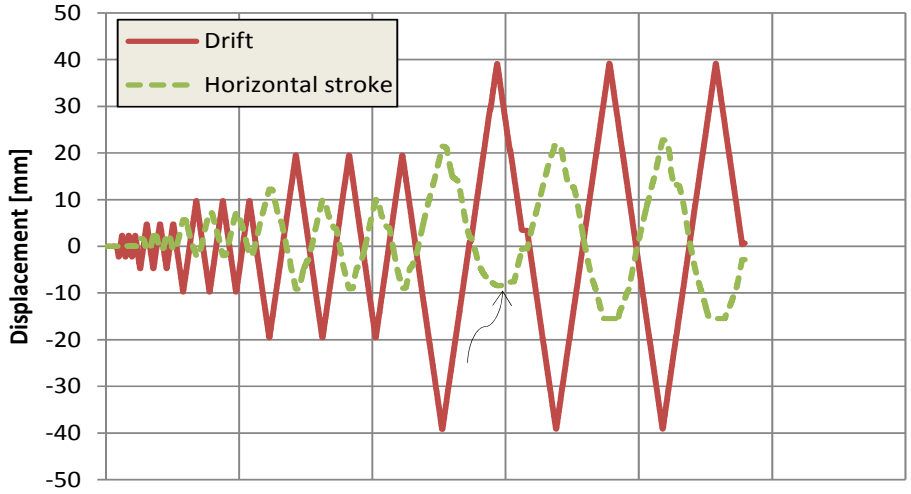

Figure 3.92 – Temporary block of horizontal displacement for cyclic protocol E on FPD 4

3.4.5. Design recommendations

If the profiles are mounted following the suggested symmetric configuration, the global behaviour turns symmetric also in case of FPD with restrained out-of-plane displacement, characterised by a single device asymmetric behaviour. The global envelope of two devices mounted symmetrically is shown in Figure 3.93 with reference to FPD 1 with both restraint conditions, by summing of two inverted experimental curves. The curve shows that the behaviour is symmetric and that it is characterised by a large plateau followed by an over-resisting branch due to second order large displacement effect, for which a pure bending behaviour turns into a combined axial-bending. However, the dimensioning of the device-to-structure connection, made with post-installed fasteners or dowels, shall be performed according to the capacity design with reference to the specific behaviour of the single connection, considering both forces and bending moments.

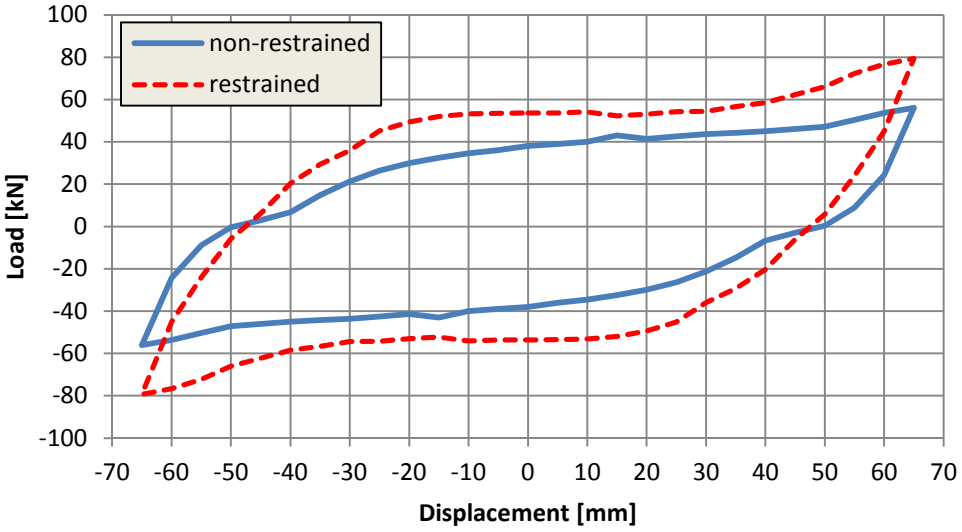

Figure 3.93 – Symmetric envelope curve for two FPD 1 with restrained horizontal displacement placed symmetrically on the panel

Chapter 4

Panel sub-assembly behaviour of dissipative systems

The present chapter contains information about the panel sub-assembly behaviour of dissipative systems and the related isostatic base configurations. The behaviour of the suggested vertical panel systems is studied experimentally, together with the influence that silicone sealant can have on the cyclic behaviour of those systems. Design rules for the sub-assembly level are provided. The influence of silicone sealant is also studied through the experimental characterisation of its local behaviour. Design recommendations are provided also for silicone sealant.

4.1. Isostatic systems

Dissipative devices are conceived as additional energetic fuse ductile connections that can dissipate energy through different mechanisms. The safest use of those connections consists in excluding them from the panel resistant mechanism, that can be provided by bearing connections properly arranged to create an isostatic system. In such a way, risk of collapse of the panels is avoided by designing the bearing connections (and the panels) to remain elastic and undamaged also while the dissipative connections are subjected to a strong use, possibly allowing their safe substitution or re-activation after the earthquake.

The study of isostatic configurations is therefore essential to create a solid base for the exploitation of improved systems. Suggested isostatic arrangements are described in the following, taking into account their ease of use in practice, both for vertical and horizontal panels. Proper procedures to evaluate the correct loads acting on primary bearing connections in case of dissipative systems are suggested, together with experimental tests aimed at verifying the correct functioning of several isostatic and dissipative systems.

The dissipative connections are assumed to be mounted on pendulum or rocking isostatic arrangement, for vertical panels, and on swaying arrangement for horizontal panels.

4.1.1. Panel sub-assembly experimental setup

An experimental campaign on panel sub-assembly isostatic and dissipative systems has been carried out at the Laboratorio Prove e Materiali of Politecnico di Milano, with the aim to investigate its cyclic behaviour and verify the correct functioning of all components.

The monoaxial test setup is made of two solid concrete panels 129 cm wide, 323 cm long and 16 cm thick, with an aspect ratio equal to 2,50, as shown in Figure 4.1. The panels are provided with a passing vertical slot in the middle of the width, providing a mechanical height (from the bottom panel-to-foundation connection to the top panel-to-beam connection) of about 260 cm, depending on the tolerances. Three recesses are placed at the thirds of the mechanical height at each side, aimed to host the dissipative connections. The top panel connections is made with round holes hosting steel pins that connect the panels to the steel articulated frame that transmits the imposed displacements to the panels. The frame is made with two HEA columns hinged at the bottom with the strong lab steel beam and at the top with the double UPN beam surrounding the panels. The physical hinges are made by steel pins. The frame is connected with the horizontal jack, which is fixed to the strong steel braced reaction frame of the lab with the centre at a height of 270 cm. A lateral displacement retainer system has been installed in correspondence of the steel beam and attached to the beam with steel spheres that are fixed to lateral stiff retaining frames.

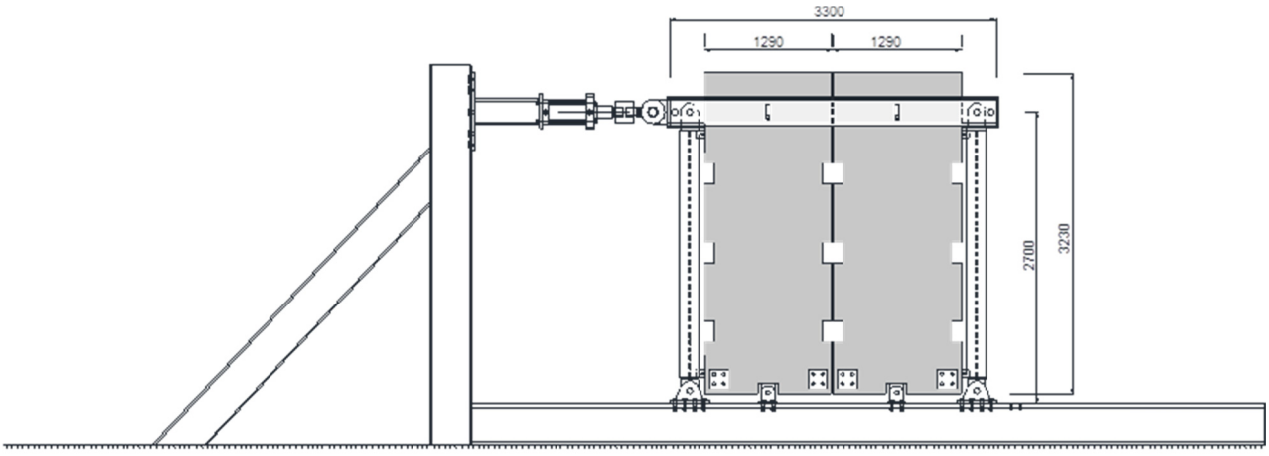

(a)

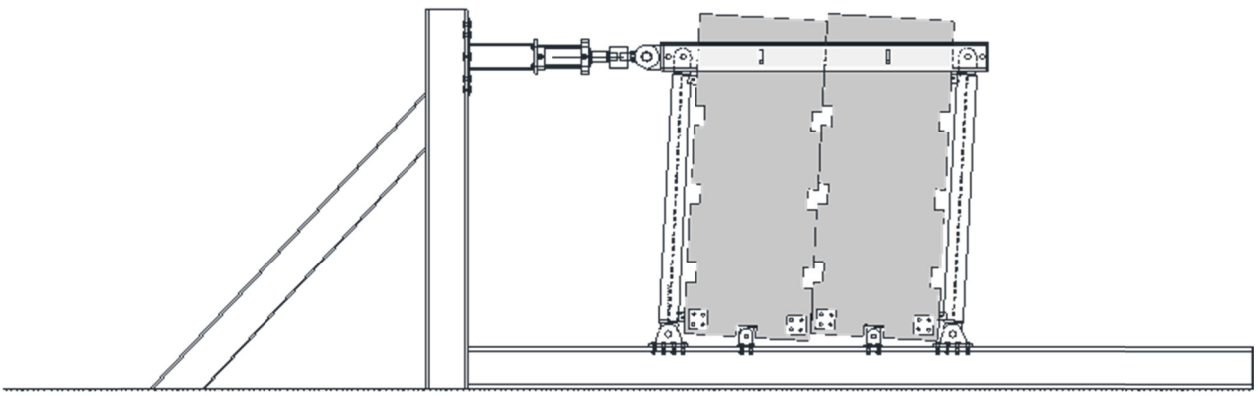

(b)

Figure 4.1 – Test setup with pinned panel-to-foundation connection: (a) technical drawing and (b) displaced configuration

Two vertical long slots are cut in the beam UPN profiles in order to create the panel-to-beam connection. The panel-to-foundation connection of the panels is pinned (pendulum system) or simply supported on the edges with shims (rocking system). Figure 4.2 shows a picture of the assembled setup.
The test instrumentation, in addition to the 750 kN jack control displacement transducer and load cell, is made by vertical displacement transducers placed at the panel base edges and connected to the base steel beam. Displacement transducers installed on concrete also measure the relative vertical sliding of the panels and their relative horizontal distancing.

Figure 4.2 – Picture of the assembled test setup

4.1.2. Pendulum arrangement

Two single cycle tests at the maximum allowed drift, equal to 5%, have been performed on the pendulum arrangement of the panels, provided with a pinned connection at their base.

Figure 4.3 shows the deformed shape of the assembled specimen. The panels rotate rigidly around their base pin. The load vs relative vertical displacement diagrams of the tests, reported in Figure 4.4, confirm that the global stiffness of the frame is practically negligible, since the maximum attained horizontal load is less than 0,6 kN. Each panel is unstable, and an imposed displacement would make negative second order horizontal forces arise, since the jack would actually hold the panels, instead of pushing or pulling them. The results of the first test confirm that a low negative stiffness has been attained, while the results of the second tests showed low positive stiffness, probably due to the effect of small frictions. The perfect rigid motion of the panels is confirmed by the displacement transducers positioned at the base of the panels, as noticeable from Figure 4.5, where each curve refers to an instrument denominated in the form “panel – edge”.

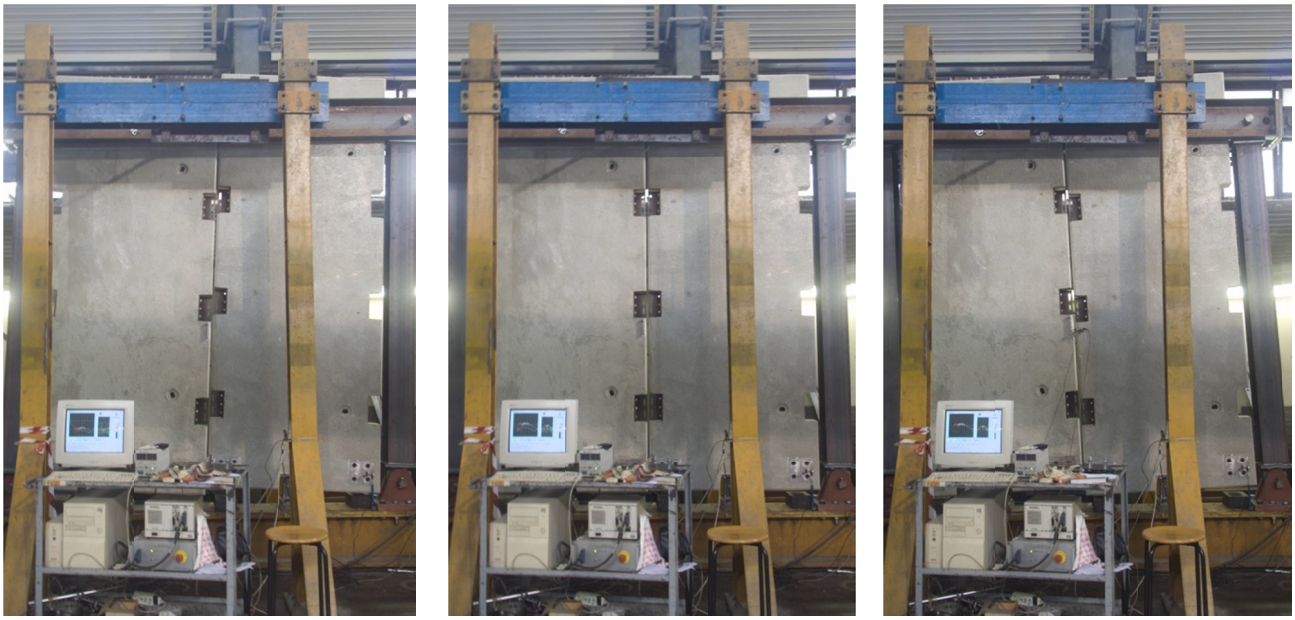

5% drift pulling 0% drift 5% drift pushing

Figure 4.3 – Isostatic pendulum configuration: deformed shape at maximum drift

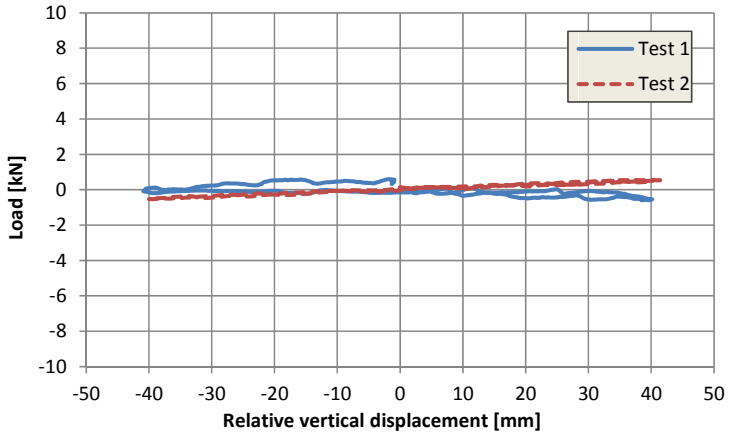

Figure 4.4 – Load vs displacement

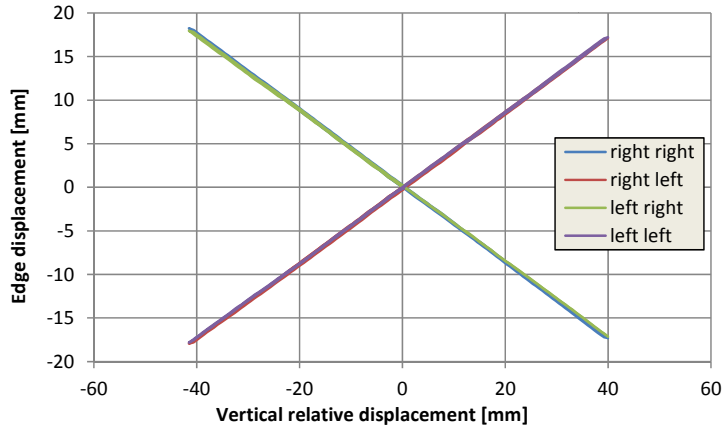

Figure 4.5 – Panel edge vertical displacement vs vertical relative displacement

4.1.3. Rocking arrangement

A single cycle test at a maximum drift of 2% has been performed on the rocking arrangement of the panels, provided with concrete cubes acting as shims at their base edges.

Figure 4.6 shows the deformed shape of the assembled specimen. The panels rotate rigidly around their base edges, moving from one edge to the opposite when changing from positive to negative displacement and viceversa. The load vs relative vertical displacement diagram of the test, reported in Figure 4.7, shows that the behaviour is practically rigid – hyper-elastic, since the panels do not lift until the overturning at their base is higher than the stabilising, as a function of their own weight. When this moment is reached, the panels lift without load increment, suddenly entering a 90° bent plateau. To further displacement increments do not correspond load increments. When the displacement turns back to the origin, the curve overcomes the loading branchs. A small dissipation of energy occurred in the experimental results, as noticeable by a small area within the cycles, probably due to small friction effects.

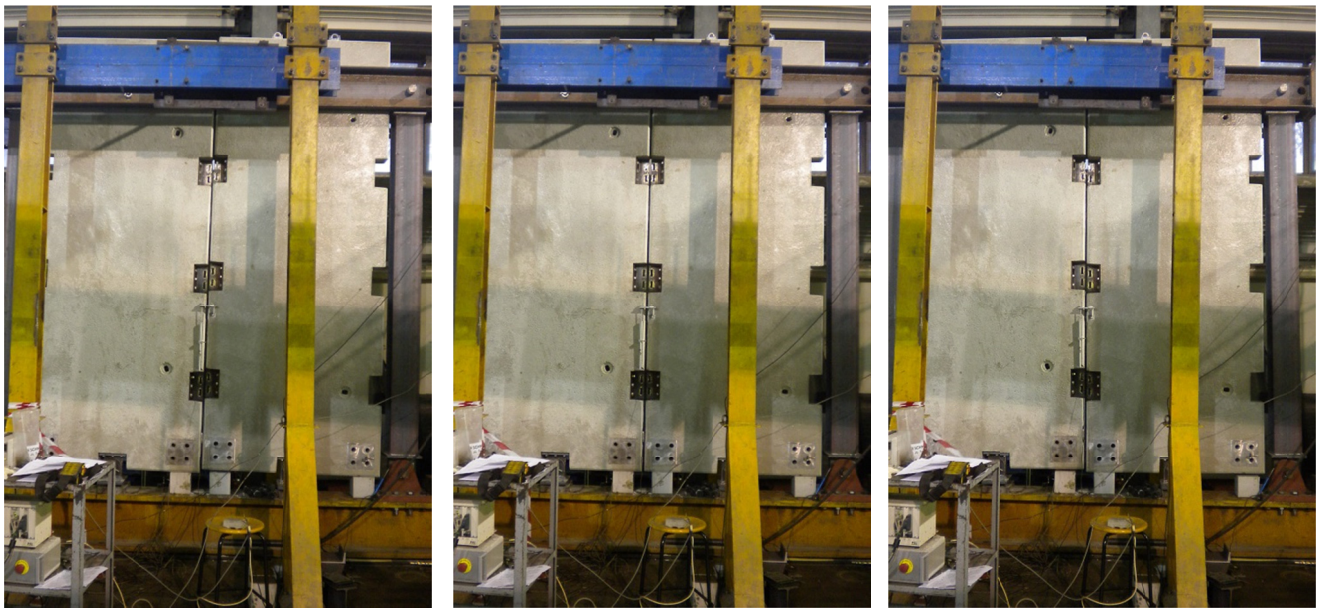

2% drift pulling 0% drift 2% drift pushing

Figure 4.6 – Isostatic rocking configuration: deformed shape at maximum drift

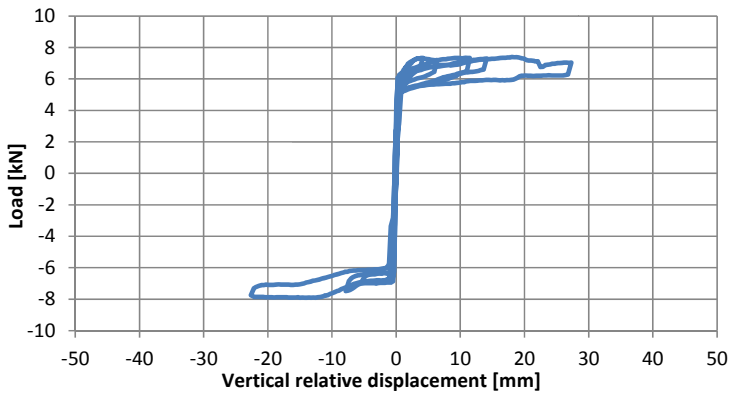

Figure 4.7 – Load vs displacement

4.2. Role of silicone sealant

Silicone sealant is a natural completion material of precast panels, since it is universally used to fill and close the joints in between panels and between panels and other components, only at the external side or at both external and internal. The main reason of its application is to provide waterproofing.

Silicone sealant is not a structural product, since its perfect receipt would allow to have a non-limited shear deformating material with null stiffness, in order to not damage even under large imposed drift and to not collaborate with the building at a structural level.

Many improvements in the field have been attained in this direction, but scarce information about the actual maximum loads and mean stiffness achievable is present in literature. In particular, Meunier *et al.* (2008) observed through experimental tests on single silicone strips that the material is characterised by a similar behaviour under shear and tension but a more rigid behaviour in compression.

In ASTP STP-1243 recommendations, Lacasse *et al.* (1995) treat the phenomenon of cyclic fatigue of silicone sealant strips subjected to tension.

In all the proposed isostatic configurations, relative sliding always occurs during an earthquake event, imposing a certain drift to long silicone sealant strips. An experimental campaign has been carried out at the Laboratorio Prove e Materiali of Politecnico di Milano in order to provide information about the influence of silicone sealant at structural level, regarding both local tests on small specimens and panel sub-assembly tests (Biondini *et al.* 2014a).

The tests are performed under different strain rates, but still quasi-static, with a much lower strain rate than those occurring during an earthquake for the proposed configurations.

Roland (2006) points out how the mechanical behaviour of rubber polymeric material is in general influenced by the strain rate to which is subjected, with both resistance and stiffness increasing with the strain rate.

4.2.1. Local tests

Several local tests on silicone strips (market available and diffused product) applied to small concrete blocks have been carried out, as listed in Table 4-1, regarding both monotonic and cyclic behaviour. The specimens are made with three concrete blocks, to which four silicone strips with different length and square cross-section sides are applied at the interface edges, as shown in Figure 4.8. In particular, three specimen geometries have been tested, namely with 10 mm side and 60 mm length, 15 mm side and 90 mm length and 20 mm side and 120 mm length, as reported in Figure 4.9.

Table 4-1 – Performed local tests on silicone sealant

TEST N.	TEST TYPE	SPECIMEN GEOMETRY		TEST ID	STRAIN RATE	AGE
		Side *s*	Length *L*			
		[mm]	[mm]		[%/s]	[days]
1	Cyclic	10	60	TO-C-10-60-F-1	0.025	105
2				TO-C-10-60-F-2	0.025	116
3		10	90	TO-C-10-90-F-1	0.025	25
4				TO-C-10-90-F-2	0.025	10
5		15	90	TO-C-15-90-F-1	0.017	5
6				TO-C-15-90-F-2	0.017	10
7		20	120	TO-C-20-120-F-1	0.013	116
8				TO-C-20-120-F-2	0.013	117
9	Monotonic	10	60	TO-M-10-60-F-1	0.025	67
10				TO-M-10-60-F-2	0.025	67
11				TO-M-10-60-S-1	0.003	5
12				TO-M-10-60-S-2	0.003	5
13			90	TO-M-10-90-S-1	0.003	12
14				TO-M-10-90-S-2	0.003	12
15				TO-M-10-90-F-1	0.025	34
16				TO-M-10-90-F-2	0.025	6
17		15	90	TO-M-15-90-S-1	0.002	46
18				TO-M-15-90-S-2	0.002	12
19				TO-M-15-90-F-1	0.017	26
20				TO-M-15-90-F-2	0.017	26
21		20	120	TO-M-20-120-S-1	0.001	46
22				TO-M-20-120-S-2	0.001	46
23				TO-M-20-120-S-3	0.001	46
24				TO-M-20-120-F-1	0.013	26
25				TO-M-20-120-F-2	0.013	26

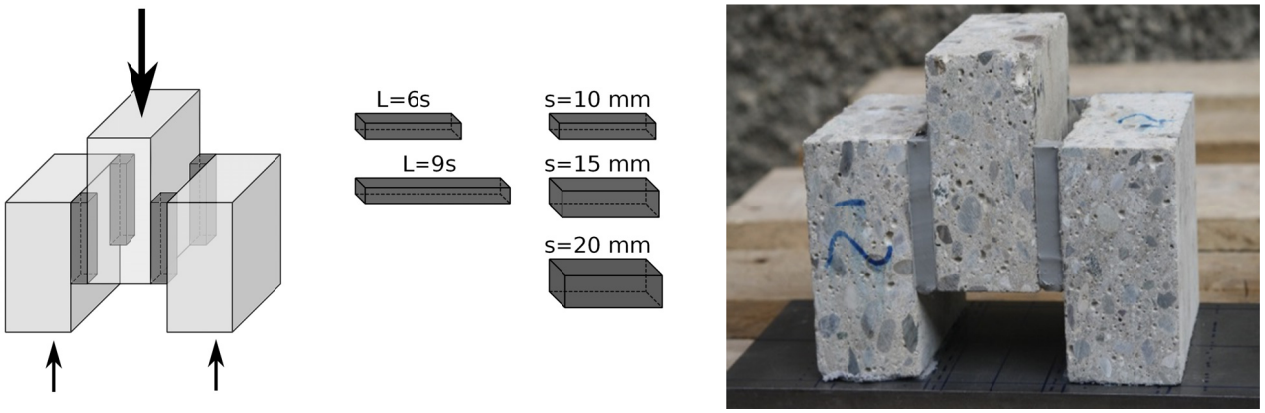

(a) (b)

Figure 4.8 – Test specimen: (a) concept and (b) picture of assembled specimen

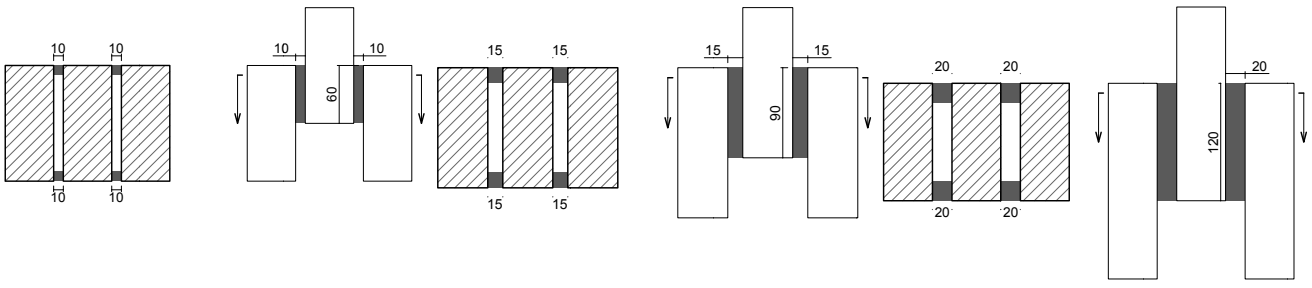

(a) (b) (c)

Figure 4.9 – Tested specimen geometries: (a) specimen 1, (b) specimen 2 and (c) specimen 3

Since the results show a large scatter, as expected from a material that is not subjected to severe production monitoring process, the considerations that can be deduced from the experimental campaign have general and indicative value. The monotonic behaviour, resumed in Figure 4.10 for larger speed, displays a very large displacement capacity of silicone, with an elastic behaviour up to about 50%~80% of drift, after which inclined struts form together with out-of-plane deformation, entering a pseudo-plastic branch. Monotonic and cyclic experimental results are resumed in Figure 4.11 for the three different specimen geometries.

The shear deformation γ and stress τ are defined as follows, with reference to the specimen geometries and an applied shear load V:

$$\gamma = \frac{d}{s} \tag{4.1}$$

$$\tau = \frac{V}{4sL} \tag{4.2}$$

Failure occurs between 150% and 300% of drift according to two observed mechanisms: for low speed tests, failure occurs at mid-span of the interface with tensile failure of the inclined struts, and for larger speed tests a combined tensile failure at mid-span and detachment from the concrete support is noticed, according to sliding surfaces that form at large drifts, as shown in Figure 4.12. The cyclic behaviour is in general more brittle, with the attainment of early failure in terms of ultimate drift. A large pinching effect is noticed, as typical for pure shear behaviour.

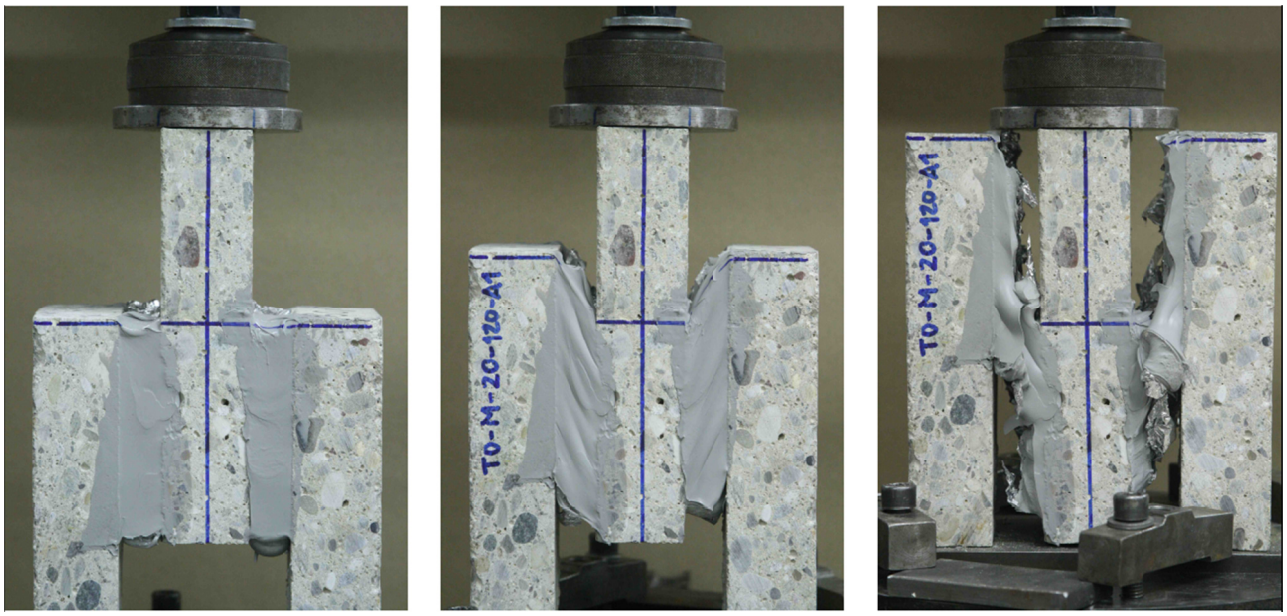

(a) (b) (c)

Figure 4.10 – Monotonic behaviour (larger speed): (a) undeformed position, (b) 200% shear deformation, (c) failure

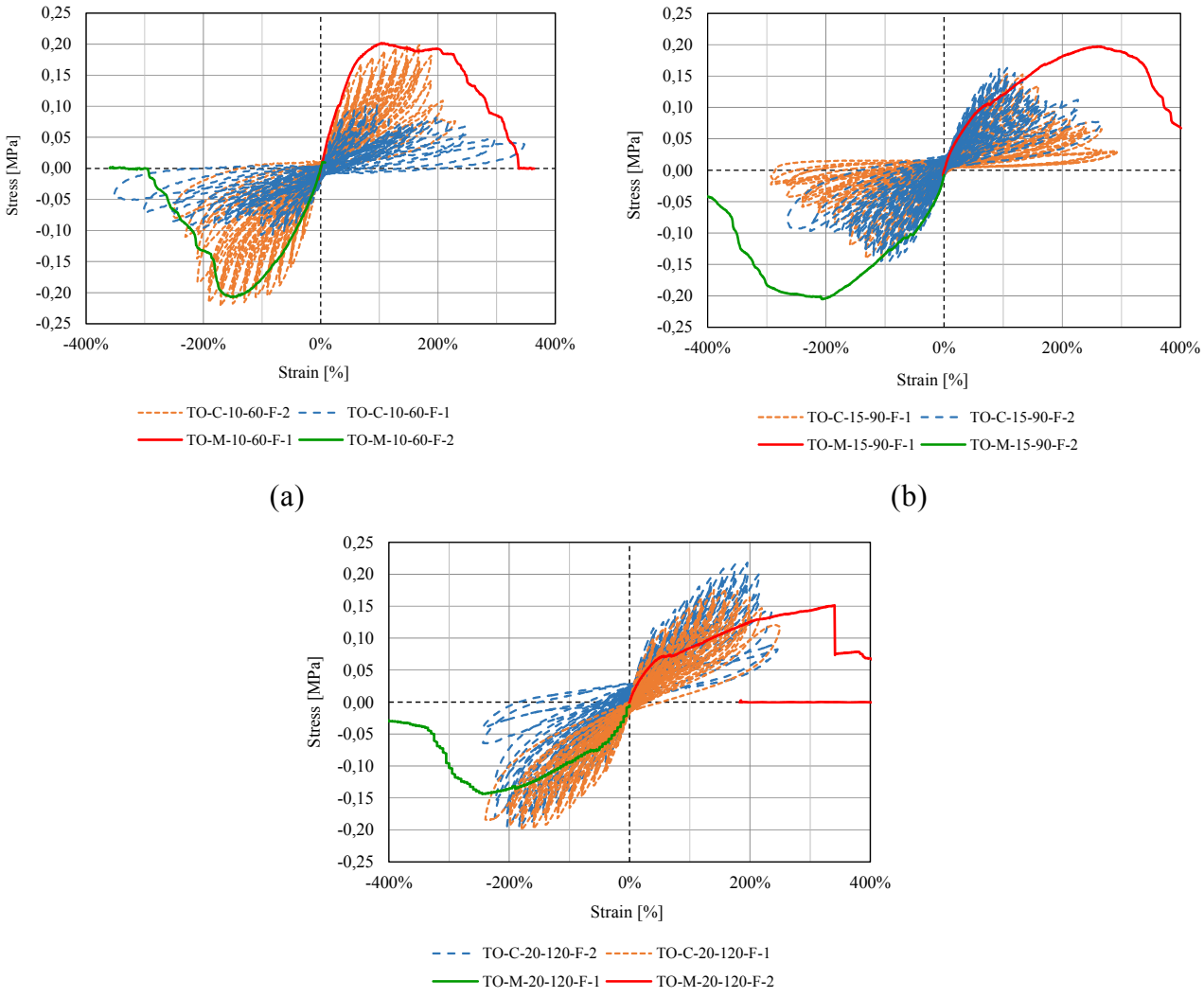

Figure 4.11 – Experimental monotonic and cyclic stress-strain relationship for (a) specimens 1, (b) specimens 2 and (c) specimens 3

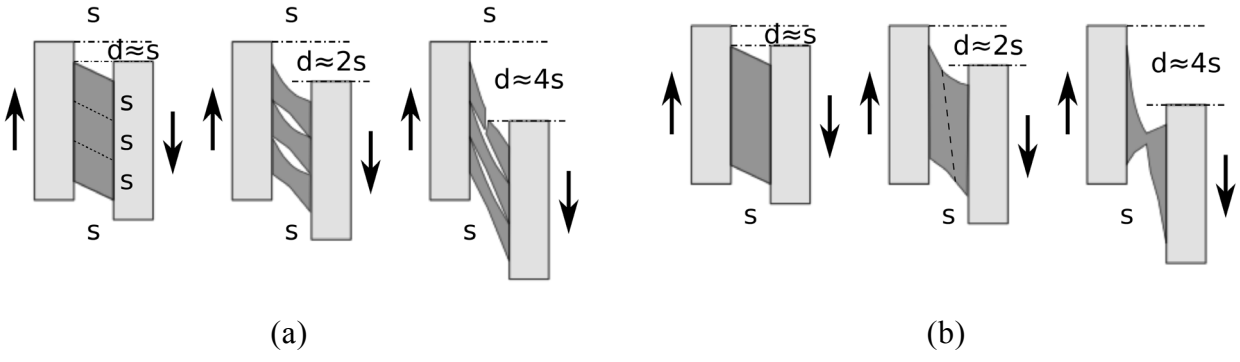

Figure 4.12 – Evolution of failure mechanisms for (a) low speed tests, with formation of inclined struts and failure at mid-span and (b) larger speed tests, with formation of sliding surfaces and combined failure at support and mid-span

All tests have been performed under a strain rate that varies from 0,01 to 0,025 s^{-1}, range corresponding to quasi-static actions. However, the comparison of the obtained results suggests that silicone sealant behaviour has a dependency on the strain rate, in particular reducing its maximum strain according to a negative logarithmic law, enlarging its maximum stress according to a positive logarithmic law and linearly enlarging its apparent shear modulus, as shown in Figure 4.13. Therefore, in case of much larger strain rate, as typical during seismic events, the obtained results are only indicative. Further experimentation with very large strain rates have to be performed, in order to cover this range, too.

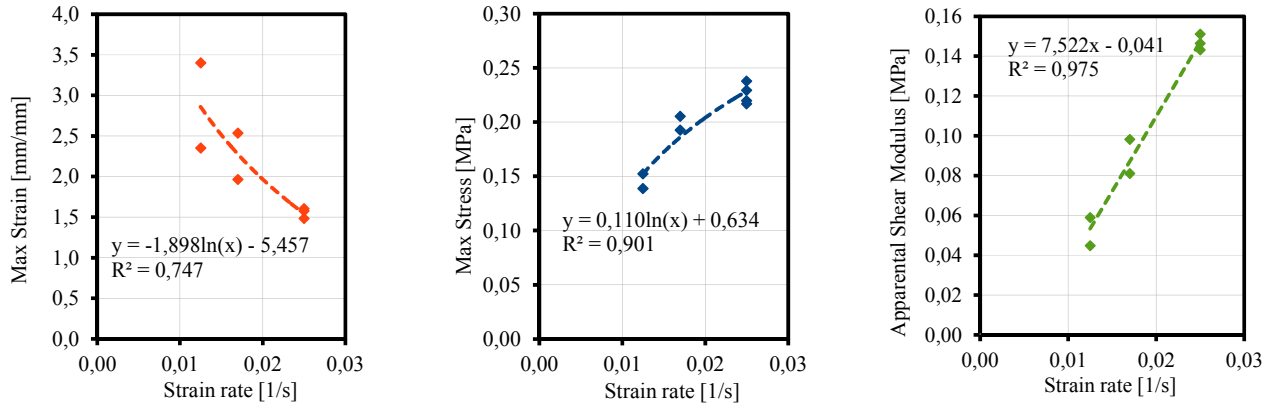

(a) (b) (c)

Figure 4.13 – Distribution of (a) maximum strain, (b) maximum stress and (c) apparental shear modulus with different strain rate and tendency curves

4.2.2. Sub-assembly test

A single sub-assembly test on silicone sealant has been performed on the pendulum connection arrangement. Silicone sealant has been placed at both sides of the panel interface along the contact lines with the exception of the upper, in which silicone has not been inserted because of the presence of the beam. Each silicone section is about 10/15 mm by 10/15 mm, depending on natural imperfections in panel position and silicone depth. The maturation period has been of 12 days.

The test is cyclic, performed in displacement control. Single cycles have been performed with the following amplitudes, in accordance with cyclic protocol B used for particular tests with modified amplitudes of 6 mm; 11 mm; 22 mm; 42 and 85 mm, corresponding roughly to 0,2; 0,4; 0,8; 1,6; 3,2 % of drift. Such displacement steps have been derived from the corresponding steps of the cyclic tests with cyclic protocol B on local specimens of silicone, assuming a rigid body motion of the panels. The cycle frequency of the actuator is controlled in such a way to represent the fast speed of the local tests, maintained constant during the whole test. Figure 4.14 shows the load vs vertical relative displacement diagram. The behaviour is stiffness degradating, with a soft initial branch with low stiffness of about 0,2 kN/mm and a progressive damage that got accentuated at the last displacement step cycles. The hysteresis shows a large pinching, as typical for shear behaviour. If considering the combination of very low stiffness and poor cyclic shape, the dissipation of energy attained is negligible with respect to that potentially dissipated by bearing structural members (even larger with dissipative

connections). The behaviour observed is similar to what found during the local tests. As shown in Figure 4.15, failure occurred for combined support and mid-span detachment after the formation of inclined struts and out-of-plane deformation.

Plotting the results in terms of stress vs strain, it is possible to note a good correspondence of the obtained behaviour with the previous test results (Figure 4.16).

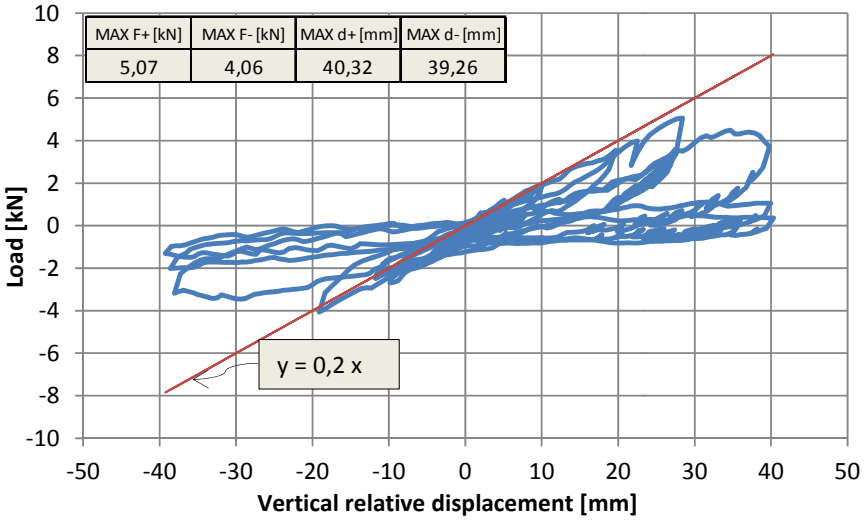

Figure 4.14 – Load vs displacement

(a) (b)

Figure 4.15 – Silicone sealant under large deformation: (a) formation of inclined struts and out of plane deformation, (b) failure for combined support and mid-span detachment

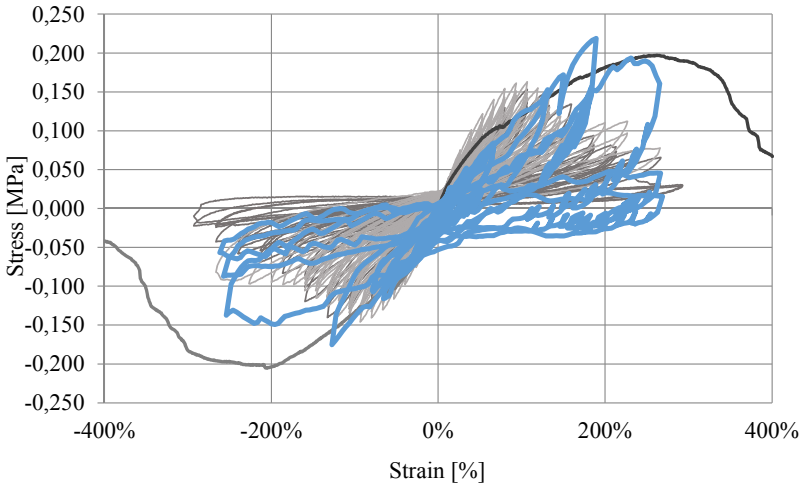

Figure 4.16 – Comparison of results

4.2.3. Design recommendations

The presence of silicone sealant can influence the serviceability limit state and increase the load on the panel connections. It is not suitable to sustain large structure drifts, tipically associated with ultimate limit state, since it tends to failure for shear strain larger than 200%. Its stiffening contribution is, however, limited and not reliable, since the mechanical characteristics of the product may largely vary. Therefore, it is suggested to consider the effect of the presence of silicone sealant only in those cases in which it is on the unsafe side, like for the calculation of actions on the panel connections. Its stiffening contribution is suggested to be disregarded when considering the possible beneficial effect on the seismic behaviour of the whole structure. Silicone sealant can reach a tangential upper bound stress τ_s up to 0,25 MPa, with an average tangential Young modulus G_s of about 0,25 MPa. Its behaviour is elastic up to about 100÷150% of strain with a pseudo-plateau up to about 200% of strain, after which the resistance rapidly decreases.

4.3. Dissipative systems with FBDs

The recesses in the panels have been designed in order to accommodate the FBDs made with symmetric T-shaped profiles and class 10.9 M14 bolts provided with Belleville washers. The support profile-to-panel connection is bolted, with six 8.8 M16 bolts that connect the profile with a steel counter-plate provided with bushes and with a bull horn bent Φ20 B450C rebar welded in its vertical portion to the counter-plate. The tests listed in Table 4-2 have been carried out with the aim to investigate the cyclic behaviour of all components in a real application, observing the general response of the sub-assembly and the evolution of the behaviour with a progressive number of connections per side, up to three. The protocol displacement amplitudes have been amplified by the mechanical aspect ratio of the panels.

Table 4-2 – Performed sub-assembly tests with FBDs

DEVICE	DEVICES PER SIDE	TEST TYPE	LOAD PROTOCOL	BOLTS	TIGHTENING TORQUE [Nm]	WASHER
FBD	1	CYCLIC	B	M14 10.9	190	BELLEVILLE
	1		E	M14 10.9	190	BELLEVILLE
	2		B	M14 10.9	190	BELLEVILLE
	2		E	M14 10.9	190	BELLEVILLE
	3		B	M14 10.9	190	BELLEVILLE
	3		E	M14 10.9	190	BELLEVILLE

4.3.1. Pendulum arrangement: three FBDs

The deformed shape of the specimen provided with three FBDs per side is shown in Figure 4.17, with a particular view of the central device in Figure 4.18. The results of the test performed with cyclic protocol B are reported in the diagram of Figure 4.19 with reference to the horizontal applied load and the vertical relative displacement directly measured between the panels, showing a very similar behaviour with respect to the particular performed tests. A very large elastic stiffness of about 120 kN/mm is recorded, which is as expected three times the stiffness value of a single device. The first cycle attains large loads, that get attenuated already at the second cycle, showing afterwards a large cyclic stability. If looking at the general response of the sub-assembly, however, as shown in Figure 4.20, it is possible to note that a largely reduced initial stiffness of about 1,5 kN/mm is obtained for a short branch, after which the stiffness increases to about 25 kN/mm. The elasticity of the loading frame and the unavoidable tolerances of all components are the cause of this reduction of elastic stiffness, that may relevantly affect energy dissipation, especially for low-displacement cycles, since the pinching branch is constant. Figure 4.21 shows that the internal base vertical transducers have a linear behaviour, while the external show the formation of a gap, which is due to a quasi-rigid body rotation of the two panels as a whole, before sliding occurs.

The results from the test carried out with cyclic protocol E are illustrated in Figure 4.22. As previously observed, largely stable cycles follow the first cycle with slight hardening behaviour.

In both tests, the mean slip load threshold is less that the predicted according to the previously presented design methodology, which is 90 kN. The design value, equal to 60 kN, seems to be over-predicted if compared with the experimental results. The reason could be found in a non-perfect vertical alignment of the support profiles, provided with an out-of-plane horizontal tolerance as low as 1 mm, which could have resulted in a bad tightening operation for one or more devices. The same phenomenon has been later observed within the full scale prototype tests. The maximum load attained is lower than the expected maximum, calculated equal to 144 kN.

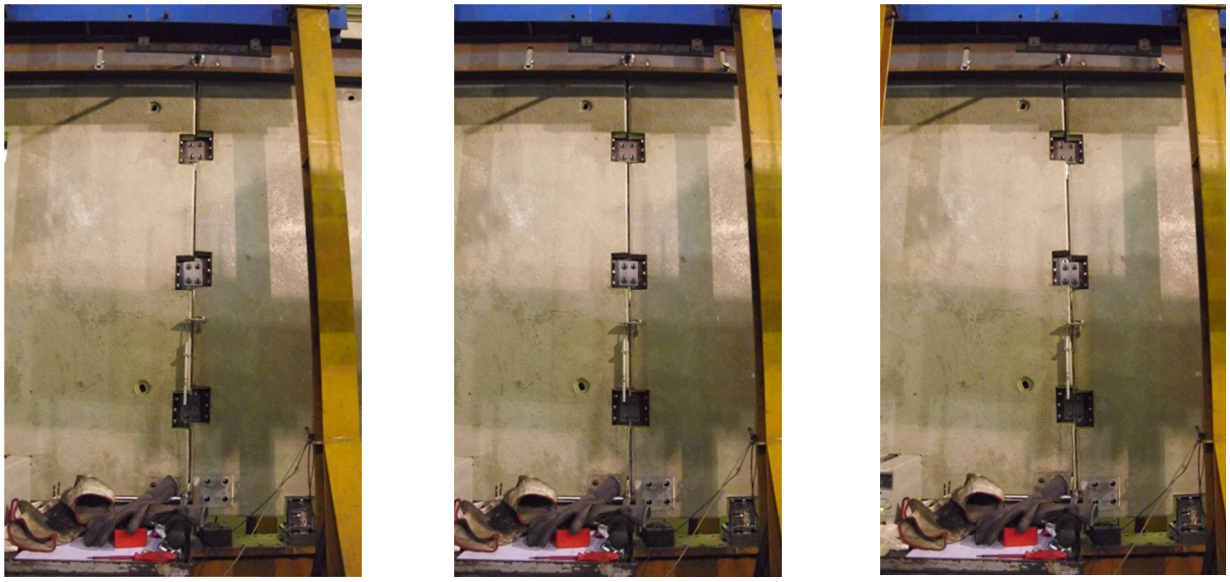

3,2 % drift pulling 0 % drift 3,2 % drift pushing

Figure 4.17 – Specimen with three FBDs in a row: deformed shape at maximum drift

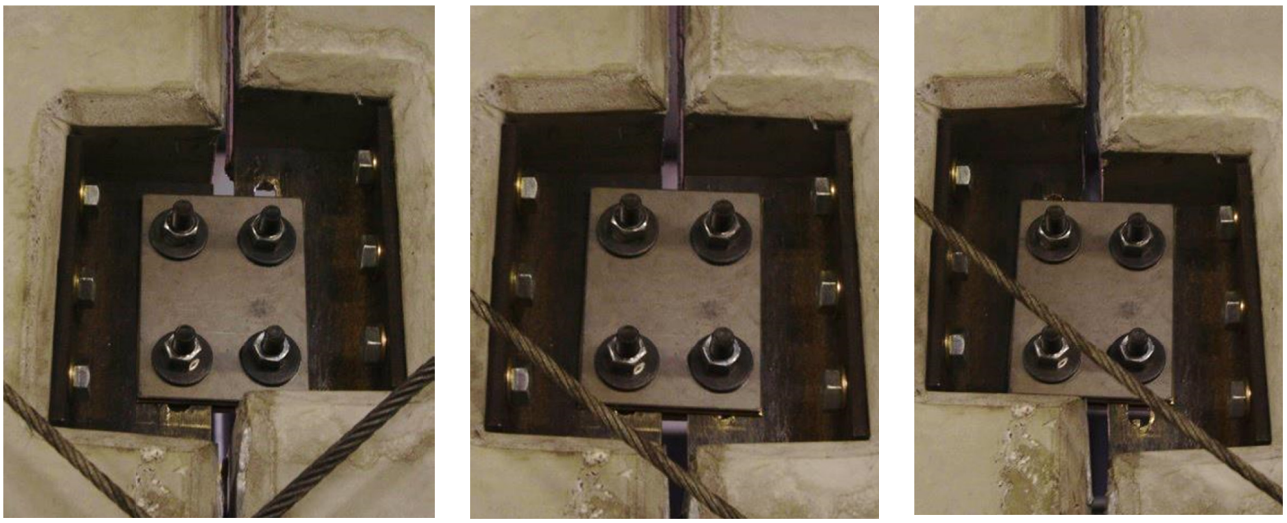

3,2 % drift pulling 0 % drift 3,2 % drift pushing

Figure 4.18 – Particular view of the central FBD

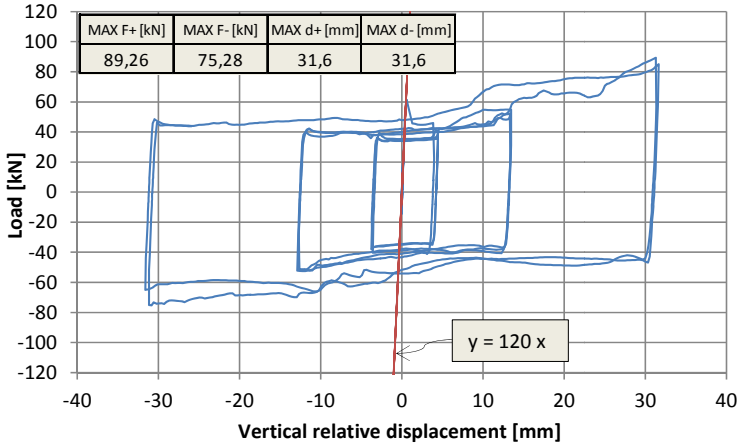

Figure 4.19 – Load vs vertical relative displacement

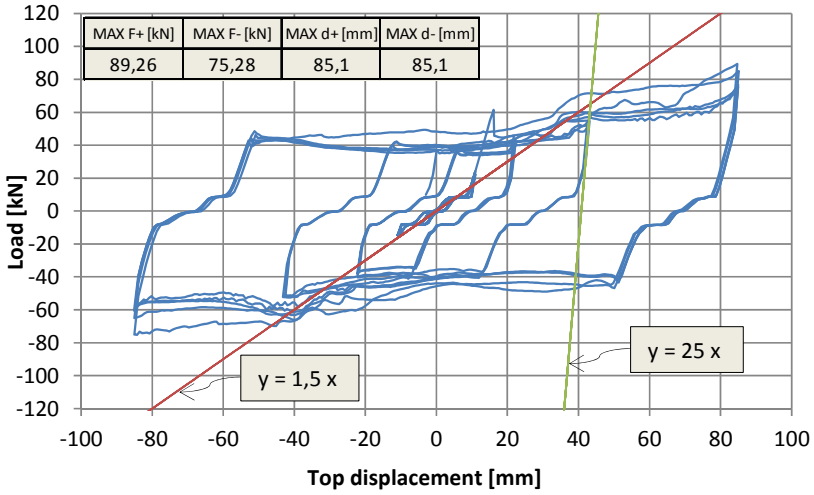

Figure 4.20 – Load vs top displacement

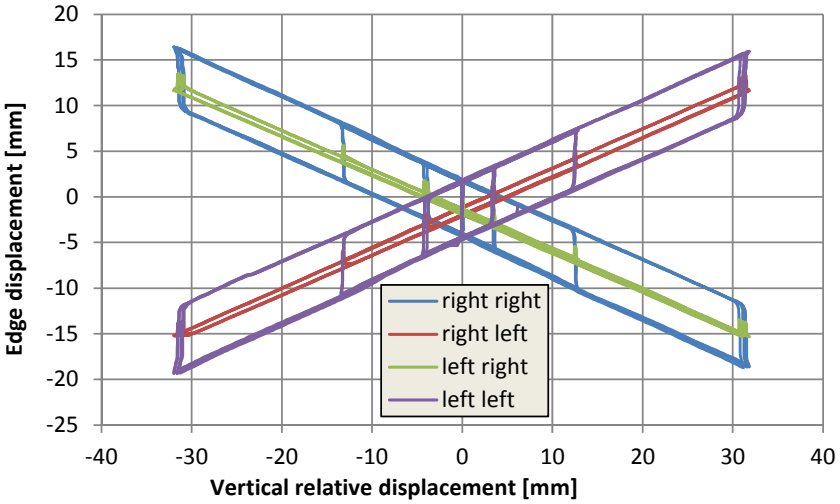

Figure 4.21 – Panel edge vertical displacement vs vertical relative displacement

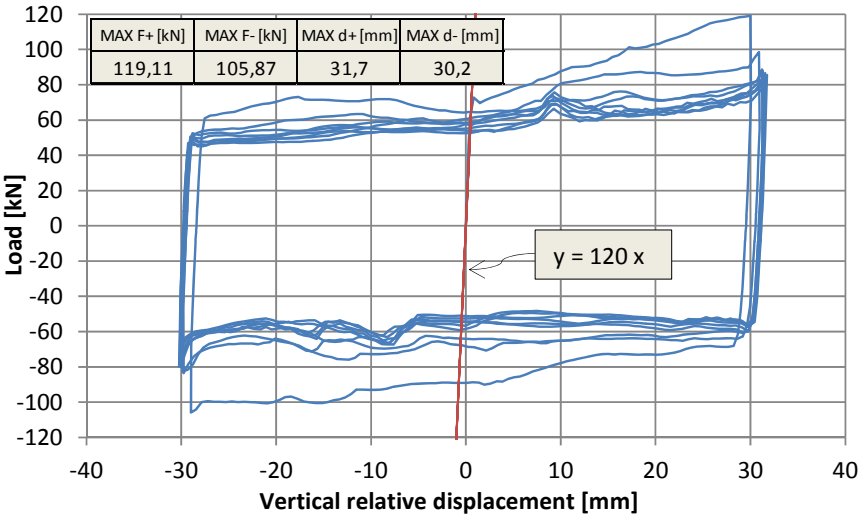

Figure 4.22 – Load vs vertical relative displacement

4.3.2. Pendulum arrangement: two FBDs

The cyclic response for the equivalent cyclic protocol B is shown in Figure 4.23 for the specimen with two connections positioned at the top and bottom recesses and in Figure 4.24 for the test with equivalent cyclic protocol E.

In both tests, slip load threshold is in between the predicted mean and the design values, 60 and 40 kN, respectively. The maximum load attained, equal to 100 kN, is very close but slightly larger than the expected maximum, equal to 96 kN.

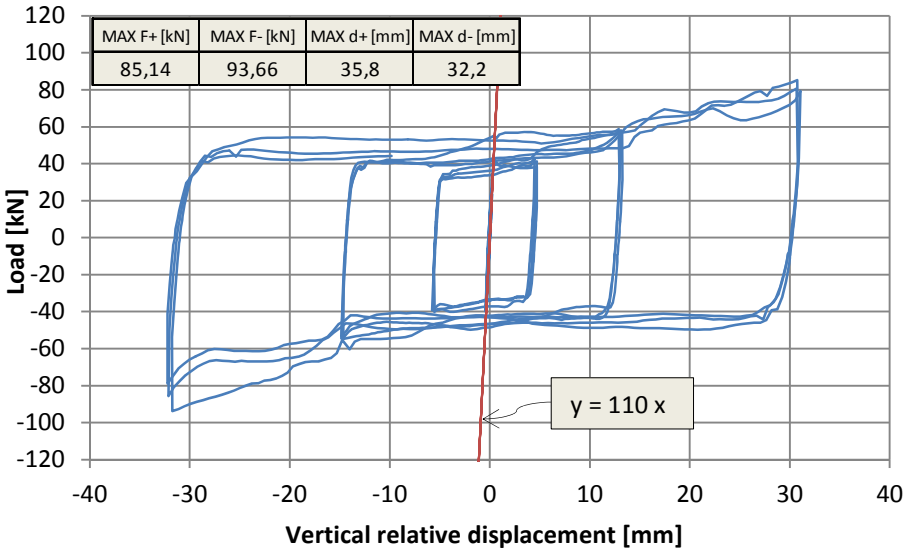

Figure 4.23 – Load vs vertical relative displacement

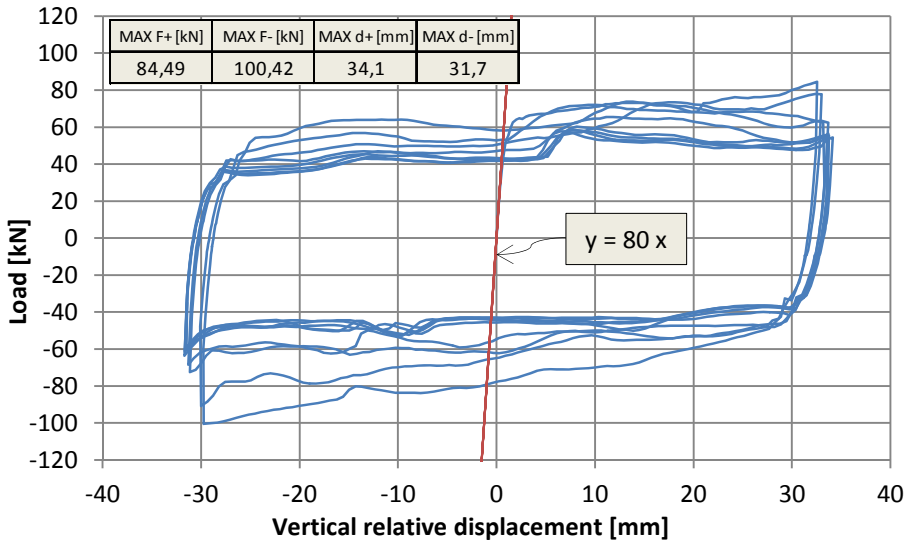

Figure 4.24 – Load vs vertical relative displacement

4.3.3. Pendulum arrangement: one FBD

The cyclic response for the equivalent cyclic protocol B is shown in Figure 4.25 for the specimen with one connections positioned at the central recess and in Figure 4.26 for the test with equivalent cyclic protocol E.

In both tests, slip load threshold is in between the predicted mean and the design values, 30 and 20 kN, respectively. The maximum predicted load, calculated as 48 kN, is equal to that experimentally attained.

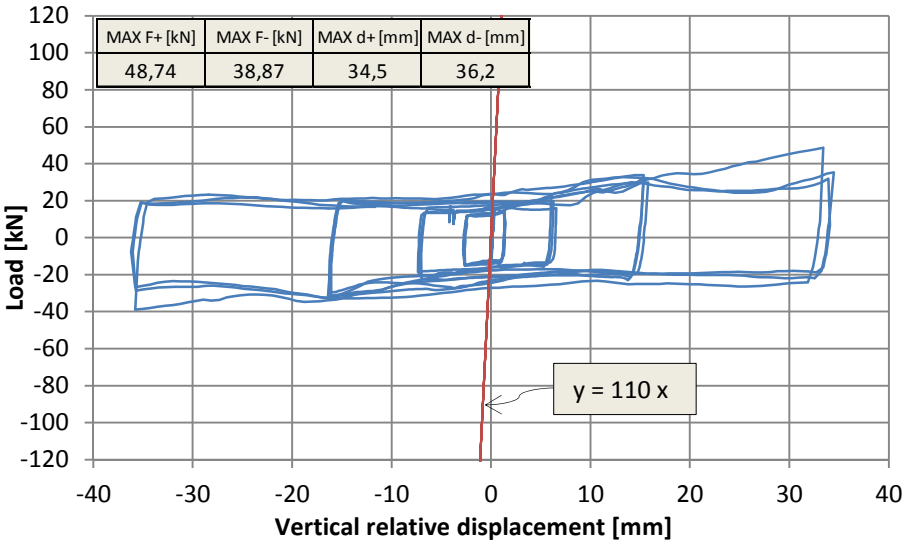

Figure 4.25 – Load vs vertical relative displacement

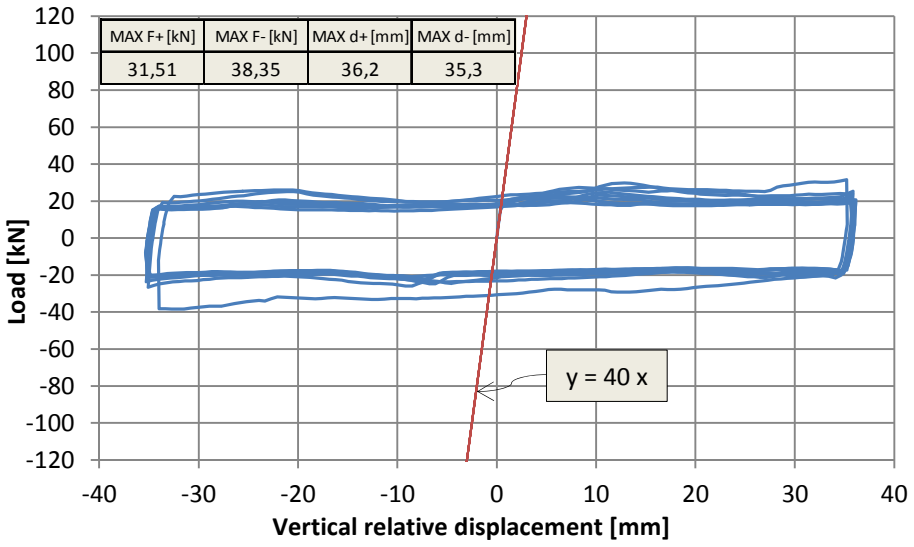

Figure 4.26 – Load vs vertical relative displacement

4.4. Dissipative systems with MSDs

Also MSDs have been mounted on the panels and tested. Hourglass-shaped beam plates with horizontal slots have been mounted in inverted configuration on UPN support profiles provided with threaded holes. Figure 4.27 shows a picture of the connection. The results of the test with a single device placed at the bottom panel recesses with adapted cyclic protocol B are summarised in the load vs displacement diagram of Figure 4.28, together with a further test performing a single cycle with the same specimen and new plates at ± 24 mm drift. An elastic local stiffness of the device of about 10 kN/mm has been obtained, with a cyclic behaviour in accordance with the results of the particular tests, very suitable for dissipation of energy and with a well-defined and repeated back-bone curve. Failure has been reached at the first negative semi-cycle with maximum displacement amplitude, due to the rupture of the beam edges, as noticeable from Figure 4.29.

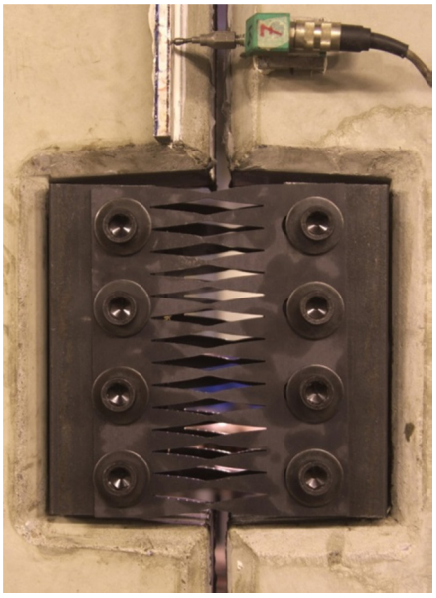

Figure 4.27 – MSD with hourglass shaped beams and horizontal slots

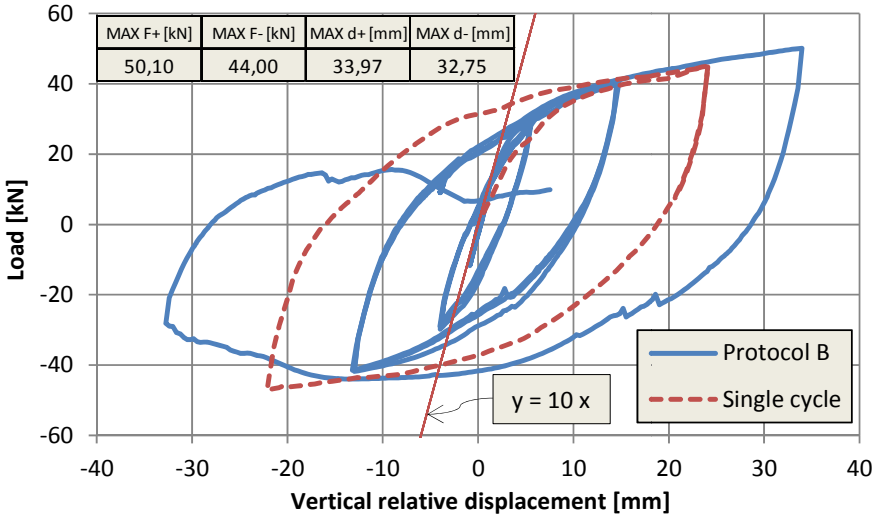

Figure 4.28 – Load vs vertical relative displacement

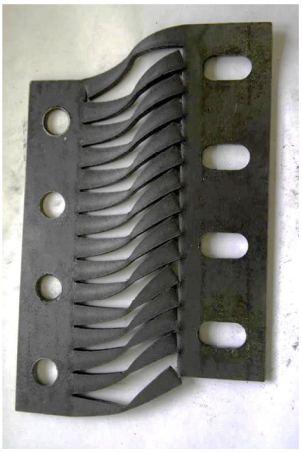

Figure 4.29 – MSD plate after the test

4.5. Design recommendations

Design recommendations are provided in the following for panel structural sub-assembly systems, both for what concerns pure isostatic arrangements and added contribution of panel-to-panel lateral forces, arising from silicone sealant and dissipative connections. Information on the cantilever isostatic system for both vertical and horizontal panels is available in Dal Lago & Ragozzini (2010) and in Dal Lago *et al.* (2012b).

4.5.1. Isostatic systems

The equilibrium equations that are presented in the following for pendulum, rocking and swaying panel connection arrangements are referred to the contemporary presence of a tri-axial seismic load and the gravity load. In fact, since the vertical load on the panel is supposed to only depend on its own weight, without live load contributions, the vertical component of the acceleration plays an important influence.

It is assumed that the seismic actions in the three axes are equal to:

$$F_{wx} = \psi_x S_x m$$
$$F_{wy} = \psi_y S_y m \qquad (4.3)$$
$$F_{wz} = \psi_z S_z m$$

where ψ_x, ψ_y and ψ_z are the contemporaneity factors, that can be considered on the base of the 30% contemporaneity rule in accordance with Eurocode 1 (EN 1991-1), S_x, S_y and S_z are the accelerations on the single panel based on its mass m. The seismic accelerations on the member can be evaluated with reference to standard calculations, as indicated in clause 2.4.5.

Correction factors Φ_2 are introduced in order to take into account the 2nd order effects with equilibrium in displaced configuration, as schematically illustrated in Figure 4.30 for a truss beam with bearing connection at the base (pendulum and rocking arrangements) and at a certain height (swaying arrangement).

The 2nd order correction factor depends on the drift imposed to the panel by the structure. It can be evaluated directly on the base of the structure displacements according to the following:

$$\Phi_2 = \delta \frac{H}{2h^2} \qquad \text{for pendulum and rocking arrangements}$$
$$\Phi_2 = \delta \frac{0{,}5H - h_1}{(h_2 - h_1)^2} \qquad \text{for swaying arrangement} \tag{4.4}$$

where δ is the horizontal relative displacement between the top and base connections, H is the gross height of the panel, h is the height of the top hinge, h_1 and h_2 are the heights of the base and top connection, respectively. The displacement δ can be considered on the safe side as an ultimate limit state drift at one direction at a time. 5% of the inter-storey height is suggested as a reference value. The imposed displacement in the secondary horizontal direction(s) is suggested to be considered equal to 1% of the inter-storey height.

Since building drift, that imposes the panel position, and horizontal seismic acceleration directions can be opposite, the horizontal load increment due to 2nd order effects is considered always positive.

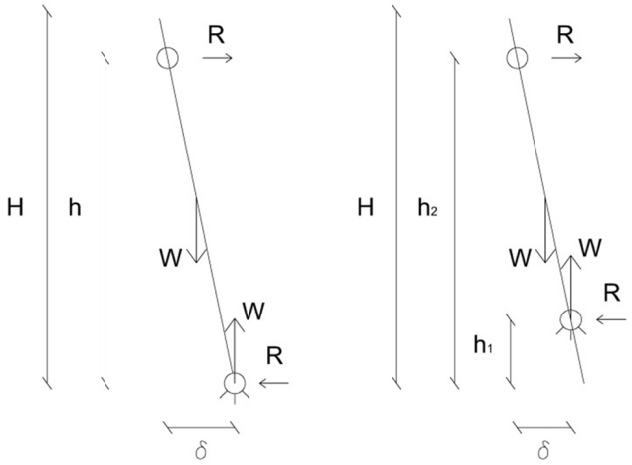

Figure 4.30 – Displaced equilibrium of a truss beam with bearing connection at its base and at a height equal to h_1

4.5.1.1. Pendulum arrangement

The equilibrium equations for the pendulum arrangements lead to the reactions illustrated in the following in the base and top connections along the three axes, with reference to Figure 4.31. The vertical reaction of the top connection is null if a small rotation around the x axis is allowed. Provided this, possible friction effects do not lead to vertical-wise force deviation.

The base joint shall be protected from accidental object introduction, since the rotation around the base joint shall not be obstructed for a correct pendulum mechanism. The length of the top connection vertical slider can be evaluated on the base of mounting tolerances and slow imposed deformation, such as beam gravity deflection or panel thermal strains.

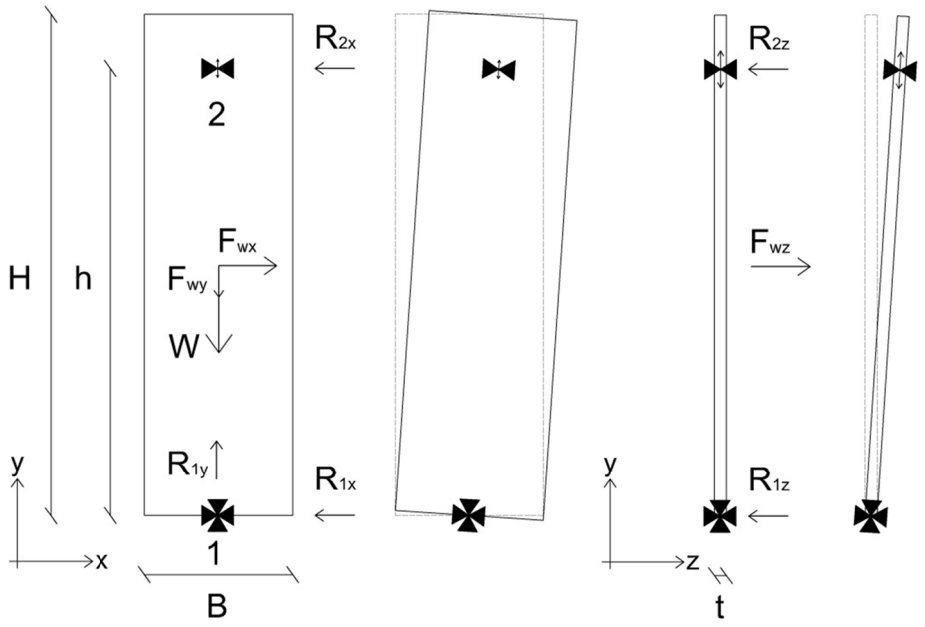

Figure 4.31 – In-plane and out-of-plane equilibrium of a pendulum panel

$$
\begin{aligned}
R_{1x} &= F_{wx}\left(1-\frac{H}{2h}\right)+(W+F_{wy})\Phi_{2x} \\
R_{1y} &= W+F_{wy} \\
R_{1z} &= F_{wz}\left(1-\frac{H}{2h}\right)+(W+F_{wy})\Phi_{2z}
\end{aligned}
\tag{4.5}
$$

$$
\begin{aligned}
R_{2x} &= F_{wx}\frac{H}{2h}+(W+F_{wy})\Phi_{2x} \\
R_{2y} &= 0 \\
R_{2z} &= F_{wz}\frac{H}{2h}+(W+F_{wy})\Phi_{2z}
\end{aligned}
\tag{4.6}
$$

4.5.1.2. Rocking arrangement

The equilibrium equations for the pendulum arrangements lead to the following reactions in the base and top connections in the three axes, with reference to Figure 4.32. The equilibrium is performed on the safe side on a displaced configuration. In-plane 2nd order effects are beneficial, and therefore they have not been considered, on the safe side. The *n* top connections shall slide in the vertical direction and are contemporarily subjected to an in-plane and an out-of-plane force. Possible friction effects can increase the actions on the connection. An experimental characterisation of the friction coefficients for shear action μ_{shear} and for axial load μ_{axial} is suggested, also to prove the avoidance of tangling of the slider (also known as

mechanical welding). Low-friction surface treatments are also suggested for the slider component.

The panel edge should be provided with an embedded steel angle in order to protect the corner from spalling. The length of the top connection vertical slider depends on the maximum structure expected drift. The top connections are suggested to be placed in a low position into the vertical slot, since imposed drift impose panel lift only. Also slow vertical displacements shall be accommodated.

The rocking configuration is often realised with panel simply supported on the foundation. Mechanical out-of-plane stoppers (i.e. steel angles) are suggested to be used, in order to avoid out-of-plane displacements that may occur due to the seismic component in the *z* direction when the panel is lifted. Mechanical in-plane stoppers (i.e. inverted T steel profiles) are suggested to be inserted at the panels interfaces at their base if the friction is not enough to avoid in-plane sliding. The following formula can be used to check this condition:

$$R_{1x} < \min(R_{1y})\mu \tag{4.7}$$

where μ is the friction coefficient for the two contact surfaces.

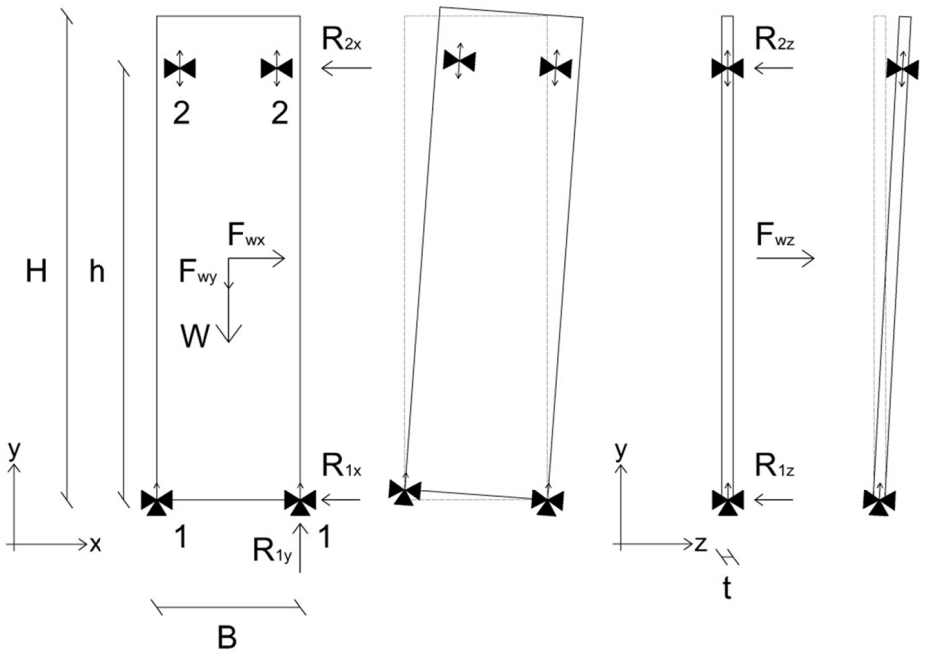

Figure 4.32 – In-plane and out-of-plane equilibrium of a rocking panel

$$R_{1x} = F_{wx}\left(1-\frac{H}{2h}\right)+W\frac{B}{2h}$$

$$R_{1y} = W \pm F_{wy} \tag{4.8}$$

$$R_{1z} = F_{wz}\left(1-\frac{H}{2h}\right)+(W+F_{wy})\Phi_{2z}$$

$$R_{2x} = \frac{1}{n}(F_{wx}\frac{H}{2h} + W\frac{B}{2h})$$
$$R_{2y} = \frac{1}{n}(R_{2x}\mu_{shear} + R_{2z}\mu_{axial}) \quad (4.9)$$
$$R_{2z} = \frac{1}{n}(F_{wz}\frac{H}{2h} + (W + F_{wy})\Phi_{2z})$$

4.5.1.3. Swaying arrangement

The equilibrium equations for the pendulum arrangements lead to the following reactions in the base and top connections in the three axes, with reference to Figure 4.33. *n* indicates the number of top connections, including both shear and tie-back connections. The base mono-directional supports shall slide horizontally during motion, but are subjected to a contemporary strong vertical action, coming from the own weight of the panel and the vertical acceleration. Low-friction surface treatments are therefore suggested for the sliding surfaces. The length of the top connection vertical slider can be evaluated on the base of mounting tolerances and slow imposed deformation, such as panel thermal strains. The equilibrium configuration of the panel is calculated under the assumption that lifting, which is not restrained, does not occur. The following formula can be used to check this condition:

$$\frac{F_{wx}}{b}(0{,}5H - h_1) < \frac{W - F_{wy}}{2} \quad (4.10)$$

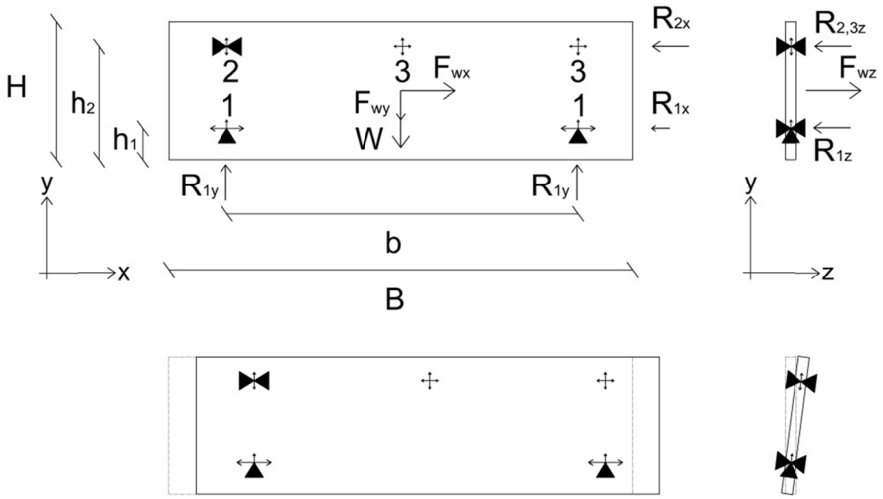

Figure 4.33 – In-plane and out-of-plane equilibrium of a swaying panel

$$
\begin{aligned}
R_{1x} &= R_{1y}\mu \\
R_{1y} &= \frac{W + F_{wy}}{2} + \frac{F_{wx}}{b}\left(0{,}5H - h_1\right) \\
R_{1z} &= \frac{F_{wz}}{2}\left(1 - 0{,}5\frac{H - h_1}{h_2 - h_1}\right) + (W + F_{wy})\Phi_{2z}
\end{aligned}
\tag{4.11}
$$

$$
\begin{aligned}
R_{2x} &= F_{wx} \\
R_{2,3y} &= 0 \\
R_{2,3z} &= \frac{F_{wz}}{n}\left(0{,}5\frac{H - h_1}{h_2 - h_1}\right) + (W + F_{wy})\Phi_{2z}
\end{aligned}
\tag{4.12}
$$

4.5.2. Addition of interface actions

The addition of interface forces in between the panels due to mechanical connecting devices or sealants leads to the introduction of additional forces in the panel bearing connections. These forces can be simply added to those arising in an isostatic configuration. Interface forces follow in general the displacement of the panels, and therefore do not increase 2nd order effects. The envelope of two conditions is considered to derive forces in the connections: the action of the maximum lateral forces F and the possible unbalance between two sides, leading to a difference in the modulus of the equivalent total load, that will be referred as ΔF. Instructions for the calculation of those two values are provided in the following with specific reference to FBDs, MSDs, FPDs and silicone sealant.

$$
\begin{aligned}
F &= n\psi_n(V + \Delta V) && \text{for FBDs} \\
F &= nV_u && \text{for MSDs and FPDs} \\
F &= \tau_u t_s H && \text{for silicone}
\end{aligned}
\tag{4.13}
$$

where $\psi_n = 1 - 0{,}1(n - 1) \geq 0{,}8$ is a contemporaneity factor that takes into account the presence of multiple (n) FBDs along a single interface and t_s indicates the gross width of the silicone strips.

$$
\begin{aligned}
\Delta F &= n\psi_n \frac{(V + \Delta V)}{2} && \text{for FBDs} \\
\Delta F &= 0 && \text{for MSDs and FPDs} \\
\Delta F &= \frac{\tau_u t_s H}{2} && \text{for silicone}
\end{aligned}
\tag{4.14}
$$

4.5.2.1. Pendulum arrangements

The presence of lateral forces leads to the following additional in-plane reactions, with reference to Figure 4.34, that are different for central and edge panels. The elastic stiffness of the connections are in series, and therefore an equivalent lateral stiffness can be calculated according to the following formula, considering pure shear deformation of the panel:

$$\frac{1}{K_{eq}} = \frac{1}{K_1} + \frac{1}{K_2} + \frac{h}{K_F B} + \frac{h}{GA^*} + \frac{b_s h}{G_s t_s H_s B} \qquad \text{for central panels}$$

$$\frac{1}{K_{eq}} = \frac{1}{K_1} + \frac{1}{K_2} + \frac{2h}{K_F B} + \frac{h}{GA^*} + \frac{2b_s h}{G_s t_s H_s B} \qquad \text{for edge panels} \tag{4.15}$$

where G_s is the tangential modulus of elasticity of silicone, b_s is the average width of the silicone joint, t_s is the width of the silicone section (generally, assuming square sections, equal to the width of the joint multiplyied by the layers, usually one or two) and H_s is the length of the silicone strip along the panel height (equal to the panel height if it is full-height sealed).

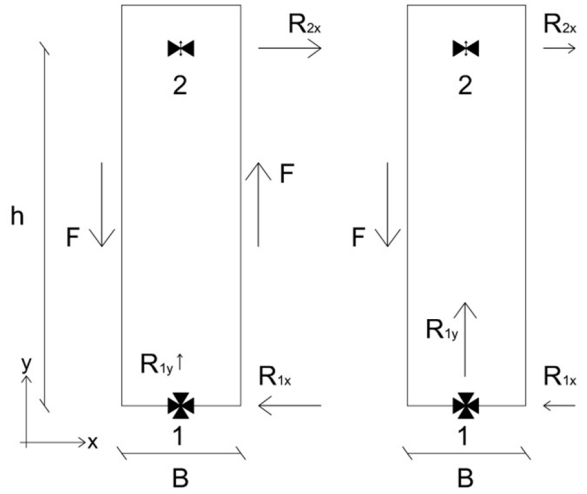

Figure 4.34 – In-plane equilibrium of a pendulum panel: contribution of interface forces on central and edge panels

$$R_{1x} = F\frac{B}{h} \qquad \text{for central panels} \tag{4.16}$$
$$R_{1y} = \Delta F$$

$$R_{1x} = F\frac{B}{2h} \qquad \text{for edge panels} \tag{4.17}$$
$$R_{1y} = F$$

$$R_{2x} = F\frac{B}{h} \qquad \text{for central panels} \tag{4.18}$$
$$R_{2,3y} = 0$$

$$R_{2x} = F\frac{B}{2h} \qquad \text{for edge panels} \qquad (4.19)$$
$$R_{2,3y} = 0$$

4.5.2.2. Rocking arrangements

The presence of lateral forces leads to the following additional in-plane reactions, with reference to Figure 4.35, that are different for central and edge panels only depending on the direction of the imposed in-plane displacement. In fact, if the displacement occurs in the force side direction, the panel rocks around that corner and the lateral force does not produce any incremental horizontal load, while if the displacement occurs in the force side opposite direction, its lever arm is exactly the same with respect to a central panel configuration. Thus, the calculation of forces in the edge panel connections is referred to that of the central panel. The elastic stiffness of the connections are in series, and therefore an equivalent lateral stiffness can be calculated according to the following formula, considering an undeformable base support and pure shear deformation for the panel:

$$\frac{1}{K_{eq}} = \frac{1}{K_2} + \frac{h}{K_F B} + \frac{h}{GA^*} + \frac{b_s h}{G_s t_s H_s B} \qquad \text{for all panels} \qquad (4.20)$$

Furthermore, large vertical actions, for instance induced by additional dissipative connections, may cause panel lifting, which shall be avoided if proper vertical tie-back connectors are not installed. The following formula can be used to check this condition:

$$R_{1y} < W \qquad (4.21)$$

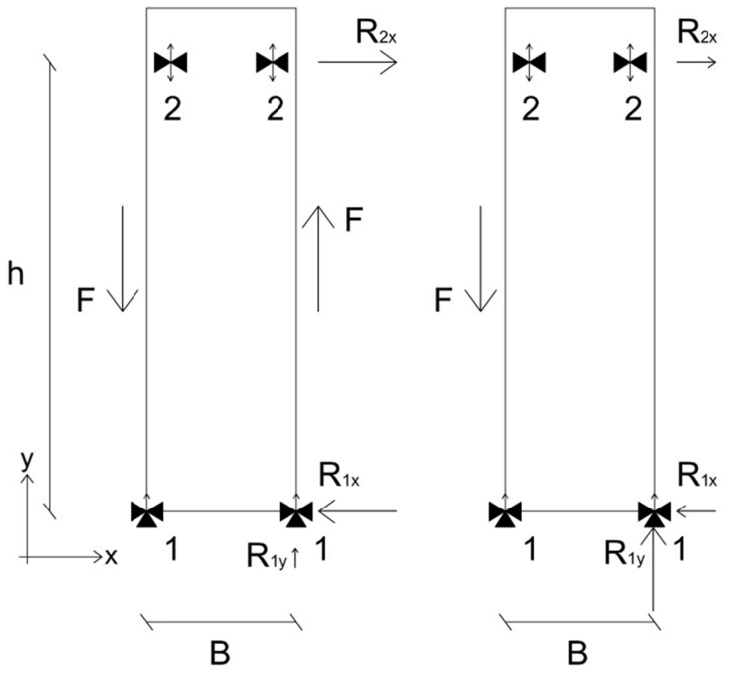

Figure 4.35 – In-plane equilibrium of a rocking panel: contribution of interface forces on central and edge panels

$$R_{1x} = F\frac{B}{h}$$
$$R_{1y} = \Delta F$$

for central panels (4.22)

$$R_{1x} = F\frac{B}{h}$$
$$R_{1y} = F$$

for edge panels (4.23)

$$R_{2x} = F\frac{B}{h}$$
$$R_{2,3y} = 0$$

for central panels (4.24)

$$R_{2x} = F\frac{B}{h}$$
$$R_{2,3y} = 0$$

for edge panels (4.25)

4.5.2.3. Swaying arrangements

The presence of lateral forces leads to the following additional in-plane reactions, with reference to Figure 4.36, that are different for central and edge panels. The horizontal elastic stiffness of the connections are in series, and therefore an equivalent lateral stiffness can be calculated according to the following formulae:

$$\frac{1}{K_{eq}} = \frac{1}{K_2} \quad \text{for central panels}$$
$$\frac{1}{K_{eq}} = \frac{1}{K_2} + \frac{1}{K_F} \quad \text{for all panels} \qquad (4.26)$$

$$R_{1x} = 0$$
$$R_{1y} = F\frac{H}{b}$$

for central panels (4.27)

$$R_{1x} = F\frac{B}{h}$$
$$R_{1y} = F\frac{H - h_1}{b}$$

for top panels (4.28)

$$R_{1x} = F\frac{B}{h}$$
$$R_{1y} = F\frac{H - h_2}{b}$$

for bottom panels (4.29)

$$R_{2x} = \Delta F$$
$$R_{2,3y} = 0$$

for central panels (4.30)

$$R_{2x} = F$$
$$R_{2,3y} = 0$$

for bottom and top panels (4.31)

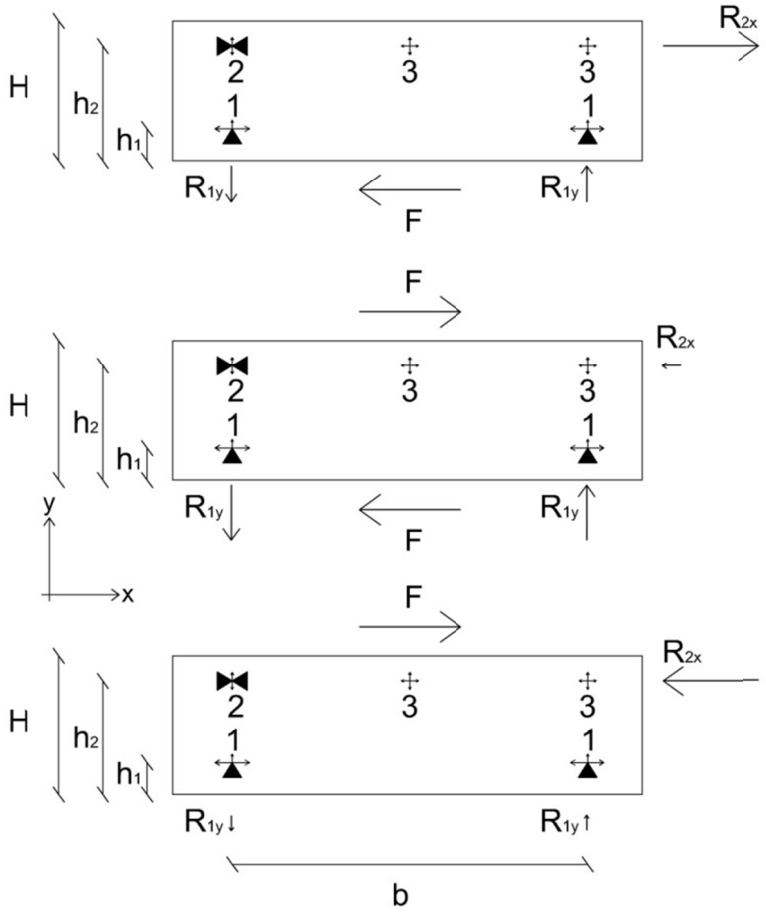

Figure 4.36 – In-plane equilibrium of a swaying panel: contribution of interface forces on central and edge panels

Chapter 5

Global structural behaviour of dissipative systems

The overall structural behaviour of structural systems provided with dissipative cladding panels is illustrated in the following for what concerns both numerical and experimental studies (Biondini *et al.* 2010, 2011, 2012a, 2013b). The present chapter refers to the behaviour of single nave structures, in which the actual flexibility of the diaphragm does not play a role. The considerations hereinafter made are, however, applicable to large structures provided with rigid diaphragm. Numerical analyses are performed on a benchmark building provided with vertical and horizontal panels at a time, with a structural arrangement representative of a typical industrial precast building, and are aimed to study the role of stiffness of the panel-to-panel dissipative connections on the seismic response of the structure.
A large experimental campaign has been carried out at ELSA/JRC laboratory at Ispra (Varese, Italy) concerning a full scale precast concrete prototype structure. The performed tests include cyclic and pseudo-dynamic with different panel connection arrangements (statically determined, integrated, dissipative) on the prototype with both vertical and horizontal panels. Results and related numerical simulations are elaborated for what concerns isostatic and dissipative arrangements on the prototype provided with FBD and FPD connections.

5.1. Numerical analyses on a benchmark building

The investigated structural prototype is a one-storey precast frame building of 40,5 by 25,0 m of dimensions in plan, made of two lines of five columns 7,0 m high and spaced by 10,0 m.

The roof is made of five transverse shed beams supporting ribbed elements. Under seismic condition the dead loads of the roof are related to:

– roof elements (including permanent finishings) = 2,8 kN/m^2;

– shed beams (average weight) = 17,5 kN/m;

– longitudinal beams (panel supporting) = 3,2 kN/m;

that lead to a vertical action of 600 kN on each of the 3 + 3 middle columns and 410 kN on each of the 2+2 end columns. All the columns have a square cross-section with side width of 60 cm and are reinforced with 12 Φ 20 mm longitudinal bars corresponding to the minimum reinforcement ratio of 1 % given by Eurocode 8 (CEN-EN 1998-1, 2004). The steel Class is B450C. The concrete Class is C45/55, with elastic modulus equal to 30 Gpa.

5.1.1. Benchmark building with vertical panels

A set of 16+16 vertical wall panels are placed along the two major sides of the building, with dimensions 2,5 by 8,0 m and an equivalent concrete thickness of 12 cm, leading to a weight of 3,0 kN/m^2. The panels are placed at the base on the foundation beam with a central hinged support that allows their free pendulum movement within the limits of the joint allowance left between the foundation beam and the panel. At the height of 7,08 m the panels are connected to the supporting beam with a central hinge. In this configuration the connection system represents a statically determined solution. In the integrated solution the panels are jointed between them by means of three connections placed in the adjacent sides at 1/4, 2/4 and 3/4 of the support height. Figure 5.1 shows the view of one cladding wall with the indication of the supports and panel connections.

These equations, applied to the total set of panels (with $F_1 \sim 0{,}8F_2$, as later shown), provide the resistance of the connections required to sustain the horizontal action H associated to the limit state to be fulfilled.

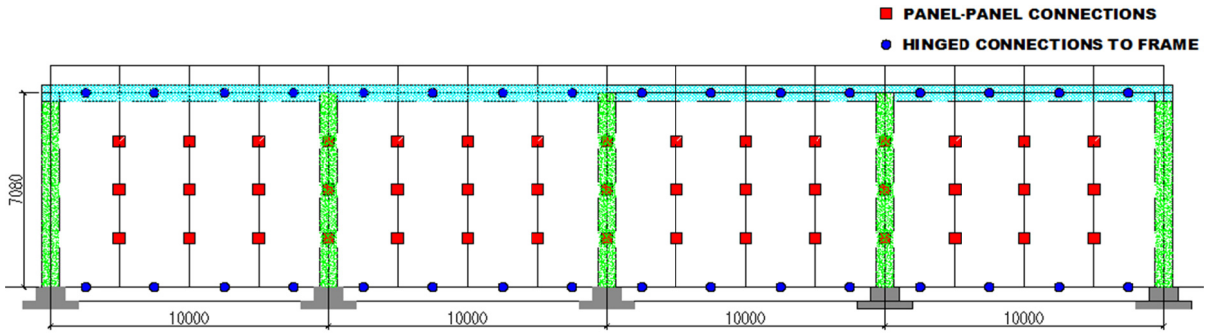

Figure 5.1 – View of the cladding walls system with vertical panels

The analysis of the structural system is carried out by means of a finite element model with beam elements for columns and shell elements for panels (Figure 5.2). A first series of linear elastic static analyses are performed on this model by applying at the top of the columns an horizontal force of 1000 kN that corresponds to a ratio of about 1/3 of the competent roof and wall weights computed as follows:

2,8 × 40,0 × 25,0 = 2,800

5 × 17,5 × 25,0 = 2,187

3,2 × 2 × 40,0 = 256

3,0 × 12,0 × 8,0/2 = 1,440

W = 6,683 kN/2=3,341 kN

where the cladding walls are considered extended to the whole perimeter less two openings of 5,0 m each.

With reference to the degree of reciprocal connection between the panels, the following two limit cases are studied: absence of connections (stiffness $k = 0$), with structural response given only by the columns, and perfectly rigid connections (stiffness $k = \infty$), with structural response

given almost only by the wall panels. Intermediate cases are also studied with different values of the elastic stiffness k of the connections. Figure 5.13 shows the deformed shape of the system without connections ($k = 0$). The top displacement is 73,0 mm and roughly corresponds to a roof drift of 1 %. The shear action on the columns is 200 kN and obviously corresponds to an equal repartition on the five columns of the global force applied at the top. The panel-to-beam fastenings do not receive any action from the roof: they can be proportioned with a local calculation based on the mass of any single panel.

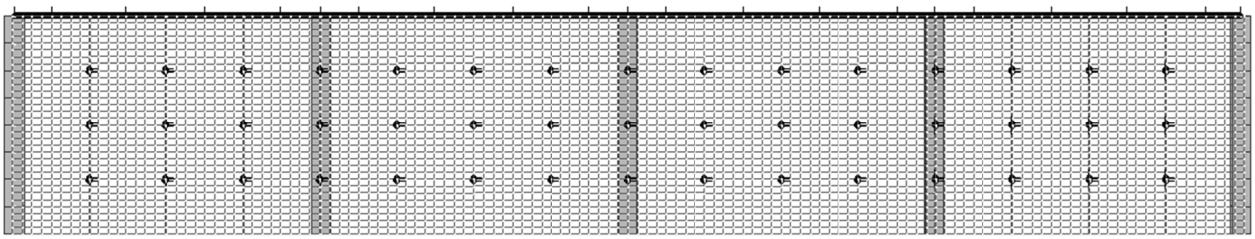

Figure 5.2 – Finite element model of the cladding wall system

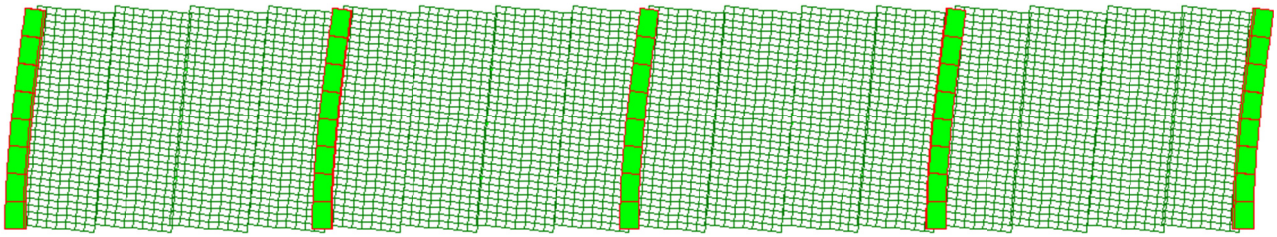

Figure 5.3 – Disconnected vertical panels (d_{top} = 73,0 mm)

For the case with perfectly rigid connections ($k = \infty$), the analysis leads to a top displacement reduced to 0,3 mm due to the much higher stiffness of the collaborating wall that takes almost all the applied action, leaving to the columns a very small portion of the base shear (0,5 kN). Figure 5.4 shows the distribution of the forces on the fastenings of the panels to the structure. An almost uniform distribution of the horizontal forces on the 16 fastenings, with values up to around 70 kN, displays for the global equilibrium of the force of 1000 kN applied at the top. At the ends of the wall there are strong vertical components on the last fastenings for the global equilibrium of the overturning moment of the top force with respect to the base. In these fastening the forces rise up to about 77 kN.

Figure 5.6 shows the distribution of the actions transmitted within the panels through their mutual connections. They are vertical reaction forces against the reciprocal sliding of the panels. The values are almost constant over all the length of the wall: 70 kN on the upper and lower connections and 55 kN on the middle connections. It can be noted that for the end panels the resultant of the forces of the three connections with the adjacent panel, missing the opposite panel, is equilibrated by the vertical resultant of the reactions of the two upper and lower fastenings to the structure. Figure 5.6 gives an indication of the concentration of the stresses on the panels over the fastenings and connections.

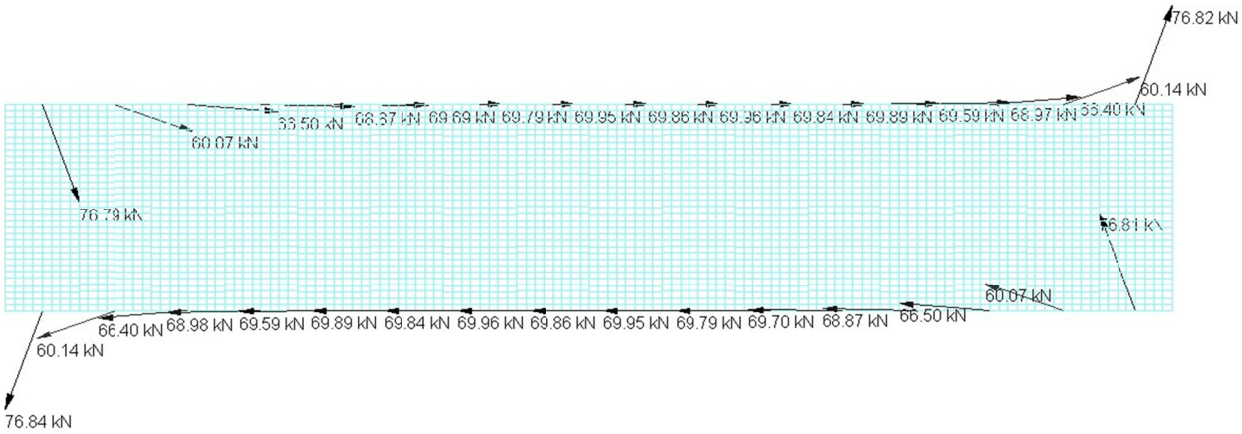

Figure 5.4 – Rigid connections: reaction forces on the fastenings (kN)

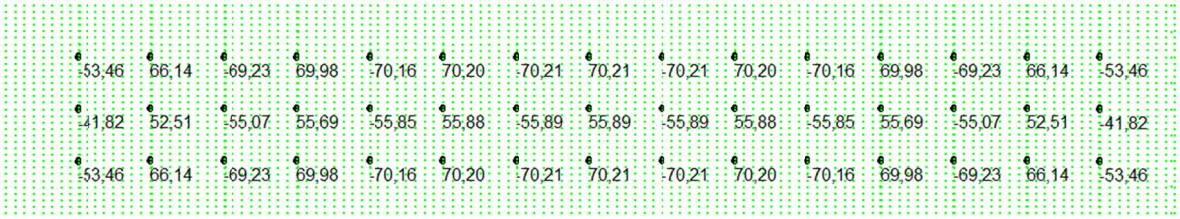

Figure 5.5 – Rigid connections: reaction forces on panel-to-panel connections (kN)

The obtained results provide an indication of the level of the forces in the connections for a seismic action applied to a very rigid structural arrangement of squat walls at the ultimate limit state of no-collapse. Following Eurocode 8 design rules (CEN-EN 1998-1 2004), for medium ductility class a behaviour factor $q = q_w q_o = 0{,}5$ by $3{,}0 = 1{,}5$ can be assumed for the squat wall system with rigid connections and, with reference to the maximum response amplification for a subsoil type B, a storey force $F_h = \alpha_g S_{max} W/q$ with $S_{max} = 1{,}2$ by $2{,}5 = 3{,}0$ can be computed. Therefore, with $F_h = 1000$ kN, a seismic capacity $\alpha_g = 1{,}5 \times 1{,}000/(3{,}0 \times 3{,}341) \approx 0{,}15$ is obtained, corresponding to a medium-low seismicity zone in the Italian territory.

The forces obtained under this moderate seismic intensity show very large values that put difficult design problems for the connections, problems that become even more critical for zones with higher seismic intensity. This emphasizes the importance of solutions able to attenuate the seismic response of the integrated wall-frame arrangement of the structure, possibly with dissipative effects of the connections.

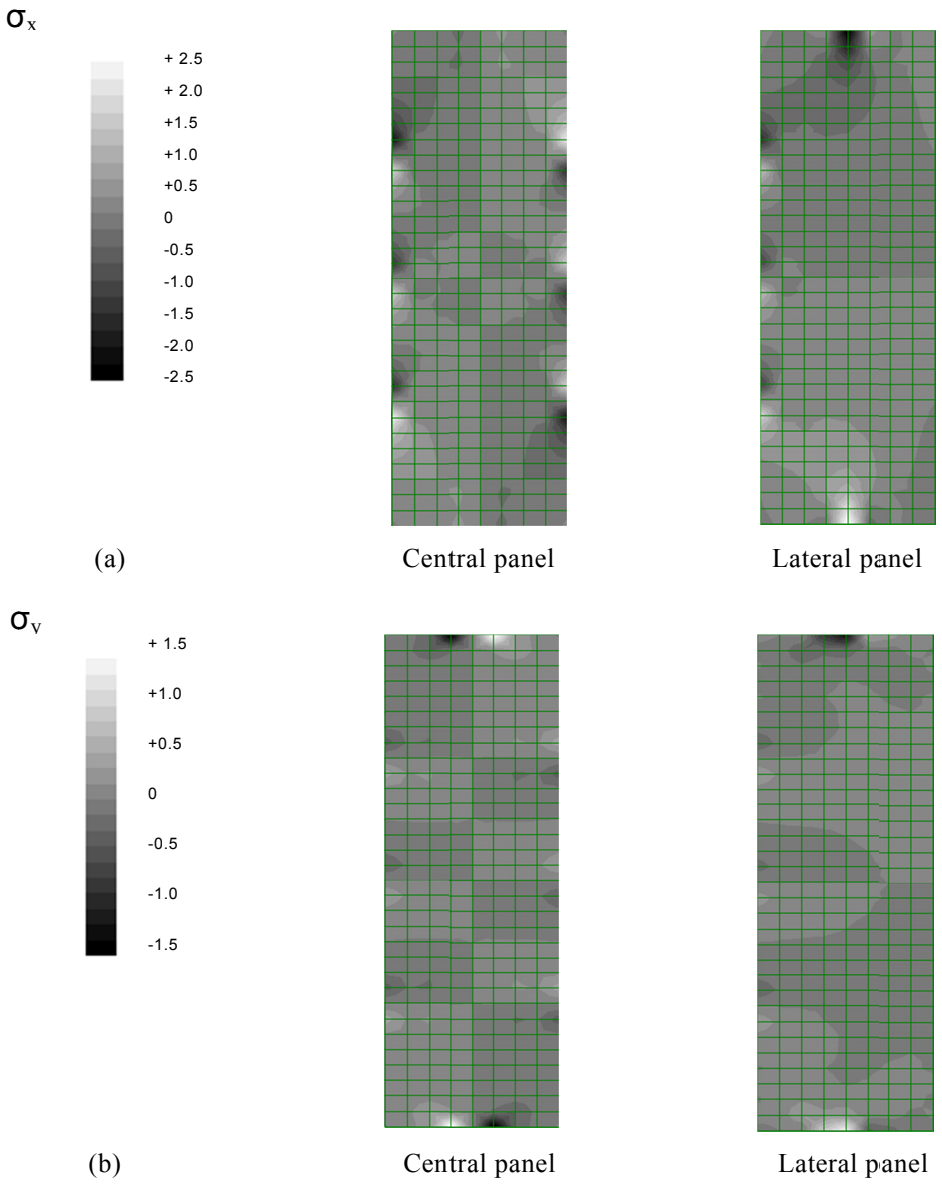

Figure 5.6 – Rigid connections: contour map of (a) horizontal normal stresses σ_{xx} and (b) vertical normal stresses σ_{yy}

The elastic stiffness of the mutual panel connections, with intermediate values $0 < k < \infty$, obviously influences the structural response. Figure 5.7 shows how the ratio between the base shear in the panels and the total base shear (columns plus wall) increases with the connection stiffness. For very low stiffness the structural response is close to a pure frame behaviour.

For intermediate values of the connection stiffness a combined behaviour typical of the dual frame-wall systems is achieved. For high stiffness values the structural response 139stabilizes on a wall system behaviour with almost total release of the column forces. Furthermore, Figure 5.7 shows the complementary stiffening effect of the connections in terms of top displacement. Finally, Figure 5.8 shows the repartition ratio of the shear force exchanged between the adjacent panels on the connections, the middle one F_1 and the upper (or lower) one F_2. For high stiffness values the middle connections have a force 0.8 time lower than the others, while for low stiffness values the forces get uniform ($F_1/F_2 \rightarrow 1$).

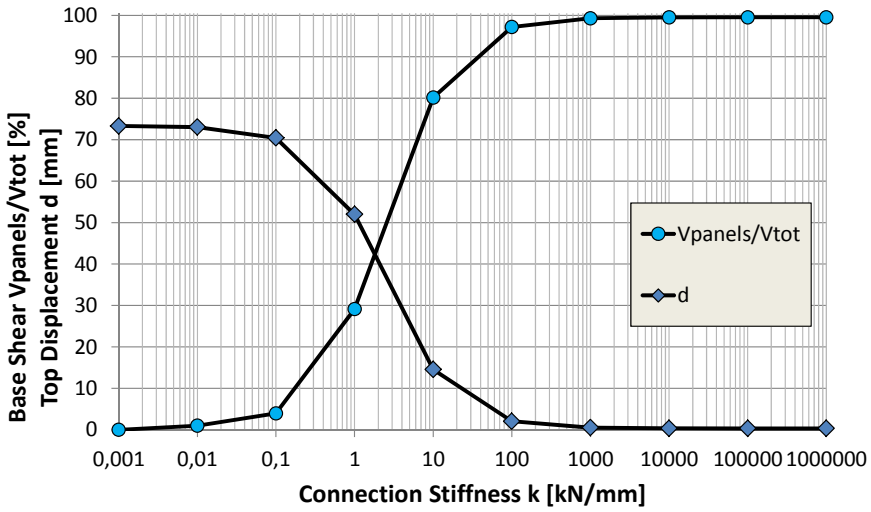

Figure 5.7 – Base shear in the panels and top displacement vs the connection stiffness

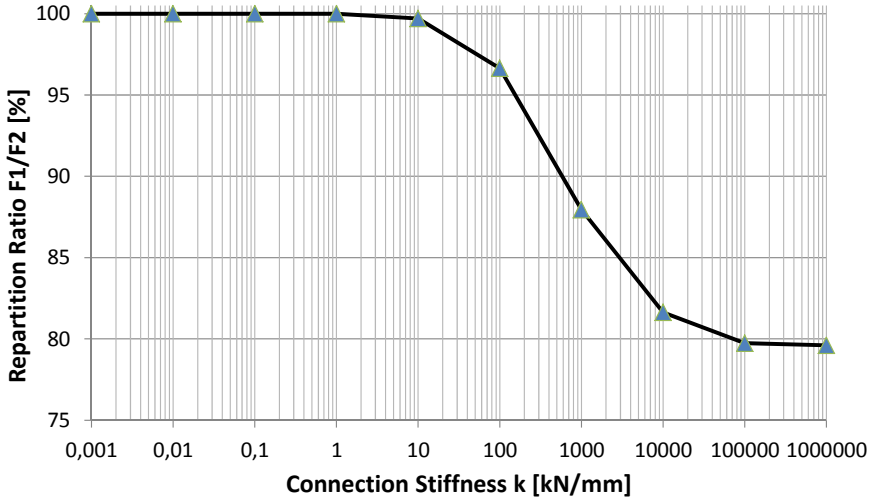

Figure 5.8 – Repartition ratio F_1/F_2 vs the connection stiffness

It is worth noting that the transition interval for the repartition ratio in the connections (Figure 5.8) is moved towards higher stiffness values with respect to both the repartition ratio of the base shear and the top displacement (Figure 5.7). The difference of the forces F_1 and F_2 is negligible for values of stiffness lower than 10 kN/mm.

The seismic response of the structure is affected by the non-linear behaviour of its members.

In particular, the effectiveness of the mutual panel connections depends primarily on their ductility capacities. To investigate this aspect a series of non-linear static analyses with monotonic loading (pushover) is performed.

Figure 5.9 shows the moment-curvature relationship of the column cross-sections for the two levels of axial forces. These diagrams are computed with a parabola-rectangle stress-strain model for concrete, neglecting its tensile strength, and with a bi-linear hardening stress-strain model for the steel reinforcement. An elastic behaviour is assumed for the wall panels relying on their over-strength with respect to the capacity of the mutual connections.

For these connections an elastic-plastic behaviour is assumed with different values of the initial elastic stiffness and of the ultimate resisting force. The ultimate deformation of the connecting devices is not specified and the plastic branch is left indefinite.

Figure 5.10 shows a family of pushover curves of the structural system for different values of the initial elastic stiffness of the connections and for a very high ultimate resisting force (R = 200 kN). From the initial slope of the curves the elastic stiffness of the structure is deduced and the natural vibration period T is evaluated. This period depends on the collaboration degree between columns and panels, provided by the stiffness of the connections, and it varies from 1,2 to 0,05 s. Figure 5.11 shows how the natural vibration period decreases with the higher values of the elastic stiffness of the connections. The same diagram also indicates the corresponding variation of the structural response in terms of ratio a/a_g between the maximum acceleration a and the peak ground acceleration a_g, computed from the elastic response spectrum given by Eurocode 8 for subsoil type B. A large increase of the seismic force can be noted in the solution with wall panels integrated in the structural assembly, with values of the ratio a/a_g that initially increases with the connection stiffness from 1.3 to 3.0 and then decrease to 1.8 for the case of rigid connections. This response factor does not consider the energy dissipation possibly offered by the structural system.

Figure 5.12 shows that the pushover curve of the structural system is limited to the level corresponding to the different possible strengths of the connections. It is worth noting that the shear ratio taken by the wall panels in the elastic stage (see Figure 5.7) decreases progressively after the yielding of the connections with the development of their plastic deformation until the yielding of the columns, as shown in Figure 5.13. From these results it is clear that, if the connections have sufficient plastic deformation capacity, the choice of their strength level can influence the energy dissipation capacity and properly regulate the structural response with reference to the intensity of the seismic action expected on site. An example of this regulation will be presented in the next section devoted to nonlinear dynamic analysis of the prototype.

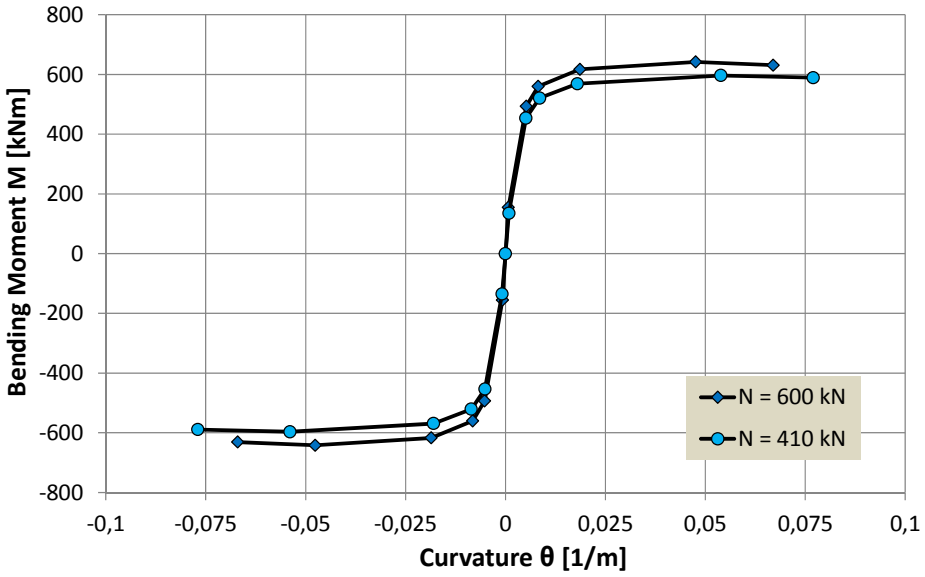

Figure 5.9 – Bending moment-curvature relationship of the column cross-sections

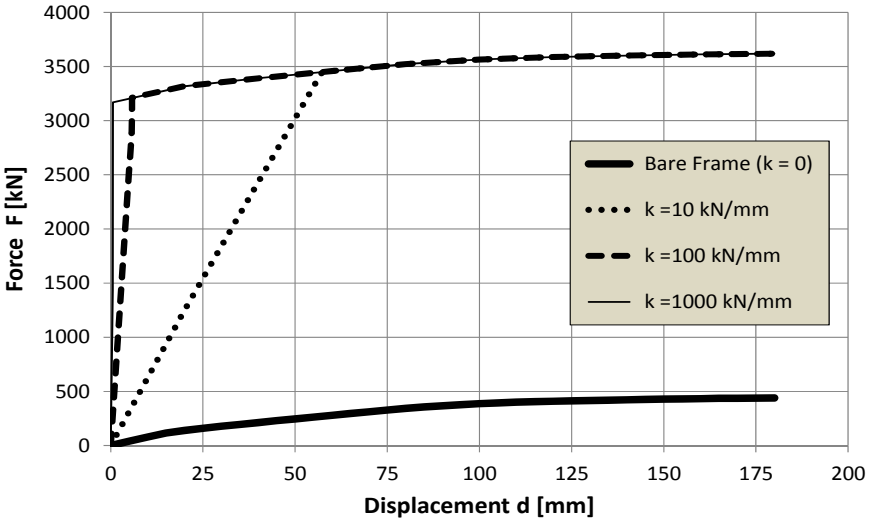

Figure 5.10 – Pushover curves for R = 200 kN

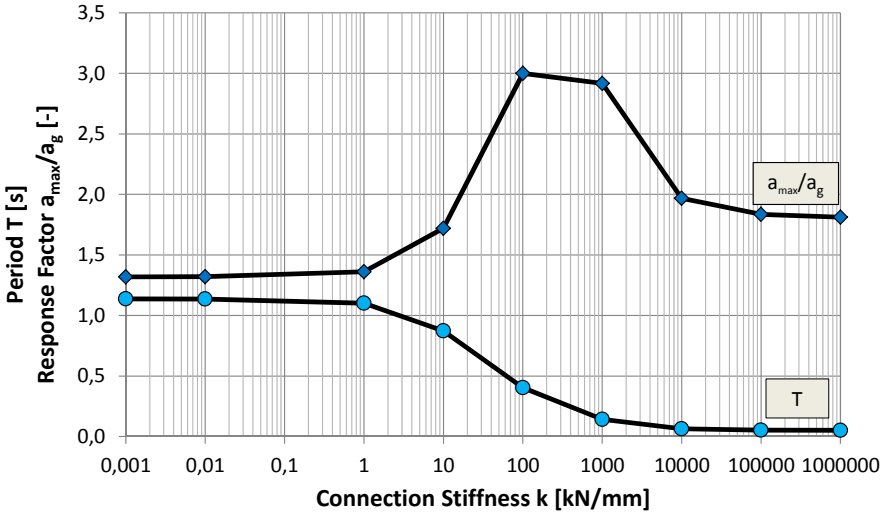

Figure 5.11 – Parameters of the dynamic response

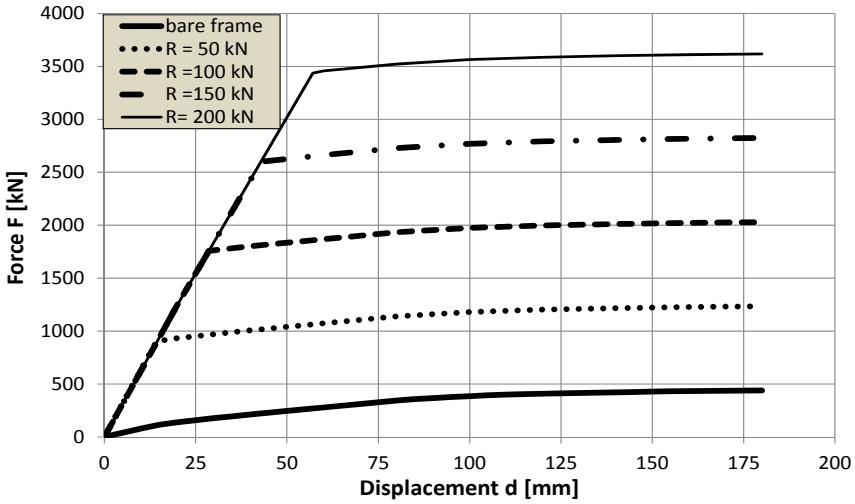

Figure 5.12 – Pushover curves for k = 10 kN/mm

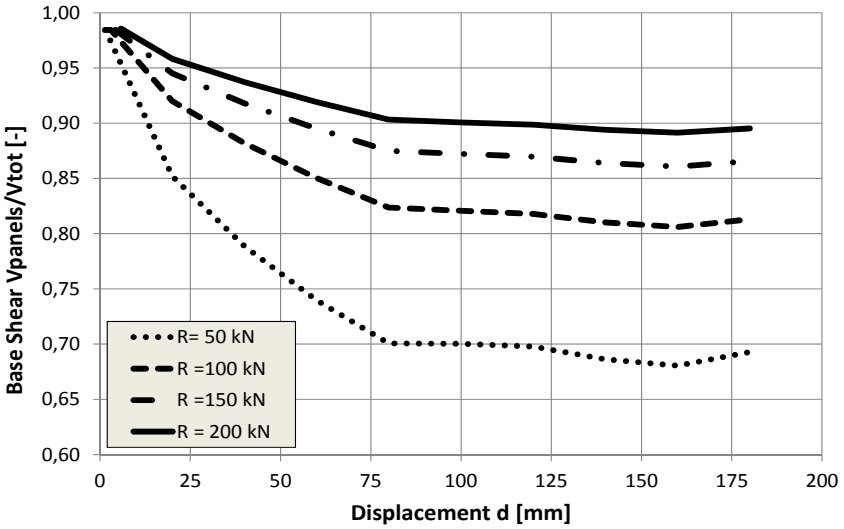

Figure 5.13 – Plastic repartition of base shear for k = 100 kN/mm

Non-linear dynamic analyses of the prototype are carried out considering the dissipative FBD connection. Figure 5.14 shows a pushover curve of the structure with SPAV connections computed with the elastic-plastic model based on an initial stiffness of 60 kN/mm, a slip resistance of 60 kN and a "functional" stroke limit of ±25 mm.

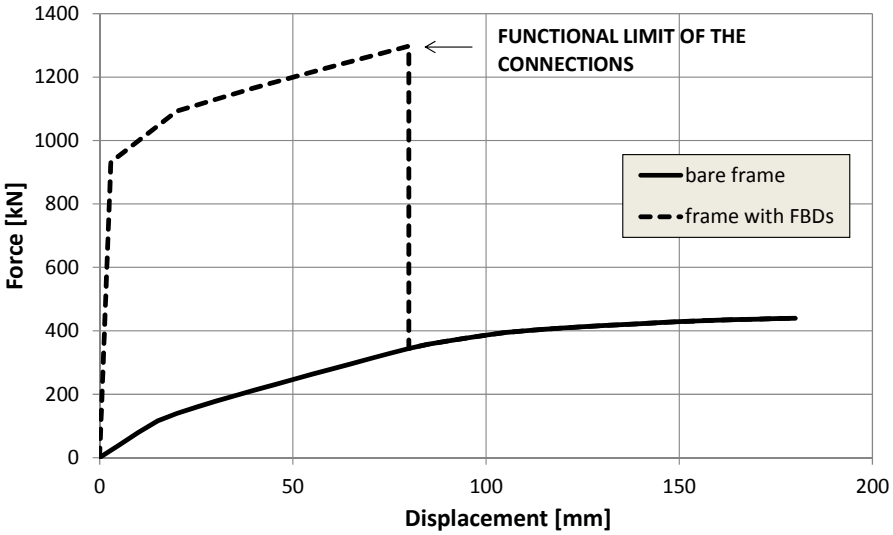

Figure 5.14 – Pushover curve with FBDs

The dynamic non-linear analyses are performed with a Takeda model (Takeda *et al.* 1970) for the columns, the elastic-plastic model described above for SPAV connections, and a linear elastic model for the panels.

The analyses are performed under a recorded accelerogram of the 2009 L'Aquila earthquake (AQK-WE) with PGA = 0,32 g, and ten artificial synthetic accelerograms (SC) compatible with the response spectrum given by Eurocode 8 for subsoil type B and scaled to PGA = 0,32 g. Figure 5.15 and Figure 5.16 show these accelerograms and their elastic response spectra

compared to the Eurocode 8 spectrum. It is worth noting that the scanty compatibility of the response spectrum of L'Aquila earthquake with the Eurocode 8 standard spectrum, due to its poor content of frequencies, could lead to a weaker impact on the actual structural response.

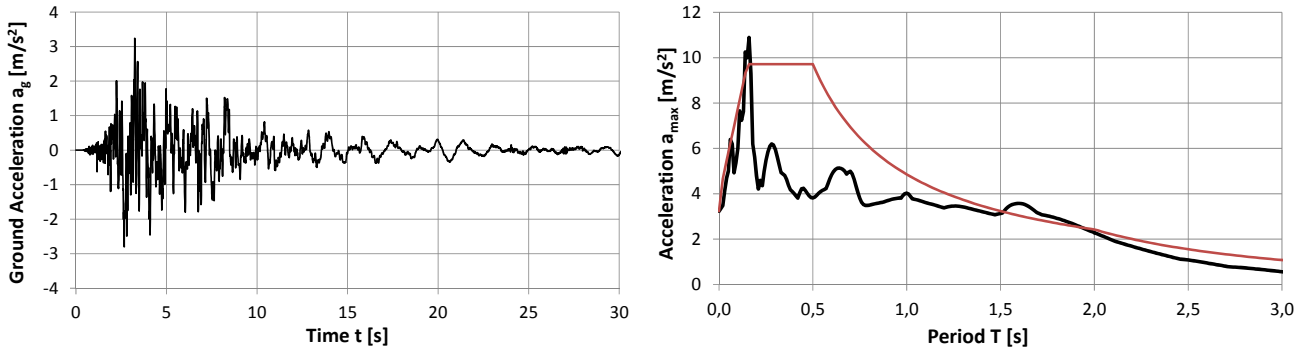

(a) (b)

Figure 5.15 – L'Aquila earthquake (AQK-WE): (a) accelerogram and (b) response spectrum compared with the model of Eurocode 8

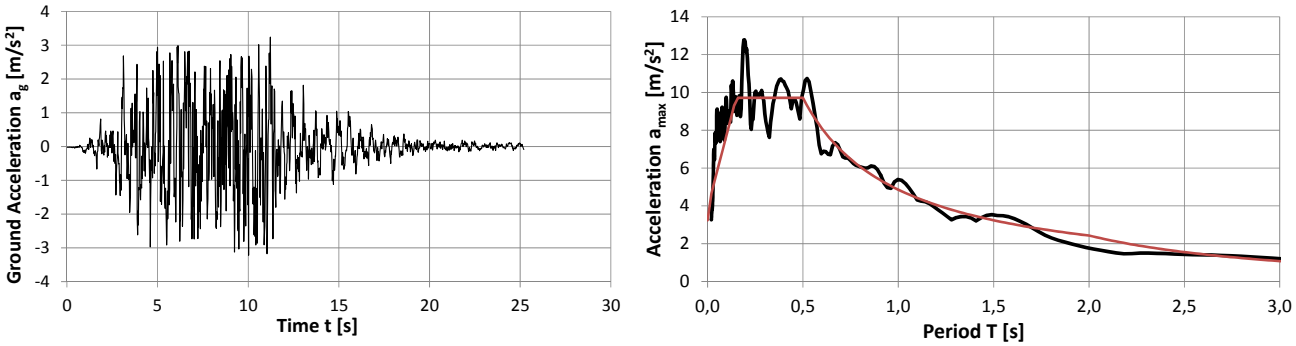

(a) (b)

Figure 5.16 – Artificial accelerogram (SC): (a) accelerogram and (b) response spectrum compared with the model of Eurocode 8

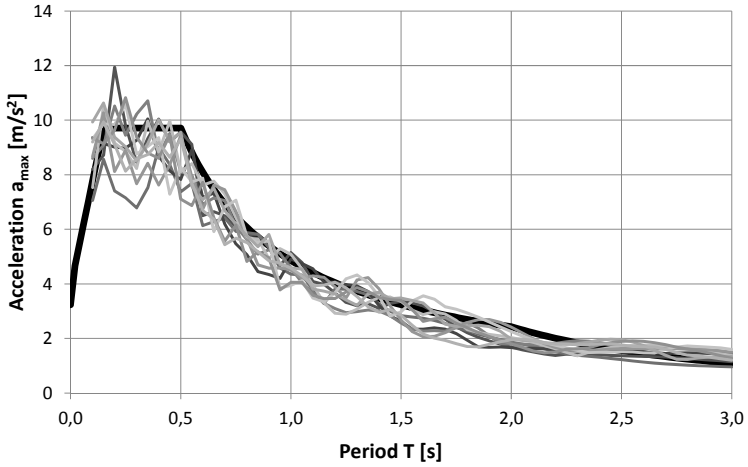

Figure 5.17 – Set of artificial earthquakes: response spectra compared with the model of Eurocode 8

The different response of the three structural configurations (statically determined, integrated and dissipative) under L'Aquila earthquake (AQK-WE) is shown in terms of vibratory curves in Figure 5.15. The diagram at the top gives the displacement time history response for a zero connection stiffness (pure frame structure), with large storey drifts; the diagram at the bottom shows the structural response with rigid connections (wall structure), with small storey drifts and high connection forces; the diagram in the middle shows the structural response with dissipative SPAV connections (dissipative structure), with intermediate storey drifts and limited connection forces. The same analyses are performed for the set of ten artificial accelerograms. Figure 5.16 shows the vibratory curves of the system under one artificial accelerogram from the set (SC, Figure 5.16a).

The strong effectiveness of the connections can be noticed in lowering the maximum storey drift of the statically determined system from 80 to 4 mm and 0,6 mm under L'Aquila earthquake, and from 80 to 6 mm and 0,8 mm under the artificial accelerogram, for SPAV connections and rigid connections, respectively. The large increase of vibration frequencies of the structural responses of the integrated systems can also be noted.

In particular, the response with rigid connections corresponds to a pure elastic behaviour of a stiff wall system.

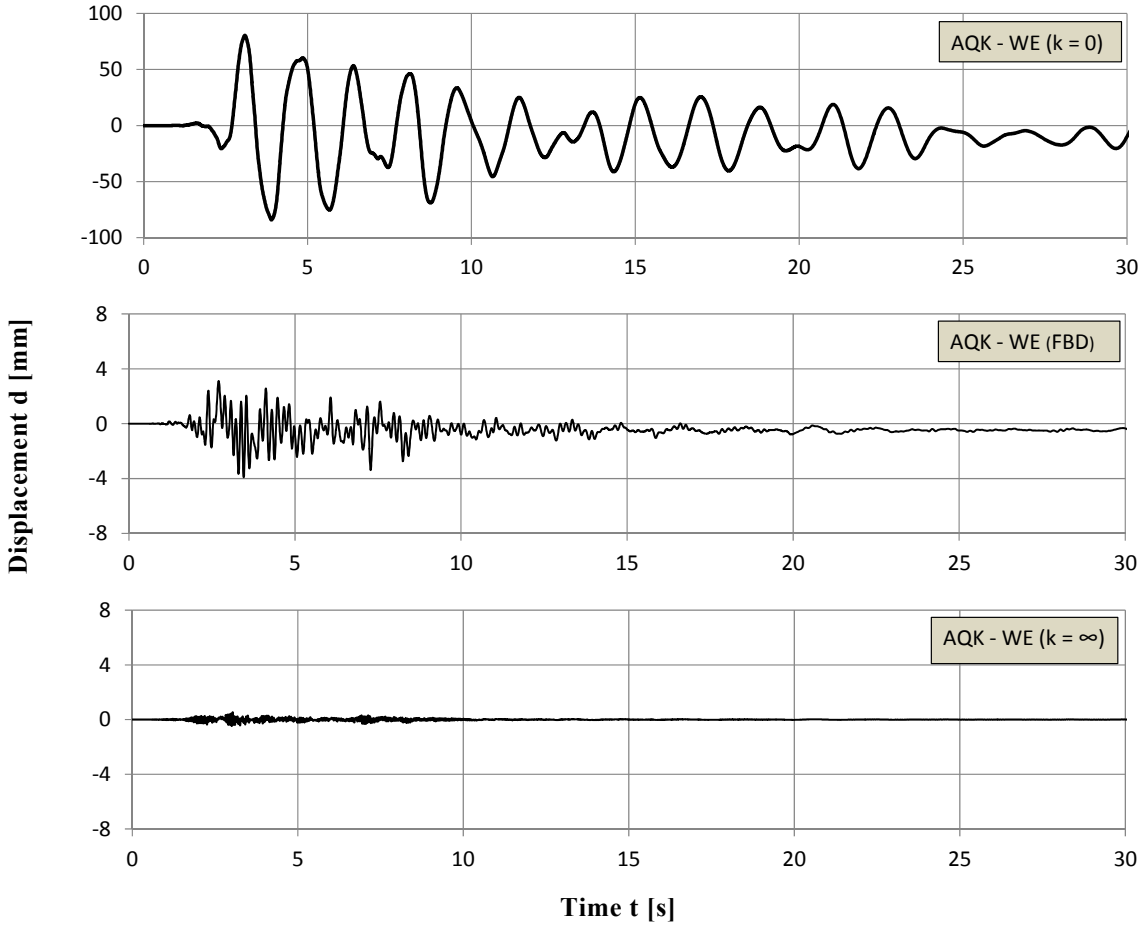

Figure 5.18 – Vibratory curves for AQK-WE accelerogram

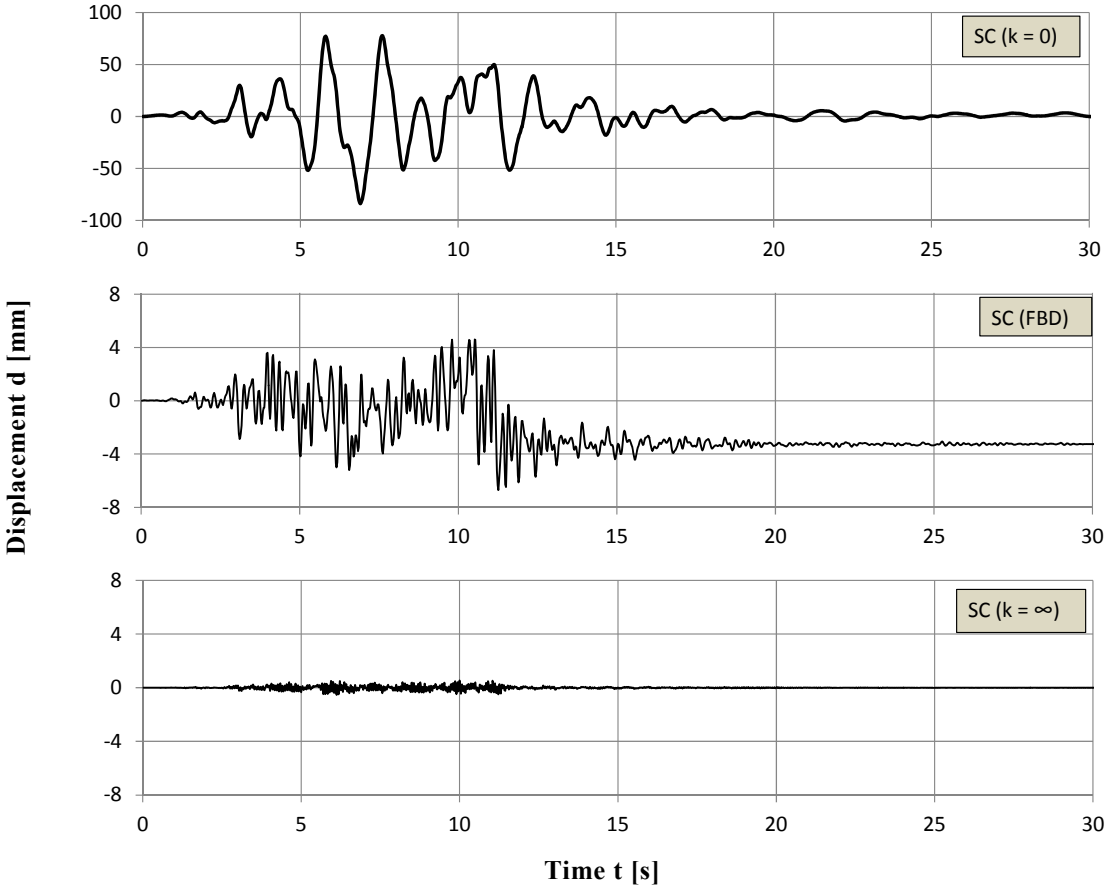

Figure 5.19 – Vibratory curves for SC accelerogram

The residual displacements of the integrated structure with dissipative connections indicate that an inelastic slide occurred in the connections and, therefore, the friction mechanism worked in dissipating energy. This is more evident for the artificial accelerograms that have, with their full content of frequencies, a stronger impact on the structure. The measure of the energy dissipation can be deduced from the force-displacement diagrams shown in Figure 5.18, where the area within the cycles is much wider for the artificial accelerogram. The vibratory curves corresponding to the whole set of artificial accelerograms are compared in Figure 5.19 for the configuration with dissipative devices. Figure 5.20 shows the absolute values of the maximum and residual displacements associated to the set of artificial earthquakes. The values of representative parameters of the structural response for the set of artificial earthquakes and L'Aquila earthquake are listed in Table 5-1. It is worth noting that the maximum displacements reached with the artificial accelerograms are much higher than with the recorded one, and are characterized by a relatively low dispersion. A mean residual displacement of 2,71 mm is expected under the artificial earthquakes, with a large scatter due to the variability of time history of each accelerogram. The energy dissipation is mainly provided by the nonlinear behaviour of the devices, while the columns remain almost linear elastic. In all the studied cases the maximum total horizontal force F_{max} applied to the structure was limited by the slip resistance (strength) of the connections:

$$F_{\max} \approx n_c (n_p - 1) R_c \frac{b}{h} \tag{5.1}$$

where:

n_c = 3 number of connections for each joint;

n_p = 16 number of the panels;

R_c = 60 kN strength of one connection;

b = 2,5 m width of a panel;

h = 7,08 m height of the upper support.

This is the maximum value of the base shear for the panels, to be added to the contribution of the columns in the overall response, which is much smaller but not negligible. It is finally noted that, with reference to the maximum force values of the elastic response with rigid connections, force reduction factors varying from 2,24 to 6,09 are deduced for the dissipative connections herein studied. This range provides an indication of the order of magnitude of the behaviour factor to be used in a typical elastic analysis of this type of systems.

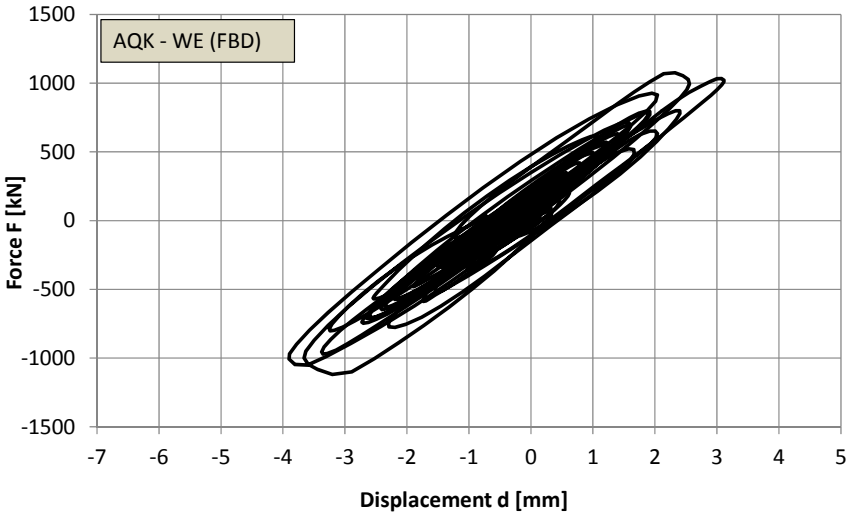

(a)

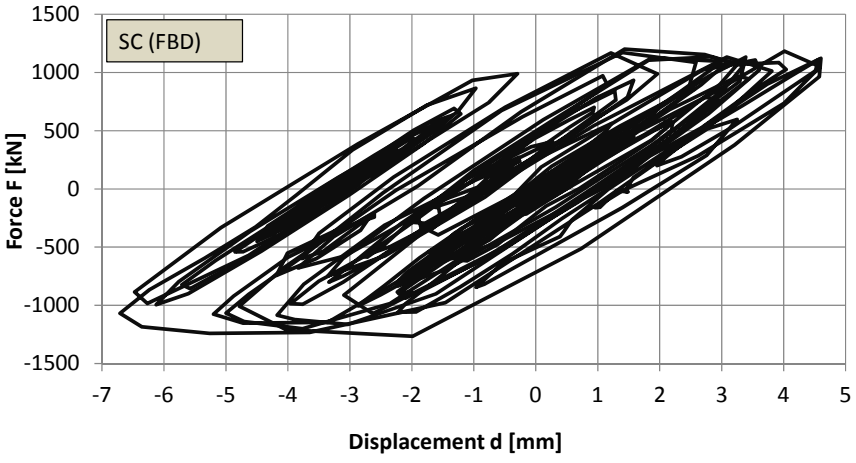

(b)

Figure 5.20 – Base shear vs displacement diagrams for (a) AQK-WE and (b) SC accelerograms

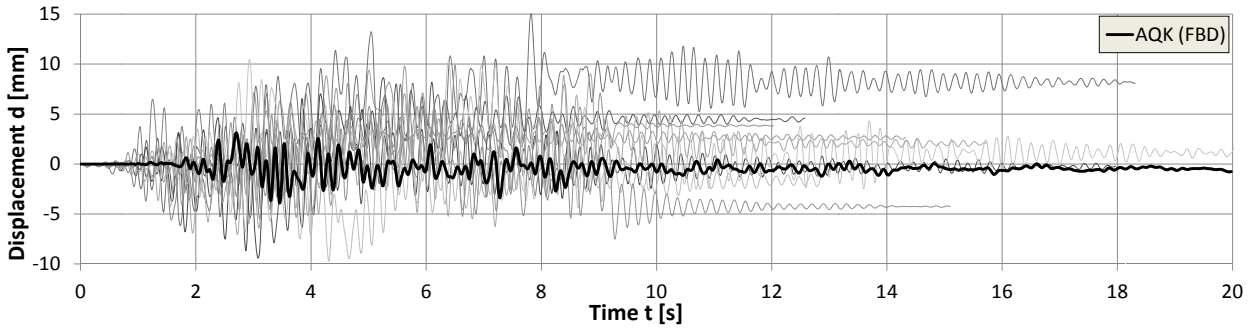

Figure 5.21 – Vibratory curves for all the set of accelerograms

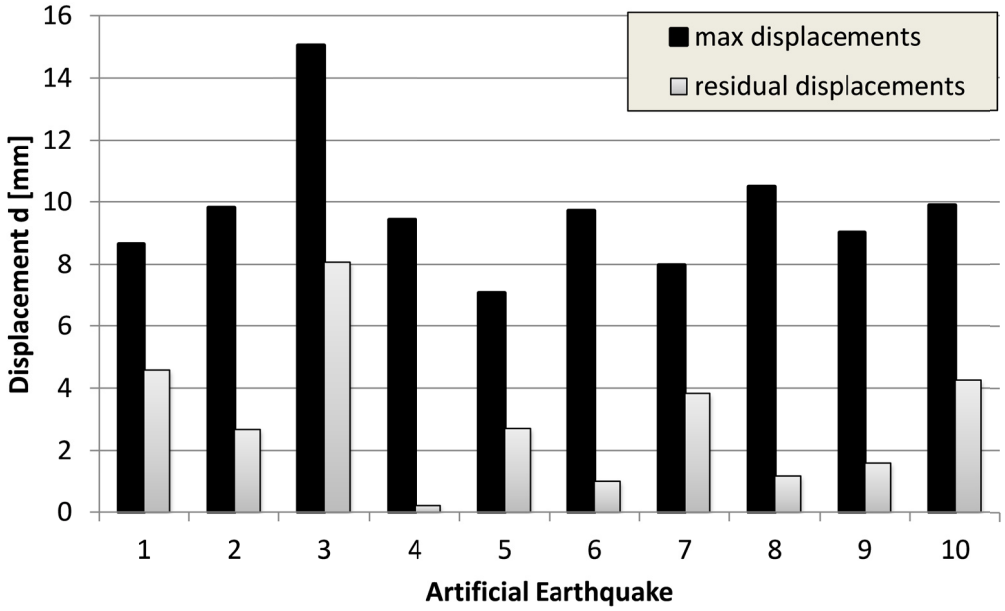

Figure 5.22 – Maxima and residual displacements

Table 5-1 – Comparison of numerical results

	ARTIFICIAL ACCELEROGRAMS				L'AQUILA AQK-WE
	MAX	MIN	MEAN	ST.DEV.	
maximum displacement (mm)	15,0	7,1	9,7	2,1	3,9
residual displacement (mm)	8,1	0,2	2,7	2,3	0,5
maximum total base shear (kN)	1577	1212	1405	113	1120
max. shear with fixed devices (kN)	8170	2920	5790	1394	2510
force reducing factor	6,09	2,92	4,59	0,91	2,24
maximum force in devices (kN)	60	60	60	0	60
maximum device slippage (mm)	5,4	2,5	3,5	0,8	1,4
energy dissipated by devices (kNm)	80,70	26,67	53,13	17,29	17,74
energy dissipated by columns (kNm)	0,03	0,00	0,00	0,01	0,00

5.1.2. Benchmark building with horizontal panels

The seismic response of the structural system previously described is now investigated by considering the cladding walls made by horizontal panels. It is assumed that the panels are linked to the frame with statically determined (double pin) connections at mid height. The panels are therefore suspended. Two lines of panel-to-panel connections are inserted at 2,35 and 4,70 m of height, in between adjacent panels, with a number of three connections for each panel contact line. By neglecting friction effects in between the contact lines, each panel is considered statically determined. The front view of the building is shown in Figure 5.23.

The structural response of the system is depending on the stiffness of the connections. For negligible stiffness, when a static horizontal load of 1000 kN applied at the top of the building, the deformed configuration is shown in Figure 5.24, where the panels are free to slide one over the other. The entity of the relative slide increases on the height of their horizontal contact surface, since they follow the deformation of the cantilever columns. For rigid connections, the panels act as a single shear wall, thus significantly reducing the top displacement (equal to that of the vertical panels case) but developing very high forces, up to 157 kN (Figure 5.25). The forces acting on the connections are different depending on the position of the devices even on the same line for such high stiffness. It can also be noticed how the upper line is subjected to higher forces. This is due to the different relative slide of the two lines. The panels act as horizontal flexural bracers, and their equilibrium brings to strong axial loads on the columns through the pinned support, which balance leads to the counter-acting bending moment. The columns are also strongly subjected to shear in the lower part, since all the base shear is carried by them.

If using FBD connections with the same parameters as descripted for the use in between vertical panels, and performing a non-linear static analysis, we obtain the curve described in Figure 5.26, where it can be noticed that the connections reach their functional limit at different drift levels for the two rows.

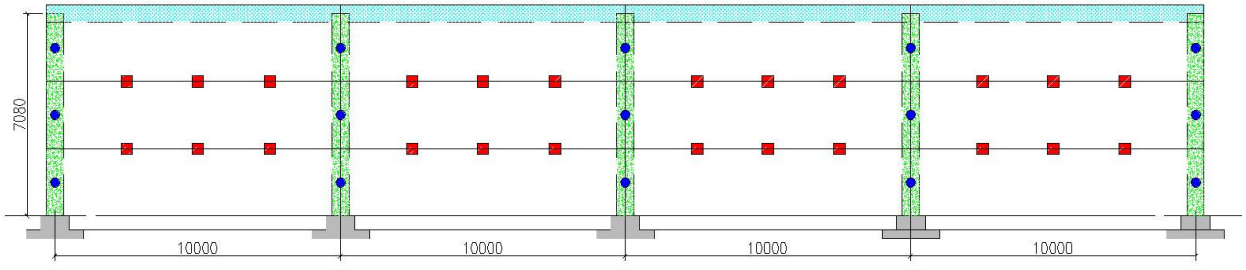

Figure 5.23 – View of the cladding walls system with horizontal panels

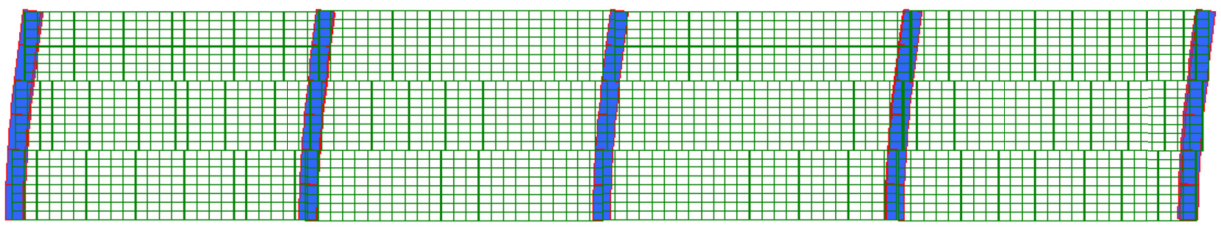

Figure 5.24 – Disconnected horizontal panels (d_{top} = 73,0 mm)

Figure 5.25 – Rigid connections: reaction forces on panel-to-panel connections (kN)

The non linear dynamic analyses performed under L'Aquila AQK-WE accelerogram and an artificially generated earthquake show that, in comparison with the response of the bare frame (equal to that of the previous case), the additional energy dissipation provided by the devices is very effective in reducing the top displacement, which decreases from 80 mm to 26 mm for L'Aquila earthquake and 13 mm for the artificial accelerogram. In both schemes a residual displacement of about 5 mm is found at the end of the earthquake. The contribution of the columns to the overall response is significant for these cases. The vibratory curves are shown in Figure 5.27. It is finally noted that, with reference to the maximum values of the elastic responses with rigid connections, equal to 2510 kN for the AQK-WE accelerogram, a force reduction factor by 3,59 is deduced for the friction connections herein studied in the case of AQK-WE earthquake.

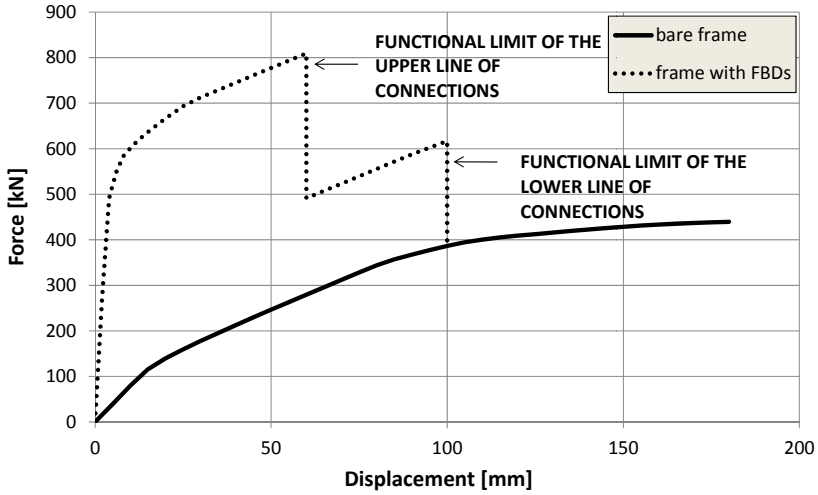

Figure 5.26 – Pushover curve with FBDs

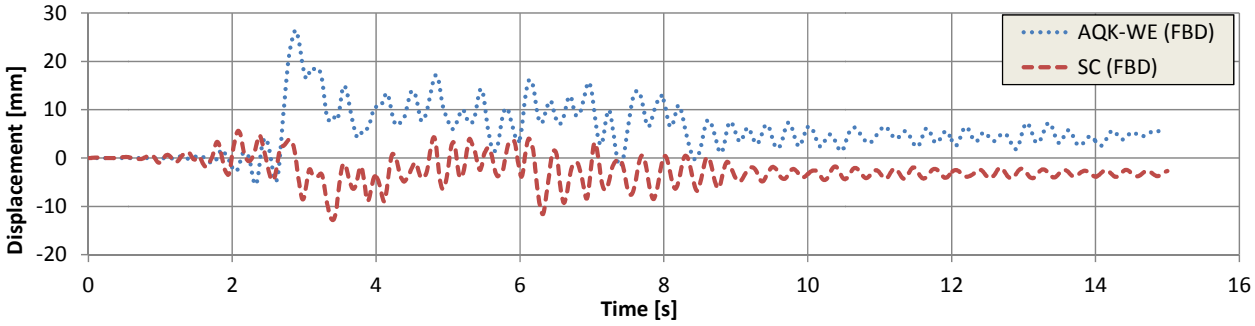

Figure 5.27 – Vibratory curves under SC and AQK-WE accelerograms

5.1.3. Concluding remarks

The results of this investigation provides important information related to the magnitude distribution of the forces that the mutual connections between the panels have to transmit. The elastic forces are obtained for a medium-low seismicity zone in the Italian territory with α_g=0,15 and would become much larger for higher risk areas. These are very high forces that put difficult problems for the design of connectors. The problems would become even more difficult for a seismic force acting in the transversal direction of the building along which its effects would be subdivided by a much lower number of panel connections, involving also the connections of the roof in its diaphragm behaviour. The dissipative solution, employing statically undetermined arrangements of connection with limited strength, leads to a large reduction of the maximum and residual drift, with a consequent avoidance of yielding at the base of the columns and structural damage in the whole structure.

5.2. Cyclic and pseudo-dynamic tests on a full scale precast prototype

An extensive experimental campaign regarding the cyclic and pseudo-dynamic behaviour of a precast building prototype has been designed by Politecnico di Milano research group and carried out by ELSA/JRC team within the SAFECLADDING project. The specimen has been designed in detail, cast and assembled by Styl-Comp company.

The prototype is a dry-assembled single-storey precast frame structure representing a typical industrial building in Southern Europe, with single 5 m wide nave and 8 m span double bay.

The prototype represents a wider building model with a 16 m nave and TT cross-section shaped floor members. In order to more easily handle the specimen and to make it fit the geometries of the ELSA laboratory, unrealistic 5 m long and 35 cm deep solid concrete plates have been used for flooring. They transmit a distributed shear reaction on beam equal to 0,35 m by 5 m by 25 kN/m^3 = 43,7 kN/m. They have been chosen in such a way to match the weight of the equivalent 16 m long TT member provided with roof finishing, weighting 2,7 kN/m^2 and applying a distributed shear reaction on beams equal to 2,7 kN/m^2 by 16 m = 43,2 kN/m, which is fairly similar to the previous, as intended. Figure 5.28 shows the basic geometry of both the laboratory prototype and the equivalent building model. The cladding panels, only placed in the building longitudinal direction, assuming large openings in the transversal direction, have been considered to have a distributed mass equal to 400 kg/m^2. Assuming an isostatic cladding connection system with a pendulum arrangement for the building with vertical panels, half of the mass of the panels is considered concentrated at the floor height. A total mass of 170 tons is computed for the building provided with vertical panels. Assuming an isostatic cladding connection system with a swaying arrangement for the building with horizontal panels, again half of the mass of the panels is considered concentrated at the floor height, for a total mass of 175 tons.

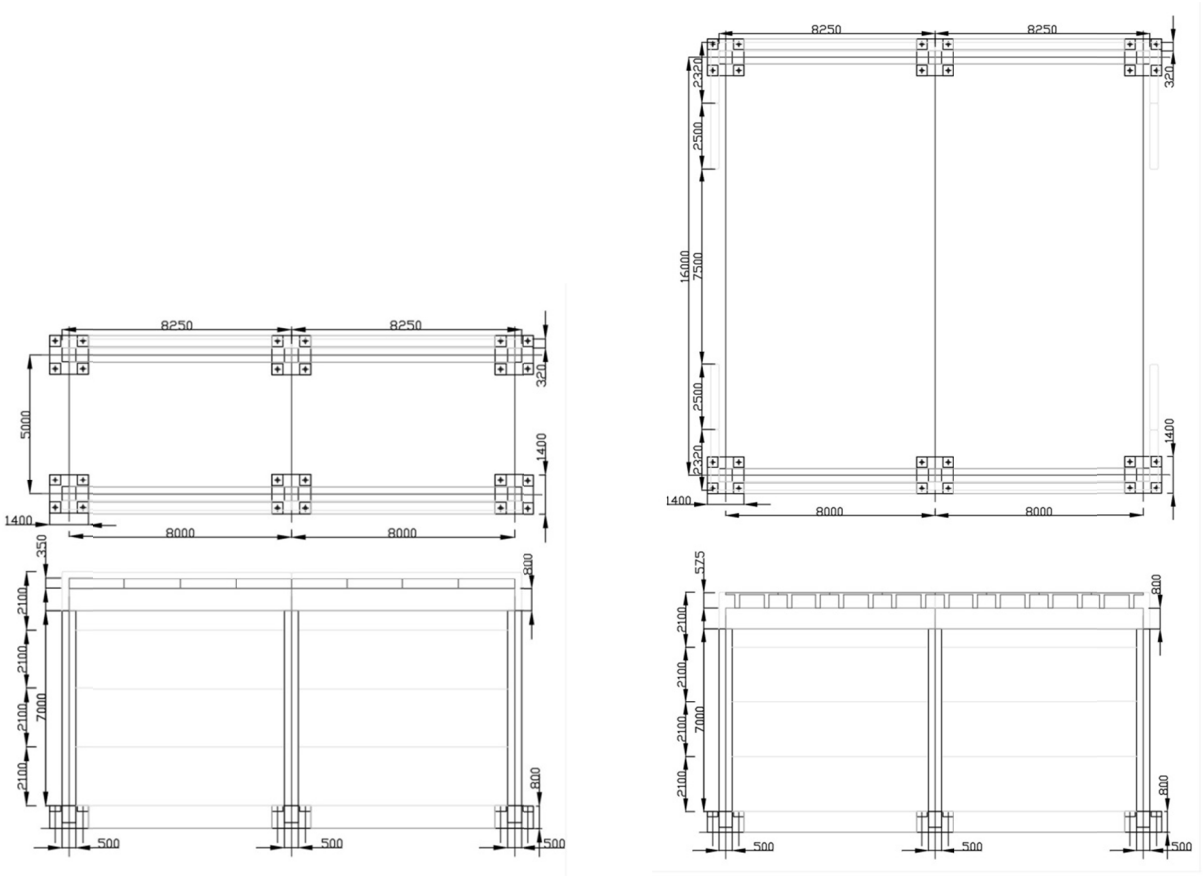

(a) (b)

Figure 5.28 – Prototype basic geometry: (a) laboratory prototype and (b) equivalent building model

The laboratory prototype members and all its components, including all connections also related to cladding panels, have been proportioned using the simple formulations illustrated in the previous chapters for both single connections and panel structural sub-systems and with safe-side non-linear dynamic numerical simulations. The frame structure, however, has been preliminary designed according to classical force-based design, in order to evaluate how the different cladding panel connection systems affect the behaviour of a non-innovative building.

The structure has been designed according to European structural standards EN 1990, EN 1991, EN 1992 and EN 1998. The concrete class is C45/55 and the reinforcing steel is class B450C for both longitudinal and transveral bars. The building is placed in a generic high seismicity area in Europe, with a subsoil classified as B. The seismic design has been performed through modal analysis with response spectrum, considering a peak ground acceleration for life safety state equal to 0,30g, which is multiplied by the subsoil amplification factor, equal to 0,2, obtaining 0,36g. Seismic loading has been considered as acting in one direction only at a time, for compatibility with the mono-axial experimental loading technique. A behaviour factor q equal to 3,00 has been adopted. Wind and snow loads have been disregarded. Table 5-2 resumes the relevant design data of the structure, with the 0,50 side square cross-section columns reinforced with 8 Φ24 rebars placed at the corners and at mid-side with a clear cover of 36 mm.

Table 5-2 – Building model design resuming table

EARTHQUAKE COMBINATION				
Period T	1,19	s		
Behaviour Factor q	3,00			
Design Spectral Acceleration	0,126	g		
Axial Load on Central Column	276,8	kN		
Axial Load on Edge Column	153,0	kN		
Theta Factor	0,115		<	0,30
2nd Order Magnification Factor	1,13			
Base Shear at ULS	242,55	kN		
Single Column Shear at ULS	40,43	kN		
Single Column Base Moment	282,98	kNm	<	337,70
ULS Displacement	151,48	mm		
SLS Displacement	60,59	mm		
ULS Drift Ratio	2,16	%		
SLS Drift Ratio	0,87	%	<	1,00

The laboratory prototype geometry is described in the following, together with the typology of member connections. The foundations are made with six large pocket elements 2,40 by 1,40 wide and 1,40 m deep, provided with 0,80 m deep pocket and with running holes for the installation on the strong floor of the laboratory with post-tensioned bars. Each pocket foundation is connected with the adjacent in the longitudinal building direction through full-depth 0,50 m wide beams with strong welded connections, for a total of 4 elements. The 6 columns have a free height of 7,00 m from the top of the pocket foundation and a square cross-section with 0,50 m of side. The connection with the foundation is cast in laboratory and is considered as a full moment-resisting joint. A picture of the connection during casting is provided in Figure 5.31. 0,50 m wide and 0,75 m deep beams are connected with the columns with dowel connections. Each joint is provided with two distanced large diameter high resistance dowels (Figure 5.32a), and it has been considered as a hinged connection for the beam gravity rotations and as a clamped connection for the beam out-of-plane bending. The slab is made with 7 solid reinforced concrete panels with 2,35 m of width, 5,22 m of length and 0,35 m of depth. It is also reinforced with two distanced large diameter dowels. The diaphragm has been further improved by performing 3 floor-to-floor welded rebar connections per interface (Figure 5.32b). Figure 5.33 shows a global view of the assembled prototype frame. The slab members are also provided with large steel plates anchored in the member that have been used to weld the lateral load transmission system that connects the structure with the large ELSA reaction wall through 4 jacks with a 1000 kN capacity each. In the transversal direction, in correspondence of the 3 column lines, out-of-plane steel bracers are installed for safety matters. They are de-coupled from the structure for a few centimeters gap, in order to start working only in case of collapse risk, without interfering with the tests.

The prototype plan views are shown in Figure 5.29 for the foundation and roof levels, while in Figure 5.30 the elevation views are collected for both longitudinal and transversal sides.

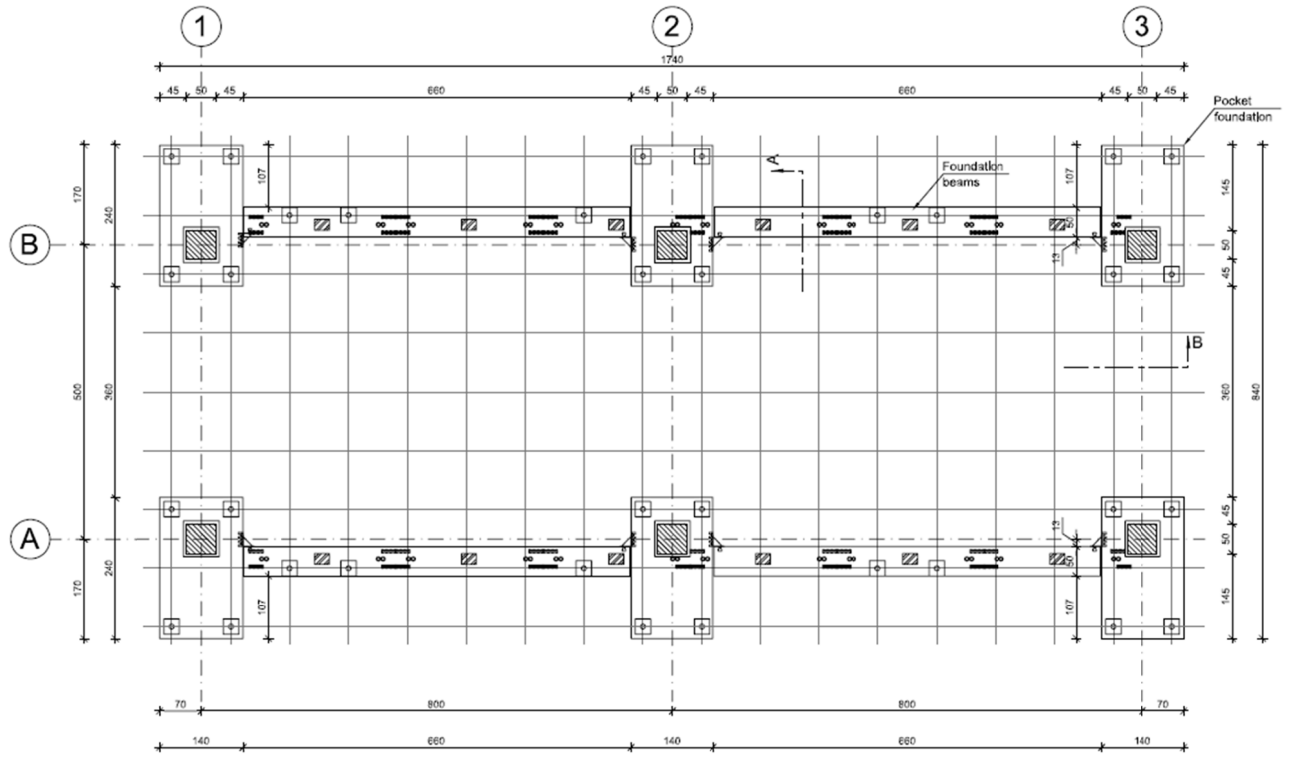

(a)

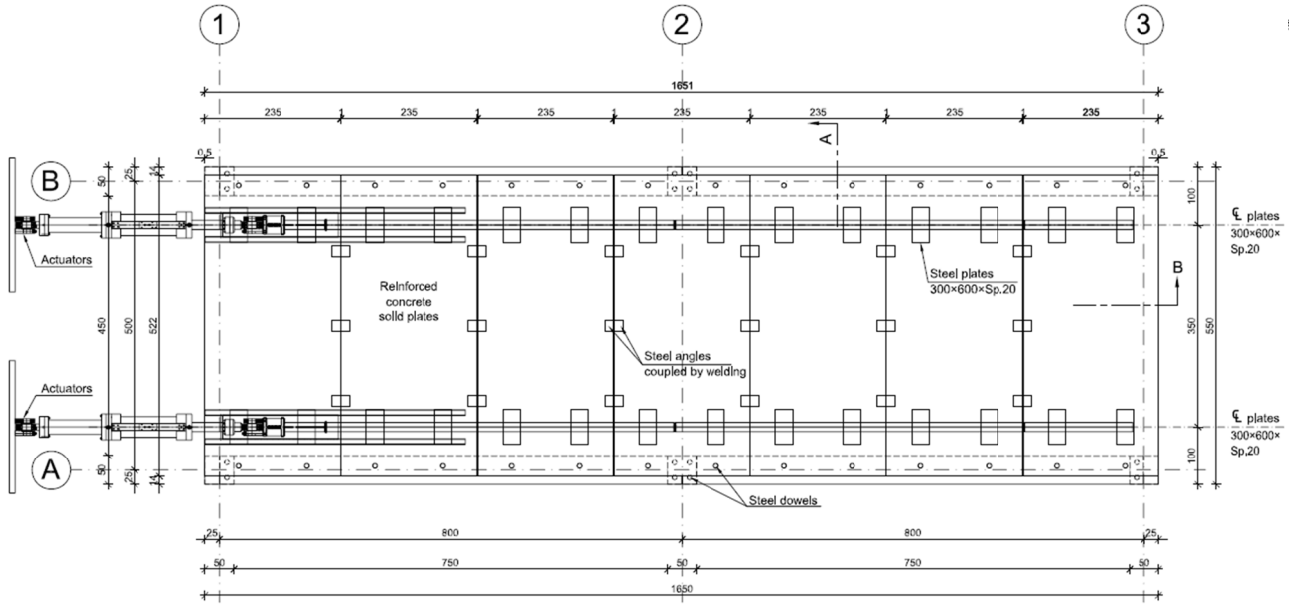

(b)

Figure 5.29 – Prototype plan views: (a) foundation view and (b) roof view

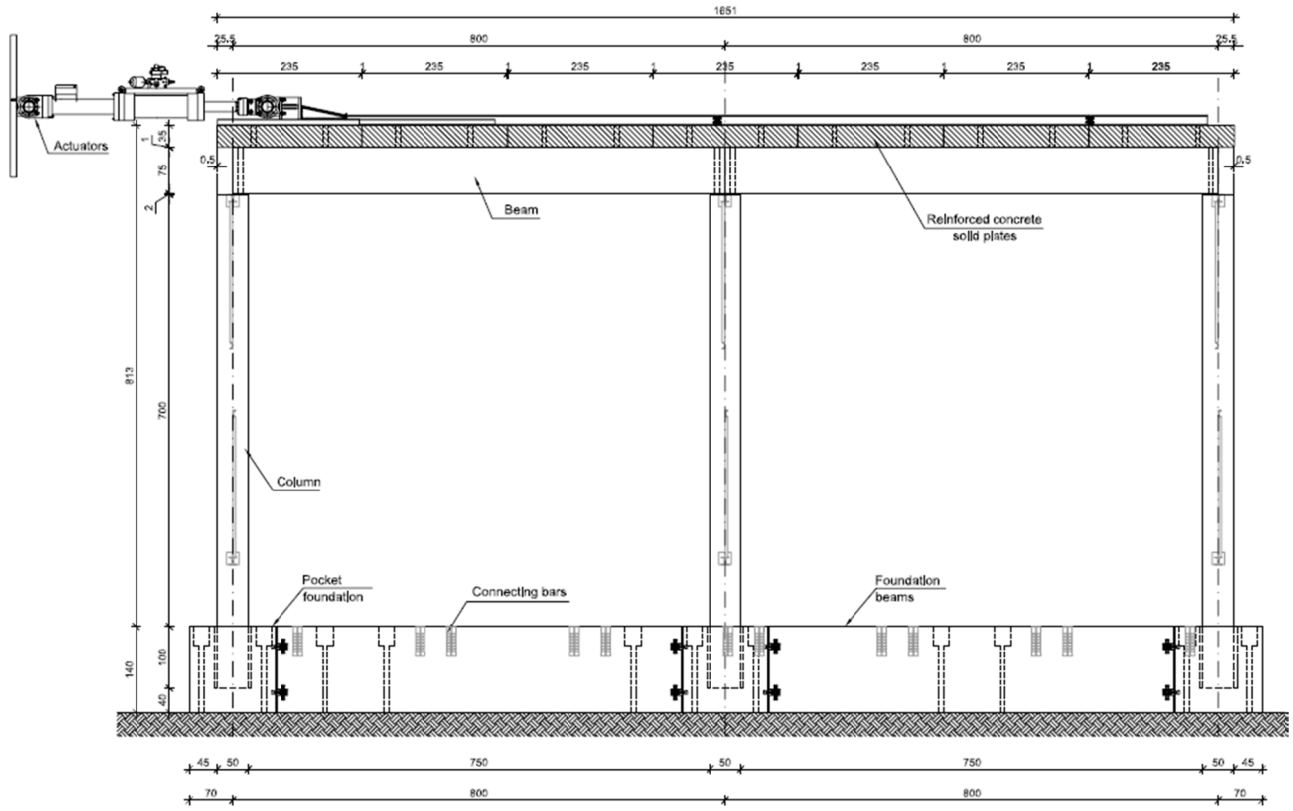

(a)

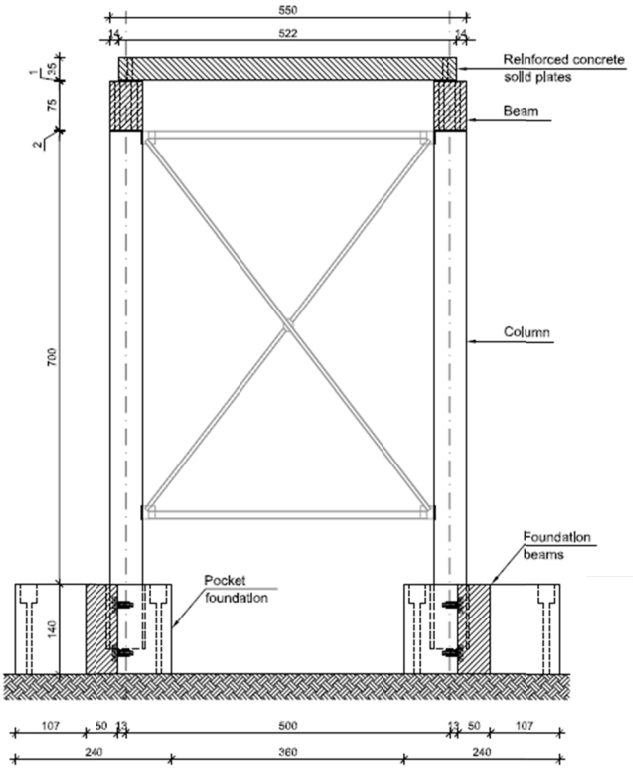

(b)

Figure 5.30 – Prototype elevation views: (a) longitudinal wise and (b**)** transversal wise

Figure 5.31 – Pocket column-to-foundation connections

(a) (b)

Figure 5.32 – (a) distanced dowel beam-to-column connection and (b) floor-to-floor welded rebar connection

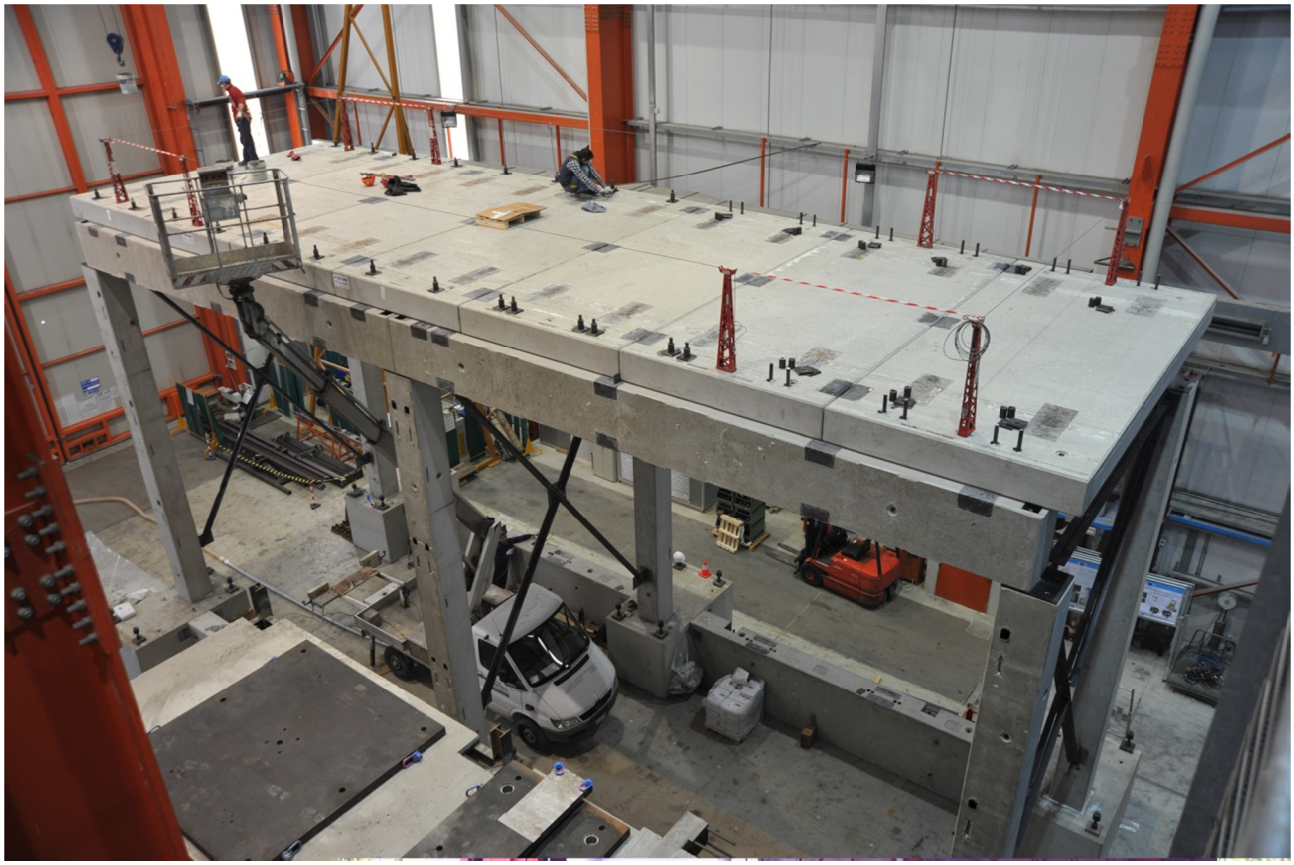

Figure 5.33 – Assembled prototype frame

The structure is tested under three geometric configurations:

- Bare frame,
- Vertical panels,
- Horizontal panels.

In the configuration with vertical panels, the frame is provided with 12 solid 2,49 m by 8,40 m wide panels with 0,20 m of depth, 6 per building longitudinal side. The panels are provided with a base recess for the accommodation of the hinged base connection and with three recesses along the interfaces with the adjacent panels for the accommodation of the FBDs. The panels are not symmetrically placed with respect to the longitudinal frame direction due to problems of geometric interference with the global connection systems. Figure 5.34 shows the elevation view of the prototype with vertical panels and Figure 5.35 shows pictures of the assembled structure.

In the configuration with horizontal panels, the frame is provided with 16 2,09 m by 8,42 m wide panels with 0,20 m of depth, 8 per longitudinal side. The panels are provided with 3 recesses per interface with the adjacent panels for the accommodation of the FBDs.

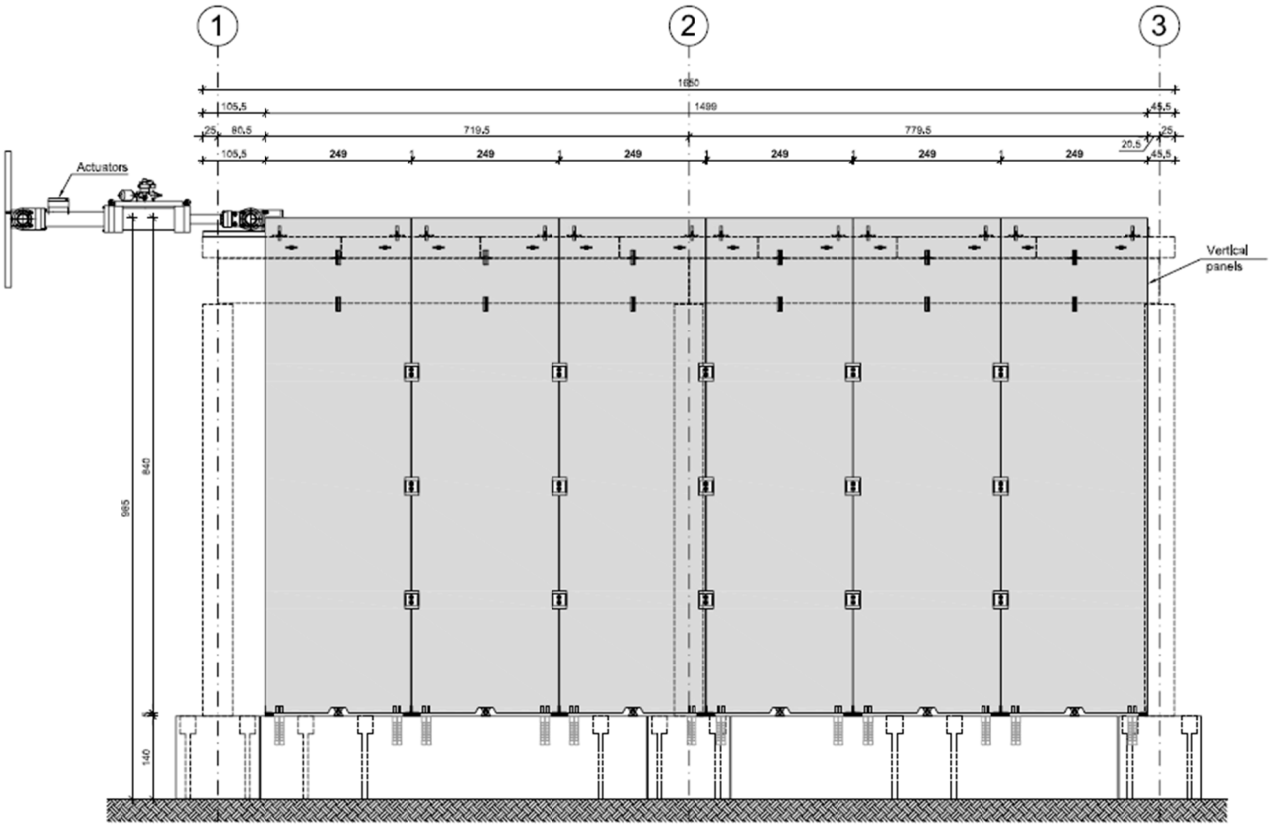

Figure 5.34 – Prototype with vertical panels: elevation longitudinal view

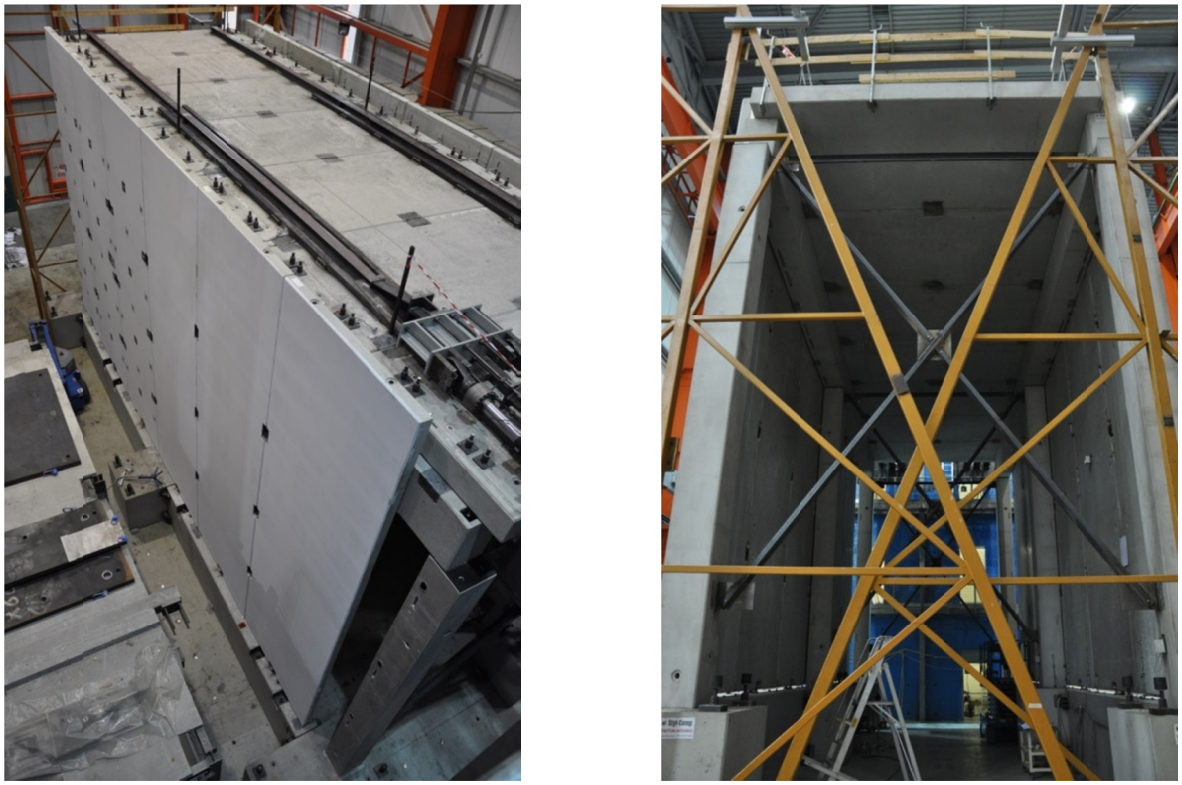

(a) (b)

Figure 5.35 – Prototype with vertical panels: (a) inclined top view and (b) transversal wise bottom view

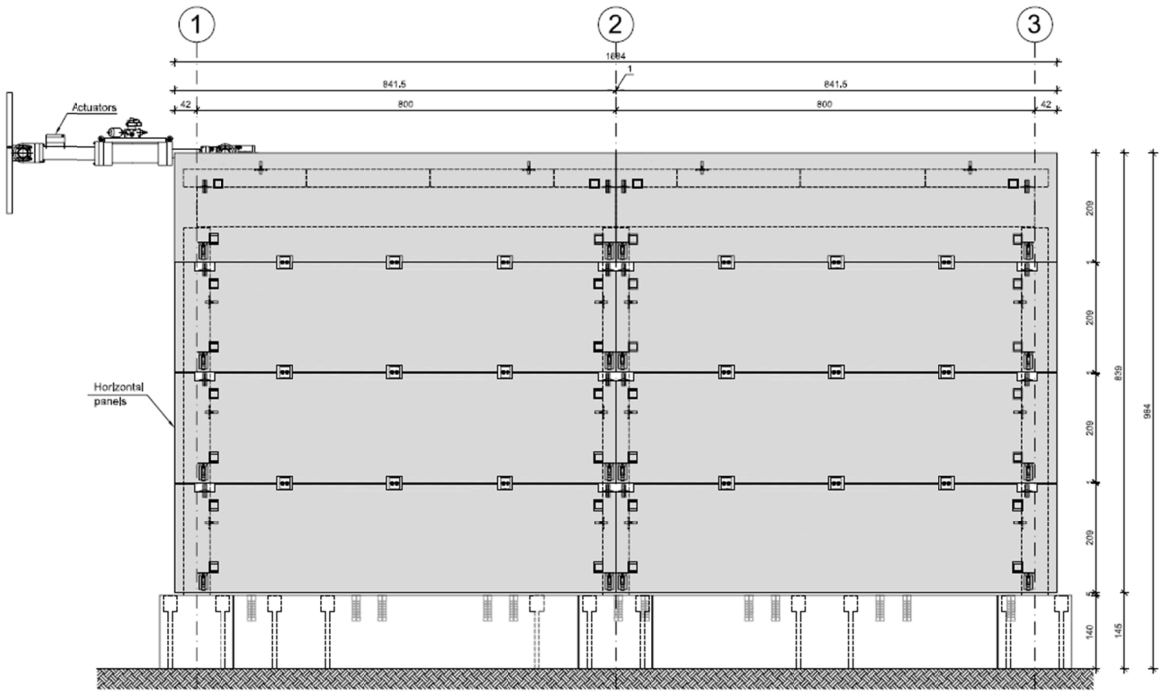

Figure 5.36 – Prototype with horizontal panels: elevation longitudinal view

5.2.1. Test sequence

A large experimental campaign has been performed on the building prototype, with the aim to verify as many proposed cladding panel connections systems as possible with regards to both influence on the dynamic seismic behaviour of the building and correct functioning of all components. The test sequence is reported in Table 5-3. Results from the tests performed on the structure with vertical panels only will be presented in detail.

Two types of test have been performed, namely cyclic and pseudo-dynamic. In all tests, potential torsional rotations of the slab are restrained by imposing an equal stroke to the actuators. The tendency to torsional effects can be observed by comparing eventual load differences between the actuators. Cyclic tests follow an increasing displacement protocol with 40% step increment and with 3 cycle repetitions. One necessary condition of all cyclic tests is to not damage the frame, since it has to be subjected to dozens of tests. Therefore, a drift ratio equal to 0,9%, to which corresponds a displacement of 63 mm, has been chosen to be the target maximum displacement during cyclic tests, since at this displacement column base yielding is expected to be safely far. The protocol is illustrated in Figure 5.37. The displacement steps are: ± 8,4 - 11,7 - 16,4 - 23,0 - 32,1 - 45,0 - 63,0 mm. At the end of the test, in case residual load occurs, it is manually returned to a zero-load position through small cycles around the zero position. In Pseudo-Dynamic tests (also indicated with the acronym PsD) the Modified Tolmezzo accelererogram is applied to the structure. This particular accelerogram is a modification of the registered signal during the Tolmezzo earthquake occurred in 1976 in Italy, enriched in frequencies in order to be compatible with the standard response spectrum. Figure 5.38 shows the un-scaled accelerogram and the response spectrum compared to that provided by EN 1998-1 for subsoil class B. Information about the hybrid numerical-experimental pseudo-dynamic test method is available in Molina & Géradin (2007), Pegon *et al.* (2008) and Molina *et al.* (2010), among others.

Table 5-3 – Test sequence

PANEL	ARRANGEMENT	SYSTEM	PANEL INTERFACE CONNECTIONS	TYPE OF TEST
VERTICAL	PENDULUM	ISOSTATIC	-	CYCLIC
		DISSIPATIVE	3 FBD	CYCLIC
				PsD 0,18g
				PsD 0,36g
				PsD 0,72g
				PsD 1,00g
			2 FBD	CYCLIC
				PsD 0,36g
				PsD 0,72g
			1 FBD	CYCLIC
				PsD 0,36g
		ISOSTATIC	-	CYCLIC
				PsD 0,10g
			SILICONE	PsD 0,10g
				CYCLIC
	ROCKING	DISSIPATIVE	1 FBD	CYCLIC
				PsD 0,36g
		ISOSTATIC	-	CYCLIC
				PsD 0,18g
	CANTILEVER			CYCLIC
		INTEGRATED		PsD 0,18g
				PsD 0,36g
				CYCLIC
HORIZONTAL	SWAYING	ISOSTATIC	-	CYCLIC
		DISSIPATIVE	2 FBD	CYCLIC
				PsD 0,36g
				PsD 0,72g
			1 FBD	CYCLIC
				PsD 0,36g
		ISOSTATIC	-	CYCLIC
				PsD 0,10g
		DISSIPATIVE	2 FPD	CYCLIC
				PsD 0,18g
				PsD 0,36g
		INTEGRATED	4 ANGLES	PsD 0,10g
				PsD 0,18g
				CYCLIC
	SWAYING STRIP WINDOWS			PsD 0,10g
				PsD 0,18g
				CYCLIC
BARE FRAME	-	-	-	PsD 0,18g
				PsD 0,36g
				CYCLIC

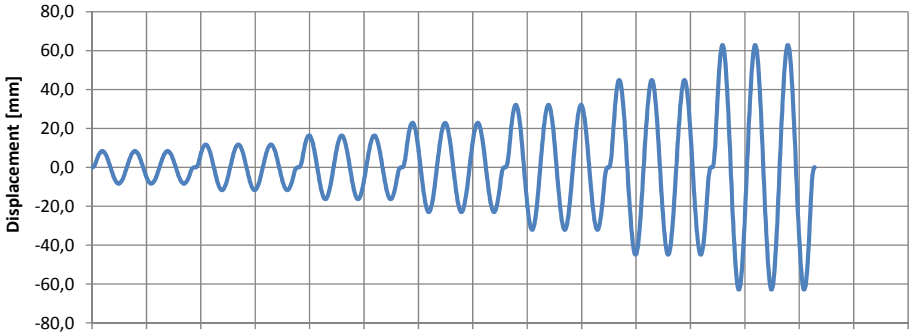

Figure 5.37 – Cyclic protocol

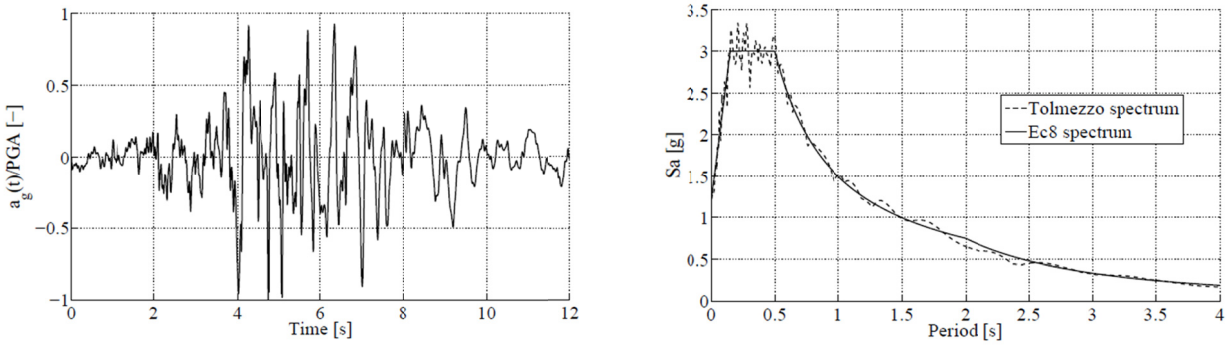

(a) (b)

Figure 5.38 – Modified Tolmezzo earthquake: (a) accelerogram, (b) response spectrum compared to that given by Eurocode 8 for subsoil B

5.2.2. Connections

Several cladding panel connections are employed in the large number of tests to be performed. In the following, a description of the complete list of connections used in the tests is given. At each particular experimental phase, the acting connections will be described.

A shear connector is used to joint cladding and structure (the beam in the vertical panel configuration and the column in the horizontal panel configuration). A commercial steel insert is adopted, specifically designed for cladding panels (Figure 5.39). A V-shaped metallic element is welded on the beam side and inserted through a high-resistance bolt to a vertical channel embedded in the panel. The connection is designed to only prevent horizontal in-plane and out-of-plane displacements.

A steel physical pinned hinge is used to connect vertical panels and foundation (Figure 5.40). A forked plate is welded in correspondence of an embedded steel counter-plate in foundation, a counter-fork plate is welded upperly to the steel plate embedded within the panel recess, and finally a cylindrical steel pin is inserted. The connection is designed to only allow in-plane panel rotations.

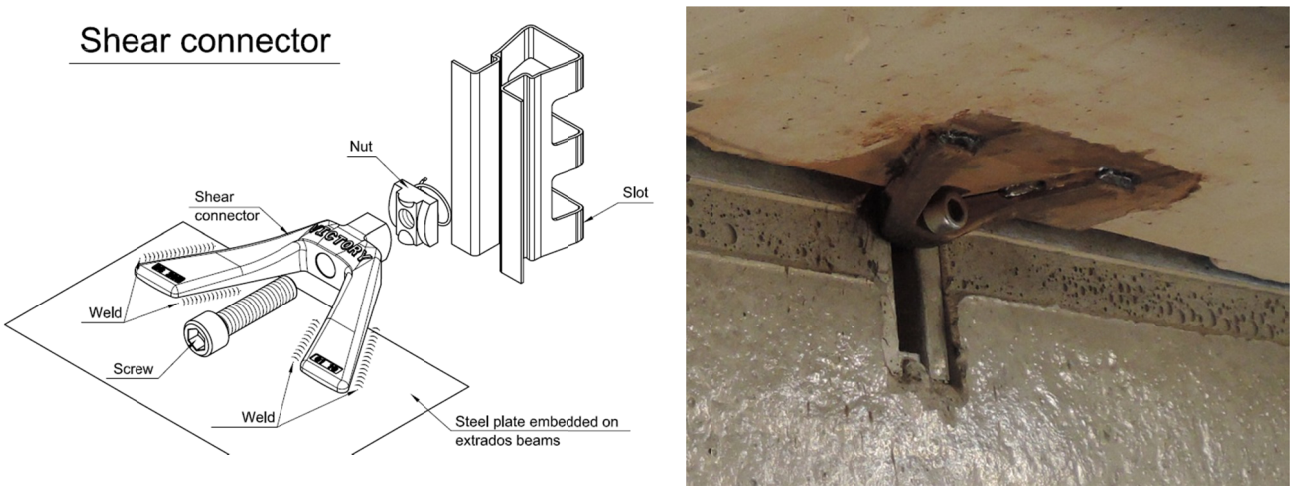

(a) (b)

Figure 5.39 – Shear connector: (a) drawing and (b) picture

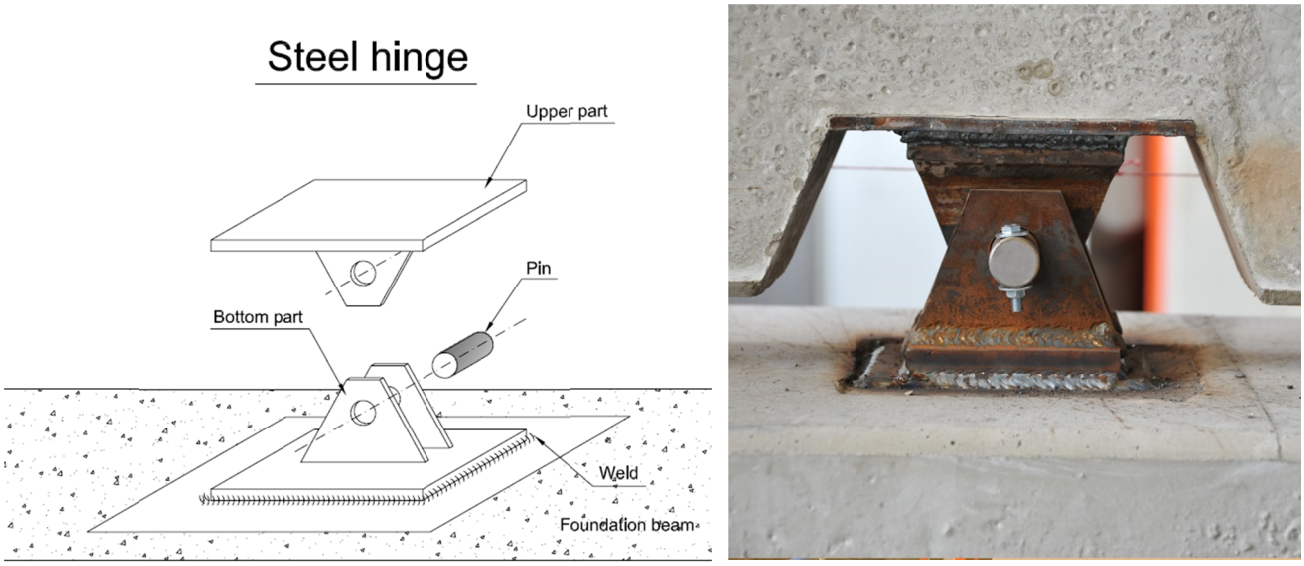

(a) (b)

Figure 5.40 – Base hinge: (a) drawing and (b) picture

Friction Based Devices are used as dissipative connections for both vertical and horizontal panels. The specific connection arrangements for vertical panels are described in Figure 5.41. In the version for vertical panels, a fillet welding has been executed in-situ between the support angle profile and the panel embedded counter-plate along the angle corner, in order to eliminate the connection tolerances and improve the cyclic behaviour.

Steel plates are used to restraint the out-of-plane and the in-plane base displacements of the vertical panels with rocking configuration. Braced angles are juxtaposed at the panel edges from both sides and welded to a base counter-plate. A further steel plate, with the function of emergency in-plane displacements retainer in case the panels tend to slide, is inserted in vertical slots left in the profiles, and then slightly welded at contact lines. A picture of the assembled connection is visible in Figure 5.42. Second-line looped-edges safety rods have been applied in between frame and panels through straight shackles linked to looped-end post-installed mechanical fasteners. A picture of the assembled connection is reported in Figure 5.43. Further push-pull safety connectors have been placed at the top of vertical panels and connected with the beams (Figure 5.44). Those connections have been used for temporary safety panel out-of-plane displacement restrainers during assemblage, but they have been left in their positions in all those test configurations in which large relative displacement between panel and beam were not expected to occur as additional safety devices.

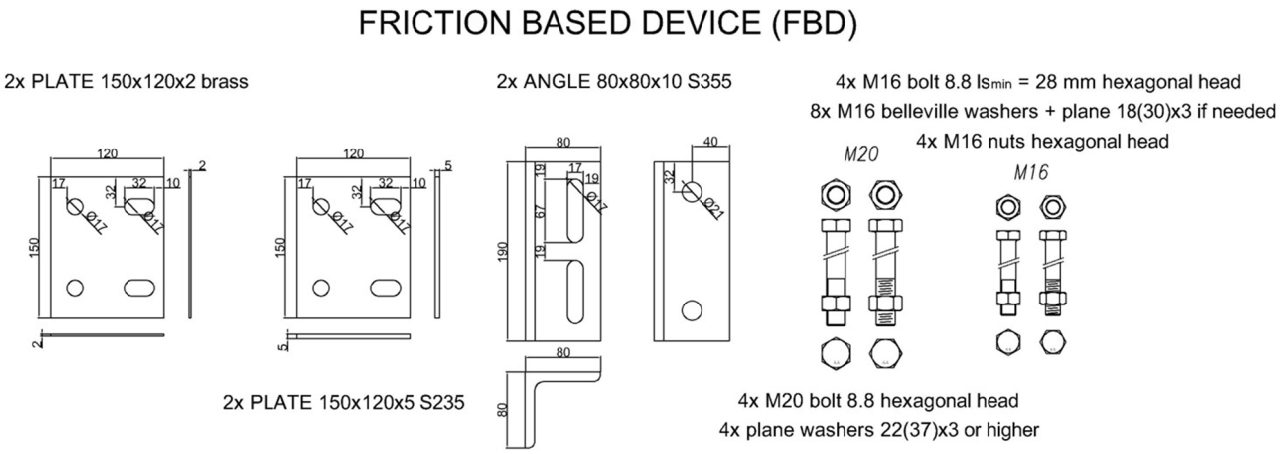

(a)

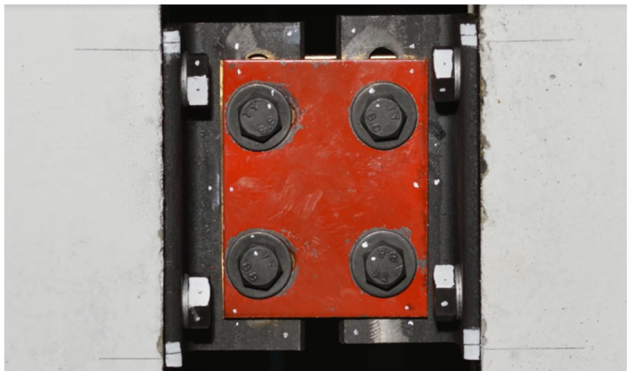

(b)

Figure 5.41 – Friction Based Device for vertical panels: (a) technical drawing and (b) picture

Figure 5.42 – Out-of-plane retainer and in-plane stopper device for rocking configurations

Figure 5.43 – Second-line safety rod

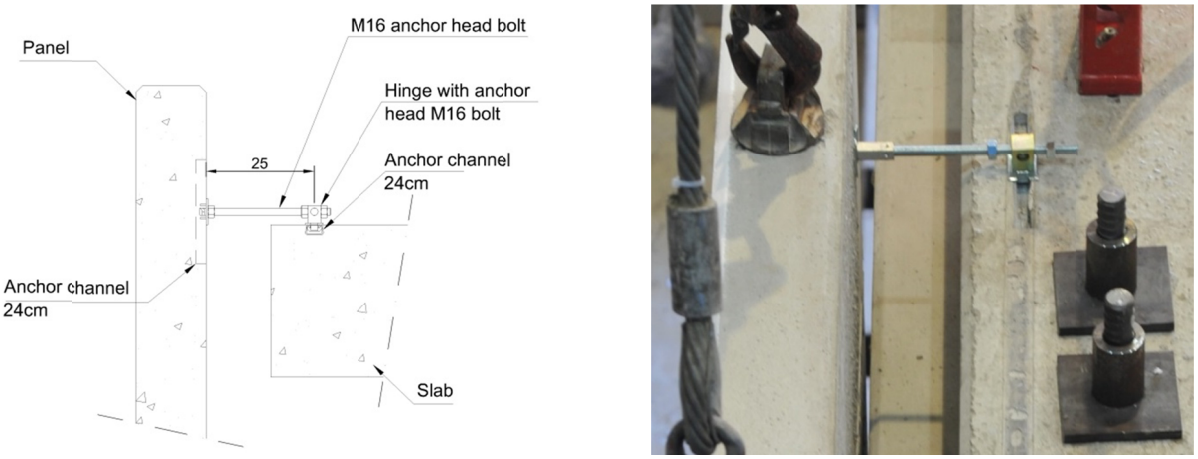

(a) (b)

Figure 5.44 – Provisional push-pull connection used as additional safety device: (a) drawing and (b) picture

5.2.3. Methods for displacement estimation

The feasibility of the experimental program has been assessed through explicit dynamic non-linear analyses and counter-checked with the ADRS (Acceleration-Displacement Response Spectrum) approach for what concerns the evaluation of the maximum displacement expected at each test. The dynamic non-linear analyses have been performed on a finite element model having the features described in the following: The mass is distributed only along the floor members, properly increased in order that the sum of all masses is equal to the design mass, corresponding to 170 tons for the prototype with vertical panels and to 175 tons for the prototype with horizontal panels. Each column is modelled with 28 beam elements, in order to accommodate the geometry. They are clamped at the base and linked to the beams with master/slave links coupling all degrees of freedom. The non-linear moment curvature relationships for external and central columns, having different axial load, are obtained from the characteristic properties of concrete and reinforcing steel. A Sargin model modified in order to take into account the core confinement has been used for concrete, while a bi-linear

elastic-hardening model has been used for steel. A Takeda cyclic model has been assigned to the elements. Each beam is divided into several beam elements, in order to accommodate the geometry. The rotation around the orthogonal horizontal axis is left free, in order to reproduce a perfectly hinged connection over the column. Each solid floor is modelled with two beam elements. They are connected with the beams through master/slave links coupling all degrees of freedom except the rotation around the orthogonal horizontal axis, which is left free in order to reproduce a perfectly hinged connection over the beam. Each panel is modelled with thick rectangular plate/shell elements, with regular sides. For the pendulum system dissipative and isostatic, they are provided with a single hinged connection at the bottom centre and a single connection at the top centre (out-of-plane and horizontal directions are coupled). Finally, the dissipative connections are modelled through a beam connection element, provided with a non-linear perfect elastic-plastic behaviour. The cyclic hysteresis model assigned is a kinematic hardening.

The ADRS approach has been chosen because of its large adaptability to different structural behaviours, such as elastic, hyper-elastic (rocking), friction damped and mixage of the previous. Actually, the method can be directly applied to the experimental results, since it does not depend on the definition of a previously defined multi-linear simplified behaviour, with the problem of indicating yielding displacement in structures in which this definition could be largely random or characterised by multiple yielding (e.g. flexible ductile frames braced with dissipative connections).

The procedure follows the following steps:

- The experimental results from the cyclic test are analysed in terms of specific dissipated energy in order to get a series of equivalent viscous damping factors on the base of the formulation: $\zeta_{eq} = \zeta_0 + E_d/(4\pi E_s)$, where ζ_0 is the explicit viscous damping of the structure (which is considered negligible for the material used and has not been included in the pseudo-dynamic testing procedure) and $E_s = \delta(Pmax + |Pmin|)/4$ is calculated according to the illustration of Figure 5.45 for a non-symmetric and non-injective cyclic behaviour, which corresponds to one eight of the specific dissipated energy calculated with reference of an equivalent perfect rigid-plastic cyclic behaviour. Since three cycle repetitions have been performed according to the cyclic load protocol, an average value is used among the three obtained.
- The experimental results from the cyclic test are plotted in terms of backbone capacity curve on an acceleration vs displacement diagram. A pushover curve correctly fitting the backbone curve can be plotted in order to estimate the behaviour at larger displacement than the maximum attained during the cyclic test.
- The demand curve is plotted according to the response spectrum of the accelerogram in the same diagram, with an initial equivalent damping ratio ζ_{eq} guess value.
- The intersection point between the capacity and the demand curve represents the performance point. The equivalent damping ratio ζ_{eq} value is then updated on the base of the corresponding displacement estimation and the interpolation (or extrapolation, if applicable) value between those experimentally obtained. This operation is repeated until convergence is attained.

- In case relevant asymmetry characterise the behaviour, both positive and negative backbone curves are plotted in the same diagram.

In order to derive extrapolated backbone curves, the definition of the yielding displacement for the precast frame has been performed according to the formulation provided in Priestley *et al.* (2007), which is not far from that calculated with a pushover analysis of the bare frame.

The experimental results of pseudo-dynamic tests illustrated in the following are all accompanied by the corresponding explicit dynamic non-linear analysis and by the displacement estimation calculated with the ADRS method.

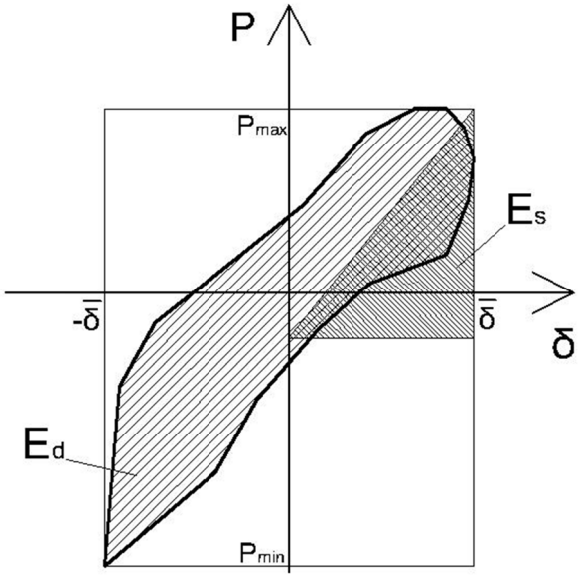

Figure 5.45 – Equivalent viscous damping factor, definition of dissipated energy and reference pattern to derive the specific energy for a non-symmetric non-injective behaviour

5.2.4. Structure with vertical panels – Isostatic systems

5.2.4.1. Pendulum arrangement

The connection configuration of the pendulum arrangement is represented in Figure 5.46 and is made with a central shear connector at the top and a central steel hinge at the bottom. The bottom hinge also prevents the rotation along the vertical axis, but two push-pull connections have been left acting at the panel top as additional safety rods. Two cyclic tests have been performed on this configuration, before and after the long series of tests with dissipative connections.

The results of the first test performed are reported in Figure 5.47, the results of the second test are reported in Figure 5.48. The behaviour of the structure is, as expected, quasi-elastic up to the maximum drift attained (0,9% of the column free height). The effect of the long series of tests may be recognised in a lower stiffness, from 3,0 kN/mm to 2,7 kN/mm from the first to the second test, probably due to a slight stiffness degradation occurred because of the large

number of cycles in which column base cracking occurred. The equivalent elastic cracked stiffness of the column is found to be 3,3 to 3,6 times lower than the non-cracked with a simple calculation based on the cantilever column scheme. The values of average equivalent viscous damping ratio per each displacement step are reported in Table 5-4 for the first test and in Table 5-5 for the second. A pseudo-dynamic test has been carried out with a PGA equal to 0,10g. The results (Figure 5.49) show a flexible behaviour, with several seconds of delay between the largest acceleration peaks and the largest drifts attained by the structure.

The numerical simulation (Figure 5.50) shows good approximation, with an apparent slight over-estimation of the column stiffness, which is in line with the cyclic behaviour of the frame shown in the first test. It is important to note that both in the test and in the model the actual shear in the panel connection is practically null, due to the fact that the mass is concentrated in correspondence of the diaphragm.

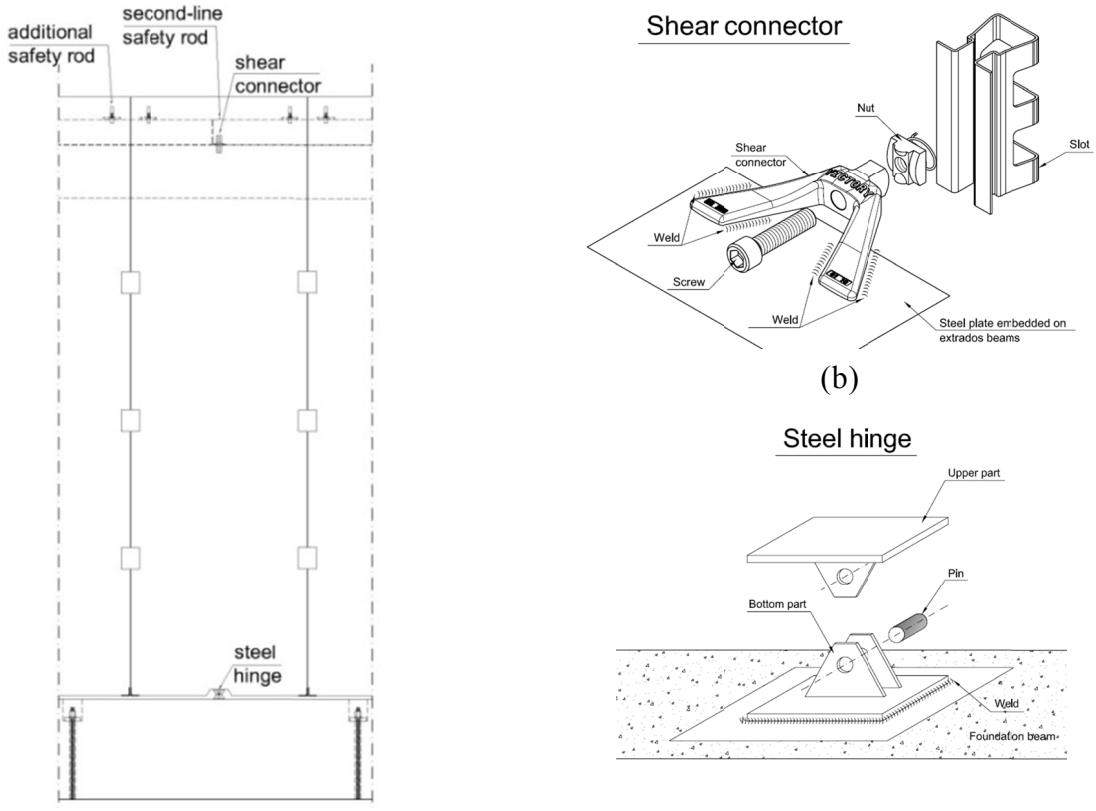

(a) (b) (c)

Figure 5.46 – Pendulum arrangement: (a) front view of the panel, (b) top shear connection, (c) base steel hinge

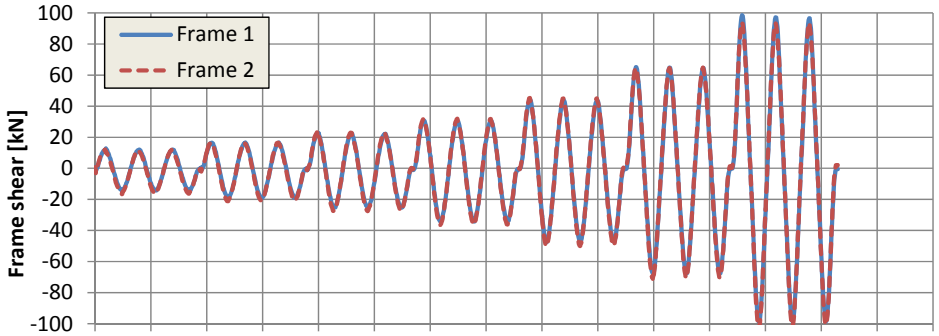

(a)

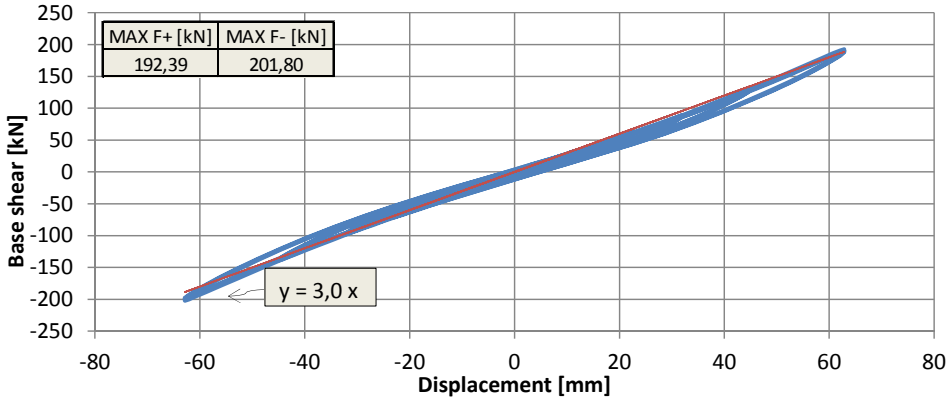

(b)

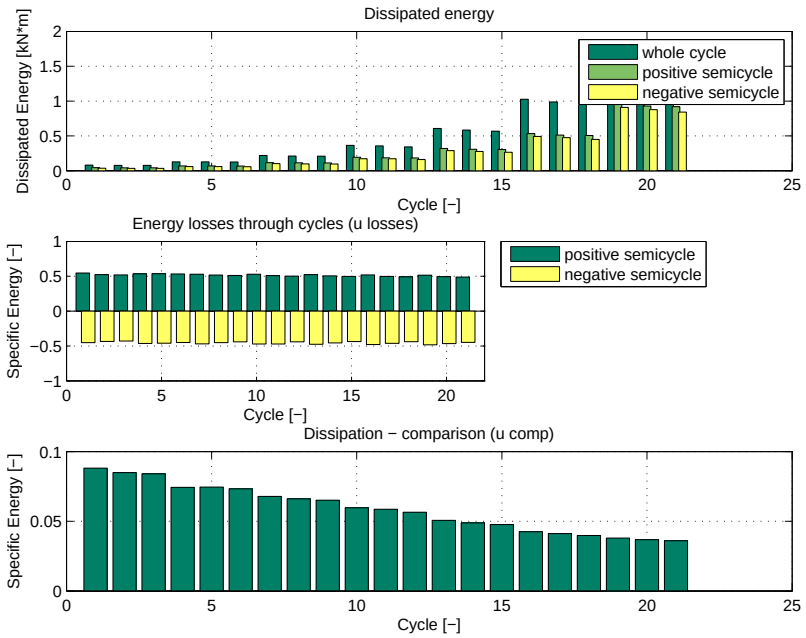

(c)

Figure 5.47 – Pendulum arrangement, cyclic test 1: (a) frame shear load history, (b) base shear vs displacement and (c) energy dissipation properties

Table 5-4 – Pendulum arrangement, cyclic test 1: equivalent viscous damping ratio

d [mm]	8,4	11,7	16,4	23,0	32,1	45,0	63,0
ζ_{eq} [%]	5,5	4,7	4,2	3,7	3,1	2,6	2,4

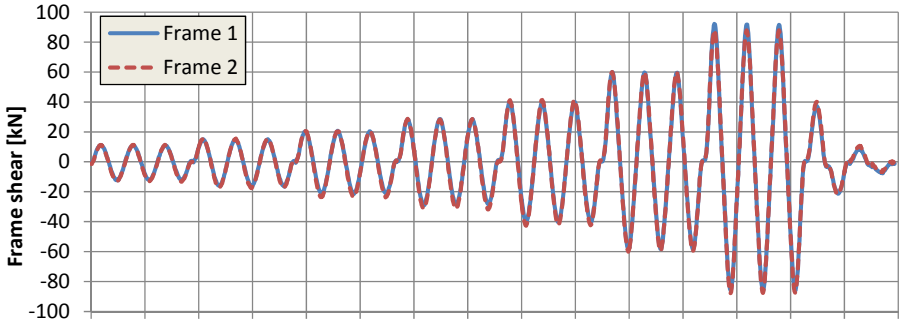

(a)

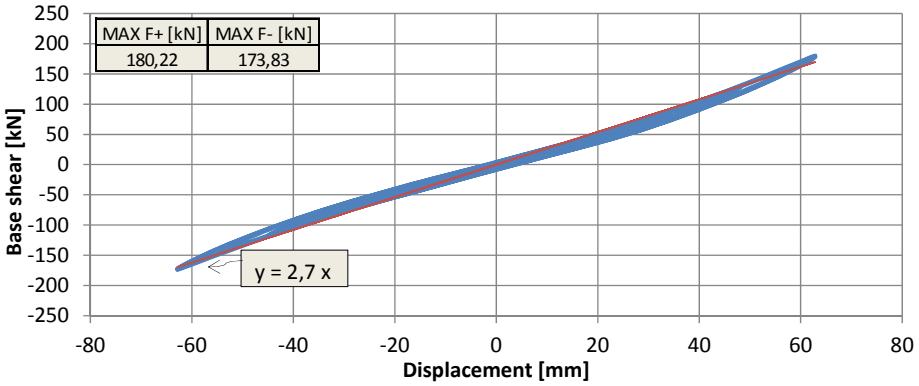

(b)

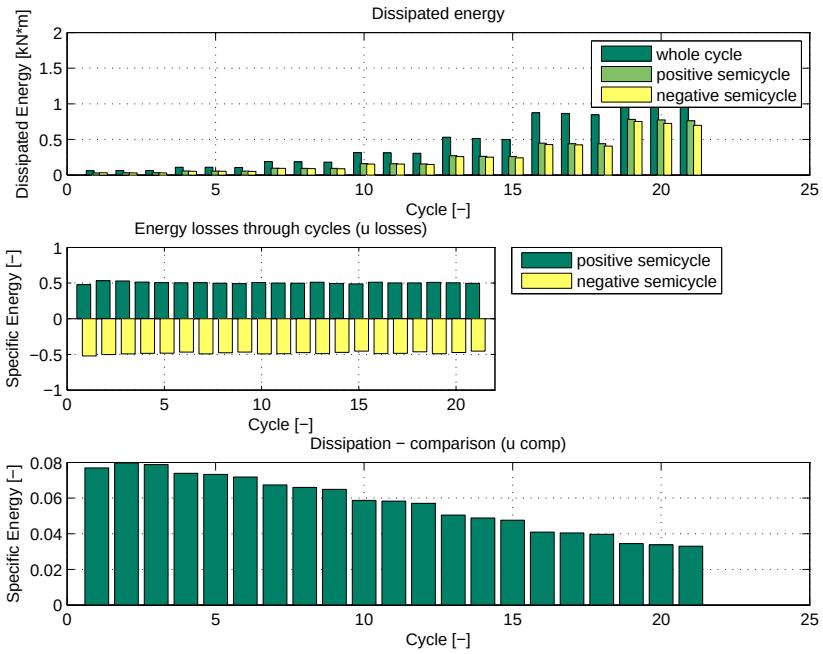

(c)

Figure 5.48 – Pendulum arrangement, cyclic test 2: (a) frame shear load history, (b) base shear vs displacement and (c) energy dissipation properties

Table 5-5 – Pendulum arrangement, cyclic test 2: equivalent viscous damping ratio per step

d [mm]	8,4	11,7	16,4	23,0	32,1	45,0	63,0
ζ_{eq} [%]	5,0	4,7	4,2	3,7	3,1	2,6	2,1

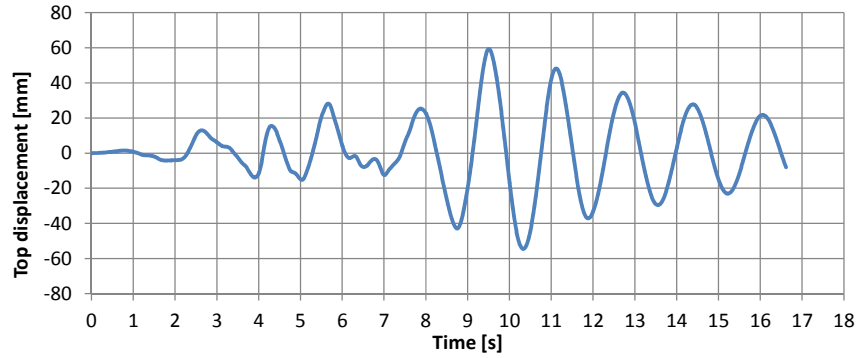

(a)

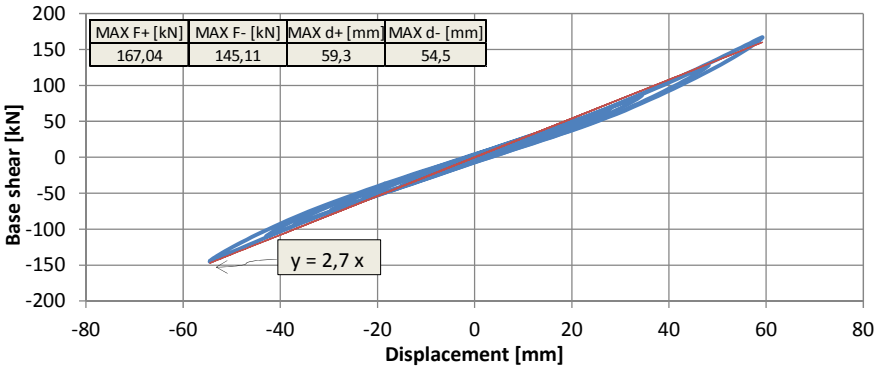

(b)

Figure 5.49 – Pendulum arrangement, PsD test with PGA = 0,10g: (a) vibratory curve and (b) base shear vs displacement

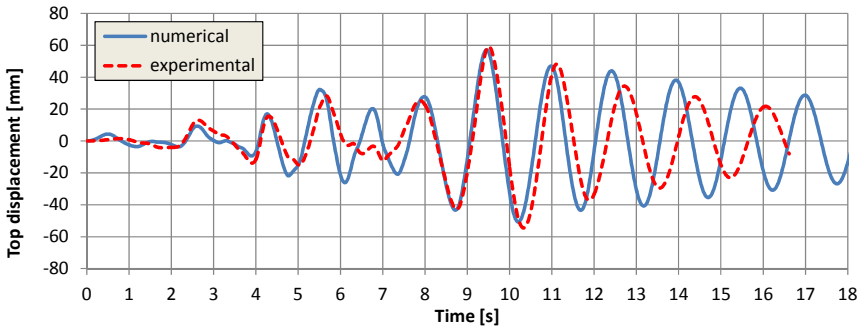

(a)

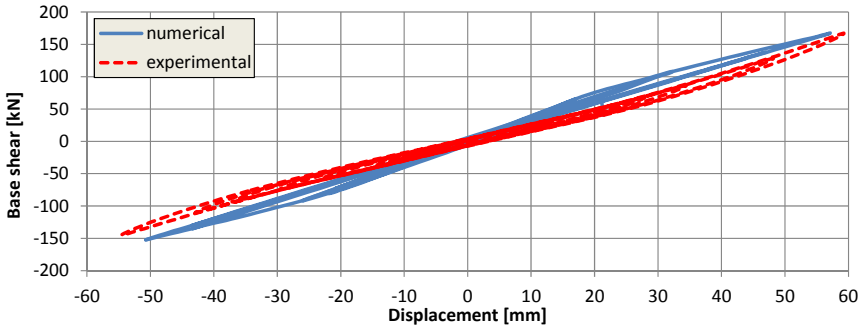

(b)

Figure 5.50 – Pendulum arrangement, numerical simulation with PGA = 0,10g: (a) vibratory curve and (b) base shear vs displacement

The ADRS procedure leads to an accurately estimated value of peak displacement for the experimental and the pushover curve, equal to 57 mm (-4% with respect to the experimental results) with an interpolated equivalent viscous damping ratio equal to 2,3% (Figure 5.51). The same procedure shows that column yielding would occur for the earthquake scaled at not less than 0,22g of PGA. The corresponding equivalent viscous damping, obtained for extrapolation of the experimental results, is very low.

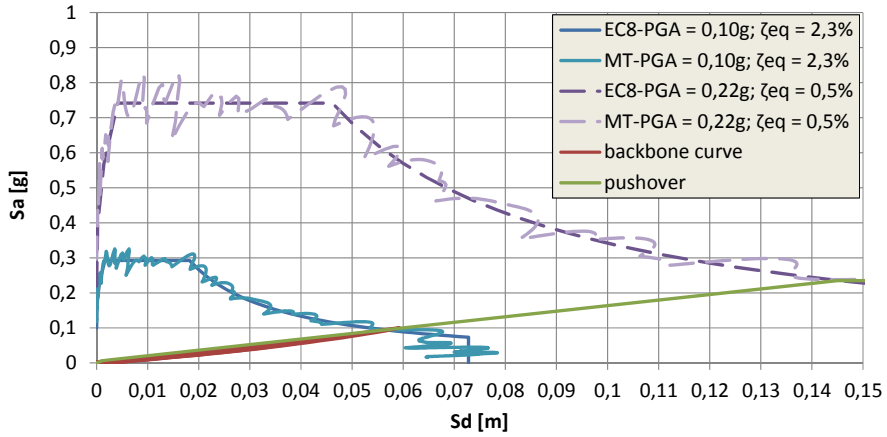

Figure 5.51 – Pendulum arrangement: maximum displacement according to ADRS procedure

5.2.4.2. Pendulum arrangement with silicone sealant

The pendulum structural configuration with added double layer of 10 mm deep silicone strips is represented in Figure 5.52. Silicone has been sprayed at the exterior and interior interfaces between panels, for a total external length of 7,5 m (8,4 m less three recesses of 0,3 m of length each) and a total internal length of 6,1 m (under beam height of 7,0 m less three recesses of 0,3 m of length each). The equivalent silicone strip length for each interface is therefore equal to 7,5 + 6,1 = 13,6 m. Silicone has been left 10 days to attain maturation, due to the strict laboratory testing program. Small samples sprayed in contemporaneity with the application to the structure and cut before the test execution suggested that the polymeration of silicone had been correctly reached before the test.

A pseudo-dynamic test has been carried out with a PGA equal to 0,10g. The numerical simulation, conducted in accordance with the panel sub-assembly design rules regarding the stiffness change in presence of silicone, which results are reported in comparison with the experimental in Figure 5.53, shows that the numerical model is able to catch with accuracy the experimental results. A direct comparison with the pure isostatic arrangement, graphed in Figure 5.54, shows that to slightly reduced displacements correspond slightly enlarged forces. The elastic stiffness is increased by about 50%. A cyclic test has been performed afterwards, in order to not risk to damage the silicone before the pseudo-dynamic test. The results, reported in Figure 5.55, show a similar behaviour with respect to what observed during the PsD test. A relevant force cyclic degradation has been observed during the maximum displacement cycle, which suggests that silicone attained its maximum reistance and entered the softening branch. The values of average equivalent viscous damping ratio per each displacement step are reported in Table 5-6. Figure 5.56 shows the displaced silicone.

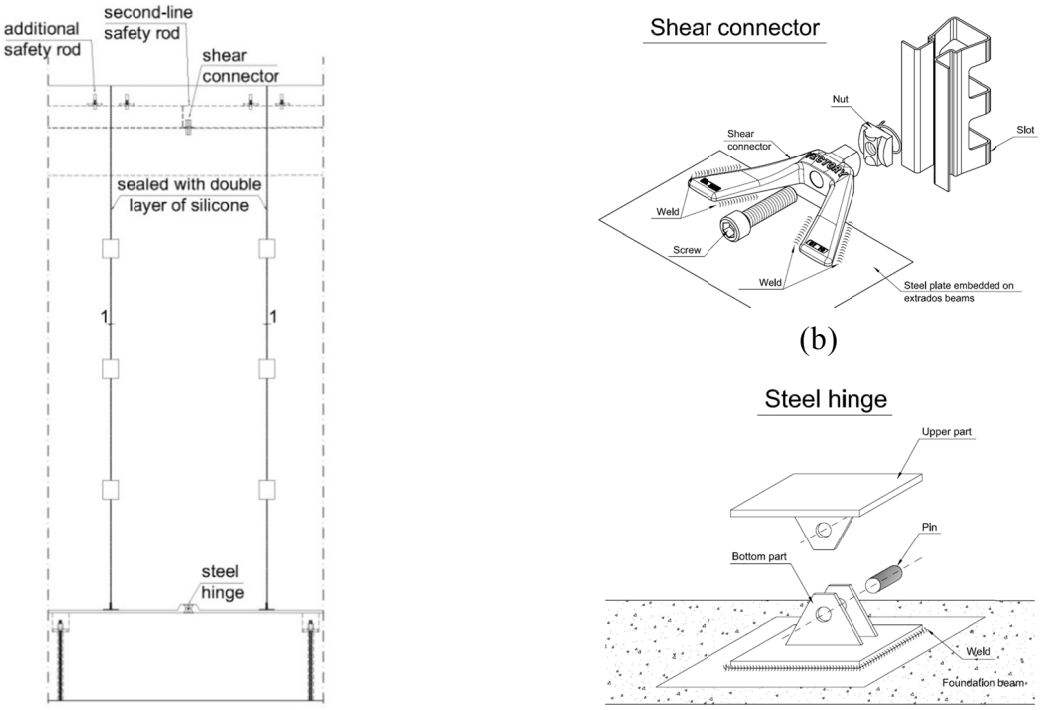

(a) (b) (c)

Figure 5.52 – Pendulum arrangement with silicone sealant: (a) front view of the panel, (b) top shear connection, (c) base steel hinge

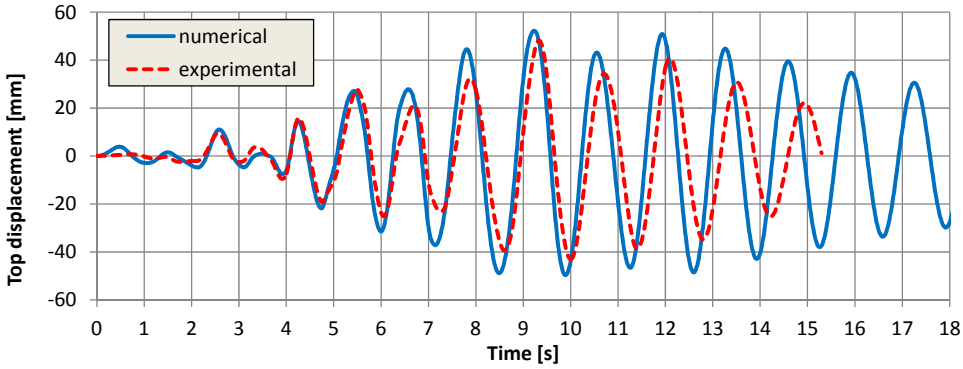

(a)

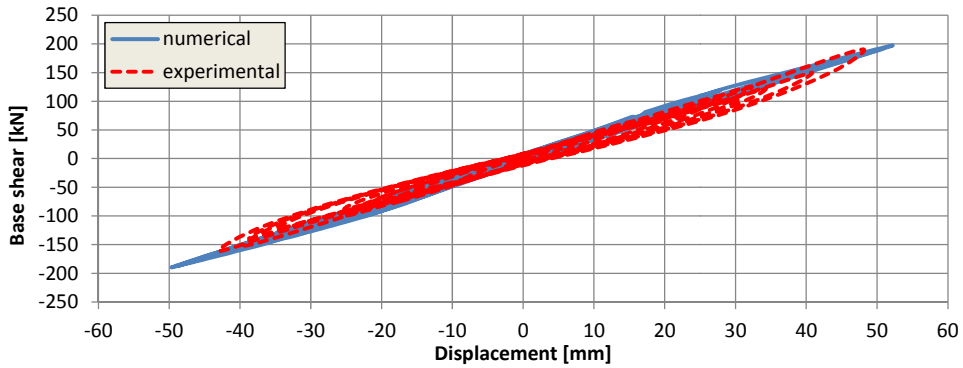

(b)

Figure 5.53 – Pendulum arrangement with silicone sealant, numerical simulation with PGA = 0,10g: (a) vibratory curve and (b) base shear vs displacement

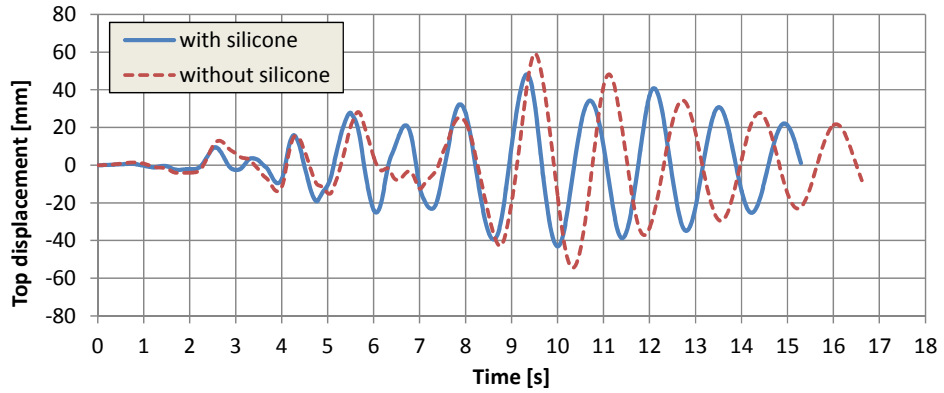

(a)

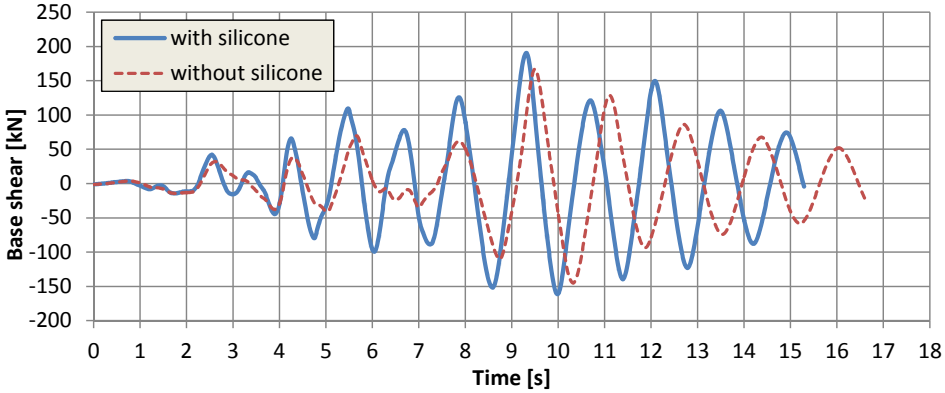

(b)

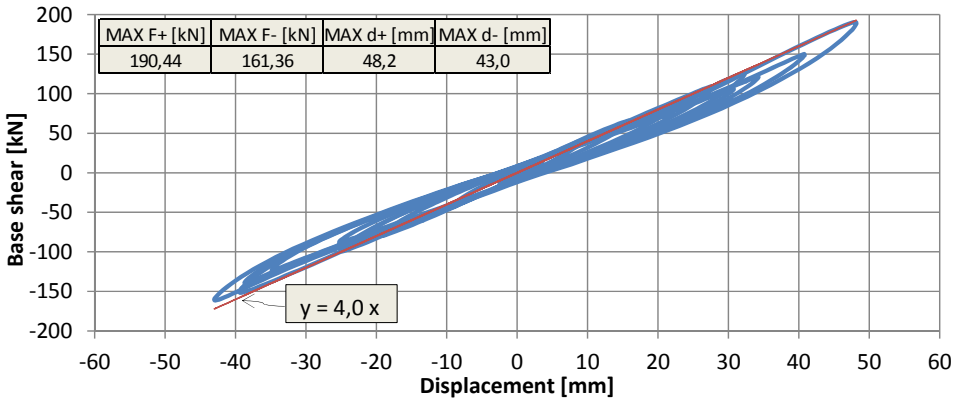

(c)

Figure 5.54 – Pendulum arrangement with silicone sealant, PsD test with PGA = 0,10g: (a) vibratory curve, (b) base shear load history and (c) base shear vs displacement

The ADRS procedure leads to the same slightly under-estimated value of peak displacement for the experimental and the pushover curve, equal to 43 mm (-11% with respect to the experimental results) with an interpolated equivalent viscous damping ratio equal to 4,0% (Figure 5.57). Since silicone is taken close to failure at this level of displacement, the simplified method for stronger earthquakes should be applied with reference to the purely isostatic connection arrangement.

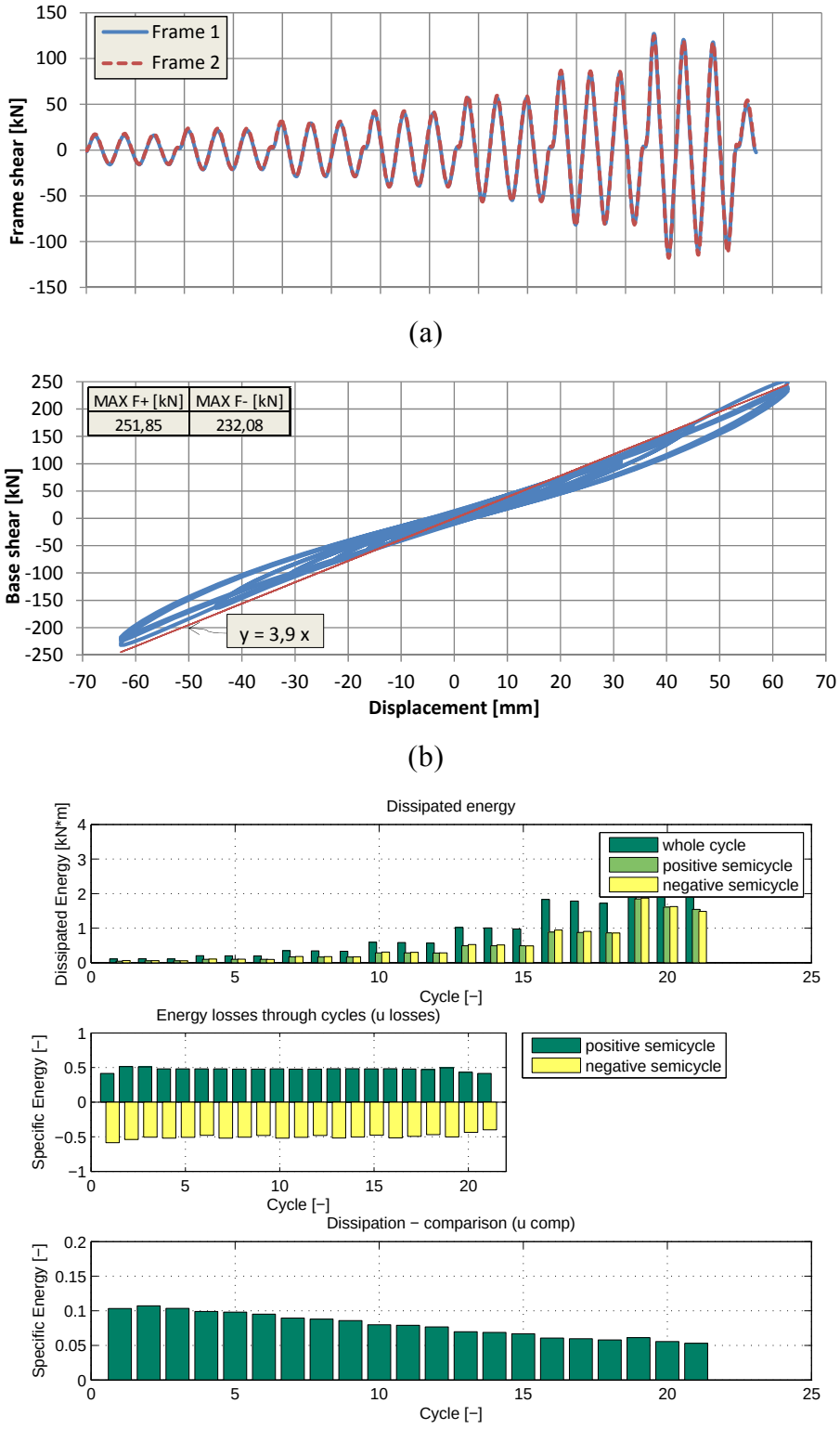

Figure 5.55 – Pendulum arrangement with silicone sealant, cyclic test: (a) frame shear load history, (b) base shear vs displacement and (c) energy dissipation properties

Table 5-6 – Pendulum arrangement with silicone sealant, cyclic test: equivalent viscous damping ratio

d [mm]	8,4	11,7	16,4	23,0	32,1	45,0	63,0
ζ_{eq} [%]	6,7	6,2	5,6	5,0	4,6	3,8	3,6

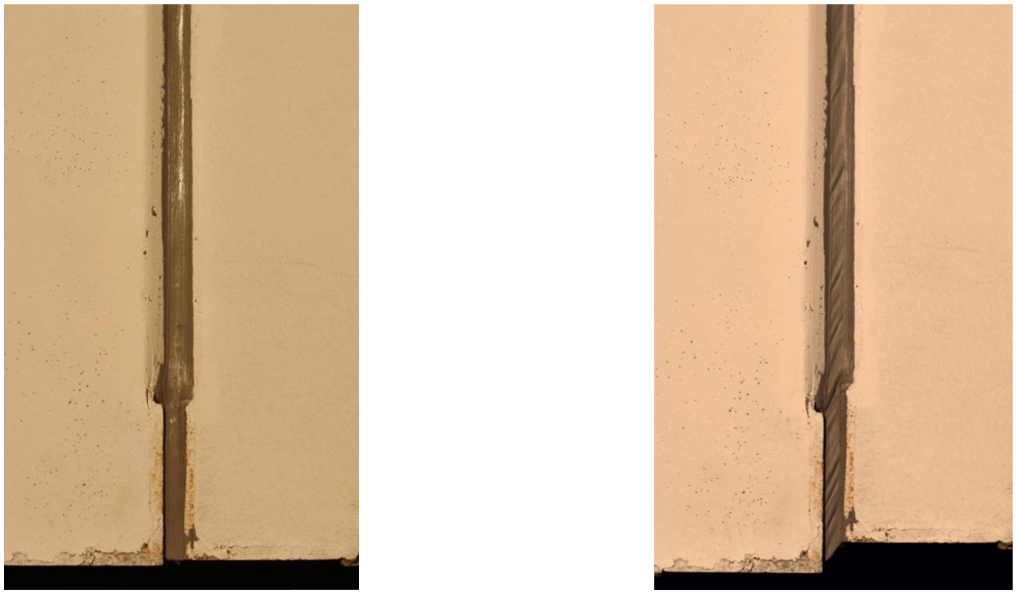

(a) (b)

Figure 5.56 – Pendulum arrangement with silicone sealant, cyclic test: (a) particular of the base portion of silicone strip before the test and (b) displaced behaviour at 0,9% of drift

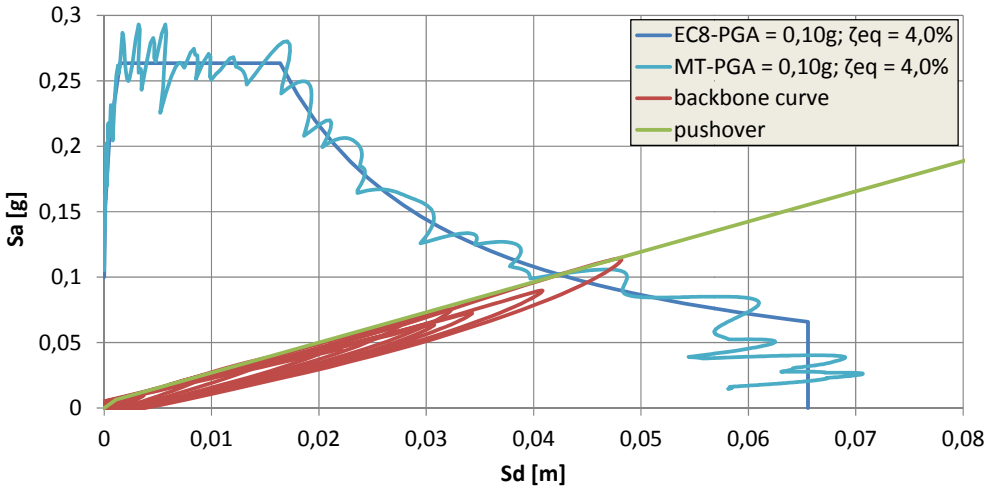

Figure 5.57 – Pendulum arrangement with silicone sealant: maximum displacement according to ADRS procedure

5.2.4.3. Rocking arrangement

The connection configuration of the rocking arrangement is represented in Figure 5.58 and is made with a central shear connector at the top and a simple support on steel shims at both bottom edges, which are also provided with out-of-plane restrainers.

The results of the cyclic test are reported in Figure 5.59 and show a flexible elastic behaviour, after which a more flexible elastic branch occurs when the panels are lifted, with a stiffness similar to that of the frame only. The global behaviour may be defined hyper-elastic, since to strong stiffness lowering does not correspond dissipation of energy.

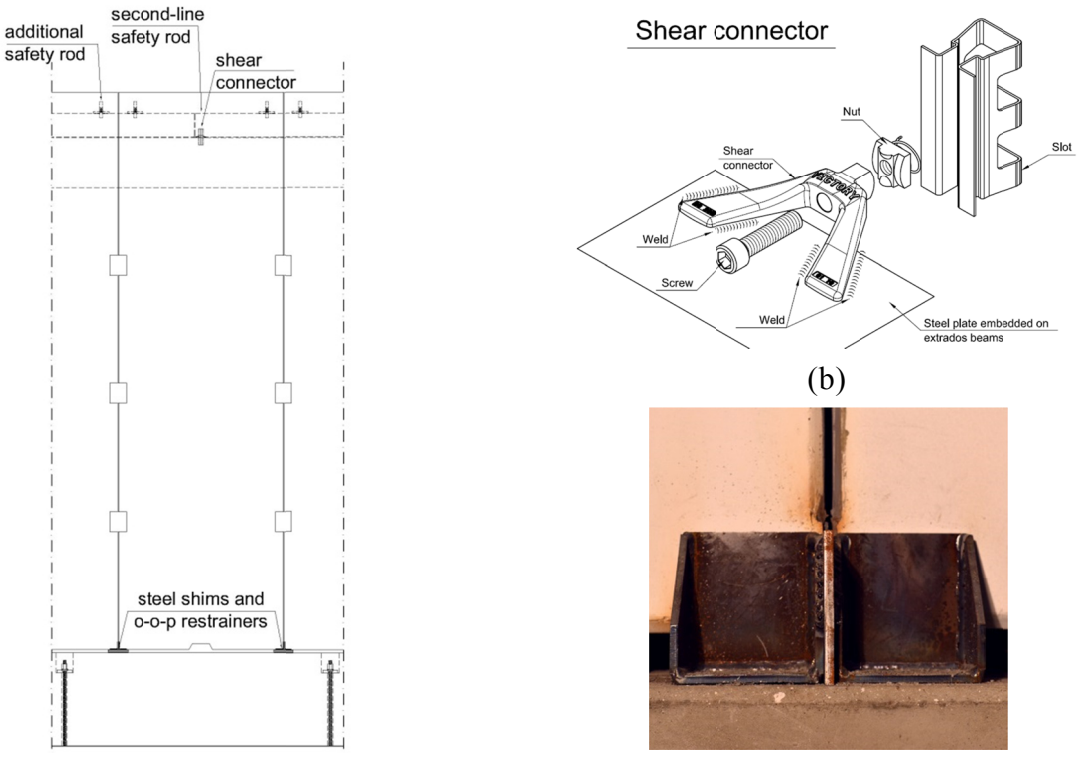

Figure 5.58 – Rocking arrangement: (a) front view of the panel, (b) top shear connection, (c) base steel shims and out-of-plane restrainers

After a visual inspection, it has been found that most of the top shear connectors suffered strong damage during the imposed vertical displacement, which is probably the cause of the low initial stiffness. The failures are likely to be occurred during the previous test carried out on the same configuration provided with a FBD per interface. The behaviour shows a slight asymmetry between the two frames parallel to the imposed displacement, as shown in Figure 5.59a. The values of average equivalent viscous damping ratio per each displacement step are reported in Table 5-7.

The PsD test with PGA equal to 0,18g, which results are collected in Figure 5.60, suggests that the panel weight is very efficient in reducing the building displacement, if compared to the equivalent structure with pendulum arrangement. However, the peculiar cyclic behaviour with enlarged initial stiffness to which does not correspond dissipation of energy is only efficient for low PGA earthquake, corresponding to serviceability limit state for the model structure. The numerical simulation (Figure 5.61) does not correctly match the initial elastic stiffness, even if considering the existing gap in the shear connections, due to the bad functioning of those connections.

The ADRS procedure leads to a very largely over-estimated value of peak displacement for the experimental and the pushover curve, equal to 72 mm (+95% with respect to the experimental results) with an interpolated equivalent viscous damping ratio equal to 2,9% (Figure 5.62). The same procedure shows that column yielding would occur for the earthquake scaled at not less than 0,31g of PGA. The corresponding equivalent viscous damping, obtained for extrapolation of the experimental results, is equal to 2,1%.

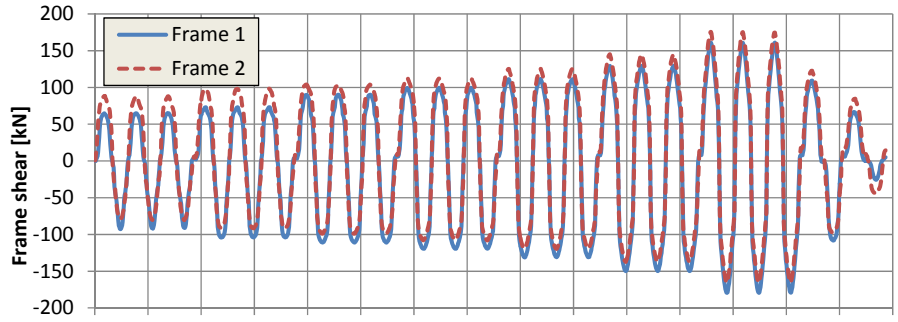

(a)

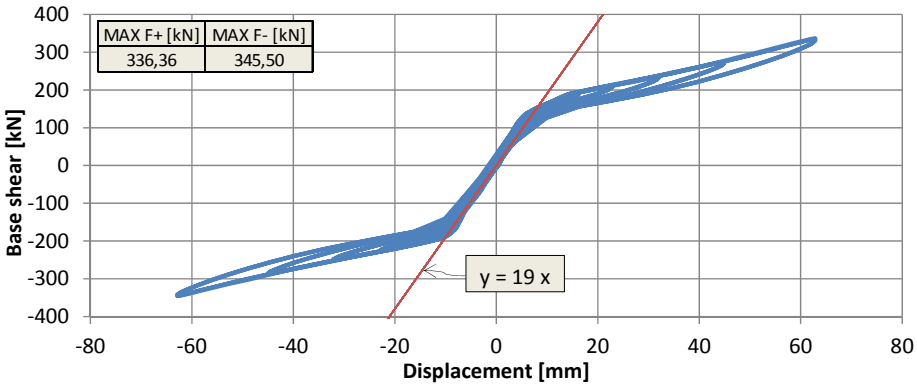

(b)

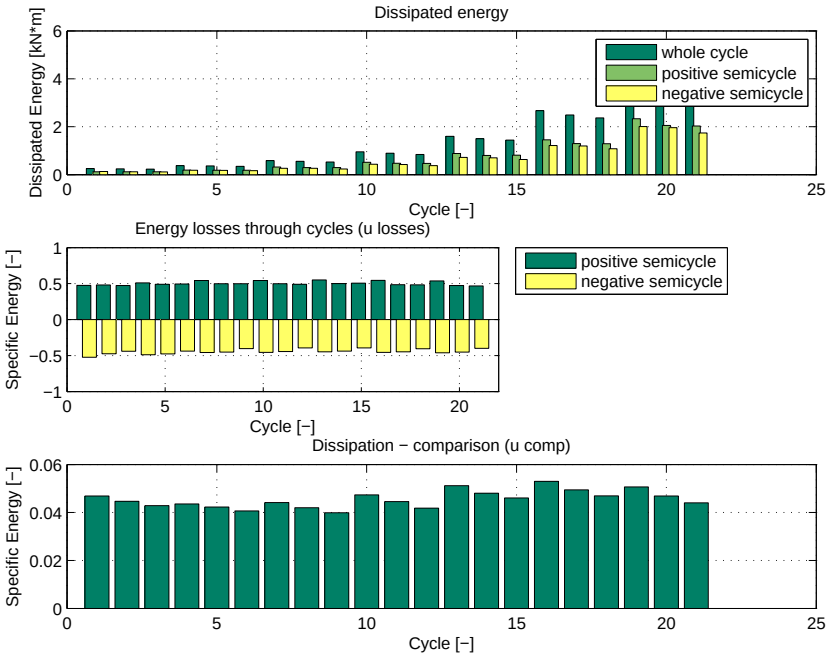

(c)

Figure 5.59 – Rocking arrangement, cyclic test: (a) frame shear load history, (b) base shear vs displacement and (c) energy dissipation properties

Table 5-7 – Rocking arrangement, cyclic test: equivalent viscous damping ratio

d [mm]	8,4	11,7	16,4	23,0	32,1	45,0	63,0
ζ_{eq} [%]	2,9	2,7	2,7	2,8	3,1	3,2	3,0

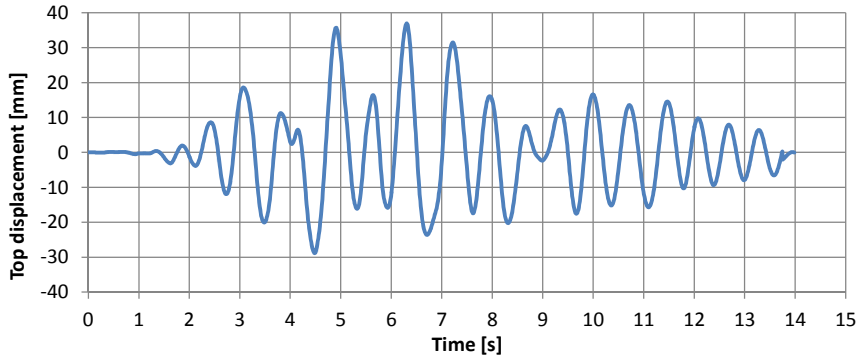

(a)

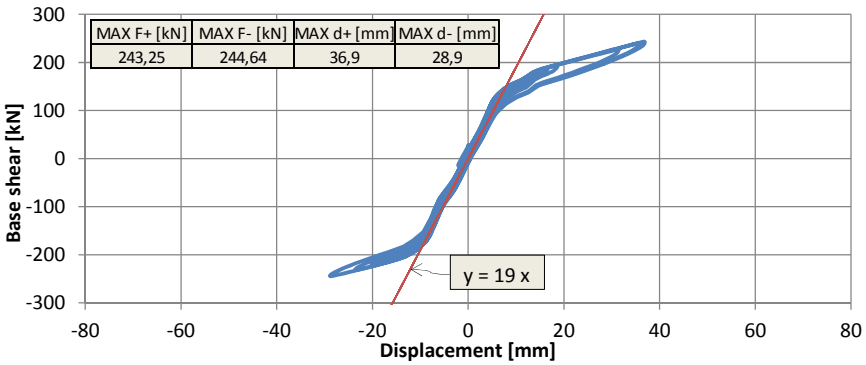

(b)

Figure 5.60 – Rocking arrangement, PsD test with PGA = 0,18g: (a) vibratory curve and (b) base shear vs displacement

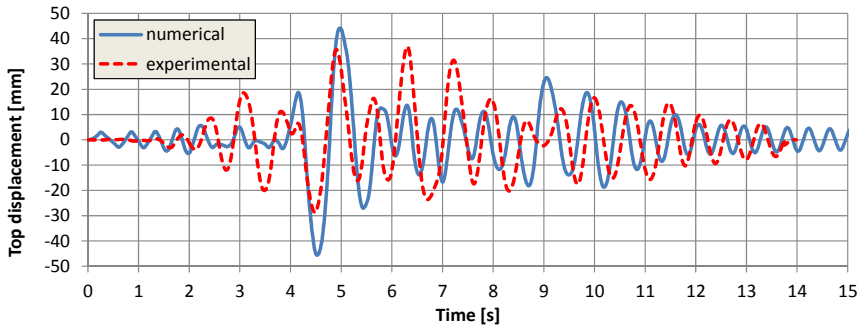

(a)

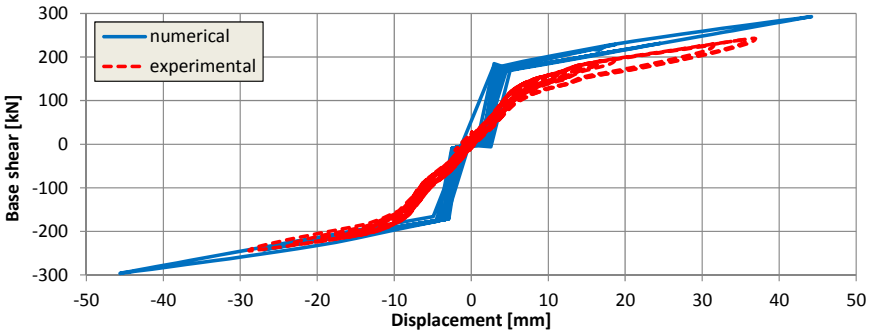

(b)

Figure 5.61 – Rocking arrangement, numerical simulation with PGA = 0,18g: (a) vibratory curve and (b) base shear vs displacement

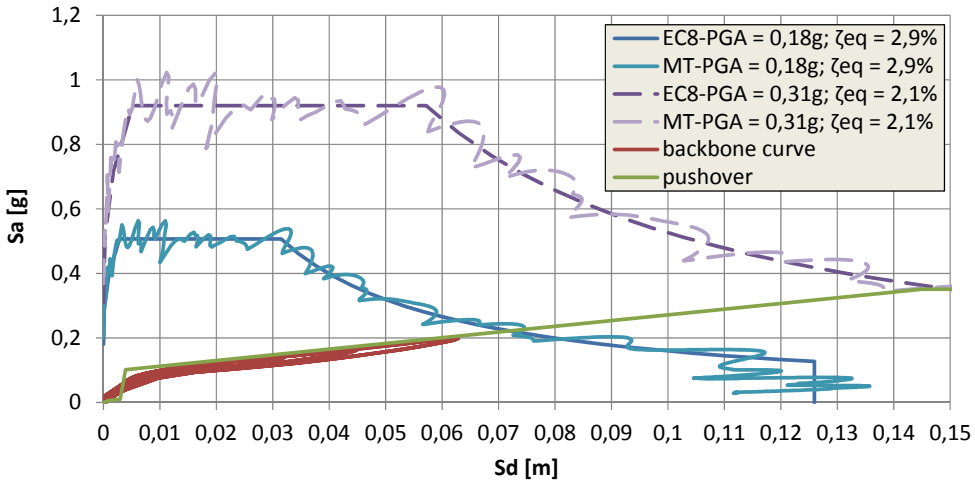

Figure 5.62 – Rocking arrangement: maximum displacement according to ADRS procedure

5.2.5. Structure with vertical panels – Dissipative systems with FBDs

5.2.5.1. Preliminary connection tuning and testing

Several problems had to be faced and solved before the FBDs installed within the full scale prototype started working as assumed during the design.

Zinc-coated bolts have been wrongly delivered to the ELSA laboratory. While applying the torque to the bolts, coupled with burnished steel Belleville washers, the technicians observed that the bolts started rotating after the application of a certain load level, without enough gripping. Tightening while holding the opposite nut with a key allowed to apply the required force, but then very large losses were measured immediately after the operation, since the additional needed torque was applied to the opposite side technician arm, instead that on the bolt itself. This effect is due to the unproper use of zinc-coated bolts for friction applications. In addition, a similar effect occurred if applying the torque to burnished bolts heads instead of nuts, due to the fact that part of the torque was lost for friction between the bolt and hole contact surface.

After substituting all zinc-coated bolts with burnished ones, some devices could not be tightened at the required level because of imperfect alignment between plates and support profiles. Horizontal tolerance in the support profile-to-panel connection, provided by the hole diameter enlargement with respect to the bolt, proved to be not enough. Therefore, horizontal short slots have been milled at the support profiles, after which tightening of all FBDs occurred successfully.

Cyclic tests performed on the building provided with three FBDs per interface led to hysteretic loops with a large pinching effect, with about 15 mm of horizontal branch, affecting energy dissipation capacity. This is due to the effect of mounting tolerances, which is in accordance with the results obtained on the panel sub-assembly experimental tests. However, an additional negative contribution to this extent is due to the vertical tolerance of the support profiles, that have been designed with a profile-to-panel bolted connection not based on friction grip.

Provided that the round hole has been executed with a two millimetre diameter tolerance instead of the single millimetre prescribed, the whole contribution of the device tolerance in terms of horizontal branch extent becomes equal to the double of the round hole diameter tolerance multiplied by the mechanical aspect ratio of the panel, in the case of the ELSA building 4 mm x 7800 / 2500 = 12,5 mm. This pinching horizontal branch remains at a constant length independently from the displacement amplitude, and this suggests that the contribution of this effect in reducing the dissipation of energy of the overall building is predominantly important for serviceability limit state seismic events, to which relative small displacements are associated, rather than for ultimate limit state seismic events.

Furthermore, the milling of the horizontal slots allowed for a certain torsional degree of freedom, complicating the mechanical behaviour of the connection. After the consideration that a friction grip connection with an angle shaped support profile, characterised by large torsional actions, was not feasible with the given geometries, it has been decided to directly weld the support angle profiles to the steel counter-plates inserted in the panel recesses. Welding has been performed on the connection already tightened with the originally used bolts, that have been left during the tests.

A comparison between the experimental cyclic behaviour of the building provided with bolted and welded connections is shown in Figure 5.63 in terms of single device average load versus panel relative vertical displacement. The single device average load has been obtained by subtracting to the experimental load history the contribution of the frame alone, as measured with the previously performed test, and dividing the load by the number of connections. With welded connections, the pinching effect is largely reduced to about 3 mm, with the only contribution from mounting tolerances of the panel bearing connections acting.

The mean slip threshold load corresponding to the FBD geometry of those inserted within the ELSA prototype with each bolt tightened at 220 Nm, calculated according to the proposed design procedure, is equal to about 75 kN. The experimental values are of about 60 kN (-20%) for the specimen with bolted support-to-panel connections and of about 90 kN (+20%) for that with welded support-to-panel. The first reduced value may be due to the vertical displacement and torsional rotation degrees of freedom, while the latter enlarged value could have occurred because of a larger friction coefficient acting on the bolt thread or within brass and steel. Another possible reason for this slip threshold load enlargement could be found in the much lower test velocity at ELSA laboratory with respect to the tests performed at Politecnico di Milano, which could have turned the response to be depending on the static burnished steel-brass friction coefficient, instead on the dynamic. With the values already considered within the FBD design methodology description, the enlargement from the dynamic to the static friction coefficient is equal to about 16%.

The comparison between the dynamic behaviour of the structure provided with three bolted or welded FBDs per panel interface when subjected to a base accelerogram with PGA equal to 0,18g is shown in Figure 5.64, highlighting how the behaviour could dramatically change for low displacement demanding seismic events. In this case, the dissipative connections barely entered into the slipping phase, maintaining the building largely within the fully operability limit state.

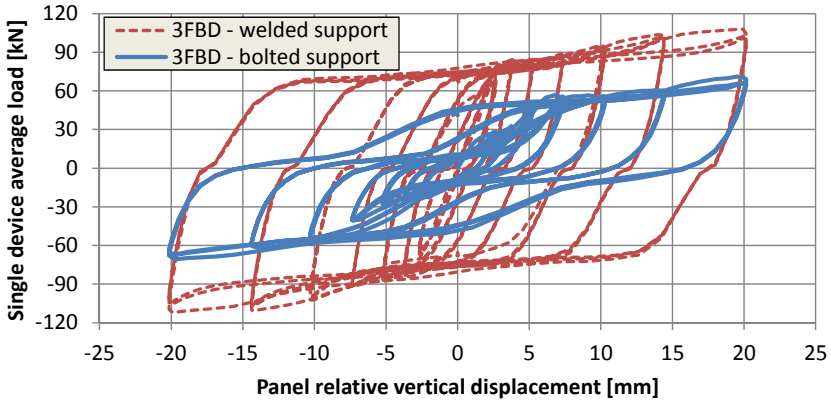

Figure 5.63 – Pendulum arrangement with three FBDs per interface: comparison between cyclic behaviour with welded and bolted support profiles

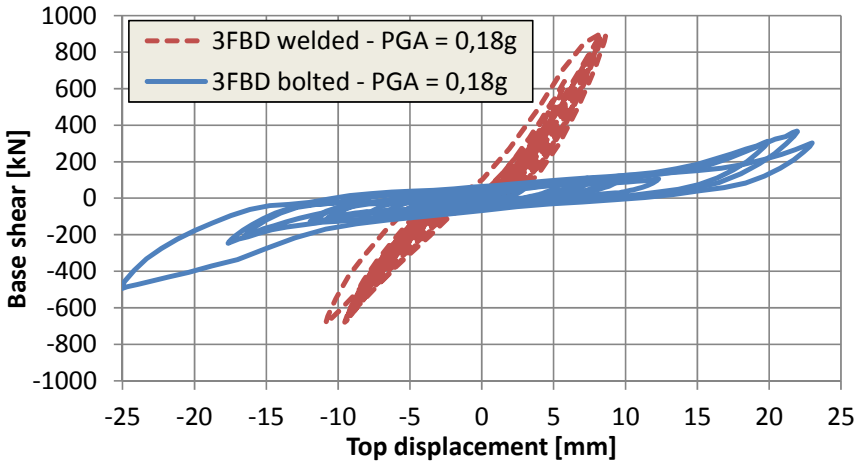

Figure 5.64 – Pendulum arrangement with three FBDs per interface: comparison between PsD tests with PGA equal to 0,18g with welded and bolted support profiles

5.2.5.2. Pendulum arrangement: three FBDs

To the pendulum arrangement, three FBDs have been added at each panel interface (Figure 5.65). Each slipping bolt of the connections has been tightened with a torque equal to 220 Nm, to which corresponds an average slip threshold shear load equal to 75 kN according to the design rules previously suggested for the single device. The results of the cyclic test, illustrated in Figure 5.66, show a highly dissipative behaviour, with a very large area included within the hysteretic cycles. The experimental slip threshold is slightly larger than what predicted, and is equal to about 90 kN per connection. This may be due to a slightly different friction coefficient of bolts and nuts, and/or to the fact that the test has been performed under relatively slow speed if compared to the particular tests on the single device. The difference between the static and the dynamic brass-steel coefficient is 16%, which is very similar to the difference between the experimental and the expected threshold (20%).

The values of average equivalent viscous damping ratio per each displacement step are reported in Table 5-8.

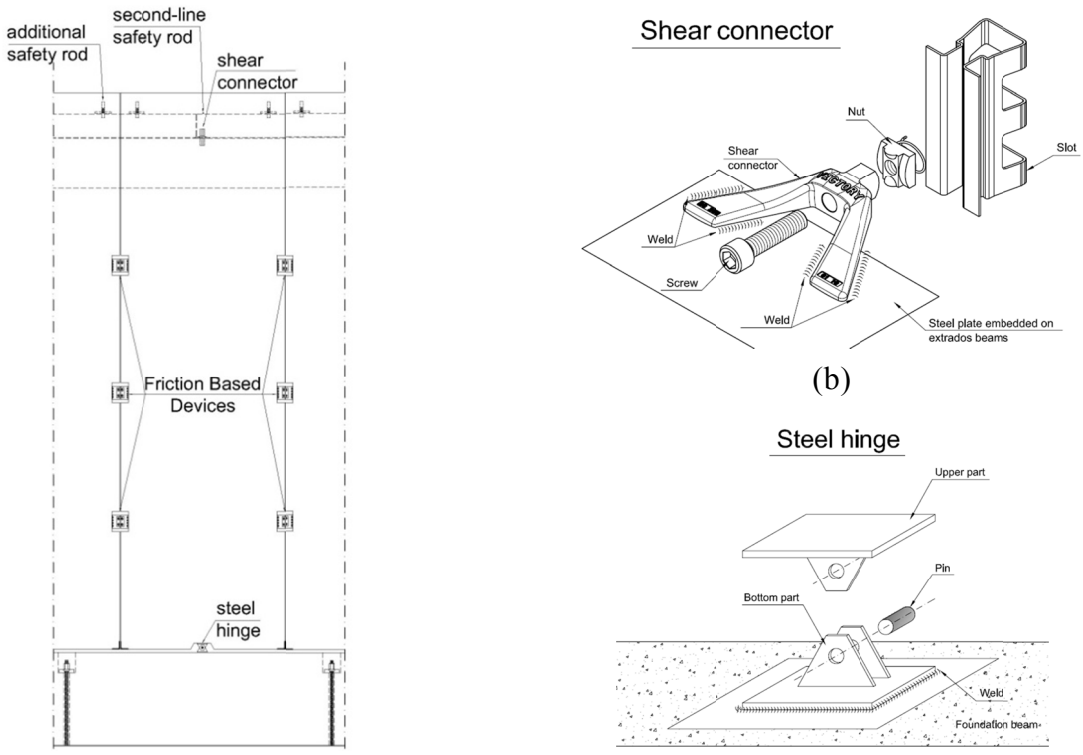

Figure 5.65 – Pendulum arrangement with 3 FBDs per interface: (a) front view of the panel, (b) top shear connection, (c) base steel hinge

While a global initial elastic stiffness equal to about 100 kN/mm has been observed, a larger unload stiffness equal to about 180 kN/mm is observed, followed by a small (±1,5~2,5 mm) pinching branch and a much lower reload stiffness. This peculiar behaviour is due to the shear connector and the base hinge, that play a role with their deformation (leading to a lower initial and reloading stiffness) and with their tolerances (causing the small pinching effect). A slight difference in terms of loads between the two parallel frames can be observed in Figure 5.66a, probably due to slight difference in local behaviour of the connections.

Several PsD tests have been carried out with this configuration. The first with a value of PGA corresponding to the serviceability limit state of the model structure, equal to 0,18g. Results are collected in Figure 5.67 and show a dramatic reduction of structure top displacement with respect to what would have been measured on the pendulum isostatic arrangement, with a much stiffer dynamic behaviour. Since the displacements are limited, the pinching effect is clearly noticeable in the hysteretic cycles. FBD slippage has been attained for very limited length and only towards the positive direction, and thus it can be stated that the dissipative connections behaved almost elastically during this seismic event. A satisfactory symmetry between the two parallel frames has been recorded during the event.

The numerical simulation, which results are collected in Figure 5.68, is characterised by a similar stiffness behaviour, but the response seems to be under-damped with respect to the experimental results, especially if comparing the free vibrations after the motion. According to the numerical results, which are on safe side in this case, columns have not even been cracked during the earthquake.

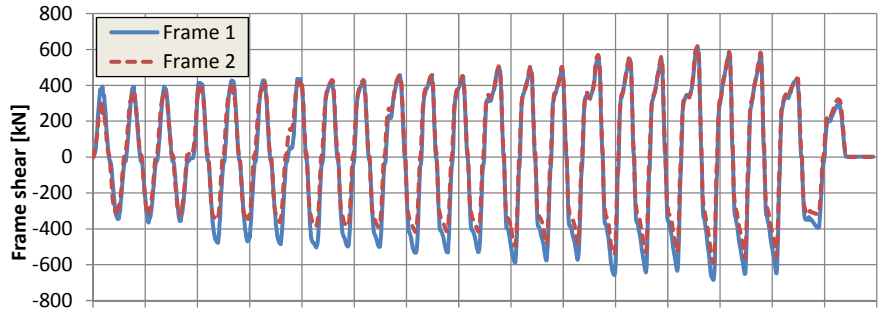

(a)

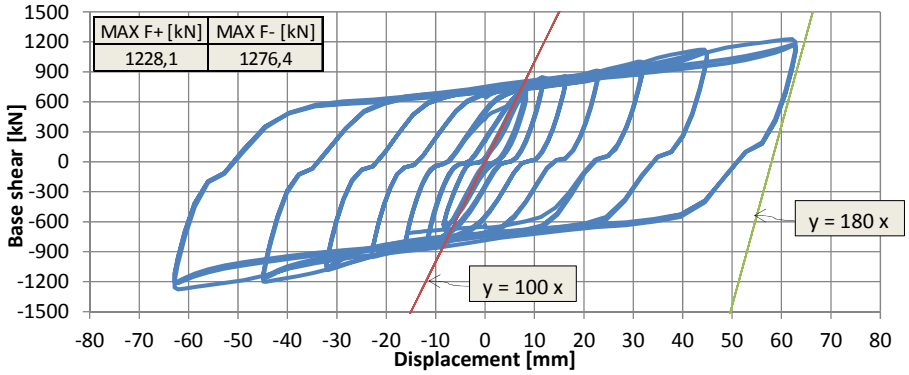

(b)

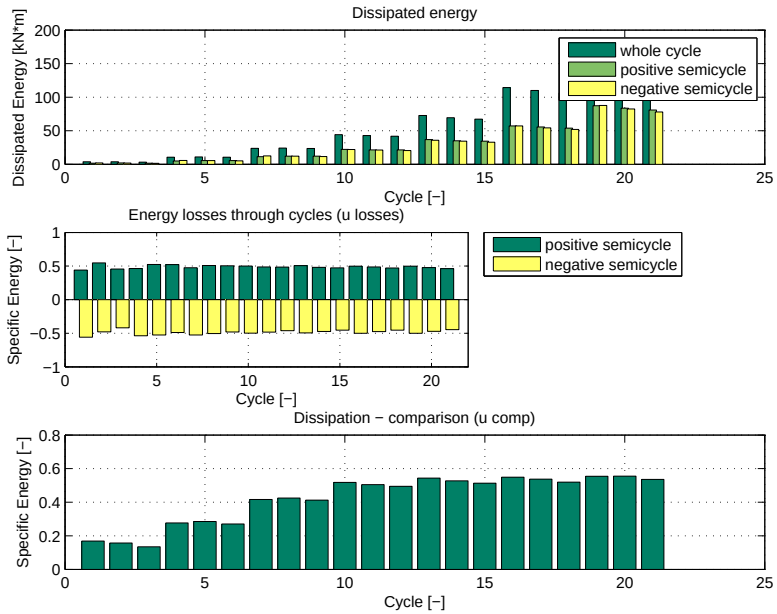

(c)

Figure 5.66 – Pendulum arrangement with 3 FBDs per interface, cyclic test: (a) frame shear load history, (b) base shear vs displacement and (c) energy dissipation properties

Table 5-8 – Pendulum arrangement with 3 FBDs per interface, cyclic test: equivalent viscous damping ratio

d [mm]	8,4	11,7	16,4	23,0	32,1	45,0	63,0
ζ_{eq} [%]	9,8	17,7	26,6	32,2	33,7	34,1	34,9

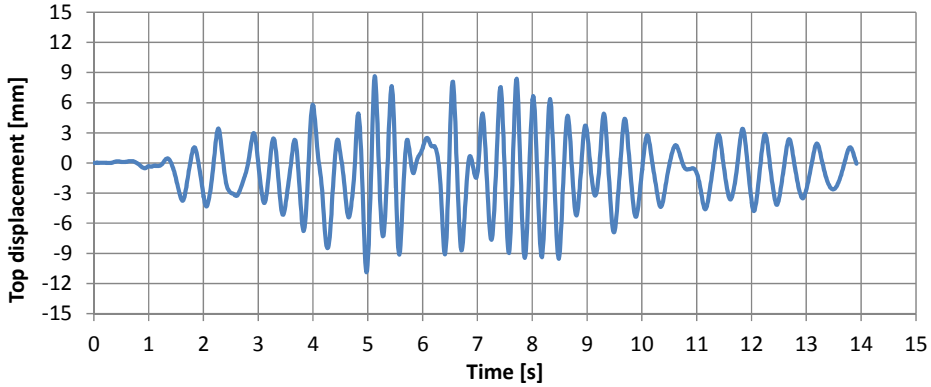

(a)

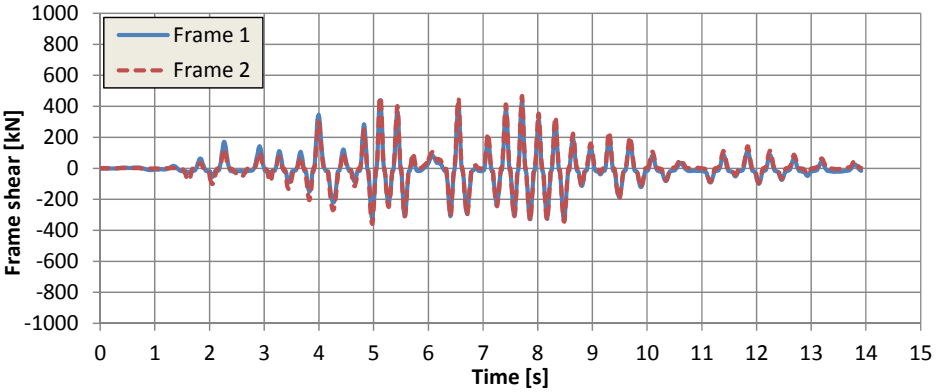

(b)

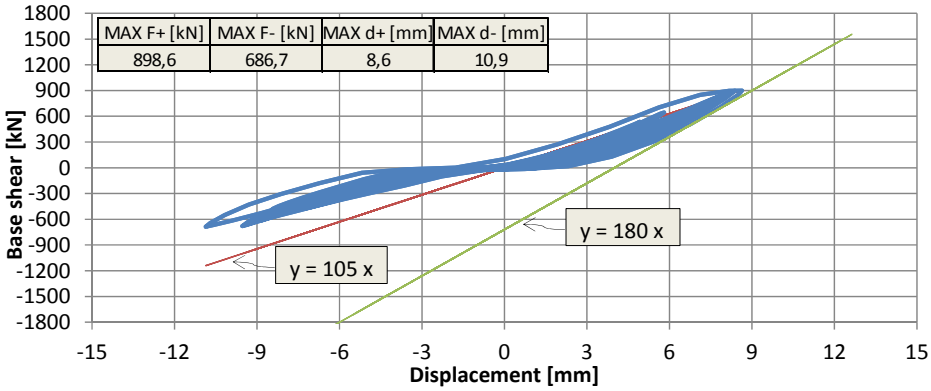

(c)

Figure 5.67 – Pendulum arrangement with 3 FBDs per interface, PsD test with PGA = 0,18g: (a) vibratory curve, (b) frame shear load history and (c) base shear vs displacement

The ADRS procedure leads to the following displacement estimations (Figure 5.78): for the test with PGA equal to 0,18g the estimated maximum displacement is 7 mm (-36% with respect to the experimental results) with an interpolated equivalent viscous damping ratio equal to 9,8%, for the test with PGA equal to 0,36g the estimated maximum displacement is 16 mm (-25% with respect to the experimental results) with an interpolated equivalent viscous damping ratio equal to 25,8% (the intersection of the capacity curve with the demand curve of the modified Tolmezzo accelerogram occurs many times within the range between 12 and 18 mm due to the spikes, leading to a difficultly predicatble exact value), for the test with PGA

equal to 0,72g the estimated maximum displacement is 82 mm (+77% with respect to the experimental results) with an interpolated equivalent viscous damping ratio of 35,7%, for the test with PGA equal to 1,00g the estimated maximum displacement is 127 mm (+45% with respect to the experimental results) with an interpolated equivalent viscous damping ratio of 35,7%. The same procedure shows that column yielding would occur for the earthquake scaled at not less than 1,10g of PGA. The corresponding equivalent viscous damping, obtained for extrapolation of the experimental results, has been taken equal to 38,5%.

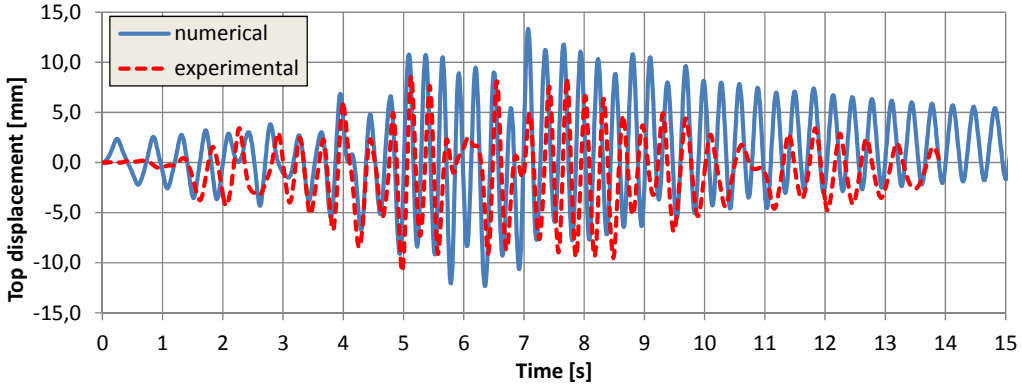

(a)

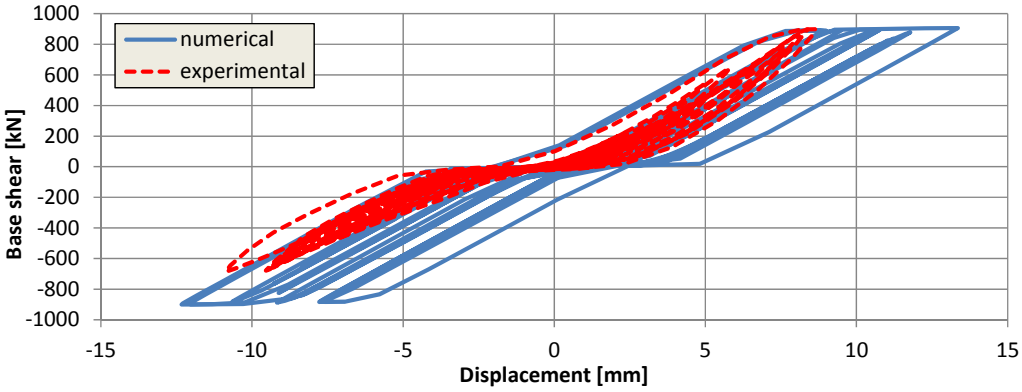

(b)

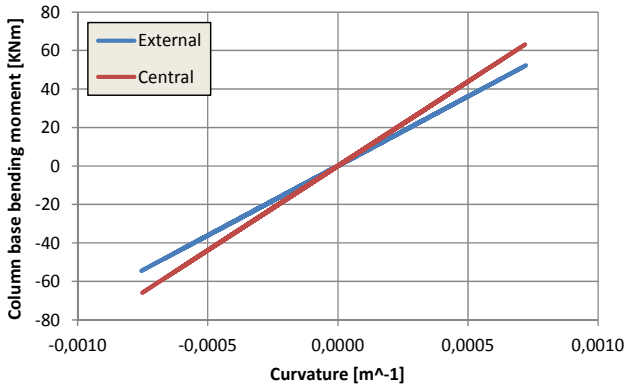

(c)

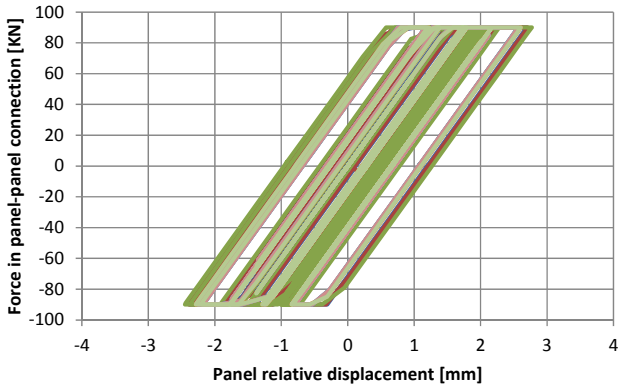

(d)

Figure 5.68 – Pendulum arrangement with 3 FBDs per interface, numerical simulation with PGA = 0,18g: (a) vibratory curve, (b) base shear vs displacement, (c) column base moment vs curvature and (d) FBD hysteretic cycles

Within the test with PGA equal to 0,36g, corresponding to the ultimate limit state of the model structure, still a very low displacement has been attained by the structure. The results (Figure 5.69) show that the hysteretic cycles of the overall structure correspond to a large dissipation of energy due to the dissipative connections, and that a satisfactory symmetry has been shown by the parallel frames. The numerical simulation, which results are collected in Figure 5.70, is characterised by a similar stiffness behaviour, but the response seems to be under-damped with respect to the experimental results in the range of free vibrations after the motion. The column bases reached cracking but they are very far from rebar yielding. By comparing the structure hysteretic cycles, it can be noticed a slight hardening of the response, which is likely to be due to difficultly predictable hardening of the dissipative connections.

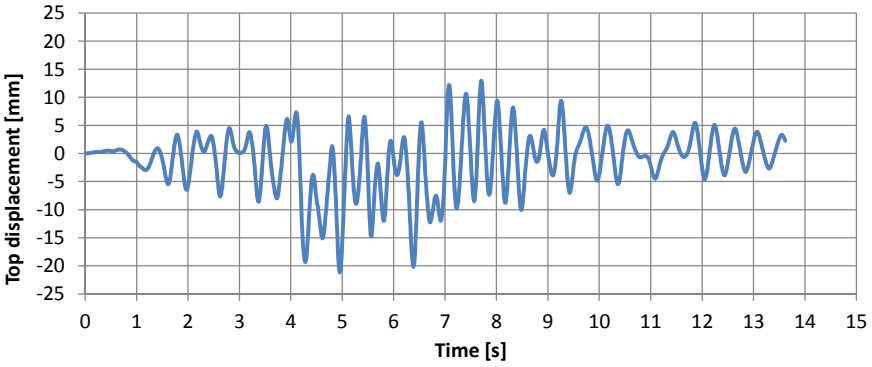

(a)

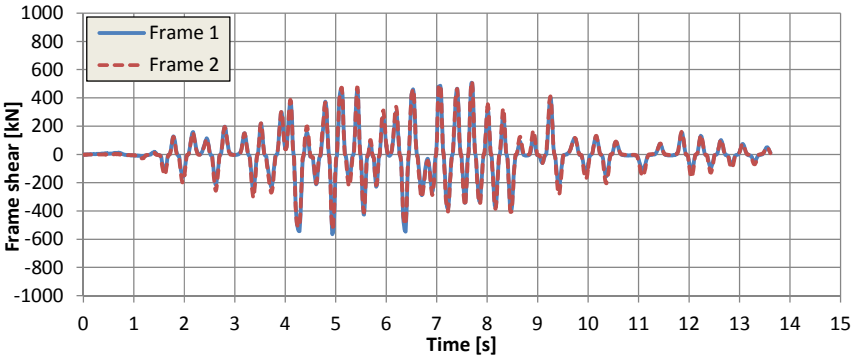

(b)

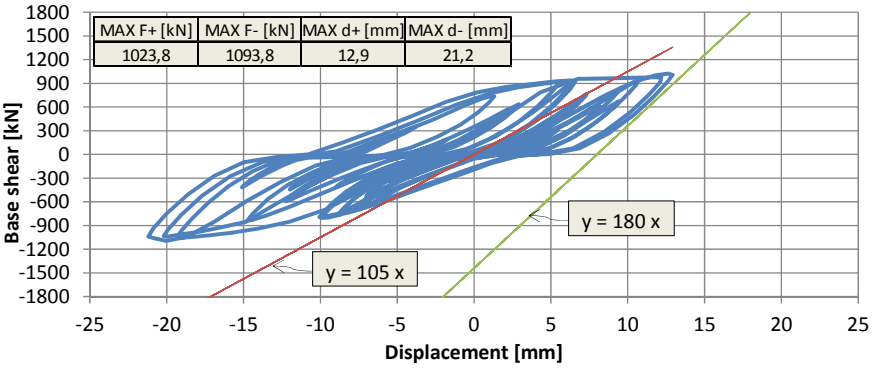

(c)

Figure 5.69 – Pendulum arrangement with 3 FBDs per interface, PsD test with PGA = 0,36g: (a) vibratory curve, (b) frame shear load history and (c) base shear vs displacement

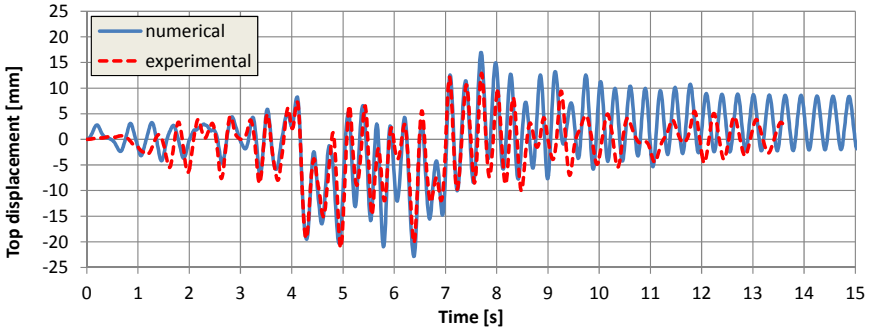

(a)

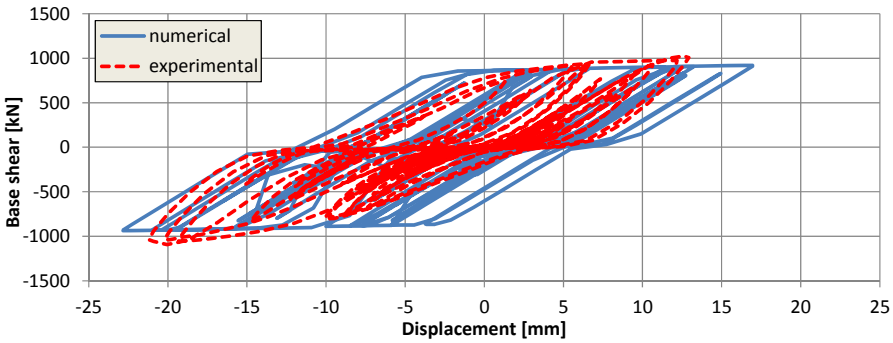

(b)

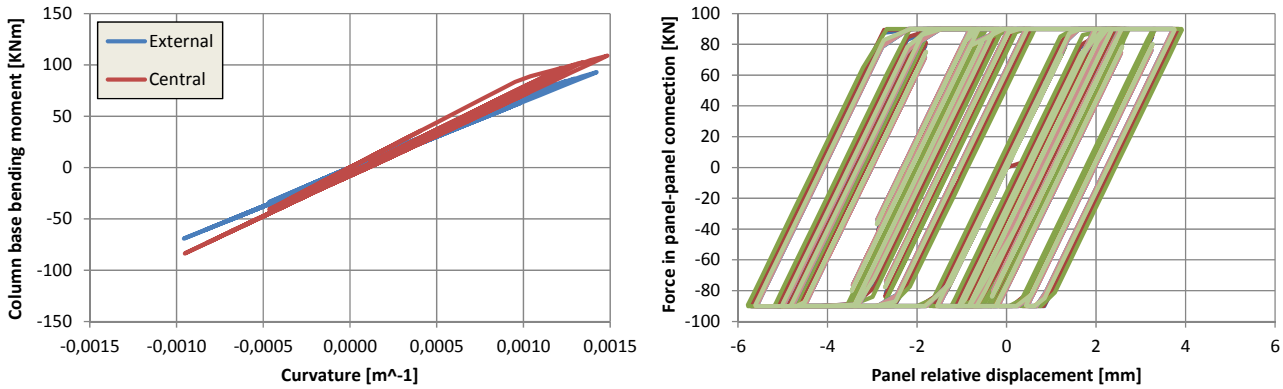

(c) (d)

Figure 5.70 – Pendulum arrangement with 3 FBDs per interface, numerical simulation with PGA = 0,36g: (a) vibratory curve, (b) base shear vs displacement, (c) column base moment vs curvature and (d) FBD hysteretic cycles

A further test with PGA equal to 0,72g, corresponding to the double of the ultimate limit state PGA of the model structure, has been confirmed and executed as scheduled in the experimental programme, since the results from the previous have been particularly positive. The results (Figure 5.71) show that the hysteretic cycles of the overall structure correspond to a large dissipation of energy due to the dissipative connections, and that a satisfactory symmetry has been shown by the parallel frames. The numerical simulation, which results are collected in Figure 5.72, is able to catch all displacement trends, with non-negligible modulus differences due to the hardening behaviour of the first large cycles, which are then followed by further cycles which slip threshold has been correctly catched by the analysis. The column bases reached cracking but they are very far from rebar yielding.

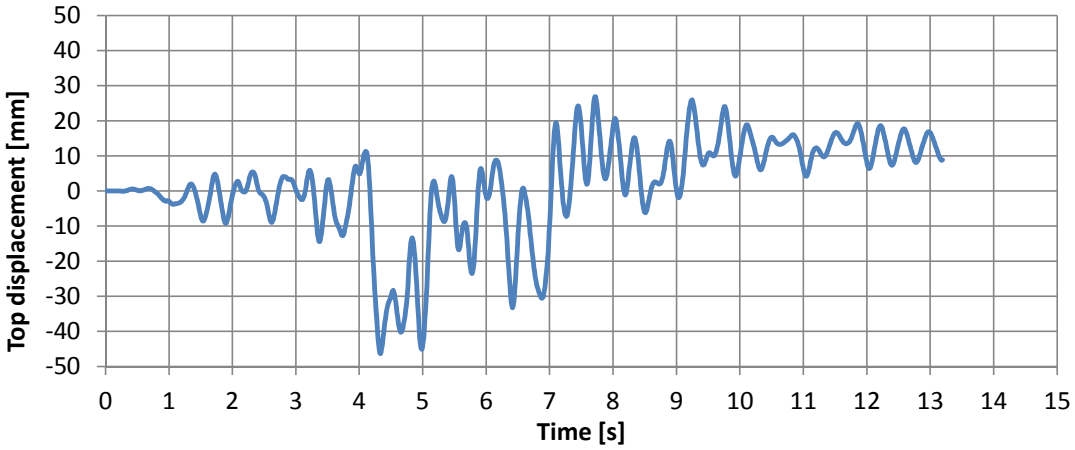

(a)

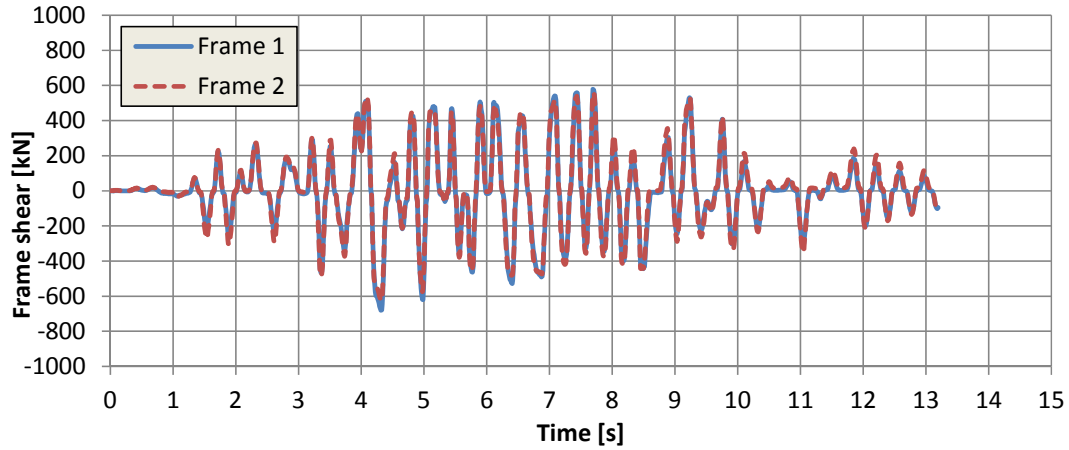

(b)

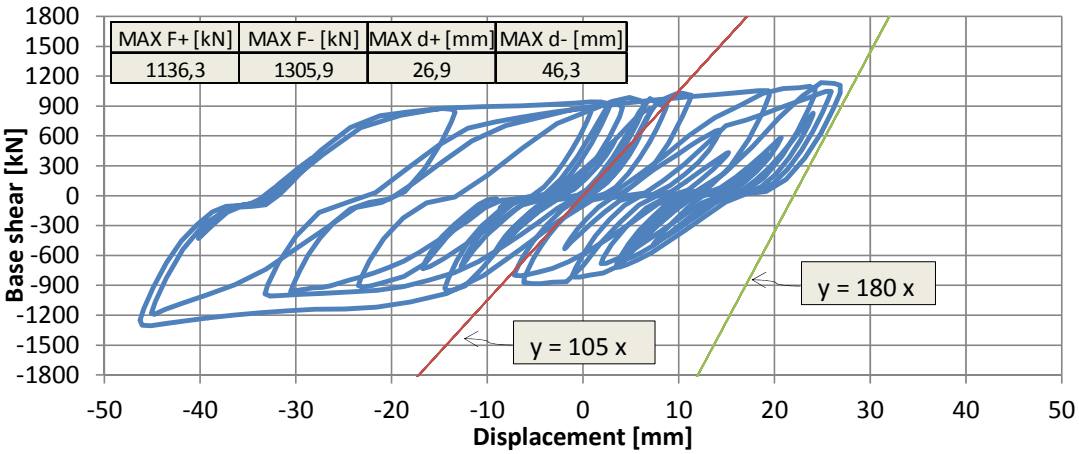

(c)

Figure 5.71 – Pendulum arrangement with 3 FBDs per interface, PsD test with PGA = 0,72g: (a) vibratory curve, (b) frame shear load history and (c) base shear vs displacement

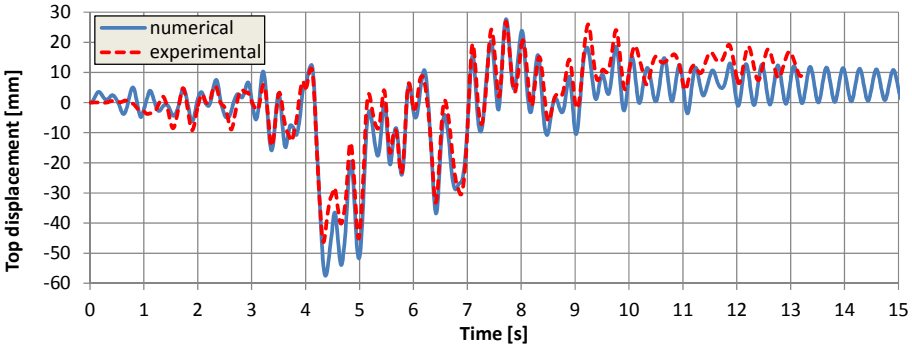

(a)

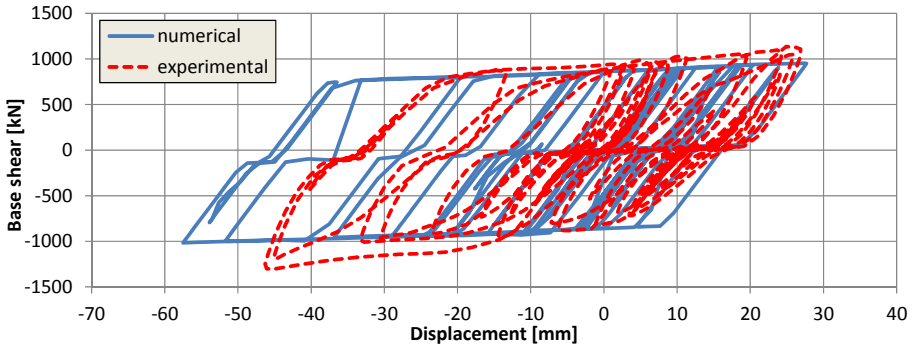

(b)

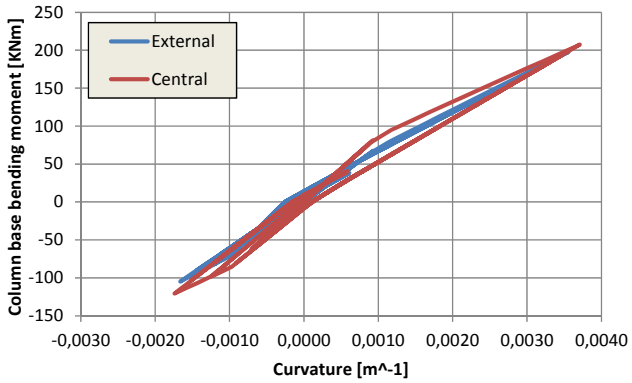

(c)

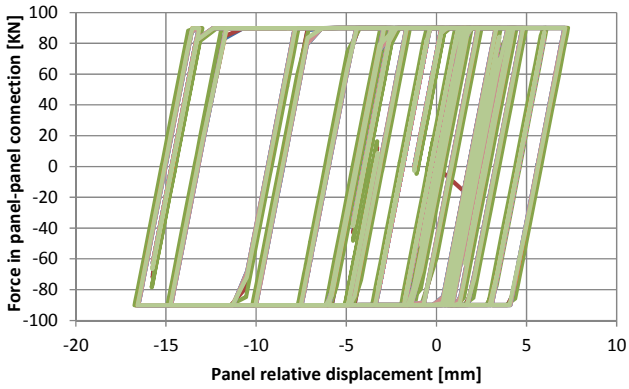

(d)

Figure 5.72 – Pendulum arrangement with 3 FBDs per interface, numerical simulation with PGA = 0,72g: (a) vibratory curve, (b) base shear vs displacement, (c) column base moment vs curvature and (d) FBD hysteretic cycles

Based on the results of the scheduled tests, it has bee decided to perform a further test with PGA equal to 1,00g, corresponding to 2,8 times the ultimate limit state PGA of the model structure, has been executed. Even to this dramatic event, the structure responds elastically. The results (Figure 5.73) show that the hysteretic cycles of the overall structure correspond to a dramatic dissipation of energy concentrated into the FBDs, with a satisfactory symmetry has been shown by the parallel frames. The maximum drift achieved is less than 88 mm, at which column base yielding is still not expected to occur. Figure 5.74 shows the initial and displaced front view of the building, highlighting the pendulum deformation mechanism of the panels. A particular of an FBD under initial and maximum drift is reported in Figure 5.75.

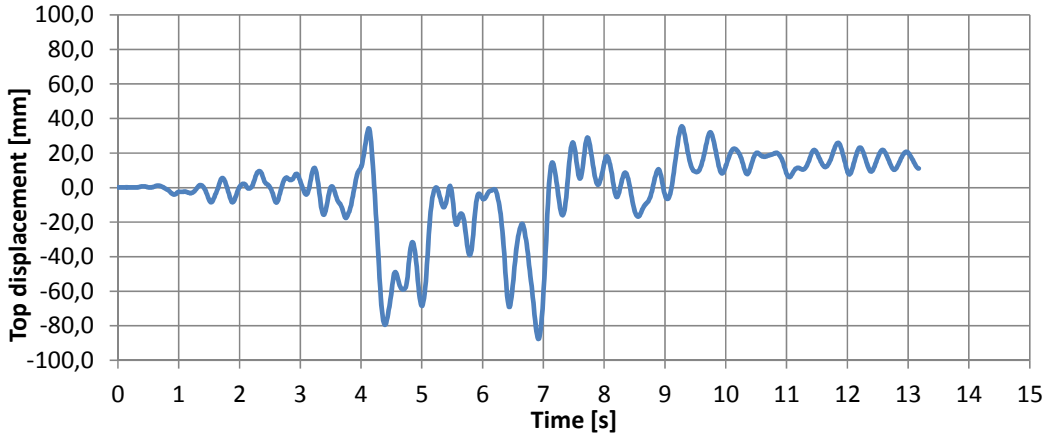

(a)

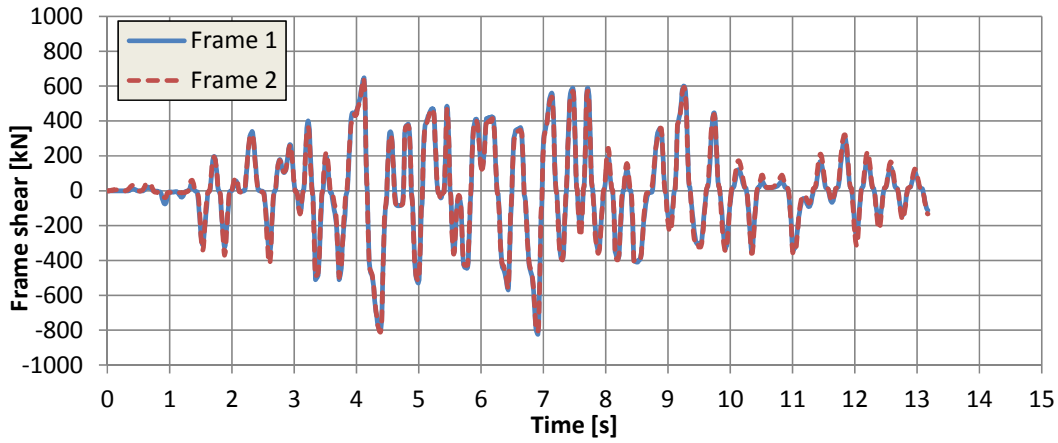

(b)

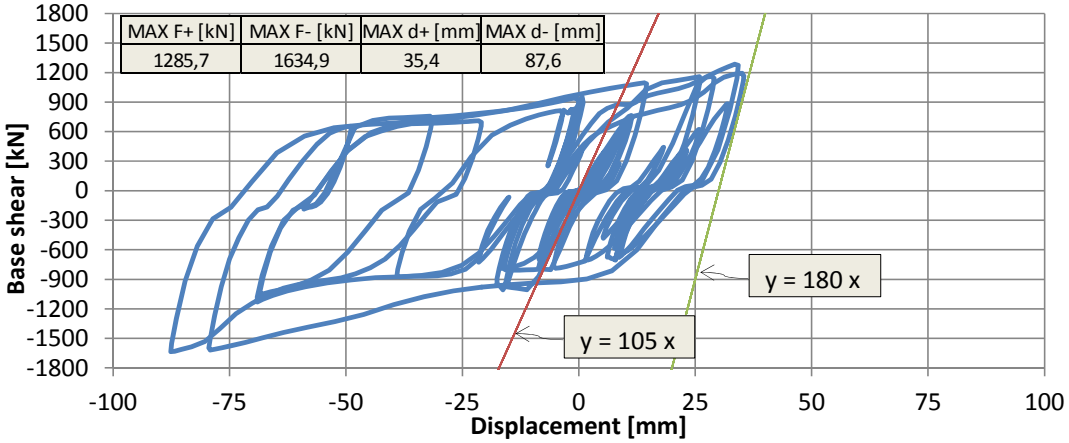

(c)

Figure 5.73 – Pendulum arrangement with 3 FBDs per interface, PsD test with PGA = 1,00g: (a) vibratory curve, (b) frame shear load history and (c) base shear vs displacement

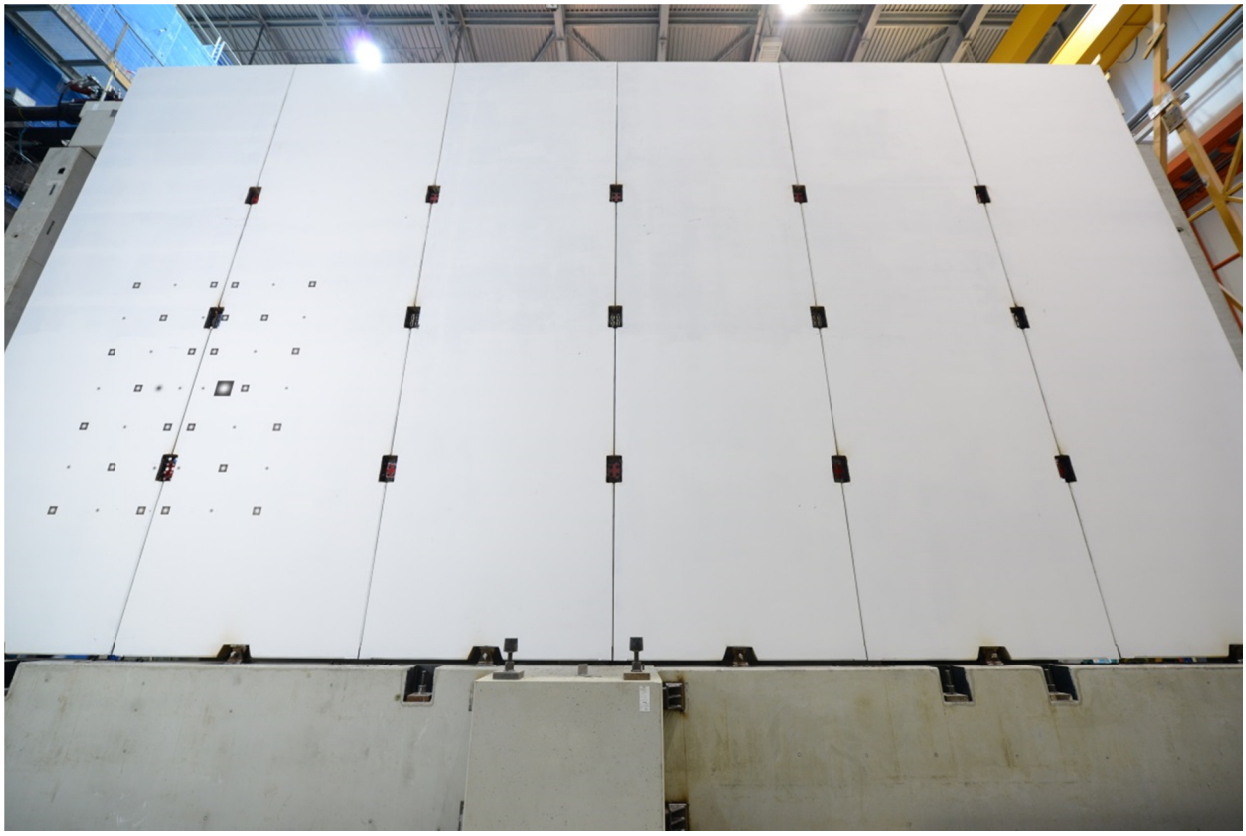

(a)

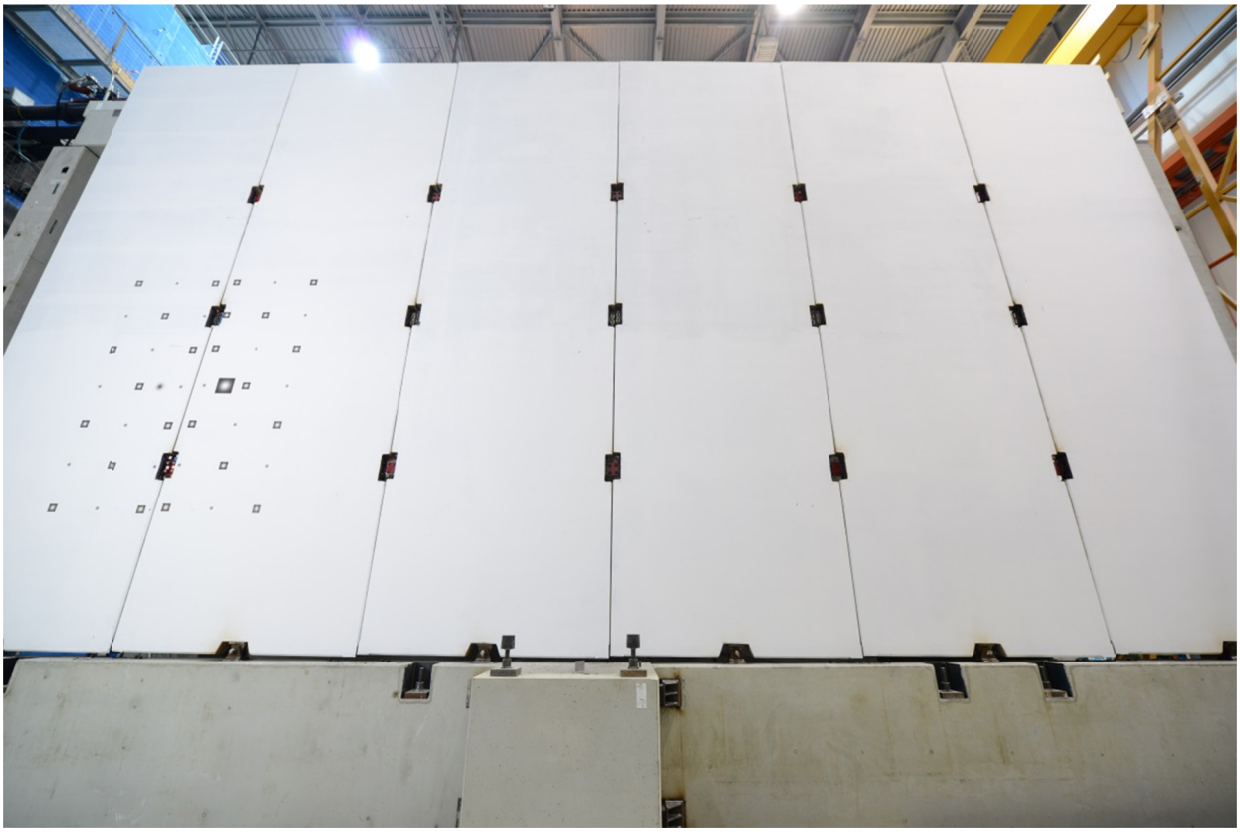

(b)

Figure 5.74 – Pendulum arrangement with 3 FBDs per interface, PsD test with PGA = 1,00g: front view at (a) beginning of the test (b) maximum drift

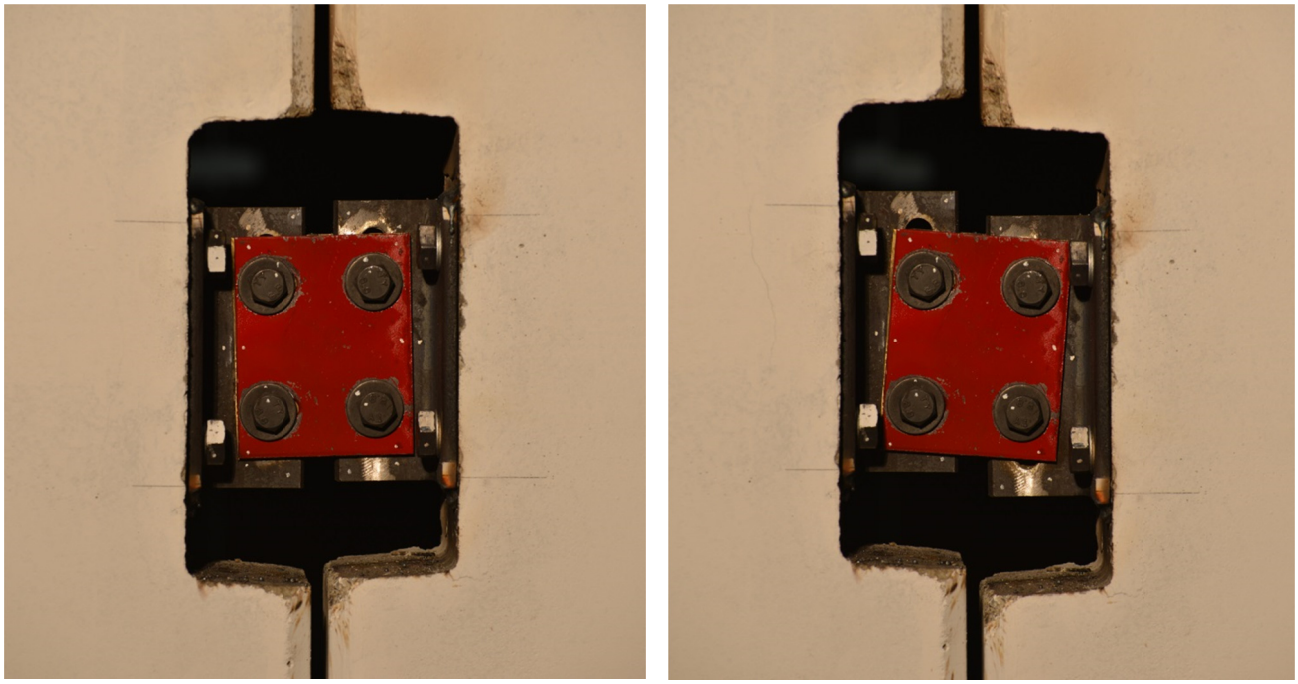

(a) (b)

Figure 5.75 – Pendulum arrangement with 3 FBDs per interface, PsD test with PGA = 1,00g: (a) particular of one FBD and (b) displaced connection at 1,25% of drift

The numerical simulation, which results are collected in Figure 5.76, is characterised by a similar stiffness behaviour and is able to catch the exact deformation trend, even with some modulus differences due to the hardening behaviour of the first cycles at large displacements. The column bases reached cracking but they are far from rebar yielding. The dissipative connections displaced with a maximum of about 27 mm, which is about a half of their capacity (50 mm).

At the end of this and the previous earthquakes on this configuration, all members behaved entirely elastically, with cracked but not yielded column bases (the cracks were back closed at the end of the earthquake) and absence of cracking in all members, included the panels. The enormous amount of energy dissipated by the earthquakes has been all afforded to the FBDs, which do not damage during correct operationality, and are therefore in perfect state at the end of the earthquakes. As shown by the local tests, also the brass sheets, that have been subjected to tremendous slippage, did not need substitution, which is confirmed by the fact that they provided similar response throughout all the test series. A picture of the brass sheets after connection dismounting is reported in Figure 5.77. Only re-tightening of the connections has been executed at the end of each test, but the JRC technicians assure that the maximum losses within all the bolts were not larger than 20 Nm, which is less than 10% of the initial torque. Also the permanent deformation of the structure, which is about 15 mm in the test with PGA equal to 1,00g, is simply related to the final position in which the FBDs have been working. In order to make the structure automatically come back to zero drift, it would be needed to realease all FBDs, and then re-tighten them.

Practically, at the end of the test with PGA equal to 1,00g, the structure was ready to immediately receive another similar earthquake with large over-resources.

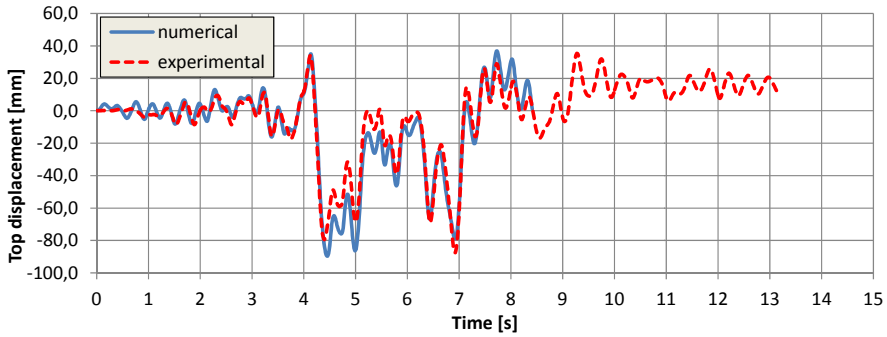

(a)

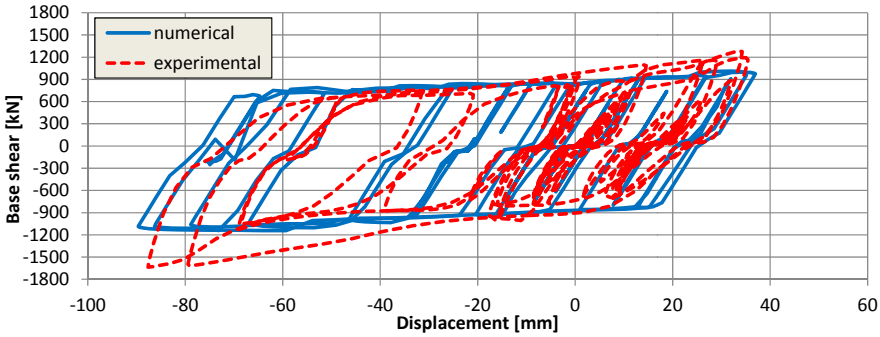

(b)

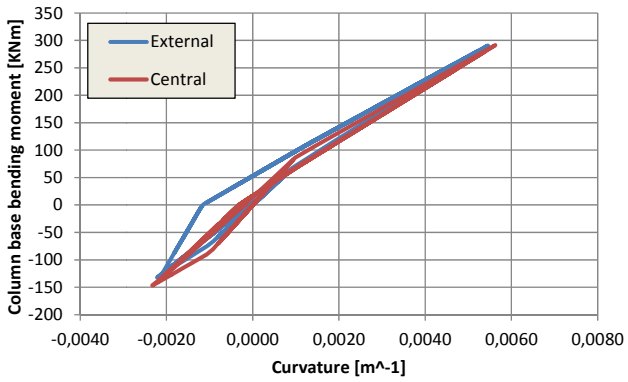

(c)

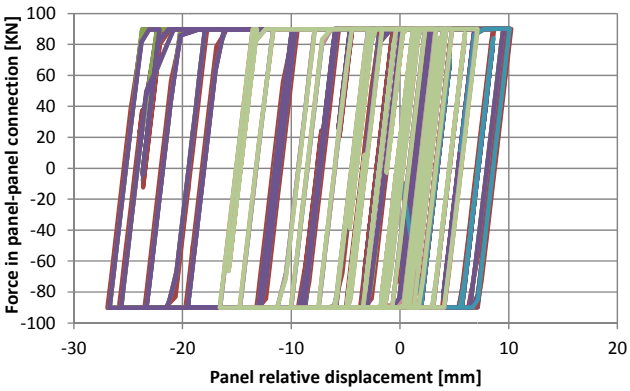

(d)

Figure 5.76 – Pendulum arrangement with 3 FBDs per interface, numerical simulation with PGA = 1,00g: (a) vibratory curve, (b) base shear vs displacement, (c) column base moment vs curvature and (d) FBD hysteretic cycles

Figure 5.77 – FBD brass plates after the whole series of tests on dissipative systems

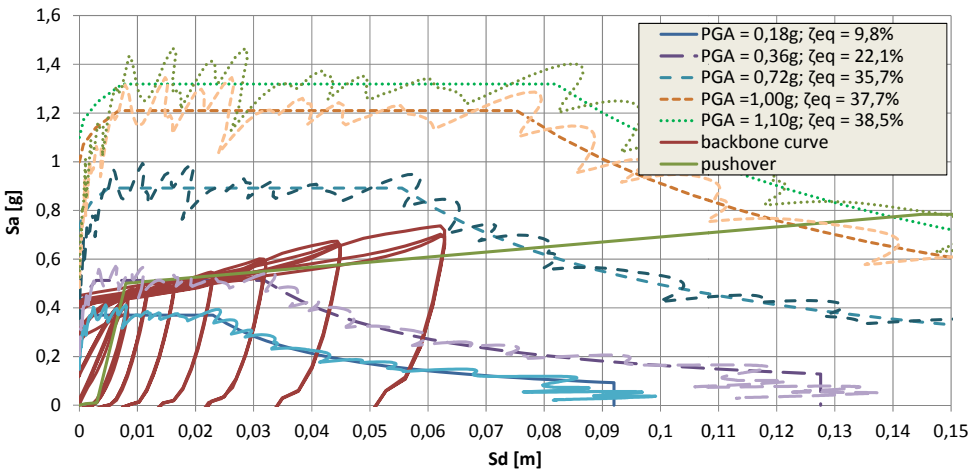

Figure 5.78 – Pendulum arrangement with 3 FBDs per interface: maximum displacement according to ADRS procedure

5.2.5.3. Pendulum arrangement: two FBDs

Two FBDs have been added at each panel interface to the pendulum arrangement (Figure 5.79), each slipping bolt of which has been tightened with a torque equal to 220 Nm. The results of the cyclic test, illustrated in Figure 5.80, show a highly dissipative behaviour, with a very large area included within the hysteretic cycles. Also in this case, the experimental slip threshold corresponds to about 90 kN per connection.

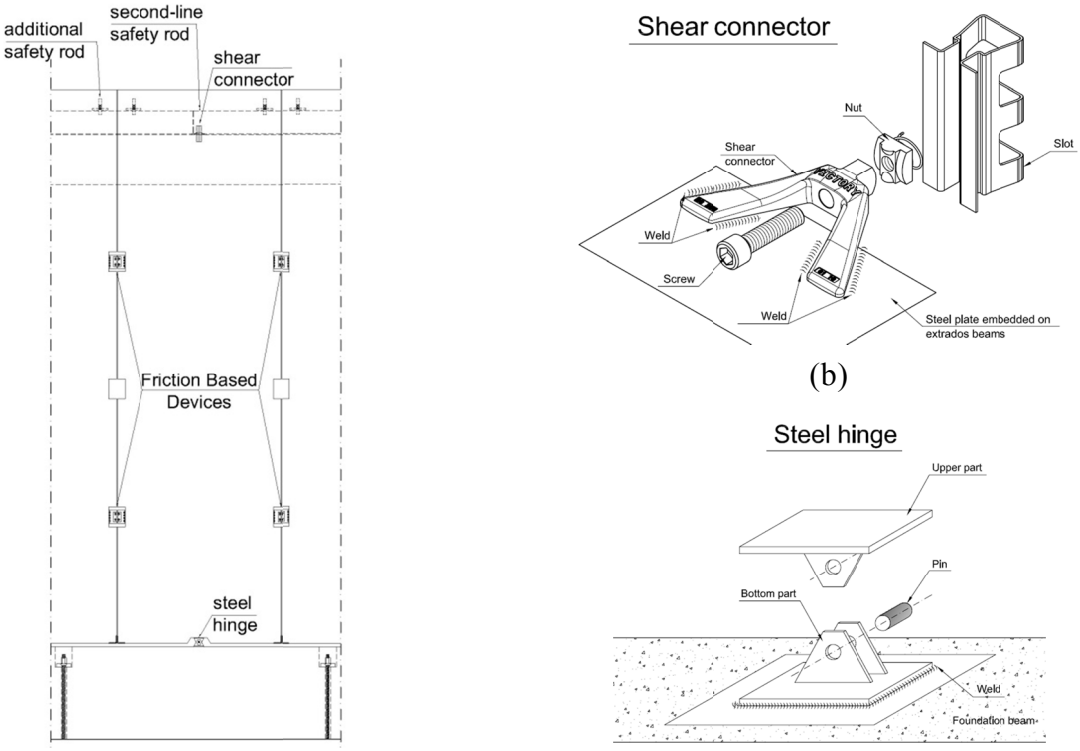

Figure 5.79 – Pendulum arrangement with 2 FBDs per interface: (a) front view of the panel, (b) top shear connection, (c) base steel hinge

The values of average equivalent viscous damping ratio per each displacement step are reported in Table 5-9. The global initial elastic stiffness is lowered to about 60 kN/mm, and still a larger unload stiffness equal to about 120 kN/mm is observed (which is two thirds of the unload stiffness of the structure with three FBDs per interface), followed by a small (±1,5~2,5 mm) pinching branch and a much lower reload stiffness. Only very slight difference in terms of loads between the two parallel frames can be observed in Figure 5.80a, probably due to slight difference in local behaviour of the connections.

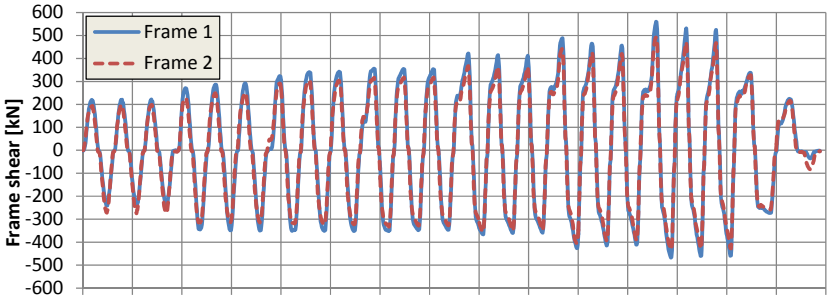

(a)

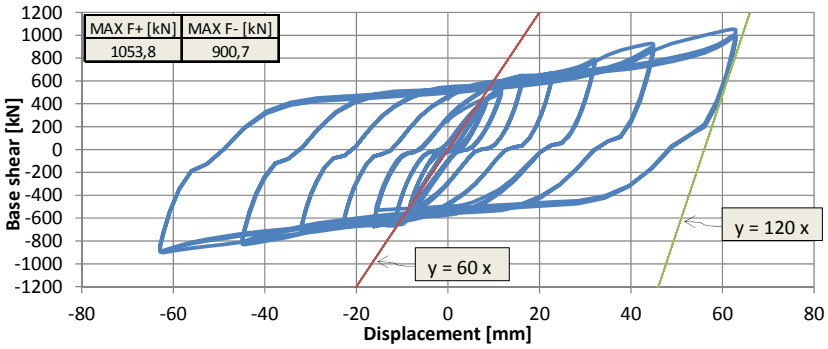

(b)

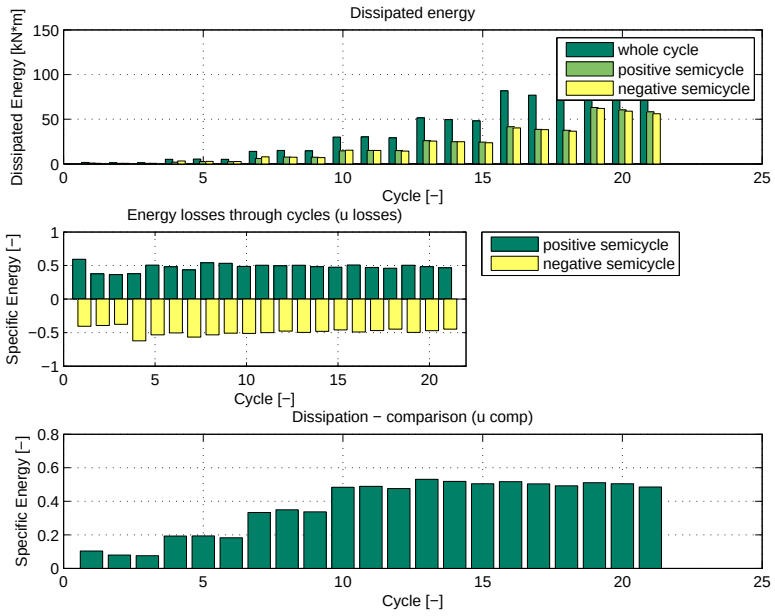

(c)

Figure 5.80 – Pendulum arrangement with 2 FBDs per interface, cyclic test: (a) frame shear load history, (b) base shear vs displacement and (c) energy dissipation properties

Table 5-9 – Pendulum arrangement with 2 FBDs per interface, cyclic test: equivalent viscous damping ratio

d [mm]	8,4	11,7	16,4	23,0	32,1	45,0	63,0
ζ_{eq} [%]	5,5	12,1	21,7	30,8	33,0	32,1	31,9

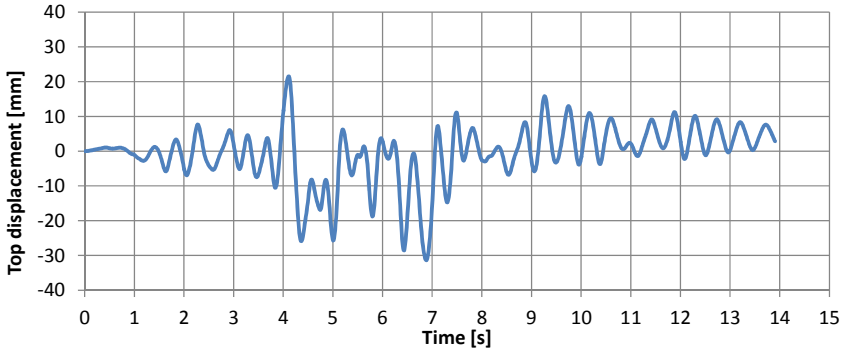

(a)

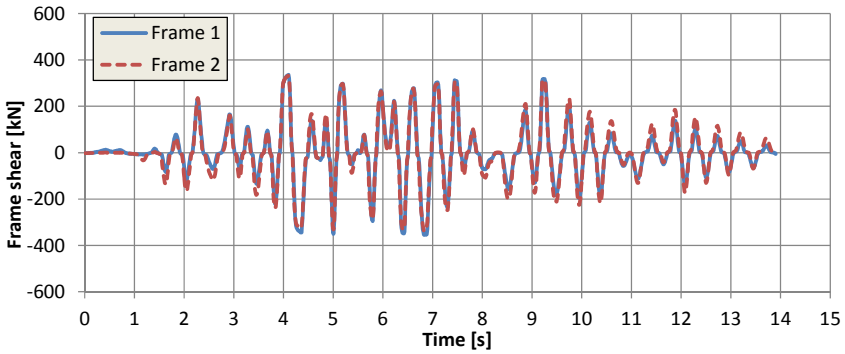

(b)

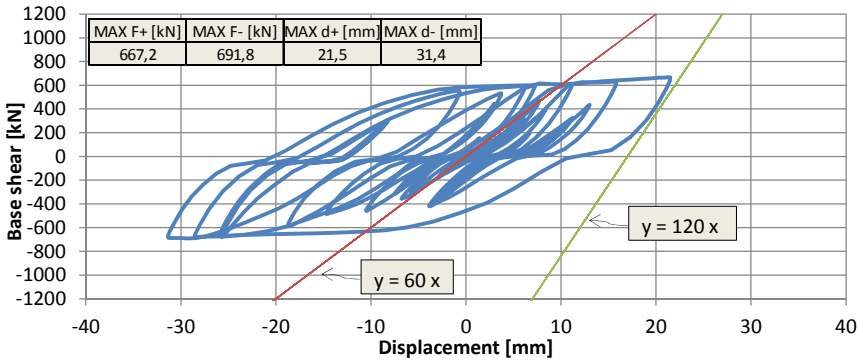

(c)

Figure 5.81 – Pendulum arrangement with 2 FBDs per interface, PsD test with PGA = 0,36g: (a) vibratory curve, (b) frame shear load history and (c) base shear vs displacement

The ADRS procedure leads to the following displacement estimations (Figure 5.85): for the test with PGA equal to 0,36g the estimated maximum displacement is 33 mm (+5% with respect to the experimental results) with an interpolated equivalent viscous damping ratio equal to 32,9%, for the test with PGA equal to 0,72g the estimated maximum displacement is 102 mm (+28% with respect to the experimental results) with an interpolated equivalent viscous

damping ratio of 31,5%. The same procedure shows that column yielding would occur for the earthquake scaled at not less than 0,95g of PGA. The corresponding equivalent viscous damping, obtained for extrapolation of the experimental results, has been taken equal to 31,0%. A pseudo-dynamic test with PGA equal to 0,36g, corresponding to the ultimate limit state PGA of the model structure, has been executed. The results (Figure 5.81) show that two FBDs per interface are still very effective in reducing the top drift and, consequently, the damage on the structure. Even with a lower number of dissipative connections, a satisfactory symmetry has been shown by the parallel frames. The numerical simulation (Figure 5.82) is able to catch the displacement history trend of the structure, even if non-negligible differences in terms of top displacement reached are noticed on the unsafe side. The structural hysteretic cycles satisfactorily juxtapone to the experimentally measured, with a good estimation of the slip load threshold.

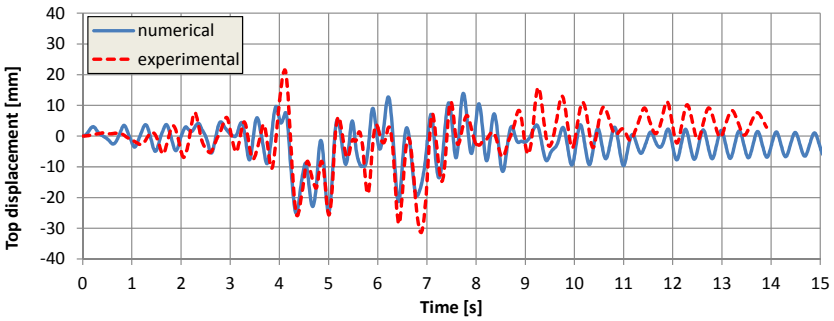

(a)

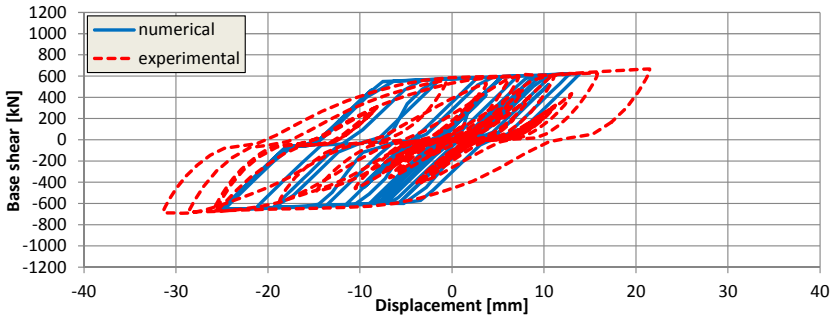

(b)

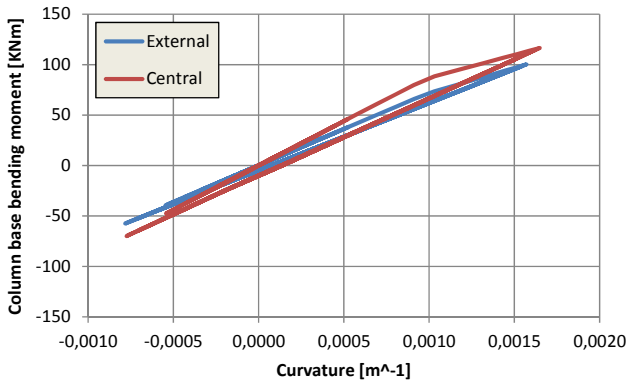

(c)

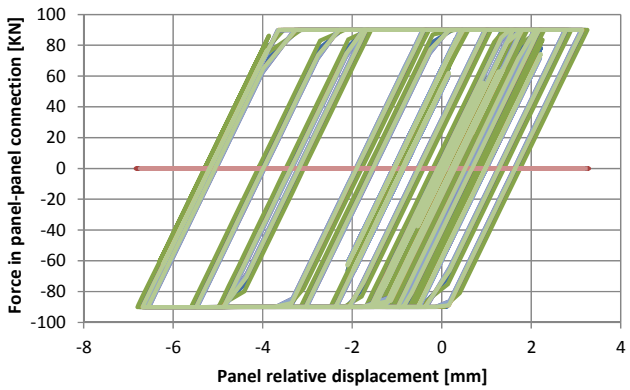

(d)

Figure 5.82 – Pendulum arrangement with 2 FBDs per interface, numerical simulation with PGA = 0,36g: (a) vibratory curve, (b) base shear vs displacement, (c) column base moment vs curvature and (d) FBD hysteretic cycles

A further pseudo-dynamic test with PGA equal to 0,72g, corresponding to the double of the ultimate limit state PGA of the model structure, has been executed, pushing the experimentation with respect to the originally scheduled 0,54g value of PGA. The results (Figure 5.83) show that the top displacement attained is less than 80 mm, to which column base yielding is still not associated. The numerical simulation (Figure 5.84) is able to catch the displacement history trend of the structure together with the maximum displacement values. As already observed in previous tests, the first cycle at large displacement is associated to a hardening behaviour, which re-alignes to the numerical analysis within further cycles. The maximum slippage of the FBDs is equal to 24 mm, which is less than half of their capacity.

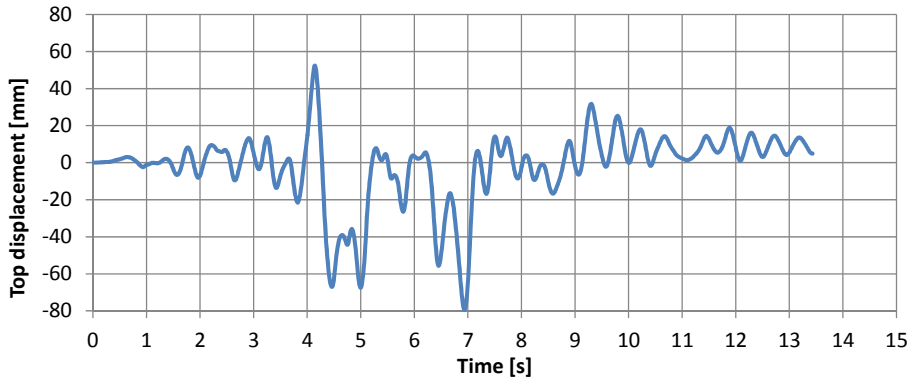

(a)

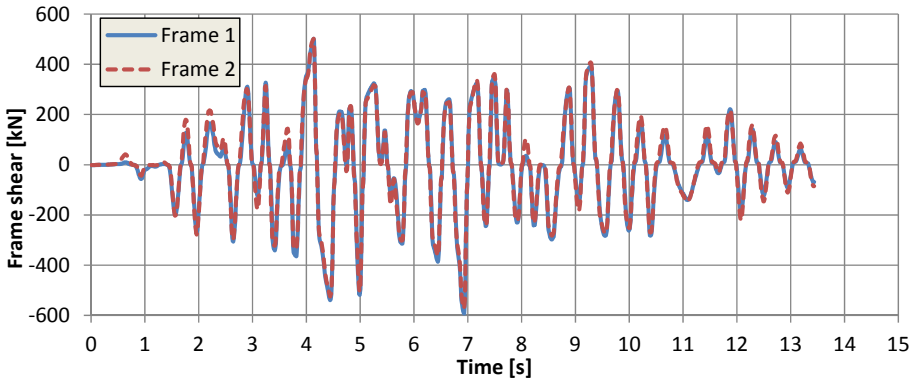

(b)

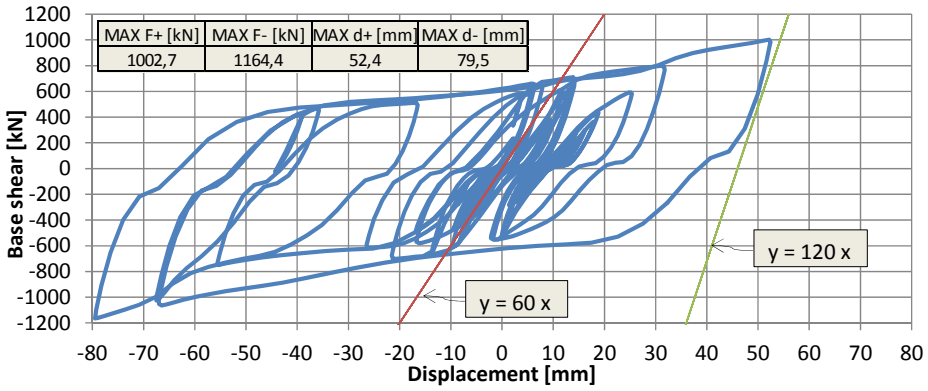

(c)

Figure 5.83 – Pendulum arrangement with 2 FBDs per interface, PsD test with PGA = 0,72g: (a) vibratory curve, (b) frame shear load history and (c) base shear vs displacement

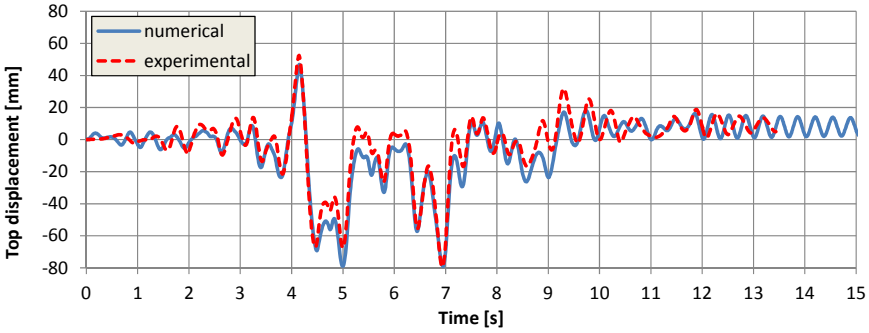

(a)

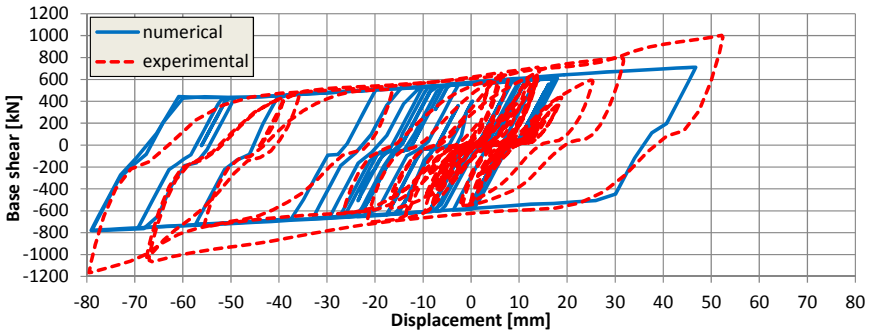

(b)

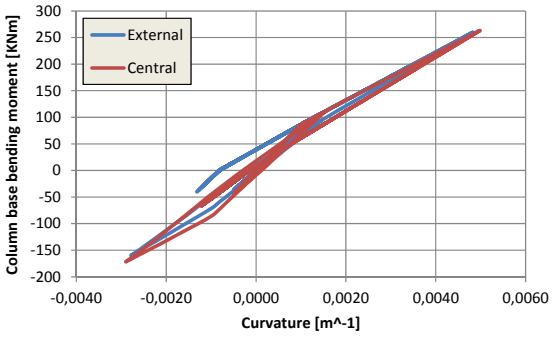

(c)

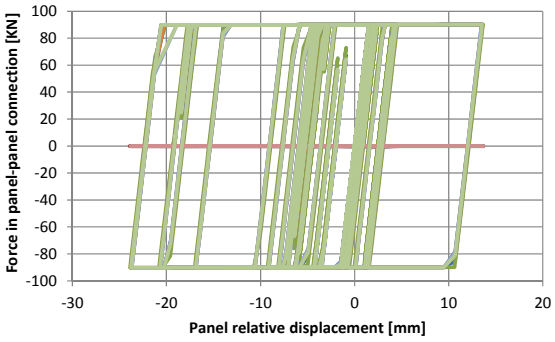

(d)

Figure 5.84 – Pendulum arrangement with 2 FBDs per interface, numerical simulation with PGA = 0,72g: (a) vibratory curve, (b) base shear vs displacement, (c) column base moment vs curvature and (d) FBD hysteretic cycles

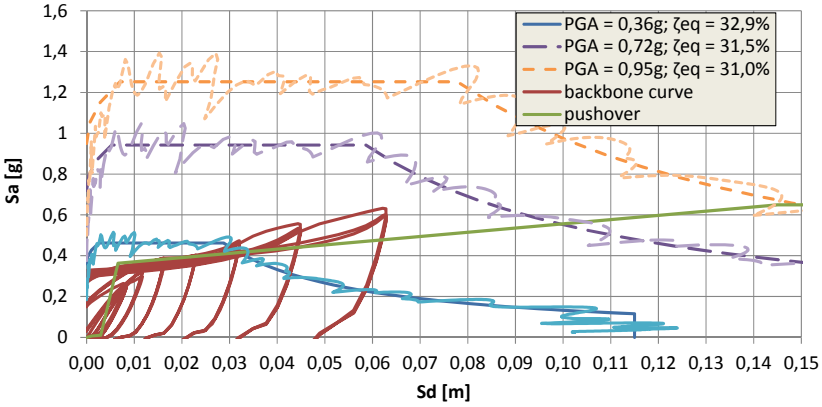

Figure 5.85 – Pendulum arrangement with 2 FBDs per interface: maximum displacement according to ADRS procedure

5.2.5.4. Pendulum arrangement: one FBD

The building with single FBD per panel interface (Figure 5.86), each slipping bolt of which has been tightened with a torque equal to 220 Nm, has been tested under cyclic and pseudo-dynamic load. The results of the cyclic test, illustrated in Figure 5.87, show a highly dissipative behaviour, with a very large area included within the hysteretic cycles. Also in this case, the experimental slip threshold corresponds to about 90 kN per connection.

The values of average equivalent viscous damping ratio per each displacement step are reported in Table 5-10.

The global initial elastic stiffness is lowered to about 38 kN/mm, and still a larger unload stiffness equal to about 60 kN/mm is observed (which is one third of the unload stiffness of the structure with three FBDs per interface), followed by a small (±1,5~2,5 mm) pinching branch and a much lower reload stiffness. Practically no difference in terms of loads between the two parallel frames can be observed in Figure 5.87a.

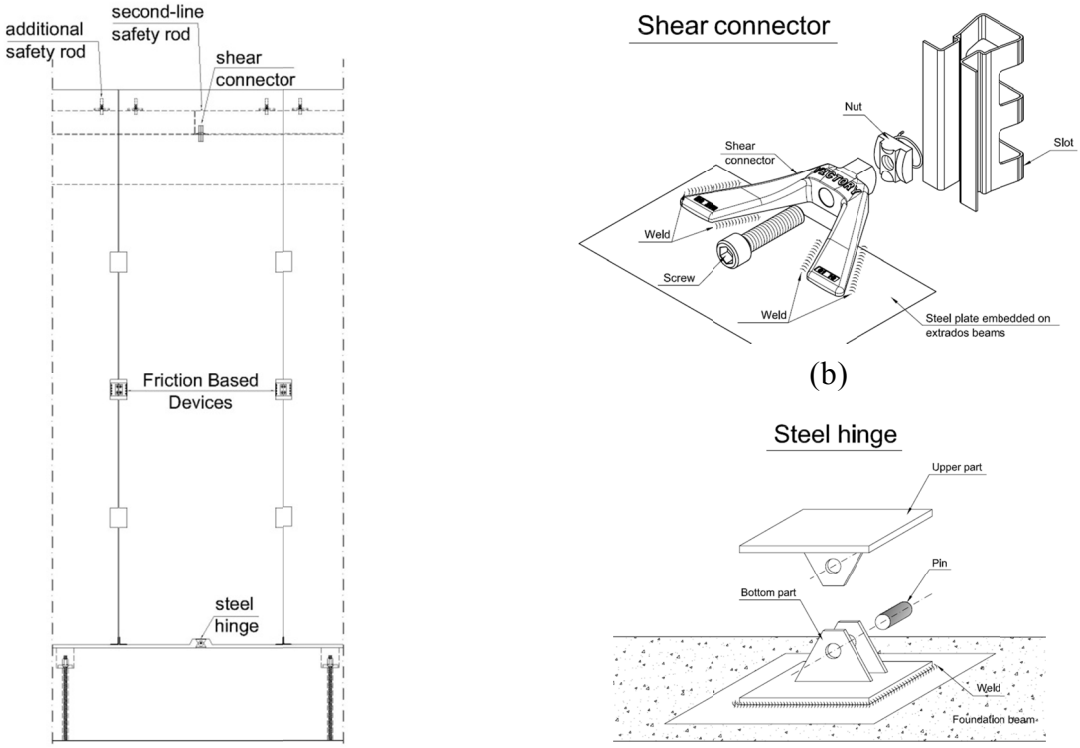

(a) (b) (c)

Figure 5.86 – Pendulum arrangement with 1 FBD per interface: (a) front view of the panel, (b) top shear connection, (c) base steel hinge

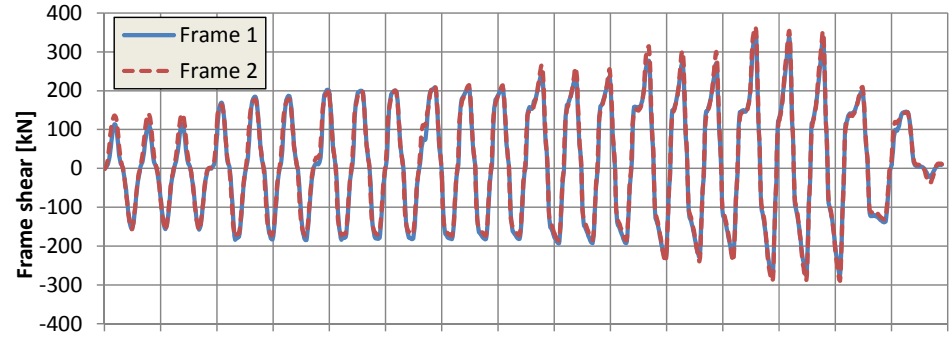

(a)

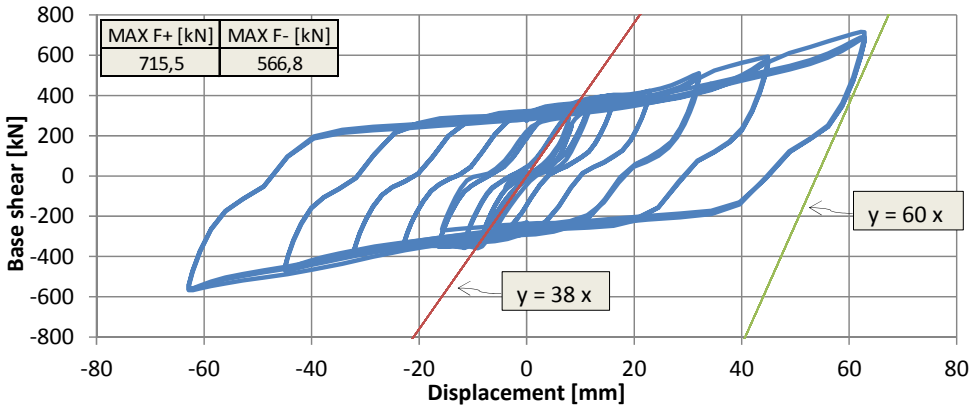

(b)

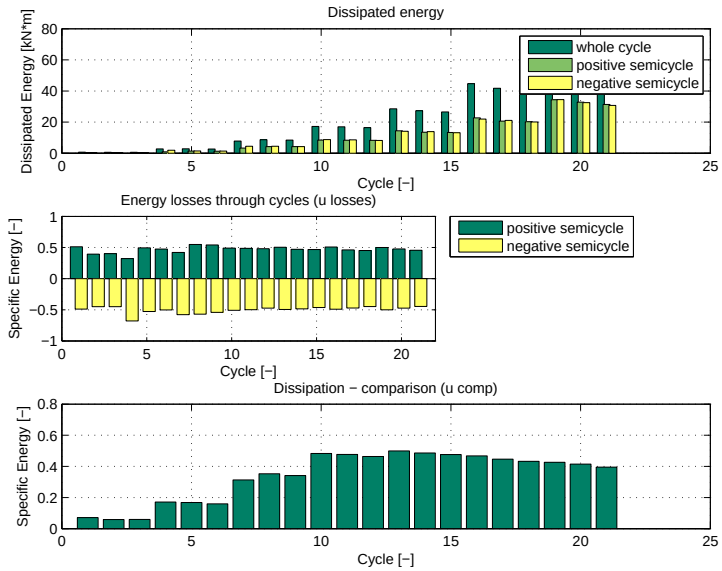

(c)

Figure 5.87 – Pendulum arrangement with 1 FBD per interface, cyclic test: (a) frame shear load history, (b) base shear vs displacement and (c) energy dissipation properties

Table 5-10 – Pendulum arrangement with 1 FBD per interface, cyclic test: equivalent viscous damping ratio

d [mm]	8,4	11,7	16,4	23,0	32,1	45,0	63,0
ζ_{eq} [%]	4,0	10,6	21,4	30,2	31,0	28,6	26,3

A single pseudo-dynamic test has been carried out with PGA equal to 0,36g, corresponding to the ultimate limit state acceleration of the building model. The experimental results are collected in Figure 5.88. The maximum top displacement attained is lower than 52 mm, and therefore all structural members have performed in elastic field. The seismic response shows a larger flexibility with respect to the tests with three connections per interface, but still much stiffer if compared to the isostatic configuration. The numerical analysis, which results are shown in Figure 5.89, provides a good estimation of the vibratory curve and the hysteresis of the building. The FBDs have been subjected to moderate slippage, equal to 14 mm, and this suggests that the structure is provided with large over-resources and that it could sustain much larger PGA earthquakes.

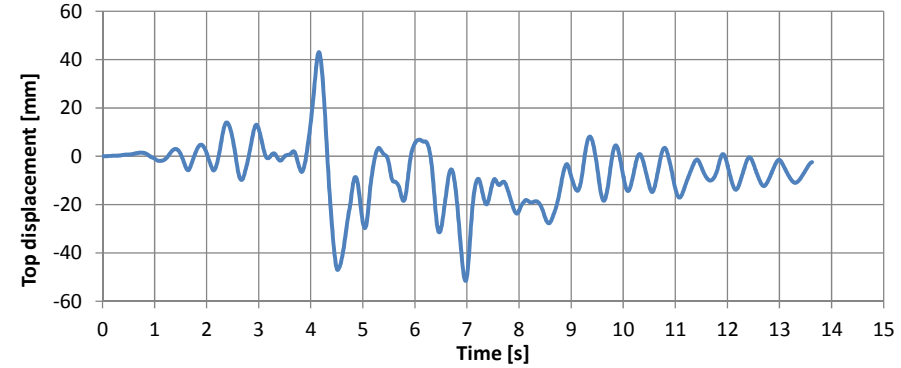

(a)

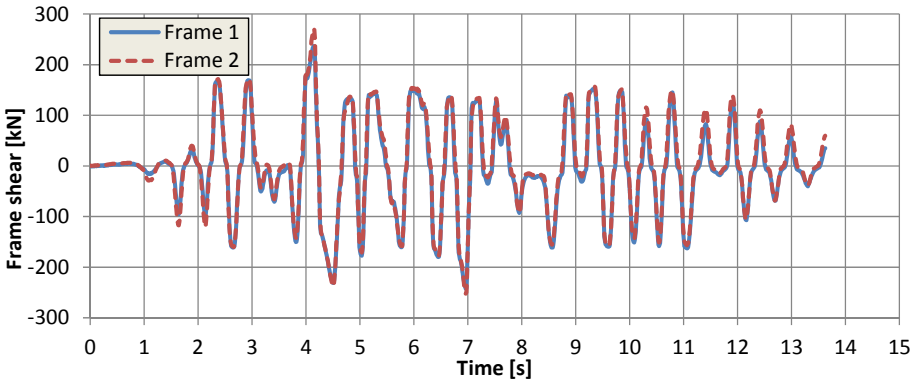

(b)

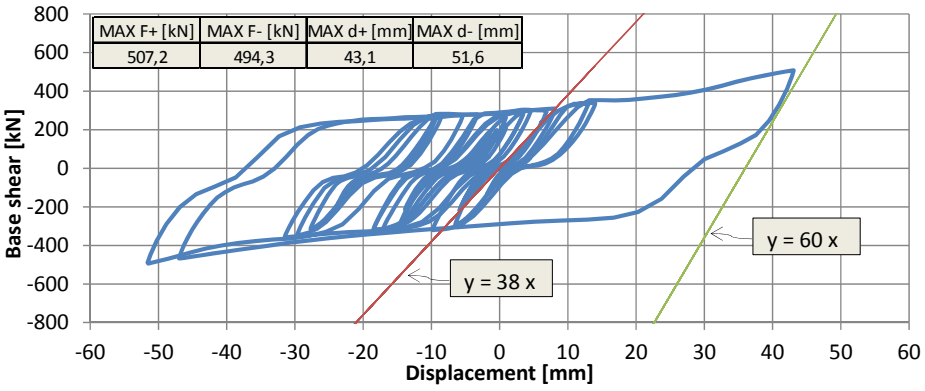

(c)

Figure 5.88 – Pendulum arrangement with 1 FBD per interface, PsD test with PGA = 0,36g: (a) vibratory curve, (b) frame shear load history and (c) base shear vs displacement

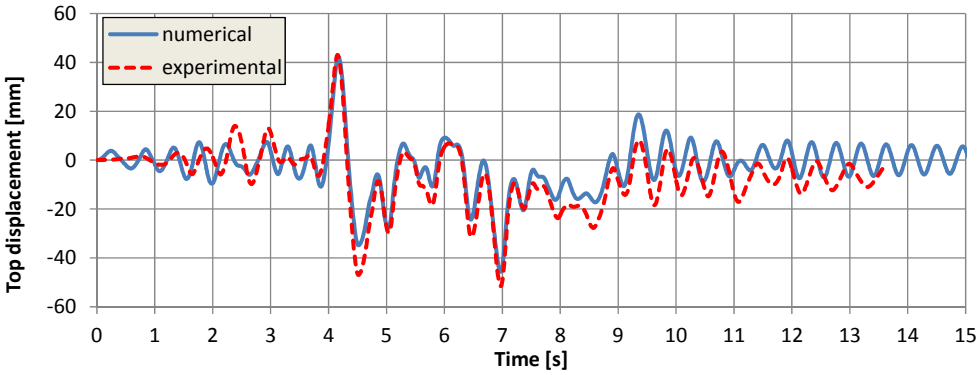

(a)

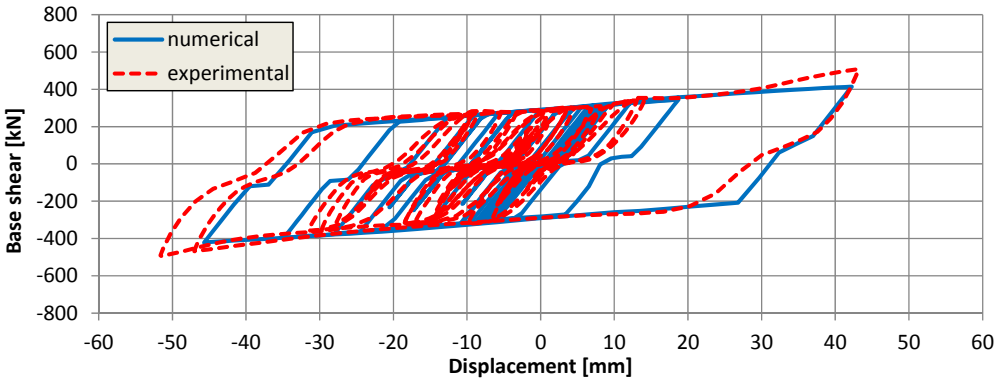

(b)

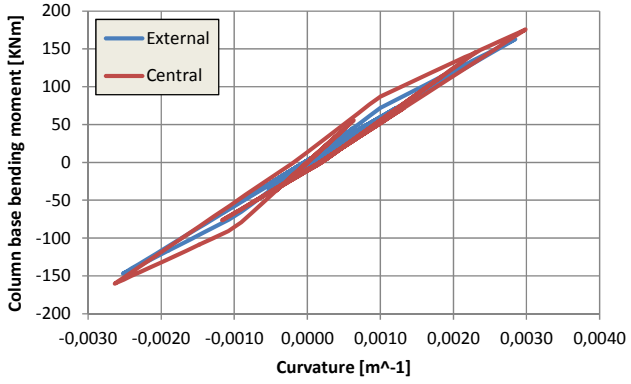

(c)

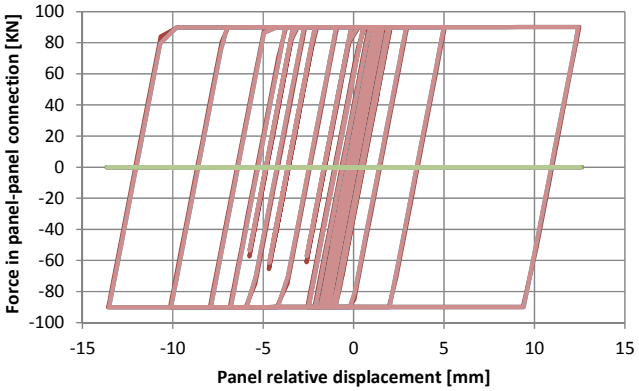

(d)

Figure 5.89 – Pendulum arrangement with 1 FBD per interface, numerical simulation with PGA = 0,36g: (a) vibratory curve, (b) base shear vs displacement, (c) column base moment vs curvature and (d) FBD hysteretic cycles

The ADRS procedure leads to the following displacement estimations (Figure 5.90): for the test with PGA equal to 0,36g the estimated maximum displacement is 58 mm (+12% with respect to the experimental results) with an interpolated equivalent viscous damping ratio equal to 26,9%. The same procedure shows that column yielding would occur for the earthquake scaled at not less than 0,57g of PGA. The corresponding equivalent viscous damping, obtained for extrapolation of the experimental results, has been taken equal to 15,8%.

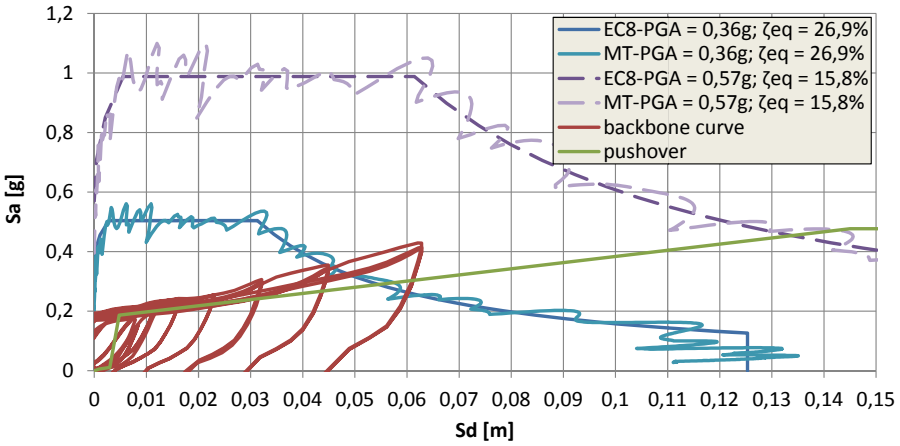

Figure 5.90 – Pendulum arrangement with 1 FBD per interface: maximum displacement according to ADRS procedure

5.2.5.5. Rocking arrangement: one FBD

The building with rocking panel connection arrangement has been provided with a single FBD per panel interface (Figure 5.91), each slipping bolt of which has been tightened with a torque equal to 150 Nm, lower than the maximum torque applied during the previous tests in order to avoid edge panel lifting due to a vertical action larger than the panel own weight. The results of the cyclic test, illustrated in Figure 5.87, show a highly dissipative behaviour, with a very large area included within the hysteretic cycles.

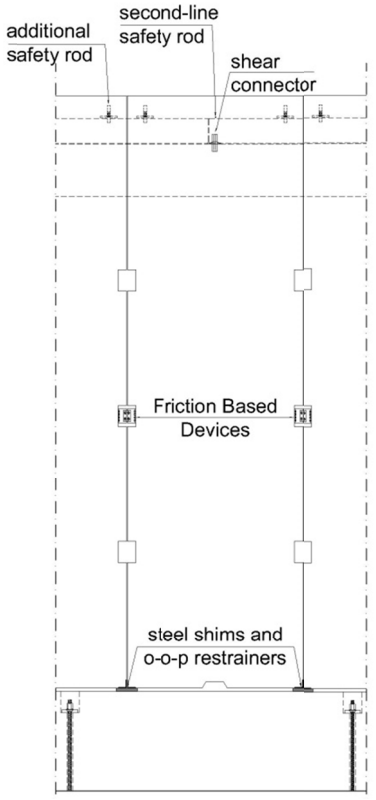

(a)

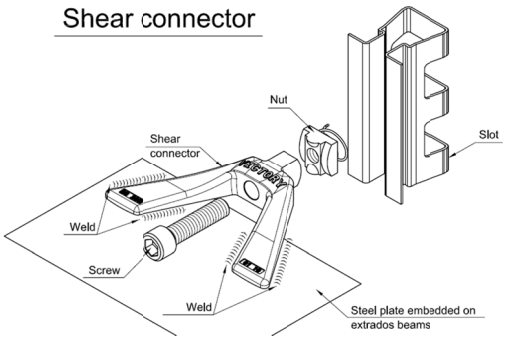

(b)

(c)

Figure 5.91 – Rocking arrangement with 1 FBD per interface: (a) front view of the panel, (b) top shear connection, (c) base steel shims and out-of-plane restrainers

The experimental slip threshold corresponds to about 30 kN horizontal per panel interface, which is composed by the self-centring effect of the panels (13 kN) and by the horizontal shear component due to the dissipative connections, that is about 17 kN, coming from a vertical slip threshold of the single connection of about 50 kN.

The hysteretic cycles are flag-shaped, since the lateral contribution provided by the panels does not correspond to dissipation of energy, which is all concentrated in the dissipative devices. The values of average equivalent viscous damping ratio per each displacement step are reported in Table 5-11. The global initial elastic stiffness is of about 38 kN/mm, and a larger unload stiffness equal to about 60 kN/mm is observed, followed by a very large pinching branch due to the peculiarity of the rocking system.

Those stiffness values are identical to the corresponding of the tests on pendulum arrangement with single FBD per interface. Practically no difference in terms of loads between the two parallel frames can be observed in Figure 5.92a.

A pseudo-dynamic test has been conducted with PGA equal to 0,36g, corresponding to ultimate limit state PGA of the building model. The vibratory curve suggests that the behaviour is very stiff while displacements are in the range in which the panels do not lift, and that for larger displacements the behaviour turns to be quite flexible. The top displacement attained is less than 58 mm, which means that all structural members behaved elastically.

Pictures with the elevation views of the panels before the test and subjected to the maximum drift are shown in Figure 5.94. The numerical simulation, which results are reported in Figure 5.95, show a very good correspondence with the experimental results in terms of vibratory curve. Also the matching of the hysteretic cycles is good, with a numerical over-estimation of the initial stiffness, probably due to non-critical damage occurred in most panel shear connections during their sliding, which may have caused an experimental decreased stiffness.

The ADRS procedure leads to the following displacement estimations (Figure 5.96): for the test with PGA equal to 0,36g the estimated maximum displacement is 62 mm (+9% with respect to the experimental results) with an interpolated equivalent viscous damping ratio equal to 19,3%. The same procedure shows that column yielding would occur for the earthquake scaled at not less than 0,53g of PGA. The corresponding equivalent viscous damping, obtained for extrapolation of the experimental results, has been taken equal to 10,0%.

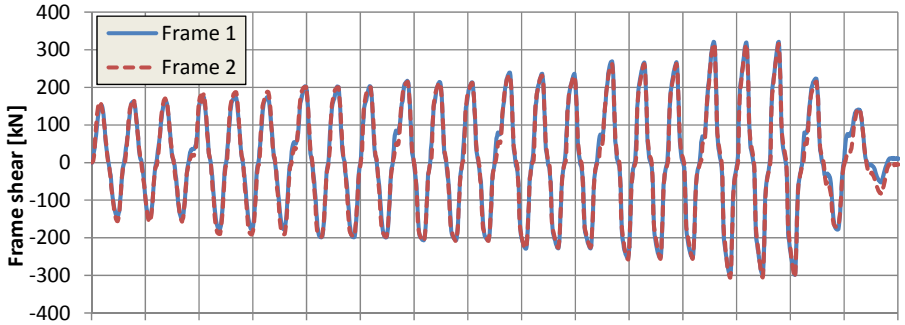

(a)

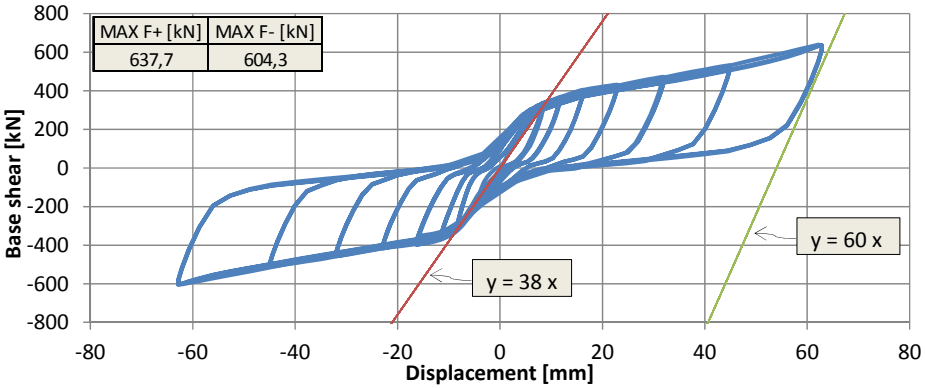

(b)

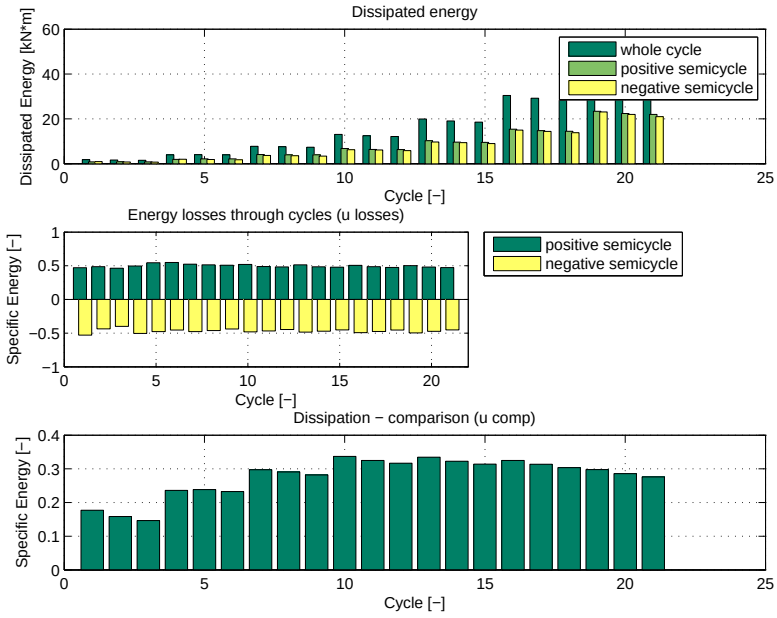

(c)

Figure 5.92 – Rocking arrangement with 1 FBD per interface, cyclic test: (a) frame shear load history, (b) base shear vs displacement and (c) energy dissipation properties

Table 5-11 – Rocking arrangement with 1 FBD per interface, cyclic test: equivalent viscous damping ratio

d [mm]	8,4	11,7	16,4	23,0	32,1	45,0	63,0
ζ_{eq} [%]	10,2	15,0	18,5	20,8	20,6	20,0	18,2

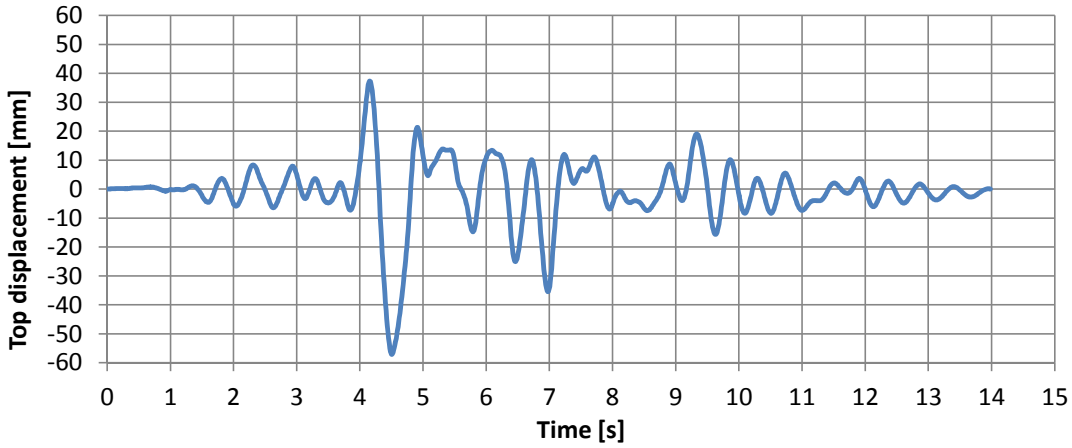

(a)

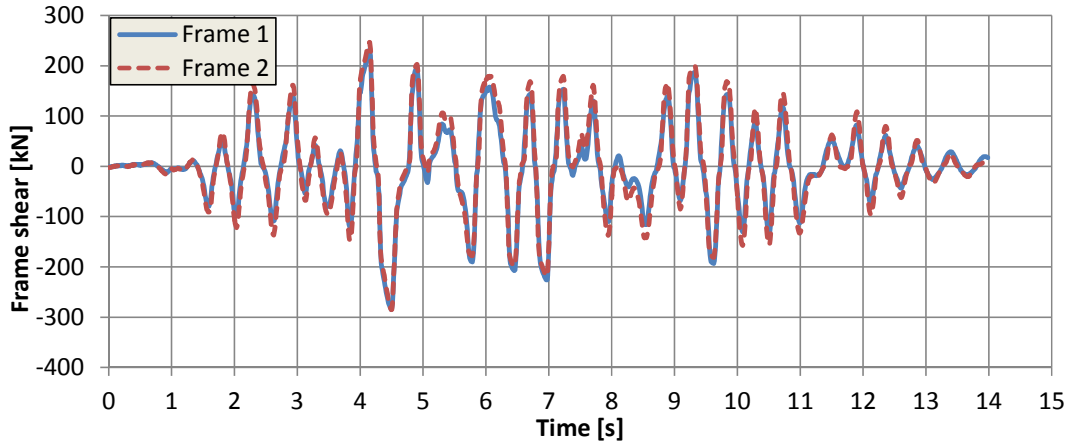

(b)

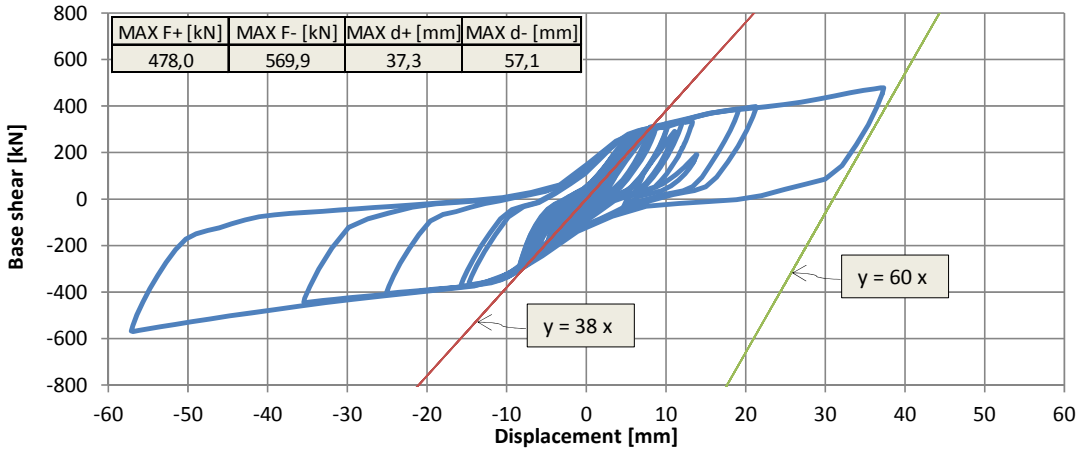

(c)

Figure 5.93 – Rocking arrangement with 1 FBD per interface, PsD test with PGA = 0,36g: (a) vibratory curve, (b) frame shear load history and (c) base shear vs displacement

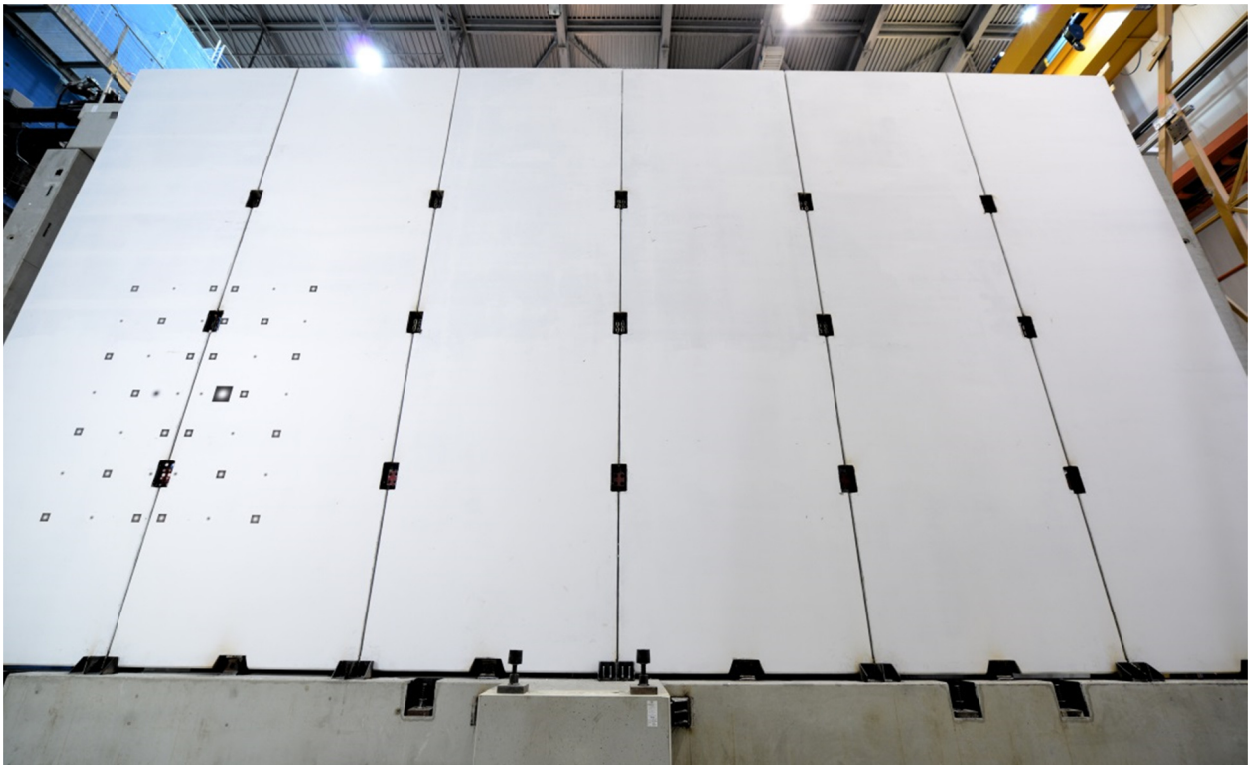

(a)

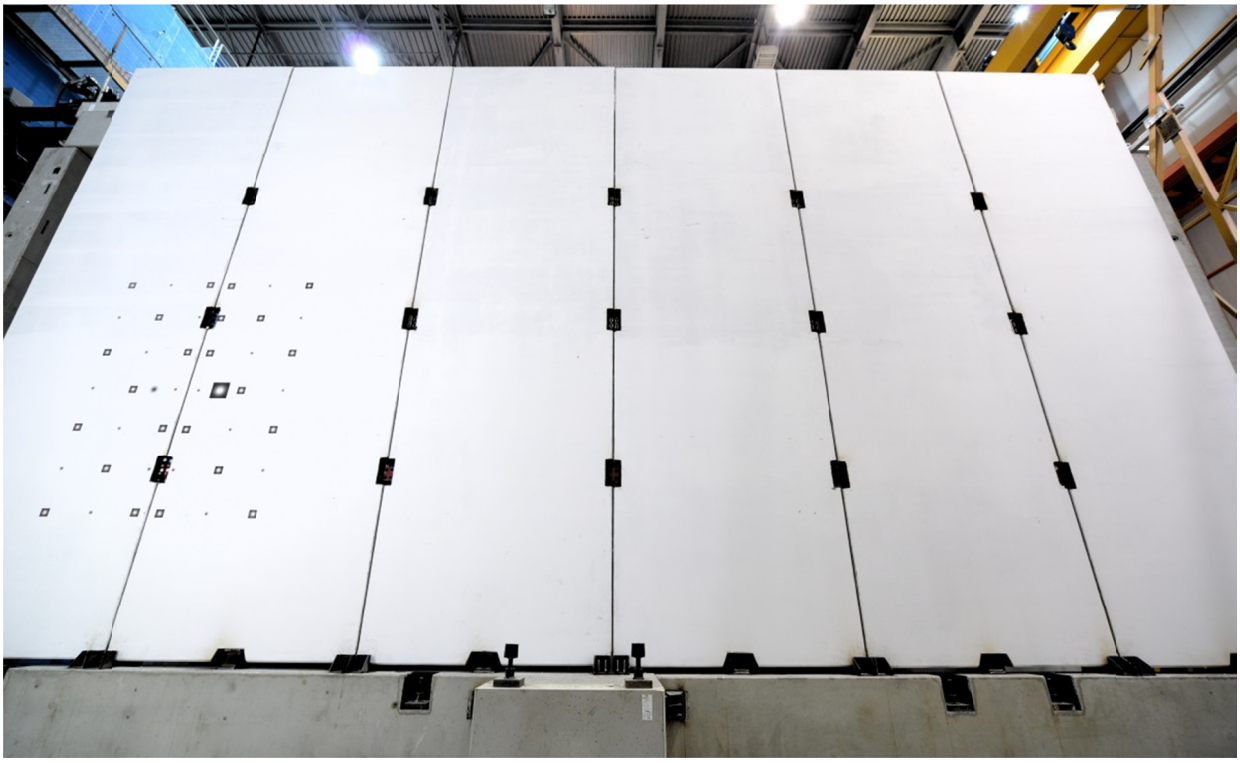

(b)

Figure 5.94 – Rocking arrangement with 1 FBD per interface, PsD test with PGA = 0,36g: front view at (a) beginning of the test (b) maximum drift

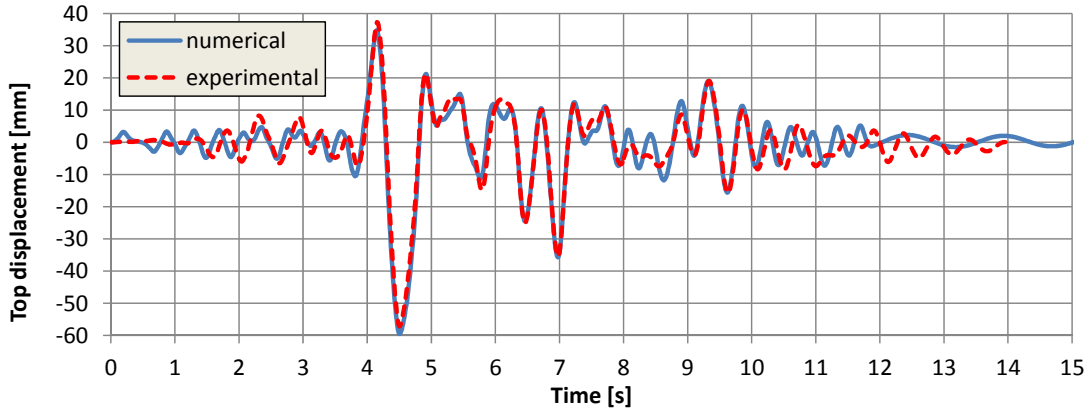

(a)

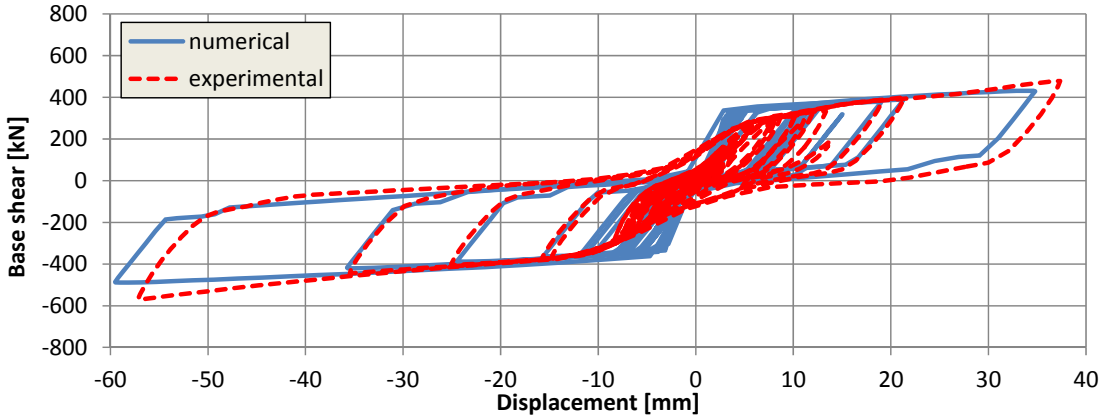

(b)

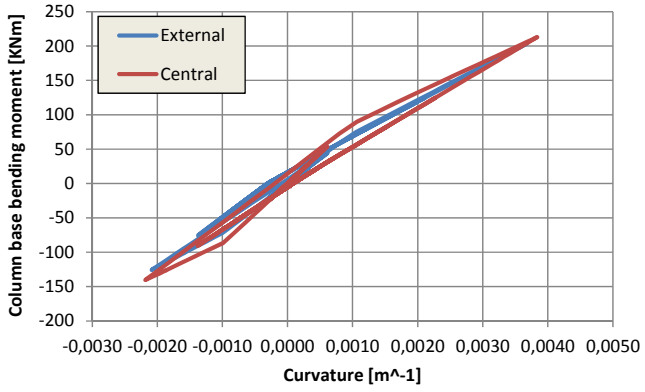

(c)

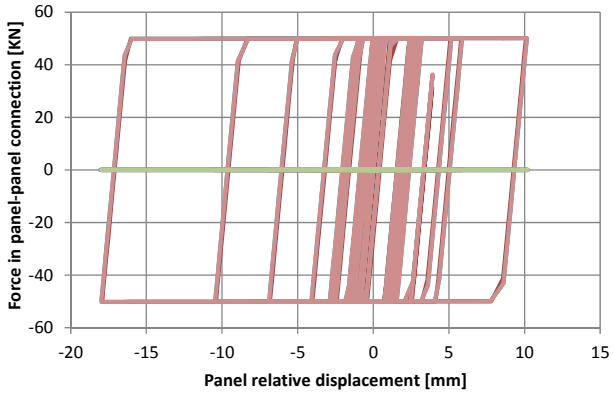

(d)

Figure 5.95 – Rocking arrangement with 1 FBD per interface, numerical simulation with PGA = 0,36g: (a) vibratory curve, (b) base shear vs displacement, (c) column base moment vs curvature and (d) FBD hysteretic cycles

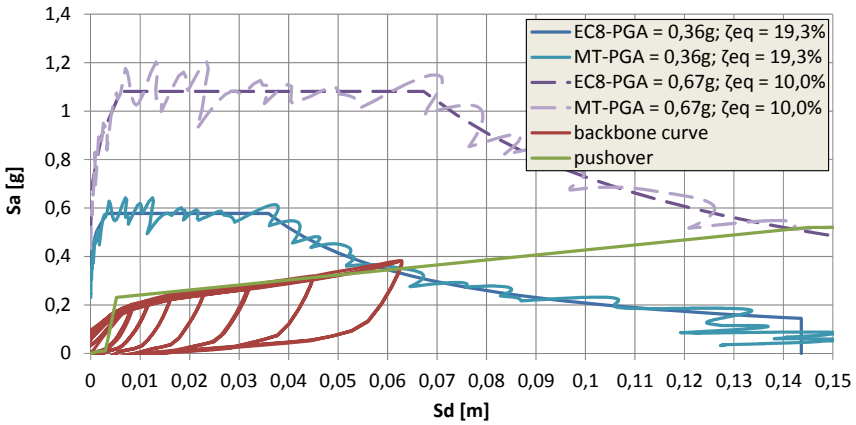

Figure 5.96 – Rocking arrangement with 1 FBD per interface: maximum displacement according to ADRS procedure

5.2.6. Design considerations

From the comparison among the experimental maximum top displacement and its estimation with the ADRS procedure (Table 5-12), it can be noticed how the method generally provides safe-side displacement predictions. The few cases of under-estimation concern only few millemetres of error. In the majority of the over-estimated cases, it can be observed that the unpredictable over-resistance of the FBDs led to a stiffer response, justifying the safe-side error. In the case of the isostatic rocking system, the response for serviceability limit state is largely over-estimated, anyway always on the safe side.

Table 5-12 – Maximum top displacement for (a) PsD test results and (b) estimation with ADRS procedure

	Experimental maximum top displacement [mm]						
	pendulum					rocking	
PGA [g]	isostatic	silicone	3FBD	2FBD	1FBD	isostatic	1FBD
0,10	59,3	48,2	-	-	-	-	-
0,18	-	-	10,9	-	-	36,9	-
0,36	-	-	21,2	31,4	51,6	-	57,1
0,72	-	-	46,3	79,5	-	-	-
1,00	-	-	87,6	-	-	-	-

(a)

	Estimated maximum top displacement with ADRS procedure [mm]						
	pendulum					rocking	
PGA [g]	isostatic	silicone	3FBD	2FBD	1FBD	isostatic	1FBD
0,10	57 (-4%)	43 (-11%)	-	-	-	-	-
0,18	-	-	7 (-36%)	-	-	72 (+95%)	-
0,36	-	-	16 (-25%)	33 (+5%)	58 (+12%)	-	62 (+9%)
0,72	-	-	82 (+77%)	102 (+28%)	-	-	-
1,00	-	-	127 (+45%)	-	-	-	-

(b)

This method may be used not only as an analysis tool to check the experimental behaviour, but also as a performance-based design tool. In particular, the design procedure according to the ADRS method may be defined with the following steps:

- The level of performance is defined.
- An initial guess of the structure geometry is draft.
- A pushover and cyclic analysis of the structure is performed.
- The distribution of equivalent viscous damping factors is calculated.
- The numerical results from the pushover analysis are plotted in terms of backbone capacity curve on an acceleration vs displacement diagram.
- The demand curve is plotted according to the response spectrum of the accelerogram in the same diagram, with an initial equivalent damping ratio ζ_{eq} guess value.
- The intersection point between the capacity and the demand curve represents the performance point. The equivalent damping ratio ζ_{eq} value is then updated on the base of the corresponding displacement estimation and the interpolation (or extrapolation, if applicable) value between those numerically obtained. This operation is repeated until convergence is attained.
- The level of performance is checked.
- In case of non-satisfactory level of performance, the design shall restart from the initial guess.

As a rapid dimensioning criteria, the concept of equivalent total dissipated energy may be used to identify the properties of the new structure. In fact, if analysing the experimental total dissipated energy, it can be noted (Table 5-13) how even structures having a very different behaviour (from isostatic to dissipative to integrated) dissipate in very general terms a comparable amount of energy.

Table 5-13 – Total experimental dissipated energy from the PsD tests on different structures

	Total dissipated energy [kJ]							
	pendulum					rocking		cantilever
PGA [g]	isostatic	silicone	3FBD	2FBD	1FBD	isostatic	1FBD	integrated
0,10	4,4	9,5	-	-	-	-	-	-
0,18	-	-	15,9	-	-	9,5	-	12,8
0,36	-	-	67,8	86,9	93,3	-	82,1	74,9
0,72	-	-	246,6	334,2	-	-	-	-
1,00	-	-	520,2	-	-	-	-	-

Chapter 6

Seismic performance of precast buildings with dissipative systems

The seismic behaviour of multi-nave or multi-span buildings is largely influenced by the diaphragm stiffness. Large plan mono-storey precast concrete buildings for industrial or commercial use are often provided with roof structures made by distanced floor members with interposed lightening openings. This type of roofing, based on the current spans of the elements, does not provide a rigid diaphragm. The actual flexibility of the roofing systems depend on the floor-to-beam connection arrangement. Also dry-assembled precast slabs with adjacent floor members can act as non-rigid diaphragm, depending on the connection stiffness and on the presence of mutual floor-to-floor connections. A non-rigid diaphragm can lead to in-plane distortions and different seismic response for the frames of the structure. A study of the influence of this phenomenon is provided in the present chapter through a case study. A more systematic parametric analysis considering mono-storey buildings with different shapes and roofing technology provided with dissipative cladding panel connections is also addressed.

6.1. Role of the diaphragm action

The horizontal actions stress the diaphragm on the base of the distribution of mass and stiffness of the different lateral force resisting systems acting in parallel.

The problem of the diaphragm behaviour of precast roofing systems has been addressed in literature, among others, by Fleischman *et al.* (2002) and Ferrara *et al.* (2004) with reference to specific dry-assembled structural arrangements.

When the diaphragmatic action cannot take place, for instance in case of mono-ribbed floor members connected with typical hinged connections or double-ribbed elements similarly connected only at one rib, each frame of the overall structural assembly behaves substantially independently from the adjacent, with dynamic behaviour depending only on its own stiffness characteristics and pertinent mass.

A structural system with homogeneous distribution of stiffness and mass behaves therefore in a more uniform way, slightly stressing the eventual diaphragm. Relevant differencies of mass and/or stiffness modifies the seismic behaviour of the building, largely stressing the diaphragm, if stiff, or creating possible out-of-phase responses with large roof distortions, if flexible.

Such a behaviour is magnificated if statically undetermined cladding panel connection arrangements are introduced in the structure, since the peripheral frames become then characterised by a much larger stiffness in comparison with the internal.

The seismic behaviour of a typical precast industrial building is studied through modal and dynamic non-linear analyses (Biondini *et al.* 2013a). The aim is to show the behaviour of the building when subjected to horizontal static loads or load histories with different properties of the diaphragm connections and of the cladding panel mutual connections, studying configurations with increasing differences in terms of stiffness between internal and external frames.

The mono-storey building, which plan and section views are shown in Figure 6.8 is composed by two 15 m span naves and four 10 m span bays. The 0,6 by 0,6 m square cross-section columns are 7 m tall, the 0,8 by 0,4 m rectangular cross-section beams run along the bays and the 0,6 m deep and 2,1 m wide double-Ts floor members run along the naves. The floor members are distanced, so to leave room for natural lightening. The roof distributed mass from floor members and non-structural dead loads is 285 kg/m^2.

The rectangular vertical cladding panels have 2,5 by 8,75 m dimensions, equivalent thickness of 12 cm and distributed mass of 300 kg/m^2. The panels are positioned exclusively along the bays. The cladding panels are connected to the structure with a pendulum arrangement, with the addition of mutual panel-to-panel connections, as indicated in Figure 6.1b. The floor members are connected to the beams with hinged connections in correspondence of the ribs. For each member edge, one connection is rigid and the other has variable stiffness.

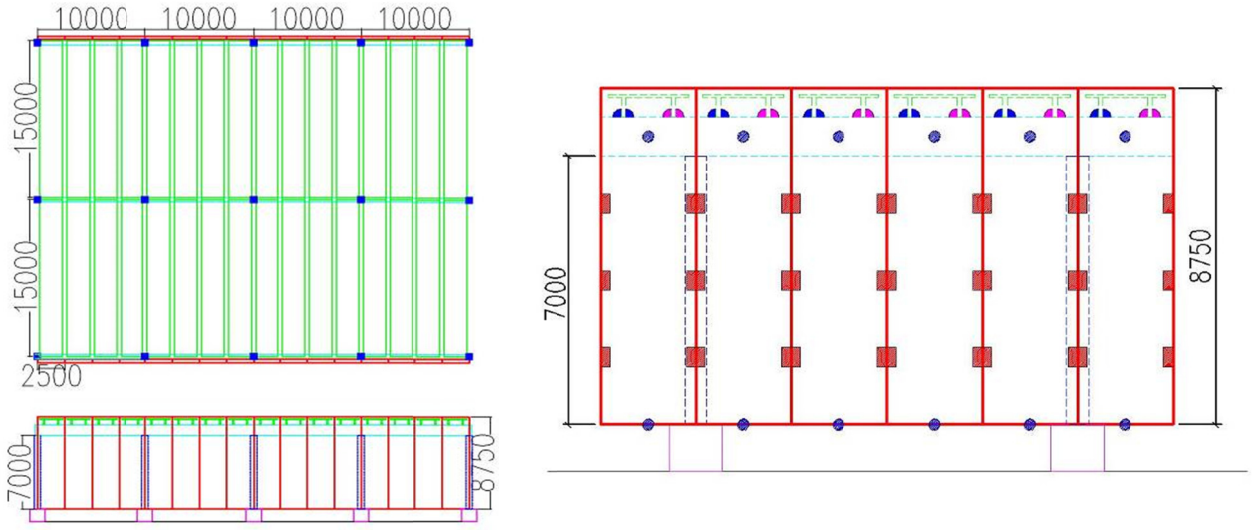

(a) (b)

Figure 6.1 – Precast industrial building prototype: a) plan and lateral view; b) particular lateral view with connection arrangement

The modal analysis is conducted considering a halved elastic stiffness of the columns, in order to take into account the effect of cracking as suggested by Eurocode 8. All other elements, in which cracking is not expected to occur, are provided with plain stiffness.

The results of modal analyses performed on the structure with variable panel-to-panel connection stiffness k_p in case of rigid diaphragm are illustrated in Figure 6.2a and in Figure 6.2b. The condition of null stiffness of the connections corresponds to a statically determined panel arrangement and a consequent pure frame behaviour of the structure, with a fundamental natural frequency equal to 0,97 Hz. The condition of maximum stiffness of the panel-to-panel connections (10^{10} kN/m) refers to a wall behaviour of the structure, with a highly rigid response, to which a fundamental natural frequency equal to 19,78 Hz is associated.

For increasing values of panel-to-panel connection stiffness, a global stiffening of the structure is observed. In particular the stiffness range between 10^4 and 10^6 kN/m represents the transtition phase from a frame behaviour to a wall type.

The sum of the participating factor associated to the fundamental vibration modes is practically constant with the connection stiffness, with a percentage of about 87% of the global mass. The missing percentage refers to local modes of panels and columns, to each of which a very small percentage of participating mass is associated.

Exploring the influence of a non-rigid diaphragm on the dynamic behaviour of the structure, the translational stiffness of the floor-to-beam connection k_t is varied through the modal analyses. In Figure 6.3a and Figure 6.3b the fundamental natural frequency and the relative participation factor are, respectively, plotted for variable k_p and k_t. For $k_t = 0$ (null diaphragm), the fundamental vibration mode eith frequency equal to 0,91 Hz only involves the central frame (the participation mode is 30%), since the lateral ones act independently.

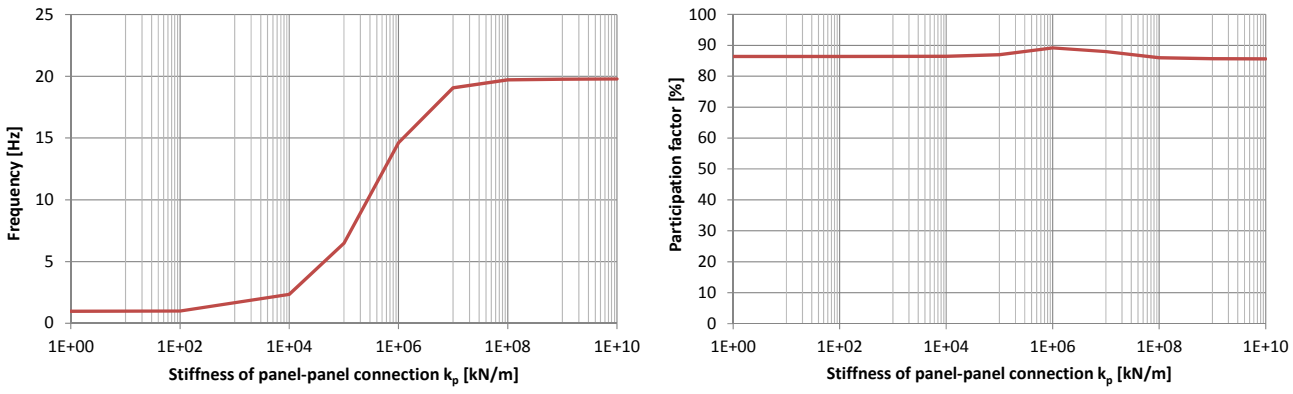

(a) (b)

Figure 6.2 – Structure with rigid diaphragm and variable panel-to-panel connection stiffness k_p: a) fundamental natural frequency, b) associated participation factor

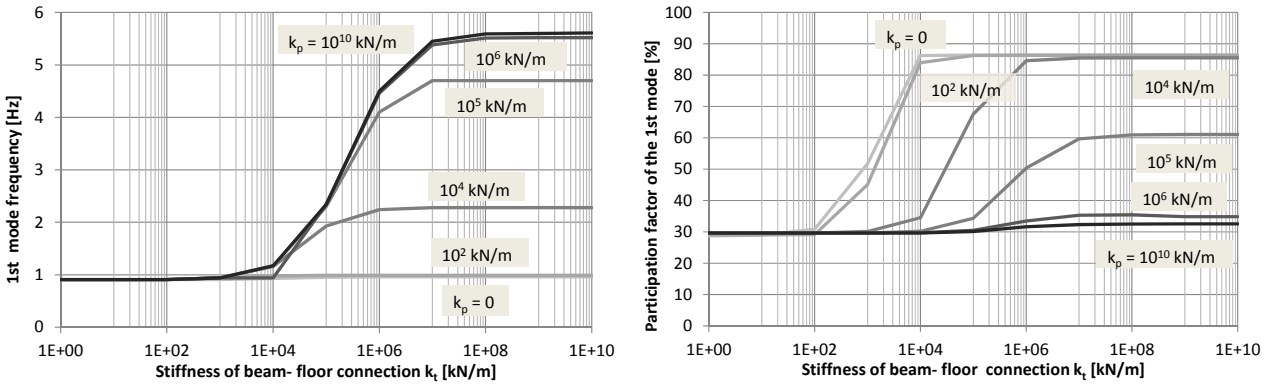

(a) (b)

Figure 6.3 – Structure with variable floor-to-beam connection stiffness k_t and panel-to-panel connection stiffness k_p: a) fundamental natural frequency, b) associated participation factor

For low stiffness panel-to-panel connections, the fundamental frequency is scarcely dependent on k_t, since all frames have similar mass and stiffness. It increases from 0,91 Hz, representing the vibration mode of the only central frame, to 0,97 Hz, which is associated to the whole building vibration mode. Anyway, the response of the frames can be uncoupled and therefore largely out-of-phase for values of k_t lower than 100 kN/m, even if a full participation of all frames is only reached after 10^4 kN/m. To increasing values of k_p corresponds a gradual stiffening of the fundamental mode with k_t. It is interesting to note that the plateau frequency value for fixed connections, equal to 5,61 Hz, is much lower than the corresponding frequency with rigid diaphragm, equal to 19,78 Hz. This is due to the out-of-plane deformability of the floor members and suggests that out-of-plane double clamped floor members cannot perform as a rigid diaphragm.

It is also possible to trace the trends of intermediate solutions: the fundamental frequency is subjected to a large variation in between 10^4 and 10^7 kN/m of k_t, stabilyzing on larger plateau values with larger stiffness k_p.

The participation factor trend shows a transition phase that is strongly depending on the stiffness k_p, in particular it develops in between 10^2 and 10^4 kN/m for low values of k_p and in between 10^5 and 10^7 kN/m for large values of k_p, stabilyzing on decreasing values with larger k_p. For what concerns the upper modes, Table 6-1 and Table 6-2 contain the most relevant results from the modal analyses on extreme cases for the direction parallel to the panels and orthogonal, respectively. Multiple frequencies indicate that the specific dynamic behaviour is individuated by different uncoupled modes within the structure. In those cases, the frequency range is indicated, together with the sum of each participation factor contribution.

In the direction parallel to the panels three dynamic behaviours are observed:

Mode 1: overall frame deformation according to cantilever deformed shape of columns

Mode 2: local flexure of columns without top displacement

Mode 3: local in-plane flexure of the panels with top displacement

Table 6-1 – Natural frequencies and associated participation factors for the relevant vibration modes in direction parallel to the cladding panels for (a) $k_p = 0$, b) $k_p = 10^{10}$ kN/m

Panel in plane direction - $k_p = 0$					
MODE	1	2	3	4	
$k_t = 0$	0,91 - 1,00	-	-	-	frequency [Hz]
	86,45	-	-	-	Part. Factor [%]
$k_t = 10^{10}$	0,97	-	-	-	frequency [Hz]
	86,35	-	-	-	Part. Factor [%]

(a)

Panel in plane direction - $k_p = 10^{10}$					
MODE	1	2	3	4	
$k_t = 0$	0,91	19,76 - 20,25	26,91 - 27,01	-	frequency [Hz]
	29,64	15,90	41,61	-	Part. Factor [%]
$k_t = 10^{10}$	5,61	19,78 - 20,27	27,46 - 27,52	-	frequency [Hz]
	32,54	13,59	41,50	-	Part. Factor [%]

(b)

Table 6-2 – Natural frequencies and associated participation factors for the relevant vibration modes in direction perpendicular to the cladding panels for (a) $k_p = 0$, b) $k_p = 10^{10}$ kN/m

Panel out of plane direction - $k_p = 0$					
MODE	1	2	3	4	
$k_t = 0$	0,91 - 1,00	1,56	5,40 - 5,42	-	frequency [Hz]
	80,99	1,81	5,93	-	Part. Factor [%]
$k_t = 10^{10}$	0,96	-	5,41 - 5,45	-	frequency [Hz]
	83,15	-	5,62	-	Part. Factor [%]

(a)

Panel out of plane direction - $k_p = 10^{10}$					
MODE	1	2	3	4	
$k_t = 0$	0,92	1,57	5,46 - 5,49	20,06	frequency [Hz]
	81,08	1,75	7,01	1,08	Part. Factor [%]
$k_t = 10^{10}$	0,96	-	5,47 - 5,50	19,38	frequency [Hz]
	83,17	-	7,33	2,14	Part. Factor [%]

(b)

It is noted how, for the building with statically determined panel connection arrangement ($k_p = 0$), the dynamic behaviour is determined by the only Mode 1. To hinged floor members corresponds however an uncoupled behaviour. For the building with rigid panel connections, the dynamic behaviour is substantially modified only for what concerns the first vibration mode, while the upper keep similar values of both frequency and participation factor (Table 6-1).

In the direction orthogonal to the panels, four dynamic behaviours are observed:

Mode 1: coordinated flexure of all frames according to cantilever deformed shape of the columns

Mode 2: counter-phase flexure of frames according to cantilever deformed shape of the columns

Mode 3: local flexure of panels with single curvature

Mode 4: local flexure of panels with double curvature

It is noted how, moving from a null diaphragm to double clamped floor members, the dynamic behaviour does not change substantially with the degree of inter-connection of the panels, except for the fact that Mode 2 disappears for stiff diaphragm, since the frames are driven to move together (Table 6-2).

The seismic behaviour of the structure is studied through non-linear time-history analysis. The non-linear behaviour of columns and FBD connections is defined in analogy with clause 6.1.1.

The modified Tolmezzo accelerogram (Figure 5.38) scaled at PGA = 0,32g is used as input motion, applied only in the direction parallel to the panels. The analyses are performed with different combinations of panel connections and diaphragm deformability.

For what concerns the panel-to-panel connections, the following solutions are examined:

- no connections (statically determined solution)
- rigid connections (integrated solution)
- FBD connections (dissipative solution)

For what concerns the diaphragm flexibility, the following solutions are examined:

- rigid diaphragm (numerically imposed)
- out-of-plane clamped floor-to-beam connection (both double-T ribs hingely connected)
- out-of-plane hinged floor-to-beam connection (only one double-T rib hingely connected)

6.1.1. Isostatic systems

Figure 6.4 shows the vibratory curves corresponding to the central and external frames of the structure with statically determined panel connection arrangement for the three diaphragm typologies.

For the case of out-of-plane clamped floor members there is no difference among the curves corresponding to different frames, as it is naturally observed in the case of rigid diaphragm. The building shows a flexible behaviour, with a maximum top displacement equal to about 18 cm. Considering an out-of-plane hinged floor-to-beam connection, corresponding to a null diaphragm, a slight out-of-phasing is observed between the responses of different frames, with moderate distortion of the slab. The difference is due to the slight difference of mass associated to the frames.

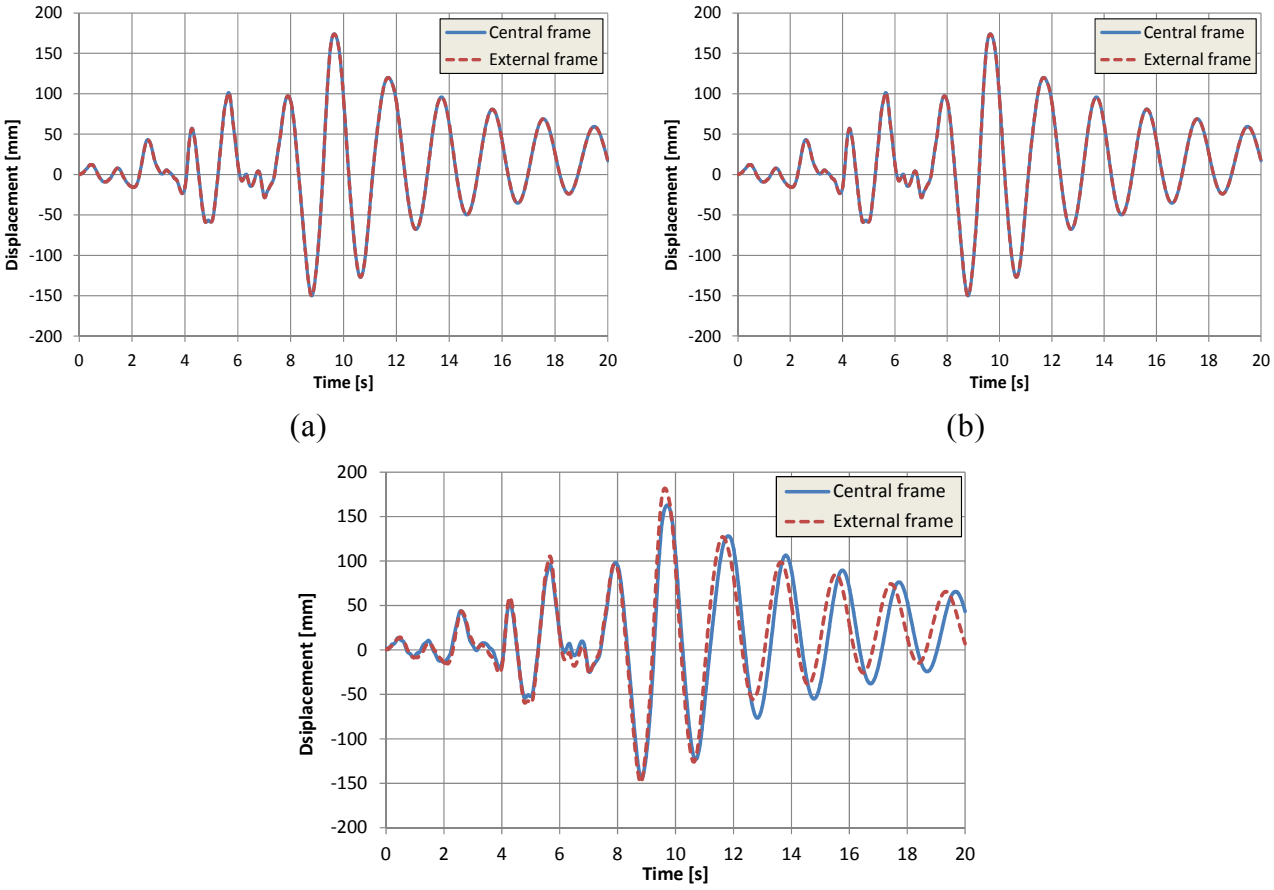

Figure 6.4 – Vibratory curves for the building with statically determined panel connection arrangement: (a) with rigid diaphragm, (b) with clamped floor member edges, (c) with hinged floor member edges

6.1.2. Integrated systems

The vibratory curves corresponding to the application of the accelerogram to the structure with integrated panel connection arrangement with the three typologies of diaphragm are illustrated in Figure 6.5.

The building with a rigid diaphragm shows a very rigid behaviour, with maximum top displacement as low as 0,36 mm.

With a deformable diaphragm, large differences between the displacement amplitudes are reported, with a maximum displacement of 8 mm for the central frame and of 0,3 mm for the external. The responses are in-phase. It is noted that, although the difference in terms of displacement is very large, its absolute value is low.

With null diaphragm, out-of-phase responses are reported, with the central frame vibrating very flexibly and in accordance with the statically determined connection curve and the external frame practically remaining still.

6.1.3. Dissipative systems

FBDs are inserted in between the panels, which behaviour is described by an elastic-plastic model with stiffness of 60 kN/mm and a threshold load of 60 kN. The corresponding vibratory curves are plotted in Figure 6.6 for the three different diaphragm typologies.

The building with rigid diaphragm is characterised by a rigid response up to the threshold limit of the connections, after which the response becomes more flexible, associated with a large energy dissipation hysteretic behaviour. The maximum drift is reduced to 13 mm with respect to the statically determined case.

With deformable diaphragm, similar responses are obtained, with the central frame moving slightly more than the external, with a maximum top displacement of 17 mm for the central and 14 mm for the external. The diaphragm effect is relevant, although the difference in the response is not negligible.

Finally, with null diaphragm, the behaviour is very different, with the central frame largely displacing and damaging according to the statically determined corresponding curve and the external remaining almost still.

The load-displacement behaviour of the dissipative connections is shown in Figure 6.7. In both cases of (a) rigid and (b) deformable diaphragm large dissipative cycles are observed, while for (c) null diaphragm cycles with lower displacement amplitude are computed, with a lower associated energy dissipation.

From the above considerations, it can be stated that dissipative cladding connections need a stiff diaphragm in order to fully activate their energy dissipation capacity and to limit the deformation of the building, to which corresponds structural damage at the base of the columns.

The maxima foces acting on the central panel connection system are reported in Table 6-3a, in particular for panel-to-panel, panel-to-beam and panel-to-foundation.

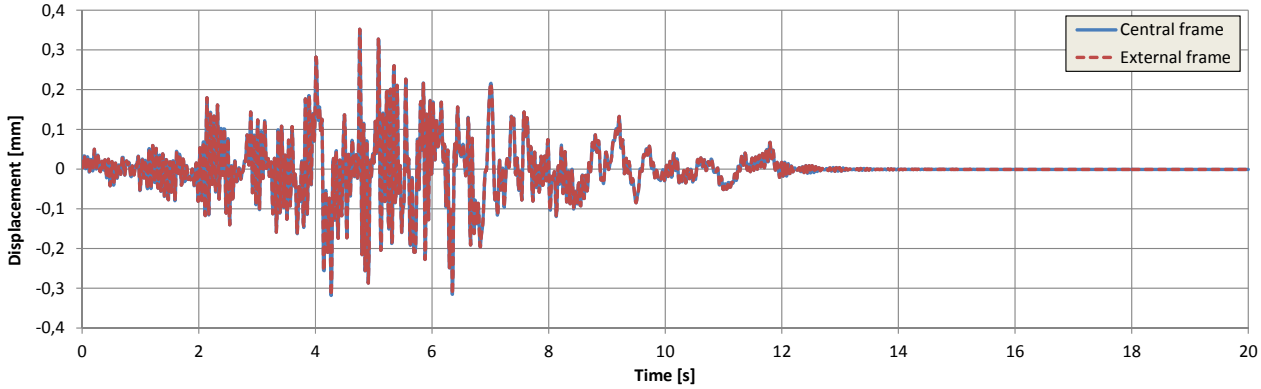

(a)

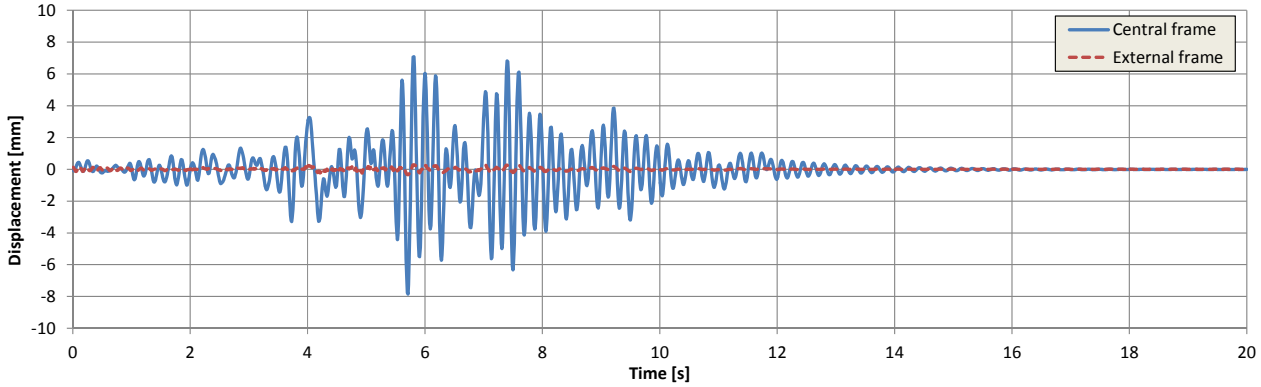

(b)

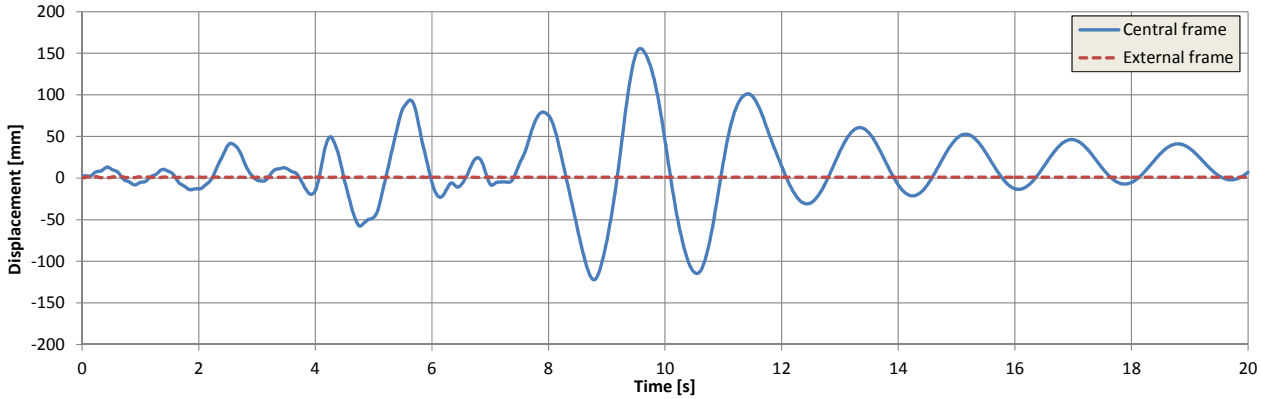

(c)

Figure 6.5 – Vibratory curves for the building with integrated panel connection arrangement: (a) with rigid diaphragm, (b) with clamped floor member edges, (c) with hinged floor member edges

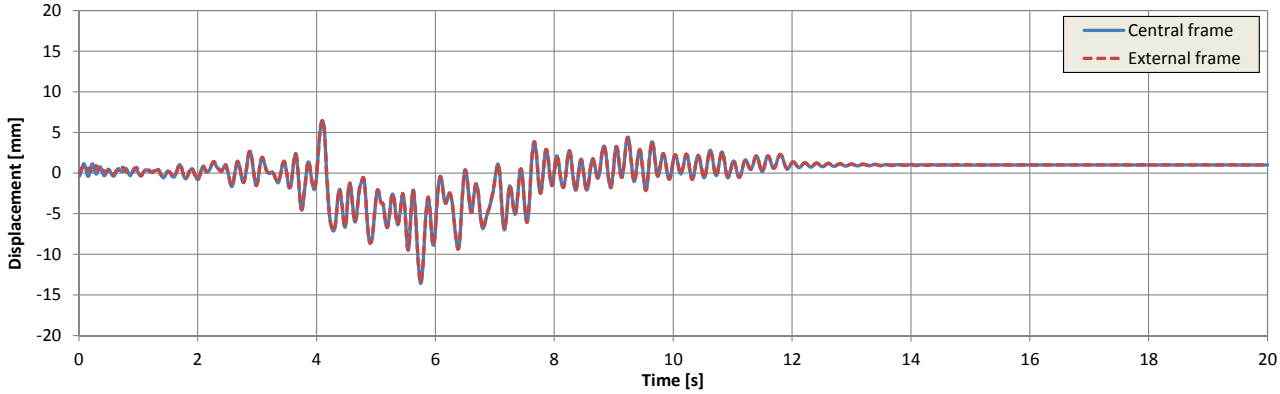

(a)

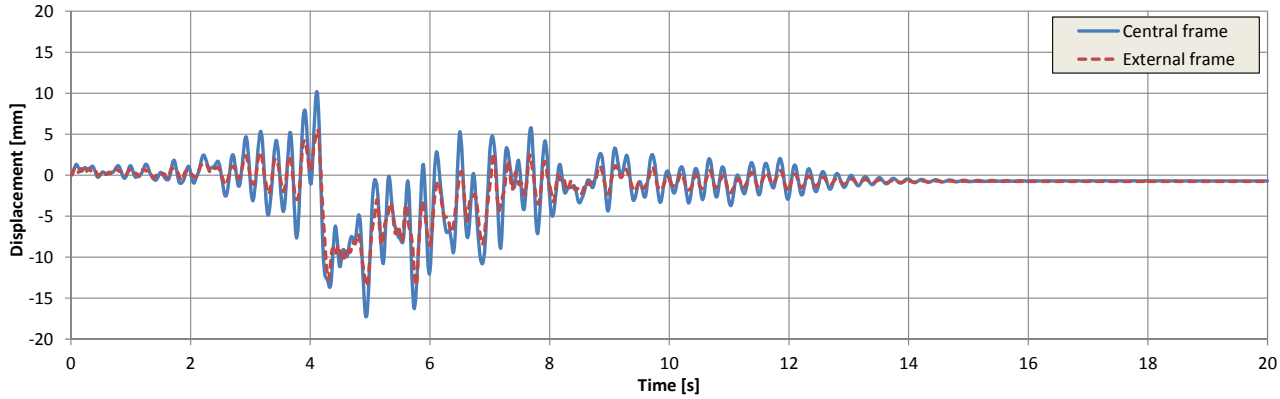

(b)

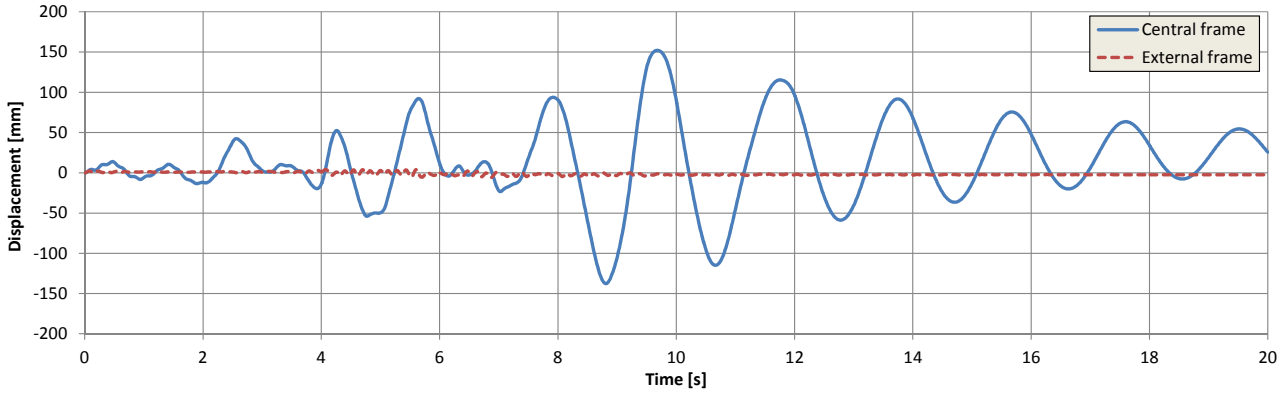

(c)

Figure 6.6 – Vibratory curves for the building with dissipative panel connection arrangement: (a) with rigid diaphragm, (b) with clamped floor member edges, (c) with hinged floor member edges

For statically determined configuration, the very low horizontal reactions are due to the second order effect of the panel in the pendulum configuration, while the vertical reaction is due to panel own weight. For integrated configuration, forces rise much higher for both panel-to-panel, reaching up to 109 kN, and for panel-to-structure, reaching up to 119 kN. For the dissipative arrangement, forces are limited according to the friction threshold and the equilibrium of the single panel.

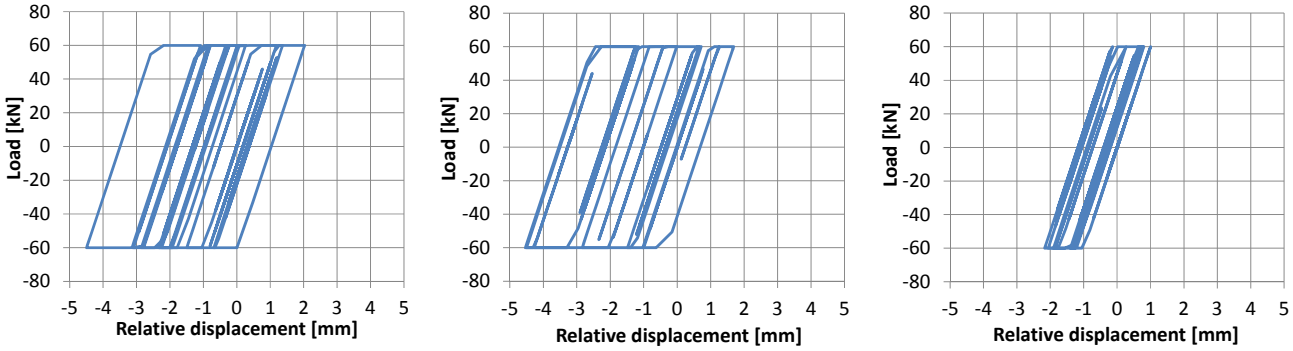

(a) (b) (c)

Figure 6.7 – Hysteretic cycles of a FBD of the central cladding panel: (a) with rigid diaphragm, (b) with clamped floor member edges, (c) with hinged floor member edges

Table 6-3b contains the maxima load values for an edge panel. With statically undetermined configurations a maximum vertical reaction of 261 kN is obtained, with limited horizontal reactions. The different force distribution with respect to the central panel is due to the presence of connections only at one side.

Table 6-4 resumes the maximum shear load on the floor-to-beam connections, that are very large in the floor direction for the statically undetermined diaphragm cases.

Table 6-3 – Maximum force in panel connections for (a) a central panel and (b) an edge panel

		MAX ACTION IN CONNECTIONS [kN]			
CLADDING CONNECTION SYSTEM	DIAPHRAGM	PANEL-PANEL	PANEL-BEAM (horizontal)	PANEL-FOUNDATION (vertical)	PANEL-FOUNDATION (horizontal)
ISOSTATIC	RIGID	0	7	64	6
	DEFORMABLE	0	7	64	6
	NULL	0	7	64	6
INTEGRATED	RIGID	98	83	64	107
	DEFORMABLE	109	98	64	119
	NULL	54	42	64	64
DISSIPATIVE	RIGID	60	48	64	69
	DEFORMABLE	60	55	64	68
	NULL	60	45	64	69

(a)

		MAX ACTION IN CONNECTIONS [kN]			
CLADDING CONNECTION SYSTEM	DIAPHRAGM	PANEL-PANEL	PANEL-BEAM (horizontal)	PANEL-FOUNDATION (vertical)	PANEL-FOUNDATION (horizontal)
ISOSTATIC	RIGID	0	7	64	6
	DEFORMABLE	0	7	64	6
	NULL	0	7	64	6
INTEGRATED	RIGID	78	13	228	40
	DEFORMABLE	85	22	261	40
	NULL	54	3	180	29
DISSIPATIVE	RIGID	60	24	253	49
	DEFORMABLE	60	31	250	47
	NULL	60	22	248	48

(b)

Table 6-4 – Maximum force in floor-to-beam connections for a central floor member

		MAX ACTION IN CONNECTIONS [kN]	
CLADDING CONNECTION SYSTEM	DIAPHRAGM	FLOOR-BEAM LONGITUDINAL SHEAR	FLOOR BEAM TRANSVERSAL SHEAR
ISOSTATIC	RIGID	-	-
	DEFORMABLE	~ 16	~ 14
	NULL	~ 9	~ 10
INTEGRATED	RIGID	-	-
	DEFORMABLE	~ 304	~ 36
	NULL	~ 20	~ 27
DISSIPATIVE	RIGID	-	-
	DEFORMABLE	~ 234	~ 28
	NULL	~ 31	~ 29

From the above considerations, the following statements can be draft:

- A homogeneous distribution of mass and stiffness leads to a uniform seismic response of the structure, even with flexible diaphragm,
- With flexible diaphragm, a non-homogeneous distribution of mass and stiffness causes relevant slab distortions and out-of-phase response of the single frames, with a vibratory motion that is amplified for the more flexible frames and reduced for the stiffer,
- With rigid diaphragm, a non-homogeneous distribution of mass and stiffness leads to large actions on the diaphragm members and connections,
- An homogeneous distribution of mass and stiffness in a precast frame structure can be achieved through the adoption of a statically determined cladding panel connection system,
- A statically undetermined cladding connection system (dissipative or integrated) leads to differences in terms of stiffness between external and internal frames,
- The adoption of an integrated cladding connection system leads to large actions in the connections,
- The forces in the connections can be limited with a dissipative cladding connection system,
- The efficiency of a dissipative cladding connection system is reduced in structures with flexible diaphragms.

6.2. Parametric investigation

In order to verify the actual influence of cladding panels on the seismic behaviour of precast buildings with different shapes, a wide parametric investigation has been performed by means of numerical analyses on several structural assemblies representing the most common typologies of precast buildings. The aim is to analyse how the different types of connection systems (isostatic and dissipative) play their role in the structural response, so to spot the situations where this role is important and address on these situations further deeper investigations on the practical applicability conditions.

Dynamic non-linear analyses have been performed with reference to both serviceability and no-collapse Limit State. The modified Tolmezzo accelerogram (Figure 5.38) has been used as input seismic action. The analyses have been elaborated with different 3D overall structural models of the structure. The panel connection arrangements have been represented with the simplified assumption of cantilever and pendulum respectively for the statically determined and the dissipative system. Frame systems of structures for one-storey buildings with industrial and commercial destination have been considered. The following construction parameters have been assumed in the parametric analyses:

- *structural arrangement:* regular
- *roof deck:* short beams with long roof elements
- *column height:* 7,5 m
- *cladding walls:* on four sides
- *type of panels:* vertical
- *panel connections* (isostatic - dissipative system)
- *shape ratio:* elongated 3/1 - medium 3/2 - compact 3/3
- *roof diaphragm:* null - deformable - rigid
- *action intensity:* 0,18g - 0,36g - 0,60g
- *action direction*: longitudinal - transversal

Details on the building typologies and on different analyses performed are given hereafter. A proportioning on sizes and reinforcement has been made following Eurocode 8 design rules, with PGA equal to 0,30g and subsoil class B. For the columns a concrete Class C45/55 is adopted with rebars made with steel grade B450C. The mean values of material strength and deformability have been assumed in the calculations. The numerical models have been built with the same features of those illustrated in Chapter 5.

The combination of all the aforementioned parameters leads to 3x3x2x3x2=108 different cases to be analysed. A reduced number of output parameters are identified as significantly representative of the structural response under earthquake, as a function of the investigated typology case. The list is specified below.

The plans and the sections of the three 3/1, 3/2 and 3/3 shape ratios are shown in Figure 6.8 (only for the rigid roof diaphragm): the lay-out consists of 1, 2 or 3 roof bays of 20,0 m in *x* direction and 8 beam spans of 7,5 m in *y* direction. The net column height is 7,5 m.

In Figure 6.9 the three type of roof diaphragm are shown as actually available in the ordinary production typologies: (a) spaced Y-shape roof elements with single rib end connections for a null diaphragm action (modelled as double hinged); (b) spaced double-Ts elements with double rib end connections for a deformable diaphragm (modelled as clamped); (c) attached double-Ts connected to each other with welds for a rigid diaphragm (modelled as clamped).

The cladding panels are all supported on their foundations and the connection with the frame is made with the frame beams in Y-direction, whilst in X-direction they are connected with the frame floor members in the case of rigid diaphragm and with an additional frame made by one column and two beams for each span in the cases of null and deformable diaphragms. The corners are provided with soft elements, in order to avoid panel contact issues.

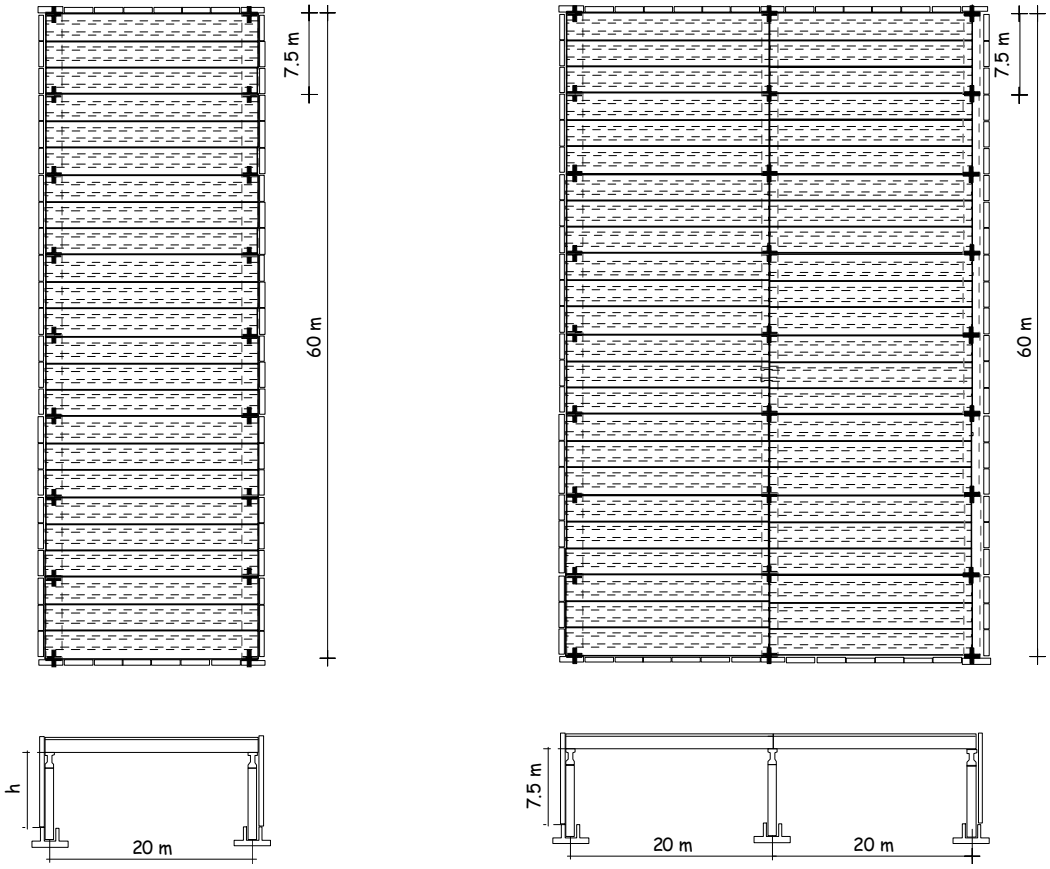

Figure 6.8 – Building plan shapes considered: (a) 3/1, (b) 3/2, (c) 3/3

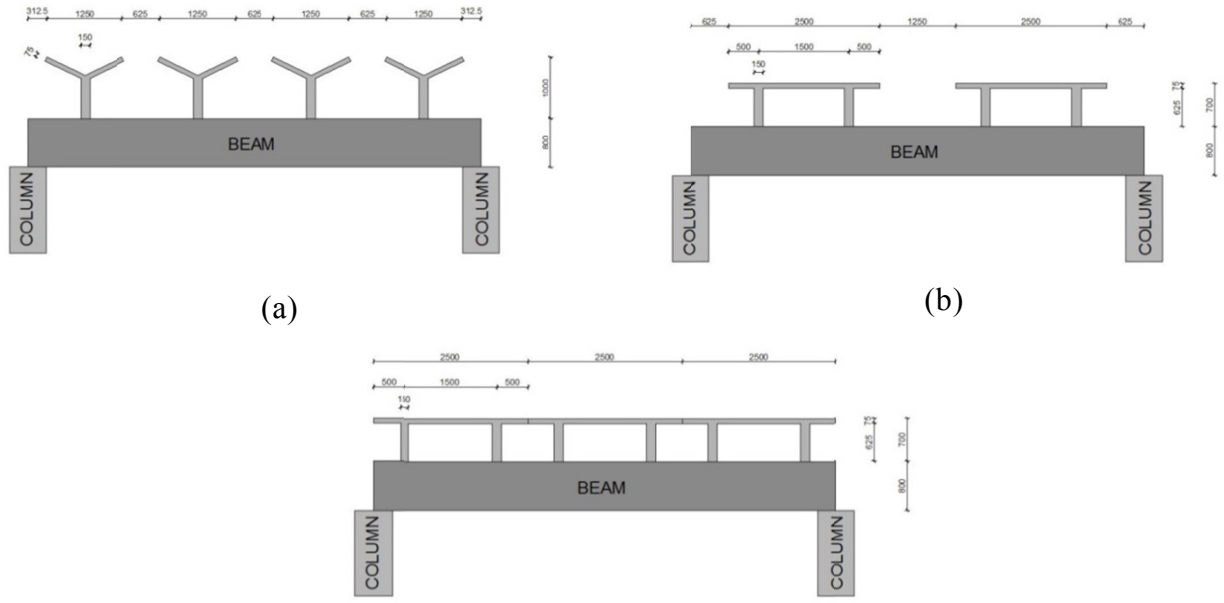

Figure 6.9 – Typologies of diaphragm considered: (a) null, (b) deformable, (c) rigid

In the following the definitions of relevant results from the analyses are provided, together with the reference values:

a1 maximum top x (or y) drift (mm): maximum top x (or y) displacement

a2 ratio (%): maximum top x (or y) displacement divided by the column height

b1 differential top x (or y) drift (mm): maximum minus minimum top x (or y) contemporary displacement

b2 ratio (%): maximum minus minimum top x (or y) contemporary displacements divided by the column height

c1 maximum top x (or y) drift (mm): maximum top x (or y) displacement (the same of *a1)*

c2 relative (-): maximum top x (or y) displacement divided by the reference x (or y) displacement

d1 maximum connection slide (mm): maximum displacement of the considered sliding connections

d2 relative (-): maximum displacement of the considered sliding connections divided by the reference x (or y) displacement

e1 maximum force roof-roof (kN): maximum force in roof-to-roof connection

e2 relative (-): maximum force in roof-to-roof connection divided by the reference x (or y) column shear

f1 maximum force roof-beam (kN): maximum force in roof-to-beam connection

f2 relative (-): maximum force in roof-to-beam connection divided by the reference x (or y) column shear

g1 maximum force beam-column (kN): maximum force in beam-to-column connection

g2 relative (-): maximum force in beam-to-column connection divided by the reference x (or y) column shear

h1 maximum force wall-structure (kN): maximum force in wall panel-to-structure connection

h2 relative (-): maximum force in wall panel-to-structure connection divided by the reference x (or y) column shear

i1 maximum force wall-wall (kN): maximum force in wall panel-to-panel connection

i2 relative (-): maximum force in wall panel-to-panel connection divided by the reference x (or y) column shear

j1 total base shear (kN): maximum sum of contemporary base x (or y) shear of columns and wall panels

j2 relative (-): total base x (or y) shear divided by the reference total x (or y) base shear

k1 total column base shear (kN): maximum sum of contemporary base x (or y) shears of columns

k2 ratio (%): sum of base x (or y) shear of columns divided by the total base x (or y) shear of columns and wall panels

l1 mean column shear (kN): total column base x (or y) shear of columns divided by the number of columns

l2 relative (-): mean column base x (or y) shear divided by the reference x (or y) column base shear

m1 maximum column shear (kN): maximum base x (or y) shear in a column

m2 ratio (%): maximum base x (or y) shear in a column divided by the mean column base x (or y) shear

Reference x (or y) displacement: is the top x (or y) displacement calculated for a given structural arrangement, roof deck and shape ratio, assuming cladding wall panels on four sides, statically determined connection system with cantilever arrangement and a rigid roof diaphragm.

Reference x (or y) column base shear: is the mean x (or y) column shear of columns calculated for a given structural arrangement, roof deck and shape ratio, assuming cladding wall panels on four sides, statically determined connection system with cantilever arrangement and a rigid roof diaphragm.

Reference x (or y) total base shear: is the maximum sum of contemporary base x (or y) shear of columns and wall panels calculated for a given structural arrangement, roof deck and shape ratio, assuming cladding wall panels on four sides, statically determined connection system with cantilever arrangement and a rigid roof diaphragm.

Table 6-5 – Reference values

Building type	**Quantity**	**x-direction**			**y-direction**		
		0.18 g	**0.36 g**	**0.60 g**	**0.18 g**	**0.36 g**	**0.60 g**
Single-bay	Reference displacement [mm]	100	191	230	96	183	236
	Reference column base shear [kN]	73	94	97	71	93	96
	Reference total base shear [kN]	1453	1886	1939	1419	1865	1910
Two-bays	Reference displacement [mm]	98	186	229	98	186	227
	Reference column base shear [kN]	75	97	99	75	96	98
	Reference total base shear [kN]	2316	2996	3074	2337	2973	3045
Three-bays	Reference displacement [mm]	104	194	238	104	196	275
	Reference column base shear [kN]	73	92	98	77	96	98
	Reference total base shear [kN]	3059	3881	4136	3239	4012	4111

Table 6-6 – single bay building, null diaphragm

	DIS3-1nul	x - direction			y - direction		
		PGA=0,18g	PGA=0,36g	PGA=0,60g	PGA=0,18g	PGA=0,36g	PGA=0,60g
a1	Maximum top drift (mm)	111	218	346	6	21	38
a2	Ratio (%)	1,5	2,9	4,6	0,1	0,3	0,5
b1	Differential top drift (mm)	113	218	375	74	132	175
b2	Ratio (%)	1,5	2,9	5,0	1,0	1,8	2,3
c1	Maximum top drift (mm)	111	218	346	6	21	38
c2	Relative (-)	1.11	1.14	1.73	0.07	1.11	1.16
d1	^Max connection slide (mm)	1	5	11	2	6	11
d2	Relative (-)	0.01	0.03	0.05	0.02	0.03	0.05
f1	Max force roof-beam (kN)	35	50	72	21	22	29
f2	Relative (-)	0.48	0.53	0.74	0.29	0.24	0.31
g1	Max force beam-column (kN)	68	90	101	21	39	60
g2	Relative (-)	0.93	0.95	1.05	0.30	0.42	0.62
h1	Max force wall-structure (kN)	300	311	319	309	315	326
h2	Relative (-)	4.11	3.31	3.29	4.36	3.38	3.39
i1	Max force wall-wall (kN)	60	60	60	60	60	60
i2	Relative (-)	0.82	0.64	0.62	0.85	0.65	0.62
j1	Total base shear (kN)	2300	4226	5622	3837	4706	5398
j2	Relative (-)	1.58	2.24	2.90	2.70	2.52	2.83
k1	Total column shear (kN)	5734	934	1174	387	406	656
k2	Relative (-)	0.25	0.22	0.21	0.10	0.09	0.12
l1	Mean column shear (kN)	29	47	59	19	20	33
l2	Relative (-)	0.39	0.50	0.61	0.27	0.22	0.34
m1	Max column shear (kN)	76	111	122	59	45	69
m2	Relative (-)	2.65	2.37	2.07	3.03	2.21	2.11
h1v	Max vert.force wall-struct.(kN)	297,98	308,17	314,71	306,66	311,59	321,56
h1h	Max hor. force wall-struct.(kN)	66,18	74,19	83,35	67,29	73,10	83,99

^ connection slides all equal

Table 6-7 – single bay building, deformable diaphragm

	DIS3-1def	x - direction			y - direction		
		PGA=0,18g	PGA=0,36g	PGA=0,60g	PGA=0,18g	PGA=0,36g	PGA=0,60g
a1	Maximum top drift (mm)	45	80	124	6	18	40
a2	Ratio (%)	0,6	1,1	1,6	0,1	0,2	0,5
b1	Differential top drift (mm)	46	67	66	74	137	165
b2	Ratio (%)	0,6	0,9	0,9	1,0	1,8	2,2
c1	Maximum top drift (mm)	45	80	124	6	18	40
c2	Relative (-)	0,45	0,42	0,54	0,06	0,10	0.17
d1	^Max connection slide (mm)	4	14	31	2	5	12
d2	Relative (-)	0,04	0,08	0,14	0,03	0,03	0,05
f1	Max force roof-beam (kN)	517	735	715	73	87	147
f2	Relative (-)	7.08	7.82	7,37	1,03	0,93	1.53
g1	Max force beam-column (kN)	79	113	129	23	48	95
g2	Relative (-)	1,08	1,20	1,33	0,32	0,51	1,00
h1	Max force wall-structure (kN)	309	315	328	312	316	334
h2	Relative (-)	4,23	3,35	3,38	4,39	3,39	3,48
i1	Max force wall-wall (kN)	60,00	60,00	60,00	60,00	60,00	60,00
i2	Relative (-)	0,82	0,64	0,62	0,85	0,65	0,62
j1	Total base shear (kN)	2435	3554	3890	3694	4930	5265
j2	Relative (-)	1,68	1,88	2,01	2,60	2,64	2,76
k1	Total column shear (kN)	824	1218	2873	415	759	813
k2	Relative (-)	0,34	0,34	0,734	0,11	0,15	0,15
l1	Mean column shear (kN)	41	61	144	21	38	41
l2	Relative (-)	0,56	0,65	1,48	0,29	0,41	0,42
m1	Max column shear (kN)	167	149	204	33	59	92
m2	Relative (-)	4,05	2,44	1,42	1,62	1,56	2,27
h1v	Max vert.force wall-struct.(kN)	307	312	323	310	313	330
h1h	Max hor. force wall-struct.(kN)	66	63	85	67	75	83

^ connection slides all equal

Table 6-8 – single bay building, rigid diaphragm

	DIS3-1rig	x - direction			y - direction		
		PGA=0,18g	PGA=0,36g	PGA=0,60g	PGA=0,18g	PGA=0,36g	PGA=0,60g
a1	Maximum top drift (mm)	32	62	113	9	30	73
a2	Ratio (%)	0,4	0,8	1,5	0,1	0,4	1,0
b1	Differential top drift (mm)	7	8	10	0	0	0
b2	Ratio (%)	0,1	0,1	0,1	0,0	0,0	0,0
c1	Maximum top drift (mm)	32	62	113	9	30	73
c2	Relative (-)	0,32	0,32	1,17	0,09	0,16	0,31
d1	^Max connection slide (mm)	9	18	34	3	10	22
d2	Relative (-)	0,09	0,10	0,15	0,03	0,05	0,09
e1	Max force roof-roof (kN)	196,40	227,06	328,84	132,37	153,72	183,49
e2	Relative (-)	2,69	2,42	3,39	1,86	1,65	1,91
f1	Max force roof-beam (kN)	31	43	43	52	56	63
f2	Relative (-)	0,42	0,46	0,45	0,73	0,60	0,66
g1	Max force beam-column (kN)	59	91	136	12	30	59
g2	Relative (-)	0,81	0,97	1,41	0,17	0,32	0,61
h1	Max force wall-structure (kN)	309	320	327	313	315	324
h2	Relative (-)	4,23	3,44	3,51	3,36	3,39	3,37
i1	Max force wall-wall (kN)	60,00	60,00	60,00	60,00	60,00	60,00
i2	Relative (-)	0,82	0,64	0,62	0,85	0,65	0,62
j1	Total base shear (kN)	2051	2978	3958	3879	4800	5349
j2	Relative (-)	1,41	1,58	2,04	2,73	2,57	2,80
k1	Total column shear (kN)	959	1589	2423	334	621	1038
k2	Relative (-)	0,47	0,53	0,61	0,09	0,13	0,19
l1	Mean column shear (kN)	53	88	135	19	35	58
l2	Relative (-)	0,73	0,94	1,39	0,26	0,37	0,60
m1	Max column shear (kN)	59	96	145	19	36	75
m2	Relative (-)	1,10	1,08	1,08	1,04	1,04	1,29
h1v	Max vert.force wall-struct.(kN)	307,17	317,24	323,24	307,97	309,62	316,10
h1h	Max hor. force wall-struct.(kN)	59,04	69,39	74,66	66,06	74,83	83,73

^ connection slides all equal

Table 6-9 – two bays building, null diaphragm

	DIS3-2nul	x - direction			y - direction		
		PGA=0,18g	PGA=0,36g	PGA=0,60g	PGA=0,18g	PGA=0,36g	PGA=0,60g
a1	Maximum top drift (mm)	114	224	321	95	209	328
a2	Ratio (%)	1,5	3,0	4,3	1,3	2,8	4,4
b1	Differential top drift (mm)	113	227	318	94	204	335
b2	Ratio (%)	1,5	3,0	4,2	1,3	2,7	4,5
c1	Maximum top drift (mm)	114	224	321	95	209	328
c2	Relative (-)	1,16	1,21	1,40	0,97	1,12	1,45
d1	^Max connection slide (mm)	1	3	5	2	7	16
d2	Relative (-)	0,01	0,01	0,04	0,02	0,04	0,07
f1	Max force roof-beam (kN)	5	11	15	39	48	70
f2	Relative (-)	0,07	0,11	0,15	0,52	0,50	0,71
g1	Max force beam-column (kN)	83	99	122	93	133	166
g2	Relative (-)	1,11	1,02	1,23	1,24	1,39	1,69
h1	Max force wall-structure (kN)	244	311	319	310	316	324
h2	Relative (-)	3,25	3,20	3,22	4,13	3,30	3,31
i1	Max force wall-wall (kN)	57	60	60	60	60	60
i2	Relative (-)	0,76	0,62	0,61	0,80	0,62	0,61
j1	Total base shear (kN)	2590	3927	5925	4043	5145	6269
j2	Relative (-)	1,12	1,31	1,93	1,73	1,73	2,06
k1	Total column shear (kN)	1485	2447	3029	1045	1322	1658
k2	Relative (-)	0,57	0,62	0,51	0,26	0,26	0,26
l1	Mean column shear (kN)	48	79	98	34	43	53
l2	Relative (-)	0,64	0,81	0,99	0,45	0,44	0,55
m1	Max column shear (kN)	78	114	129	95	137	230
m2	Relative (-)	1,63	1,45	1,32	2,83	3,21	4,30
h1v	Max vert.force wall-struct.(kN)	241	307	314	308	313	320
h1h	Max hor. force wall-struct.(kN)	59	74	83	68	75	83

^ connection slides all equal

Table 6-10 – two bays building, deformable diaphragm

	DIS3-2def	x - direction			y - direction		
		PGA=0,18g	PGA=0,36g	PGA=0,60g	PGA=0,18g	PGA=0,36g	PGA=0,60g
a1	Maximum top drift (mm)	69	120	133	41	54	82
a2	Ratio (%)	0,9	1,6	1,8	0,5	0,7	1,1
b1	Differential top drift (mm)	46	67	66	38	45	54
b2	Ratio (%)	0,6	0,9	0,9	0,5	0,6	0,7
c1	Maximum top drift (mm)	69	120	133	41	54	82
c2	Relative (-)	0,71	0,65	0,58	0,42	0,29	0,36
d1	^Max connection slide (mm)	3	11	29	2	9	23
d2	Relative (-)	0,03	0.06	0,13	0,01	0,05	0,10
f1	Max force roof-beam (kN)	-	-	1007	362	-	541
f2	Relative (-)	-	-	10,17	4,82	-	5,52
g1	Max force beam-column (kN)	-	-	163	38	-	66
g2	Relative (-)	-	-	1,65	0,51	-	0,67
h1	Max force wall-structure (kN)	308,39	317,34	327,34	312,50	315,77	331,67
h2	Relative (-)	4,11	3,27	3,31	4,17	3,29	3,38
i1	Max force wall-wall (kN)	60	60	60	60	60	60
i2	Relative (-)	0,80	0,62	0,61	0,80	0,62	0,61
j1	Total base shear (kN)	2345	3426	4391	4086	5585	6594
j2	Relative (-)	1,01	1,14	1,43	1,75	1,88	2,17
k1	Total column shear (kN)	2246	3444	4117	825	1149	1714
k2	Relative (-)	0,96	1,01	0,94	0,20	0,20	0,26
2	Mean column shear (kN)	72	111	133	27	37	55
2	Relative (-)	0,97	1,15	1,34	0,35	0,39	0,56
m1	Max column shear (kN)	121	163	192	65	81	124
m2	Relative (-)	1,67	1,47	1,44	2,43	2,18	2,24
h1v	Max vert.force wall-struct.(kN)	306	314	323	310	317	328
h1h	Max hor. force wall-struct.(kN)	67	74	83	67	75	84

^ connection slides all equal

Table 6-11 – two bays building, rigid diaphragm

	DIS3-2rig	x - direction			y - direction		
		PGA=0,18g	PGA=0,36g	PGA=0,60g	PGA=0,18g	PGA=0,36g	PGA=0,60g
a1	Maximum top drift (mm)	26	57	106	17	50	93
a2	Ratio (%)	0,3	0,8	1,4	0,2	0,7	1,2
b1	Differential top drift (mm)	5	7	7	3	5	4
b2	Ratio (%)	0,1	0,1	0,1	0,0	0,1	0,1
c1	Maximum top drift (mm)	26	57	106	17	50	93
c2	Relative (-)	0,27	0,31	0,46	0,17	0,27	0,41
d1	^Max connection slide (mm)	6,61	14,83	28,95	4,14	6,80	26,66
d2	Relative (-)	0,07	0,08	0,13	0,04	0,04	0,12
e1	Max force roof-roof (kN)	309	354	383	151	235	208
e2	Relative (-)	4,13	3,65	3,87	2,02	2,45	2,13
f1	Max force roof-beam (kN)	58,46	67,07	70,74	69,13	93,77	87,50
f2	Relative (-)	0,78	0,69	0,71	0,92	0,98	0,89
g1	Max force beam-column (kN)	48	88	138	23	46	73
g2	Relative (-)	0,64	0,91	1,40	0,30	0,48	0,74
h1	Max force wall-structure (kN)	311	320	324	311	321	329
h2	Relative (-)	4,15	3,30	3,27	4,15	3,34	3,36
i1	Max force wall-wall (kN)	60	60	60	60	60	60
i2	Relative (-)	0,80	0,62	0,61	0,80	0,62	0,61
j1	Total base shear (kN)	2950	4147	5391	4586	5638	5969
j2	Relative (-)	1,27	1,38	1,75	1,96	2,00	1,96
k1	Total column shear (kN)	1419	2337	3350	665	1603	1874
k2	Relative (-)	0,48	0,56	0,62	0,14	0,28	0,31
l1	Mean column shear (kN)	53	87	124	25	59	69
l2	Relative (-)	0,70	1,15	1,25	0,33	0,62	0,71
m1	Max column shear (kN)	54	93	143	29	76	107
m2	Relative (-)	1,03	1,07	1,16	1,19	1,27	1,55
h1v	Max vert.force wall-struct.(kN)	309	318	320	307	315	322
h1h	Max hor. force wall-struct.(kN)	61	66	76	67	72	86

^ connection slides all equal

Table 6-12 – three bays building, null diaphragm

	DIS3-3nul	x - direction			y - direction		
		PGA=0,18g	PGA=0,36g	PGA=0,60g	PGA=0,18g	PGA=0,36g	PGA=0,60g
a1	Maximum top drift (mm)	116	200	315	96	201	313
a2	Ratio (%)	1,5	2,7	4,2	1,3	2,7	4,2
b1	Differential top drift (mm)	115	199	316	98	202	320
b2	Ratio (%)	1,5	2,6	4,2	1,3	2,7	4,3
c1	Maximum top drift (mm)	116	200	315	96	201	313
c2	Relative (-)	1,11	1,03	1,32	0,92	1,03	1,14
d1	^Max connection slide (mm)	1	1	3	2	5	13
d2	Relative (-)	0,01	0,01	0,01	0,02	0,03	0,05
f1	Max force roof-beam (kN)	93	169	230	124	212	373
f2	Relative (-)	1,28	1,84	2,34	1,60	2,20	3,81
g1	Max force beam-column (kN)	83,15	103,03	125,43	68,67	94,97	102,67
g2	Relative (-)	1,14	1,12	1,28	0,89	0,99	1,05
h1	Max force wall-structure (kN)	203	306	316	312	312	319
h2	Relative (-)	2,78	3,32	3,23	4,05	3,25	3,25
i1	Max force wall-wall (kN)	33	59	60	60	60	60
i2	Relative (-)	0,45	0,64	0,61	0,78	0,62	0,61
j1	Total base shear (kN)	3378	6531	8871	4949	6051	8450
j2	Relative (-)	1,10	1,68	2,14	1,53	1,51	2,06
k1	Total column shear (kN)	1247	1749	2378	1425	1850	2174
k2	Relative (-)	0,37	0,27	0,27	0,29	0,31	0,26
l1	Mean column shear (kN)	30	42	57	34	44	52
l2	Relative (-)	0,41	0,45	0,58	0,44	0,46	0,53
m1	Max column shear (kN)	81	116	133	82	117	152
m2	Relative (-)	2,72	2,78	2,35	2,41	2,65	2,93
h1v	Max vert.force wall-struct.(kN)	201	302	311	310	309	314
h1h	Max hor. force wall-struct.(kN)	26	50	66	67	74	82

^ connection slides all equal

Table 6-13 – three bays building, deformable diaphragm

	DIS3-3def	x - direction			y - direction		
		PGA=0,18g	PGA=0,36g	PGA=0,60g	PGA=0,18g	PGA=0,36g	PGA=0,60g
a1	Maximum top drift (mm)	78	111	161	56	76	119
a2	Ratio (%)	1,0	1,5	2,1	0,7	1,0	1,6
b1	Differential top drift (mm)	80	110	121	46	76	80
b2	Ratio (%)	1,1	1,5	1,6	0,6	1,0	1,1
c1	Maximum top drift (mm)	78	111	161	56	76	119
c2	Relative (-)	0,75	0,57	0,67	0,53	0,39	0,43
d1	^Max connection slide (mm)	2	10	31	3	10	34
d2	Relative (-)	0,02	0,05	0,13	0,03	0,05	0,12
f1	Max force roof-beam (kN)	319	423	538	354	497	559
f2	Relative (-)	4,37	4,60	5,49	4,60	5,17	5,70
g1	Max force beam-column (kN)	84	125	145	54	55	83
g2	Relative (-)	1,15	1,36	1,48	0,70	0,58	0,85
h1	Max force wall-structure (kN)	314,39	321,96	324,95	312,37	313,39	343,17
h2	Relative (-)	4,31	3,50	3,32	4,06	3,26	3,50
i1	Max force wall-wall (kN)	60,00	60,00	60,00	60,00	60,00	60,00
i2	Relative (-)	0,82	0,65	0,61	0,78	0,62	0,61
j1	Total base shear (kN)	5275	7164	9873	5594	5964	8042
j2	Relative (-)	1,72	1,85	2,39	1,35	1,49	1,96
k1	Total column shear (kN)	1776	3144	5002	1116	1804	3288
k2	Relative (-)	0,34	0,44	0,51	0,20	0,30	0,41
l1	Mean column shear (kN)	42	75	119	27	43	78
l2	Relative (-)	0,58	0,81	1,22	0,35	0,45	0,80
m1	Max column shear (kN)	113	146	169	47	69	95
m2	Relative (-)	2,68	1,95	1,42	1,76	1,60	1,21
h1v	Max vert.force wall-struct.(kN)	312	319	320	310	310	339
h1h	Max hor. force wall-struct.(kN)	65	48	85	66	74	83

^ connection slides all equal

Table 6-14 – three bays building, rigid diaphragm

	DIS3-3rig	x - direction			y - direction		
		PGA=0,18g	PGA=0,36g	PGA=0,60g	PGA=0,18g	PGA=0,36g	PGA=0,60g
a1 *a2*	Maximum top drift (mm) Ratio (%)	29 0,4	60 0,8	110 1,5	22 0,3	55 0,7	98 1,3
b1 *b2*	Differential top drift (mm) Ratio (%)	5 0,1	7 0,1	7 0,1	6 0,10	6 0,1	7 0,1
c1 *c2*	Maximum top drift (mm) Relative (-)	29 0,27	60 0,31	110 0,46	22 0,22	56 0,28	96 0,35
d1 *d2*	^Max connection slide (mm) Relative (-)	7 0,07	15 0,08	30 0,13	6 0,06	15 0,08	30 0.11
e1 *e2*	Max force roof-roof (kN) Relative (-)	229 3,14	252 2,74	265 3,44	285 3,70	285 2,96	293 2,99
f1 *f2*	Max force roof-beam (kN) Relative (-)	65,39 0,90	68,13 0,74	88,31 0,90	76,83 1,00	88,45 0,92	104,74 1,07
g1 *g2*	Max force beam-column (kN) Relative (-)	39,02 0,53	75,06 0,82	121,23 1,24	25,42 0,33	43,80 0,46	75,45 0,77
h1 *h2*	Max force wall-structure (kN) Relative (-)	328 4,50	329 3,58	335 3,42	314 4,07	319 3,33	326 3,33
i1 *i2*	Max force wall-wall (kN) Relative (-)	60 0,82	60 0,65	60 0,61	60 0,78	60 0,62	60 0,61
j1 *j2*	Total base shear (kN) Relative (-)	4892 1,60	6316 1,63	8928 2,16	4849 1,50	6635 1,65	6777 1,65
k1 *k2*	Total column shear (kN) Relative (-)	2279 0,47	4236 0,67	6081 0,68	1392 0,29	2132 0,32	3324 0,49
l1 *l2*	Mean column shear (kN) Relative (-)	63 0,87	118 1,28	169 1,72	39 0,50	59 0,62	92 0,94
m1 *m2*	Max column shear (kN) Relative (-)	87 1,37	169 1,44	248 1,47	63 1,63	90 1,52	148 1,60
h1v *h1h*	Max vert.force wall-struct.(kN) Max hor. force wall-struct.(kN)	326 73	326 79	330 87	309 66	314 73	319 83

^ connection slides all equal

The most relevant results of the structural analyses can be summerised as follows:

- At service (0,18g) limit conditions, maximum drifts varying from 1,5% to 1,0% and 0,4% have been evaluated respectively for null, deformable and rigid diaphragm (that is from 116 to 78 and to 29 mm).
- At no-collapse (0,36g) limit conditions, maximum drifts varying from 3,0% to 1,6% and 0,8% have been evaluated respectively for null, deformable and rigid diaphragm (that is from 224 to 120 and to 57 mm).
- With a rigid diaphragm, in roof-to-roof connections maximum forces from 196 kN to 309 kN have been evaluated at service (0,18g) limit conditions and from 227 kN to 354 kN at no-collapse (0,36g) limit conditions.
- At service (0,18g) limit conditions, in roof-to-beam connections maximum forces from 35 kN to 124 kN have been evaluated for null and rigid diaphragm, from 354 kN to 517 kN for deformable diaphragm.
- At no-collapse (0,36g) limit conditions, in roof-to-beam connections maximum forces from 35 kN to 124 kN have been evaluated for null and rigid diaphragm, from 497 kN to 735 kN for deformable diaphragm.
- In general the forces in roof-to-roof and roof-to-beam connections are really high especially for deformable diaphragm and this causes problems for their design.
- At service (0,18g) limit conditions, in beam-to-column connections maximum forces from 39 kN to 84 kN have been evaluated for all types of diaphragm.
- At no-collapse (0,36g) limit conditions, in beam-to-column connections maximum forces from 75 kN to 125 kN have been evaluated for all types of rigid diaphragm.
- At both in service (0,18g) and no-collapse (0,36g) limit conditions, an almost constant value of the force (from 309 kN to 328 kN) in the panel-to-structure connections derives from the slide limit of friction devices.

A comparison of the maxima displacements attained is graphed in Figure 6.10.

For 1-bay the diaphragm action is not relevant in y (longitudinal) direction, is very important in x (transverse) direction.

For 2 and 3-bays the diaphragm action is always very important in reducing the maximum displacements.

Also deformable diaphragms have a relevant influence in reducing the maximum displacements.

It has to be pointed out that additional panel-supporting frames in X-direction for null and deformable structures showed very large out-of-plane displacements with seismic action insisting on the Y-direction, due to their independent dynamics with respect to the main frame structure. This solution would require special attention during the design.

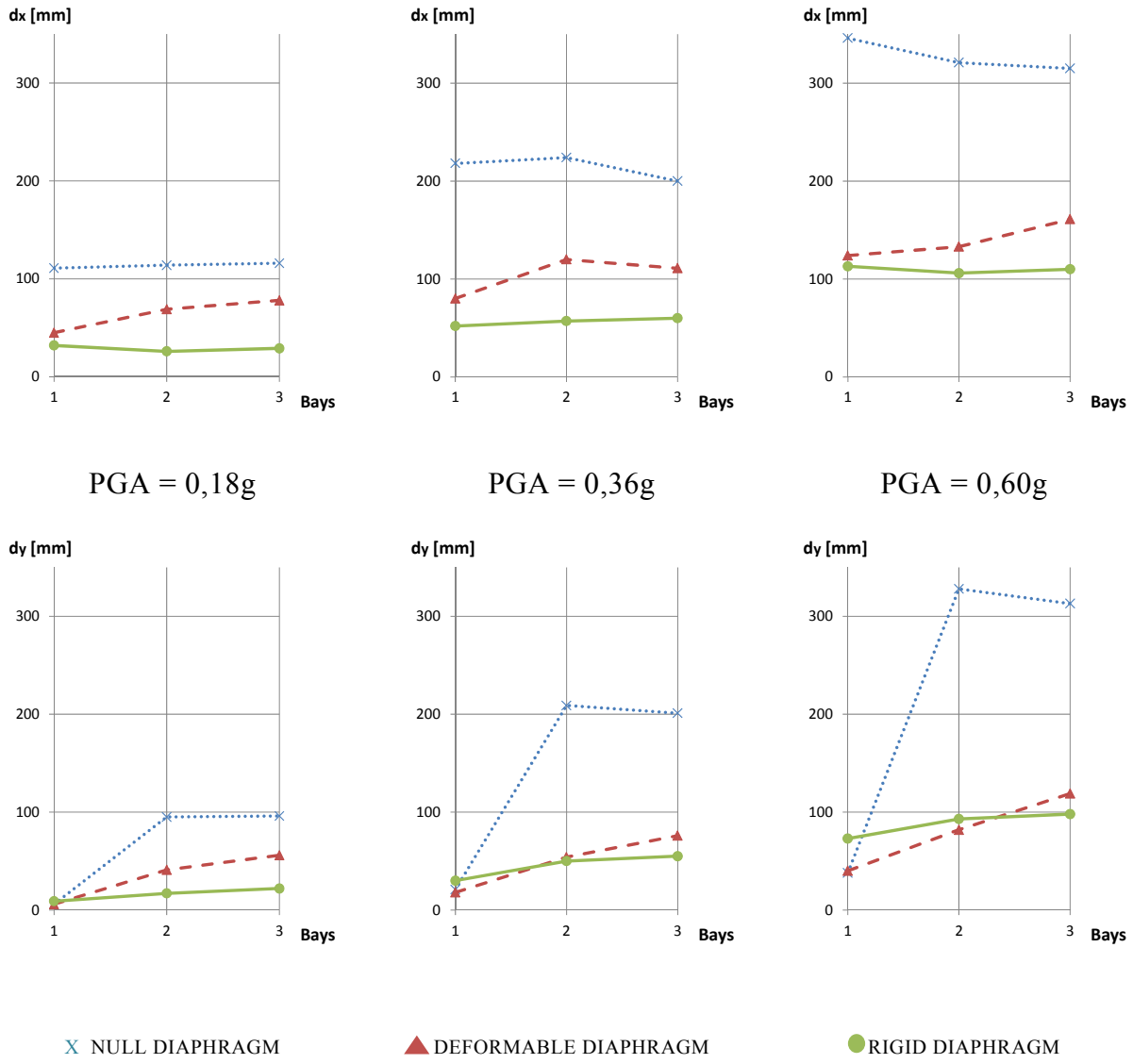

Figure 6.10 – Comparison of maximum displacement attained

A comparison of the maximum base shear attained is graphed in Figure 6.11.

The influence of the roof diaphragm on the global response of the structure is small.

At service (0,18g) and no-collapse (0,36g) limit conditions for 1 and 2-bays the global response is higher in y (longitudinal) than in x (transverse) direction because of the higher stiffening influence of the wall panels.

Close to collapse (0,60g) conditions the above difference lowers and changes, being affected by the actual distribution of the plastic resources in the structural elements.

In general the global response for increasing number of bays grows less than proportionally to the correspondent involved masses.

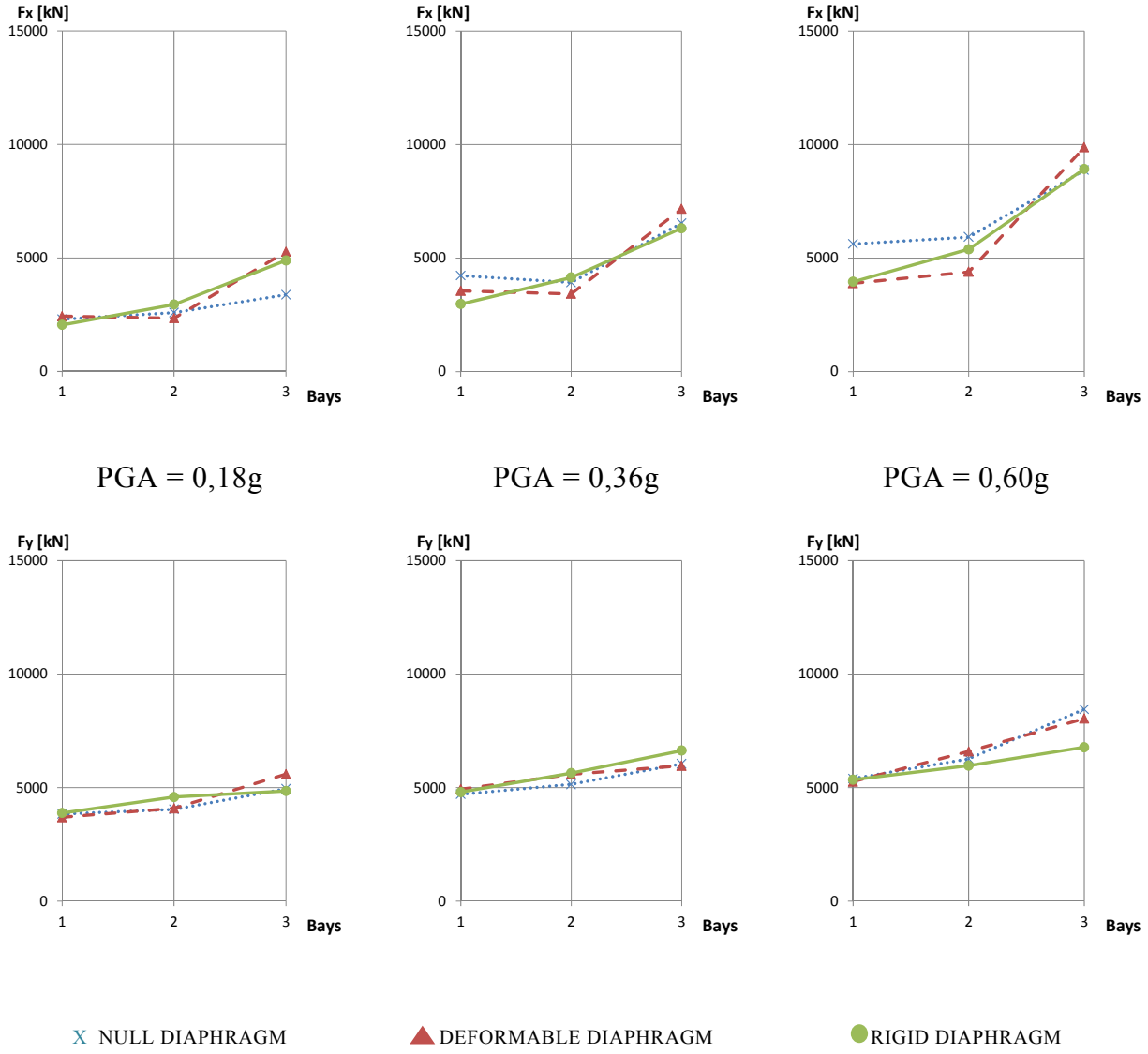

Figure 6.11 – Comparison of maximum base shear attained

A direct comparison with the reference values coming from the analyses on the same buildings provided wth isostatic cantilever panel connection arrangement is graphed in Figure 6.12.

With respect to the isostatic arrangement the stiffening effect of wall panels leads to higher responses that arrive to almost 3 times for 1-bay in y (longitudinal) direction.

In general the above effect decreases with the higher number of bays in y (longitudinal) direction.

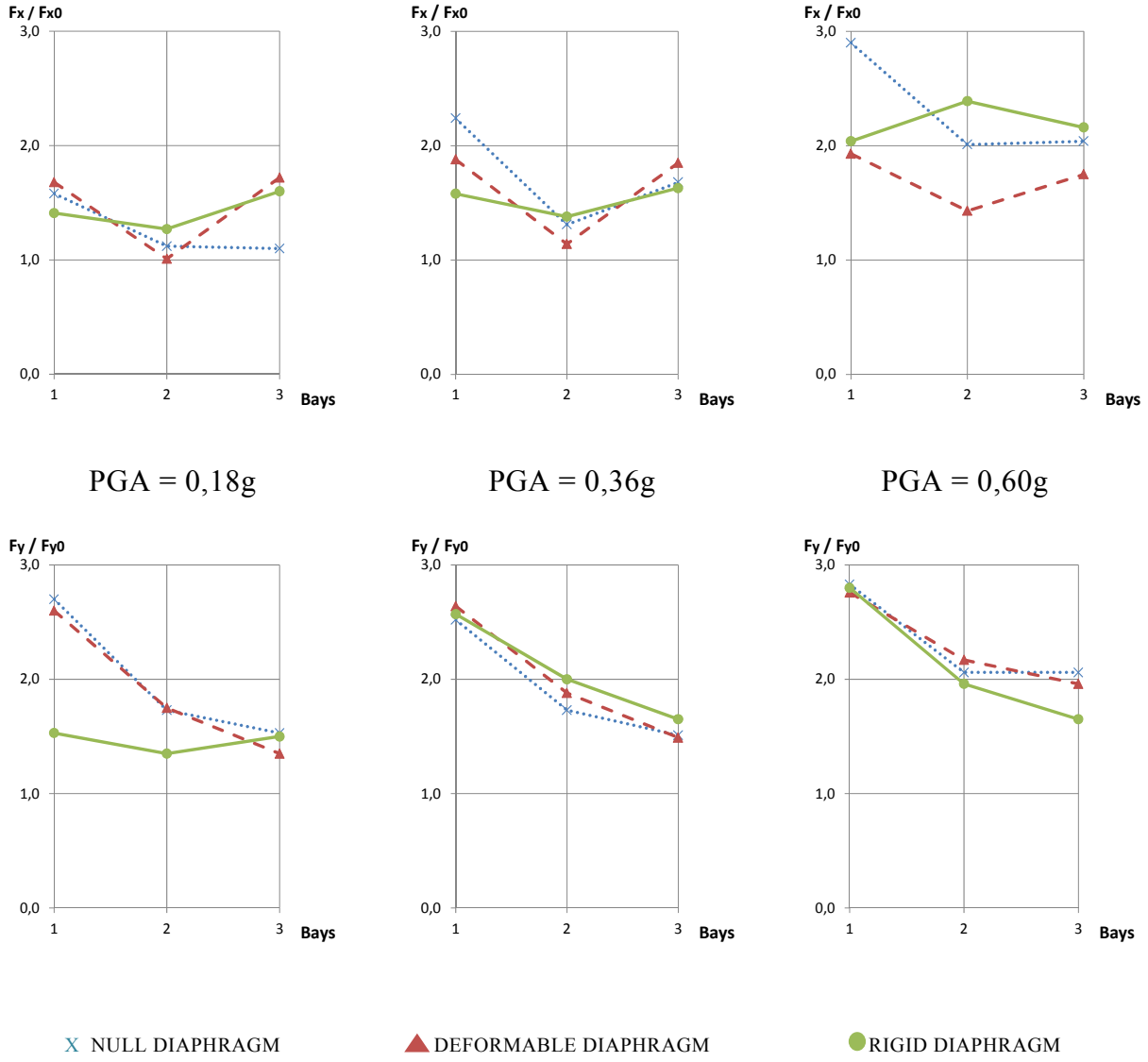

Figure 6.12 – Comparison of relative base shear attained

Finally, a comparison of complementary data, including serviceability limit state displacement over reference values, base shear at no-collapse limit state over reference values and differential drift ratio for PGA equal to 0,60g, is graphed in Figure 6.13.

Except for 1-bay in y (longitudinal) direction, at service (0,18g) limit conditions the null diaphragm corresponds to the isostatic arrangement in terms of maximum displacements.

At the service (0,18g) limit condition the deformable and rigid diaphragms lead to a relevant reduction of displacements in both directions with respect to the isostatic arrangement.

The stiffening effect of wall panels, at the no-collapse (0,36g) limit condition, leads to a relevant reduction of the shear in columns in y (longitudinal) direction with respect to the isostatic arrangement.

The above effect is not so relevant in general in x (transverse) direction.

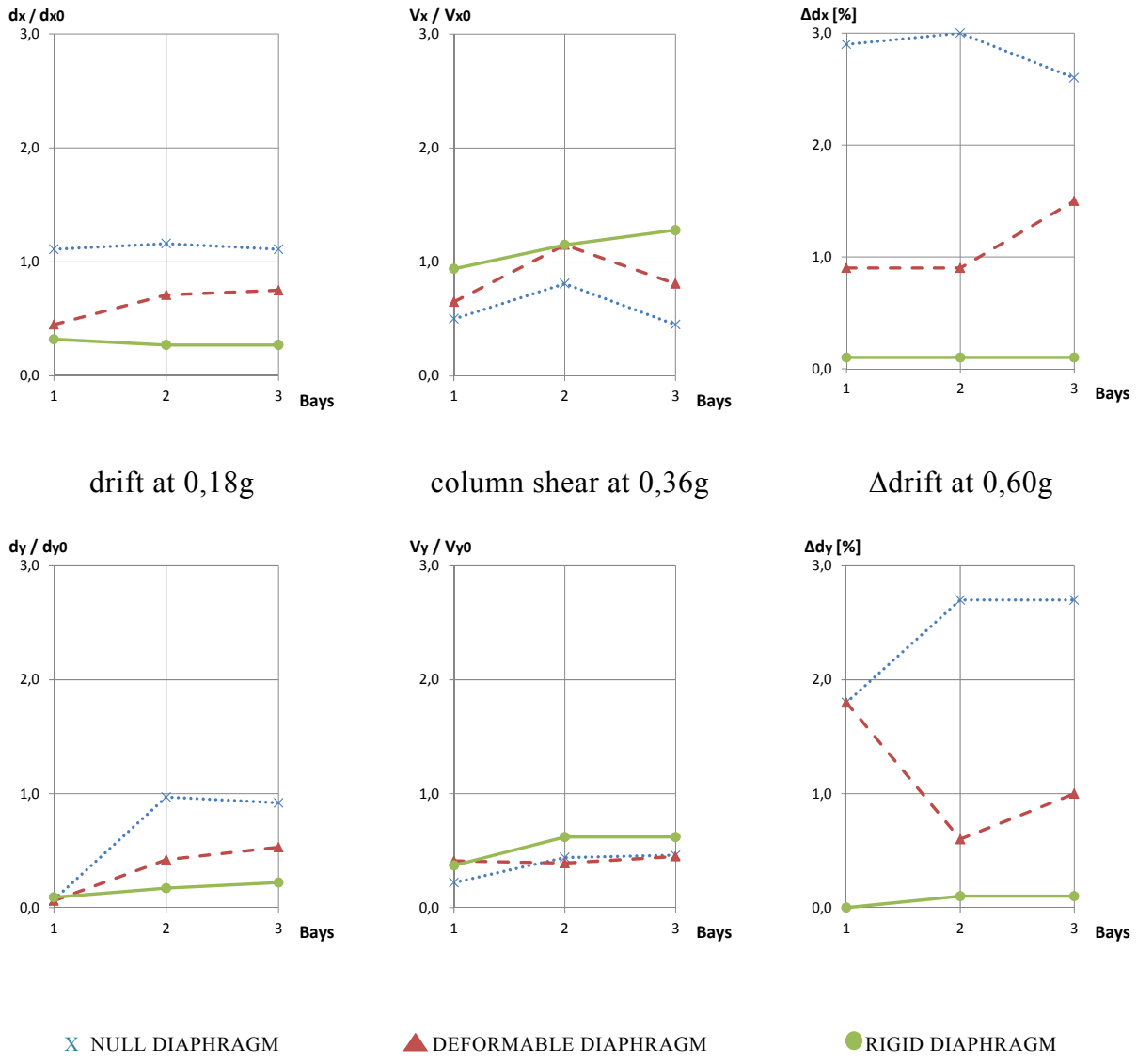

Figure 6.13 – Comparison of complementary data

The results obtained from the parametric analysis confirm the validity of the statements drafted with regards to the case study. As also noted within the case study analysis, very large forces arise in the slab connections, both the floor-to-beam and the floor-to-floor, if adopted. Those forces are an outcome of the analyses in which perfect elastic elements have been used to model them. The possibility of using ductile connections could be exploited to limit the forces in the connections, providing though a larger flexibility to the diaphragm. Dissipative ductile connections could also allow to participate in the energy absorption during the seismic motion. This solution will be the subject of further studies.

Chapter 7

Conclusions

7.1. Objectives achieved

A general framework for the structural conception and seismic assessment of precast structures with cladding panels has been proposed, with several cladding connection systems based on the panel sub-assembly static scheme that fully incorporate the panels within the design of the structure. Dissipative cladding solutions are found to be very effective, exploiting both the large flexibility of typical precast frames and the large stiffness of typical cladding wall panels to improve the seismic behaviour of the whole structure.

Three innovative dissipative cladding connections have been conceived, designed and experimentally characterised. They are Friction Based, Multiple Slit and Folded Plate devices. The experimentation allowed to define optimal technological features for the single devices. Simple design guidelines for single connections have been provided.

FBDs provide a quasi rigid-plastic behaviour to which a very large dissipation of energy is associated, with a typical friction-type hysteresis. The connection provided with brass sheets exhibited a very large cyclic reliability, to which also corresponds the possibility of re-use of the same connection after many large amplitude cycles. It has been shown that the connection does not suffer from damage up to its maximum drift, which is a design parameter depending on the length of the vertical slots, and that the brass sheets can be re-used even if subjected to strong abrasion. Since the abrasion causes friction load threshold losses, which can be strongly limited with the use of belleville washers, the connections only need to be re-tightened after use. Moderate uncertainty is associated with the definition of the slip load threshold due to the friction mechanism, which has been taken into account in the definition of the design rules.

MSDs can provide large elastic stiffness and a smooth well-defined strongly hardening behaviour, due to the diffusion of plasticity along the rectangular section of each elementary beam and to the material hardening. The device shows a large cyclic stability only for beam drift not larger than about 10%, after which the behaviour turns unstable, even if monotonic drift up to about 50% have been attained prior to failure. Devices with optimised hourglass-shaped beams allow to distribute the plasticity along the whole member, instead of locating it at the beam edges, as noticed for straight beam profiles. Despite the large relative displacement capacity of the device, the maximum displacement attained is relatively low due to the small dimensions, that are needed in order to easily apply the device in between cladding panels.

A mixed friction-plastic solution has been conceived and tested, showing that the length of the vertical slots directly increase the displacement capacity, still ensuring a largely dissipative behaviour, if the friction load threshold is calibrated in between MSD yielding and unstable branch load thresholds.

FPDs provide an in-plane flexible behaviour with large displacement capacity, to which good energy dissipation properties are associated, ensuring a contemporary large out-of-plane strength and stiffness. The device is characterised by a large cyclic stability and a smooth and well-defined elastic-plastic backbone curve. Even if the mechanical behaviour of the single device is largely influenced by the out-of-plane restraints and can turn to be strongly asymmetric, the global response is always symmetric, due to the selected installation scheme. Plate thickness larger than 8 mm installed with a single line of bolts has been shown to introduce pinching effects that jeopardise the energy dissipation properties of the device.

Silicone sealant has also been experimentally characterised, showing a very large shear flexibility and deformation capacity, up to about 200% of drift, with a typical hysteretic shear behaviour. Since the strength of silicone is very low and its drift accommodation capacity is typically overcome at ULS drift, its contribution may be omitted when favourable. However, the very long strips typically sprayed in between the panels can produce a non-negligible increase of actions on the bearing connections of the panel in case of seismic event. Design guidelines are provided to take into account its influence based on capacity design.

The behaviour of panel structural sub-assemblies with dissipative connection systems has been characterised through experimental testing for selected configurations. Design guidelines of the panel bearing connections for different dissipative systems based on capacity have been drafted, together with indications on the design features of the basic isostatic systems. The experimentation highlighted the effect of mounting tolerances on the global behaviour of the sub-assembly, that may significantly affect the hysteretic shape especially for low drift. The tested panel-to-panel dissipative devices performed as expected and any local damage of the panels has been observed, even at large attained drift.

A case study performed on a typical precast structure shows how the dissipative cladding panel solution allows to dramatically reduce the drift under a seismic event while controlling the forces, largely improving the seismic performance of the overall structural system.

A full-scale prototype of precast structure has been subjected to a wide experimental campaign at ELSA laboratory of the Joint Research Centre of the European Commission concerning cyclic and pseudo-dynamic tests with both isostatic and dissipative panel connection arrangements. The results confirm the large effectiveness of the dissipative solution in enhancing the seismic behaviour of the whole structure, with reliable and predictable behaviour that confirm the remarkable advantages induced by the added stiffness and dissipation of energy. The adoption of dissipative cladding solutions allowed the structure to remain in elastic field even under a seismic event with a PGA six times larger than the SLS design of the same structure with isostatic panel connection arrangement.

Numerical analysis, performed on the base of the given guidelines for single devices and panel sub-assemblies, shows a very satisfactory matching with the experimental results. A simplified design procedure based on the ADRS (Acceleration-Displacement Response Spectrum) method

has been applied to the experimental results and has been verified to provide a rough safe-side estimation of the maximum attained drift.

The study has been extended to large plan structures, exploring the influence of the diaphragm flexibility on the seismic behaviour of a set of mono-storey buildings provided with dissipative cladding connections. A parametric analysis has been performed on a set of buildings with different plan geometry. The results confirm the remarkable improvement of the seismic performance of precast structures based on the beneficial effects of cladding dissipative connections, which can provide suitable energy dissipation capacity and limit at the same time forces and displacements when relevant stiffness of the horizontal diaphragms is ensured.

7.2. Future developments and challenges

The results of numerical analyses pointed out that large forces arise in rigid and flexible diaphragms of buildings provided with cladding panel dissipative connections. Traditional mechanical floor-to-beam post-installed angle connections seem to be inadequate to carry those forces and provide the required stiffness, which could be provided by strong dowel connections, depending on the specific cases. The adoption of floor-to-floor connections relevantly help increasing the dry-assembled diaphragms stiffness, contemporarily reducing the actions on the floor-to-beam connections. However, the traditional welded connections, that provide large stiffness and resistance, are subjected to very large forces, which are hardly compatible with the resistance of surrounding concrete. Ductile floor-to-floor mechanical connections with load threshold may represent a good balance between added stiffness and control of forces. New connection devices are required in order to achieve this objective, and some dissipative devices considered in the present work may be adapted to this use.

Furthermore, the cladding panels considered in the present work are very stiff, while panels provided with openings or realised with different technology may provide a non-negligible flexibility and modify the response of the cladding provided with dissipative connections. Their distribution in the building may also introduce in-plane non-regularities, leading to torsional effects. Future research along these lines is necessary.

References

Aaleti, S., Henry, R.S., Liu, K.Y., Sritharan, S., Tsai, K.C. (2008). "Experimental investigation on a precast wall with end columns (PREWEC) system", *11th East Asia-Pacific Conference on Structural Engineering and Construction Conference (EASEC)*, Taipei, Taiwan, November 19-21, 1-10.

Aiken, I.D., Nims, D.K., Whittaker, A.S., Kelly, J.M. (1993). "Testing of passive energy dissipation systems", *Earthquake Spectra*, **9**(3), 335-369.

Antoniou, S., Pinho, R. (2004a). "Advantages and limitations of adaptive and non-adaptive force-based pushover procedures", *Journal of Earthquake Engineering*, **8**(4), 497-522.

Antoniou, S., Pinho, R. (2004b). "Development and verification of a fully adaptive pushover procedure", *Journal of Earthquake Engineering*, **8**(5), 643-661.

Architectural Institute of Japan (AIJ). (1998). *Japanese Architectural Standard Specifications (JASS) 21*, ALC Panel work, AIJ, Tokyo, Japan.

Arnold, C. (1989). "Cladding Design: Recent Architectural Trends and Their Impact on Seismic Design", *International Symposium on Architectural Precast Concrete Cladding - Its Contribution to Lateral Resistance of Buildings*, Chicago, Illinois, USA, November, 8-9, 14-31.

ATC-40 (1996). Seismic evaluation and retrofit of concrete buildings, Applied Technology Council (ATC), Redwood City, California, USA, **1**, pp. 346.

Bachman, R., Dowty, S. (2008). "Is it a nonstructural component or a nonbuilding structure?", *Structure Magazine*, July, 18-21.

Baird, A., Diaferia, R., Palermo, A., Pampanin, S. (2011a). "Parametric Investigation of Seismic Interaction between Precast Concrete Cladding Systems and Moment Resisting Frames", *Structures Congress 2011*, Las Vegas, Nevada, USA, April 14-16.

Baird, A., Diaferia, R., Palermo, A., Pampanin, S. (2011b). "Numerical Modelling of Local Cladding-Structure Interaction", *4th Structural Engineers World Congress (SEWC)*, Como, Italy, April 4-6, Paper No. 92.

Baird, A., Palermo, A., Pampanin, S. (2012). "Understanding cladding damage: A numerical investigation into a Christchurch earthquake case study", *2012 New Zealand Society for Earthquake Engineering (NZSEE) Conference,* Christchurch, New Zealand, April 13 – 15.

Belleri, A., Piras, D., Riva, P. (2010). "Seismic Performance of Precast Cladding Panels", *14th European Conference of Earthquake Engineering (ECEE)*, Ohrid, FRY Macedonia, August 30 - September 4.

Belleri, A., Riva, P. (2008). "Direct displacement based design and force based design of precast concrete structures", *Life-Cycle Civil Engineering*, Fabio Biondini & Dan M. Frangopol editors, CRC Press/Balkema, AK Leiden, Netherlands, 273-378.

Bhaskararao, A.V., Jangid, R.S. (2006). "Seismic analysis of structures connected with friction dampers", *Engineering Structures*, **28**, 690-703.

Biondini, F. (2009). "Seismic Design Criteria for Precast Concrete Structures", in: *Advances on Reinforced Concrete and Precast Constructions*, M. Di Prisco (Ed.), Starrylink, 73-84.

Biondini, F., Dal Lago, B., Lamperti, M., Toniolo, G. (2014a). "Qualificazione sperimentale di materiali siliconici per giunti di pannelli prefabbricati", *Giornate AICAP 2014 (Associazione Italiana Cemento Armato e Precompresso)*, Bergamo, Italy, May 22-24, 391-398 (in Italian).

Biondini, F., Dal Lago, B., Toniolo, G. (2010a). "Influenza delle connessioni tra pannelli sulla risposta sismica di costruzioni prefabbricate", *18° Congresso C.T.E. (Collegio dei Tecnici della industrializzazione Edilizia)*, Brescia, Italy, November 11-13, **2**, 739-748 (in Italian).

Biondini, F., Dal Lago, B., Toniolo, G. (2011a). "Seismic behaviour of precast structures with dissipative connections of cladding wall panels", *XIV Congresso ANIDIS – L'Ingegneria Sismica in Italia (Associazione Nazionale Italiana Di Ingegneria Sismica)*, Bari, Italy, September 18-22, paper No. 189.

Biondini, F., Dal Lago, B., Toniolo, G. (2012a). "Seismic behaviour of precast buildings with cladding panels", *15th World Conference of Earthquake Engineering (WCEE)*, Lisbon, Portugal, September 24-28.

Biondini, F., Dal Lago, B., Toniolo, G. (2013a). "Azione diaframma in strutture prefabbricate con pannelli di parete", *XV Congresso ANIDIS – L'Ingegneria Sismica in Italia (Associazione Nazionale Italiana Di Ingegneria Sismica)*, Padova, Italy, June 30 - July 4 (in Italian).

Biondini, F., Dal Lago, B., Toniolo, G. (2013b). "Role of wall panel connections on the seismic performance of precast structures", *Bulletin of Earthquake Engineering*, **11**, 1061-1081.

Biondini, F., Dal Lago, B., Toniolo, G. (2014b). "Connettori dissipativi ad attrito tra pannelli prefabbricati: sperimentazione e criteri di impiego", *Giornate AICAP 2014 (Associazione Italiana Cemento Armato e Precompresso)*, Bergamo, Italy, May 22-24, 399-406 (in Italian).

Biondini, F., Dal Lago, B., Toniolo, G. (2014c). "Angolari dissipativi per il collegamento dei pannelli in strutture prefabbricate", *20° Congresso C.T.E. (Collegio dei Tecnici della industrializzazione Edilizia)*, Milano, Italy, November 6-8, 533-542 (in Italian).

Biondini, F., Dal Lago, B., Toniolo, G. (2014d). "Comportamento sperimentale di connettori dissipativi elasto-plastici tra pannelli prefabbricati", *20° Congresso C.T.E. (Collegio dei Tecnici della industrializzazione Edilizia)*, Milano, Italy, November 6-8, 513-520 (in Italian).

Biondini, F., Dal Lago, B., Toniolo, G. (2014e). "Experimental and numerical assessment of dissipative connections for precast structures with cladding panels", *2nd European Conference on Earthquake Engineering and Seismology (ECEES)*, Istanbul, Turkey, August 25-39, pp. 12.

Biondini, F., Ferrara, L., Negro, P., Toniolo, G. (2004). "Results of Pseudodynamic Test on a Prototype of Precast R.C. Frame". *International Conference on Advances in Concrete and Structures* (ICACS), Beijing-Xuzhou-Shanghai, China, May 25-27, 2004.

Biondini, F., Palermo, A., Toniolo, G. (2011b). "Seismic performance of concrete structures exposed to corrosion: case studies of low-rise precast buildings", *Structure and Infrastructure Engineering*, **7**(1-2), 109-119.

Biondini, F., Titi, A., Toniolo, G. (2012b). "Pseudodynamic Tests and Numerical Simulations on a Full-Scale Prototype of a Multi-Storey Precast Structure", *15th World Conference of Earthquake Engineering (WCEE)*, Lisbon, Portugal, September 24-28, Paper No. 1468.

Biondini, F., Titi, A., Toniolo, G. (2012c). "Simulazione numerica di prove pseudodinamiche su prototipo in scala reale di una struttura prefabbricata multipiano", *19° Congresso C.T.E. (Collegio dei Tecnici della industrializzazione Edilizia)*, Bologna, Italy, November 8-10, 91-100 (in Italian).

Biondini, F., Titi, A., Toniolo, G. (2013c). "Prestazioni sismiche di strutture prefabbricate con connessioni trave-pilastro ad attrito", *XV Congresso ANIDIS – L'Ingegneria Sismica in Italia (Associazione Nazionale Italiana Di Ingegneria Sismica)*, Padova, Italy, June 30 - July 4, pp. 8 (in Italian).

Biondini, F., Toniolo, G. (2002). "Probabilistic Parameters of the Seismic Performance of Reinforced Concrete Frames", *1st fib Congress 2002 (Fédération Internationale du Béton / International Federation for Structural Concrete)*, Osaka, Japan, October 13-19, Paper E-228.

Biondini, F., Toniolo, G. (2003). "Seismic Behaviour of Concrete Frames: Experimental and Analytical Verification of EC8 Design Rules", *fib Symposium on Concrete Structures in Seismic Regions (Fédération Internationale du Béton / International Federation for Structural Concrete)*, Athens, Greece, May 6-9, 2003.

Biondini, F., Toniolo, G. (2004). "Validation of seismic design criteria for concrete frames based on Monte Carlo simulation and full scale pseudodynamic tests", *13th World Conference on Earthquake Engineering (WCEE),* Vancouver, British Columbia, Canada, August, 1-6, paper No. 2581, pp. 15.

Biondini, F., Toniolo, G. (2008). "Results of an Experimental Research on Precast Structures under Seismic Actions", *fib Symposium "Tailor Made Concrete Structures: New Solutions for Our Society"*, *(Fédération Internationale du Béton / International Federation for Structural Concrete)* Amsterdam, The Netherlands, May 19-22, 2008.

Biondini, F., Toniolo, G. (2009). "Probabilistic calibration and experimental validation of seismic design criteria for one storey concrete frames", *Journal of Earthquake Engineering*, **13**(4), 426-462.

Biondini, F., Toniolo, G. (2010). "Experimental research on seismic behavior of precast structures", *Industria Italiana del Cemento*, **854**, 74-79.

Biondini, F., Toniolo, G. (2011). "Pseudodynamic tests on full-scale prototype of a multistorey precast structure", *XIV Congresso ANIDIS – L'Ingegneria Sismica in Italia (Associazione Nazionale Italiana Di Ingegneria Sismica)*, Bari, Italy, September 18-22.

Biondini, F., Toniolo, G., Tsionis, G. (2010b). "Capacity design and seismic performance of multi-storey precast structures", *European Journal of Environmental and Civil Engineering*, **14**(1), 11-28.

Biondini, F., Toniolo, G., Zaho, B. (2008). "Pseudodynamic tests on full scale prototypes of precast structures", *14th World Conference on Earthquake Engineering (WCEE)*, Beijing, China.

Bonfanti, C., Carabellese, A., Toniolo, G. (2008). "Strutture prefabricate: catalogo delle tipologie esistenti", Report from DPC, ReLUIS, Assobeton, pp. 78 (in Italian).

Bournas, D.A., Negro, P. (2012a). "Pseudodynamic Testing of the SAFECAST Building: Seismic Performance of the Mechanical Connections", *15th World Conference of Earthquake Engineering (WCEE)*, Lisbon, Portugal, September 24-28, paper No. 1053.

Bournas, D.A., Negro, P. (2012b). "Full scale testing of the SAFECAST three-storey precast building", *19° Congresso C.T.E. (Collegio dei Tecnici della industrializzazione Edilizia)*, Bologna, Italy, November 8-10, 113-120.

Bournas, D.A., Negro, P., Molina, J. (2013a). "Pseudodynamic Tests on a full-scale 3-storey precast concrete building: global response", *Engineering Structures*, **57**, 594-608.

Bournas, D.A., Negro, P., Molina, J. (2013b). "Pseudodynamic Tests on a full-scale 3-storey precast concrete building: behaviour of the mechanical connections and floor diaphragms", *Engineering Structures*, **57**, 609-627.

Building Center of Japan (BCJ). (1997). *Building Standard Law of Japan*.

Camnasio, E. (2013). "Lifetime performance and seismic resilience of concrete structures exposed to corrosion", *PhD Thesis dissertation,* Department of Structural Engineering, Politecnico di Milano.

Cao, L., Naito, C. (2009). "Precast concrete double-tee connections, part 2: shear behaviour", *PCI Journal,* Precast Concrete Institute, Spring, 97-115.

Capozzi, V., Magliulo, G., Manfredi, G. (2010). "Test on beam-column pin connections in precast buildings", *14th European Conference on Earthquake Engineering (ECEE)*, Ohrid, Macedonia, paper No. 1185.

CEB-FIP (2003). Seismic Design of Precast Concrete Building Structures. fib Bulletin 27. State of the art report prepared by Task Group 7.3. Fédération Internationale du Béton / International Federation for Structural Concrete, Lausanne, Switzerland, pp. 262.

CEB-FIP (2008). Structural Connections for Precast Concrete Buildings. fib Bulletin 43. State of the art report prepared by Task Group 7.3. Fédération Internationale du Béton / International Federation for Structural Concrete, Lausanne, Switzerland, pp. 254.

CEN-EN 1998-1:2004 (2004). Eurocode 8: Design of structures for earthquake resistance – Part 1 General rules, seismic actions and rules for buildings, European Committee for Standardization, Brussels, Belgium.

Chan, R.W.K. (2003). "Experimental investigation of push-pull precast cladding connections", *Master Thesis at San Jose State University*, San Francisco, California, USA.

Chan, R.W.K., Albermani F., Kitipornchai, S. (2013). "Experimental study of perforated yielding shear panel device for passive energy dissipation", *Journal of Constructional Steel Research*, **91**, 14-25.

Chan, R.W.K., Albermani F., Williams, M.S. (2009). "Evaluation of yielding shear panel device for passive energy dissipation", *Journal of Constructional Steel Research*, **65**, 260-268.

Chan, R.W.K., Albermani, F. (2008). "Experimental study of steel slit damper for passive energy dissipation", *Engineering Structures*, **30**, 1058-1066.

Charney, F.A., Harris, J.R. (1989). "The Effect of Architectural Precast Concrete Cladding on the Lateral Response of Multistory Buildings", *International Symposium on Architectural Precast Concrete Cladding - Its Contribution to Lateral Resistance of Buildings*, Chicago, Illinois, USA, November, 8-9, 80-96.

Chen *et al*. (2010). "Design and Construction of a Full-scale 5-story Base Isolated Building outfitted with Nonstructural Components for Earthquake Testing at the UCSD-NEES Facility", *2010 Structures Congress*, Orlando, Florida, USA.

Cherry, S., Filiatrault, A. (1993). "Seismic response control of building using friction dampers", *Earthquake Spectra*, **9**(3), 447-466.

Chopra, A.K. (2006). Dynamics of structures: theory and application to earthquake engineering, Prentice Hall College Division, 3rd edition, pp. 876.

Chopra, A.K., Goel, R.K. (1999). "Capacity-demand-diagram methods for estimating seismic deformations of inelastic structures: SDF systems", *Report No. PEER-1999/02*, Pacific Earthquake Engineering Research Center, College of Engineering, University of California, Berkeley, California, USA, pp. 55.

Chopra, A.K., Goel, R.K. (2002). "A modal pushover analysis procedure for estimating seismic demands for buildings", *Earthquake Engineering and Structural Dynamics*, **31**, 561-582.

Circolare Ministero L.P. 4 luglio 1996 n. 156. *Istruzioni per l'applicazione delle Norme tecniche di cui al decreto ministeriale 16 gennaio 1996* (in Italian).

Cohen, J.M. (1995). "Seismic Performance of Cladding: Responsibility Revisited", *Journal of Performance of Constructed Facilitie*s, American Society of Civil Engineers (ASCE), November, 154-269.

Cohen, J.M., Powell, G.H. (1993). "A design study of an energy dissipating cladding system", *Earthquake Engineering and Structural Dynamics*, **22**(7), 617-632.

Colombo, A., Toniolo, G. (2010). "Problemi di progettazione sismica delle connessioni dei pannelli di tamponamento", *18° Congresso C.T.E. (Collegio dei Tecnici della industrializzazione Edilizia)*, Brescia, Italy, November 11-13, **2**, 799-806 (in Italian).

Colombo, A., Toniolo, G. (2012a). "Precast concrete structures: the lesson learnt from L'Aquila earthquake", *Structural Concrete,* **13**(2), 73-83.

Colombo, A., Toniolo, G. (2012b). "Costruzioni prefabbricate: la lezione appresa dal terremoto d'Abruzzo", *18° Congresso C.T.E. (Collegio dei Tecnici della industrializzazione Edilizia)*, Brescia, Italy, November 11-13, **2**, 807-818 (in Italian).

Colombo, A., Toniolo, G. (2012c). "Problems of seismic design of the cladding panels of precast buildings", *2012 New Zealand Society for Earthquake Engineering (NZSEE) Conference,* Christchurch, New Zealand, April 13-15, paper No. 129, pp. 8.

Craig, J.I., Goodno, B.J., Keister, M.J., Fennell, C.J. (1986). "Hysteretic Behavior of Precast Cladding Connections", *Dynamic Response of Structures*, Ed. by G.C. Hart and R.B. Nelson, In 3rd Conference of Engineering Mechanics Division, American Society of Civil Engineers (ASCE), Los Angeles, CA, USA, March 31-April 2, 817-826.

Craig, J.I., Goodno, B.J., Pinelli, J.P., Moore, C. (1992). "Modelling and evaluation of ductile cladding connection systems for seismic response attenuation in buildings". *10th World conference on Earthquake Engineering (WCEE)*, Madrid, Spain, July 19-24, **7**.

Craig, J.I., Leistikow, R., Fennell, C.J. (1988). "Experimental Studies of the Performance of Precast Concrete Cladding Connections", *9th World Conference on Earthquake Engineering (WCEE)*, Tokyo-Kyoto, Japan, August 2-9, **6**, 201-206.

D.M.L.P. 16 gennaio 1996. *Norme tecniche relative ai «Criteri generali per la verifica di sicurezza delle costruzioni e dei carichi e sovraccarichi»* (in Italian).

Dal Lago, A., Dal Lago, B. (2011). "Telai prefabbricati ad assetto variabile", *XIV Congresso ANIDIS – L'ingegneria Sismica in Italia (Associazione Nazionale Italiana Di Ingegneria Sismica)*, Bari, Italy, September 18-22, paper No. 190 (in Italian).

Dal Lago, A., Dal Lago, B. (2012a). "Progetto SAFECAST: problematiche riscontrate confrontando progetto e prove sismiche", *19° Congresso C.T.E. (Collegio dei Tecnici della industrializzazione Edilizia)*, Bologna, Italy, November 8-10, 553-562 (in Italian).

Dal Lago, A., Ragozzini, R. (2010). "Fissaggio dei pannelli alla struttura prefabbricata in zona sismica", *18° Congresso C.T.E. (Collegio dei Tecnici della industrializzazione Edilizia)*, Brescia, Italy, November 11-13, **1**, 345-352 (in Italian).

Dal Lago, B. (2014). "Studio sperimentale su piastre piegate per collegare i pannelli orizzontali in strutture prefabbricate", *ACI Italy Chapter Workshop: tecniche innovative per il miglioramento sismico di edifici prefabbricati*, Bologna, Italy, October 22 (in Italian).

Dal Lago, B., Dal Lago, A. (2012b). "Precast structures with adaptable restraints", *15th World Conference of Earthquake Engineering (WCEE)*, Lisbon, Portugal, September 24-28.

Dal Lago, B., Lamperti, M.G.L., Dal Lago A. (2012a). "Comportamento a strappo di estremità di tegoli prefabbricati con connessioni meccaniche", *19° Congresso C.T.E. (Collegio dei Tecnici della industrializzazione Edilizia)*, Bologna, Italy, November 8-10, 141-150 (in Italian).

Dal Lago, B., Lamperti, M.G.L., Dal Lago A. (2012b). "Studio sul comportamento bidirezionale di connessioni meccaniche scorrevoli pannello-telaio", *19° Congresso C.T.E. (Collegio dei Tecnici della industrializzazione Edilizia)*, Bologna, Italy, November 8-10, 131-140 (in Italian).

Dal Lago, B., Lamperti, M.G.L., Toniolo G. (2013). "Experimental behaviour of semi-dry column-foundation connections for precast buildings", *Studi e Ricerche*, Scuola di Specializzazione F.lli Pesenti, Politecnico di Milano, **32**, 249-268.

Dal Lago, B., Lamperti, M.G.L., Toniolo, G. (2010). "Verifica sperimentale di connessioni prefabbricate pilastro-fondazione soggette a carichi ciclici: risultati preliminari", *18° Congresso C.T.E. (Collegio dei Tecnici della industrializzazione Edilizia)*, Brescia, Italy, November 11-13, **2**, 915-922 (in Italian).

Dal Lago, B., Lamperti, M.G.L., Toniolo, G. (2012c). "Studio sperimentale su connessioni pilastro-fondazione per strutture prefabbricate", *19° Congresso C.T.E. (Collegio dei Tecnici della industrializzazione Edilizia)*, Bologna, Italy, November 8-10, 121-130 (in Italian).

De Matteis, G. (2005). "Effect of lightweight cladding panels on the seismic performance of moment resisting steel frames", *Engineering Structures*, **27,** 1662-1676.

Dei Poli, S., Di Prisco, M., Gambarova, P.G. (1992). "Shear Response, deformations, and subgrade stiffness of a dowel bar embedded in concrete", *ACI Structural Journal*, American Concrete Institute, **89**(6), 665-675.

Dei Poli, S., Di Prisco, M., Gambarova, P.G. (1993). "Cover and stirrup effects on the shear response of dowel bar embedded in concrete", *ACI Structural Journal*, American Concrete Institute, **90**(4), 441-450.

Diaferia, R., Baird, A., Palermo, A., Pampanin, S. (2011). "Numerical Study on the Seismic Interaction Between 2D Seismic Resisting Frames and Claddings", *4th Structural Engineers World Congress (SEWC),* Como, Italy, April 4-6, Paper No. 91.

Eberhard, M.O., Sozen, M.A. (1993). "Behavior-based method to determine design shear in earthquake-resistant walls", *Journal of Structural Engineering*, American Society of Civil Engineers (ASCE), **119**(2), 619-639.

EN 1990:2002. *Eurocode 0: Basis of structural design.* European Committee for Standardization, Brussels, Belgium.

EN 1991-1:2004. *Eurocode 1: Actions on structures. Part 1: General actions.* European Committee for Standardization, Brussels, Belgium.

EN 1992-1-1:2004. *Eurocode 2: Design of concrete structures. Part 1-1: General rules and rules for buildings.* European Committee for Standardization, Brussels, Belgium.

EN 1993-1-8:2005. *Eurocode 3: Design of steel structures. Part 1-8: Design of joints.* European Committee for Standardization, Brussels, Belgium.

EN 1998-1:2004. *Eurocode 8: Design of structures for earthquake resistance. Part 1: General rules, seismic actions and rules for buildings.* European Committee for Standardization, Brussels, Belgium.

Ercolino, M., Capozzi, V., Magliulo, G., Manfredi, G. (2013). "Influence of cladding panels on dynamic behavior of one-storey precast buildings", *Precast Design*, **7**, 197-205.

Espín, A.T. (2011). "Primeras inspecciones aftershock – consideraciones y visión general de los daños ocasionados por el sismo de Lorca", *Jornada de Ingeniería sísmica – el terremoto de Lorca*, Murcia, Spain, June 23 (in Spanish).

Fabbrocino, G., Magliulo, G., Manfredi, G. (2006). "Seismic response of existing precast industrial buildings with poor member connections", *2nd fib Congress (Fédération Internationale du Béton / International Federation for Structural Concrete)*, Napoli, Italy, June 5-8.

Fajfar, P. (1999). "Capacity spectrum method based on inelastic demand spectra", *Earthquake Engineering and Structural Dynamics*, **28**, 979-993.

Fajfar, P. (2000). "A non-linear analysis method for performance-based seismic design", *Earthquake Spectra*, **16**(3), 573-592.

Fajfar, P., Fischinger, M. (1988). "N2 – a method for non-linear seismic analysis of regular buildings", *9th World Conference on Earthquake Engineering (WCEE)*, Tokyo-Kyoto, Japan, August 2-9, **5**, 111-116.

Fajfar, P., Gaspersic, P. (1996). "The N2 method for the seismic analysis of RC buildings", *Earthquake Engineering and Structural Dynamics*, **25**, 31-46.

Felicetti, R., Lamperti, M.G.L., Toniolo, G. (2008). "Analisi sperimentale del comportamento sismico di connessioni tegolo-trave di strutture prefabbricate", *17° Congresso C.T.E. (Collegio dei Tecnici della industrializzazione Edilizia)*, Roma, Italy, November 5-7 (in Italian).

FEMA (2007). "Interim testing protocols for determining seismic performance characteristics of structural and non-structural components through laboratory testing", *FEMA 461 Document*, Washington, DC (USA).

Ferrara, L., Felicetti, R., Toniolo G., Zenti C. (2011). "Friction dissipative devices for cladding panels in precast buildings", *European Journal of Environmental and Civil Engineering*, **15**(9), 1319-1338.

Ferrara, L., Mola, E., Negro, P. (2006). "Cyclic test on a full scale prototype of r/c one storey industrial building", *2nd fib Congress (Fédération Internationale du Béton / International Federation for Structural Concrete)*, Napoli, Italy, June 5-8.

Ferrara, L., Toniolo, G., Tsionis, G. (2004). "Sulla azione diaframma dei sistemi di copertura in edifici industriali prefabbricati in calcestruzzo armato", *15° Congresso C.T.E. (Collegio dei Tecnici della industrializzazione Edilizia)*, Bari, Italy, November 4-6 (in Italian).

Filiatrault, A., Christopoulos, C., Stearns, C. (2001). "Guidelines, specifications and seismic performance characterization of nonstructural building components and equipments", *Pacific Earthquake Engineering Research Center (PEER) Report 2003/05*, College of Engineering, University of California, Berkeley, California (USA).

Filiatrault, A., Sullivan, T. (2014). "Performance-based design of nonstructural building components: the next frontier of earthquake engineering", *Earthquake Engineering and Engineering Vibration*, **13**(1), 17-46.

Filiatrault, A., Tremblay, R., Christopoulos, C., Folz, B., Pettinga, D. (2013). Elements of earthquake engineering and structural dynamics, Presses Internationales Polytechnique, 3rd edition, pp. 874.

Fischinger, M., Kramar, M., Isakovic, T. (2008). "Cyclic response of slender RC columns typical of precast industrial buildings", *Bulletin of Earthquake Engineering*. **6**(3), 519-534.

Fischinger, M., Kramar, M., Isaković, T. (2012a). "Seismic Risk Assessment of Multi-Storey Precast Structures", *15th World Conference of Earthquake Engineering (WCEE)*, Lisbon, Portugal, September 24-28, paper No. 2161.

Fischinger, M., Zoubek, B., Kramar, M., Isaković, T. (2012b). "Cyclic Response of Dowel Connections in Precast Structures", *15th World Conference of Earthquake Engineering (WCEE)*, Lisbon, Portugal, September 24-28, paper No. 2127.

Fischinger, M., Zoubek, M., Isaković, T. (2013). "Seismic behaviour of the beam-to-column dowel connections: FEM analysis", *4th European Community on Computational Methods in Applied Sciences (ECCOMAS) Thematic Conference on Computational Methods in Structural Dynamics and Earthquake Engineering*, Kos Island, Greece, June, 12-14, pp. 8.

Fleischman, R.B., Farrow, K.T. (2001). "Dynamic response of perimeter lateral-system structures with flexible diaphragms", *Earthquake Engineering and Structural Dynamics*, **30**(5), 745-763.

Fleischman, R.B., Farrow, K.T. (2003). "Seismic design recommendations for precast concrete diaphragms in long floor span constructions", *PCI Journal,* Precast Concrete Institute, November-December, 46-62.

Fleischman, R.B., Farrow, K.T., Eastman, K. (2002). "Seismic performance of perimeter lateral-system structures with highly flexible diaphragms", *Earthquake Spectra*, **18**(2), 251-286.

Fleischman, R.B., Ghosh, S.K., Naito, C.J., Wan, G., Restrepo, J., Sause, R., Cao, L. (2005a). "Seismic design methodology for precast concrete diaphragms part 2: research program", *PCI Journal,* Precast Concrete Institute, November-December, 14-31.

Fleischman, R.B., Naito, C.J., Restrepo, J., Sause, R., Ghosh, S.K. (2005b). "Seismic design methodology for precast concrete diaphragms part 1: design framework", *PCI Journal,* Precast Concrete Institute, September-October, 68-83.

Fleischman, R.B., Sause, R., Pessiki, S., Rhodes, A.B. (1998). "Seismic behavior of precast parking structure diaphragms", *PCI Journal,* Precast Concrete Institute, **43**(1), 38-53.

Freeman, S.A. (1978). "Prediction of Response of Concrete Buildings to Severe Earthquake Motion", *Douglas McHenry International Symposium on Concrete and Concrete Structures*, SP-55, ACI, American Concrete Institute, Detroit, Michigan, USA, 589-605.

Freeman, S.A. (1998). "The capacity spectrum method as a tool for seismic design", *11th European Conference on Earthquake Engineering (ECEE)*, Paris, France, September 6-11, pp. 8.

Fu Y., Cherry S. (2000). "Design of friction damped structures using lateral force procedure", *Earthquake Engineering and Structural Dynamics*, **29**, 989-1010.

Gaiotti, R., Smith, B.S. (1992). "Stiffening of Moment-Resisting Frame by Precast Concrete Cladding", *PCI Journal,* Precast Concrete Institute, PCI, **37**(5), 80-92.

Getz, D.R., Memari, A.M. (2006). "Static and Cyclic Racking Performance of Autoclaved Aerated Concrete Cladding Panels", *Journal of Architectural Engineering*, American Society of Civil Engineers (ASCE), March, 12-23.

Ghabraie, K., Chan, R., Huang, X., Xie, Y.M. (2010). "Shape optimization of metallic yielding devices for passive mitigation of seismic energy", *Engineering structures*, **32**, 2258-2267.

Gjelvik, A. (1973). "Interaction between Frames and Precast Panel Walls", *Journal of Structural Division*, American Society of Civil Engineers (ASCE), **100**(2), 405-426.

Goodno, B.J., Craig, J.I. (1989). "Historical Overview of Studies on the Contribution of Cladding to Lateral Resistance of Buildings", *International Symposium on Architectural Precast Concrete Cladding - Its Contribution to Lateral Resistance of Buildings*, Chicago, Illinois, USA, November, 8-9, 36-47.

Goodno, B.J., Craig, J.I. (1998). "Ductile Cladding Connection Systems for Seismic Design", *A report to Building and Fire Research Laboratory*, NIST, Gaithersburg, Maryland, USA, pp. 176.

Goodno, B.J., Craig, J.I., Meyyappa, M. (1983). "Cladding-Structure Interaction in High-Rise Buildings", *Report No. CEE-7704269*, Georgia Institute of Technology, Atlanta, Georgia, USA.

Goodno, B.J., Meyyappa, M., Nagarajaiah, S. (1988). "A Refined model for Precast Concrete Cladding and Connections", *9th World Conference on Earthquake Engineering (WCEE),* Tokyo-Kyoto, Japan, August 2-9, **6**, 195-200.

Goodno, B.J., Palsson, H. (1986). "Analytical Studies of Building Cladding", *Journal of Structural Engineering*, American Society of Civil Engineers (ASCE), **112**(4), 665-676.

Goodno, B.J., Will, K.M., Palsson, H. (1980). "Effect of Cladding on Building Response to Moderate Ground Motion", *7th World Conference on Earthquake Engineering (WCEE)*, Istanbul, Turkey, September, **2**, 449-456.

Grigorian, C.E., Yang, T.S., Popov, E.P. (1987). "Slotted Bolted Connection Energy Dissipators" *Earthquake Spectra*, **9**(3), 491-504.

Hegle, R.L. (1989). "Connection of Cladding to Multi-Story Structures," *International Symposium on Architectural Precast Concrete Cladding - Its Contribution to Lateral Resistance of Buildings*, Chicago, Illinois, USA, November, 8-9, 192-201.

Henry, R.M., Roll, F. (1986). "Cladding-Frame Interaction", *Journal of Structural Engineering*, American Society of Civil Engineers (ASCE), **112**(4), 815-834.

Hobelmann, J.P., Schachter, M., Cooper, M.C. (2012). "Architectural precast concrete panel systems used for lateral-force resistance", *PCI Journal,* Precast Concrete Institute, Winter, 124-134.

Hunt, J.P., Stojadinović, B. (2010). "Seismic Performance Assessment and Probabilistic Repair Cost Analysis of Precast Concrete Cladding Systems for Multistory Buildings", *PEER Report 2010/110*. Pacific Earthquake Engineering Research Center, College of Engineering, University of California, Berkeley, California, USA, pp. 347.

Hutchinson, T., Restrepo, J., Conte, J. (2012). "Shake Table Response of a Fully Furnished Full-scale Five-story Building", *NEES QuakeSummit*, Boston, Massachusetts, USA, July 9-12.

Itoh, K., Nishida, K., Hamazaki, H., Mizutani, Y., Aiko, T., Hironami, J., Takahashi, M., Tomita, K. (1998). "Full-scale seismic test of ALC rocking installation systems", *Summary of Technical Papers of Annual Conventions*, Architectural Institute of Japan, paper No. 1054-1060**,** 107-120.

Iverson, J.K. (1989). "Concrete Cladding Connections in Earthquake Country", *International Symposium on Architectural Precast Concrete Cladding - Its Contribution to Lateral Resistance of Buildings*, Chicago, Illinois, USA, November, 8-9, 202-216.

Iverson, J.K., Hawkins, N.M. (1994). "Performance of Precast/Prestressed Concrete Building Structures During Northridge Earthquake", ASME-APM-52-15, 169-181.

Iwan, W.D., Gates, N.C. (1979). "Estimating earthquake response of simple hysteretic structures", *Journal of the Engineering Mechanics Division*, American Society of Civil Engineers (ASCE), **105**(3), 391-405.

Jacobsen, L.S. (1930). "Steady forced vibration as influenced by damping", *PCI Journal,* Precast Concrete Institute, March/April.

Kam, W.Y., Pampanin, S., Palermo, A., Carr, A.J. (2010). "Self-centering structural systems with combination of hysteretic and viscous energy dissipations", *Earthquake Engineering and Structural Dynamics,* **39**, 1083-1108.

Karadogan, F., Yuksel, E., Bal, E.I. (2012). "The Seismic Behavior of An Asymmetric Exterior Precast Beam-Column Connection", *15th World Conference of Earthquake Engineering (WCEE)*, Lisbon, Portugal, September 24-28.

Karavasilis, T.L., Kerawala, S., Hale, E. (2012). "Hysteretic model for steel energy dissipation devices and evaluation of a minimal-damage seismic design approach for steel buildings", *Journal of Constructional Steel Research*, **70**, 358-367.

Keintzel, E. (1992). Advances in the design of shear for RC structural walls under seismic loading. Nonlinear seismic analysis and design of reinforced concrete buildings, Elsevier, New York, USA.

Kim J., Choi, H., Min, K. (2003). "Performance-based design of added viscous dampers using capacity spectrum method", *Journal of Earthquake Engineering*, **7**(1), 1-24.

Kramar, M., Isakovic, T., Fischinger, M. (2010). "Seismic collapse risk of precast industrial buildings with strong connections", *Earthquake Engineering and Structural Dynamics*. **39**(8), 847-868.

Krawinkler, H., Seneviratna, G.P.D.K. (1998). "Pros and cons of a pushover analysis of seismic performance evaluation", *Engineering Structures*. **20**(4-6), 452-464.

Kurama, Y.C. (2001). "Simplified Seismic Design Approach for Friction-Damped Unbonded Post-Tensioned Precast Concrete Walls", *ACI Structural Journal*, American Concrete Institute, **98**(5), 705-716.

Kurama, Y.C. (2000). "Seismic Design of Unbonded Post-Tensioned Precast Concrete Walls with Supplemental Viscous Damping", *ACI Structural Journal*, American Concrete Institute, **97**(4), 648-658.

Lacasse, M.A., Bryce, J.E., Margeson, J.C. (1995). "Evaluation of cyclic fatigue as a mean of assessing the performance of construction joints", *Science and Technology of Building Seals, Sealants, Glazing and Waterproofing (ASTM STP 1243),* **4**, 49-64.

Levy, R., Marianchik, E., Rutenberg, A., Segal, F. (2001). "A simple approach to the seismic design of friction damped braced medium-rise frames", *Engineering Structures*, **23**, 250-259.

Ma, X., Borchers, E., Pena, A., Krawinkler, H., Billington, S., Deierlein, G.G. (2010). "Design and behavior of steel shear plates with openings as energy dissipating fuses", *Report 173*, Department of Civil and Environmental Engineering, Stanford University, March 2010.

Magliulo, G., Capozzi, V., Fabbrocino, G., Manfredi, G. (2011). "Neoprene-concrete fiction relationships for seismic assessment of existing precast buildings", *Engineering Structures*, **33**(2), 532–538.

Magliulo, G., Ercolino, M., Manfredi, G. (2014a). "Influence of cladding panels on the first period of one-story precast buildings", *Bulletin of Earthquake Engineering,* DOI: 10.1007/s10518-014-9657-2, pp. 25.

Magliulo, G., Ercolino, M., Petrone, C., Coppola, O., Manfredi, G. (2014b). "Emilia earthquake: the sesmic performance of precast RC buildings", *Earthquake Spectra,* **30**(2), 891-912.

Magliulo, G., Fabbrocino, G., Manfredi, G. (2008). "Seismic assessment of existing precast industrial buildings using static and dynamic nonlinear analyses", *Engineering Structures,* **30**, 2580-2588.

Mandelli Contegni, M., Palermo, A., Toniolo, G. (2007). "Strutture prefabricate: schedario dei collegamenti", Report from DPC, ReLUIS, Assobeton, pp. 71 (in Italian).

Mandelli Contegni, M., Palermo, A., Toniolo, G. (2008). "Strutture prefabricate: schedario di 255difice prefabbricati in c.a.", Report from DPC, ReLUIS, Assobeton, pp. 206 (in Italian).

Maneetes, H. (2007). "Development of a seismic dissipating mechanism for precast concrete cladding panels", *PhD Thesis dissertation,* College of Engineering, Pennsylvania State University.

Martinelli, E., Faella, C. (2010). "Confronto parametrico tra metodi di analisi static non-lineare per la determinazione della duttilità richiesta", *18° Congresso C.T.E. (Collegio dei Tecnici della industrializzazione Edilizia)*, Brescia, Italy, November 11-13, **2**, 673-682 (in Italian).

Martinelli, P., Mulas, M.G. (2010). "An innovative passive control technique for industrial precast frames", *Engineering Structures,* **32**, 1123-1132.

Matsumiya, T., Suita, K., Nakashima, M., Liu, D., Inoue, M., Takehara, S. (2004). "Effect of ALC panel finishes on structural performance-test on full scale three story frame for evaluation of seismic performance", *Journal of Structural and Construction Engineering,* Architectural Institute of Japan, **581**, 145-151.

McCann, R.A. (1991). "Architectural precast Concrete Cladding Connections", *Seminar on Implementation and Performance of Structural Details*, Structural Engineers Associaction of Northern California, October 31st, pp. 21.

McMullin, K., Nguyen, H. (2008). "Drift Controlled Damage to Precast Concrete Cladding Panels – Expected Damage Patterns", *6th Network for Earthquake Engineering Simulation (NEES) Annual Meeting*, Portland, Oregon, USA, June 18-20.

McMullin, K., Ortiz, M. (2009). "Drift-Sensitive Damage to Precast Concrete Cladding Panels - Preliminary Results", *2009 National Science Foundation (NSF) Engineering Research and Innovation Conference*, Honolulu, Hawaii, USA.

McMullin, K., Wong, Y., Choi, C., Chan, K. (2004). "Seismic performance states of precast concrete cladding connections", *13th World Conference on Earthquake Engineering (WCEE)*, Vancouver, British Columbia, Canada, August 1-6, paper No. 3379.

Memari, A.M., Maneetes, H., Bozorgnia, Y. (2004). "Study of the Effect of Near-Source Vertical Ground Motion on Seismic Design of Precast Concrete Cladding Panels", *Journal of Architectural Engineering*, American Society of Civil Engineers (ASCE), December, 167-183.

Menegotto, M. (2010). "Experiences from L'Aquila 2009 earthquake", *3rd fib Congress (Fédération Internationale du Béton / International Federation for Structural Concrete),* Washington DC, USA, 29 May - 2 June.

Metelli, G., Beschi, C., Riva, P. (2011). "Cyclic Behaviour of a Column-to-Foundation Joint for Precast Structures". *European Journal of Environmental and Civil Engineering*, **15**(9), 1297-1318.

Meunier, L., Chagnon, G., Favier, D., Orgeas, L., Vacher, P. (2008). "Mechanical experimental characterization and numerical modelling of an unfilled silicone rubber", *Polymer testing*, **29**, 765-777.

Meyyappa, M., Palsson, H., Craig, J.I. (1981). "Modal Parameter Estimation for a Highrise Building Using Ambient Response Data Taken During Construction", *2nd Specialty Conference on Dynamic Response of Structures: Experimentation, Observation, Prediction and Control,* Atlanta, Georgia, USA, 141-151.

Miranda, E., Bertero, V.V. (1994). "Evaluation of strength reduction factors for earthquake resistant design", *Earthquake Spectra*, **10**(2), 357-379.

Molina, F.J., Géradin, M. (2007). "Earthquake Engineering experimental research at JRC-ELSA", *North-Atlantic Treaty Organization (NATO) workshop on Extreme Man-Made and Natural Hazards in Dynamics of Structures*, NATO Security through Science Series C: Environmental Security, ed. Ibrahimbegovic, A. and Kozar, I., (Springer), 311-351.

Molina, F.J., Magonette, G., Viaccoz, B. (2010). "Linear model of a pseudo-dynamic testing system", *Joint Research Centre (JRC) Scientific and Technical Reports*, EUR 24313 EN, European Commission, Joint Research Centre, IPSC, ELSA, Laboratory, Ispra (VA), Italy, pp. 54.

Morgen, B.G., Kurama, Y.C. (2007). "Seismic design of frction-damped precast concrete frame structures", *Journal of Structural Engineering*, American Society of Civil Engineers (ASCE), **133**, November, 1501-1511.

Mualla, I.H. (1999). "Experimental and numerical evaluation of a novel friction damper device", *PhD Thesis dissertation*, Department of Structural Engineering and Materials, Technical University of Denmark.

Mualla, I.H., Nielsen, L.O., Belev, B., Liao, W.I., Loh, C.H., Agrawal, A. (2002). "Numerical predictions of shaking table tests on a full scale friction-damped structure", *12th European Conference on Earthquake Engineering (ECEE)*, London, UK, September 9-13, paper No. 109.

Naito, C., Cao, L., Wesley, P. (2009). "Precast concrete double-tee connections, part 1: tension behaviour", *PCI Journal,* Precast Concrete Institute, Winter, 49-66.

Nakaki, S.D. (1998). "Design guidelines for precast and cast-in-place concrete diaphragms", *National Earthquake Hazards Reduction Program (NEHRP) Professional Fellowship Report*, Earthquake Engineering Research Institute, April.

National Institue of Standards and Technology (NIST), (1995). "Literature review on seismic performance of building cladding systems", *FEMA GCR 95-681 Document*, Gaithersburg, Maryland, USA.

Negro, P., Toniolo, G. (editors) (2012). Design Guidelines for Connections of Precast Structures under the Seismic Action. *European Commission Joint Research Centre Institute for the Protection and Security of the Citizen*, Luxembourg: Publications Office of the European Union.

Norme Tecniche per le Costruzioni. Decreto Ministeriale D.M. January 14, 2008 (in Italian).

NPCA (2012). "Architectural precast concrete wall panels: connection guide", *National Precast Concrete Association (NPCA) Document*, Carmel, Illinois, USA, pp. 70.

Oh, S.H., Kim, Y.J., Ryu, H.S. (2009). "Seismic performance of steel structures with slit dampers", *Engineering Structures*, **31**, 1997-2008.

Okazaki, T., Nakashima, M., Suita, K., Matsumiya, T., (2007). "Interaction between cladding and structural frame observed in a full-scale steel building test", *Earthquake Engineering and Structural Dynamics,* **36**, 35-53.

Oppenheim, I.J. (1973). "Dynamic Behavior of Tall Buildings with Cladding", *5th World Conference on Earthquake Engineering*, Rome, Italy, June, 2769-2773.

Pall, A.S., (1989). "Friction Damped Connections for Precast Concrete Cladding", *International Symposium on Architectural Precast Concrete Cladding - Its Contribution to Lateral Resistance of Buildings*, Chicago, Illinois, USA, November, 8-9, 300-310.

Palsson, H., Goodno, B.J. (1982). "A Degrading Stiffness model for Precast Concrete Cladding", *7th European Conference of Earthquake Engineering (ECEE)*, Athens, Greece, September 20-25, **5**, 135-142.

Palsson, H., Goodno, B.J. (1988). "Influence of Interstory Drift on Cladding Panels and Connections", *9th World Conference on Earthquake Engineering (WCEE)*, Tokyo-Kyoto, Japan, August 2-9, **6**, 213-218.

Palsson, H., Goodno, B.J., Craig, J.I., Will, K.M. (1984). "Cladding Influence on Dynamic Response of Tall Buildings", *Earthquake Engineering and Structural Dynamics*, **12**(2), 215-228.

Pampanin, S. (2000). "Alternative design philosophies and seismic response of precast concrete buildings", *PhD Thesis dissertation,* Department of Structural Engineering, Politecnico di Milano.

Pampanin, S., Priestley, M.J.N., Sritharan, S. (2001). "Analytical Modelling of the Seismic Behaviour of Precast Concrete Frames Designed with Ductile Connections", *Journal of Earthquake Engineering*, **5**(3), 329-367.

Pantoli, E., Chen, M., Hutchinson, T., Underwood, G.A., Hildebrand, M. (2013). "Shake table testing of a full-scale five-story building: seismic performance of precast concrete cladding panels", *4th European Community on Computational Methods in Applied Sciences (ECCOMAS) Thematic Conference on Computational Methods in Structural Dynamics and Earthquake Engineering*, Kos Island, Greece, June, 12-14, pp. 19.

Pegon, P., Molina, F.J., Magonette, G. (2008). "Continuous pseudo-dynamic testing at ELSA", in Hybrid Simulation; Theory, Implementation and Applications, ed. Saouma V.E. and Sivaselvan M. V. (Taylor & Francis/Balkema), 79-88.

Pinelli, J.P., Craig, J.I., (1989). "Experimental studies on the performance of Mexican precast cladding connections", *International Symposium on Architectural Precast Concrete Cladding - Its Contribution to Lateral Resistance of Buildings*, Chicago, Illinois, USA, November, 8-9, 159-176.

Pinelli, J.P., Craig, J.I., Goodno, B.J. (1995). "Energy based seismic design of ductile cladding systems", *Journal of Structural Engineering*, American Society of Civil Engineers (ASCE), **121(**3), 567 – 577.

Pinelli, J.P., Craig, J.I., Goodno, B.J., Hsu, C.C. (1993). "Passive Control of Building Response Using Energy Dissipating Cladding Connections", *Earthquake Spectra*, **9**(3), 529-546.

Pinelli, J.P., Moore, C., Craig, J.I., Goodno, B.J. (1992). "Experimental testing of ductile cladding connections for building façades", *The Structural Design of Tall Buildings*, **1**(1), 57-72.

Pinelli, J.P., Moore, C., Craig, J.I., Goodno, B.J. (1996). "Testing of Energy Dissipating Cladding Connections", *Earthquake Engineering and Structural Dynamics*, **25**, 129-147.

Piras, D., Belleri, A., Riva, P. (2010). "Prove sperimentali sul comportamento sismico di pannelli di tamponamento orizzontali prefabbricati", *18° Congresso C.T.E. (Collegio dei Tecnici della industrializzazione Edilizia)*, Brescia, Italy, November 11-13, **1**, 13-20.

Priestley, M.J.N., Calvi, G.M., Kowalsky, M.J. (2007). Displacement based seismic design of structures, Istituto Universitario per gli Studi Superiori (IUSS) press, Pavia, Italy, 1st edition, pp. 733.

Priestley, M.J.N., Seible, F., Calvi, G.M. (1996). Seismic design and retrofit of bridges, Wiley-Interscience Editor, 1st edition, pp. 686.

Priestley, M.J.N., Sritharan, S., Conley, J.R., Pampanin, S. (1999). "Preliminary Results and Conclusions From the PRESSS Five-Story Precast Concrete Test Building", *Special Report in PCI Journal,* Precast Concrete Institute, **44**(6), 42-67.

Priestley, M.J.N. (1996). "The PRESSS Program - Current Status and Proposed Plans for Phase III", *Special Report in PCI Journal,* Precast Concrete Institute, **41**(2), 22-40.

Priestley, M.J.N. (1991). "Overview of PRESSS Research Program", *PCI Journal,* Precast Concrete Institute, **36**(4), 50-57.

Protezione Civile, (2012). "Linee di indirizzo per interventi locali e globali su edifice industriali monopiano non pogettati con criteri antisismici", Report from DPC, ReLUIS, CNI, Assobeton, 78 pp. (in Italian).

Psycharis, I., Mouzakis, H. (2012a). "Monotonic, cyclic and shaking table tests on pinned beam-column connections", *15th World Conference of Earthquake Engineering (WCEE)*, Lisbon, Portugal, September 24-28, paper No. 3070.

Psycharis, I., Mouzakis, H. (2012b). "Shear resistance of pinned connections of precast members to monotonic and cyclic loading", *Engineering Structures*, **41**, 413-427.

Restrepo, J., Park, R., Buchanan, A. (1993). The Seismic Behaviour of Connections between Precast Concrete Elements, *Research Report 93-3*, Department of Civil Engineering, University of Canterbury, Christchurch, Canterbury, New Zealand.

Rihal, S.S. (1988). "Earthquake resistance and behavior of heavy facades/claddings and connections in medium-rise steel-framed buildings", *9th World Conference on Earthquake Engineering (WCEE)*, Tokyo-Kyoto, Japan, August 2-9, **6**.

Rihal, S.S. (1989). "Earthquake resistance and behaviour of APCC and connections", *International Symposium on Architectural Precast Concrete Cladding - Its Contribution to Lateral Resistance of Buildings*, Chicago, Illinois, USA, November, 8-9, 110-140.

Roh, H., Reinhorn, A.M. (2009). "Analytical modeling of rocking elements", *Engineering Structures*, **31**, 1179-1189.

Roland, C.M. (2006). "Mechanical behaviour of rubber at high strain rates", *Rubber Chemistry and Technology*, **79**, 429-459.

Sack, R.L., Beers, R.J., Thomas, D.L. (1989). "Seismic Behavior of Architectural Precast Concrete Cladding", *International Symposium on Architectural Precast Concrete Cladding - Its Contribution to Lateral Resistance of Buildings*, Chicago, Illinois, USA, November, 8-9, 141-158.

SAFECAST (2009). Performance of Innovative Mechanical Connections in Precast building structures under seismic conditions, FP7-SME-2007, Grant agreement number 218417.

Saisi, A., Toniolo, G. (1998). "Precast r.c. columns under cyclic loading: an experimental programme oriented to EC8", *Studi e Ricerche*, Scuola di Specializzazione F.lli Pesenti, Politecnico di Milano.

Sakamoto, I., Oohashi, Y., Yamada, M., Watanabe, H., Yokogi, K. (1987). "An experimental study on seismic performance of external ALC wall panels", *Summary of Technical Papers of Annual Conventions*, Architectural Institute of Japan, paper No. 1101-1103**,** 201-206.

Savoia, M., Mazzotti, C., Buratti, N., Ferracuti, B., Bovo, M., Ligabue, V., Vincenzi, L. (2012). "Damages and collapses in industrial precast buildings after the Emilia earthquake", *Ingegneria Sismica*, **29**(2-3), 120-131.

Schoettler, M.J., Belleri, A., Zhang, D., Restrepo, J.I., Fleischman, R.B. (2009). "Preliminary results of the shake-table testing for the development of a diaphragm seismic design methodology", *PCI Journal,* Precast Concrete Institute, Winter, 100-124.

Schoettler, M.J., Restrepo, J.I., Fleischman, R.B., Nigbor, R., Deutsch, D. (2012). "Mapping damage in precast concrete buildings from the February 2011 Christchurch, New Zealand earthquake", *Network for Earthquake Engineering Simulation (NEES)*.

Schultz, A.E., Magana, R.A., Tadros, M.K., Huo, X. (1994). "Experimental study of joint connections in precast concrete walls", *5th U.S. National Conference on Earthquake Engineering*, Chicago, Illinois, USA, July 10-14, 1994, **2**, 579-587.

Sheppard, D.A. (1981). "Connections for seismic resistant precast concrete construction", *Workshop on Design of Prefabricated Concrete Buildings for Earthquake Loads*, ATC-08.

Shibata, A., Sozen, M.A. (1976). "Substitute-structure method for seismic design in R/C", *Journal of Structural Division*, American Society of Civil Engineers (ASCE), **102**, January, 1-18.

Shiohara, H., Watanabe, F. (2000). "The Japan PRESS precast concrete connection design", *12th World Conference on Earthquake Engineering (WCEE)*, Auckland, New Zealand, January 30 - February 4, paper No. 2348, pp. 8.

Sielaff, B.J. (2005). "Evolution of design code requirements for exterior elements and connections", *Earthquake Spectra*, **21**(1), 213-224.

Simeonov, S. *et al.* (1985). Building Construction Under Seismic Conditions in The Balkan Region – Design and Construction of Prefabricated Reinforced Concrete Building Systems, UNDP/UNIDO project RER/79/015.

Singh, M.P., Moreschi, L.M., Suarez, L.E., Matheu, E.E. (2006a). "Seismic design forces. I: Rigid nonstructural components", *Journal of Structural Engineering*, ASCE, **132**(10), 1524-1532.

Singh, M.P., Moreschi, L.M., Suarez, L.E., Matheu, E.E. (2006b). "Seismic design forces. II: Flexible nonstructural components", *Journal of Structural Engineering*, ASCE, **132**(10), 1533-1542.

Smith, B.J., Kurama, Y.C., McGinnis, M.J. (2011). "Design and Measured Behavior of a Hybrid Precast Concrete Wall Specimen for Seismic Regions", *Journal of Structural Engineering*, ASCE, **137**(10), 1052-1062.

Smith, B.S., Gaiotti, R. (1989). "Interaction of Precast Concrete Cladding with a Story-Height Frame Module", *International Symposium on Architectural Precast Concrete Cladding - Its Contribution to Lateral Resistance of Buildings*, Chicago, Illinois, USA, November, 8-9, 48-61.

Soong, T.T., Spencer Jr, B.F. (2002). "Supplemental energy dissipation: state-of-the-art and state-of-the-practice", *Engineering Structures*, **24**, 243-249.

Soroushian, P., Obaseki, K., Rojas, M., Najm, H.S. (1987a). "Behaviour of bars in dowel action against concrete cover", *ACI Structural Journal*, American Concrete Institute, **84**(2), 170-176.

Soroushian, P., Obaseki, K., Rojas, M., Sim, J. (1987b). "Analysis of dowel bar acting against concrete core", *ACI Structural Journal*, American Concrete Institute, **83**(4), 642-649.

Stanton, J.F., Hawkins, N.M., Hicks, T.R. (1991). "PRESSS II Project 1.3: Connection Classification and Evaluation", *PCI Journal,* Precast Concrete Institute, **36**(5), pp 62-71.

Strand7 Pty Limited (2005). Strand7 (Straus7) software – theoretical manual, version 1.

Strand7 Pty Limited (2010). Using Strand7 (Straus7) – introduction to the Strand7 finite element analysis system, edition 3.

Sullivan, T.J., Priestley, M.J.N., Calvi, G.M. (2005). "Development of an innovative seismic design procedure for frame-wall structures", *Journal of Earthquake Engineering,* **9**(2), 279-307.

Symans, M.D., Charney, F.A., Whittaker, A.S., Constantinou, M.C., Kircher, C.A., Johnson, M.W., McNamara, M.J. (2008). "Energy dissipation systems for seismic applications: current practice and recent developments", *Journal of Structural Engineering*, American Society of Civil Engineers (ASCE), January, 3-21.

Symans, M.D., Cofer, W.F., Fridley, K.J. (2002). "Base isolation and supplemental damping systems for seismic protection of wood structures: literature review", *Earthquake Spectra*, **18**(3), 549-572.

Takeda, T., Sozen, M.A., Nielsen, N.N. (1970). "Reinforced Concrete Response to Simulated Earthquakes", *Journal of the Structural Division*, American Society of Civil Engineers (ASCE), **96**(12), 2557-2573.

Tena-Colunga, A., Abrams, D. (1996). "Seismic Behavior of Structures with Flexible Diaphragms", *Journal of Structural Engineering*, American Society of Civil Engineers (ASCE), **122**(4), 439-445.

Thiel, C.C., Elsesser, E., Lindsay, J., Kelly, T., Bertero, V.V., Filippou, F., McCann, R. (1986). "Seismic Energy Absorbing Cladding System: A Feasibility Study", *ATC-17 Seminar and Workshop on Base Isolation and Passive Energy Dissipation*, ATC, San Francisco, California, USA, March 12-14, 251-260.

Titi, A. (2012). "Lifetime probabilistic seismic assessment of multistory precast buildings", *PhD Thesis dissertation,* Department of Structural Engineering, Politecnico di Milano.

Titi, A., Biondini, F. (2013). "Resilience of concrete frame structures under corrosion", *11th International Conference on Structural Safety and Reliability* (ICOSSAR 2013), New York, NY, USA, June 16-20, 2013. In: *Safety, Reliability, Risk and Life-Cycle Performance of Structures and Infrastructures*, G. Deodatis, B.R. Ellingwood & D.M. Frangopol (Eds.), CRC Press, Taylor & Francis Group, 2014, 597-604.

Titi, A., Biondini, F. (2014). "Probabilistic seismic assessment of multistory precast concrete frames exposed to corrosion", *Bulletin of Earthquake Engineering*, **12**(6), 2665-2681.

Toniolo, G. (2012). "Regole di progetto per le connessioni delle strutture prefabbricate", *19° Congresso C.T.E. (Collegio dei Tecnici della industrializzazione Edilizia)*, Bologna, Italy, November 8-10, 515-522 (in Italian).

Toniolo, G. (2012). "SAFECAST project: European research on seismic behaviour of the connections of precast structures", *15th World Conference of Earthquake Engineering (WCEE)*, Lisbon, Portugal, September 24-28, paper No.1389.

Toniolo, G. (2014). "Ruolo dei sistemi di connessione dei pannelli di tamponamento nel comportamento sismico degli edifici prefabbricati", *20° Congresso C.T.E. (Collegio dei Tecnici della industrializzazione Edilizia)*, Milano, Italy, November 6-8, 521-531 (in Italian).

Towashiraporn, P., Park, J., Goodno, B.J., Craig, J.I. (2002). "Passive control methods for seismic response modification", *Progress in Structural Engineering and Materials,* **4**, 74-86.

Tsopelas, P., Constantinou, M.C., Kircher, C.A., Whittaker, A.S. (1997). "Evaluation of simplified method of analysis for yielding structures", *Technical Report NCEER-97-0012*, National Center for Earthquake Engineering Research, State University of New York, Buffalo, New York, USA, pp. 194.

Tsoukantas, S.G., Tassios, T.P. (1989). "Shear resistance of connections between reinforced concrete linear precast elements", *ACI Structural Journal*, American Concrete Institute, **86**(3), 242-249.

Tyler, R.G., (1977). "Damping in Building Structures by Means of PTFE Sliding Joints", *Bulletin of the New Zealand Society for Earthquake Engineering (NZSEE)*, **10**(3), 139-142.

Valente, M. (2010). "Valutazione dell'azione diaframma della copertura sulla risposta sismica di edifici monopiano prefabbricati", *18° Congresso C.T.E. (Collegio dei Tecnici della industrializzazione Edilizia)*, Brescia, Italy, November 11-13, 2, 819-828.

Valente, M. (2013). "Improving the seismic performance of precast buildings using dissipative devices", *The 2nd International Conference on Rehabilitation and Maintenance in Civil Engineering, Procedia Proceedings,* **54**(2013), 795-804 (in Italian).

Villaverde, R. (1997). "Seismic design of secondary structures: state of the art", *Journal of Structural Engineering*, ASCE, **123**(8), 1011-1019.

Vintzeleou, E.N., Tassios, T.P. (1987). "Behavior of dowels under cyclic deformations", *ACI Structural Journal*, American Concrete Institute, **84**(1), 18-30.

Vintzeleou, E.N., Tassios. T.P. (1985). "Mechanics of load transfer along interfaces in reinforced concrete, prediction of shear force vs. shear displacement curves", *Studi e Ricerche*, Scuola di Specializzazione F.lli Pesenti, Politecnico di Milano, **7**, 121-161.

Wan, G., Fleischman, R.B., Zhang, D. (2012). "Effect of spandrel beam to double tee connection characteristic on flexure-controlled precast diaphragms", *Journal of Structural Engineering*, American Society of Civil Engineers (ASCE), February, 247-257.

Wang, M.L. (1986a). "Nonstructural elements test phase: U.S.-Japan cooperative research project on a full scale steel test frame", Center of Environmental Design Research, University of California Berkeley, pp. 140.

Wang, M.L. (1986b). "Full scale tests of cladding components", *3rd Conference on Engineering and Mechanical Division*, American Society of Civil Engineers (ASCE), Los Angeles, California, USA, March 31- April 02, 497-504.

Wang, M.L. (1987). "Cladding Performance on a Full Scale Test Frame", *Earthquake Spectra*, **3**(1), 119-173.

Wang, M.L. (1992). Design of cladding for earthquakes, in: *Tall Building Systems and Concepts*, Council on Tall Buildings and Urban Habitat, Committee 12a, McGraw-Hill, Inc., New York, USA, Chapter 4.

Weidlinger, P. (1973). "Shear Field Panel Bracing", *Journal of Structural Division*, American Society of Civil Engineers (ASCE), **99**(7), 1615-1631.

Whittaker, A., Costantinou, M. (2004). Seismic energy dissipation systems for buildings, in: *Earthquake engineering: From engineering seismology to performance-based engineering*, Boca Raton (FL), CRC, chapter 12.

Wiebe, L., Chritopoulos, C. (2014). "Controlled rocking systems for enhanced seismic resilience: State of the art", *IC-SDCI 2014*, Shanghai, China, May 16-18, 496-503.

Wolz, M.W., Hsu, C.C., Goodno, B.J. (1992). "Nonlinear Interaction between Building Structural Systems and Nonstructural Cladding Components", *ATC-29 Seminar and Workshop on Seismic Design and Performance of Equipment and Nonstructural Elements in Buildings and Industrial Structures*, ATC, Irvine, California, USA, October 3-5, 329-340.

Zoubek, B., Fischinger, M., Isakovic, T. (2014). "Seismic response of dowel connections in precast industrial buildings", *2nd European Conference on Earthquake Engineering and Seismology (ECEES)*, Istanbul, Turkey, August 25-39, pp. 11.